M.A. Hayat
Editor

Tumors of the Central Nervous System

Volume 12
Molecular Mechanisms, Children's Cancer, Treatments, and Radiosurgery

Springer

Tumors of the Central Nervous System
Volume 12

For further volumes:
http://www.springer.com/series/8812

Tumors of the Central Nervous System
Volume 12

Tumors of the Central Nervous System

Molecular Mechanisms, Children's Cancer, Treatments, and Radiosurgery

Edited by

M.A. Hayat
Distinguished Professor
Department of Biological Sciences,
Kean University, Union, NJ, USA

Springer

Editor
M.A. Hayat
Department of Biological Sciences
Kean University
Room 213, Library building
Morris Avenue 1000
Union, NJ 07083, USA

ISBN 978-94-007-7216-8 ISBN 978-94-007-7217-5 (eBook)
DOI 10.1007/978-94-007-7217-5
Springer Dordrecht Heidelberg New York London

Library of Congress Control Number: 2013953935

Printed on acid-free paper

Springer is part of Springer Science+Business Media (www.springer.com)

Although touched by technology, surgical pathology always has been, and remains, an art. Surgical pathologists, like all artists, depict in their artwork (surgical pathology reports) their interactions with nature: emotions, observations, and knowledge are all integrated. The resulting artwork is a poor record of complex phenomena.

Richard J. Reed, MD

One Point of View

All small tumors do not always keep growing, especially small breast tumors, testicular tumors, and prostate tumors. Some small tumors may even disappear without a treatment. Indeed, because prostate tumor grows slowly, it is not unusual that a patient may die at an advanced age of some other causes, but prostate tumor is discovered in an autopsy study. In some cases of prostate tumors, the patient should be offered the option of active surveillance followed by PSA test or biopsies. Similarly, every small kidney tumor may not change or may even regress. Another example of cancer or precancer reversal is cervical cancer. Precancerous cervical cells found with Pap test, may revert to normal cells. Tumor shrinkage, regression, dormancy, senescence, reversal, or stabilization is not impossible. Can prosenescence therapy be an efficient alternative strategy to standard therapies for cancer prevention and treatment?

Another known example of cancer regression is found in pediatric neuroblastoma patients. Neuroblastoma shows one of the highest rates of spontaneous regression among malignant tumors. In addition to the well-known spontaneous regression in stage 4S disease, the high incidence of neuroblastoma remnants found during autopsy of newborns suggest that localized lesions may undergo a similar regression (Guin et al. 1969). Later studies also indicate that spontaneous regression is regularly seen in infants with localized neuroblastoma and is not limited to the first year of life (Hero et al. 2008). These and other studies justify the "wait and see" strategy, avoiding chemotherapy and radiotherapy in infants with localized neuroblastoma, unless MYCN gene is amplified. Infants with nonamplified MYCN and hyperdiploidy can be effectively treated with less intensive therapy. Infants with disseminated disease without MYCN have excellent survival with minimal or no treatment. Another example of spontaneous shrinkage and loss of tumors without any treatment is an intradural lipoma (Endoh et al. 1998).

Although cancers grow progressively, various lesions such as cysts and thyroid adenomas show self-limiting growth. Probably, cellular senescence occurs in many organ types following initial mutations. Cellular senescence, the growth arrest seen in normal mammalian cells after a limited number of divisions, is controlled by tumor suppressors, including p53 and p16, and so this phenomenon is believed to be a crucial barrier to tumor development. It is well-established that cell proliferation and transformation induced by oncogene activation are restrained by cellular senescence.

Metastasis is the main cause of death from cancer. Fortunately, metastasis is an inefficient process. Only a few of the many cancer cells detached from the primary tumor succeed in forming secondary tumors. Metastatic inefficiency varies depending on the location within an organ, but the malignancy may continue to grow preferentially in a specific tissue environment. Some of the cancer cells shed from the primary tumor are lost in the circulation due to hemodynamic forces or the immune system, macrophages, and natural killer cells.

Periodic rejection of a drug by FDA, which was previously approved by the FDA, is not uncommon. Most recently, the FDA ruled that Avastin should not be used to treat advanced breast cancer, although it remains on the market to treat other cancers, including colon and lung malignancies. Side-effects of Avastin include high blood pressure, massive bleeding, heart attack, and damage to the stomach and intestines.

Unwanted side effects of some drug excipients (e.g., propylene glycol, menthol) may also pose safety concerns in some patients. Excipients are defined as the constituents of the pharmaceutical formulation used to guarantee stability, and physicochemical, organoleptic and biopharmaceutical properties. Excipients frequently make up the majority of the volume of oral and parenteral drugs. Not all excipients are inert from the biological point of view. Although adverse drug reactions caused by the excipients are a minority of all adverse effects of medicinal products, the lack of awareness of the possible risk from excipients should be a concern for regulatory agencies, physicians, and patients (Ursino et al. 2011). Knowledge of the potential side effects of excipients is important in clinical practice.

It is known that chemotherapy can cause very serious side-effects. One most recent example of such side-effects was reported by Rubsam et al. (2011). Advanced hepatocellular carcinoma (HCC) induced by hepatitis C virus was treated with Sorafenib. It is an oral multikinase inhibitor that interferes with the serine/threonine kinases RAF-1 and B-Raf and the receptor tyrosine kinases of the vascular endothelial growth factor receptors and the platelet-derived growth factor receptor-beta. Although sorafenib is effective in regressing HCC, it shows serious side-effects including increasingly pruritic and painful skin changes (cutaneous eruption).

An example of unnecessary surgery is the removal of all the armpit lymph nodes after a biopsy when a sentinel node shows early stage breast cancer; removal of only the sentinel node may be needed. Limiting the surgery to the sentinel node avoids painful surgery of the armpit lymph nodes, which can have complications such as swelling and infection (such limited surgery is already being practiced at the Memorial Sloan-Kettering Cancer Research Center). Radiation-induced second cerebral tumors constitute a significant risk for persons undergoing radiotherapy for the management of cerebral neoplasms. High-grade gliomas are the most common radiation-induced tumors in children (Pettorini et al. 2008). The actual incidence of this complication is not known, although it is thought to be generally low.

Medical Radiation

Chromosome aberrations induced by ionizing radiation are well-known. Medical radiation-induced tumors are well-documented. For example, several types of tumors (sarcomas, meningiomas) can develop in the CNS after irradiation of the head and neck region (Parent 1990). Tumorigenic mechanisms underlying the radiation therapy of the CNS are discussed by Amirjamshidi and Abbassioun (2000) (See below).

Radiation therapy is commonly used to treat, for example, patients with primary and secondary brain tumors. Unfortunately, ionizing radiation has limited tissue specificity, and tends to damage both neoplastic and normal brain tissues. Radiation-induced brain injury, in fact, is a potential, insidious later cerebral side-effect of radiotherapy. Most commonly it consists of damage in small arteries and capillaries, resulting in secondary processes of ischemia.

After radiation therapy, imaging techniques (CT, MRI, SPECT) can be used to assess treatment response and detect radiation-induced lesions and recurrent tumors. Optical spectroscopy has also been used for detecting radiation damage (Lin et al. 2005). The F_{500} nm spectral peak allows accurate selection of tissues for biopsy in evaluating patients with new, contrast enhancing lesions in the setting of previous irradiation. This peak is highly correlated with a histological pattern of radiation injury. Deep lesions require a stereotactic biopsy to be conclusive. Also, much of the radiation effect is mediated by acute and chronic inflammatory cellular reactions. Biopsy samples supplement pathological differentiation of radiation effect from tumor progression. It should be noted that most of the biopsies show radionecrosis as well as scattered tumor cells.

Women treated with therapeutic chest radiation may develop cancer. This possibility becomes exceedingly serious considering that 50,000–55,000 women in the United States have been treated with moderate to high-dose chest radiation (~20 Gy). This possibility is much more serious for pediatric or young adult cancer patients, because these women are at a significantly increased risk of breast cancer and breast cancer mortality following cure of their primary malignancy (Martens et al. 2008). A recent study also indicates that such young women develop breast cancer at a young age, which does not appear to plateau (Henderson et al. 2010). In this high risk population, ironically there is a benefit associated with early detection. In other words, young women with early stage breast cancer following chest radiation have a high likelihood for favorable outcome, although life-long surveillance is needed.

Presently, although approximately 80 % of the children with cancer are cured, the curative therapy could damage a child's developing organ system; for example, cognitive deficits following cranial radiotherapy are well known. Childhood survivors of malignant diseases are also at an increased risk of primary thyroid cancer (Sigurdson et al. 2005). The risk of this cancer increases with radiation doses up to 20–29 Gy. In fact, exposure to radiation therapy is the most important risk factor for the development of a new CNS tumor in survivors of childhood cancer, including leukemia and brain tumors.

The higher risk of subsequent glioma in children subjected to medical radiation at a very young age reflects greater susceptibility of the developing brain to radiation. The details of the dose-response relationships, the expression of excess risk over time, and the modifying effects of other host and treatment factors have not been well defined (Neglia et al. 2006).

A recent study indicates that childhood brain tumor survivors are at an increased risk of late endocrine effects, particularly the patients treated with cranial radiation and diagnosed at a younger age (Shalitin et al. 2011). Among children with cancer, the application of radiotherapy, therefore, should not be taken lightly, and it should be administered only when absolutely necessary to successfully treat the primary tumor. When radiotherapy is administered, use of the minimum effective dose tends to minimize the risk of second CNS neoplasms (late effect). Prolonged follow-up of childhood cancer survivors (particularly those treated with radiation) is necessary because of the long period between treatment and the development of malignancy. This practice should be a part of the effective therapy of the primary disease.

It is well established that radiation doses are related to risk for subsequent malignant neoplasms in children with Hodgkin's disease. It has been reported that increasing radiation dose was associated with increasing standardized incidence ratio ($p = 0.0085$) in survivors of childhood Hodgkin's disease (Constine et al. 2008). Approximately, 75 % of subsequent malignancies occurred within the radiation field. Although subsequent malignancies occur, for example, in breast cancer survivors in the absence of radiotherapy, the rise increases with radiation dose.

The pertinent question is: Is it always necessary to practice tumor surgery, radiotherapy, chemotherapy or hormonal therapy or a combination of these therapies? Although the conventional belief is that cancer represents an "arrow that advances unidirectionally", it is becoming clear that for cancer to progress, it requires cooperative microenvironment (niche), including immune system and hormone levels. However, it is emphasized that advanced (malignant) cancers do not show regression, and require therapy. In the light of the inadequacy of standard treatments of malignancy, clinical applications of the stem cell technology need to be expedited.

Prostate Cancer

There were an estimated 217,730 new cases of prostate cancer in the United States in 2010 with 32,050 deaths, making it the second leading cause of cancer deaths in men. Currently, there are more than 2,000,000 men in the United States who have had radical or partial prostate surgery performed. Considering this huge number of prostate surgeries and the absence of a cumulative outcome data, it seems appropriate to carefully examine the benefits of radical surgery, especially in younger men.

Clinical prostate cancer is very rare in men of the ages younger than 40 years. In this age group the frequency of prostate malignancy is 1 in 10,000 individuals. Unfortunately, the incidence of malignancy increases over the ensuing decades, that is, the chance of prostate malignancy may reach to 1 in

7 in men between the ages of 60 and 79 years. Reactive or aging-related alterations in the tumor microenvironment provide sufficient influence, promoting tumor cell invasion and metastasis. It has been shown that nontumorigenic prostate epithelial cells can become tumorigenic when cocultured with fibroblasts obtained from regions near tumors (Olumi et al. 1999).

Prostate cancer treatment is one of the worst examples of overtreatment. Serum prostate specific antigen (PSA) testing for the early detection of prostate cancer is in wide use. However, the benefit of this testing has become controversial. The normal cut-off for serum levels of PSA is 4 ng/ml, so a man presenting with a PSA above this level is likely to require a rectal biopsy, but only in 25 % of men with serum levels of PSA between 4 and 10 ng/ml have cancer (Masters 2007). The PSA threshold currently being used for biopsy ranges between 2.5 and 3.4 ng/ml. Up to 50 % of men presenting with prostate cancer have PSA levels within the normal range. It is apparent that screening of prostate cancer using PSA has a low specificity, resulting in many unnecessary biopsies, particularly for gray zone values (4–10 ng/ml). According to one point of view, the risks of prostate cancer overdetection are substantial. In this context, overdetection means treating a cancer that otherwise would not progress to clinically significant disease during the lifetime of the individual. Overdetection results in overtreatment. The advantages and limitations of PSA test in diagnosing prostate cancer were reviewed by Hayat (2005, 2008).

Androgen deprivation therapy (ADT) is an important treatment for patients with advanced stage prostate cancer. This therapy is carried out by blocking androgen receptor or medical or surgical castration. Although ADT is initially very effective, treated tumors inevitably progress to androgen-independent prostate cancer (AIPC); which is incurable. One possible mechanism responsible for the development of AIPC is modulation of the tissue microenvironment by neuroendocrine-like cancer cells, which emerge after ADT (Nelson et al. 2007).

Recently, Pernicova et al. (2011) have further clarified the role of androgen deprivation in promoting the clonal expansion of androgen-independent prostate cancer. They reported a novel linkage between the inhibition of the androgen receptor activity, down-regulation of S-phase kinase-associated protein 2, and the formation of secretory, senescent cells in prostate tumor cells. It is known that several components of the SASP secretome, such as IL-6, IL-8, KGH, and epidermal growth factor, are capable of transactivating androgen receptor under androgen-depleted conditions (Seaton et al. 2008). It needs to be pointed out that androgen deprivation therapy, used in high-risk patients with prostate cancer, may cause reduced libido, erectile dysfunction, fatigue, and muscle loss; osteoporosis is also a late complication. Therefore, periodic bone density scanning needs to be considered.

Recently, the FDA cleared the use of NADiA (nucleic acid detection immunoassay) ProsVue prognostic cancer test. This proprietary nucleic acid detection immunoassay technology identifies extremely low concentrations of proteins that have not been routinely used as a diagnostic or prognostic aid. It is an in vitro diagnostic assay for determining the rate of change of serum total PSA over a period of time. The assay can quantitate PSA at levels <1 ng/ml.

This technique can be used as a prognostic marker, in conjunction with clinical evaluation, to help identify patients at reduced risk for recurrence of prostate cancer for years following prostatectomy. It targets the early detection of proteins associated with cancer and infectious diseases. This technique combines immunoassay and real-time PCR methodologies with the potential to detect proteins with femtogram/ml sensitivity (10–15 g/ml). Additional clinical information is needed regarding its usefulness in predicting the recurrence.

A significant decrease in the risk of prostate cancer-specific mortality is observed in men with few or no comorbidities. Indeed, active surveillance in lieu of immediate treatment (surgery or radiation, or both) is gaining acceptance. Most men with prostate cancer, even those with high-risk disease, ultimately die as a result of other causes (Lu-Yao et al. 2009). Debate on this controversy is welcome, but narrow opinions and facile guidelines will not lead to facts and new information; men worldwide deserve it (Carroll et al. 2011). Automatic linking positive diagnosis with treatment, unfortunately, is a common clinical practice. Unfortunately, even men who are excellent candidates for active surveillance in the United States often undergo some treatment. Deferment of treatment is advised in men with low-risk disease, especially of a younger age.

Active surveillance is proposed for patients with low-risk prostate cancer in order to reduce the undesirable effects of overdiagnosis. Prostate specific antigen serum level lower than 10 ng/L and Gleason score lower than 7 are the main criteria to select patients for active surveillance. The correct use of these two criteria is essential to differentiate between aggressive and nonaggressive prostate cancer. Autopsy studies indicate that approximately one out of three men older than 50 years show histological evidence of prostate cancer (Klotz 2008). Thus, a large proportion of prostate cancers are latent, never destined to progress, or affect the life of the patient. It is estimated that the percentage of low-risk prostate cancer is between 50 % and 60 % of newly diagnosed cases. A large number of patients die having prostate cancer, but not because of this cancer (Filella et al. 2011).

First whole genome sequences of prostate tumors were recently published online in *Nature journal* (vol. 470: 214–220, 2011). This study revealed that rather than single spelling errors, the tumor has long "paragraphs" of DNA that seem to have broken off and moved to another part of the genome (rearrangement of genes), where they are most active. These portions of DNA contain genes that help drive cancer progression. The mutated genes involved include PTEN, CADM2, MAG12, SPOP, and SPTA1. This information may lead to the development of more efficient, less invasive ways to diagnose and treat this cancer. Such information, in addition, should lead to personalized therapeutics according to sequencing results of different gene mutations or chromosomal rearrangements. The urgent need of such studies becomes apparent considering the huge number of new cases of prostate problems reported every year.

In contrast to prostate cancer, cardiovascular disorders take the heavier toll of life. In other words, the risk of death for men in the United States between the ages of 55 and 74 years due to cardiovascular disease surpasses that of

prostate cancer. Cardiovascular disease is the most common of the chronic non-communicable diseases that impact global mortality. Approximately, 30 % of all deaths worldwide and 10 % of all healthy life lost to disease are accounted for by cardiovascular disease alone.

In conclusion, initial treatment with standard surgery, irradiation, chemotherapy, or hormonal therapy, or combination of these protocols can result in both local and systemic sequalae. Therefore, surveillance for late recurrence and secondary primary malignancies is recommended for most cancer patients. Patients with breast, lung, prostate, colorectal, and head and neck cancers constitute the largest groups requiring long-term monitoring and follow-up care.

Eric Hayat

References

Amirjamshidi A and Abbassioun K (2000) Radiation-induced tumors of the central nervous system occurring in childhood and adolescence. Childs Nerv Syst 16:390–397

Carroll PR, Whitson JH, Cooperberg MR (2011) Serum prostate-specific antigen for the early detection of prostate cancer; always, never, or only sometimes? J Clin Oncol 29:345–346

Constine LS, Tarbell N, Hudson MM et al (2008) Subsequent malignancies in children treated for Hodgkin's disease: associations with gender and radiation dose. Int J Radiat Oncol Biol Phys 72:24–33

Endoh M, Iwasaki Y, Koyanagi I, Hida K, Abe H (1998) Spontaneous shrinkage of Iumbosacral lipoma in conjunction with a general decrease in body fat: case report. Neurosurgery 43(1):150–151; discussion 151–152

Filella X, Alcover J, Molina R (2011) Active surveillance in prostate cancer: the need to standardize. Tumor Biol 32:839–843

Guin P, Gilbert E, Jones B (1969) Incidental neuroblastoma in infants. Am J Clin Pathol 51:126–136

Hayat MA (2005) Prostate carcinoma: an introduction. In: Immunohistochemistry and in situ hybridization of human carcinomas, vol. 2. Elsevier, San Francisco, pp 279–297

Hayat MA (2008) Prostate carcinoma. In: Methods of cancer diagnosis, therapy, and prognosis, vol. 2. Springer Science, New York, pp 391–396

Henderson TO, Amsterdam A et al (2010) Surveillance for breast cancer in women treated with chest radiation for a childhood, adolescent or young adult cancer: a report from Children's Oncology Group. Ann Intern Med 152:1–22

Hero S, Simon T, Spitz R, Ernestus K, Gnekow A, Scheel-Walter H, Schwabe D, Schilling F, Benz-Bohm G, Berthold F (2008) Localized infant neuroblastomas often show spontaneuous regression: results of the prospective trials NB95-S and NB 97. J Clin Oncol 26:1504–1510

Klotz L (2008) Low-risk prostate cancer can and should often be managed with active surveillance and selective delayed intervention. Nat Clin Pract Urol 5:2–3

Lin W-C, Mahadevan-Jansen A, Johnson MD, Weil R, Toms SA (2005) *In vivo* optical spectroscopy detects radiation damage in brain tissue. Neurosurgery 57:518–525

Lu-Yao GL, Albertsen PC, Moore DF et al (2009) Outcomes of localized prostate cancer following conservative management. JAMA 302:1202–1209

Masters JR (2007) Clinical applications of expression profiling and proteomics in prostate cancer. Anticancer Res 27:1273–1276

Mertens AC, Liu Q, Neglia JP et al (2008) Cause-specific late mortality among 5-year survivors of childhood cancer: the Childhood Cancer Survivor Study. J Natl Cancer Inst 100:1368–1379

Neglia JP, Robison LL, Stovall M, Liu Y, Packer RJ et al (2006) New primary neoplasms of the central nervous system in survivors of childhood cancer: a report from the childhood cancer survivor study. J Natl Cancer Inst 98:1528–1537

Nelson EC, Cambio AJ, Ok JH, Lara PN Jr, Evans CP (2007) Clinical implications of neuroendocrine differentiation in prostate cancer. Prostate Cancer Prostatic Dis 10:6–14
Olumi AF, Grossfeld GD, Hayward SW, Carroll PR, Tlsty TD, Cunha GR (1999) Carcinoma-associated fibroblasts direct tumor progression of initiated human prostatic epithelium. Cancer Res 59:5002–5011
Parent AD (1990) Late complications of radiation-induced neoplasms. Neurosurgery 26:1090–1091
Pernicova Z, Slabakova E, Kharaishvill G, Bouchal J, Kral M, Kunicka Z, Machalam M, Kozubik A Soucek K (2011) Androgen depletion induces senescence in prostate cancer cells through down-regulation of SKp2. Neoplasia 13:526–536
Pettorini BL, Park Y-S, Caldarelli M, Massimi L, Tamburrini G, DiRocco C (2008) Radiation induced brain tumors after central nervous system irradiation in childhood: a review. Child's Nerv Syst 24:793–805
Rubsam K, Flaig MJ, Ruzicka T, Prinz JC (2011) Erythema marginatum hemorrhagicum: a unique cutaneous side effect of sorafenib. J Am Acad Dermatol 64:1194–1196
Seaton A, Scullin P, Maxwell PJ, Wilson C, Pettigrew J, Gallagher R, O'Sullivan JM, Johnston PG, Waugh DJ (2008) Interleukin-8 signaling promotes androgen-independent proliferation of prostate cancer cells via induction of androgen receptor expression and activation. Carcinogenesis 6:1148–1156
Shalitin S, Gal M, Goshen Y, Cohen I, Yaniv I, Philip M (2011) Endocrine outcome in long-term survivors of childhood brain tumors. Horm Res Paediatr 76:113–122
Sigurdson AJ, Ronckers CM, Mertens AC et al (2005) Primary thyroid cancer after a first tumor in childhood (the childhood cancer survivor study): a nested case-control study. Lancet 365:2014–2023
Ursino MG, Poluzzi E, Caramella C, DePonti F (2011) Excipients in medicinal products used in gastroenterology as a possible cause of side effects. Regul Toxicol Pharmacol 60:93–105

Preface

It is recognized that scientific journals and books not only provide current information but also facilitate exchange of information, resulting in rapid progress in the medical field. In this endeavor, the main role of scientific books is to present current information in more details after careful additional evaluation of the investigational results, especially those of new or relatively new therapeutic methods and their potential toxic side-effects.

Although subjects of diagnosis, drug development, therapy and its assessment, and prognosis of tumors of the central nervous system, cancer recurrence, and resistance to chemotherapy are scattered in a vast number of journals and books, there is need of combining these subjects in single volumes. An attempt will be made to accomplish this goal in the projected fourteen-volume series of handbooks.

In the era of cost-effectiveness, my opinion may be minority perspective, but it needs to be recognized that the potential for false-positive or false-negative interpretation on the basis of a single laboratory test in clinical pathology does exist. Interobservor or intraobservor variability in the interpretation of results in pathology is not uncommon. Interpretative differences often are related to the relative importance of the criteria being used.

Generally, no test always performs perfectly. Although there is no perfect remedy to this problem, standardized classifications with written definitions and guidelines will help. Standardization of methods to achieve objectivity is imperative in this effort. The validity of a test should be based on the careful, objective interpretation of the tomographic images, photo-micrographs, and other tests. The interpretation of the results should be explicit rather than implicit. To achieve accurate diagnosis and correct prognosis, the use of molecular criteria and targeted medicine is important. Equally important are the translation of molecular genetics into clinical practice and evidence-based therapy. Translation of medicine from the laboratory to clinical application needs to be carefully expedited. Indeed, molecular medicine has arrived.

This is the twelfth volume in the series, Tumors of the Central Nervous System. As in the case of the eleven previously published volumes, this volume mainly contains information on the diagnosis, therapy, and prognosis of brain and spinal cord tumors. Various aspects of a large number of tumor types, including neuroblastoma, medulloblastoma, meningioma, and chordoma, are discussed. The contents are divided into four subheadings: molecular mechanisms, children's cancer, treatments, and radiosurgery, for the convenience of the readers. Molecular profiling of brain tumors to select

appropriate therapy in clinical trials of brain tumors is discussed in detail. The classification/diagnosis of brain tumors based on function analysis is presented. CDK6 as the molecular regulator of neuronal differentiation in the adult brain, and the role of aquaporins in human brain tumor growth are explained. Children's tumors, including neuroblastoma and medulloblastoma, are discussed. Molecular genetic alterations in medulloblastoma are explained. Survival differences between children and adults with medulloblastoma are pointed out. The use of various types of imaging methods to diagnose brain tumors is explained. Important, effective treatments for patients with brain and spinal tumors are included. Treatments, such as stereotactic radiosurgery, endoscopic neurosurgery, electrochemotherapy, transsphenoidal surgery, focal ablation, whole brain radiation therapy, and recraniotomy, are detailed. The remaining volumes in this series will provide additional recent information on these and other aspects of CNS malignancies.

By bringing together a large number of experts (oncologists, neurosurgeons, physicians, research scientists, and pathologists) in various aspects of this medical field, it is my hope that substantial progress will be made against this terrible disease. It would be difficult for a single author to discuss effectively the complexity of diagnosis, therapy, and prognosis of any type of tumor in one volume. Another advantage of involving more than one author is to present different points of view on a specific controversial aspect of the CNS cancer. I hope these goals will be fulfilled in this and other volumes of this series. This volume was written by 92 contributors representing 11 countries. I am grateful to them for their promptness in accepting my suggestions. Their practical experience highlights their writings, which should build and further the endeavors of the reader in this important area of disease. I respect and appreciate the hard work and exceptional insight into the nature of cancer provided by these contributors. The contents of the volume are divided into three subheadings: Pineal Tumors, Pituitary Tumors, and Spinal Tumors for the convenience of the reader.

It is my hope that the current volume will join the preceding volumes of the series for assisting in the more complete understanding of globally relevant cancer syndromes. There exists a tremendous, urgent demand by the public and the scientific community to address to cancer diagnosis, treatment, cure, and hopefully prevention. In the light of existing cancer calamity, financial funding by governments must give priority to eradicating this deadly malignancy over military superiority.

I am thankful to Dr. Dawood Farahi and Philip Connelly for recognizing the importance of medical research and publishing through an institution of higher education. I am also thankful to my students for their contribution to the preparation of this volume.

M.A. Hayat

Contents

Contents of Volume 1

Contents of Volume 2

Contents of Volume 3

Contents of Volume 4

Contents of Volume 5

Contents of Volume 6

Contents of Volume 7

Contents of Volume 8

Contents of Volume 9

Contents of Volume 10

Contents of Volume 11

Contributors

Birgit Agerholm-Larsen Department of Oncology 54B1, Copenhagen University Hospital Herlev, Herlev, Denmark

Loukas G. Astrakas Department of Medical Physics, Medical School, University of Ioannina, Ioannina, Greece

Donald S. Backos Department of Pharmaceutical Sciences, Skaggs School of Pharmacy and Pharmaceutical Sciences, University of Colorado Anschutz Medical Campus, Aurora, CO, USA

Garni Barkhoudarian John Wayne Cancer Institute at Saint John's Health Center, Santa Monica, CA, USA

Stefan Bauer Institute for Surgical Technology and Biomechanics, University of Bern, Bern, Switzerland

Jürgen Becker Department of Anatomy and Cell Biology, University Medicine Goettingen, Goettingen, Germany

Damasia Becu-Villalobos Institute of Experimental Biology and Medicine – CONICET, Buenos Aires, Argentina

Silvia Inés Berner Hospital Santa Isabel, Buenos Aires, Argentina

Pierre Beukelaers GIGA-Neurosciences, Developmental Neurobiology Unit, University of Liege, Liege, Belgium

Nicolas Caron GIGA-Neurosciences, Developmental Neurobiology Unit, University of Liege, Liege, Belgium

Ricardo L. Carrau Department of Otolaryngology - Head & Neck Surgery, The Ohio State University Wexner Medical Center, Columbus, OH, USA

Eric L. Chang Department of Radiation Oncology, University of Southern California, Los Angeles, CA, USA

Sam T. Chao Department of Radiation Oncology, Cleveland Clinic, Cleveland, OH, USA

Alfredo Conti Department of Neurosurgery, Cyber Knife Center, University of Messina, Messina, Italy

Carolina Cristina Institute of Experimental Biology and Medicine – CONICET, Buenos Aires, Argentina

Aaron Cutler John Wayne Cancer Institute at Saint John's Health Center, Santa Monica, CA, USA

Giuseppe D'Aliberti Department of Neurosurgery, Niguarda Ca'Granda Hospital, Milan, Italy

Rafael V. Davalos Virginia Tech – Wake Forest University, School of Biomedical Engineering and Sciences, Blacksburg, VA, USA

Alberto Debernardi Department of Neurosurgery, Niguarda Ca'Granda Hospital, Milan, Italy

Leo F.S. Ditzel Filho Department of Neurosurgery, The Ohio State University Wexner Medical Center, Columbus, OH, USA

Thomas L. Ellis Virginia Tech – Wake Forest University, School of Biomedical Engineering and Sciences, Blacksburg, VA, USA

Claudia Faria Division of Neurosurgery, The Hospital for Sick Children, Toronto, ON, Canada

Christopher C. Franklin Department of Pharmaceutical Sciences, Skaggs School of Pharmacy and Pharmaceutical Sciences, University of Colorado Anschutz Medical Campus, Aurora, CO, USA

Gregory J. Gagnon Radiation Oncology, Georgetown University Hospital, Washington, DC, USA

Paulo A. Garcia Virginia Tech – Wake Forest University, School of Biomedical Engineering and Sciences, Blacksburg, VA, USA

Julie Gehl Department of Oncology 54B1, Copenhagen University Hospital Herlev, Herlev, Denmark

Emmanuelle C. Genin GIGA-Neurosciences, Developmental Neurobiology Unit, University of Liege, Liege, Belgium

M.A. Hayat Biological Science Department, Kean University, Union, NJ, USA

Eirik Helseth Department of Neurosurgery, Oslo University Hospital, Oslo, Norway

Fraser C. Henderson Department of Neurosurgery, Georgetown University Hospital, Washington, DC, USA

Morten Høyer Oncological Department, Aarhus University Hospital, Aarhus, Denmark

Karen Huscher Department of Neurosurgery, Cyber Knife Center, University of Messina, Messina, Italy

Timothy Huyck Department of Medicine, Section Hematology/Oncology, Northwestern University, Chicago, IL, USA

Maria Ines Institute of Experimental Biology and Medicine – CONICET, Buenos Aires, Argentina

Helle K. Iversen Department of Oncology 54B1, Copenhagen University Hospital Herlev, Herlev, Denmark

Hideyuki Iwayama Department of Pediatrics, Neonatology and Congenital Disorders, Nagoya City University, Nagoya, Japan

Siavash Jabbari Department of Radiation Oncology, The Doug and Nancy Barnhart Cancer Center, Sharp Chula Vista Medical Center, Chula Vista, CA, USA

Steven Kalkanis Department of Neurosurgery, Henry Ford Center for Cancer Surgery, Detroit, MI, USA

Alex Karotki Department of Radiation Oncology, Sunnybrook Health Sciences Centre, University of Toronto, Toronto, ON, Canada

Amin B. Kassam Division of Neurosurgery, University of Ottawa, Ottawa, Ontario, Canada

Daniel F. Kelly Brain Tumor Center, John Wayne Cancer Institute at Saint John's Health Center, Santa Monica, CA, USA

David A. Larson Department of Radiation Oncology, University of California, San Francisco, CA, USA

Benjamin Lassen Department of Neurosurgery, Oslo University Hospital, Oslo, Norway

Yasmin Lassen-Ramshad Oncological Department, Aarhus University Hospital, Aarhus, Denmark

Daniel Letourneau Department of Radiation Oncology, Princess Margaret Hospital, University of Toronto, Toronto, ON, Canada

Mette Linnert Department of Oncology 54B1, Copenhagen University Hospital Herlev, Herlev, Denmark

Simon S. Lo Department of Radiation Oncology, University Hospitals Cancer Center, Case Comprehensive Cancer, Case Western Reserve University, Cleveland, OH, USA

Lijun Ma Department of Radiation Oncology, University of California, San Francisco, CA, USA

Faisal Mahmood Department of Oncology 54B1, Copenhagen University Hospital Herlev, Herlev, Denmark

Brigitte Malgrange GIGA-Neurosciences, Developmental Neurobiology Unit, University of Liege, Liege, Belgium

Giulia Maurizi Department of Medical and Surgical Sciences, Clinic of Hematology, Educational Centre, Marche Polytechnic University, Ancona, Italy

Kyle McCool Departments of Neurosurgery, Georgetown University Hospital, Washington, DC, USA

Nancy McLaughlin Department of Neurosurgery, University of California, Los Angeles, Los Angeles, CA, USA

Torstein R. Meling Department of Neurosuregry, Oslo University Hospital, Oslo, Norway

Perez Millán Institute of Experimental Biology and Medicine – CONICET, Buenos Aires, Argentina

Mustafa Nadi Division of Neurosurgery, The Hospital for Sick Children, Toronto, ON, Canada

Joseph P. Neglia University of Minnesota, Minneapolis, MN, USA

Laurent Nguyen GIGA-Neurosciences, Developmental Neurobiology Unit, University of Liege, Liege, Belgium

Beatrice Nico Department of Human Anatomy and Histology, University of Bari Medical School, Bari, Italy

Lauren Nye Department of Medicine, Section Hematology/Oncology, Northwestern University, Chicago, IL, USA

Melvin Omodon Department of Neurosurgery, Henry Ford Center for Cancer Surgery, Detroit, MI, USA

James Perry Department of Neurology, Sunnybrook Health Sciences Centre, University of Toronto, Toronto, ON, Canada

Jørgen B. Petersen Department of Medical Physics, Aarhus University Hospital, Aarhus, Denmark

Thomas Picht Department of Neurosurgery and Neurology, Charite-University Medicine, Berlin, Germany

Robyn L. Poerschke Department of Pharmaceutical Sciences, Skaggs School of Pharmacy and Pharmaceutical Sciences, University of Colorado Anschutz Medical Campus, Aurora, CO, USA

Antonella Poloni Department of Medical and Surgical Sciences, Clinic of Hematology, Educational Centre, Marche Polytechnic University, Ancona, Italy

Daniel M. Prevedello Department of Neurosurgery, The Ohio State University Wexner Medical Center, Columbus, OH, USA

Jeffrey Raizer Department of Medicine, Medical Neuro-Oncology, Northwestern University, Chicago, IL, USA

Philip Reigan Department of Pharmaceutical Sciences, Skaggs School of Pharmacy and Pharmaceutical Sciences, University of Colorado Anschutz Medical Campus, Aurora, CO, USA

Mauricio Reyes Institute for Surgical Technology and Biomechanics, University of Bern, Bern, Switzerland

Domenico Ribatti Department of Human Anatomy and Histology, University of Bari Medical School, Bari, Italy

Pantaleo Romanelli Cyberknife Center, Milano, Italy

John H. Rossmeisl Virginia Tech – Wake Forest University, School of Biomedical Engineering and Sciences, Blacksburg, VA, USA

Simona Ruggieri Department of Human Anatomy and Histology, University of Bari Medical School, Bari, Italy

James T. Rutka Division of Neurosurgery, The Hospital for Sick Children, Toronto, ON, Canada

Akmal Safwat Oncological Department, Aarhus University, Aarhus, Denmark

Arjun Sahgal Department of Radiation Oncology, Sunnybrook Health Sciences Centre, Princess Margaret Hospital, University of Toronto, Toronto, ON, Canada

Paul Sanghera Department of Radiation Oncology, Hall-Edwards Radiotherapy Research Group, University Hospital Birmingham, Birmingham, UK

Juliet Seigle Radiation Oncology, Georgetown University Hospital, Washington, DC, USA

Henrik Pagh Schultz Oncological Department, Aarhus University Hospital, Aarhus, Denmark

Johannes Slotboom Institute for Surgical Technology and Biomechanics, University of Bern, Bern, Switzerland

Nicolas Smoll Department of Clinical Neurosciences and Neurosurgery, Faculty of Medicine, University Hospitals of Geneva, Geneva, Switzerland

Domenico Solari Department of Neurosurgery, Università degli Studi di Napoli Federico II, Naples, Italy

Hany Soliman Department of Radiation Oncology, Sunnybrook Health Sciences Centre, University of Toronto, Toronto, ON, Canada

Andreas M. Stark Department of Neurosurgery, Schleswig Holstein University Medical Center, Kiel, Germany

Magdalena Szczerbowska-Boruchowska Faculty of Physics and Applied Computer Science, AGH University of Science and Technology, Krakow, Poland

Satoshi Takahashi Department of Neurosurgery and Neurology, Charite-University Medicine, Campus Virchow Clinic, Berlin, Germany

Giuseppe Talamonti Department of Neurosurgery, Niguarda Ca'Granda Hospital, Milan, Italy

Lucie M. Turcotte University of Minnesota, Minneapolis, MN, USA

A. Aria Tzika Department of Medical Physics, Medical School, University of Ioannina, Ioannina, Greece

Norishi Ueda Department of Pediatrics, Neonatology and Congenital Disorders, Nagoya City University, Nagoya, Japan

Renaud Vandenbosch GIGA-Neurosciences, Developmental Neurobiology Unit, University of Liege, Liege, Belgium

Roland Wiest Institute for Surgical Technology and Biomechanics, University of Bern, Bern, Switzerland

Part I

Molecular Mechanisms

Classification/Diagnosis of Brain Tumors Using Discriminant Function Analysis

1

Magdalena Szczerbowska-Boruchowska

Contents

Abstract

The occurrence of brain tumors is one of the most important causes of morbidity and mortality in young adults and children. The accurate classification of a tumor is crucial for finding the best treatment of the patient. Therefore, the development of diagnostic methods that may improve classification of brain tumors is of grate importance. In this work, a review of current method applied to the diagnosis of brain tumors is presented. Special attention is paid to the remarkable opportunities provided by using discriminant function analysis as a tool that may support classification of brain tumors. The examples of applications of selected techniques of modern physics such us magnetic resonance imaging, magnetic resonance spectroscopy, synchrotron radiation based X-ray fluorescence, infrared spectroscopy and small angle X-ray scattering technique for classification of brain tumors are discussed. Moreover, the usefulness of morphological features of neoplastic tissues including blood vessel shape and morphometric features of cell nuclei for diagnosis of brain tumors with the use of discriminant function analysis is presented. As the literature studies show, very high predictive abilities are achieved if the analytical and imaging results are supported by discriminant function analysis. Therefore, the potential diagnostic methods in combination

M. Szczerbowska-Boruchowska (✉)
AGH University of Science and Technology,
Faculty of Physics and Applied Computer Science,
Al. Mickiewicza 30, Krakow 30-059, Poland
e-mail: Magdalena.Boruchowska@fis.agh.edu.pl

M.A. Hayat (ed.), *Tumors of the Central Nervous System, Volume 12*,
DOI 10.1007/978-94-007-7217-5_1,

with discriminant function analysis would be recommended to be included to standard clinical examinations.

Introduction

Brain tumors remain an important cause of mortality in the world (Farley et al. 2008). The World Health Organization (WHO) recognizes a variety of primary brain tumor types. A new comprehensive classification of neoplasms affecting central nervous system was ratified by the WHO in 2007 and can be found elsewhere (Louis et al. 2007). A grading system for each tumor type is also provided there. In general, the classification is presented as the standard for the characterization of brain tumors to the clinical oncology and cancer research communities world-wide. The 2007 WHO classification is based on the consensus of an international experts including amongst other pathologists and geneticists. However, in spite of well defined standards for brain tumor classification the difficult and questionable cases still exist in the neuro-oncology. Therefore, various techniques that could be served as an accessory diagnostic tool are of grate importance.

Nowadays, both clinical history and radiological investigation can be used to detect the presence of a brain tumor and provide clue about its location. However, to decide about the tumor type and grade of malignancy with absolute certainty additional laboratory tests have to be included. Typically, for diagnosing brain tumors the following techniques are used (Simonetti 2004):

- Computed Tomography,
- Magnetic Imaging Resonance,
- Positron Emission Tomography,
- Biopsy followed by histopathological examination.

Routinely, diagnosis given by histopathologist base on a biopsy sample is a final step in confirming the tumor type and grade of malignancy. However, it should be emphasized that biopsy is an invasive surgical procedure and does not always enables the correct recognition. This is mainly due to the fact that a biopsy provides only local information from the tumor, which structure can be heterogeneous and infiltrative. Moreover, even for specimens taken intraoperatively from a tumor, some diagnosing difficulties may occur. As it is known the process of histopathological diagnosis of tumors is based on the verbatim interpretation of the pictures (the microscopic ones) of tissue samples. A histopathologist uses their expertise and knowledge gained from literature to diagnose each case. This helps not only in classification of brain tumor but also in taking a clinical decision as to its treatment. However, diagnosis given by histopathologist is not objective. Moreover, nothing is directly given in a microscopic picture of the tumor sample. In many cases evaluation and histopathological diagnosis are at variance. Probably, oligodendroglial tumors are among the most susceptible with regard to the differences in neuropathological interpretation and prognostication (Giannini et al. 2008). Moreover, difficulties in differentiation between reactive, i.e., non-neoplastic glial reaction and low grade astrocytoma should to be mentioned (Burger and Scheithauer 2007). Routinely, hematoxylin-eosin (HE) staining of tissue samples embedded in paraffin is used for histopathological examination. However, studies include also immunohistochemical methods (most frequently with antibodies against glial fibrillary acidic protein – GFAP, epithelial membrane antigene – EMA, vimentin, cytokeratins, CD34 and others, accordingly to the specific requirements of differential diagnosis). Since histopathological diagnosis still come up against difficult or disputable cases it is very important to develop new tools that can aid in the diagnosis of brain tumor type and grade. For that reason, efforts toward implementation of innovative techniques that could improve accuracy of diagnostic procedures in relation to brain tumors are of grate importance. The usefulness of interdisciplinary studies including spectroscopy and imaging techniques of modern physics should be emphasized. What is more, increasingly special methods of data analysis are coupled with both the techniques used routinely for diagnosing of brain tumors and these not commonly used yet in

the clinic. The potential usefulness of such methods in supporting the classification of brain tumors as well as in providing novel biomarkers of prognosis is verified.

The morphological, biochemical or genetic pattern of tissues may constitute a source of the unique fingerprint of different types of brain tumors. Therefore, the techniques used for study of neoplastic tissues have to be supported by appropriate data mining methods. The use of supervised pattern recognition methods such as discriminant function analysis on complex data provides a powerful tool for characterizing different classes of brain tumors according to their features, determined with the use of various analytical techniques. Discriminant function analysis is one of the promising procedures of data processing. In general, this method of statistical analysis is used to determine which variables (here: brain tumor features) discriminate between two or more naturally occurring groups (here: brain tumor types or grade of malignancy) (Carroll et al. 1997). Another major role of discriminant analysis is predictive classification of cases which may support brain tumor diagnosis. Mathematically, discriminant function analysis is aimed to find a set of linear combinations of the variables, which are called discriminant functions. The values of such linear combinations have to be as close as possible within groups included to analysis and as far apart as possible between groups. The discriminant functions are calculated for a sample of cases for which group membership is known and then can be applied to new cases with measurements on the same set of variables, but unknown group membership. This allows for the classification of new, unknown cases that have to be diagnosed based on the constructed classification model. The detailed theoretical basis of DA technique was presented elsewhere (Carroll et al. 1997). Generally, discriminant function analysis is a well-known technique for data simplification, feature extraction and case classification. This method has found many applications including various aspects of neuro-oncology. Some of them are discussed in this work.

Brain Tumor Diagnosis Using Nuclear Magnetic Resonance

Magnetic resonance imaging (MRI) is one of the most commonly used techniques in clinical diagnosis of brain tumors (Simonetti 2004). The recording of stocked images throughout the total volume of the brain allows for the assessment of anatomical location, morphology and size of tumor tissue. The nuclear magnetic resonance (NMR) intensities of various tissue types are determined by three parameters, i.e., proton density, the spin – lattice (T_1) and spin – spin (T_2) relaxation times. Sensitivities if these factors depend on two acquisition parameters such us echo time and repetition time. Signal intensity in each voxel is determined by all these parameters. The magnetic resonance imaging The MRI methods include imaging with contrast agents (T_1-eighted, T_2- weighted, proton density weighted MR images), diffusion-weighted imaging (analysis of water movement within brain tissue at the molecular level) and functional MRI (visualization of specific brain structure participating in a specific function). The application of the MRI technique to brain tumor diagnosis was described in details by Simonetti (2004).

A new technique based on nuclear magnetic resonance that could assist brain tumor diagnosis and classification is magnetic resonance spectroscopy (MRS) (Simonetti 2004). This technique is not commonly used in the clinic. However, most of 1.5 T MRI spectrometers are also appropriate for MRS measurements. Two methods of measurements are commonly applied in magnetic resonance spectroscopy. The first one is based on the spectra obtained from a specific selected region (voxel or volume element) in the brain. Therefore, this method is called single voxel spectroscopy (SVS). Typically, in brain tumor diagnosis the voxel includes neoplastic tissue. Apart from single voxel measurements, the spectra can be collected from a two- (or three-) dimensional grid. This method is referred to magnetic resonance spectroscopic imaging (MRSI) or chemical shift imaging. In this case, changes in metabolic levels determined in measured volume of the tissue may identify heterogeneity of tumor.

The MRS spectra provide information about the concentrations and chemical properties of various metabolites. The MRS is particularly useful for biomedical applications. It is due to the fact that MRS can be performed with the several nuclei such as ^{1}H, ^{31}P, ^{13}C, and ^{19}F. All of them are important from a medical point of view (Negendank 1992). The ^{31}P-MRS may assist tumor diagnosis by the studies of energy metabolism as the content of phosphocreatine, adenosine-5′-triphosphate (ATP) and inorganic phosphate can be determined. Moreover, phosphomonoesters, which level was found to be increased in tumors in compare with normal tissue, can be followed using the ^{31}P-MRS. It should be also mentioned that this technique allows for the calculation of intracellular pH, which is an important parameter in the study of neoplastic tissues. Also the proton nucleus is important in the diagnosis of brain tumors. As a large number of brain metabolites contain protons, they can be followed in the ^{1}H-MRS. The following important brain metabolites can be examined using proton MRS: glutamate, choline, creatine, N-acetyl aspartate, fatty acids, myo-inosinol and lactate. Despite that the quantification of single metabolite is in practice, a multivariate approach is highly suited. Since spectral features of spectra acquired in neoplastic tissue differ from these obtained from normal tissue, the proton MRS can assist noninvasive diagnostic of brain tumors. This technique is also useful for differentiation of tumor types and grades, as spectra obtained from tumors of various types and grades reveal significantly different spectral patterns.

Since the spectroscopic data is very different in comparison with imaging data the application of MRS is hampered in clinical diagnostic. This is also due to a large amount of spectroscopic data generated. Therefore, there is a need for implementation of statistical tools that simplify the data interpretation and therefore reduce time consuming. Because the linear discriminant analysis (LDA) is one of the best-known statistical techniques for pattern recognition, is often used to assist MRI and MRS studies (Simonetti 2004). In general, LDA utilizes a subset of data from original MR images or spectra of known tissue type, as training set, and calculate a classification model. The calculated linear combinations (discriminant functions) of MR images (or spectral patterns) discriminate between the tissue classes defined in the training set. It should be emphasized that application of the LDA to classification of brain tumors using MRSI is problematic. It due to the fact, that accurate histological characterization of all spectroscopic voxels is difficult. In spite of that, linear discriminant analysis applied to MRI and MRS results has found application in classification of brain tumors. Both in vivo and in vitro studies were conducted. Exemplary applications of MRI and MRS to diagnosis of brain tumors are presented in further paragraphs.

In Vivo Spectroscopy and Imaging

As non-invasive diagnostic tests could reduce the necessity for biopsy and its associated risks of morbidity and mortality various MRI and MRS sequences have been studied in an attempt to recognize brain tumor type without biopsy.

The studies using a combination of MRI and MRSI features for non-invasive classification of brain tumors were reported by Devos et al. (2005). This work was aimed to investigate the discriminatory value of MRI intensities and metabolic data extracted from MRSI for automated brain tumor diagnosis. Moreover, the usefulness of several classification techniques including linear discriminant analysis was tested. The analysis was carried out for 25 patients with a brain tumor and four volunteers as a control group. The following specimens were studied: 10 grade II gliomas, 4 grade III gliomas, and 7 grade IV gliomas, and 3 meningiomas. All of them were assigned to four classes of brain tumors. From each patient, data were taken from several voxels within the tumor area. Additionally, data from both cerebrospinal fluid from patients and normal brain tissue from patients and volunteers were selected. Data from all cases with the same histopathological recognition were combined into one class. Finally, seven classes of pathologies were obtained. The following MRI and MRSI features were taken into account for the classification

procedures: water normalized magnitude spectra, metabolite amplitudes obtained by peak integration, and imaging intensities. The comparison of MR spectra from MRSI, MR imaging intensities, peak integration values obtained from the MR spectra and a combination of the latter two was used to test the influence of imaging intensities and metabolic data. As mentioned above LDA based on binary classification was performed. Prior to LDA, the use of principal component analysis as a feature extraction technique was required. As the area under the receiver operating characteristic curve (AUC) is a good summary measure of the test accuracy, the test performance was measured by the mean AUC and its pooled standard error calculated from 100 randomizations. In general, all classification techniques including LDA obtained a high performance when using peak integration values with or without MR imaging intensities. Particularly, for healthy versus tumor tissue, low- versus high-grade tumors, low- versus high-grade gliomas and gliomas versus meningiomas, the mean test AUC was higher than 99 %, 91 %, 95 %, and 99 %, respectively, when both MR imaging intensities and peak integration values were used. It was found that the use of metabolic data derived from MRSI significantly improved classification of brain tumor types in comparison with the use of MR imaging intensities solely. The studies showed clearly that ^{1}H MRSI is an important adjunct to the MRI techniques that increase classification ability of brain tumors significantly. Imaging intensities derived from MRI and MRS metabolic data provide complementary information for the accurate discrimination between brain tissue types. Therefore combination of both techniques should be included to the standard clinical examination.

The ability of diffusion tensor MR imaging (DTI) metrics combined with tractography to discriminate between the three most common brain tumor types i.e. glioblastoma, meningioma, and metastasis was studied by Byrnes et al. (2006). The analysis was carried out for 36 brain tumor patients. They were proven histopathologicaly to be glioblastoma, meningioma or metastasis. The three tumor types were described by the DTI metrics. Principal component analysis and subsequently a linear discriminant analysis using the derived principal components were applied to determine the variables that differentiate tumor types most significantly and to classify the cases. It was found that mean diffusivity calculated for tumor region, linear tensor shape metrics in tumor, mean diffusivity calculated for oedema around the tumor, fractional anisotropy in oedema and streamline density separate the tumor types most significantly. The results of case classification showed that 86.1 % of cases were correctly classified at all data included to the analysis. Whilst, in cross validation using the 'leave one out' method, 80.6 % of cases were classified according to their histpathological recognition. Particularly, glioblastoma was correctly classified in 69 %, meningioma in 75 % and metastasis in 100 % of cases. This shows that DTI combined with tractography and linear discriminant analysis are useful in the diagnosis of brain tumor in vivo and could potentially reduce the requirement for invasive biopsy.

Dynamic contrast-enhanced MRI (DCE-MRI) was combined with immunohistochemical studies to determine the possibility of brain glioma grading (Awasthi et al. 2012). The classification was supported by discriminant function analysis. Seventy six brain tumors were included to the studies. Fifty five of them were found to be high grade on histopathology (41 glioblastoma, 4 gliosarcoma, and 10 III grade astrocytoma). Twenty one low-grade tumors were diagnosed histopathologically as II grade tumors (16 cases), and I grade tumors (5 cases). DCE-MRI perfusion indices, i.e., relative cerebral blood volume (rCBV), relative cerebral blood flow (rCBF), permeability (k^{trans} and k_{ep}), and leakage (v_e) were quantified and used in discriminant function analysis. The mmunohistochemical markers applied included: vascular endothelial growth factor (VEGF), hypoxia inducible factor (HIF), matrix metalloproteinases (MMP), phosphatase of regenerating liver 3 (PRL-3). MMP-9-, PRL-3-, HIF-1α-, and VEGF- expressing cells were quantified from the excised tumor tissues prior to the statistical analysis. Using Pearson's correlation the following significantly correlated pairs

were found: VEGF expression and rCBV, VEGF expression and rCBF, MMP-9 expression and k_{ep}, HIF-1α expression and rCBV, HIF-1α expression and VEGF expression. Base on these correlation results, one of the variables from each of these correlated pairs (i.e., VEGF, MMP-9, and HIF-1α) was removed to use only non-invasive markers in farther discriminant analysis. Variables rCBV, k_{ep}, and v_e were found to be significant discriminators of the tumor grade and were included to construct a classification model. Using the calculated discriminant functions, 49 of 55 high grade tumor cases (89.1 %) and 21 of 21 low-grade tumor cases (100 %) were correctly classified. The classification procedure showed that over 92 % of correct classifications were achieved for all analyzed cases (70 correctly classified of 76 analyzed). The authors showed (Awasthi et al. 2012) that the DCE-MRI is able to differentiate between high and low-grade gliomas. This suggests utility of the DCE-MRI method in better noninvasive imaging assessment of these pathologies in comparison to conventional MRI imaging. Moreover, the significant positive correlation of selected DCE-MRI indices and immunohistochemical markers indicates that appropriate DCE-MRI indices can imitate the expression of these immunohistochemical markers.

Metabolic Characterization In Vitro

A multivariate discriminant analysis procedure was applied by Roda et al. (2000) to classify human cerebral tumors in vitro, combining the use of proton MRS with automatic amino acid analysis of biopsy extracts. Eighty-one samples were taken surgically. The following eight classes, determined in histopathological examination, were studied: high-grade astrocytomas (19 cases), low-grade astrocytomas (10 cases), normal brain (9 cases), medulloblastomas (4 cases), meningiomas (18 cases), metastases (8 cases), neurinomas (9 cases), and oligodendrogliomas (4 cases). Perchloric acid extracts were prepared from every biopsy and analyzed with the use of proton MRS to obtain a fingerprint of the metabolite profiles of every tissue class. Additionally, amino acid profiles of the biopsies were studied in the same extracts used for proton MRS analysis by automatic ion exchange chromatography. The details concerning the sample preparation and measurement conditions can be found elsewhere (Roda et al. 2000). In general, 44 variables (27 resonances or ratios of resonances measured by proton MRS, and 17 amino acid concentrations determined by ionic exchange chromatography) were used to statistical analysis. A step-wise discriminant analysis was carried out to found the linear combination of variables that the best discriminate between the classes compared. It was observed, that inositol and acetate are the metabolites of the highest importance to the discrimination between biopsy extracts of high-grade and low-grade astrocytomas. Moreover, the studies showed that tyrosine and proline are relevant contributors to the discrimination between high- and low-grade gliomas. Whilst, glutamine has been found as the most significant variable in the discrimination between: high-grade astrocytomas and meningiomas, low-grade astrocytomas and normal brain, and low-grade astrocytomas and medulloblastomas. The highest importance in the discrimination between low-grade astrocytomas and neurinomas and between low-grade astrocytomas and oligodendrogliomas was noticed for glycine. To conclude, valine, methionine, cysteine, tyrosine, and proline were shown by Roda et al. (2000) to contribute importantly to discrimination between analyzed groups. Moreover, the applied multilateral classification procedure enabled to achieve the following scores of correct classifications: normal brain, 100 %; neurinomas, 100 %; medulloblastomas, 100 %; meningiomas, 94.5 %; metastases, 86 %; low-grade astrocytomas, 80 %; oligodendrogliomas, 75 %; and high-grade astrocytomas, 74 %. The results presented by Roda et al. (2000) provide a promising background for the implementation of nonhistological protocols for in vitro tumor diagnosis in clinical practice.

High resolution spectra acquired in vitro using ^{1}H MRS are particularly useful to determine the chemical components of tissue extracts (Faria et al. 2011). The spectral features of brain tissue extract at high field strengths are comparable to

proton MRS in vivo. This means that despite the degradation of tissues before the extraction process and the fact that the analyses rely only on water soluble metabolites most biochemical information is retrieved. The work reported by Faria et al. (2011) was aimed to the application of discriminant function analysis to high resolution proton MRS spectra in order to refine the identification of their metabolic profile and to find possible markers for various types of brain tumors. Human brain tumor biopsies were used in the analysis. Forty three extracts of brain tissue from 39 patients with brain tumors and 4 patients (as control group) operated for drug-resistant partial epilepsy were studied. The histological examination of each specimen was carried out for the same part of the tumor that was taken to prepare extracts for ^{1}H MRS. The tumor samples were divided into four groups: high-grade neuroglial tumors (Hg), including glioblastomas and anaplastic oligoastrocytomas; low-grade neuroglial tumors (Lg), including non-anaplastic oligoastrocytomas and grade II astrocytomas; non-neuroglial tumors (NN), including meningiomas, adenomas, schwannomas and papilloma, and metastasis from breast, lung and kidney adenocarcinomas. Nine metabolites such as acetoacetate (Ac), alanine (Ala), creatine (Cr), choline compounds [composed of free choline (Cho), glycerophosphocholine (GPC) and phosphocholine (PC)], γ-aminobutyric acid (GABA), glycine (Gly), glutamine and glutamate (Gln/Glu), myo-inositol (m-Ins), and N-acetyl aspartate (NAA) were responsible for the sample discrimination. It was found that Hg tumors showed a relative abundance of Gly, Ala, and Gln/Glu. Moreover, m-Ins was increased in Lg compared to Hg tumors. NN tumors revealed lower levels of Cr and NAA in comparison to both Lg and Hg tumors. NN was also characterized by a higher relative abundance of Ala and Gly in relation to Lg tumors and Ac when compared with Hg tumors. m-Ins and Gln/Glu levels in NN tumors were relatively increased in Lg and Hg tumors, respectively. Metastasis showed lower levels of m-Ins and Gln/Glu in comparison with both NN and Hg tumors. The comparison between metastasis and Lg tumors showed that metastasis had higher levels of Ala and Gly and lower levels of m-Ins, Cr and NAA compare with Lg tumors. Moreover, it was observed that tumors revealed higher level of Ala and PC and reduced level of Cr, m-Ins, NAA, and GABA when compared with control group. The classification of specimens using 'leave-one-out' method showed that from all discriminant function analyses only two incorrect classifications occurred, i.e., two metastasis samples were classified as Hg tumor. This proves the efficiency of proton MRS coupled with discriminant function analysis in group characterization.

Differentiation/Classification of Brain Tumors Based on Elemental and Macromolecular Characteristic

Microscopic examination of brain tumor sections clearly shows variability of morphological features between various tumor types. As an example, white-light microscope images of hematoxylin-eosin stained tissue section of selected brain tumors are shown in Fig. 1.1. In that light the question arises: whether the morphological features of brain tumors are mirrored by their biochemical composition? To answer this question both elemental and macromolecular characteristics of neoplastic tissues seems to be useful. Monitoring of biochemical processes and interactions within the neoplastic tissues may be directly realized by recognition of their organic and inorganic components. It should be emphasized that investigations of biochemical features in biological specimens require analytical techniques that enable precise, microscale probing. It is due to the complex nature of the tumor, which apart from the "intrinsic" heterogeneity of the neoplasm, frequently shows admixture of necrotic areas, components of the host tissue, reactive gliosis and secondary constituents such as lymphocytes, monocytes, blood vessels, calcifications, macrophages, neutrophils etc. Moreover, trace level detectability is required for the determination of low concentrations of chemical elements that are typical of biological

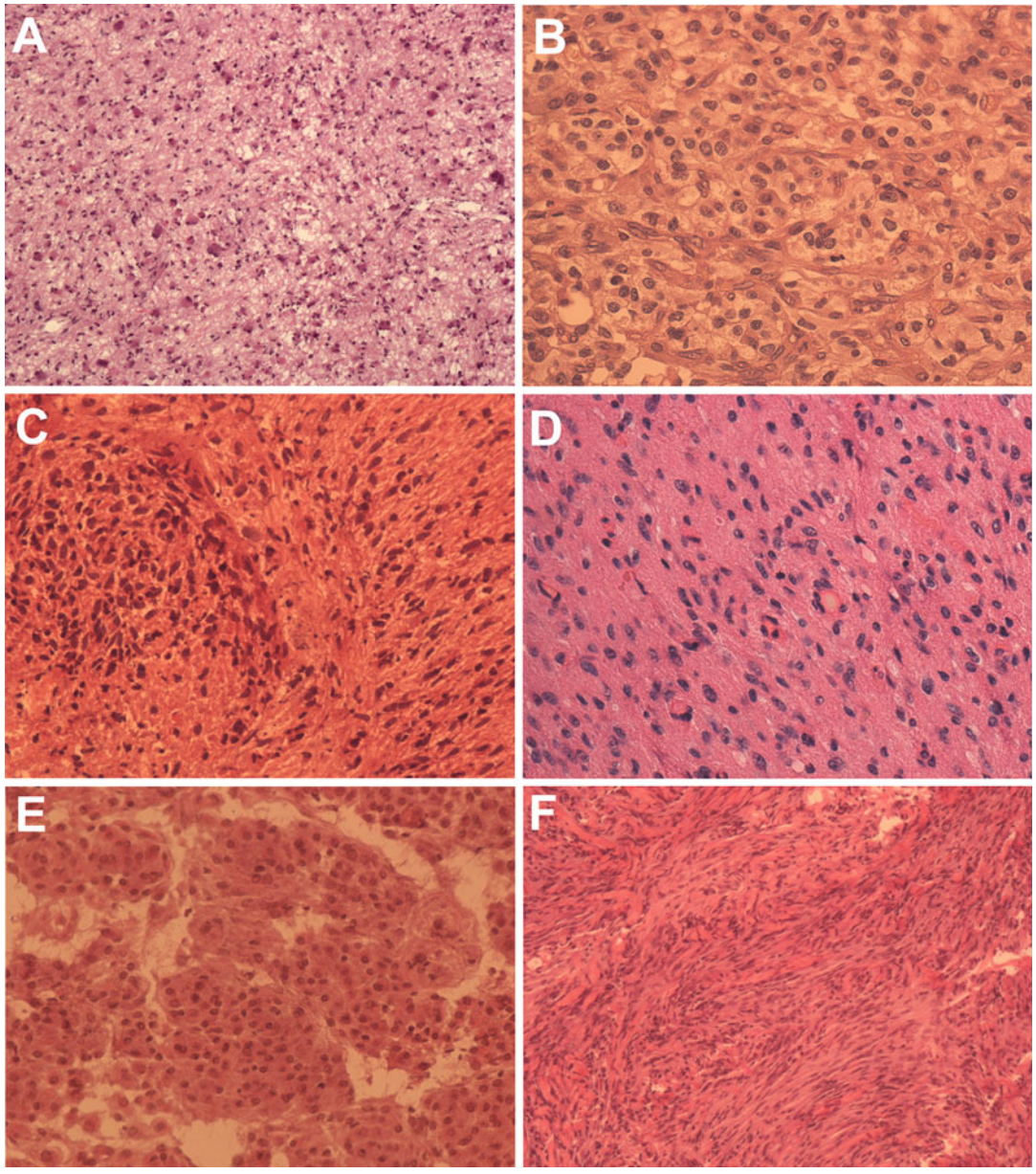

Fig. 1.1 White-light microscope images of hematoxylin-eosin stained tissue section of selected brain tumors: (**a**) – gemistocytic astrocytoma (III grade); (**b**) – oligodendroglioma (II grade); (**c**) – glioblastoma multiforme (IV grade); (**d**) – anaplastic astrocytoma (III grade); (**e**) – meningothelial meningioma (I grade); (**f**) – fibrous meningioma (I grade)

tissues. For example, it was found that the mass fractions of trace elements in gray matter of brain cortex, in mg/kg (in parentheses) were the following: Fe (250), Cu (20), Zn (80), Rb (3) (Boruchowska et al. 2001). This shows that only the analytical technique, which ensures the traceability of mg/kg (ppm) may be used in probing of neoplastic tissue (assuming that levels of trace elements in both tumor and host tissues are in the same range).

Elemental "Signature" of Brain Tumors

The X-ray fluorescence (XRF) technique, especially based on synchrotron radiation (SRXRF), offers a nondestructive qualitative and quantitative analysis of chemical elements. The principles of the XRF technique can be found elsewhere (Markowicz 1993). The XRF technique including the SRXRF method has been used in a number of applications in biology and medicine (Szczerbowska-Boruchowska et al. 2011; Ducić et al. 2011; Ortega et al. 2007).

The usefulness of the SRXRF technique for classification (diagnosis) of brain tumors was studied by Szczerbowska-Boruchowska et al. (2011). The following tumor types were investigated: glioblastoma multiforme (11 cases), gemistocytic astrocytoma (2 cases), oligodendroglioma (4 cases), anaplastic oligodendroglioma (2 cases), ganglioglioma (1 case), fibrillary astrocytoma (1 case) and atypical transitional meningioma (1 case). The specimens, taken intraoperatively, were diagnosed histopathologically at the Department of Neuropathology at the Jagiellonian University Medical College in Krakow. The sample preparation procedures for both routine histopathological examination and spectroscopic studies were described in details by Szczerbowska-Boruchowska et al. (2011).

Elemental analysis of unstained tissue section representing various brain tumors was carried out using the SR-XRF technique. The measurements were performed at the bending magnet beamline L at HASYLAB (Hamburger Synchrotrostrahlunglabor, Hamburg, Germany). The primary X-ray energy was set to 17 keV. The incidence beam was focused to a size of 15 μm in diameter with the use of a half-lenses polycapillary. Each tissue section was scanned in two directions at a step size of 15 μm both horizontally and vertically. A typical size of the area of scanning was from 300 to 500 μm in one direction.

The SR-XRF technique allowed for the determination of elements such as P, S, Cl, K, Ca, Fe, Cu, Zn, Br and Rb in all analyzed neoplastic tissues. Based on the masses per unit areas of elements, determined for each point within the scanned area of the tissue sections, two-dimensional maps of elemental distribution were prepared. An example of XRF maps for oligodendroglioma case is shown in Fig. 1.2. For each sample data from 100 measurement points were selected for further statistical analysis. Multiple discriminant analysis (MDA) was used for two purposes: (1) detecting the variables (elements) that allow for discrimination between different tumor types, and (2) classifying cases into groups related to histopathological recognition. In the analysis, the samples were discriminated into groups based on their histopathological diagnosis. It was found that the most significant elements in the general discrimination of tumor type are as follows: S, Cl, Cu, Fe, K, Br and Zn. This means, that the contents of these elements and their relative ratios in neoplastic tissues may be a source of the unique elemental fingerprint of different types of brain tumors. Moreover, the largest difference in elemental composition was observed between atypical transitional meningioma and fibrillary astrocytoma (c.f. Fig. 1.3). As one can noticed from Fig. 1.3 the smallest differentiation, taking into account the elemental composition of neoplastic tissues, was noted between glioblastoma multiforme and oligodendroglioma. The usefulness of the calculated discriminant functions was examined via their ability to correctly classify each data point to their a priori groups. The mean percentage of correct predictions determined according to the a posteriori probabilities procedure was equal to 99.93 %. This means that almost 100 % agreement with histopathological diagnosis was achieved. Apart from the classification of tumor cases used previously for construction of discriminant function model the validation procedure was also carried out for ten new samples. In this case, the mean percentage of correct predictions obtained for the new cases of brain gliomas was 87.6 %. These results show that the elemental studies coupled with multiple discriminant analysis allowed for the classification of different types of brain tumors into separate groups and also even for classification/diagnosis of the unknown cases. Very high predictive accuracies of MDA that were achieved in the study described

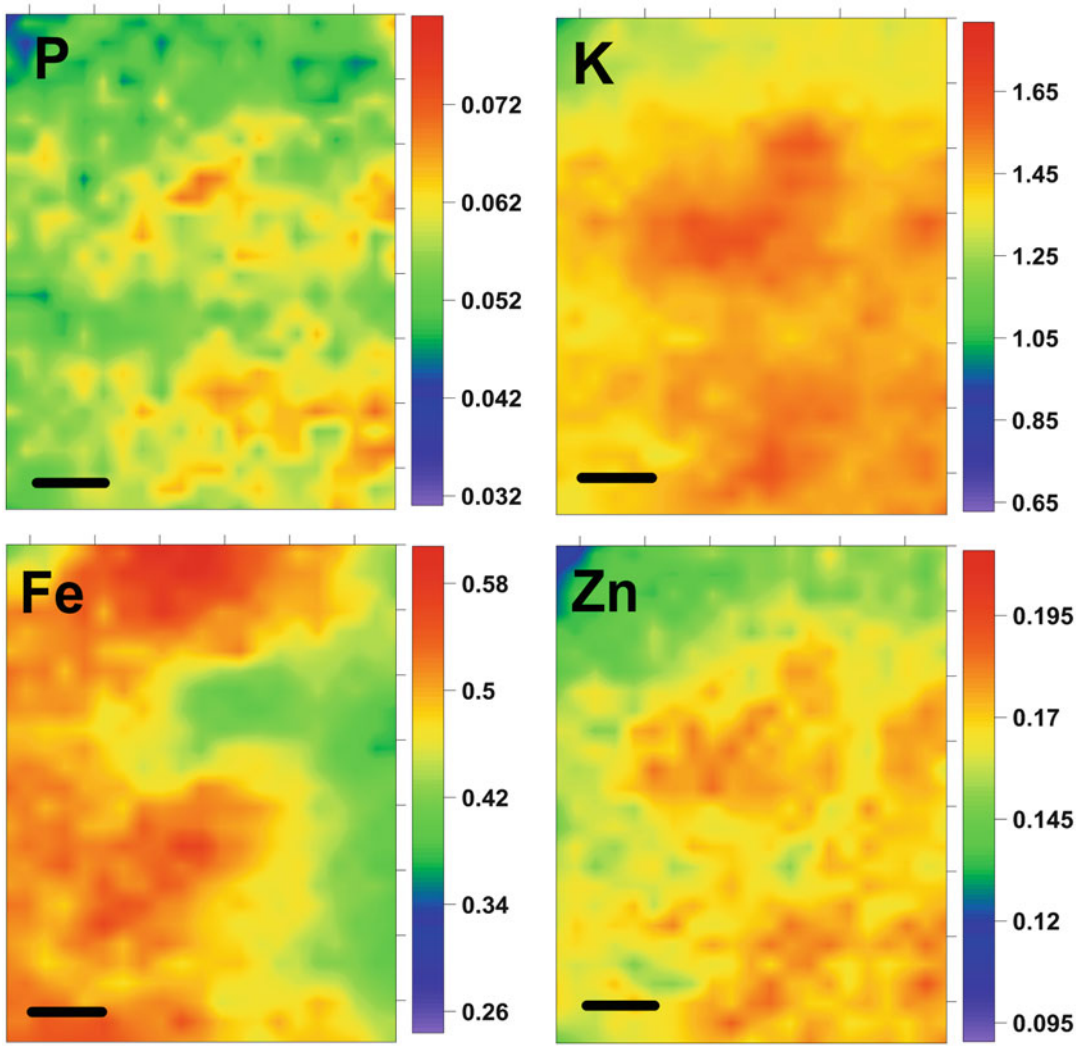

Fig. 1.2 Distribution of selected elements in oligodendroglioma (II grade) tissue section. Data presented in (μg/cm^2). Scale bar: 50 μm

by Szczerbowska-Boruchowska et al. (2011) should be emphasized. As the authors suggest, the created elemental fingerprinting may be a very useful tool in assisting the process of histopathological diagnosis/classification of brain tumors. Moreover, it was pointed out that the elemental composition of a relatively small fragment of neoplastic tissue represents satisfactorily the elemental "signature" of cancer and using multiple discriminant analysis enables differentiation of various types of brain tumors.

Macromolecular Fingerprint of Brain Tumors

Apart from elemental composition of brain tumors an organic components seem to be potential markers of various neoplastic tissues. The main biological macromolecules such as proteins, lipids, nucleic acids and carbohydrates can be satisfactorily identified with the use of infrared (IR) spectroscopy (Miller et al. 2002). Due to unique fingerprinting capabilities, this technique

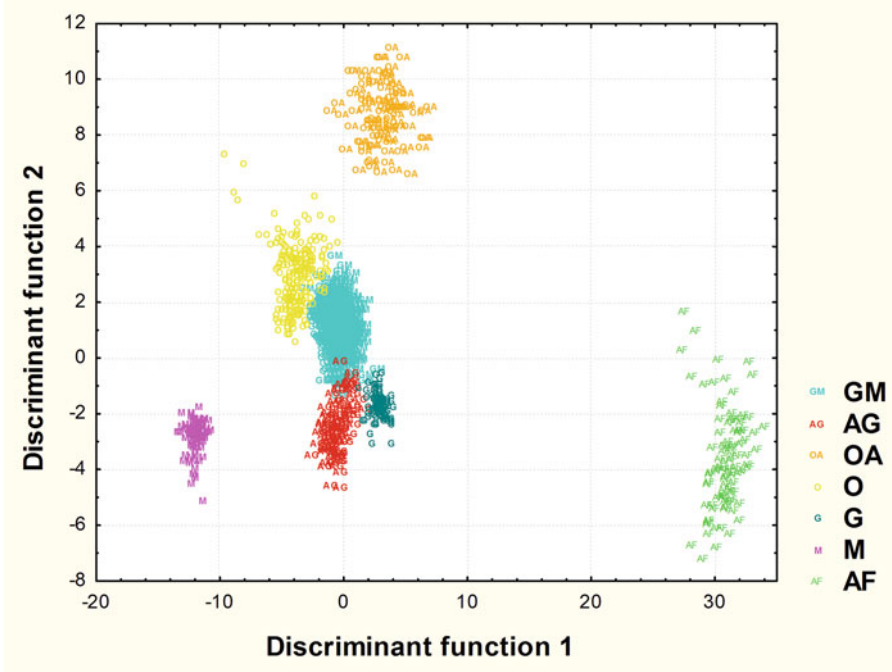

Fig. 1.3 The scatterplot of observations in the space of discriminant variables for different types of brain tumors (*OA* anaplastic oligodendroglioma, *AG* gemistocytic astrocytoma, *AF* fibrillary astrocytoma, *GM* glioblastoma multiforme, *G* ganglioglioma, *O* oligodendroglioma, *M* atypical transitional meningioma)

is a very valuable tool for biomolecular investigations. Moreover, IR spectroscopy allows for the probing of tissues and cells at the molecular level. Therefore, it was suggested as a diagnostic method for clinical applications. The selected advantages of IR spectroscopy such us minimal sample preparation required, non-destructive characteristic, no external markers required, and rapidity should be emphasized (Krafft et al. 2006). The IR imaging allows for the determination of two-dimensional distribution of biological macromolecules in tissues and cells. Moreover, molecular structure information can be also obtained from the same analysis, for protein secondary structure and fatty acyl chain peroxidation level. Therefore, several cancer markers can be identified based on IR spectroscopy. Potential applications of IR spectroscopy imaging coupled with linear discriminant analysis as a complement tool for diagnosis of brain tumors were discussed by Krafft et al. (2006, 2007). The authors (Krafft et al. 2006) used IR spectroscopic maps of multiple tissue samples from two patients (with an astrocytoma of III grade and a multifocal glioblastoma brain tumor) to construct a classification model. For this purpose linear discriminant analysis was applied. The chemical properties of training samples were described by the lipid-to-protein ratio (band intensity ratio 2,850–1,655 cm^{-1}), two additional molecular descriptors identified at 1,545 cm^{-1}/1,655 cm^{-1} (amide II to amide I intensities ratio) and (1,231 + 1,450) cm^{-1}/1,655 cm^{-1}, which are associated with hemoglobin and collagen, respectively. The model was applied to classify normal brain tissue, II grade astrocytoma, III grade astrocytoma, glioblastoma, hemorrhage, and leptomeninges. For each class, three IR spectra were taken as a training set from IR spectroscopic maps of two patients corresponding to the average spectrum, the minimum magnitude, and the maximum magnitude of the spectral features within the metric. Then the LDA model was used to whole IR spectroscopic images obtained for the analyzed

tissue sections. The majority of the IR spectra from IR maps were correctly assigned according to their histopathological recognition. However, it was found that glioma tissues are inhomogeneous and might encompass several grades of malignancy. In the same work (Krafft et al. 2006) additional samples were used in the frame of an independent test of the previously constructed LDA classification model. For this purpose tissue sections taken from 15 patients with astrocytoma of III WHO grade, 31 patients with glioblastoma brain tumors, and 5 patients without brain tumor were analyzed. Single IR spectra from these sections were subjected to the LDA model. The results showed that for five normal samples 100 % accuracy was achieved. Fifteen III grade astrocytoma samples were assigned according to their histopathological recognition with 80 % accuracy. For 31 glioblastoma samples 74.2 % accuracy was achieved. Moreover, 20 % of III grade astrocytoma samples were assigned to glioblastoma and 19.4 % of glioblastoma samples were assigned to III grade astrocytoma. This may result from similar chemical composition of lipids and proteins. 6.4 % of glioblastoma samples were incorrectly classified as hemorrhage or leptomeninges. In general, 100 % of III grade astrocytoma and 93.6 % of glioblastoma were recognized as malignant gliomas. No malignant glioma was assigned to normal tissue or II grade astrocytoma. The high score (over 93 % of correct classifications) of the independent test samples shows that linear discriminant analysis based on molecular composition of tissue may be a potentially valuable method assisting classification of brain tumors. The usefulness of IR spectroscopic imaging coupled with linear discriminant analysis for classification of malignant gliomas was also studied by Krafft et al. (2007). In this work multiple IR images obtained for three tissue sections from one patient with a malignant glioma are acquired and assigned to the six classes normal brain tissue, II grade astrocytoma, III grade astrocytoma, glioblastoma multiforme (IV WHO grade), hemorrhage, and other tissue. For the diagnosis of new samples the LDA classification model trained as described by Krafft et al. (2006) was used. The usefulness of such procedure was verified additionally by using different IR detector (the focal plane array detector) for collecting new data than this (the single-channel detector) applied to probe the training samples. Based on the classification of IR spectra it was found that on average 95 % of the tissue cryosection was assigned to malignant glioma (that means III grade astrocytoma or glioblastoma) which points to a location within the tumor. From 12 % to 34 % of specimens classified as malignant gliomas and increased cell density were consistent with a location of the section near the tumor margins. Only single malignant glioma cells (less than 0.2 %) within mostly normal brain tissue of regular cellularity were detected in the cryosection which most likely originated from outside of the tumor. The presented results pinpoint the high accuracy of the LDA model which was trained by IR spectra from different patients and with different detectors. This demonstrates that the IR spectral patterns used to distinguish normal brain tissue and tumors are conserved among patients. Moreover, the LDA model is able to describe and recognize these spectral fingerprints. It should be also emphasized that the chemical information used in LDA model as the selected descriptors is identical in IR spectra which were recorded by single- or multi-channel IR detector. The work described by Krafft et al. (2007) pointed out that the chemical and molecular differences between normal brain tissue and brain tumors are sufficiently large and the appropriate LDA classification model may assist diagnosis/classification of brain tumors.

Myelin Structure Based Differentiation of Brain Tumors

Different forms of brain tumors, particularly glioblastoma and meningioma reveal distinct difference in myelin structure (Falzon et al. 2007). It was reported that malignant gliomas infiltrate the brain along myelinated tracts. Contrary, meningioma infiltration is inhibited along myelinated fibres. Moreover, meningiomas are strongly affected by the inhibitory proteins present in

myelin of the central nervous system, whilst glioblastomas are not as sensitive. The alteration of the structure of myelin between brain tumor types was examined using small angle X-ray scattering (SAXS) technique by Falzon et al. (2007). Due to the differences in myelin structures of brain tumors, particularly between glioblastoma and meningioma, selected SAXS features would indicate differences in tissue structure. These may include a change in the scattering ring intensity, the presence of new scattering rings, shifts in the position of the scattering rings, and changes in the relative intensities of the scattering rings. Statistical recognition techniques including flexible discriminant analysis (FDA) have been used to identify differences in SAXS images obtained for various brain tumors. The following cases were studied: schwannoma (5 samples from 5 patients), meningioma (12 samples from 11 patients), and glioblastoma multiforme (12 samples from 9 patients). In general, 29 SAXS patterns from 25 patients were included to the analysis. Independent component analysis was applied to find a feature set representing the SAXS images. Differences in the features were related to differences in the myelin scattering rings, the number of scattering rings at low d-values and differences in the amorphous background. In the next step, three mixing coefficients were used to present the contribution of each feature in the image. This allowed for the using of flexible discriminant analysis to discover a hidden order in the data set. Both the spectral and intensity content of the second and fourth order myelin scattering rings changes from benign to malignant conditions were observed. The change in peak intensity would result from a change in the structural order of myelin or a decrease in the amount of myelin in the tissue. Using a FDA model that was assessed using the 'leave-one out' cross validation, an excellent separation of classes (schwannoma, meningioma and glioblastoma) was achieved. This indicates significant changes in the myelin content or structure within the analyzed tissues. Moreover, a very good classification score (almost 100 %) was reached. Only one glioblastoma case was classified is a schwannoma. The results of FDA analysis shows that separation of the schwannoma, meningioma and glioblastoma tissue can be achieved based upon the properties of the myelin scattering rings. This means that fundamental differences between these tumor types are related to myelin and that successful classification of brain tumors can be achieved using X-ray scattering.

Differentiation and Grading of Brain Tumors Using Morphological Features of Neoplastic Tissue

Vessel Shape Analysis

Malignancy of brain tumors was determined based on vessel shape by Bullit et al. (2004). Histological examinations show that blood vessels associated with malignant tumors reveal characteristic shape abnormalities. Changes in vessel tortuosity were proposed as a potential marker for incipient malignancy. This is due to the fact that vessel tortuosity precedes sprout formation. Moreover vessel shape may be normalized by successful tumor treatment. Therefore, the quantification of such vessel shape changes in vivo could offer a powerful, noninvasive means of estimating tumor malignancy. Bullit et al. (2004) reported a study that used measures of vessel shape to diagnose malignancy brain tumors based on magnetic resonance high-resolution 3D images. In general, the study was aimed to noninvasively discriminate malignant from benign tumors including cases difficult to diagnose by other imaging methods. The analyzed disputable cases included hemorrhagic lesions, pinpoint abnormalities, irradiated tumors, and hypervascular benign lesions. The study was carried out for 21 brain lesions in 19 patients scheduled for tumor removal. Additionally, images of sixteen healthy subjects were used to establish the healthy database. On all subjects the following sentences were performed: T1, T2, and MRA. Moreover, the tumor patients received additionally a gadolinium enhanced T1 sequence. Typically, voxel spacing was $0.5 \times 0.5 \times 0.8\ \mathrm{mm}^3$.

However bigger spacing values were also applied for selected patients. Vessel extraction involved definition of a seed point, automatic extraction of an image intensity ridge representing the vessel's central skeleton, and automatic determination of vessel radius at each skeleton point. Such extracted vessels were then processed to construct connected vessel trees and to exclude noise. For each tumor patient, an automated analysis of vessel shape was performed only upon those vessels lying within the tumor boundaries. Next, the same region of interest was mapped into the coordinate space of each healthy patient. A similar, regional analysis was carried out upon each healthy subject's vasculature. A minimum vessel number was set to 4. The following vessel attributes of interest were defined: vessel density measure, tortuosity type II characterized by a "bag of worms" configuration, and tortuosity type III characterized by high-frequency, low-amplitude coils or sine waves. A quadratic discriminant analysis and a nonparametric discriminant analysis were performed for automate diagnosis. Classification of each tumor achieved based on vessel shape was compared to the final pathological report. All of the 21 tumors (12 malignant and 9 benign) were classified correctly into the benign or malignant group during the blinded study. Potentially difficult cases were properly labeled. Four benign and three malignant lesions had been treated by months or years earlier. Moreover, it was found prior surgery and radiation therapy did not appear to disrupt vessel analysis. The authors describe one example of a grade III glioma, which exhibited abnormal vessel tortuosity but no significant neovascularity. This shows that vessel analysis as a means of early detection of incipient cancers seems possible. Moreover, in spite of vessel density, malignancy was related to vasculature bearing high-frequency tortuosity abnormalities. These vascular changes were displayed by glioma grade IV, glioma grade III, lymphoma, metastatic melanoma, metastatic breast carcinoma, and pinealoblastoma. It was found that abnormal vessel tortuosity occurs not only within the enhancing margins of malignant tumors but also in the surrounding tissue. This means that even tiny lesions can be classified as malignant or benign via examination of vessels in the surrounding tissue. The work described by Bullit et al. (2004) clearly points out the usefulness of vessel shape computerized analysis and discriminant analysis methods for specific diagnosis of brain tumors. However, the observations should be verified for a larger series.

Studies of Tumor Cell Nuclei

As mentioned above, brain tumors reveal differences in morphological features at the single cell level. Therefore, appropriate methods of statistical analysis based on the information provided by morphometric studies of neoplastic tissue sections seems to be promising tool assisting classification of brain tumors. Nuclear shape studies with reference to the differentiation and grading of brain tumors using discriminant function analysis was carried out by Nafe et al. (2006). For this purpose a digital image analysis system was used to measure tumor cell nuclei. Typically, at least 300 per case were included to the study. The following tumor types were investigated: II grade oligodendrogliomas (13 cases), III grade oligodendrogliomas (11 cases), IV grade medulloblastomas (14 cases), III grade anaplastic ependymomas (12 cases). Moreover, Ki-67- positive vs. Ki-67 – negative tumor cell nuclei in the 14 medulloblastomas were included to the analysis. For each cell nucleus, Fourier amplitudes no. 1–15, moments no. 1–7 according to Hu, ellipse shape factor, concavity factor, roundness factor, Feret ratio, fractal dimension and bending energy were determined. The comparisons of the discriminatory power of these parameters were tested in three pairwise: II grade oligodendrogliomas vs. III grade oligodendrogliomas; IV grade medulloblastomas versus III grade anaplastic ependymomas; and Ki-67- positive versus Ki-67 – negative medulloblastomas cell nuclei. Using data from Fourier analysis 100 % correct classifications were achieved when comparing both II grade oligodendrogliomas versus III grade oligodendrogliomas and IV grade medulloblastomas versus III grade anaplastic ependymomas. 75 % correct

classifications were obtained in comparison between Ki-67-positive and Ki-67-negative nuclei from medulloblastomas. Including the other shape parameters to the discriminant function analysis resulted in a lower percentage of correctly reclassified cases for all three pairwise comparisons. The studies presented by Nafe et al. (2006) clearly show that Fourier analysis allowed for the optimal statistical discrimination between different brain tumors. As was reported, nuclear shape is an important criterion for the investigation of brain tumors. Therefore, the use of Fourier shape analysis in combination with discriminant function analysis is recommended for quantification of histological examinations.

In conclusion, the diversity of diagnostic methods now available allows for the determination of unique features of neoplastic tissues. Interdisciplinary studies including these based of techniques of modern physics and clinical practice open new opportunities for current oncology. As an accurate initial diagnosis of brain tumors has important consequences for therapeutic decisions and prognosis, methods assisting brain tumor classification/diagnosis are of grate importance. Literature studies show that various techniques, including these not commonly used in the clinic, provide valuable information that may improve current diagnostic of brain tumors. What is more, the appropriate methods of statistical analysis such us discriminant function analysis can be applied to gain the usefulness of diagnostic techniques. Undoubtedly, such interdisciplinary approach to the problem of the classification of brain tumors requires a remarkable commitment of clinicians. Often, the close cooperation between clinicians, radiologist, physicists, analysts and statistics is necessary. In selected cases, the need for the complex research facilities (such as synchrotrons) can provide also some limitations for such studies. However, as was reported in this work, in most cited cases very high predictive abilities were achieved. Therefore, the potential diagnostic methods in combination with discriminant function analysis would be recommended to be included to standard clinical examination.

Acknowledgements This work was supported by the "Polish Ministry of Science and Higher Education and its grants for Scientific Research."

References

Awasthi R, Rathore RK, Soni P, Sahoo P, Awasthi A, Husain N, Behari S, Singh RK, Pandey CM, Gupta RK (2012) Discriminant analysis to classify glioma grading using dynamic contrast-enhanced MRI and immunohistochemical markers. Neuroradiology 54:205–213

Boruchowska M, Lankosz M, Adamek D, Korman A (2001) PIXE analysis of human brain tissue. X-Ray Spectrom 30:174–179

Bullitt E, Jung I, Muller K, Gerig G, Aylward S, Joshi S, Smith K, Lin W, Ewend MC (2004) Determining malignancy of brain tumors by analysis of vessel shape. In: Barillot C, Haynor DR, Hellier P (eds) Medical Image Computing and Computer-Assisted Intervention – MICCAI 2004, LNCS 3217, Springer, Berlin/Heidelberg, pp 645–653

Burger PC, Scheithauer BW (2007) In: Silverberg SG, Sobin LH (eds) Tumors of the central nervous system, AFIP atlas of tumor pathology. Tumors of neuroglia and choroid plexus. ARP Press, Washington, DC, pp 33–208

Byrnes TJ, Barrick TR, Ladroue C, Bell BA, Clark CA (2006) DTI and tractography metrics discriminate between brain tumour types in vivo. Proc Intl Soc Mag Reson Med 14:608

Carroll JD, Green PE, Chaturvedi A (eds) (1997) Mathematical tools for applied multivariate analysis. Academic Press, New York

Devos A, Simonetti AW, van der Graaf M, Lukas L, Suykens JA, Vanhamme L, Buydens LM, Heerschap A, Van Huffel S (2005) The use of multivariate MR imaging intensities versus metabolic data from MR spectroscopic imaging for brain tumour classification. J Magn Reson 173:218–228

Ducić T, Quintes S, Nave KA, Susini J, Rak M, Tucoulou R, Alevra M, Guttmann P, Salditt T (2011) Structure and composition of myelinated axons: a multimodal synchrotron spectro-microscopy study. J Struct Biol 173:202–212

Falzon G, Pearson S, Murison R, Hall C, Siu K, Round A, Schültke E, Kaye AH, Lewis R (2007) Myelin structure is a key difference in the x-ray scattering signature between meningioma, schwannoma and glioblastoma multiforme. Phys Med Biol 52:6543–6553

Faria AV, Macedo FC, Marsaioli A, Ferreira MMC, Cendes F (2011) Classification of brain tumor extracts by high resolution (1)H MRS using partial least squares discriminant analysis. Braz J Med Biol Res 44:149–164

Farley J, Shin HR, Bray F, FormanD, Mathers C, Parkin DM (2008) GLOBOCAN 2008: cancer incidence and mortality worldwide in 2008, IARC CancerBase, Lyon, no 10

Giannini C, Burger PC, Berkey BA, Cairncross JG, Jenkins RB, Mehta M, Curran WJ, Aldape K (2008) Anaplastic oligodendroglial tumors: refining the correlation among histopathology, 1p 19q deletion and clinical outcome in Intergroup Radiation Therapy Oncology Group Trial 9402. Brain Pathol 18:360–369

Krafft C, Sobottka SB, Geiger KD, Schackert G, Salzer R (2007) Classification of malignant gliomas by infrared spectroscopic imaging and linear discriminant analysis. Anal Bioanal Chem 387: 1669–1677

Krafft C, Thümmler K, Sobottka SB, Schackert G, Salzer R (2006) Classification of malignant gliomas by infrared spectroscopy and linear discriminant analysis. Biopolymers 82:301–305

Louis DN, Ohgaki H, Wiestler OD, Cavenee WK (eds) (2007) WHO classification of tumours of the central nervous system. IARC, Lyon

Markowicz AA (1993) X-ray physics. In: Van Grieken RE, Markowicz AA (eds) Handbook of X-ray spectrometry. Methods and techniques. Marcel Dekker, New York/Basel/Hong Kong, pp 1–73

Miller LM, Dumas P, Jamin N, Teillaud J-L, Miklossy J, Forro L (2002) Combining IR spectroscopy and fluorescence imaging in a single microscope: biomedical applications using a synchrotron infrared source. Rev Sci Instr 73:1357–1360

Nafe R, Yan B, Schlote W, Schneider B (2006) Application of different methods for nuclear shape analysis with special reference to the differentiation of brain tumors. Anal Quant Cytol Histol 28:69–77

Negendank W (1992) Studies of human tumors by MRS: a review. NMR Biomed 5:303–324

Ortega R, Cloetens P, Devès G, Carmona A, Bohic S (2007) Iron storage within dopamine neurovesicles revealed by chemical nano-imaging. PLoS One 2:e925. doi:10.1371/journal.pone.0000925

Roda JM, Pascual JM, Carceller F, González-Llanos F, Pérez-Higueras A, Solivera J, Barrios L, Cerdán S (2000) Nonhistological diagnosis of human cerebral tumors by 1H magnetic resonance spectroscopy and amino acid analysis. Clin Cancer Res 6:3983–3993

Simonetti AW (2004) Investigation of brain tumor classification and its reliability using chemometrics on MR spectroscopy and MR imaging data. PhD thesis, University of Nijmegen

Szczerbowska-Boruchowska M, Lankosz M, Adamek D (2011) First step toward the "fingerprinting" of brain tumors based on synchrotron radiation X-ray fluorescence and multiple discriminant analysis. J Biol Inorg Chem 6:1217–1226

Neuronal Differentiation in the Adult Brain: CDK6 as the Molecular Regulator

2

Nicolas Caron, Emmanuelle C. Genin, Renaud Vandenbosch, Pierre Beukelaers, Laurent Nguyen, and Brigitte Malgrange

Contents

Abstract

The occurrence of adult neurogenesis within the subgranular zone (SGZ) of the dentate gyrus (DG) of the hippocampus and the subventricular zone (SVZ) of the lateral ventricles is now well established. However the molecular mechanisms involved in proliferation, differentiation, migration and functional integration newborn neurons in pre-existing neural network remain largely unknown. The cyclin-dependent kinases (Cdks) belong to a family of serine/threonine kinases, which control the progression of cells through several phases of the cell cycle. Cdk4 and Cdk6, and then Cdk2, with their specific cyclins (cyclins D for Cdk4/6, cyclins E for Cdk2), control the G1/S phase transition by phosphorylating retinoblastoma family proteins ultimately releasing E2F transcription factors, which are essential for cell cycle progression. In the adult brain, Cdk6 also controls the length of G1 phase, which is a critical step for balancing proliferation with neuronal differentiation.

Adult Neurogenesis

Introduction

For a century, it was established that brain ceased to grow "new nerve cells after birth". However, in the late 1960s, thanks to a new method developed to label dividing cells with H^3-thymidine, Altman

N. Caron • E.C. Genin • R. Vandenbosch
P. Beukelaers • L. Nguyen • B. Malgrange (✉)
GIGA-Neurosciences, Developmental Neurobiology Unit, University of Liege, Avenue de l'Hopital, 1 BatB36, 1er etage, Liège 4000, Belgium
e-mail: bmalgrange@ulg.ac.be

M.A. Hayat (ed.), *Tumors of the Central Nervous System, Volume 12*,
DOI 10.1007/978-94-007-7217-5_2,

showed the production of new cells in the rat adult brain (Altman and Das 1965). Subsequently, new techniques have been developed to study cell proliferation and highlight the birth of new neurons during adulthood. In the 1990s, the use of bromodeoxyuridine (BrdU) and immunohistochemical techniques coupled with confocal microscopy allowed the definite identification of adult neurogenesis in mammals including human beings (Reynolds and Weiss 1992). Indeed, neural stem cells (NSCs) were isolated from the adult brain and cultured. These cells could be expanded and showed self-renewal ability and multipotentiality in vitro, two characteristics of stemness. NSCs were the likely source of new neurons in vivo as they were able to differentiate in culture into all cell types of the brain, including neurons. Neurogenesis takes place throughout life in two discrete brain areas: the dentate gyrus of the hippocampus (DG) and the subventricular zone of the lateral ventricle (SVZ). The process of adult neurogenesis encompasses the proliferation of resident neural stem and progenitor cells and their subsequent differentiation, migration, and functional integration into the pre-existing synaptic network. In the DG, excitatory granule neurons are generated throughout life from stem and progenitor cells in the subgranular zone (SGZ). While in the SVZ, highly proliferative progenitors give rise to new neurons that migrate through the rostral migratory stream (RMS) to reach the olfactory bulb (OB) where they predominantly differentiate into GABAergic inhibitory interneurons.

Adult Neurogenesis in the Dentate Gyrus

The hippocampus is a cortical structure that belongs to the limbic system. It is folded onto itself and it locates in the medial temporal lobe of the brain. It is composed of two major structures: the Ammon's horn (CA1, CA2, and CA3), the DG divided into three main parts: the hilus, the granular zone (GCL) and the SGZ. The process of adult hippocampal neurogenesis encompasses the slow proliferation of early stem or progenitor cells located in the SGZ, the subsequent faster proliferation of more restricted progenitors (expansion phase), the selection for survival or elimination of young neurons, the integration of the surviving neurons into the pre-existing neuronal network of the GCL. The last phases of postmitotic development include gradually increasing neuronal connectivity and changes in physiological neuronal properties. Newly integrated granule neurons project their axons to CA3 and are electrophysiologically functional.

Type-1 Cells: Radial Glia-Like Stem Cells

The development of new neurons in the adult DG is now well defined. Indeed, several cell stages have been described and can be differentiated by antigenic and morphological criteria. Hippocampal adult neurogenesis originates in the SGZ from astrocyte-like type-1 cells whose soma is triangular-shaped and. These cells possess a radial glia-like morphology as they send a long apical extension into the molecular layer that contacts blood vessels through vascular end feet. Numerically, type-1 cells represent the most abundant precursor cell type but rarely divide. These quiescent astrocyte-like type-1 cells express glial fibrillary acidic protein (GFAP), as well as nestin, an intermediate filament protein, and the transcription factor, Sox2 (Fig. 2.1). However, these cells do not express S100B, a protein specifically present in the postmitotic astrocytic population.

Type-2 Cells: Progenitors Cells

Type-1 cells divide asymmetrically and give rise to type-2 precursor cells, also known as transit amplifying precursors (TAP) or intermediate progenitor cells (IPC). Indeed, these cells possess an intense mitotic activity, thereby amplifying the pool of highly proliferating progenitors. Type-2 cells are morphologically distinct from type-1 cells: their processes are short and horizontally oriented. Type-2 cells are often subdivided in early progenitors, i.e. type-2a cells, and more mature type-2b cells. Type-2a cells still express markers of radial glia including nestin and Sox2 but no longer GFAP, a specific marker for type-1

cells. Type-2b cells show the first antigenic signs of neuronal differentiation and express several neuroblast markers such as doublecortin (DCX), a microtubule-associated protein involved in differentiation and neuronal migration, and the transcription factors NeuroD and Tbr2. The first synaptic inputs are GABAergic and recorded in type-2 cells, which suggest that these cells are wired to the pre-existing hippocampal network.

Type-3 Cells: Neuroblasts

Type-3 precursor cells correspond to a transition from a proliferative stage (type-2b cells) to postmitotic immature neurons. These cells are the most neuronally committed precursors and possess restricted proliferative capacity as compared to type-2b cells. Type-3 cells express markers of the neuronal lineage such as DCX, PSA-NCAM, NeuroD and Prox1 but lack the expression of glial markers. They exit the cell cycle and migrate on a short distance into the GCL, where they give rise to immature DCX neurons expressing calretinin, a calcium-binding protein, and neuronal nuclei (NeuN), a postmitotic neuronal marker. Most immature neurons produced will not survive and only few newborn granule cells will be stably integrated into the synaptic network of the DG.

Stem Cells or Not in the Dentate Gyrus?

Initially, hippocampal precursor cells were found to be multipotent in vitro and able to differentiate into electrophysiologically functional granule excitatory neurons. This persistent neuronal production in the adult DG arise from type-1 radial glial precursors (Doetsch et al. 1999), however whether these cells are able to self-renew by symmetric and/or asymmetric division remains under debate.

Indeed, it has been demonstrated, both in vitro and in vivo, that type-1 cells enter the cell cycle to generate, through asymmetric divisions, type-2 cells that in turn become neuroblasts, which then differentiate into mature neurons. Nevertheless, several teams were unsuccessful in identifying true stem cells in the SGZ. Seaberg and van der Kooy (2002) followed by Bull and Bartlett (2005) failed to isolate cells with self-renewal ability and multipotentiality in the adult DG (Bull and Bartlett 2005; Seaberg and Van Der Kooy 2002). More recently, Clarke et al. used in vitro clonal assay to challenge the stem cell properties (self-renewal and multipotentiality) of postnatal DG precursors. They found that type-1 cells are lineage-restricted progenitors with limited proliferative capacity and never detected colonies with abilities of self-renewing and multipotentiality (Clarke and Van Der Kooy 2011). Likewise, Encinas et al. showed in vivo that, after a limited number of asymmetric divisions, type-1 cells exit the cell cycle and start acquiring the astrocytic morphology, therefore leading to exhaustion of the "stem cell" pool (Encinas et al. 2011). However, among type-1 cells, some have a long-term ability to generate neurons and glia as well as to undergo self-renewing symmetric divisions, and therefore are true stem cells (Bonaguidi et al. 2011).

Adult Neurogenesis in the SVZ

The SVZ is composed of three main cell types: neuroblasts (Type-A cells), radial glia-like cells (Type-B cells), and TAPs (IPCs, Type-C cells) (Fig. 2.1). This heterogeneous population of cells exists in a dedicated environment, mainly composed of multiciliated ependymal cells (type-E cells) lining the ventricular surface as well as specialized vascular network (Ming and Song 2011). Arrangement of this "niche" is spatially defined, in that ependymal cells are organized in a pinwheel-like fashion surrounding monociliated type-B cells touching the ventricular surface (Mirzadeh et al. 2010). This «pinwheel structure» is only present in the ventricular wall of the neurogenic SVZ region suggesting an important role for intercellular interactions in neurogenesis (Mirzadeh et al. 2010). In addition, SVZ NSCs (i.e. type-B cells) extend basal processes that terminate on blood vessels that lie beneath the ependymal layer.

During lineage progression, astrocytic-like type-B stem cells produce TAPs that in turn give rise to type-A neuroblasts. These cells are immature proliferating neurons that migrate

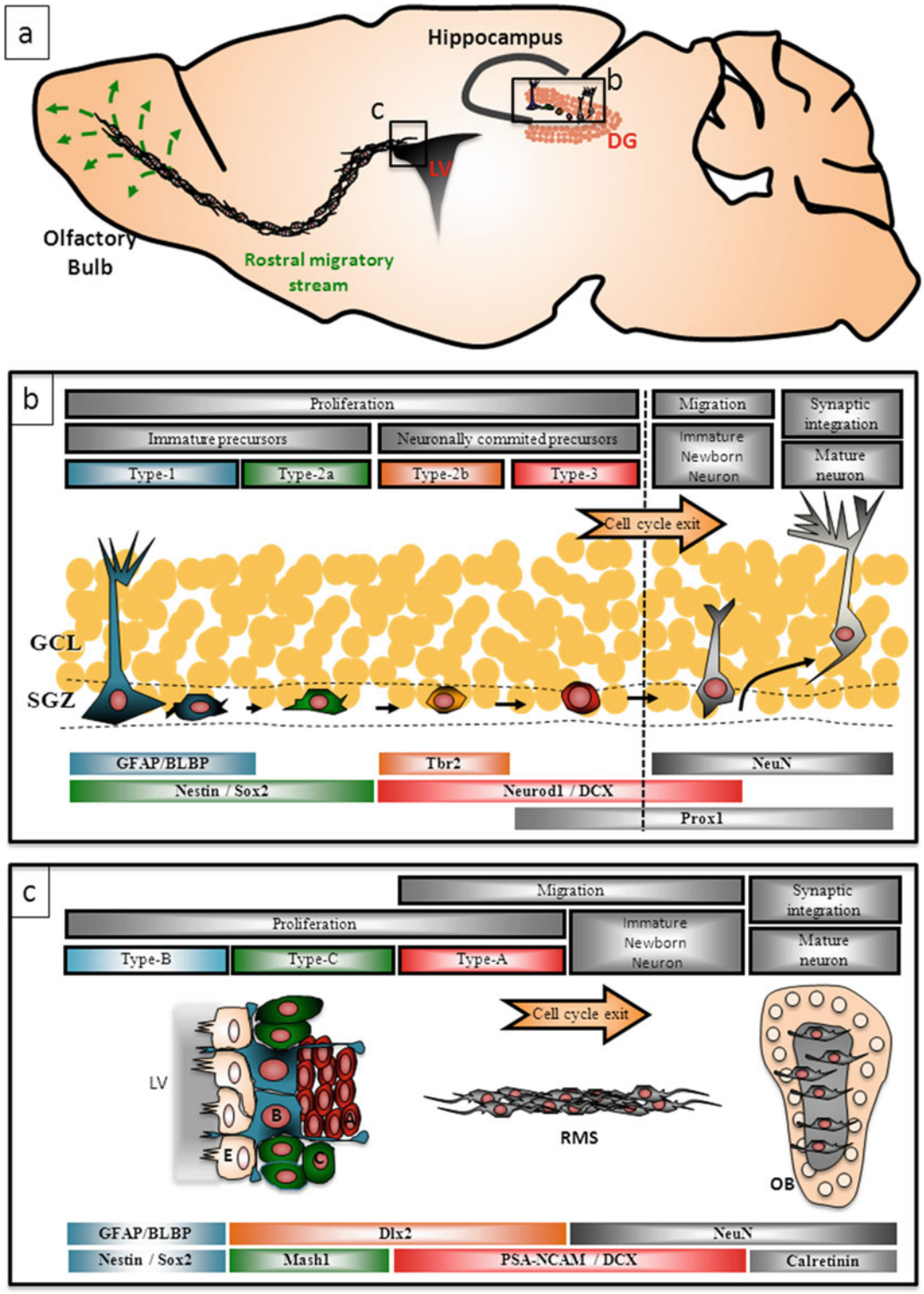
a
Hippocampus
b
c
DG
LV
Olfactory Bulb
Rostral migratory stream
b
Proliferation
Migration
Synaptic integration
Immature precursors
Neuronally commited precursors
Immature Newborn Neuron
Mature neuron
Type-1
Type-2a
Type-2b
Type-3
Cell cycle exit
GCL
SGZ
GFAP/BLBP
Tbr2
NeuN
Nestin / Sox2
Neurod1 / DCX
Prox1
c
Migration
Synaptic integration
Proliferation
Immature Newborn Neuron
Mature neuron
Type-B
Type-C
Type-A
Cell cycle exit
LV
B
E
RMS
OB
GFAP/BLBP
Dlx2
NeuN
Nestin / Sox2
Mash1
PSA-NCAM / DCX
Calretinin

over long distances (several millimetres) from the SVZ bordering the lateral ventricles of the brain via the rostral migratory stream (RMS) toward the olfactory bulb (OB) through a tube formed by astrocytes. In the OB, type-A cells detach from the RMS and migrate radially toward glomeruli where they differentiate and becoming GABAergic granule or periglomerular interneurons.

Type-B Cells: Radial Glia-Like Stem Cells

Type-B cells extend an apical ending that contact the ventricle and a long basal process ending on blood vessels. The number of contacts in the ventricle appears to increase when SVZ proliferation is stimulated (Mirzadeh et al. 2010). Type-B cells are considered to be the NSCs with ultrastructural characteristics of astroglial cells such as irregular contours that profusely fill the spaces between neighbouring cells, a long basal process that terminates on blood vessels and a single primary cilium that reaches the ventricle lumen. The function of the single primary cilium remains to be understood. This cilium can have a mechanosensory function, suggesting that the force of CSF flow itself may exert an influence on the proliferative state of the stem cell (Singla and Reiter 2006). This organelle has also been implicated in Sonic Hedgehog (Shh), Wnt, and PDGF signaling pathways, which are important for the stemness maintenance (Ihrie and Alvarez-Buylla 2011).

Type-B cells express, like type-1 cells in the DG, GFAP, nestin and sox2 but, importantly, not S100B an astrocytic marker also expressed by ependymal cells (Ming and Song 2011). In the RMS, all type-B cells ensheath migrating neuroblasts. Type-B cells divide to generate by successive asymmetric or symmetric division TAPs (type-C cells).

Type-C Cells: Transient Amplifying Cells

Type-C cells represent the most important pool of proliferating progenitors within the SVZ, as type-2 cells in the DG. These cells are larger and more spherical than type-B cells and are intimately connected to blood vessels. Type-B cells form a tubular sheath surrounding type-C cells. Initial observations revealed that in vitro "neurospheres" were derived from type-B NSCs (Doetsch et al. 2002), however, a new study indicates that this neurosphere-forming ability is also an intrinsic property of type-C cells (Pastrana et al. 2009). In vivo, these cells still lack a specific clear-cut molecular marker that differentiate them from other cells (Doetsch et al. 1999). It was reported recently that type-C cells express specifically transcription factor Mash1 and a homeobox transcription factor, Distal less 2 (Dlx2), which is also express in type-A cells (Ming and Song 2011). Type-C cells will give rise to neuroblasts also named type-A cells.

Type-A Cells: Neuroblasts

The ultimate precursor type in the lineage progression of the adult SVZ is type-A cell. These cells express Dlx2 and are also characterized by the expression of proteins related to migration as DCX and PSA-NCAM (PolySialic Acid – Neuronal Cell Adhesion Molecule) – the embryonic form of NCAM. In the RMS, type-A cells form chains and migrate toward the OB through glial tube formed by astrocytes.

Fig. 2.1 Schematic representation of adult rodent neurogenesis. (**a**) Illustration of a sagittal section through the mouse brain showing location of neurogenic zones: the subgranular zone (*SGZ*) of the dentate gyrus (*DG*) in the hippocampus and the subventricular zone of the lateral ventricles (*LV*) where neurons are produced and migrate to the olfactory bulb (*OB*) via the rostral migratory stream (*RMS*). (**b**) Schematic summary of the neuronal differentiation cascade in the adult dentate gyrus. Each cell type is characterized by the expression of specific markers. (**c**) Representation of progenitor cell types and neurons in the SVZ/RMS/olfactory system based on the expression of localization and expression of specific markers. *GFAP* Glial Fibrillary acid protein, *BLBP* Brain lipid-binding protein, *Tbr2* T-box brain protein 2, *DCX* Doublecortin, *Prox1* prospero homeobox 1, *NeuN* Neuronal Nuclei, *Dlx2* distal-less homeobox2, *Mash1* mammalian achaete scute homolog 1, *PSA-NCAM* Poly-Sialated Neural Cell Adhesion Molecule, *E* ependymal cells

Six days after their birth in the SVZ, the first neuroblasts arrive in the OB and migrate radially into the layers where they differentiate into mature interneurons. A majority of neuroblasts differentiate into GABAergic granule neurons while a minority differentiate into GABAergic periglomerular neurons and a small portion into dopaminergic neurons. Finally, new granule cells with mature morphologies display spontaneous synaptic potentials (Carleton et al. 2003).

Cell Cycle

Introduction

The cell cycle consists in a series of sequential phases that takes place in a cell leading to its division and replication. The duration of the cell cycle varies from 2 to 3 h in unicellular organisms (such as *Saccharomyces cerevisiae*) to 24 h in eukaryotic cells. In prokaryotic cells, which lack a nucleus, the cell cycle occurs through binary fission: circular DNA is replicated, and then the cell splits into two identical cells which contain an exact copy of the original DNA. In eukaryotic cells, the cell cycle is an elaborate replication process divided in two periods: interphase and mitosis (M). Interphase leads to DNA duplication and comprises three distinct phases: G1 (Gap 1), S phase (DNA synthesis) and G2 (Gap 2). During G1, the expression of genes required for G1 progression and S phase entry results mostly from the initial Rb phosphorylation. After DNA replication that occurs in S phase, the cell enters in G2 where significant proteic biosynthesis occurs, mainly involving in the generation of microtubules necessary for mitosis. The process of mitosis comprises five phases: prophase, metaphase, anaphase, telophase and cytokinesis (a cytoplasmic division). Errors in mitosis often lead to cell cycle arrest and apoptotic cell death to avoid genomic instability and accumulation of mutations. Dependent of environmental and development signals, cells in G1 may stop their division and, temporarily or permanently, leave the cell cycle to enter in a quiescence or senescence state, i.e. G0 phase (Gap 0). During this stage, cells may remain quiescent for long periods of time (like skin fibroblasts or liver hepatic cells), possibly permanently (i.e. neurons or cardiac cells); or cells may enter in senescence in response to DNA damage or degradation.

The progress through the cell cycle requires the assembly of complexes of cyclin-dependent kinase (CDK, catalytic subunit) and a cyclin (regulator subunit) (Fig. 2.2). Functional heterodimer enters into the cell nucleus where it gets phosphorylated by a CDK-activating kinase (CAK) to activate or inhibit its target proteins and allows the entry into the next phase of the cell cycle. In mammals, they are at least 15 different cyclins known from Cyclin A to Cyclin Y, and 21 genes encoding CDKs among which a few (CDK1, CDK2, CDK4, CDK6) are exclusively associated with cell cycle regulation (Malumbres and Barbacid 2009). Each cyclin can bind one or two CDKs and each CDK can be associated with one or two cyclins. CDKs are constitutively expressed in cells whereas cyclins are synthesized in a cyclic manner in response to various molecular signals at specific cell cycle stages.

When quiescent cells (G0) enter into the cell cycle (in G1), the D-type cyclins (i.e. cyclin D1, D2 and D3) are expressed in response to mitogenic signals and bind to their catalytic partners, CDK4 or CDK6. The kinase activity of these complexes results in the expression of genes whose products are involved in G1/S transition and S phase progression. The G1/S transition requires the binding of CDK2 to cyclin E. CDK2 activity is also implicated in S phase progression through binding with cyclin A. Cyclin A is also important for G2/M transition through its association with CDK1. Finally, during M phase, cyclin B/CDK1 phosphorylates several important structural components of the cell that are responsible for nuclear envelope breakdown and reorganization of the microtubule and actin filaments.

Redundancy exists between cyclins: in the absence of cyclin E-Cdk2, cyclin A-Cdk2 can promote G1/S transition while cyclin D-CDK4/6 and cyclin E-CDK2 play redundant roles during G1/S progression. The degradation of cyclins A

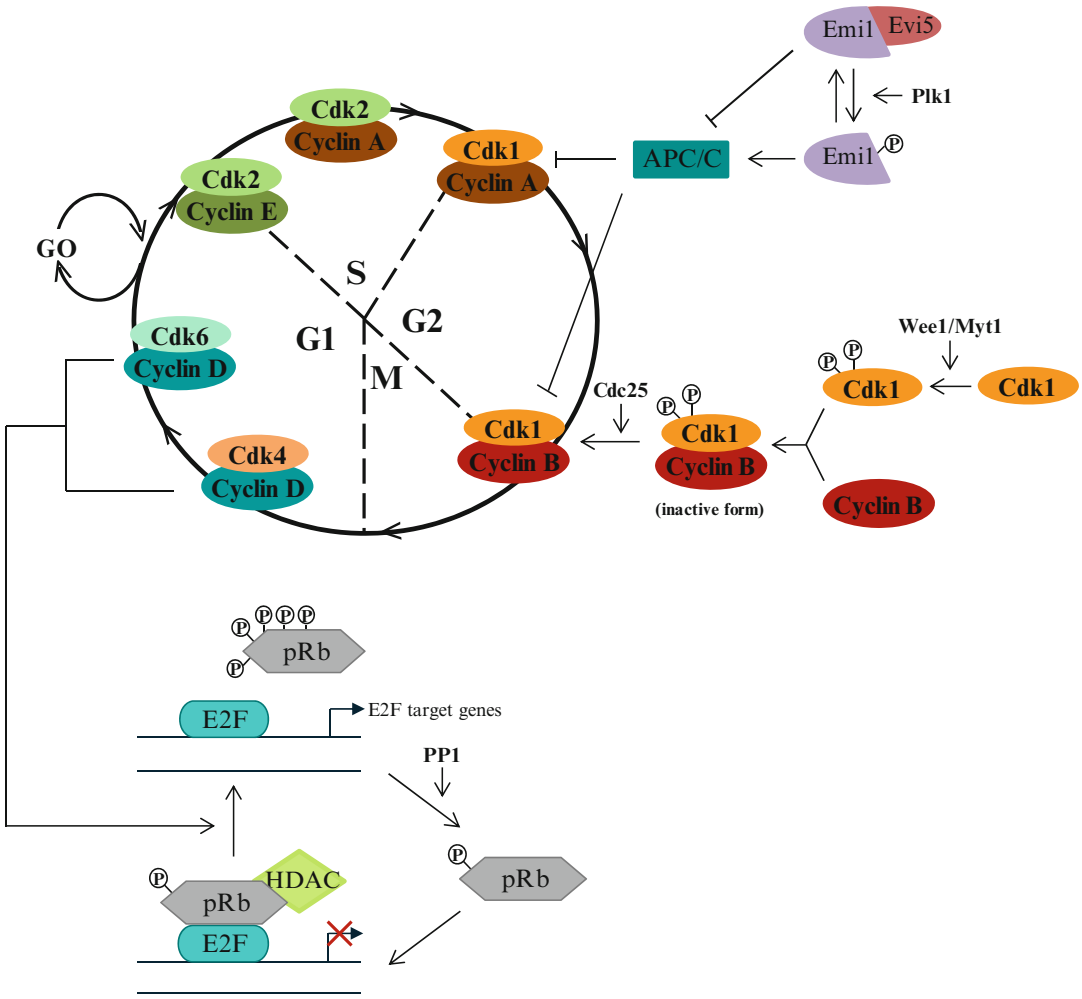

Fig. 2.2 Different aspects of cell cycle regulation. Modulation of cell cycle progression by CDK/cyclins, Rb/E2F pathway and M-phase promoting factor (MPF, i.e. CDK1/CyclinB) modulators

and B is regulated by the APC/C complex (Anaphase-Promoting Complex/Cyclosome) and the APC/C inhibitor Emi1 (Early Mitotic Inhibitor 1). The APC/C complex is an ubiquitin multisubunit E3 ligase, which contribute to the degradation of cyclins A and B by promoting poly-ubiquitinylation. Expression of these cyclins in S phase and G2 requires the inactivation of APC/C by Emi1 whose transcription is induced by E2F transcription factors. Emi1 is stabilized through binding to Evi5, while its degradation occurs after phosphorylation by Plk1 (Polo-like kinase 1).

CDKs Modulators

The activity of CDKs is regulated by both activating and inhibitory phosphorylations due to their association with cyclins, but also with "non-cyclin" CDK activators or CDK inhibitors.

CDK Inhibitors

The cell cycle is negatively regulated by two families of CDK inhibitors (CKIs): INK4 and CIP/KIP (Sherr and Roberts 1999). CKIs inhibit CAK phosphorylation of CDK by conformational changes, but without binding to CAK.

- The INK4/ARF Family

The INK4/ARF (Inhibitor of Kinase 4/Alternative Reading Frame) family exclusively binds and inhibits CDK4 and CDK6 by blocking their binding to D-type cyclins during G1 phase progression. This family contains four members: INK4A (also named p16), INK4B (p15 or CDKN2B), INK4C (p18 or CDKN2C) and INK4D (p19 or CDKN2D). A unique gene encodes all INK4 proteins, which are 15- to 19-kDa polypeptides containing several ankyrin repeats implicated in their interaction with CDK4 and CDK6. These proteins show poor sequence homology (approximately 40 %), however they are highly conserved among species (for example, each of the INK4 proteins in the mouse shares 90 % identity with the corresponding proteins in human). INK4 proteins are equally potent as inhibitors, but are differentially expressed during mouse development and show diversity in their pattern of expression suggesting cell-lineage specificity or tissue-specific functions.

- The CIP/KIP Family

Members of CIP/KIP (CDK Interacting Protein/Kinase Inhibitory Protein) family are negative regulators of the cell cycle progression. The CIP/KIP family is composed of three members: $p21^{Cip1}$ (CDKN1A), $p27^{Kip1}$ (p27, CDKN1B) and $p57^{Kip2}$ (CDKN1C), which are negative regulators of cyclin E/CDK2, cyclin A/CDK2 and cyclin B/CDK1, and negative or positive regulators of cyclin D/CDK4-6 (Besson et al. 2008). Contrary to the INK4/ARF family, the action of Cip/Kip members depends on their binding to both cyclins and Cdks subunits, that occurs on a specific N-terminal domain conserved in all CIP/KIP members, the "LFG" domain. The remainder of their sequence is poorly conserved, suggesting that each of these proteins present specific functions in the regulation of the cell cycle. Under physiological conditions, p27 is highly expressed during G0 and early G1 phase, and then rapidly decrease in late G1 and S phase. p27 blocks S phase progression through inhibition of cyclin E/CDK2 and cyclin A/CDK2. p21 is less specific, it inhibits the activity of cyclin E-A/CDK2 and cyclin B/CDK1 complexes, and also cyclin D/CDK4 that controls G1 checkpoint. Moreover, p21 can bind PCNA (Proliferating Cell Nuclear Antigen) subunit of δ DNA polymerase and inhibits this enzyme activity to block DNA replication. p57 seems more implicated in the regulation of the cell cycle during the embryonic development, and it present a tissue-specificity expression.

Cip/Kip proteins could also act as non-inhibitory or positive modulators of cell cycle progression by facilitating the transition between the G1 and the S phase. Their progressive binding to increasing amount of cyclin D/CDK4 dimers releases their inhibitory activity on cyclin E/CDK2 and thus favors cell cycle progression. The balance between inhibitory and non-inhibitory functions of CIP/KIP could be linked to their phosphorylation state within specific domains. For example, p27 is an inhibitor of cyclin D/Cdk4 complexes in cell cycle-arrested cells, while it is associated with active cyclin D/Cdk4 complexes in proliferating cells. Indeed, p27 is preferentially tyrosine phosphorylated (Tyr88 and 89) in proliferating cells, causing it to bind cyclin D/Cdk4 in a non-inhibitory mode. In quiescent cells, p27 is dephosphorylated while bound to cyclin D/Cdk4 and therefore inhibits complexes activity (James et al. 2008). It is also possible that CIP/KIP role as inhibitor or non-inhibitor could depend directly on their expression level (Labaer et al. 1997).

Other CDK Modulators

In addition to activation by cyclins and inhibition by CKIs, CDKs can also be modulated by other proteins, such as CDK activating kinase (CAK), RINGO/Speedy family of proteins, Wee1/Myt1 kinases and Cdc25 phosphatases.

- CDK Activating Kinase (CAK)

The CDK/cyclin complexes are activated by phosphorylation at specific sites on the CDKs by CDK activating kinase (CAK). CAK is formed by the association of CDK7, cyclin H and the assembly factor MAT1. It activates CDK1, CDK2, CDK4 and CDK6 by phosphorylation on a conserved threonine residue. This phosphorylation is responsible for an increase binding of CDK to its substrate. The activation of CAK requires the binding of CDK7 to cyclin H, which

allows the phosphorylation of CDK7 on a conserved Thr170 residue in the activation loop. But, contrary to the others CDKs, which need to be phosphorylated to be active, the phosphorylation of CDK7 on its activation segment is not essential for CAK activity. Indeed, MAT1 can substitute Thr170 phosphorylation and is sufficient to activate CDK7/cyclin H complex. CDK7 presents a second site of phosphorylation at Ser164 in Human, whose activation by phosphorylation due to CDK7/cyclin H complex enhances activity and cyclin binding. CAK is also a subunit of the transcription factor TFIIH, which predominantly phosphorylates proteins involved in transcription, including the RNA polymerase II large subunit C-terminal domain involved in the transition to transcriptional pre-initiation from transcriptional initiation stage. TFIIH can phosphorylate CDK2, but less efficiently than free CAK.

- RINGO/Speedy Family

Speedy or RINGO (Rapid Induced of G2/M progression in Oocytes) proteins are direct activators of CDK1 and CDK2. They also bind CDK5, but not CDK4 or CDK6. To date, five mammalian RINGO/Speedy family members have been identified, RINGO A to E. These proteins contain a conserved central region of about 100 residues called the 'Speedy-box' essential for CDK binding and activation, although with different affinities: the binding and the activation of CDK2 is more efficient than CDK1. Unlike cyclins, RINGO/Speedy proteins do not phosphorylate CDKs in the activation loop of the kinase domain. Therefore, unconventional not yet identified roles for RINGO/Speedy proteins in the regulation of cell cycle are suggested.

- M-phase Promoting Factor (MPF) Modulators: Wee1/Myt1 Kinases and Cdc25 Phosphatases

The entry of cell in mitosis is controlled by the M-phase promoting factor (MPF, Nobel Price of Physiology and Medicine 2001 shared by Paul Nurse, Tim Hunt and Leland Hartwell). MPF is a complex of two proteins, cyclin B and CDK1. This complex is necessary for G2/M transition but must be rapidly inactivated during mitosis to avoid several mitosis cycles. CDK1 is expressed at constant level during the whole cell cycle, whereas cyclin B has a cyclic expression with an initiation of synthesis at the end of S phase. Cyclin B accumulates during G1, S, G2, M phases but decreases rapidly at the end of mitosis (at the checkpoint). The increase of cyclin B concentration allows the formation of CDK1/cyclin B complex, whose activity is determined by the phosphorylation state of CDK1 (Fig. 2.2). To be active, CDK1 must be phosphorylated on Thr161 by CAK. In interphase, after its association with cyclin B, CDK1 is held in a relatively inactive state by simultaneous phosphorylation of Thr14 and Tyr15 residues located within the ATP-binding site by Wee1 and Myt1. These two residues must be dephosphorylated for the activation of the cyclin B/CDK1 complex and thus to promote the initiation of mitosis. Dephosphorylation is ensured by the Cdc25 phosphatases (CDC25 A, CDC25 B and CDC25 C, in humans). Thus, the active heterodimer cyclin B/CDK1 (phosphorylated on Thr161) inhibits Wee1 and Myt1 kinases and activates Cdc25 phosphatases, therefore increasing CDK1 activity, and favors the entry of cell in mitosis by phosphorylation of its target proteins such as histone H1, lamin or microtubule-associated proteins, responsible for chromosome condensation during mitosis, fragmentation and solubilization of nuclear lamina or microtubules dynamic stability, respectively. When mitosis is initiated, CDK1 activates the degradation of cyclin B by poly-ubiquitinylation, and then CDK1 is dephosphorylated on Thr161 by a phosphatase: a new cycle can begin.

Rb/E2F Pathway

The primary function of cyclin D-dependent kinases – CDK4 and CDK6 – is phosphorylation of a retinoblastoma tumor suppressor protein (pRb), encoded by the retinoblastoma susceptibility gene (RB1). The retinoblastoma tumor suppressor family (also named "pocket proteins"), pRb, together with the related proteins p107 and p130, plays a critical role in cell cycle regulation. pRb proteins have approximately 50 % of sequence homology, and contain a specific and conserved domain named the "pocket domain" that is responsible for their repressor function. pRb are transcriptional repressors that regulates the cell cycle through their ability to bind and

sequestrate E2F transcription factors (Swiss and Casaccia 2010). pRb interacts and inhibits E2F through its specific "pocket domain" to coordinate the initiation of S phase by mitogenic signaling molecules (Mcclellan and Slack 2007). To this end, pRb activity is modulated by a balance of phosphorylation/dephosphorylation that arises from kinase and phosphatase activities in a cell cycle-dependent manner (Fig. 2.2). Indeed, at G0 and early G1, Rb is hypophosphorylated allowing its binding to E2F factors blocking their transactivation domain and inhibiting the recruitment of co-repressors (as histone deacetylase 1 (HDAC1) or Brg1/hBRM, members of the SWI/SNF nucleosome remodeling complex) as well as the expression of E2F target genes. The cyclin/CDK complexes responsible for the cell cycle progression hyperphosphorylate pRb from late G1 to mitosis, thus relieving the constraints on E2F proteins and allowing the expression of genes required for DNA synthesis and cell cycle progression. Towards the end of M phase, the protein phosphatase 1 (PP1), which is also necessary for mitotic exit, dephosphorylates pRb. E2Fs are required during cell cycle progression, as they contribute to irreversibility of G1/S transition via a positive feedback loop: E2Fs activate the overexpression of cyclin E, which interacts with Cdk2, resulting in activation of pRb phosphorylation.

"Cell Cycle" CDKs in Neurogenesis

The mechanisms involved in proliferation, neuronal differentiation, migration and functional integration in the adult brain remain largely unknown. Initially identified as core cell cycle regulators, some Cdks have emerged as multifaceted proteins with functions beyond cell cycle regulation. Recently, accumulating evidence ascribed crucial roles to regulators of Cdk4/6 activity in controlling adult neurogenesis.

Cdk1

Contrary to other "cell cycle" Cdks, the lack of Cdk1 expression in mice leads the death at morula stage (E2.5) (Santamaria et al. 2007). Thus, Cdk1 seems to be the only cell cycle Cdk whose loss is not compensated by the others Cdks during early stages of embryonic development. In absence of the other cell cycle Cdks, such as Cdk2, Cdk4 and/or Cdk6, Cdk1 seems to be able to form functional complexes with all cyclins implicated in the embryonic cell cycle division, resulting in the activation of the pRb/E2F pathway and therefore in the cell cycle progression (Santamaria et al. 2007). A possible role of Cdk1 in adult neurogenesis remains to be elucidated.

Cdk2

Cdk2 was thought to be indispensable to drive cells through the transition from G1 to S phases and for the progression in S phase. The generation of $Cdk2^{-/-}$ mice has changed this theory. Indeed, $Cdk2^{-/-}$ mice are viable and develop normally with a minor body weight reduction (Ortega et al. 2003), therefore suggesting that Cdk2 is not essential for proliferation in embryonic or adult mice. However $Cdk2^{-/-}$ mice are sterile, shedding light on Cdk2 importance in germ cells.

Regarding brain cells, Cdk2 is required for oligodendrocyte progenitor cells (OPCs) proliferation in vitro (Belachew et al. 2002), suggesting that Cdk2 may have a similar role in adult neurogenesis. In the absence of Cdk2 in adult mice, a decrease of density and proliferation of NSCs is observed in the SVZ (Jablonska et al. 2007) while no significant difference is detected in the DG (Vandenbosch et al. 2007). Under pathological conditions, such as demyelinating lesions, the absence of Cdk2 in adult mice is associated with increase OPCs renewal and differentiation, thus resulting in promotion of remyelination (Caillava et al. 2011). In numerous organs, the absence of Cdk2 can be compensated by other Cdks. In $Cdk2^{-/-}$ cells, Cdk1 binds to Cyclin E, and this active complex regulates efficiently G1/S transition. Indeed, the absence of Cdk2 in perinatal mice is associated with Cdk4 overexpression in SVZ cells, suggesting that CDK4 compensate for the loss of CDK2 expression (Jablonska et al. 2007). This compensatory effect is absent at later postnatal stages, leading to impaired neurogenesis.

Cdk4

Knockout mice for Cdk4 are viable but infertile and show growth retardation. Moreover, these mice develop insulin-deficient diabetes due to a degeneration of beta-islet pancreatic cells (Rane et al. 1999). In adult mice, Cdk4 expression is exclusively restricted to dividing NSCs in the DG and SVZ (Beukelaers et al. 2011). Cdk4, in association with its cyclin partner (i.e. cyclin D1), play a critical role in adult neurogenesis by modulating the length of G1 phase. Indeed, overexpression of Cdk4 and cyclin D1 is associated with a reduction of G1 length, which results in inhibition of adult neurogenesis and increases of NSCs population (Artegiani et al. 2011; Lange et al. 2009). However, the absence of Cdk4 does not impact on adult neurogenesis in adult mice (Beukelaers et al. 2011).

Cdk5

Although Cdk5 does not act as a checkpoint kinase during cell cycle progression, it can regulate several proteins implicated in the cell cycle, such as pRb. Mice lacking Cdk5 die in utero around E16.5 (Ohshima et al. 1996). In the brain, Cdk5 plays a critical role in corticogenesis and neuronal migration during embryonic development (Ohshima et al. 1996). Cdk5 plays also a critical role in adult neurogenesis where it is implicated in the migration of neuroblasts in the SVZ, in the migration and maturation of newborn neurons, and also in the regulation of adult-generated neuron survival in the hippocampus (Lagace et al. 2008). However, the molecular mechanisms of its role in adult neurogenesis remain unknown.

Cdk6 a Key Molecular Regulator for Adult Neurogenesis

Cdk6-deficient mice are viable, but present a reduced proliferation of erythroid lineage and a decrease in the size of thymus and spleen. In the adult brain, the expression pattern of Cdk6 is restricted to the two zones of adult neurogenesis and more precisely to the proliferating cells (i.e. Ki67+ cells) (Beukelaers et al. 2011). Our laboratory showed that the lack of Cdk6 results in reduced number of proliferating cells in both the adult DG and SVZ, suggesting that Cdk6 is essential to control the biology of progenitor cell in these neurogenic areas. More precisely, the quantification of the different subpopulations of proliferating cells revealed that only neuronally committed progenitor cell population, i.e. type-2b and type-3 in the DG and Type C and A in the SVZ, are impaired in the absence of Cdk6. The immature population of progenitor cells, i.e. type-B (SVZ) and type-1 and 2a (DG) cells remains unaffected in both wild type and $Cdk6^{-/-}$ mice. The decrease of neuronally committed cells observed in $Cdk6^{-/-}$ neurogenic areas could affect neuronal cell production. Indeed, the authors showed a reduction of the number of young postmitotic neurons (DCX+/NeuN+) in the two neurogenic areas, consistent with the decreased proliferation.

It has been shown that neuronally committed precursors undergo a define number of cell divisions prior exiting the cell cycle and differentiating into neurons. Thus, the selective reduction of neuronal committed precursors likely arises from a premature exhaustion of progenitor through increased rate of cell cycle exit. Beukelaers et al. (2011) showed that the absence of Cdk6 increased the cell cycle exit in the DG and in the anterior part of the RMS of $Cdk6^{-/-}$ animals. Altogether, Cdk6 controls the proliferation and cell cycle exit of neuronally committed precursors.

Recently, Lange et al. demonstrated that a lengthening of G1 by Cdk4/cyclin D1 downregulation is sufficient to promote the exit of the cell cycle of cortical progenitors and their differentiation into projection neurons (Lange et al. 2009). In addition, Malumbres et al. demonstrated a lengthening of G1 in $Cdk6^{-/-}$ T lymphocytes (Malumbres et al. 2004). Using cumulative S-phase labelling with BrdU, Beukelaers et al. (2011) demonstrated that the overall duration of the cell cycle (T_C) in DG cycling precursors was increased in $Cdk6^{-/-}$ (22 h32′ in the DG ; 12 h34′ in the SVZ) compared to WT (19 h55′ in the DG ; 9 h58′ in the SVZ). Importantly, this increase was linked to a specific increase of G1 length in neuronally committed precursors (+28.08 % in the DG and +82.21 % in the SVZ).

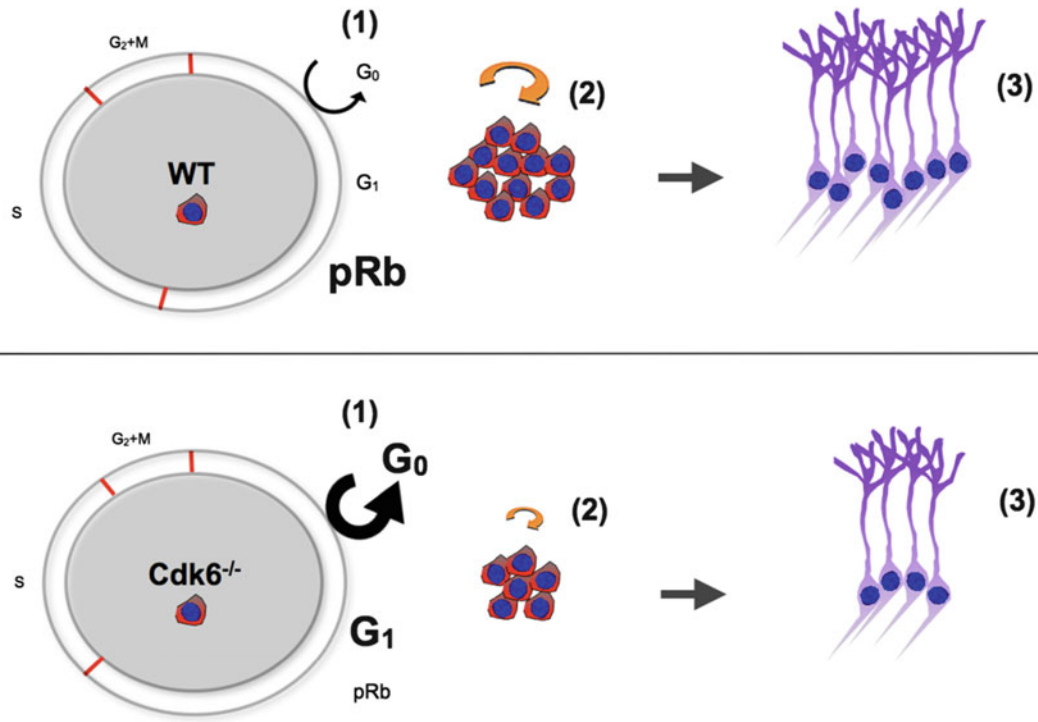

Fig. 2.3 Schematic representation of the phenotype of adult neurogenesis in Cdk6$^{-/-}$ mice. Cdk6$^{-/-}$ adult neural precursors display increased G1 phase length concomitant with pRb hypophosphorylation. Lengthening of G1 leads to premature cell cycle exit into G0 (*1*), reduces precursor expansion (*2*) and, finally, neurogenesis (*3*) (from Beukelaers et al. 2011)

During the G1 phase, Cdk6 phosphorylates pRb on Ser780, leading to the release of E2F and S phase entry. In the absence of Cdk6 a decrease of phosphorylation of Rb was observed in the DG and the SVZ (Beukelaers et al. 2011). Therefore, Cdk6 controls the expansion of neuronally committed precursors by controlling the hyperphosphorylation of pRb and the G1 phase length (Fig. 2.3).

Conclusion

It has been experimentally demonstrated that lengthening of G1 is sufficient to induce neurogenesis and that shortening G1 inhibits neurogenesis and increases the formation and proliferation of NSCs (Artegiani et al. 2011; Beukelaers et al. 2011). Moreover, the switch between proliferation and differentiation of neuronal production in the adult brain is partly controlled by CDK6 via the modulation of G1 phase duration. Therefore, the manipulation of Cdk/Cyclin complexes could be used as a new cell-based therapeutic approach to restore neuronal loss in several neurodegenerative disorders such as Parkinson's disease, Alzheimer's disease, Huntington's disorder or multiple sclerosis. The aim of this strategy would be to induce endogenous neural cells in the adult nervous system to form new neurons, by controlling their proliferation versus differentiation.

The crucial advantage of this therapeutic strategy is to enhance the proliferation of endogenous adult NSCs to avoid the danger of immunological graft rejection. Indeed, until now, several therapeutic approaches using neural cells have been studied, such as transplantation of oligodendrocyte progenitor cells or phenotypically restricted neuronal progenitor cells or mixed progenitor

pools, but all of these present high risks of immunological graft rejection. Moreover, a part of the challenge in cell replacement therapy is to produce new cells (i.e. neurons) with the precise characteristics needed to restore brain function that has been compromised during the disease (e.g. the specific loss of GABAergic neurons in Huntington's disease or the progressive decrease of dopaminergic neurons in Parkinson's disorder). The nervous system has an intrinsic capacity to produce new neural progenitor cells, which can restore the connectivity with existing networks in the patient's brain. This capacity can be used as therapeutic approach for a multiple of neurodegenerative disorders.

It is known that genetic modifications, in particular cell cycle modifications, enhance the risk of tumor formation. However, the balance between proliferation and differentiation of neural cells can be temporarily manipulated to avoid the deregulation of the cell cycle and formation of cancer stem cells. Indeed, after stroke, it has been shown that G1 phase is dynamically and transiently modified, with an early expansion of the SVZ neural progenitor pool due to a decrease of G1 length and an increase of neurogenesis that is not associated with tumorigenic effect.

References

Altman J, Das GD (1965) Autoradiographic and histological evidence of postnatal hippocampal neurogenesis in rats. J Comp Neurol 124:319–335

Artegiani B, Lindemann D, Calegari F (2011) Overexpression of cdk4 and cyclinD1 triggers greater expansion of neural stem cells in the adult mouse brain. J Exp Med 208:937–948

Belachew S, Aguirre AA, Wang H, Vautier F, Yuan X, Anderson S, Kirby M, Gallo V (2002) Cyclin-dependent kinase-2 controls oligodendrocyte progenitor cell cycle progression and is downregulated in adult oligodendrocyte progenitors. J Neurosci 22:8553–8562

Besson A, Dowdy SF, Roberts JM (2008) CDK inhibitors: cell cycle regulators and beyond. Dev Cell 14:159–169

Beukelaers P, Vandenbosch R, Caron N, Nguyen L, Belachew S, Moonen G, Kiyokawa H, Barbacid M, Santamaria D, Malgrange B (2011) Cdk6-dependent regulation of G(1) length controls adult neurogenesis. Stem Cells 29:713–724

Bonaguidi MA, Wheeler MA, Shapiro JS, Stadel RP, Sun GJ, Ming GL, Song H (2011) In vivo clonal analysis reveals self-renewing and multipotent adult neural stem cell characteristics. Cell 145:1142–1155

Bull ND, Bartlett PF (2005) The adult mouse hippocampal progenitor is neurogenic but not a stem cell. J Neurosci 25:10815–10821

Caillava C, Vandenbosch R, Jablonska B, Deboux C, Spigoni G, Gallo V, Malgrange B, Baron-Van Evercooren A (2011) Cdk2 loss accelerates precursor differentiation and remyelination in the adult central nervous system. J Cell Biol 193:397–407

Carleton A, Petreanu LT, Lansford R, Alvarez-Buylla A, Lledo PM (2003) Becoming a new neuron in the adult olfactory bulb. Nat Neurosci 6:507–518

Clarke L, Van Der Kooy D (2011) The adult mouse dentate gyrus contains populations of committed progenitor cells that are distinct from subependymal zone neural stem cells. Stem Cells 29:1448–1458

Doetsch F, Caille I, Lim DA, Garcia-Verdugo JM, Alvarez-Buylla A (1999) Subventricular zone astrocytes are neural stem cells in the adult mammalian brain. Cell 97:703–716

Doetsch F, Petreanu L, Caille I, Garcia-Verdugo JM, Alvarez-Buylla A (2002) EGF converts transit-amplifying neurogenic precursors in the adult brain into multipotent stem cells. Neuron 36:1021–1034

Encinas JM, Michurina TV, Peunova N, Park JH, Tordo J, Peterson DA, Fishell G, Koulakov A, Enikolopov G (2011) Division-coupled astrocytic differentiation and age-related depletion of neural stem cells in the adult hippocampus. Cell Stem Cell 8:566–579

Ihrie RA, Alvarez-Buylla A (2011) Lake-front property: a unique germinal niche by the lateral ventricles of the adult brain. Neuron 70:674–686

Jablonska B, Aguirre A, Vandenbosch R, Belachew S, Berthet C, Kaldis P, Gallo V (2007) Cdk2 is critical for proliferation and self-renewal of neural progenitor cells in the adult subventricular zone. J Cell Biol 179:1231–1245

James MK, Ray A, Leznova D, Blain SW (2008) Differential modification of p27Kip1 controls its cyclin D-cdk4 inhibitory activity. Mol Cell Biol 28:498–510

Labaer J, Garrett MD, Stevenson LF, Slingerland JM, Sandhu C, Chou HS, Fattaey A, Harlow E (1997) New functional activities for the p21 family of CDK inhibitors. Genes Dev 11:847–862

Lagace DC, Benavides DR, Kansy JW, Mapelli M, Greengard P, Bibb JA, Eisch AJ (2008) Cdk5 is essential for adult hippocampal neurogenesis. Proc Natl Acad Sci U S A 105:18567–18571

Lange C, Huttner WB, Calegari F (2009) Cdk4/cyclinD1 overexpression in neural stem cells shortens G1, delays neurogenesis, and promotes the generation and expansion of basal progenitors. Cell Stem Cell 5:320–331

Malumbres M, Barbacid M (2009) Cell cycle, CDKs and cancer: a changing paradigm. Nat Rev Cancer 9:153–166

Malumbres M, Sotillo R, Santamaria D, Galan J, Cerezo A, Ortega S, Dubus P, Barbacid M (2004) Mammalian cells cycle without the D-type cyclin-dependent kinases Cdk4 and Cdk6. Cell 118:493–504

Mcclellan KA, Slack RS (2007) Specific in vivo roles for E2Fs in differentiation and development. Cell Cycle 6:2917–2927

Ming GL, Song H (2011) Adult neurogenesis in the mammalian brain: significant answers and significant questions. Neuron 70:687–702

Mirzadeh Z, Han YG, Soriano-Navarro M, Garcia-Verdugo JM, Alvarez-Buylla A (2010) Cilia organize ependymal planar polarity. J Neurosci 30:2600–2610

Ohshima T, Ward JM, Huh CG, Longenecker G, Veeranna, Pant HC, Brady RO, Martin LJ, Kulkarni AB (1996) Targeted disruption of the cyclin-dependent kinase 5 gene results in abnormal corticogenesis, neuronal pathology and perinatal death. Proc Natl Acad Sci U S A 93:11173–11178

Ortega S, Prieto I, Odajima J, Martin A, Dubus P, Sotillo R, Barbero JL, Malumbres M, Barbacid M (2003) Cyclin-dependent kinase 2 is essential for meiosis but not for mitotic cell division in mice. Nat Genet 35:25–31

Pastrana E, Cheng LC, Doetsch F (2009) Simultaneous prospective purification of adult subventricular zone neural stem cells and their progeny. Proc Natl Acad Sci U S A 106:6387–6392

Rane SG, Dubus P, Mettus RV, Galbreath EJ, Boden G, Reddy EP, Barbacid M (1999) Loss of Cdk4 expression causes insulin-deficient diabetes and Cdk4 activation results in beta-islet cell hyperplasia. Nat Genet 22:44–52

Reynolds BA, Weiss S (1992) Generation of neurons and astrocytes from isolated cells of the adult mammalian central nervous system. Science 255:1707–1710

Santamaria D, Barriere C, Cerqueira A, Hunt S, Tardy C, Newton K, Caceres JF, Dubus P, Malumbres M, Barbacid M (2007) Cdk1 is sufficient to drive the mammalian cell cycle. Nature 448:811–815

Seaberg RM, Van Der Kooy D (2002) Adult rodent neurogenic regions: the ventricular subependyma contains neural stem cells, but the dentate gyrus contains restricted progenitors. J Neurosci 22:1784–1793

Sherr CJ, Roberts JM (1999) CDK inhibitors: positive and negative regulators of G1-phase progression. Genes Dev 13:1501–1512

Singla V, Reiter JF (2006) The primary cilium as the cell's antenna: signaling at a sensory organelle. Science 313:629–633

Swiss VA, Casaccia P (2010) Cell-context specific role of the E2F/Rb pathway in development and disease. Glia 58:377–390

Vandenbosch R, Borgs L, Beukelaers P, Foidart A, Nguyen L, Moonen G, Berthet C, Kaldis P, Gallo V, Belachew S, Malgrange B (2007) CDK2 is dispensable for adult hippocampal neurogenesis. Cell Cycle 6:3065–3069

Prolactinomas: Role of VEGF, FGF-2 and CD31

3

Maria Ines, Perez Millán, Carolina Cristina, Silvia Inés Berner, and Damasia Becu-Villalobos

Contents

Abstract

Pituitary tumors rarely produce metastasis, but cause considerable morbidity and mortality. Each pituitary tumor of clonal origin represents the multifactorial result of failure of different regulatory events where growth and angiogenic factors may play critical roles in hormone secretion and cell proliferation. Prolactinomas, pituitary tumors which secrete prolactin, are generally treated successfully with dopamine agonists, even though a 10–15 % are resistant to this pharmacological therapy.

The role of angiogenesis in pituitary tumor development has been questioned, as pituitary tumors have been usually found to be less vascularized than the normal pituitary tissue. Nevertheless, a significantly higher degree of vasculature has been shown in invasive pituitary prolactinomas when compared to noninvasive prolactinomas. Furthermore, it has also been described that macroprolactinomas are more vascular than microprolactinomas.

Many growth factors and their receptors are involved in pituitary tumor development. For example, VEGF, FGF-2, FGFR1 and PTTG, which give a particular vascular phenotype, are modified in pituitary adenomas. Inhibitors of angiogenesis, Thrombospondin-1 and FGF-2 endogenous antisense have also been detected. In particular, vascular endothelial growth factor (VEGF) the central mediator of angiogenesis in endocrine glands, was encountered in experimental and human pituitary tumors at different levels of expression, and in particular,

M. Ines • P. Millán • D. Becu-Villalobos (✉)
Institute of Experimental Biology and Medicine – CONICET, Buenos Aires 1428, Argentina
e-mail: dbecu@dna.uba.ar

C. Cristina
BioResearch Center-National University of NorthWest of Buenos Aires, Junin, Buenos Aires, 6000, Argentina

S.I. Berner
Santa Lucia Hospital and Santa Isabel Clinic, Buenos Aires, Argentina

M.A. Hayat (ed.), *Tumors of the Central Nervous System, Volume 12*,
DOI 10.1007/978-94-007-7217-5_3,

in dopamine resistant prolactinomas. Even though the role of angiogenesis in pituitary adenomas is contentious, VEGF, making permeable pituitary endothelia, might contribute to adequate temporal vascular supply and mechanisms other than endothelial cell proliferation. The study of angiogenic factor expression in aggressive prolactinomas with resistance to dopamine agonists will yield important data in the search of therapeutical alternatives.

Introduction

Pituitary Tumors

Pituitary tumors rarely produce metastasis, but cause considerable morbidity and mortality. In general, they result from monoclonal growth and intrinsic genetic defects which are related to oncogenes, suppressor genes, and genes responsible for differentiation. On the other hand, growth factors of hypothalamic or pituitary origin may act on aberrant cells, contributing to their proliferation (Ezzat 2001). Point mutations identified up till now can only account for a small percentage of pituitary tumors, and the mechanism of pituitary tumorigenesis is still unraveling.

Prolactinomas

Prolactin secreting adenomas are the most frequent type among pituitary tumors. Patients with prolactinoma usually present endocrinological symptoms resulting from hyperprolactinemia and, less commonly, with visual defects due to compression of the optic chiasm. Macroprolactinomas are benign, slowly proliferating tumors, although they may be locally highly aggressive, particularly in males, and invade adjacent structures. Giant prolactinomas (tumor volume exceeding 4 cm in diameter, and/or with prolactin levels higher than 3,000 ng/ml and mass effect) are a rare subcategory of macroprolactinomas, remain one of the greatest challenges in neurosurgery. Because of invasive growth, giant adenomas can compress or destroy adjacent structures, resulting in neurological dysfunction, and cavernous sinus compression. Pharmacological therapy with dopamine agonists remains the mainstay of treatment. This therapy is effective in >85 % of patients with prolactin-secreting pituitary tumors. A minority of patients show no primary response to either bromocriptine or cabergoline (Molitch 2005), and the development of dopamine agonist resistance in an initially responsive prolactinoma is unusual.

Angiogenesis in Pituitary Tumors

The formation of new blood vessels within neoplasms, termed angiogenesis, provides the tumor tissues with oxygen and basic energetic compounds. An increase in tumor size necessarily requires a corresponding increase in vascularization that is assured by means of the complex dynamic process of angiogenesis. In most human tumors, including breast, bladder, and stomach, angiogenesis has been shown to be correlated with tumor behavior. On the other hand, pituitary tumors are usually less vascularized than the normal pituitary tissue, as suggested by Schechter (Schechter 1972), and later confirmed by other authors (Jugenburg et al. 1995; Turner et al. 2000b). Differences in the angiogenic pattern of pituitary adenomas have yielded highly controversial results concerning hormonal phenotypes, size or invasion. In most studies, immunohistochemistry evaluation of different markers of microvascular density (MVD) such as cluster differentiation molecules (CD 31 and CD 34), Factor VIII (factor eight-related antigen), and ulex europaeus agglutinin I have been used. Nevertheless, the appraisal of MVD by immunohistochemistry has a number of substantial limitations, which are mainly due to the complex biology of tumor vasculature, and the irregular geometry of the vascular system (Vidal et al. 2003).

Some data point to increased angiogenesis in pituitary adenomas. For example, it has been described that macroprolactinomas are significantly more vascular than microprolactinomas (Jugenburg et al. 1995), and Turner et al. (2000a) demonstrated a significantly higher degree of

vasculature of invasive pituitary prolactinomas. Inhibitors of angiogenesis were effective in the suppression of growth of experimental prolactinomas and in angiographic studies the presence of additional arteries (which were not part of the portal system) were found in 66 % of patients with pituitary adenomas (Schechter et al. 1988). Nevertheless, the role of angiogenesis in pituitary tumor development has been questioned, as the normal pituitary is a highly vascularized gland.

Vascular Endothelial Growth Factor

Experiments over the past decades indicate that vascular endothelial growth factor-A (VEGF-A or VEGF) is a central regulator of angiogenesis in endocrine glands. VEGF-A is the founding member of a family of closely related cytokines that exert critical functions in vasculogenesis and in both pathologic and physiologic angiogenesis and lymphangiogenesis. The VEGF-A gene is located on the short arm of chromosome 6 and is differentially spliced to yield several different isoforms, the three most prominent of which encode polypeptides of 189, 165, and 121 amino acids in human cells. The protein has a hydrophobic leader sequence, typical of secreted proteins. It was discovered in the late 1970s as a tumor-secreted protein that potently increased microvascular permeability to plasma proteins. We can summarize its unique properties:

1. It is essential for normal developmental vasculogenesis and angiogenesis, as both null (*VEGF-A*$^{-/-}$) and heterozygote (*VEGF-A*$^{+/-}$) animals are embryonic lethals.
2. It increases vascular permeability to plasma and plasma proteins, a characteristic trait of the tumor microvasculature and a critical early step in tumor stroma generation.
3. It is a selective mitogen for vascular endothelium because its major tyrosine kinase receptors are selectively (though not exclusively) expressed on vascular endothelium.
4. It is overexpressed in a variety of human cancer cells (in human vascular tumors, including brain, colon, gastrointestinal tract, ovary, breast, and others).
5. It has a potential for evaluating prognosis in individual patients and as a therapeutic target.

Vascular Endothelial Growth Factor in the Pituitary Gland

VEGF expression has been described in all cell types in the normal pituitary, with greater expression in somatotroph and follicle-stellate cells. Using immunohistochemistry higher VEGF expression has been shown in the normal gland compared with adenomas (Lloyd et al. 1999), while the opposite has also been published. In a group of pituitary adenomas, ACTH and GH secreting adenomas, pituitary carcinomas had the strongest VEGF immunoreactivity (Lloyd et al. 1999). On the other hand, Viacava et al. (2003) found no differences in VEGF expression among tumors of different histotype, and McCabe et al. (2002) comparing VEGF in a series of adenomas composed of 77 % non functioning adenomas, and only 4 % of prolactinomas, found highest expression in nonfunctioning adenomas and GH producing adenomas. Elevated serum VEGF concentrations have been demonstrated in patients harboring pituitary tumors, and approximately 90 % of human pituitary tumors cultured in vitro show measurable VEGF secretion.

Using Western blot analysis of pituitary adenomas we found that VEGF protein expression was higher in prolactinomas compared to nonfunctioning (NF), GH, and ACTH secreting adenomas (Cristina et al. 2010). This finding may be related to the high percentage of macroprolactinomas in the series studied (11/12). In this respect, using angiogenic markers, it has been described that macroprolactinomas are significantly more vascularized than microprolactinomas. Furthermore, lower VEGF found in ACTH-producing adenomas may be consistent with the finding that VEGF production can be suppressed by glucocorticoids which are potent inhibitors of VEGF production in vitro (Lohrer et al. 2001). On the other hand, pituitary adenoma VEGF expression was similar in both sexes and was not influenced by age or years of adenoma evolution, when all adenomas were considered. This is in agreement with most studies which reveal that sex,

age or even rate of recurrence did not influence VEGF expression in pituitary tumors.

These data indicate that even though the role of angiogenesis in pituitary adenomas is contentious, VEGF might contribute to adequate temporal vascular supply with mechanisms other than endothelial cell proliferation. Tumor angiogenesis in the pituitary, as well as in other endocrine neoplasms, probably reflects the basic observation that tumors require neovascularization to grow; however, the changes that occur may be somewhat different from some other tissues that are less highly vascularized in the nonneoplastic state. Some data suggest that VEGF may prolong cell survival by inducing expression of the anti-apoptotic protein bcl-2 in pituitary adenomas, suggesting that part of its angiogenic activity is related to protection of endothelial cells from apoptosis. VEGF has been associated to intratumoral hemorrhage (Arita et al. 2004), and might also participate in the occurrence of pituitary peliosis, a form of vasculogenic mimicry. Peliosis may be linked to the permeabilizing function of this growth factor, and to the increased fenestration induced in blood vessels stimulated by VEGF overexpression. Peliosis occurrence has been related to high VEGF expression in hepatocarcinogenesis, spleen damage, and in a lethal hepatic syndrome in mice. This process may be seen in prolactinomas and other pitutitary adenomas, though it usually goes unrecognized. In dopamine D2 receptor knockout (*Drd2*$^{-/-}$) mice which develop lactotroph hyperplasia and eventually prolactinomas, we have described increased peliosis occurrence in these pituitary tumors in association with increased VEGF expression (Cristina et al. 2005).

Fibroblast Growth Factor-2

Basic fibroblast growth factor-2 (basic FGF, or FGF2), a potent angiogenic factor, was originally isolated from the bovine pituitary and has a pleiotropic activity affecting both vasculature and parenchyma cell proliferation and differentiation. It belongs to a large family of heparin-binding growth factors comprising at least 22 structurally related members. FGF2 expression is complex; at least four FGF2 isoforms (18, 22, 22.5, and 24 kDa) in human, and three (18, 21, and 22 kDa) in mouse are synthesized through alternative translation initiation from CUG codons. The 18 kDa isoform is predominantly cytoplasmic but can also be found in the extracellular matrix, while the higher-molecular-weight isoforms are localized in nuclei and ribosomes. The 18 kDa FGF2 isoform is highly expressed in the normal human pituitary, while pituitary adenomas produce predominantly the 24 kDa form. Recently, a 34 kDa isoform was reported with the most upstream CUG codon among all FGF2 forms. None of the isoforms have a typical secretory signal sequence, but alternative pathways have been described for their export from the cell. The biological effects of FGF2 are mediated through four high-affinity transmembrane receptors (FGFR1 – FGFR4) that have intrinsic tyrosine kinase activity. They can be found on a wide variety of cell membrane surfaces including endothelial cells where FGF2 exerts its proangiogenic functions.

Fibroblast Growth Factor-2 and FGFR1 in the Pituitary

FGF2 participates in pituitary development and proliferation and regulates hormone synthesis and secretion, affecting prolactin and TSH production. It is mainly produced by folliculostellate cells (FS) (Ferrara et al. 1987), although somatotrophs and gonadotrophs have also been reported to be sources of this growth factor. FGF2 participates in estradiol-mediated prolactinoma induction in rats under both physiological and pharmacological conditions. In the hyperplastic pituitaries of *Drd2*$^{-/-}$ mice, it induces prolactin secretion and cellular proliferation, and, interestingly has a differential subcellular distribution compared to that of wild-type pituitaries, which could be associated with different biological roles of this angiogenic factor in both genotypes (Cristina et al. 2007a). FGF2 is also expressed by human pituitary adenoma cells in vitro, and high levels of serum FGF2 were found in patients bearing pituitary tumors, declining following surgical adenomectomy. In the case of a giant invasive prolactinoma with loss of

response to dopamine agonist therapy we have recently reported strong immunoreactivity for both angiogenic factors VEGF and FGF2, as well as immunoreactivity for the endothelial cell marker CD31 indicating high vascularization of the adenoma (Mallea-Gil et al. 2009).

FGFR1 is found in the normal human pituitary as well as in pituitary adenomas, and its mRNA was described in the rat neural and anterior lobe. Furthermore, FGFR1 has been proposed as a candidate marker of pituitary tumors together with FGF2 and pituitary tumor transforming gene (PTTG); indeed, the FGF2 receptor FGFR1 was found to be highly expressed in pituitary tumors compared to the normal gland (McCabe et al. 2003). Furthermore, significantly increased FGFR1 mRNA expression was described in functioning tumors that invaded the sphenoid bone compared with those that did not, thus raising the possibility of using the FGFR1 as a molecular marker of tumor biological behavior (McCabe et al. 2003). On the other hand, it has also been determined that cytoplasmic FGFR1 immunoreactivity was inversely correlated with maximum pituitary tumor diameter.

Proteins and Genes Related to FGF2 in Prolactinomas

FGF4: DNA derived from human prolactinomas expresses transforming activity in heterologous cells and has sequences in close resemblance with those of *hst* gene. Overexpression of *hst* gene leads to increased production of FGF4. Shimon et al. (1996) demonstrated the function of the *hst* gene in rat lactotroph tumor formation and prolactin secretion. They were able to show that lactotrophs in 5 of 14 prolactinomas stained strongly with anti-FGF-4 monoclonal antibodies. Immunoreactive hst product in adenoma cells was observed in invasive prolactinomas. These findings imply a role of *hst* gene, and its product FGF4, in cellular proliferation, growth and aggressive behavior in prolactinomas.

PTTG: Estrogen promotes experimental prolactinoma development via induction of a pituitary tumour transforming gene (*pttg*) (Cristina et al. 2007b) that is located on chromosome 5q33. PTTG has been shown to be tumorigenic in vivo, by regulating basic fibroblast growth factor (FGF2) secretion and inhibiting chromatid separation.

Thrombospondin-1: (TSP-1) is a modular glycoprotein secreted by different cell types, including endothelial cells. It is composed of multiple active domains that bind to soluble factors, cell receptors, and extracellular components. TSP-1 was the first endogenous inhibitor of angiogenesis to be identified and its effect is due, at least in part, to its capacity to bind FGF2. TSP-1 agonists can inhibit experimental prolactinoma development (Sarkar et al. 2007).

FGF2 Endogenous Antisense (GFG) RNA: In *Xenopus laevis* oocytes, a 1.5 kb *FGF2* antisense (GFG) RNA complementary to the third exon and 3′UTR of FGF-2 mRNA has been implicated in FGF2 mRNA regulation. The human homolog has been localized to the same chromosomal site as FGF2 (chromosome 4, JO4513 adjacent to D4S430), confirming this as a human endogenous anti-sense gene. This GFG anti-sense gene also encodes a 35 kDa protein, and regulates cell proliferation and hormone secretion. Pituitary tumors have been shown to express FGF2 and GFG while the normal human pituitary expresses GFG but not FGF2; GFG protein levels are higher in the normal gland than in most tumors. Aggressive pituitary adenomas appear to express more FGF-2 than GFG mRNA (Ezzat 2001).

Truncated FGFR4: Altered FGF receptor expression has been found in pituitary adenomas (Ezzat 2001), and FGFR4 undergoes alternative transcription initiation in pituitary adenomas, giving rise to an oncogenic protein in pituitary adenomas of various subtypes. Expression of this pituitary tumor-derived (ptd)-FGFR4 protein is more frequent in macroadenomas than in microadenomas and correlates with the Ki-67 labeling index. Recent data suggest that ptd-FGFR4 alters cell adhesion by a mechanism that explains the loss of reticulin, which is the hallmark of pituitary adenomas. Taken together, these data suggest that deregulated FGF/FGFR function plays a role in pituitary tumorigenesis, and particularly in prolactinoma development.

CD31 and CD34

Different markers of MVD such as CD 31 and CD 34, Factor VIII (factor eight-related antigen), and ulex europaeus agglutinin I, have been used to evaluate angiogenesis. CD31 and CD34, both endothelial cell antigens, are sensitive markers of microvessels. They stain the majority of tumor vessels, both mature and new vessels. Even though antibodies to CD31 are not completely specific for endothelial cells, as they may also detect plasma cells, they are widely used for MVD appraisal, and results generally correlate with those obtained with CD34. Using these endothelial cell markers, some authors have found more prominent vasculature in prolactinomas, and others found that these tumors had the lowest while TSH secreting adenomas had the highest MVD. It has also been reported that ACTH secreting tumors had the lowest MVD, while other authors found that GH secreting adenomas had the lowest, or the highest MVD. Finally, some authors did not find any significant difference in MVD between the hormonal subtypes. These results point to the complexity of evaluation of vascularity in the adenomatous pituitary, and, as suggested by Itoh et al. (2003) angiogenesis may be revealed in the alteration of diameter or shape of the blood vessels.

With regard to the relation between MVD and sex or age of the patients, contradictory findings have also been reported. Jugenburg et al. (1995) reported no significant correlations, whereas Turner et al. (2000a) found tumor MVD clearly decreased with age in GH producing adenomas, and there was a trend in other tumor types from older patients to have lower MVD. In contrast, a positive correlation between age and MVD has also been reported. We described that in pituitary adenomas: CD31 expression was not different between sexes, and did not correlate with patients' age when all adenomas were considered. Nevertheless, if only non functioning adenomas were analyzed we found a positive correlation of CD31 with increasing age (Cristina et al. 2010), in agreement with other authors (Vidal et al. 2001), and therefore age may have an influence on the extent of neovascularization of non functioning adenomas.

Interestingly enough, we described a high correlation of VEGF and CD31 expression for all adenoma types, and for prolactinomas and nonfunctioning adenomas in particular (Cristina et al. 2010). This is in contrast to results published by other authors in which MVD did not correlate with VEGF expression. Therefore, the strong positive association of VEGF and CD31 expression found in pituitary adenomas suggests the participation of tumor vascularization in adenoma development.

On the other hand, proliferation markers (PCNA and Ki67) do not correlate with the angiogenic markers CD31 and VEGF, as described by us and others. This suggests that the rate of epithelial and tumor cell proliferation in pituitary tumors is not directly related to neovascularization, and other factors, such as primary genetic alterations or alteration of apoptotic pathways, may directly affect the rate, invasiveness and tumor behavior. In this respect, a positive relationship was observed between the expression of bcl-2, an antiapoptotic protein, and increasing MVD, suggesting an association between angiogenesis and cell survival.

Dopamine D2 Receptors and Angiogenesis

A relationship between the dopaminergic D2 receptor (D2R) and endothelial cell proliferation within tumors has been proposed. Dopamine and other related catecholamine neurotransmitters that interact with the D2R selectively inhibit VEGF–induced angiogenesis and inhibit the growth of malignant tumors as well as the vascular permeabilizing and angiogenic activities of VEGF. Besides, in two outbred lines of Wistar rats, which present high and low dopaminergic reactivity, respectively, VEGF expression was lower in the first group, and this group was more resistant to tumor implantation and developed significantly fewer lung metastases.

It is well established that D2R is the principal receptor involved in prolactin inhibition at the pituitary level, and in αMSH regulation at the intermediate pituitary lobe. Therefore, as expected, D2R knockout (*Drd2*$^{-/-}$) mice generated by targeted

mutagenesis have chronic hyperprolactinemia, pituitary hyperplasia, and a moderate increase in serum αMSH. We also showed that they are growth retarded evidence and alteration in the GH-IGF-I axis. After 16 months of age, highly vascularized adenomas develop, especially in females, but also in males. Prominent vascular channels as well as extravasated red blood cells are not contained in capillaries or peliosis, a common finding in the hyperplastic and adenomatous *Drd2*$^{-/-}$ pituitaries. As described, peliosis has been found in different tumors that secrete VEGF.

We found that VEGF mRNA and protein expression were increased in pituitaries from *Drd2*$^{-/-}$ female mice when compared to age-matched wild-type female mice (Cristina et al. 2005). Pituitary VEGF production is stimulated by estrogen in rat pituitaries and the somatolactotroph cell line GH3. Nevertheless, estrogen levels are not increased in *Drd2*$^{-/-}$ female mice, indicating that increased pituitary VEGF expression is mainly dependent on the lack of dopaminergic control. In experiments with wild-type female mice we found that prolonged treatment with the D2R antagonist, haloperidol, enhanced pituitary VEGF protein content and prolactin release (Cristina et al. 2005), and there was a significant correlation between pituitary VEGF levels and serum prolactin after haloperidol treatment. These results support the notion that dopamine acting at the D2R inhibits pituitary VEGF expression.

Interestingly, we found that the main source of VEGF in the hyperplastic pituitary were follicle stellate cells and not lactotrophs (Cristina et al. 2005). Follicle stellate cells represent 5–10 % of pituitary cells and are an important component of paracrine communication within the pituitary. They are detected by their content of the glial protein S100, they form follicles, are star shaped, and have long processes in between the secretory cells of the pituitary. They also contain FGF-2, follistatin, and interleukin 6. Because D2Rs have been described in lactotropes and not in follicle stellate cells it may be inferred that a paracrine-derived factor from lactotropes is acting on follicle stellate cells to increase VEGF expression. These data indicate that the D2R is linked to pituitary VEGF expression. In dopamine agonist resistant prolactinomas a decrease in number or function of D2Rs has been proposed (Caccavelli et al. 1994), and we have found highly expressed VEGF in a dopamine agonist giant prolactinoma (Mallea-Gil et al. 2009).

VEGF and its receptor may become supplemental therapeutic tools in dopamine-resistant prolactinomas. In this regard, in recent years, antiangiogenesis has been publicized as a novel alternative or supplement to conventional cancer therapy, and a variety of regimens that prevent tumor angiogenesis and/or that attack tumor blood vessels have met with remarkable success in treating mouse cancers.

Overexpression of VEGF by tumour cells can be targeted by:

- Antibodies against VEGF (Bevacizumab).
- Antibodies against VEGF receptors.
- Soluble VEGF receptors (VEGF-TRAP) that bind circulating VEGF.
- Catalytic RNA molecules (ribozymes), which cleave VEGF receptor mRNA.
- Orally available molecules that selectively block or prevent activation of VEGF receptor tyrosine kinases.

Despite the spectacular successes reported in the treatment of mouse tumors, the first clinical trials were discouragingly negative. This could be related to the fact that most of the patients treated in the beginning had advanced disease and had already failed conventional treatments. Also, antiangiogenesis therapy differs fundamentally from chemotherapy, and optimal implementation was needed.

Several agents targeting the VEGF ligand are now being developed in different clinical trials around the world to treat colon, rectal, breast, lung and other cancers. Bevacizumab (Avastin™), an anti-VEGF monoclonal antibody that inhibits formation of neovasculature and tumor growth in many human cancer cell lines, has a proven survival benefit in metastatic colon rectal cancer, and has now been approved by the FDA in combination with intravenous 5-FU-based chemotherapy as a treatment for patients with first-line metastatic cancer of the colon or rectum (Hurwitz et al. 2004).

Conclusions

In pituitary adenomas an altered expression of growth factors and their receptors has been observed (Asa and Ezzat 2002; Ezzat 2001; Melmed 2003; Renner et al. 1996; Turner et al. 2003). Although it is unlikely that these alterations play a causative role in pituitary tumor pathogenesis, intratumoral changes of these factors at their receptors may result in a permissive microenvoronment that contributes to excessive hormone production and loss of growth control in pituitary adenomas. Each pituitary tumor of clonal origin represents the multifactorial result of failure of different regulatory events. In this regard, pro- and anti-angiogenic growth factors such as FGF-2, VEGF, and others, may determine the final angiogenic phenotype of pituitary tumors, and thus subsequent tumor behavior. Furthermore, we believe that the study of angiogenic factor expression in aggressive prolactinomas with resistance to dopamine agonists will yield important data in the search of therapeutical alternatives.

References

Arita K, Kurisu K, Tominaga A, Sugiyama K, Eguchi K, Hama S, Yoshioka H, Yamasaki F, Kanou Y (2004) Relationship between intratumoral hemorrhage and overexpression of vascular endothelial growth factor (VEGF) in pituitary adenoma. Hiroshima J Med Sci 53:23–27

Asa SL, Ezzat S (2002) The pathogenesis of pituitary tumours. Nat Rev Cancer 2:836–849

Caccavelli L, Feron F, Morange I, Rouer E, Benarous R, Dewailly D, Jaquet P, Kordon C, Enjalbert A (1994) Decreased expression of the two D2 dopamine receptor isoforms in bromocriptine-resistant prolactinomas. Neuroendocrinology 60:314–322

Cristina C, Diaz-Torga G, Baldi A, Gongora A, Rubinstein M, Low MJ, Becu-Villalobos D (2005) Increased pituitary vascular endothelial growth factor-A in dopaminergic D2 receptor knockout female mice. Endocrinology 146:2952–2962

Cristina C, Diaz-Torga G, Gongora A, Guida MC, Perez-Millan MI, Baldi A, Becu-Villalobos D (2007a) Fibroblast growth factor-2 in hyperplastic pituitaries of D2R knockout female mice. Am J Physiol Endocrinol Metab 293:E1341–E1351

Cristina C, Diaz-Torga GS, Goya RG, Kakar SS, Perez-Millan MI, Passos VQ, Gianella-Neto D, Bronstein MD, Becu-Villalobos D (2007b) PTTG expression in different experimental and human prolactinomas in relation to dopaminergic control of lactotropes. Mol Cancer 6:4

Cristina C, Perez-Millan MI, Luque G, Berner S, Dulce RA, Sevlever G, Becu-Villalobos D (2010) VEGF and CD31 association in pituitary adenomas. Endocr Pathol 21(3):154–160

Ezzat S (2001) The role of hormones, growth factors and their receptors in pituitary tumorigenesis. Brain Pathol 11:356–370

Ferrara N, Schweigerer L, Neufeld G, Mitchell R, Gospodarowicz D (1987) Pituitary follicular cells produce basic fibroblast growth factor. Proc Natl Acad Sci U S A 84:5773–5777

Hurwitz H, Fehrenbacher L, Novotny W, Cartwright T, Hainsworth J, Heim W, Berlin J, Baron A, Griffing S, Holmgren E, Ferrara N, Fyfe G, Rogers B, Ross R, Kabbinavar F (2004) Bevacizumab plus irinotecan, fluorouracil, and leucovorin for metastatic colorectal cancer. N Engl J Med 350:2335–2342

Itoh J, Serizawa A, Kawai K, Ishii Y, Teramoto A, Osamura RY (2003) Vascular networks and endothelial cells in the rat experimental pituitary glands and in the human pituitary adenomas. Microsc Res Tech 60:231–235

Jugenburg M, Kovacs K, Stefaneanu L, Scheithauer BW (1995) Vasculature in nontumorous hypophyses, pituitary adenomas, and carcinomas: a quantitative morphologic study. Endocr Pathol 6:115–124

Lloyd RV, Scheithauer BW, Kuroki T, Vidal S, Kovacs K, Stefaneanu L (1999) Vascular endothelial growth factor (VEGF) expression in human pituitary adenomas and darcinomas. Endocr Pathol 10:229–235

Lohrer P, Gloddek J, Hopfner U, Losa M, Uhl E, Pagotto U, Stalla GK, Renner U (2001) Vascular endothelial growth factor production and regulation in rodent and human pituitary tumor cells in vitro. Neuroendocrinology 74:95–105

Mallea-Gil MS, Cristina C, Perez-Millan MI, Ballarino MC, Rodriguez Villafañe AM, Stalldecker G, Becu-Villalobos D (2009) Invasive giant prolactinoma with loss of therapeutic response to cabergoline: expression of angiogenic markers. Endocr Pathol 20:35–50

McCabe CJ, Boelaert K, Tannahill LA, Heaney AP, Stratford AL, Khaira JS, Hussain S, Sheppard MC, Franklyn JA, Gittoes NJ (2002) Vascular endothelial growth factor, its receptor KDR/Flk-1, and pituitary tumor transforming gene in pituitary tumors. J Clin Endocrinol Metab 87:4238–4244

McCabe CJ, Khaira JS, Boelaert K, Heaney AP, Tannahill LA, Hussain S, Mitchell R, Olliff J, Sheppard MC, Franklyn JA, Gittoes NJ (2003) Expression of pituitary tumour transforming gene (PTTG) and fibroblast growth factor-2 (FGF-2) in human pituitary adenomas: relationships to clinical tumour behaviour. Clin Endocrinol (Oxf) 58:141–150

Melmed S (2003) Mechanisms for pituitary tumorigenesis: the plastic pituitary. J Clin Invest 112:1603–1618

Molitch ME (2005) Pharmacologic resistance in prolactinoma patients. Pituitary 8:43–52

Renner U, Pagotto U, Arzt E, Stalla GK (1996) Autocrine and paracrine roles of polypeptide growth factors, cytokines and vasogenic substances in normal and tumorous pituitary function and growth: a review. Eur J Endocrinol 135:515–532

Sarkar AJ, Chaturvedi K, Chen CP, Sarkar DK (2007) Changes in thrombospondin-1 levels in the endothelial cells of the anterior pituitary during estrogen-induced prolactin-secreting pituitary tumors. J Endocrinol 192:395–403

Schechter J (1972) Ultrastructural changes in the capillary bed of human pituitary tumors. Am J Pathol 67:109–126

Schechter J, Goldsmith P, Wilson C, Weiner R (1988) Morphological evidence for the presence of arteries in human prolactinomas. J Clin Endocrinol Metab 67:713–719

Shimon I, Huttner A, Said J, Spirina OM, Melmed S (1996) Heparin-binding secretory transforming gene (hst) facilitates rat lactotrope cell tumorigenesis and induces prolactin gene transcription. J Clin Invest 97:187–195

Turner HE, Harris AL, Melmed S, Wass JA (2003) Angiogenesis in endocrine tumors. Endocr Rev 24:600–632

Turner HE, Nagy Z, Gatter KC, Esiri MM, Harris AL, Wass JA (2000a) Angiogenesis in pituitary adenomas – relationship to endocrine function, treatment and outcome. J Endocrinol 165:475–481

Turner HE, Nagy Z, Gatter KC, Esiri MM, Harris AL, Wass JA (2000b) Angiogenesis in pituitary adenomas and the normal pituitary gland. J Clin Endocrinol Metab 85:1159–1162

Viacava P, Gasperi M, Acerbi G, Manetti L, Cecconi E, Bonadio AG, Naccarato AG, Acerbi F, Parenti G, Lupi I, Genovesi M, Martino E (2003) Microvascular density and vascular endothelial growth factor expression in normal pituitary tissue and pituitary adenomas. J Endocrinol Invest 26:23–28

Vidal S, Horvath E, Kovacs K, Lloyd RV, Scheithauer BW (2003) Microvascular structural entropy: a novel approach to assess angiogenesis in pituitary tumors. Endocr Pathol 14:239–247

Vidal S, Kovacs K, Horvath E, Scheithauer BW, Kuroki T, Lloyd RV (2001) Microvessel density in pituitary adenomas and carcinomas. Virchows Arch 438:595–602

Human Brain Tumor Growth: Role of Aquaporins

4

Beatrice Nico, Simona Ruggieri, and Domenico Ribatti

Contents

Abstract

The aquaporins (AQPs) are a family of transmembrane water channel proteins widely distributed and play a major role in transcellular and transepithelial water movement. Moreover, recent evidence indicates that AQPs may be involved in cell migration and angiogenesis. This review article summarizes literature data concerning the involvement of AQPs in human brain tumor growth, angiogenesis and metastatic process and suggests a potential therapeutic approach by antagonizing their biological activity.

Introduction

The aquaporins (AQPs) represent a family of transmembrane water channel proteins widely distributed in various tissues throughout the body and play a major role in transcellular and transepithelial water movement. There are at least 13 AQPs present in many epithelial, endothelial and other tissues of mammals and other animal species. AQPs are divided in two groups: AQP1, AQP2, AQP4, AQP5 and AQP8 are primarily water selective, whereas AQP3, AQP7, AQP9 and AQP10 (called 'aqua-glyceroporins') also transport glycerol and other small solutes, such as lactic acid. Much of our understanding of AQPs functions in mammalian physiology has come from phenotype analysis of mice lacking each of the AQPs.

B. Nico • S. Ruggieri • D. Ribatti (✉)
Department of Basic Medical Sciences, Neurosciences and Sensory Organs, University of Bari Medical School, Piazza G. Cesare 11, Policlinico, 70124 Bari, Italy
e-mail: domenico.ribatti@uniba.it

M.A. Hayat (ed.), *Tumors of the Central Nervous System, Volume 12*,
DOI 10.1007/978-94-007-7217-5_4,

AQPs are localized in the plasma membrane but some isoforms are present in the cytoplasmic compartments, and their translocation to the plasma membrane is crucial in the regulation of water transfer (Saadoun et al. 2002a). Besides their role in transport fluid and regulating the osmotic balance, AQPs may be involved in cell migration (Verkman 2005). Whereas the expression and role of AQPs in secretion and absorption across epithelial barriers, their role in growth and motility of tumor cells is less clearly understood. AQPs have been found to be expressed in high-grade tumors and their expression in some tumors has been correlated with their metastatic potential (Hoque et al. 2006). AQPs in tumors allow water to rapidly penetrate into the growing tumor mass and tumor AQP expression may cause tumor expansion by exacerbating tumor-associated edema. Moreover, AQP-1 is involved also in tumor angiogenesis, tumor cell proliferation and migration. Thus, AQP-1-null mice showed impaired angiogenesis and considerable growth reduction of melanoma cells implanted subcutaneously, as compared to control animals (Saadoun et al. 2005a). Other studies show that AQPs may influence cell motility and localize to areas of focal plasma membrane shape change and protrusions.

Three AQPs have been clearly identified in the brain, namely AQP-1, AQP-4 and AQP-9. A positive correlation has been established between histological tumor grade and the amount of AQPs expression in brain tumors and human glioblastoma (Saadoun et al. 2002a, b; Warth et al. 2007). The control of brain water balance between different compartments is mainly maintained by astrocytes via AQPs. Edema and the consequent increase in intracranial pressure is one of the most serious consequence of brain tumor growth, where both vasogenic and cytotoxic edema are recognizable (Marmarou 2007). In high-grade gliomas, vasogenic edema, which drives fluids from blood vessels into the surrounding tissue, is associated with blood brain barrier (BBB) damage, interendothelial tight junction opening and an increased vascular permeability (Schneider et al. 2004). This review article will be focused on the analysis of the literature data concerning the role of AQP-1 and AQP-4 in human brain tumor growth.

Aquaporin 1

AQP-1 is expressed in endothelial cells of nonfenestrated capillaries and human arteries. Moreover, the involvement of AQP-1 in transendothelial water transport of nonfenestrated endothelium has been shown in descending vasa recta and in peritoneal capillaries. Expression of AQP-1 has been related with lung and colon cancers, mammary carcinomas, brain tumors, hemangioblastomas and multiple myeloma (Verkman et al. 2008).

In an experimental model in which wild-type and AQP-1-null mice were subcutaneously implanted with B16F10 melanoma cells, it has been demonstrated that tumor growth was reduced in AQP-1-null mice due to impaired angiogenesis (Saadoun et al. 2005a). A consistent histological finding in tumors of AQP-1 null mice was a much lower density of microvessels and the presence of islands of viable tumor cells surrounded by necrotic tissue. Tumor cell migration and metastatic potential greatly increased in two mouse tumor cell lines with AQP-1 expression as compared to the same cell lines without AQP-1 expression (Hu and Verkman 2006).

AQP-1 is strongly expressed in proliferating tumor microvessels in human (Saadoun et al. 2002a, b) and rat and in the chick embryo chorioallantoic membrane (CAM) microvessels. The AQP-1 chicken sequence has been clones and then AQP-1 specific dsRNA oligonucleotides (siRNA) has been generated that caused a significant reduction in the growth of new blood vessels in the CAM, providing evidence that AQP-1 is involved in angiogenesis. A positive correlation between AQP-1 expression and intratumoral microvascular density has been demonstrated in endometrial adenocarcinoma, ovarian cancer, and multiple myeloma.

AQP-1 is expressed at the apical membrane of endothelial cells and its deletion significantly reduces tumor growth and migration (Saadoun et al. 2005a) while up-regulation of AQP-1 increases the migration and metastatic potential of melanoma cells (Papadoupolos et al. 2008). In the brain, capillaries have no immunohistochemical signal in anti-AQP-1 staining. However, an induction of AQP-1 mRNA in immortalized

rat brain microvascular endothelial cells is reported following dexametasone treatment. AQP-1 is localized in the apical membrane of the choroid plexus epithelium.

Impaired fluid secretion has been found in AQP-1 knockout mice in choroid plexus where cerebrospinal fluid is produced and is up-regulated in choroid plexus tumors, which are associated with increased cerebrospinal fluid production (Hasegawa et al. 1994). AQP-1 expression is up-regulated in glioblastoma multiforme (GBM) in tumor cells and peritumoral astrocytes (Saadoun et al. 2002a; Oshio et al. 2005) and may have a role in the formation of cerebral edema (Papadopoulos et al. 2004a). Moreover, AQP-1 was found expressed in pathological brain endothelium when AQP-4 expression on astrocyte foot has disappeared.

Saadoun et al. (2005a) reported impaired angiogenesis and endothelial cell migration in AQP-1-null mice and suggested that AQP-dependent cell migration might be a general cellular phenomenon. They demonstrated the presence of slowed lamellipodial dynamics in AQP-1 null mice and AQP-1 polarization to the leading edge of migrating cell, and proposed a mechanism of AQP-facilitated cell migration in which actin cleavage and ion uptake at the tip of lamellipodium create local osmotic gradients that drive water influx, facilitating lamellipodial extension and cell migration. The formation of pseudopodial protrusions at the leading edge of migrating cells is the earliest step in locomotion. The molecular mechanism responsible for AQP-1 polarization in migrating cells is not known, but might involve interaction between water channels and actin cytoskeleton. In this context, AQP-1 accelerates cell migration by facilitating the rapid turnover of membrane protrusions at the leading edge. Monzani et al. (2009) have investigated the possible relationship between AQP-1 and cytoskeleton in endothelial and melanoma cells (both expressing AQP-1), demonstrating the involvement of Lin proteins, which are plasma membrane-associated proteins containing one or several PDZ domains required for the organization of the cytoskeleton (Craven and Bredt 1998).

Hu and Verkman (2006) transfected B16F10 and 4T1 tumor cells with AQP-1 and demonstrated an increase in their plasma membrane osmotic water permeability by five- to ten-fold. In vitro analysis of cell migration by transwell assay, wound healing and video microscopy showed a two- to three-fold accelerated migration of the AQP-1-expressing tumor cells compared to control ones. AQP-1 is expressed in the plasma membrane of human HT20 colon cancer cells and adenovirus-mediated high expression of AQP-1 increased relative plasma membrane water permeability and migration rate in both wound healing and invasive transwell migration assay (Jiang 2009). AQP-1 also is up-regulated by increased glucose consumption and glycolysis in glioma cells. If AQP-1 contributes to the glycolysis-dependent acidification of the extracellular environment, the coordinate up-regulation of AQP-1 and cathepsin B in the perivascular area at the tumor periphery provides a favourable microenvironment for glioma cells invasion.

Aquaporin 4

In the brain, AQP-4 is expressed at the glia limitans everywhere, ependymal lining, cerebellum, hippocampal dentate gyrus, and in the supraoptic and paraventricular nuclei of the hypothalamus (Badaut et al. 2002). Low AQP-4 expression has also been found in the neocortex, hippocampal areas, nucleus of the stria terminalis, and the medial habenular nucleus (Badaut et al. 2002). AQP-4 is expressed in a polarized way by astrocytic foot processes at the borders between major water compartments and the brain parenchyma (Nielsen et al. 1997) and the perivascular expression of AQP4 coincides with the K^+ channel protein Kir 4.1 at BBB level (Nagelhus et al. 1999). Otherwise, in glioma cells co-localization of AQP4 with K^+ channel protein Kir 4.1 is abolished and a misallocation of both Kir channels and AQP4 has been reported (Warth et al. 2007), suggesting that this molecular rearrangement occurs as a reaction to BBB damages, facilitating edema fluid flow. Furthermore, AQP4 colocalizes with α-β dystroglycan proteins, which, in turn, are receptors for the basement membrane proteins laminin and agrin. In glioma cells, agrin deficiency is coupled with redistribution of AQP4 and loss in

α-dystroglycan (Warth et al. 2007), indicating a key role for the extracellular matrix in the polarity and functions of the astroglial endfeet. Mice lacking AQP-4 showed improved outcome and reduced brain water accumulation compared with wild type mice in models of cytotoxic brain edema including water intoxication and ischemic stroke (Manley et al. 2000) and the diffusion rate of FITC-labeled dextran in the brain of AQP-4 gene-knockout mice was accelerated.

AQP-4 is involved in the clearance of extracellular fluid from the brain parenchyma in vasogenic edema. AQP-4 null mice have a significantly greater increase in brain water content and intracranial pressure than the wild type, indicating that brain water elimination is defective after AQP-4 deletion (Papadopoulos et al. 2004b; Papadopoulos and Verkman 2007). AQP-4 may be involved also in cytotoxic brain edema; in fact, swelling of astrocytic foot processes is a major finding in cytotoxic edema and water intoxicated AQP-4-null mice show a significant reduction in astrocytic foot processes swelling and a decrease in brain water content (Manley et al. 2000). It is to note that AQP-4 not only facilitates water influx in edema formation, but also serves as an efflux route for water in edema elimination, in line with the bidirectional flow of water through the AQP-4 water channel (Saadoun and Papadopoulos 2010).

AQP-4 is up-regulated in several brain tumors. In glioma, AQP-4 is highly concentrated at the cell membrane covering the surface of tumor cells and is strongly up-regulated and redistributed across the surface of glioma cells (Warth et al. 2007). AQP-4 is up-regulated in GBM (Saadoun et al. 2002a), its distribution is not restricted to astrocytic endfeet and its up-regulation in tumor cells and reactive astrocytes surrounding gliomas plays a role in vasogenic edema formation (Warth et al. 2005, 2007). High-grade gliomas are characterized by peritumoral vasogenic edema and AQP-4 has been found to be strongly up-regulated and redistributed across the surface of glial tumor cells (Saadoun et al. 2002b; Warth et al. 2007), so AQP-4 could be considered as a protective factor in reducing cerebral fluid accumulation in glioma. We have evaluated AQP-4 expression and content in GBM and have demonstrated that chemotherapy and radiotherapy induce a down-regulation in AQP-4 expression restoring its perivascular rearrangement suggesting its potential role in the resolution of brain edema (Fig. 4.1) (Nico et al. 2009).

Mou et al. (2010) investigated changes of AQP-4 protein expression in normal brain and in brain glioma tumor and peritumoral edematous tissues and analyzed the relationship of AQP-4 protein with edema index, vascular endothelial growth factor (VEGF) and hypoxia inducible factor 1 alpha (HIF-1α) protein. They demonstrated that expression of AQP-4 was higher in the tumor and highest in the peritumor tissue. Moreover, AQP-4 protein in tumor tissue of gliomas of different grades was not statistically different. In normal brain tissues, AQP-4 was mainly expressed in the foot processes of atsrocytes, but rare in the parenchyma. Finally, the degree of peritumoral edema positively correlated with the expression level of AQP-4 protein and this latter correlated with VEGF and HIF-1α expression. Over-expression of AQP-4 in human meningiomas was associated with significant peritumoral edema. Noël et al. (2012) combining freeze-fracture electron microscopy, immunohistochemistry and Western blotting, described alterations of expression and distribution of AQP-4, dystroglycan, agrin, and matrix metalloproteinases (MMP)-2, -3, and -9 in human primary glioblastomas. They demonstrated an increase in AQP-4 and MMPs expression, and a loss of agrin and dystroglycan expression in glioblastoma compared to control tissue.

AQP-4 knockdown in rat and human astrocytes was associated with a depolymerization of F-actin cytoskeleton with changes of morphology (Nicchia et al. 2005). AQP-4–facilitated astroglial cell migration involves increased plasma membrane osmotic water permeability, which enhances water transport into the cell at its leading edge (Saadoun et al. 2005b). AQP-4 deletion in astroglial cells markedly impaired cell migration toward a stab wound in adult mouse brain and glial scar formation was impaired in AQP-4-null mice with reduced migration of reactive astroglia towards a site of brain injury (Auguste et al. 2007; Saadoun et al. 2005b).

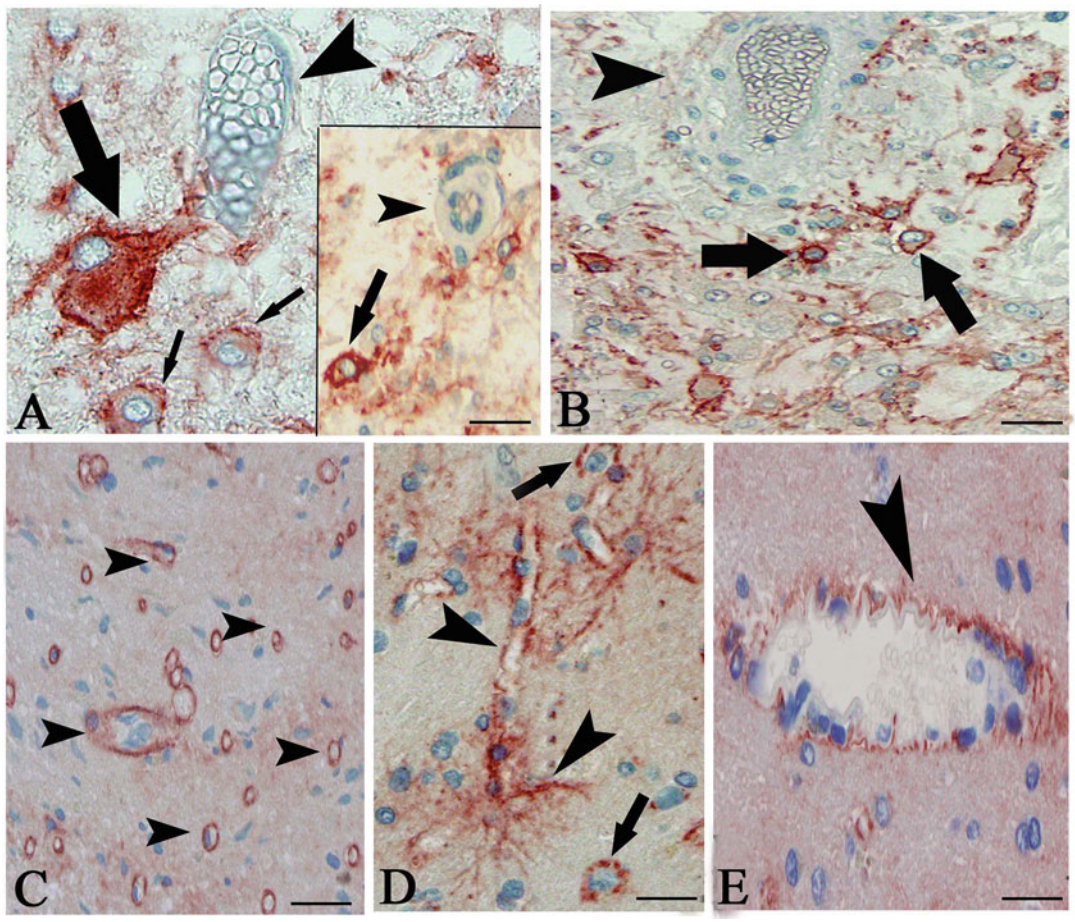

Fig. 4.1 AQP-4 immunocytochemical localization in the peripheral areas of glioblastoma nultiforme primary surgical specimens (**a**), in relapsed surgical specimens from patients treated with radiotherapy (**b**) and with chemiotherapy and radiotherapy (**c**–**e**). (**a**). Primary tumor shows a vessel faintly labeled by AQP-4 (*arrowhead*), or unlabeled (inset, *arrowhead*), surrounded by tumor cells expressing AQP-4 on the membranes (*thin arrows*) and connected with a cytoplasmic extension of an adjacent tumor cell, strongly expressing AQP-4 in both the cytoplasm and plasmamembrane (*thick arrow*). Note in the inset, an AQP-4 labeled tumor cell (*arrow*) near to an unlabeled, thick vessel wall (*arrowhead*). (**b**) A faintly AQP-4 labeled vessel (*arrowhead*) is surrounded by stained tumor cells (*arrows*). (**c**–**e**) Numerous thin walled vessels with a continuous AQP-4 perivascular arrangement (*arrowheads*) are surrounded by astrocytes labeled processes (**d**, *arrowheads*) and by a few tumor cells, with stained plasmamembranes (**d**, *arrows*). Scale bar: **a**, **d**, **e**, 25 **μ**m; **c**, 50 **μ**m; **b**, 33.3 **μ**m [Reproduced from Nico et al. 2009]

AQP-4 could be also involved in brain tumor migration and invasion and may accelerate glioma migration by facilitating the rapid changes in cell volume that accompany changes in cell shape. We have observed in the peripheral areas of primary tumors isolated glioma cells strongly labeled by AQP-4, indicative of their migratory activity (Nico et al. 2009). Glioma cells show cytoskeleton alterations and a rearrangement of actin filaments (Zhou et al. 2008) and it may be hypothesized that cytoskeleton alterations occurring during glioma transformation induce an up-regulation and mislocalization of AQP-4 favouring tumor cell detachment and migration. Nicchia et al. (2005) have shown that AQP-4 knockdown in rat and human cells was associated

with a depolymerization of actin with a change of morphology characterized by a remarkable F-actin cytoskeleton rearrangement in AQP-4 knock-down mouse astrocytes. Moreover, AQP-4 can interact with α-syntrophin, a member of the dystrophin-dystroglycan complex, indicating an involvement of AQP-4 protein in altering the cell cytoskeleton. Accordingly, we have recently demonstrated that in the brain of mdx mouse, an animal model of the Duchenne muscular dystrophy, glial cells showed a significant reduction in both protein and mRNA content of the dystrophin-associated proteins (DAPs), including AQP-4, Kir 4.1, syntrophin and α-β-dystroglycan, coupled with a decrease in dystrophin isoform (Dp71) (Nico et al. 2010). Moreover, we have shown alterations of the vascular basement membrane and reduction of the expression of its components laminin and agrin and trasnslocation of α-β-dystroglycan receptors in the glial cytolasmic endfeet.

Therapeutic Perspectives

AQPs have been considered new candidates for potential drug targets, but there are at the present no AQPs inhibitors that are suitable for clinical development (Monzani et al. 2007). Inhibition of AQP-1 and AQP-4 expression (by small interference RNA technology) or their function (with a blocking antibody or a small inhibitory molecule) may result in increased intracellular acidosis and cytotoxicity and reduced invasive potential of glioma cells. Ding et al. (2011), using small-interference RNA and a pharmaceutical inhibitor to knock down the expression of AQP-4, demonstrated a specific and massive impairment of glioblastoma cell migration and invasion in vitro and in vivo. Moreover, they showed that down-regulation of MMP-2 expression coincides with decreased cell invasive ability. Accordingly, Badaut et al. (2011) using RNA interference has demonstrated that brain water motility decreases after astrocyte AQP-4 inhibition.

Acetazolamide inhibits the osmotically induced water swelling and can suppress tumor metastasis, in part by inhibiting AQP-1 gene expression. The suppressive action of carbonic anydrases inhibitors on AQP-1 might contribute to their inhibitory effect on cancer invasion and metastasis. Topiramate, an antiepilectic agent, inhibits AQP-1 expression and attenuates water influx at the leading edge, thereby affecting membrane protrusion, cell migration and metastasis. Corticosteroids are largely used in combination with chemotherapy and contribute to significantly reduced peritumoral brain edema by decreasing the permeability of tumor vessels and/or enchance the clearance of extracellular water. Animal experiments showed a decrease of cerebral AQP-4 protein expression upon dexamethasone treatment, suggesting that AQP-4 may be considered one of the major molecular targets of the well-functioning steroid treatment in brain edema formation. Moreover, corticosteroids reduced AQP-4 mRNA level in experimental brain tumor model and after intracerebral hemorrhage in rats (Heiss et al. 1996; Gu et al. 2007).

The evidence that AQP-4 facilitates the migration of reactive astrocytes towards an injury site and the infiltration of malignant astrocytes in glioblastoma (Verkman et al. 2008) suggests that AQP-4 inhibitors may reduce reactive gliosis and infiltration of astrocytes.

Acknowledgments This work was supported by European Union Seventh Framework Programme (FPT7/2007-2013) under grant agreement no. 278570 to DR.

References

Auguste KI, Jin S, Uchida K, Yan D, Manley GT, Papadopoulos MC, Verkman AS (2007) Greatly impaired migration of implanted aquaporin-4-deficient astroglial cells in mouse brain toward a site of injury. FASEB J 21:108–116

Badaut J, Lasbennes F, Magistretti PJ, Regli L (2002) Aquaporins in brain: distribution, physiology and pathophysiology. J Cereb Blood Flow Metab 22:367–378

Badaut S, Ashwal S, Adami A, Tone B, Recker R, Spagnoli D, Ternon B, Obenaus A (2011) Brain water motility decreases after astrocytic aquaporin-4 inhibition using RNA interference. J Cereb Blood Flow Metab 31:819–831

Craven SE, Bredt DS (1998) PDZ proteins organize synaptic signaling pathways. Cell 93:495–498

Ding T, Ma Y, Liu W, Ying G, Fu L, Gu F (2011) Role of aquaporin-4 in the regulation of migration and invasion of human glioma cells. Int J Oncol 38:1521–1531

Gu YT, Zhang H, Xue YX (2007) Dexamethasone treatment modulates aquaporin-4 expression after intracerebral hemorrhage in rats. Neurosci Lett 413:126–131

Hasegawa H, Ma T, Skach W, Matthay MA, Verkman AS (1994) Molecular cloning of a mercurial-insensitive water channel expressed in selected water-transporting tissues. J Biol Chem 269:5497–5500

Heiss JD, Papavassiliou E, Merrill MJ, Nieman L, Knightly JJ, Walbridge S, Edwards NA, Oldfield EH (1996) Mechanisms of dexamethasone suppression of brain tumor-associated vascular permeability in rats. Involvement of the glucocorticoid receptor and vascular permeability factor. J Clin Invest 98:1400–1408

Hoque MO, Soria JC, Woo J, Lee T, Lee J, Jang SJ, Upadhyay S, Trink B, Monitto C, Desmaze C, Mao L, Sidransky D, Moon C (2006) Aquaporin is overexpressed in lung cancer and stimulates NIH-3T3 cell proliferation anchorage-independent growth. Am J Pathol 168:1345–1353

Hu J, Verkman AS (2006) Increased migration and metastatic potential of tumor cells expressing aquaporin water channels. FASEB J 20:1892–1894

Jiang Y (2009) Aquaporin-1 activity of plasma membrane affects HT20 colon cancer migration. IUBMB Life 61:1001–1009

Manley GT, Fujimura M, Ma T, Noshita N, Filiz F, Bollen AW, Cahn P, Verkman AS (2000) Aquaporin-4 deletion in mice reduces brain edema after acute water intoxication and ischemic stroke. Nat Med 6:159–163

Marmarou A (2007) A review of progress in understanding the pathophysiology and treatment of brain edema. Neurosurg Focus 22:E1

Monzani E, Shtil AA, La Porta CA (2007) The water channels, new drug gable targets to combat cancer cell survival, invasiveness and metastasis. Curr Drug Targets 8:1132–1137

Monzani E, Bazzotti R, Perego C, La Porta CA (2009) AQP1 is not only a water channel: it contributes to cell migration through Lin7/beta-catenin. PLoS One 4:6167

Mou K, Chen M, Mao Q, Wang P, Ni R, Xia X, Liu Y (2010) AQP-4 in peritumoral edematous tissue is correlated with the degree of glioma and expression of VEGF and HIF-alpha. J Neurooncol 100:375–383

Nagelhus EA, Horio Y, Inanobe A, Fujita A, Haug FM, Nielsen S, Kurachi Y, Ottersen OP (1999) Immunogold evidence suggests that coupling of K+ siphoning and water transport in rat retinal Müller cells is mediated by a co enrichment of Kir4.1 and AQP4 in specific membrane domain. Glia 26:147–154

Nicchia GP, Srinivas M, Li W, Brosnan CF, Frigeri A, Spray DC (2005) New possible roles for aquaporin-4 in astrocytes: cell cytoskeleton and functional relationship with connexin 43. FASEB J 19:1674–1676

Nico B, Mangieri D, Tamma R, Longo V, Annese T, Crivellato E, Pollo B, Maderna E, Ribatti D, Salmaggi A (2009) Aquaporin-4 contributes to the resolution of peritumoral brain oedema in human glioblastoma multiforme after combined chemotherapy and radiotherapy. Eur J Cancer 45:3315–3325

Nico B, Tamma R, Annese T, Mangieri D, De Luca A, Corsi P, Benagiano V, Longo V, Crivellato E, Salmaggi A, Ribatti D (2010) Glial dystrophin-associated proteins, laminin and agrin, are downregulated in the brain of mdx mouse. Lab Invest 90:1645–1660

Nielsen S, Nagelhus EA, Amiry-Moghaddam M, Bourque C, Agre P, Ottersen OP (1997) Specialized membrane domains for water transport in glial cells: high resolution immunogold cytochemistry of aquaporin-4 in rat brain. J Neurosci 17:171–180

Noël S, Wolburg-Buchholz K, Mach AF, Ritz R, Tatagiba M, Beschorner R, Wolburg H, Falleir-Becker P (2012) Dynamic of expression patterns of AQP4, dystroglycan, agrin and matrix metalloproteinases in human glioblastomas. Cell Tissue Res [Epub ahead of print] 347:429–441

Oshio K, Binder DK, Liang Y, Bollen A, Feuerstein B, Berger MS, Manley GT (2005) Expression of the aquaporin-1 water channel in human glial tumors. Neurosurgery 56:375–381

Papadopoulos MC, Saadoun S, Binder DK, Manley GT, Krishna S, Verkman AS (2004a) Molecular mechanism of brain tumor edema. Neuroscience 129:1011–1020

Papadopoulos MC, Manley GT, Krishna S, Verkman AS (2004b) Aquaporin-4 facilitates reabsorption of excess fluid in vasogenic brain edema, FASEB J 18:1291–1293

Papadopoulos MC, Verkman AS (2007) Aquaporin-4 and brain edema. Pediatr Nephrol 22:778–784

Papadopoulos MC, Saadoun S, Verkman AS (2008) Aquaporin and cell migration. Pflugers Arch 456:693–700

Saadoun S, Papadopoulos MC, Davies DC, Krishna S, Bell BA (2002a) Aquaporin-4 expression is increased in edematous human brain tumours. J Neurol Neurosurg Pscychiatry 72:262–265

Saadoun S, Papadopoulos MC, Davies DC, Bell BA, Krishna S (2002b) Increased aquaporin 1 water channel expression in human brain tumors. Br J Cancer 87:621–623

Saadoun S, Papadoulos MC, Hara-Chikuma M, Verkman AS (2005a) Impairment of angiogenesis and cell migration by targeted aquaporin-1 gene disruption. Nature 434:786–792

Saadoun S, Papadopoulos MC, Watanabe H, Yan D, Manley GT, Verkman AS (2005b) Involvement of aquaporin-4 in astroglial cell migration and glial scar formation. J Cell Sci 118:5691–5698

Saadoun S, Papadopoulos MC (2010) Aquaporin-4 in brain and spinal cord oedema. Neuroscience 168: 1036–1104

Schneider SW, Ludwig T, Tatenhorst L, Braune S, Oberleithner H, Senner V, Paulus W (2004) Glioblastoma cells release factors that disrupt blood–brain barrier features. Acta Neuropathol 107:272–276

Verkman AS (2005) More than just water channels: unexepected cellular roles of aquaporins. J Cell Sci 118:3225–3232

Verkman AS, Hara-Chikuma M, Papadopoulos MC (2008) Aquaporins-new players in cancer biology. J Mol Med 86:523–529

Zhou D, Jiang X, Xu R, Cai Y, Hu J, Xu G, Zou Y, Zeng Y (2008) Assessing the cytoskeleton system and its elements in C6 glioma cells and astrocytes by atomic force microscopy. Cell Mol Neurobiol 28:895–905

Warth A, Mittelbronn M, Wolburg H (2005) Redistribution of the water channel protein aquaporin-4 and the K^+ channel protein Kir 4.1 differ in low- and high-grade human brain tumors. Acta Neuropathol 109:418–426

Warth A, Simon P, Capper D, Goeppert B, Tabatabai G, Herzog H, Dietz K, Stubenvoll F, Ajaaj R, Becker R, Weller M, Meyermann R, Wolburg H, Mittelbronn M (2007) Expression pattern of the water channel aquaporin-4 in human gliomas is associated with blood–brain barrier disturbance but not with patient survival. J Neurosci Res 85:1336–1345

Molecular and Functional Characterization of Human Adipocytes

5

Antonella Poloni and Giulia Maurizi

Contents

Abstract

Adipose tissue, consisting mainly of adipocytes, functions as a critical organ for energy regulation, inflammation and immune response through intricate signals.

Mature adipocytes were considered to be in the terminal stage of differentiation and stationary, having lost their proliferative ability. Recently, the capability of mature adipocytes to reprogram their gene expression profile and transform into different cytotypes has been demonstrated.

Here, data of both mature and dedifferentiated adipocytes were collected and compared to underline structural and functional features of these cells. In particular, morphology, structure, molecular and immunophenotype markers, and dedifferentiation process of mature isolated adipocytes are analyzed. In addition, molecular and phenotype characterization of dedifferentiated fat cells is described, reporting important results on pluripotent differentiation ability, immunoregulatory and hematopoietic supporting functions of these cells. These findings highlight the concept that adipose lineage cells represent a suitable new cell source for clinical applications in such fields as cell therapy and regenerative medicine.

A. Poloni (✉) • G. Maurizi
Department of Medical and Surgical Sciences, Clinic of Hematology, V Floor, Educational Centre, Marche Polytechnic University, Ancona, Italy
e-mail: a.poloni@univpm.it

M.A. Hayat (ed.), *Tumors of the Central Nervous System, Volume 12*,
DOI 10.1007/978-94-007-7217-5_5,

Introduction

Human adipose tissue is no longer considered simply as a storage depository of lipids, but as a critical organ involved in energy regulation, whole-body insulin action and inflammation, through intricate endocrine, paracrine and autocrine signals (Dandona et al. 2004). Adipose tissue contains adipocytes and non-adipose cells. Mature adipocytes are functionally the most important cell type in adipose tissue, while the stromal vascular fraction contains several cell types and represents a reservoir not only of specific adipocyte precursor cells but also of multipotent stem cells (Gimble and Guilak 2003).

The literature give higher attention to stromal stem cells than to mature adipocytes which demonstrated to have stem cells properties. The stemness features of fat and its in vitro dedifferentiation process is largely unknown, despite the potential clinical applications of both mature adipocytes and dedifferentiated adipocytes in such fields, as regenerative medicine.

White adipose tissue has attracted attention because of its great and reversible capacity for expansion, which appears to be permanent throughout adult life (Planat-Bernard et al. 2004). The process of cellular differentiation in terminally differentiated mammalian cells is thought to be irreversible, but recent data suggest that the mature adipocytes, when under physiological stimuli, are able to reversibly change their phenotype and directly transform into cells with a different morphology and physiology (De Matteis et al. 2009; Poloni et al. 2012a).

Mature adipocytes are functionally the most important cell type in adipose tissue. White adipocytes are spherical cells with a single large lipid droplet formed by triacylglycerols that accounts for >90 % of the cell's volume (Cinti 2009). They have a variable size that depends mainly on the size of the lipid droplet stored in them. Even on electron microscopy there seems to be no distinct structure separating it from the thin rim of cytoplasm by a non-membranous electron-dense barrier containing functionally important proteins such as perilipin (Blanchette-Mackie et al. 1995). The thin cytoplasm contains the nucleus, characteristically squeezed by the large lipid vacuole, an usually under-developed Golgi apparatus, rough endoplasmic reticulum made up of short, isolated cisternae and rare lysosomes. Mitochondria are thin and elongated, with randomly oriented cristae, and variable in amount: in general, they are less numerous in the larger cells. Several caveolae are found on the outer surface. Numerous pinocytotic vesicles are found at the level of the outer cytoplasmic membrane, where a distinct basal membrane is present. Other organelles are usually poorly represented (Cinti 2009). Mature adipocytes should be studied using their buoyant property (Fig. 5.1).

To obtain isolated mature adipocytes free of stromal-vascular elements, after collagenase digestion, the disrupted tissues were filtered through a 200 μm nylon sieve. The filtered cells should be washed 4–5 times and eventually re-filtered if it is necessary. Only the floating top layer was collected after each washing step (Zhang et al. 2000).

The confocal microscopy analysis of adipogenic cellular fraction isolated is a good and easy way to exclude any contamination coming from other cell types contained in the whole tissue. These cells are large (50–70 μm), unilocular, perilipin-immunoreactive with a peripheral flattened nucleus.

The ceiling culture is the method that uses the buoyant property of adipocytes, allowing them to adhere to the top inner surface of a culture flask which is completely filled with medium (Sugihara et al. 1987). In this way, mature adipocytes adhere to the ceiling surface, then the flask should be reinverted to allow normal observation and the subsequent manipulation of the culture.

The aim of this chapter is to collect and compare the literature data about both mature and dedifferentiated adipocytes to better underline their stem cells properties. In addition to well characterize adipocytes morphologically and structurally, this chapter reports on the pluripotent differentiation ability, immunoregulatory and hematopoietic supporting functions of these cells. These findings open new perspectives on adipose tissue plasticity and highlight the way for cellular therapy and regenerative medicine based on the administration of adipose tissue stem cells.

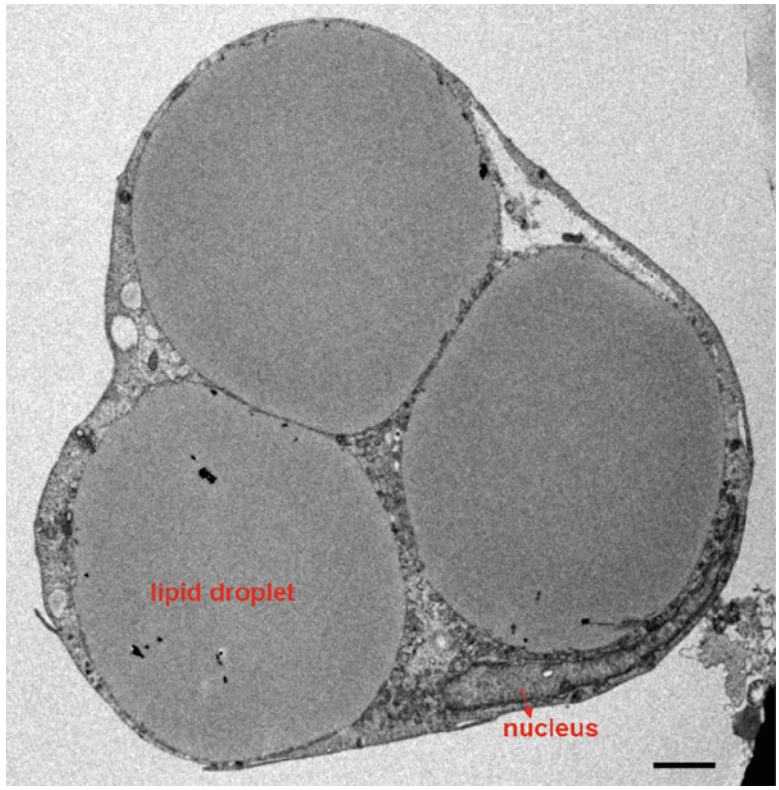

Fig. 5.1 Electron microscopy analysis. Mature adipocyte has thin cytoplasm and a nucleus characteristically squeezed by the large lipid vacuoles. The cytoplasmatic organelles are poorly represented. Scale bar = 4 μm

The Dedifferentiation Process of Mature Adipocytes

Mature adipocytes are generally considered terminally differentiated because they have lost their proliferative abilities, but recent data suggest that the process of cellular differentiation in terminally differentiated mammalian cells is not irreversible.

When maintained in culture, mature adipocytes undergo spontaneously a process of dedifferentiation (Matsumoto et al. 2008). Adipocytes lost their intracytoplasmatic lipid droplet, the nuclei became more centralized and the cells became elongated in shape, assuming a fibroblast-like morphology. At this step, the cells enter a proliferative log phase until cellular senescence (Fig. 5.2).

At molecular level, data revealed significant changes in gene expression during the dedifferentiation process (Ono et al. 2011; Poloni et al. 2012a). Adipocytes downregulated many genes that play a role in lipid and fatty acid metabolism, while concomitantly upregulated genes involved in cell proliferation, altered cell morphology, movement and migration of cells, and regulation of differentiation.

As murine adipocytes (De Matteis et al. 2009), recent data demonstrated that also human mature adipocytes expressed genes required for the cell reprogramming process, which include Oct4, Klf4, c-myc and Sox2 (Poloni et al. 2012a). Moreover, these cells expressed transcripts for embryonic stem cell genes that are required for self-renewal and pluripotency. Thus, recent data underline the potential role of mature adipocytes as stem cells (Poloni et al. 2012a; Cinti 2009). The reprogramming of genes in isolated as well as cultivated adipocytes is in line with the plastic properties of these cells.

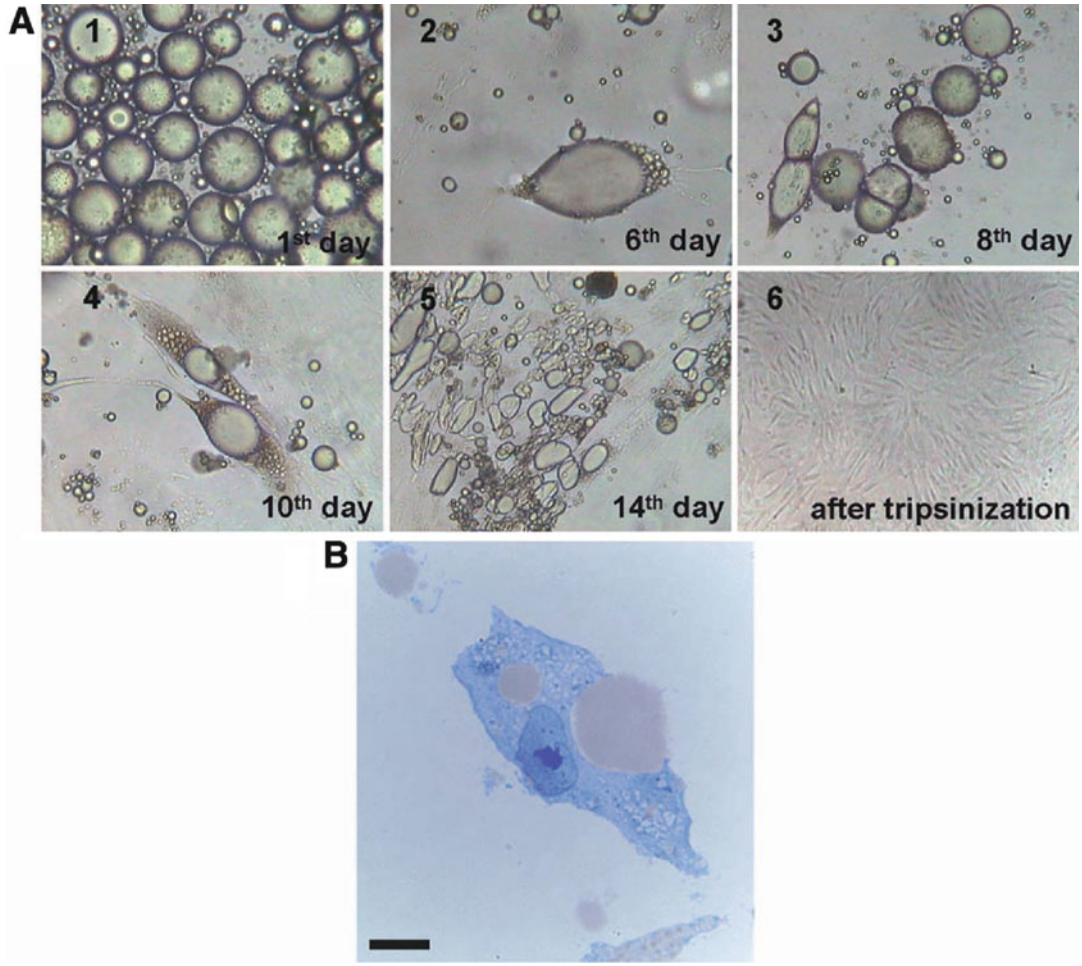

Fig. 5.2 Dedifferentiation process of mature adipocytes. During culturing, the cells attached to the upper surface of the flasks, followed by conversion to fibroblast-like dedifferentiated adipocytes, reached a morphology similar to BM-derived MSCs. (**a**) Morphological changes at different time points from mature adipocytes to dedifferentiated adipocytes. (**b**) Mature adipocytes lose their lipid droplets. Cells were stained by toluidine blue. Scale bar in **b** is equal to 4 μm, in **a**1 equal to 80 μm, in **a**2 equal to 40 μm, in **a**3 equal to 80 μm, in **a**4 equal to 80 μm, in **a**5 equal to 120 μm, and in **a**6 equal to 150 μm

Immunophenotype Characterization and Pluripotential Properties of Mature and De-differentiated Adipocytes

While dedifferentiated fat cells are well characterized (Matsumoto et al. 2008), there are only few studies that provided the cell-surface antigen profile of human mature adipocytes (Poloni et al. 2012a). The stemness markers expressed by mature adipocytes at the molecular level are also present as surface antigens. These cells are positive stained by some stem cells markers, CD34 (hematopoietic progenitor cell antigen 1, HPCA 1), CD133 (prominin 1), CD90 (Thy-1), CD105 (endoglin), CD271 (NGFR) and CD117 (c-kit). During the dedifferentiation process, the typical mesenchymal stem cells markers are highly preserved at the molecular and antigenic levels, while CD34 and CD133 are lost as antigens.

After the dedifferentiation process, adipocytes are easy to isolate and cultivate, so there are many

studies that described their immunophenotype. The cell-surface antigen profile of dedifferentiated cells was analyzed (Matsumoto et al. 2008) and this profile is consistent with previous findings for bone marrow MSCs (Pittenger et al. 1999) with uniformly positive expression of CD13 (aminopeptidase N), CD29 (integrin β1), CD44 (hyaluronate receptor), CD49b (integrin α4-subunit), CD90, CD105, CD271, CD73 (ecto-5′-nuclotidase) and HLA-A, -B, -C, but negative for CD11b (integrin αM), CD31 (platelet endothelial cell adhesion molecule), CD34, CD133, CD45 (leukocyte common antigen), CD106 (vascular cell adhesion molecule-1) and HLA-DR.

These findings suggest that the dedifferentiated adipocytes are an homogeneous population expressing the same markers as bone marrow-derived MSCs and adipose tissue-derived MSCs. Data showed that dedifferentiated adipocytes are a highly homogeneous population of cells respect to adipose-derived stem cells, that contained a variety of cell types: high number of smooth muscle cells (19 %), endothelial cells (3 %) and blood cells (13 %) (Yoshimura et al. 2006). These observations are convincing because dedifferentiated adipocytes originate from a fraction of highly pure mature adipocytes, whereas adipose-derived stem cells are an heterogeneous population.

Electron microscopy (EM) analysis of dedifferentiated adipocytes is shown in Fig. 5.3a, b. The images show most organelles described during the early stages of developing stromal vascular fraction-derived MSCs in primary cultures, i.e., well-developed Golgi complexes, short strands of rough endoplasmic reticulum, small lipid droplets, small mitochondria, lysosomes and small granules of glycogen. Nuclei were fusiform with smooth edges. Thus, the EM features of dedifferentiated adipocytes were very similar to developing stromal vascular fraction-derived MSCs (Fig. 5.3c). The spontaneous dedifferentiation process represents the manifestation of morphological, molecular and functional changes of mature adipocytes, that might be interpreted as a return back to a noncommitted status of the cells.

The methylation status of cells is the most common epigenetic modification of genome in mammalian cells (Bibikova and Fan 2010). Data showed that there are significant difference between the methylation statuses of mature adipocytes and dedifferentiated adipocytes, while there are no difference between dedifferentiated adipocytes and bone marrow-derived MSCs (Poloni et al. 2012a). These findings suggested that during the dedifferentiation process a gene reprogramming event takes place, which leads to changes in cellular epigenetic status. Dedifferentiated adipocytes achieve the DNA methylation status of bone marrow-derived MSCs by this process.

Recent advances in regenerative medicine have created a broad spectrum of stem cell research. Among them, tissue stem cell regulations are important issues to clarify the molecular mechanism of differentiation. Tissue engineering and cell therapy techniques have been developed to reconstitute different tissues. Attention has been focused on cells that might be useful in regenerative medicine (Barrilleaux et al. 2006). However, because stem cells only represent a minor population of the cells in the body, invasive procedures are frequently needed to obtain the amount of stem cells required for cell therapy. Therefore, adult stem cells sources are needed to be easily isolated and expanded with high purity.

Several studies have demonstrated that mesenchymal progenitor cells from various tissues have the potential to differentiate into other cells, suggesting that pre-committed and committed cells have plasticity in cell fate determination (Sudo et al. 2007).

Mature adipocytes are the most abundant cell type in adipose tissue and they can be easily isolated without painful procedures or donor site injury. Recent data demonstrated that mature adipocytes are able to transdifferentiate into another cell type, suggesting a great plasticity of these cells. This process implies an in vivo phenomenon of physiological and reversible reprogramming of genes in mature cells (Cinti 2009). During this process a differentiated cell turns phenotypically and functionally into a differentiated cell of another type without undergoing dedifferentiation. Some other include the additional step of dedifferentiation (Tosh and Slack 2002).

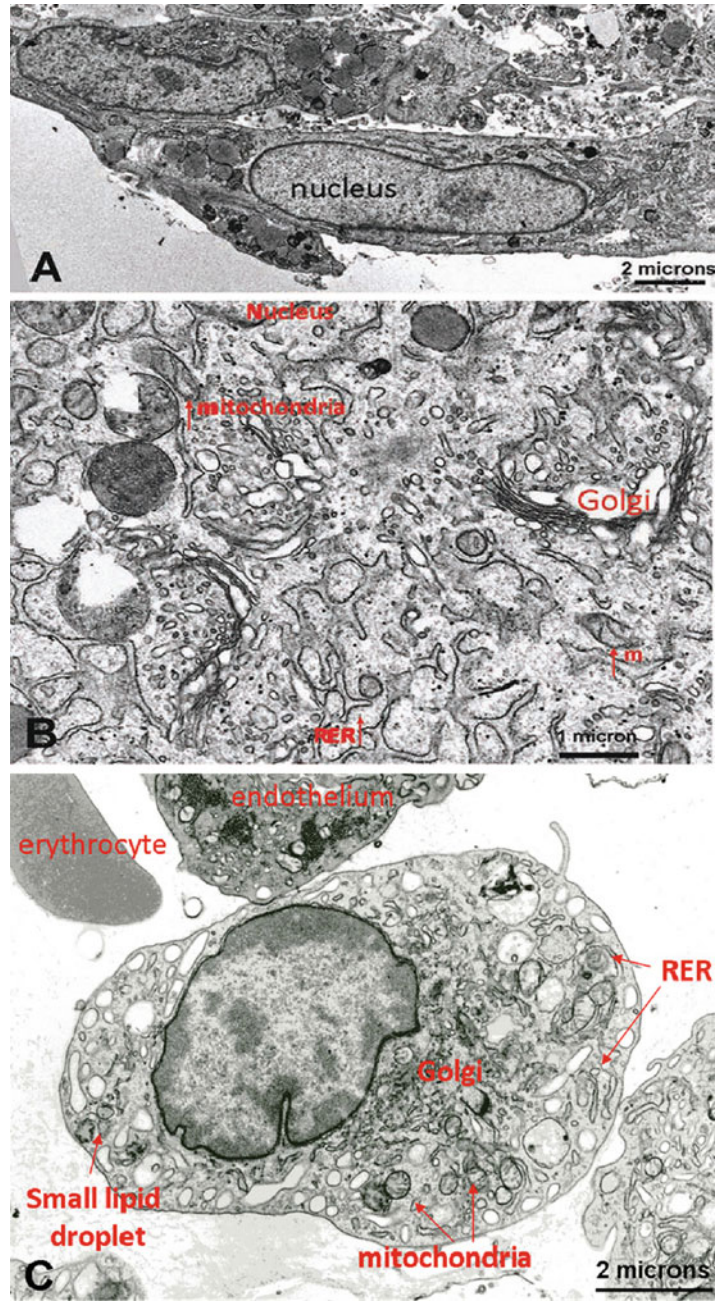

Fig. 5.3 Electron microscopy analysis. (**a**) Dedifferentiated adipocytes displayed structural organelle similarities (cytoplasm enlarged in **b**) to stromal vascular fraction-derived MSCs (**c**); RER = rough endoplasmic reticulum, m = mitochondria

Data showed two important examples of physiological and reversible transdifferentiation. In conditions of chronic cold exposure the amount brown adipose tissue (BAT) in the organ could increase via white-to-brown transdifferentiation and, vice versa, BAT could turn into WAT in case of exposure to an obesogenic diet, to enable greater energy accumulation (Cinti 2011). Moreover, murine mature adipocytes undergo a reversible process of adipocytic/epithelial differentiation during pregnancy and lactation. During pregnancy, adipocytes seem to transform progressively into epithelial cells, forming the lobulo-alveolar part of the mammary glad responsible

for milk production. At the end of lactation the lobolo-alveolar component disappears and a new adipocyte population restores the prepregnancy anatomy (Cinti 2011).

While little is known about the potential differentiation of mature adipocytes, more informations are available regarding the dedifferentiated population. Because adipose tissue is abundant and easily accessible tissue at most ages, dedifferentiated cells may be an attractive source of mesenchymal lineages for tissue engineering and other cell-based therapy (Matsumoto et al. 2008). The plastic properties of mature adipocytes are present also in dedifferentiated adipocytes.

In line with these observations, results showed that dedifferentiated adipocytes can be converted into fully differentiated cells, like adipocytes both in vitro and in vivo (Fernyhough et al. 2008), chondrocytes and skeletal myocytes in vitro (Kazama et al. 2008) under the appropriate culture conditions. In particular, dedifferentiated cells may be applicable to bone tissue engineering strategies and cell-based therapies, because they could convert into differentiated osteoblasts in vitro only by transient all-trans retinoic acid stimulation. Thus, dedifferentiated cells can undergo terminal osteoblast differentiation and osteoblast matrix formation, following subcutaneous injection into the peritoneal cavity of mice (Oki et al. 2008).

Moreover, dedifferentiated adipocytes also have the potential to rapidly acquire the endothelial phenotype in vitro and to promote neovascularization in ischemic tissue and vessel-like structure formation, suggesting that cells of endothelial and adipocyte phenotype may have a common precursor (Planat-Benard et al. 2004). These results also highlight the concept that adipose lineage cells represent a suitable new source for therapeutic angiogenesis in ischemic disease.

Data of literature demonstrated that dedifferentiated fat cells can differentiate into smooth muscle cell lineages under specific culture conditions (Sakuma et al. 2009). Green fluorescence protein labelled dedifferentiated fat cells were injected into cryo-injured bladder walls in mice, examining the ability of the fat cells to regenerate smooth muscle tissue after 14 and 30 days after transplantation. Significantly a larger amount of cell expressing α-smooth muscle actin plus green fluorescence protein were observed at the bladder wall injection sites in transplanted mice than in saline injected control mice.

Furthermore, some studies have suggested a close relationship between mature white adipocytes and cardiovascular cells, providing evidence that adipocytes and endothelial cells have a common progenitor cells (Jumabay et al. 2010). Results showed that dedifferentiated adipocytes can act as sources of spontaneously contracting cardiomyocytes in vitro, in which cardiomyocyte phenotype was identified by morphological observations, expression of cardiomyocyte-specific markers and pacemaker activity revealed by electrophysiological studies. These results support a possible link between adipocyte and cardiomyocyte differentiation that might be of importance for pathology and cardiac regeneration.

Moreover, data showed that dedifferentiated adipocytes could differentiated even in cells different from mesenchymal lineages, like neurogenic differentiation. Dedifferentiated cells displayed the capability of forming neurosphere-like structures with significantly increased of nestin expression level respect to non treated control cells (Hermann et al. 2004).

Furthermore, results achieved megakaryocytes and platelets from adipocyte cells with a similar ultrastructures of cells obtained from bone marrow CD34-positive cell. In addition, adipocyte-derived platelets exhibited surface expression of P-selectin and bound fibrinogen upon stimulation with platelet agonists, suggesting that these platelets were functional (Matsubara et al. 2012).

Taken together, the results shown above indicate the capability of the dedifferentiated adipocytes to differentiate into multiple cell lineages. This results might be interpreted as a return back to a noncommitted status for dedifferentiated adipocytes, which was favoured by the culture conditions. These findings suggest that de-differentiated cells have the molecular signature of a reprogrammed cell with features similar to stem cells.

Mature and Dedifferentiated Adipocytes Maintain the Survival and Differentiation of Hematopoietic Stem Cells

Experiments performed in mice demonstrated the presence of hematopoietic progenitors in adipose tissue able to reconstitute hematopoiesis in lethally irradiated animals by systemic infusion of adipose-derived stem cells (Cousin et al. 2003). This beneficial effect could be assigned to the presence of hematopoietic stem cells in the graft, the differentiation of injected mesenchymal stem cells into hematopoietic repopulating cells or the ability of the donor adipose cells to promote the differentiation of residual endogenous hematopoietic progenitors in the host (Corre et al. 2006). In line with this latter hypothesis, results showed that dedifferentiated adipocytes support the complete in vitro differentiation of hematopoietic progenitors without a significant difference in the well-known hematopoietic-supporting capacity of adipose tissue-derived mesenchymal stem cells (Poloni et al. 2012a).

Other data compared the hematopoietic supporting capacity of adipocytes differentiated in culture and adipose-derived MSCs (Ookura et al. 2007; Corre et al. 2006). Umbelical cord blood CD34+CD38- cells were co-cultured on MSCs or adipocytes and the results showed that the hematopoietic-supporting capacity of MSCs decreased with adipocyte differentiation. However, CD34+CD38- cells co-cultured with adipocytes preserved the ability to engraft in NOD/SCID mice, suggesting that adipocytes maintain the ability to support transplantable SCID-repopulating cells.

Moreover, a co-culture system of CD34+ cells seeded onto BM-derived adipocytes was studied to investigated their role in supporting hematopoiesis (Corre et al. 2004). These differentiated cells supported complete myeloid and lymphoid differentiation from hematopoietic stem cells, but they not supported the proliferation of immature progenitors. Moreover, the same authors showed that adipocytes differentiated from adipose-derived stem cells secreted cytokines promoting the differentiation of hematopoietic committed progenitors, like IL-6, G-CSF and GM-CSF, and cytokines inhibiting the proliferation of stem cells, like MIP1α (Corre et al. 2006).

Recently data demonstrated that isolated mature adipocytes co-cultured for long time with CD34+ cells has the ability to support the differentiation of hematopoietic stem cells as adipose tissue-derived MSCs (Poloni et al. 2012a, 2013). Because it is abundant and accessible, adipose tissue could be a convenient source of cells for the short-term reconstitution of hematopoiesis.

For many years adipose tissue was regarded as just a heat insulator and store of excess free fatty acids that could be released when needed. Now, it is considered a critical organ involved in energy regulation, inflammation, immune response thought intricate signals and interrelationships with other cells (Kershaw and Flier 2004). The immunoregulatory capacity of mature adipocytes during the dedifferentiation process was analyzed, studying their behaviour in co-cultures with allogeneic lymphocytes. Results showed that the morphological changes of mature adipocytes during the culture time were associated with functional changes. Indeed, dedifferentiated adipocytes were able to inhibit the proliferation of stimulated lymphocytes in direct co-culture, while mature fat cells stimulated their growth. These features may be associated with the ability of adipose tissue to promote inflammation via cytokine production and with the immunoregulatory capacity of MSCs (Gregor and Hotamisligil 2011) derived from different sources such as adipose tissue (Kronsteiner et al. 2011) bone marrow, amniotic fluid and chorionic villi (Krampera et al. 2006; Poloni et al. 2011, 2012b).

References

Barrilleaux B, Phinney DG, Prockop DJ, O'Connor KC (2006) Review: ex vivo engineering of living tissues with adult stem cells. Tissue Eng 12(11):3007–3019

Bibikova M, Fan JB (2010) Genome-wide DNA methylation profiling. Wiley Interdiscip Rev Syst Biol Med 2(2):210–223

Blanchette-Mackie EJ, Dwyer NK, Barber T, Coxey RA, Takeda T, Rondinone CM, Theodorakis JL, Greenberg AS, Londos C (1995) Perilipin is located on the surface layer of intracellular lipid droplets in adipocytes. J Lipid Res 36:1211–1226

Cinti S (2011) Between brown and white: novel aspects of adipocyte differentiation. Ann Med 43(2):104–115

Cinti S (2009) Transdifferentiation properties of adipocytes in the adipose organ. Am J Physiol Endocrinol Metab 297(5):E977–E986

Corre J, Barreau C, Cousin B, Chavoin JP, Caton D, Fournial G, Penicaud L, Casteilla L, Laharrague P (2006) Human subcutaneous adipose cells support complete differentiation but not self-renewal of hematopoietic progenitors. J Cell Physiol 208(2):282–288

Corre J, Planat-Benard V, Corberand JX, Pénicaud L, Casteilla L, Laharrague P (2004) Human bone marrow adipocytes support complete myeloid and lymphoid differentiation from human CD34 cells. Br J Haematol 127(3):344–347

Cousin B, André M, Arnaud E, Pénicaud L, Casteilla L (2003) Reconstitution of lethally irradiated mice by cells isolated from adipose tissue. Biochem Biophys Res Commun 301(4):1016–1022

Dandona P, Aljada A, Bandyopadhyay A (2004) Inflammation: the link between insulin resistance, obesity and diabetes. Trends Immunol 25(1):4–7

De Matteis R, Zingaretti MC, Murano I, Vitali A, Frontini A, Giannulis I, Barbatelli G, Marcucci F, Bordicchia M, Sarzani R, Raviola E, Cinti S (2009) In vivo physiological transdifferentiation of adult adipose cells. Stem Cells 27(11):2761–2768

Fernyhough ME, Hausman GJ, Guan LL, Okine E, Moore SS, Dodson MV (2008) Mature adipocytes may be a source of stem cells for tissue engineering. Biochem Biophys Res Commun 368(3):455–457

Gimble J, Guilak F (2003) Adipose-derived adult stem cells: isolation, characterization, and differentiation potential. Cytotherapy 5(5):362–369

Gregor MF, Hotamisligil GS (2011) Inflammatory mechanisms in obesity. Annu Rev Immunol 29:415–445

Hermann A, Gastl R, Liebau S, Popa MO, Fiedler J, Boehm BO, Maisel M, Lerche H, Schwarz J, Brenner R, Storch A (2004) Efficient generation of neural stem cell-like cells from adult human bone marrow stromal cells. J Cell Sci 117(Pt 19):4411–4422

Jumabay M, Zhang R, Yao Y, Goldhaber JI, Boström KI (2010) Spontaneously beating cardiomyocytes derived from white mature adipocytes. Cardiovasc Res 85(1):17–27

Kazama T, Fujie M, Endo T, Kano K (2008) Mature adipocyte-derived dedifferentiated fat cells can transdifferentiate into skeletal myocytes in vitro. Biochem Biophys Res Commun 377(3):780–785

Kershaw EE, Flier JS (2004) Adipose tissue as an endocrine organ. J Clin Endocrinol Metab 89(6):2548–2556

Krampera M, Cosmi L, Angeli R, Pasini A, Liotta F, Andreini A, Santarlasci V, Mazzinghi B, Pizzolo G, Vinante F, Romagnani P, Maggi E, Romagnani S, Annunziato F (2006) Role for interferon-gamma in the immunomodulatory activity of human bone marrow mesenchymal stem cells. Stem Cells 24(2):386–398

Kronsteiner B, Wolbank S, Peterbauer A, Hackl C, Redl H, van Griensven M, Gabriel C (2011) Human mesenchymal stem cells from adipose tissue and amnion influence T-cells depending on stimulation method and presence of other immune cells. Stem Cells Dev 20(12):2115–2126

Matsubara Y, Murata M, Ikeda Y (2012) Culture of megakaryocytes and platelets from subcutaneous adipose tissue and a preadipocyte cell line. Methods Mol Biol 788:249–258

Matsumoto T, Kano K, Kondo D, Fukuda N, Iribe Y, Tanaka N, Matsubara Y, Sakuma T, Satomi A, Otaki M, Ryu J, Mugishima H (2008) Mature adipocyte-derived dedifferentiated fat cells exhibit multilineage potential. J Cell Physiol 215(1):210–222

Oki Y, Watanabe S, Endo T, Kano K (2008) Mature adipocyte-derived dedifferentiated fat cells can transdifferentiate into osteoblasts in vitro and in vivo only by all-trans retinoic acid. Cell Struct Funct 33(2):211–222

Ono H, Oki Y, Bono H, Kano K (2011) Gene expression profiling in multipotent DFAT cells derived from mature adipocytes. Biochem Biophys Res Commun 407(3):562–567

Ookura N, Fujimori Y, Nishioka K, Kai S, Hara H, Ogawa H (2007) Adipocyte differentiation of human marrow mesenchymal stem cells reduces the supporting capacity for hematopoietic progenitors but not for severe combined immunodeficiency repopulating cells. Int J Mol Med 19(3):387–392

Pittenger MF, Mackay AM, Beck SC, Jaiswal RK, Douglas R, Mosca JD, Moorman MA, Simonetti DW, Craig S, Marshak DR (1999) Multilineage potential of adult human mesenchymal stem cells. Science 284:143–147

Planat-Benard V, Silvestre JS, Cousin B, André M, Nibbelink M, Tamarat R, Clergue M, Manneville C, Saillan-Barreau C, Duriez M, Tedgui A, Levy B, Pénicaud L, Casteilla L (2004) Plasticity of human adipose lineage cells toward endothelial cells: physiological and therapeutic perspectives. Circulation 109(5):656–663

Poloni A, Maurizi G, Leoni P, Serrani F, Mancini S, Frontini A, Zingaretti MC, Siquini W, Sarzani R, Cinti S (2012a) Human dedifferentiated adipocytes show similar properties to bone marrow-derived mesenchymal stem cells. Stem Cells 30(5):965–974

Poloni A, Maurizi G, Serrani F, Mancini S, Discepoli G, Tranquilli AL, Bencivenga R, Leoni P (2012b) Human AB serum for generation of mesenchymal stem cells from human chorionic villi: comparison with other source and other media including platelet lysate. Cell Prolif 45(1):66–75

Poloni A, Maurizi G, Serrani F, Mancini S, Zingaretti MC, Frontini A, Cinti S, Olivieri A, Leoni P (2013) Molecular functional characterization of human bone marrow adipocytes. Exp Hematol 41(6):558–566

Poloni A, Maurizi G, Babini L, Serrani F, Berardinelli E, Mancini S, Costantini B, Discepoli G, Leoni P (2011) Human mesenchymal stem cells from chorionic villi and amniotic fluid are not susceptible to transformation after extensive in vitro expansion. Cell Transplant 20(5):643–654

Sakuma T, Matsumoto T, Kano K, Fukuda N, Obinata D, Yamaguchi K, Yoshida T, Takahashi S, Mugishima H (2009) Mature, adipocyte derived, dedifferentiated

fat cells can differentiate into smooth muscle-like cells and contribute to bladder tissue regeneration. J Urol 182(1):355–365

Sudo K, Kanno M, Miharada K, Ogawa S, Hiroyama T, Saijo K, Nakamura Y (2007) Mesenchymal progenitors able to differentiate into osteogenic, chondrogenic, and/or adipogenic cells in vitro are present in most primary fibroblast-like cell populations. Stem Cells 25:1610–1617

Sugihara H, Yonemitsu N, Miyabara S, Toda S (1987) Proliferation of unilocular fat cells in the primary culture. J Lipid Res 28(9):1038–1045

Tosh D, Slack JMW (2002) How cells change their phenotype. Nat Rev Mol Cell Biol 3:187–194

Yoshimura K, Shigeura T, Matsumoto D, Sato T, Takaki Y, Aiba-Kojima E, Sato K, Inoue K, Nagase T, Koshima I, Gonda K (2006) Characterization of freshly isolated and cultured cells derived from the fatty and fluid portions of liposuction aspirates. J Cell Physiol 208:64–76

Zhang HH, Kumar S, Barnett AH, Eggo MC (2000) Ceiling culture of mature human adipocytes: use in studies of adipocyte functions. J Endocrinol 164(2): 119–128

Part II

Children's Cancer

Inhibition of Neuroblastoma Progression by Targeting Lymphangiogenesis: Role of an Endogenous Soluble Splice-Variant of VEGFR-2

6

Jürgen Becker

Contents

Abstract

The endogenous-soluble-vascular-endothelial-growth-factor-receptor-2 (esVEGFR-2) is a novel member of the VEGFR-family. It is generated from the VEGFR-2 gene by alternative splicing and was shown to bind VEGF-C with high affinity, therefore acting as an endogenous inhibitor of lymphangiogenesis. Still little is known about its functions in development and disease. We explored the distribution patterns of esVEGFR-2 in human embryonic tissues and found it expressed in many organs and structures throughout the developing organism. Most interestingly, sympathetic ganglia and the adrenal medulla were positive for the inhibitor, too. Neuroblastoma is an embryonic tumor, developing from sympathetic progenitor cells of the neural crest, which in normal development form the sympathetic nervous system as well as the adrenal medulla. Immunohistology revealed that in neuroblastoma with a differentiating type of histopathology and in differentiated tumors of the ganglioneuroblastoma type, esVEGFR-2 was expressed regularly, whereas in highly malignant neuroblastoma with an undifferentiated phenotype it could be rarely detected. All-trans-retinoic acid (ATRA) is known as crucial compound in embryonic differentiation processes. It has also been shown to induce differentiation of neuroblastoma in vitro, and is a part of clinical regimen for neuroblastoma treatment. Neuroblastoma cells treated with ATRA showed increased expression of esVEGFR-2,

J. Becker (✉)
Department of Anatomy and Cell Biology, University Medicine Goettingen, 37075 Goettingen, Germany
e-mail: Juergen.becker@med.uni-goettingen.de

M.A. Hayat (ed.), *Tumors of the Central Nervous System, Volume 12*,
DOI 10.1007/978-94-007-7217-5_6, © Springer Science+Business Media Dordrecht 2014

suggesting that high expression of esVEGFR-2 may indicate differentiated neuroblastoma and vice versa. Real-time RT-PCR analyses revealed that INSS stage 1 and 2 neuroblastomas express higher amounts of esVEGFR-2 transcripts than stage 3 and 4 tumors. Intriguingly, the down-regulation of the transcripts inversely correlates with lymph-node involvement and metastasis formation.

Together, esVEGFR-2 may indicate differentiation in neuroblastoma and provide new insights into cancer progression mechanisms where not only expression of pro-angiogenic molecules may facilitate tumor progression, but also the down regulation of anti-(lymphangiogenic)-molecules could drive malignancy.

Introduction to Tumor Angiogenesis

Angiogenesis, the formation of blood- and lymphatic vessels from preexisting vessels, can be observed under physiological conditions whenever regeneration of blood vessels is needed, namely during the proliferative phase of the endometrial mucosa or during wound healing. In tumor pathology, the supply with nutrients and oxygen via blood vessels is a key prerequisite for tumor growth beyond the borders of normal diffusion. Tumor lymphatics drain interstitial fluid from the tumor. Therefore many clinically relevant tumor entities share the ability to induce and stimulate vessel outgrowth from existing surrounding capillaries or larger vessels and to attract the newly formed vessels to the tumor. This process is termed tumor angiogenesis. Both, angiogenesis and tumor angiogenesis are mediated by secreted molecules and signaling pathways which are often found deregulated in malignancies. Molecules involved are the Hypoxia-Inducible transcription factor (HIFs), Angiopoietins (Ang-1, Ang-2) and their receptors (TIE-1; TIE-2), Integrins, Fibroblast Growth Factors (FGFs) or Transforming Growth Factor beta (TGFbeta), just to mention some of them (Carmeliet 2003). However the strongest regulators in angiogenesis and tumor angiogenesis are the Vascular Endothelial Growth Factor family members, which are VEGF-A, VEGF-B, VEGF-C, VEGF-D and Placenta growth factor (PlGF) in collaboration with their appropriate tyrosin-kinase receptors VEGFR-1 (Flt-1), VEGFR-2 (KDR/Flk1) and VEGFR-3 (Flt-4).

The VEGF-Family and its Receptors

VEGF-family members are predominantly active as homo-dimers, but heterodimers between various VEGF members have also been observed. The complexity of this system is further increased by the fact that several splicing-forms or proteolytic fragments exist for most of the VEGFs. As there are excellent recent reviews only a short overview will be provided here (for review see Adams and Alitalo 2007; Koch et al. 2011). In brief, VEGF-A is the main inducer of blood vessels. It binds to VEGFR-2 homodimers, which are assisted by the co-receptor neuropilin 1 (NRP1). The activation of VEGFR-2 is regulated by VEGFR-1, which has tenfold higher affinity to VEGF-A but only weak signaling capacity. VEGFR-1 seems to have mainly regulatory properties such as the induction of VEGFR-2 expression or attenuation of VEGF-A signaling by trapping the ligand. Of VEGF-B, two isoforms are generated by alternative splicing, both binding exclusively to VEGFR-1. The function of VEGF-B still remains a matter of debate but there is emerging evidence that it is involved in cardiac angiogenesis during development. PlGF is expressed strongly in the placenta, but can also be found in other tissues. It also binds exclusively to VEGFR-1 and its role is not fully understood, however it seems to potentiate VEGF-A induced angiogenesis. VEGF-C and VEGF-D both bind to VEGFR-3 and are the main inducers of lymphangiogenesis.

Since VEGF-C and VEGF-D were identified, it became evident that members of the VEGF-family orchestrate not only hemangiogenesis but also lymphangiogenesis. In tumors, lymphangiogenesis was considered to be non-existing for a long time, until VEGF-C-induced lymphangiogenesis was demonstrated by using VEGF-C expressing tumor cells on the chorioallantoic membrane of the chicken embryo (Papoutsi et al. 2000).

Subsequently a series of experiments could show that this also holds true for mouse models, where VEGF-C induced lymphangiogenesis correlates positively with the formation of lymphnode-metastases (Karpanen et al. 2001; Skobe et al. 2001; Stacker et al. 2001). Even though many human tumor entities also show a positive correlation between the expression of VEGF-C and VEGF-D and lymphnode involvement, this is not the case for all human malignancies (Pepper et al. 2003). Therefore it is reasonable to assume that lymphangiogenesis is not only controlled by activators but could also be counterbalanced by inhibitory molecules.

Despite intensive investigations by many groups the VEGF-system is not fully understood yet. Nevertheless, the discovery of VEGF-A opened the door to access a mighty system of angiogenic regulators, which were consequently identified as targets for anti-angiogenic therapy of cancer and other diseases, although, at least so far, not with the expected success (Leung et al. 1989; Carmeliet 2003; Sitohy et al. 2012).

EsVEGFR-2 is a Novel Endogenous Inhibitor of Lymphangiogenesis

For both, VEGFR-1 and VEGFR-2, soluble fragments, which can be detected in blood and interstitial fluid, are known (sVEGFR-1 and sVEGFR-2). These fragments are often derived by enzymatic shedding of the membrane-bound receptor. Thereby sVEGFR-1 is considered to be a major negative regulator of VEGF-A-induced haemangiogenesis, and it has been shown that especially in the cornea the soluble fragment is not a product of proteinase activity but rather synthesized by alternative splicing from the VEGFR-1 mRNA (Ambati et al. 2006).

Recently, Albuquerque and colleagues also identified a novel soluble splice variant of VEGFR-2, termed sVEGFR-2, in mouse cornea and also in human tissues (Albuquerque et al. 2009). To make strictly clear that this molecule is not a shedded proteolytic fragment, it is subsequently termed endogenous soluble VEGFR-2 (esVEGFR-2) by the author as proposed by Shibata et al. (2010). EsVEGFR-2 is characterized by a unique C-terminal 13 amino-acid sequence in mice or 16 amino-acid sequence in human, and a complete lack of the membrane-spanning and intracellular signalling components of the full-lengthVEGFR-2. The C-terminal amino acid stretches are generated by the use of an alternative stop-codon in intron 13 and proved suitable for the production of specific antibodies as well as specific primers for real-time RT-PCR. Surprisingly, esVEGFR-2 does not seem to bind VEGF-A, but exhibits high binding affinity for VEGF-C. In a series of elegant experiments Albuquerque et al. (2009), demonstrated that tissue specific knock-down of esVEGFR-2 in the mouse cornea, using the PAX6 promotor in a cre-lox system, leads to proliferation and growth of lymphatic vessels into the (normally avascular) cornea (Albuquerque et al. 2009). Additionally, keratin 14 promotor-based cre-lox VEGFR-2 knock-out causes edema in the skin due to dilation and hyperplasia of lymphatics. Cell culture experiments revealed that esVEGFR-2 inhibits VEGF-C induced proliferation of human lymphatic endothelial cells in vitro.

EsVEGFR-2 in Embryonic Development

The above discussed experiments published by Albuquerque et al. (2009), were performed using the offspring of transgenic mice and suggest that esVEGFR-2 exerts its functions during embryonic development. We used sections of human embryos and fetuses for immunohistology in order to determine esVEGFR-2 expression patterns (Becker et al. 2012).

In 8 weeks-old embryos positive staining is detectable in the epithelium of the choroid plexus, the floor plate of the neural tube, the anterior spinal artery and distinct cells of the notochord. In the liver hematopoietic cells (Fig. 6.1a, b) and scattered cells in the adventitia of the portal vein stain positive for esVEGFR-2. Scattered positive cells are also detectable in the developing dermis, and the epidermis of 8 weeks-old embryos stains

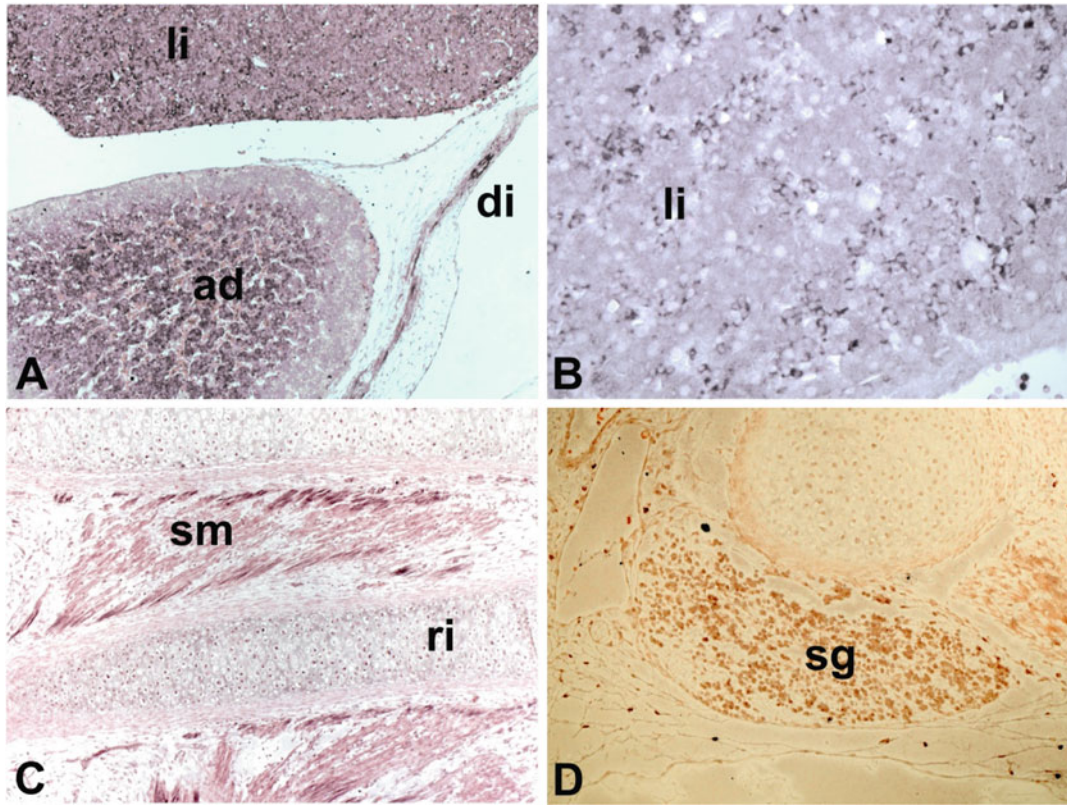

Fig. 6.1 Immunostaining for esVEGFR-2 in tissues of human, 8–10 weeks old, embryos and fetuses. (**a**) adrenal gland (ad), liver (li) and diaphragm (di). (**b**) liver. (**c**) intercostal muscles (im), ribs (ri), note strong immunoreactivity of tendineous parts of the intercostal muscle. (**d**) sympathetic ganglion (sg)

nicely positive, too. However, the identity of the scattered cells found in many tissues is not clear yet. Additional positive organs are the gut mucous-membrane, skeletal muscle cells, the tendons of skeletal muscles (Fig. 6.1c), the adrenal gland (Fig. 6.1a) and sympathetic paravertebral ganglia (Fig. 6.1d). Most strikingly, we could show that arterial endothelial cells are positive for esVEGFR-2 whereas venous endothelial cells are not (Becker et al. 2012). This phenomenon may be explained with regard to co-localization patterns of blood and lymphatic vessels. Larger arteries are accompanied by lymphatics that drain exudates, produced due due to high arterial fluid pressure. Additionally, larger lymphatics and lymphatic trunks, which drain a tributary region, are in most cases co-localized with the arteries that supply this region. Blood endothelial cells are a source of VEGF-C and therefore it can be speculated, that esVEGFR-2 might be expressed and secreted by arterial endothelial cells to block VEGF-C on the abluminal side in order to prevent attraction of lymphatic endothelial cells and thereby preventing formation of anastomoses between lymphatics and blood vessels.

EsVEGFR-2 in Neuroblastoma

Neuroblastoma is an embryonic tumor originating from neural crest cells, which belong to the sympathetic neuroblast lineage. In normal development, these cells migrate from the neural crest and form the sympathetic nervous system. Therefore neuroblastomas usually develop within or nearby sympathetic ganglia, for example along the sympathetic trunk or the adrenal medulla. Both of the latter tissues display esVEGFR-2 positivity in human embryos and fetuses (Fig. 6.1a, d). It remains unclear whether the malignantly

transformed cells follow their normal pathways in the embryo or whether the malignant transformation occurs when the cells have reached their final destination.

VEGF-C-induced lymphangiogenesis and the existence of lymphatic vessels in primary neuroblastoma specimens and experimental tumors has been shown some time ago (Lagodny et al. 2007). The international neuroblastoma staging system (INSS) refers to the lymphnode status as one of the main criteria for the clinical evaluation of tumor progression and prognosis. Albeit this system has currently been revised and transferred into the International Neuroblastoma Risk Group Staging System (INRGSS), which covers more clinical imaging data, the impact of the lymphnode status is still undoubted (Monclair et al. 2009).

Therefore, we decided to investigate the expression of esVEGFR-2 in primary neuroblastoma and the clinical relevance of the expression pattern (Becker et al. 2010). Additionally, neuroblastoma cell-lines were screened for VEGFs and VEGF-receptors, including esVEGFR-2. All tested molecules were expressed in the cell-lines, but as expected for neuroblastoma, a wide heterogeneity of the expression levels could be observed. When we used the same primer sets on untreated (which means without adjuvant chemotherapy before surgery) primary tumor samples, a slight increase of VEGF-A transcripts in stage 4 s tumors and a lower expression of VEGF-D transcripts in tumors of stages 3, 4 and 4 s could be detected. Other VEGFs did not show remarkable differences between clinical stages, except for esVEGFR-2, which was expressed significantly lower in tumor stages 3, 4 and 4 s, whereas membrane-bound VEGFR-2 (mbVEGFR-2) did not show any alterations (Becker et al. 2010).

The most significant marker for neuroblastoma progression is the amplification of the transcription factor MYCN, which strongly correlates with unfavorable outcome (Westermann and Schwab 2002). MYCN amplification can be found in 20–25 % of neuroblastomas and amplification levels may reach up to several hundred copies. This leads to a massive over-expression of MYCN at transcript and protein level. Neuroblastomas with high MYCN expression are aggressive, fast growing, well vascularized and frequently metastasizing to other organs and lymphnodes. In our studies, we could not find differences between MYCN-amplified and non-amplified primary stage 4 neuroblastoma specimens for VEGF-C, VEGFR-2 and VEGFR-1 at mRNA level. However, VEGF-A and VEGF-D transcripts are moderately increased in the MYCN-amplified samples and the inhibitory soluble receptors sVEGFR-1 and esVEGFR-2 are clearly, yet not statistically significantly, down-regulated. Of note, in 26 neuroblastoma cell-lines, mainly derived from primary tumors or metastases, there were no differences between MYCN-amplified and non-amplified specimens detectable, suggesting that in vitro data and cell-line experiments may not adequately reflect tumor behavior in this aspect (Becker et al. 2010).

However, in vitro experiments using WAC2, which are MYCN-transfected and over-expressing cells derived from the neuroblastoma cell line SH-EP, confirmed the correlation between MYCN expression and down-regulation of esVEGFR-2 (Becker et al. 2010). Other Groups reported earlier that MYCN amplified neuroblastomas up-regulate VEGF-C and that VEGF-A is down-regulated after siRNA-mediated knock-down of MYCN (Eggert et al. 2000; Kang et al. 2008). These data suggest that up-regulation of pro-angiogenic factors is one feature that facilitates neuroblastoma progression, but on the other hand, down-regulation of inhibitors of angiogenesis namely esVEGFR-2 and sVEGFR-1 may also severely disrupt the balance of pro- and anti-angiogenic factors and may strongly contribute to neuroblastoma progression.

EsVEGFR-2 Expression Correlates with Differentiation in Neuroblastoma

Typically for embryonic tumors, most neuroblastomas are diagnosed in the first 2 years of life or, with the help of modern imaging techniques even before birth. The median age of neuroblastoma patients is about 24 months. Interestingly many neuroblastomas of younger patients respond better to chemotherapy or even differentiate spontaneously to benign ganglioneuroma or

undergo complete regression. Therefore statistically, younger age strongly correlates with favorable outcome. In the neuroblastoma staging system, attention has been given to this fact with the introduction of the stage 4 s, which encloses children with progressed neuroblastoma including some degree of metastases to the skin and liver, but with an age not exceeding 12 months. Despite metastases formation these patients share an excellent prognosis and can often be cured. In older children with high risk neuroblastoma, retinoic acid derivatives have successfully been used to increase survival when applied together with or after conventional chemo-therapy (Masetti et al. 2012). The differentiating effect of retinoic acid on neuroblasoma cells in vitro has been shown in 1982 by Sidell and was refined in the years since (Sidell 1982; Reynolds et al. 1994).

We sought to identify whether esVEGFR-2 expression is correlated with differentiation in neuroblastoma. By immunohistology using an antibody raised against the specific C-terminal intronic peptide of esVEGFR-2, we found expression predominantly in low grade neuroblastomas (Hughes Grade I), which are stroma-rich with large tumor cells resembling differentiated neuronal cells (Fig. 6.2b). This tumor type is associated with no or only minor, regional lymph node involvement and good prognosis. In contrast, undifferentiated lesions with small round tumor cells (Hughes Grade III; WHO Grade III, IV) are often associated with distant lymph node metastases and dissemination to other organs like bone marrow or liver. This type of neuroblastoma is associated with poor prognosis and in the specimens we probed, no positive staining for esVEGFR-2 was detectable (Fig. 6.2a) (Becker et al. 2012). Especially in neuroblastoma with a histology of the differentiating phenotype, expression was detectable in the cytoplasm of maturing neurons, and in ganglioneuroblastoma and ganglioneuroma (Hughes Grade I) most of the ganglionic cells were strongly positive. This suggests that sympathetic neuroblasts might be able to inhibit tumor lymphangiogenesis by the production of esVEGFR-2.

Therapy with ATRA induces differentiation of the neuroblastoma cells and can stop malignant progression of the tumor especially in children younger than 18 months of age (Reynolds et al. 2003). Treatment of neuroblastoma cell-lines with 5–10 μM ATRA induced the maturation of the cells in vitro, which is depicted microscopically by the formation of neurite-like protrusions and by a proliferation delay or even arrest. Screening of ATRA-treated neuroblastoma cells by real-time RT-PCR revealed that esVEGFR-2 is constantly up-regulated over 12 days of treatment in SMS-KAN cells, however not all of the tested cells responded at the same degree (Becker et al. 2012).

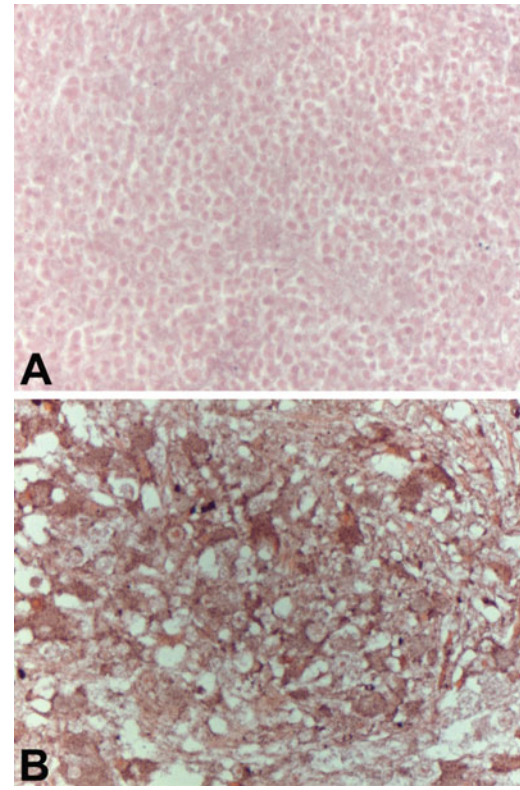

Fig. 6.2 Expression of esVEGFR-2 in human primary neuroblastoma. Paraffin sections of primary neuroblastoma specimens were subjected to immuno-histochemistry using anti-esVEGR-2 antibodies and horseradish peroxidase-coupled secondary antibodies. (**a**) Neuroblastoma of the undifferentiated small round cells type shows no immunoreactivity for esVEGFR-2. (**b**) Neuroblastoma of the differentiating type: large neuron-like cells show up with strong immunoreactivity for esVEGFR-2 in the cytoplasm

EsVEGFR-2 in Other Cancers

So far, the effects of esVEGFR-2 have not been studied in other human cancer entities. Shibata and colleagues used a mouse model with virally inducible mamma carcinoma (Shibata et al. 2010). They treated the experimental mouse tumors with plasmid vectors containing esVEGFR-2 cDNA, introduced into the carcinoma cells by in vivo electroporation. After such treatment, tumor volumes were reduced by 30 % while survival rates increased from 60 % in controls to 90 % in esVEGFR-2-treated animals. Also, metastases to lymph nodes and the number of metastatic foci in organs like the lung were reduced by 50 %. However the number of organs (lung, kidney, adrenal and ovaries) with metastases was not altered, suggesting that the hematogenic spread of tumor cells was not affected. Remarkably, only the number of lymphatics was significantly decreased in treated tumors, while the blood vessel number was not altered. Even more interestingly, the number of lymphatics with tumor cells in the lumen decreased by about 25 % in treated tumors, which is far more than one would assume by the mere reduction of vessel number, indicating that esVEGFR-2 may also affect tumor-vessel interactions. For carcinoid cancer, a tumor derived from enterochromaffin cells of the gut, Silva et al. (2011) reported that migration in vitro is enhanced by VEGF-C binding to VEGFR-3. The authors speculate that the observed expression of esVEGFR-2 in carcinoid tumor cells may bind VEGF-C and thus slow down tumor progression (Silva et al. 2011).

Induction of Alternative Splicing

In 2011 Vorlova and co-workers published their studies on the induction of alternative splicing in tyrosine-kinase receptors (RTK). They show that alternative splicing like in VEGFR-2 can be found regularly in most of the RTK-family members (Vorlova et al. 2011). More interestingly, using VEGFR-2 in human umbilical vein endothelial cells (HUVEC), they demonstrated that alternative splicing can be induced with appropriate morpholino oligonucleotides which block the U1 small nuclear ribonucloparticle (U1 snRNP, here U1) binding site at the 5′ splicing site. As shown both at mRNA and protein levels this led to specific and efficient inhibition of splicing at intron 13 and complete replacement of membrane-bound VEGFR-2 by secreted esVEGFR-2. The authors conclude that their morpholino approach may have new therapeutic prospects by targeting RTK signaling at three levels: (i) the induction of alternative splicing substitutes membrane bound receptor by the soluble inactive form; (ii) secreted soluble receptor may bind ligands and act as a decoy receptor and (iii) the secreted soluble isoforms may dimerize with their membrane-bound counterparts and form binding-active receptors with reduced or even absent signaling capacity (Vorlova et al. 2011).

Lately, Uehara and colleagues (2013) were able to confirm the results published by Vorlova and co-workers (Vorlova et al. 2011; Uehara et al. 2013). They used a similar morpholino specific for the splicing site at the exon 13 – intron 13 boundary and forced polyadenylation at the latent polyA-site of intron 13. The resulting product was correctly glycosylated and exported to the culture fluid. In vivo intravitreal injection of morpholinos induced esVEGFR-2 expression and suppressed neovascularization of the choroidea after laser treatment, therefore the effects of esVEGFR-2 on hemangiogenesis may following the mechanisms proposed by Vorlova et al. (2011). Also in cornea suture experiments, morpholinos injected under the conjunctiva inhibited hemangiogenesis and lymphangiogenesis during cornea healing. Additionally, after cornea transplantation, morpholino-treatment prevented graft rejection effectively (Uehara et al. 2013).

In sum, morpholino based induction of esVEGFR-2 seems to be a promising tool to control lymphangiogenesis and hemangiogenesis in the future.

Conclusions

The novel soluble splice variant of VEGFR-2 is a potent inhibitor of VEGF-C-mediated processes. There is evidence that in neuroblastoma, the down-regulation of esVEGFR-2 correlates with

tumor progression and lymph node involvement. There are several scenarios to explain this assumption. Firstly, with regard to the findings in the human embryonic tissues, esVEGFR-2 expression seems to be a marker of normally differentiating sympatho-adrenal cells and progenitor cells. The down-regulation of the inhibitor may therefore be a sign that the cells have left their differentiation pathway into a malignant direction. This notion is supported by our experiments with the retinoic acid derivative ATRA, which induces differentiation of tumor cells and increases the levels of esVEGFR-2. Secondly, the loss of esVEGFR-2 expression in neuroblastomas of progressed stages may elicit indirect effects in the stroma such as increased lymphatic endothelial proliferation, which facilitates the lymphatic spread of tumor cells. Beside anti-angiogenic effects, the molecule may have further properties, which influence tumor outcome, for example the modulation of immune responses. A connection between the immune system and VEGF-C has earlier been described (Chen et al. 2005). When siRNA directed against VEGF-C was applied to mice bearing experimental mammary-carcinoma the authors found that the knock-down of VEGF-C causes increased infiltration of CD 8^+ T-cells and dendritic cells, indicating an increased immune response, but also decreased lymphangiogenesis. Their anti-VEGF-C treatment resulted in an overall increased survival of the animals. A similar effect may be postulated for esVEGFR-2, which may offer an additional valuable therapeutic option. However further studies are required to fully elucidate the therapeutic value of this promising molecule.

References

Adams RH, Alitalo K (2007) Molecular regulation of angiogenesis and lymphangiogenesis. Nat Rev Mol Cell Biol 8(6):464–478

Albuquerque RJ, Hayashi T, Cho WG, Kleinman ME, Dridi S, Takeda A, Baffi JZ, Yamada K, Kaneko H, Green MG, Chappell J, Wilting J, Weich HA, Yamagami S, Amano S, Mizuki N, Alexander JS, Peterson ML, Brekken RA, Hirashima M, Capoor S, Usui T, Ambati BK, Ambati J (2009) Alternatively spliced vascular endothelial growth factor receptor-2 is an essential endogenous inhibitor of lymphatic vessel growth. Nat Med 15(9):1023–1030

Ambati BK, Nozaki M, Singh N, Takeda A, Jani PD, Suthar T, Albuquerque RJ, Richter E, Sakurai E, Newcomb MT, Kleinman ME, Caldwell RB, Lin Q, Ogura Y, Orecchia A, Samuelson DA, Agnew DW, St Leger J, Green WR, Mahasreshti PJ, Curiel DT, Kwan D, Marsh H, Ikeda S, Leiper LJ, Collinson JM, Bogdanovich S, Khurana TS, Shibuya M, Baldwin ME, Ferrara N, Gerber HP, De Falco S, Witta J, Baffi JZ, Raisler BJ, Ambati J (2006) Corneal avascularity is due to soluble VEGF receptor-1. Nature 443(7114):993–997

Becker J, Pavlakovic H, Ludewig F, Wilting F, Weich HA, Albuquerque R, Ambati J, Wilting J (2010) Neuroblastoma progression correlates with downregulation of the lymphangiogenesis inhibitor sVEGFR-2. Clin Cancer Res 16(5):1431–1441

Becker J, Frohlich J, Hansen J, Zelent C, Perske C, Wilting J (2012) The lymphangiogenesis inhibitor esVEGFR-2 in human embryos: expression in sympatho-adrenal tissues and differentiation-induced up-regulation in neuroblastoma. Histol Histopathol 27(6):721–733

Carmeliet P (2003) Angiogenesis in health and disease. Nat Med 9(6):653–660

Chen Z, Varney ML, Backora MW, Cowan K, Solheim JC, Talmadge JE, Singh RK (2005) Down-regulation of vascular endothelial cell growth factor-C expression using small interfering RNA vectors in mammary tumors inhibits tumor lymphangiogenesis and spontaneous metastasis and enhances survival. Cancer Res 65(19):9004–9011

Eggert A, Ikegaki N, Kwiatkowski J, Zhao H, Brodeur GM, Himelstein BP (2000) High-level expression of angiogenic factors is associated with advanced tumor stage in human neuroblastomas. Clin Cancer Res 6(5):1900–1908

Kang J, Rychahou PG, Ishola TA, Mourot JM, Evers BM, Chung DH (2008) N-myc is a novel regulator of PI3K-mediated VEGF expression in neuroblastoma. Oncogene 27(28):3999–4007

Karpanen T, Egeblad M, Karkkainen MJ, Kubo H, Ylä-Herttuala S, Jaattela M, Alitalo K (2001) Vascular endothelial growth factor C promotes tumor lymphangiogenesis and intralymphatic tumor growth. Cancer Res 61(5):1786–1790

Koch S, Tugues S, Li X, Gualandi L, Claesson-Welsh L (2011) Signal transduction by vascular endothelial growth factor receptors. Biochem J 437(2):169–183

Lagodny J, Juttner E, Kayser G, Niemeyer CM, Rossler J (2007) Lymphangiogenesis and its regulation in human neuroblastoma. Biochem Biophys Res Commun 352(2):571–577

Leung DW, Cachianes G, Kuang WJ, Goeddel DV, Ferrara N (1989) Vascular endothelial growth factor is a secreted angiogenic mitogen. Science 246(4935):1306–1309

Masetti R, Biagi C, Zama D, Vendemini F, Martoni A, Morello W, Gasperini P, Pession A (2012) Retinoids in pediatric onco-hematology: the model of acute promyelocytic leukemia and neuroblastoma. Adv Ther 29(9):747–762

Monclair T, Brodeur GM, Ambros PF, Brisse HJ, Cecchetto G, Holmes K, Kaneko M, London WB, Matthay KK, Nuchtern JG, von Schweinitz D, Simon T, Cohn SL, Pearson AD (2009) The International Neuroblastoma Risk Group (INRG) staging system: an INRG Task Force report. J Clin Oncol 27(2):298–303

Papoutsi M, Siemeister G, Weindel K, Tomarev SI, Kurz H, Schachtele C, Martiny-Baron G, Christ B, Marme D, Wilting J (2000) Active interaction of human A375 melanoma cells with the lymphatics in vivo. Histochem Cell Biol 114(5):373–385

Pepper MS, Tille JC, Nisato R, Skobe M (2003) Lymphangiogenesis and tumor metastasis. Cell Tissue Res 314(1):167–177

Reynolds CP, Schindler PF, Jones DM, Gentile JL, Proffitt RT, Einhorn PA (1994) Comparison of 13-cis-retinoic acid to trans-retinoic acid using human neuroblastoma cell lines. Prog Clin Biol Res 385:237–244

Reynolds CP, Matthay KK, Villablanca JG, Maurer BJ (2003) Retinoid therapy of high-risk neuroblastoma. Cancer Lett 197(1–2):185–192

Shibata MA, Ambati J, Shibata E, Albuquerque RJ, Morimoto J, Ito Y, Otsuki Y (2010) The endogenous soluble VEGF receptor-2 isoform suppresses lymph node metastasis in a mouse immunocompetent mammary cancer model. BMC Med 8:69

Sidell N (1982) Retinoic acid-induced growth inhibition and morphologic differentiation of human neuroblastoma cells in vitro. J Natl Cancer Inst 68(4):589–596

Silva SR, Bowen KA, Rychahou PG, Jackson LN, Weiss HL, Lee EY, Townsend CM Jr, Evers BM (2011) VEGFR-2 expression in carcinoid cancer cells and its role in tumor growth and metastasis. Int J Cancer 128(5):1045–1056

Sitohy B, Nagy JA, Dvorak HF (2012) Anti-VEGF/VEGFR therapy for cancer: reassessing the target. Cancer Res 72(8):1909–1914

Skobe M, Hawighorst T, Jackson DG, Prevo R, Janes L, Velasco P, Riccardi L, Alitalo K, Claffey K, Detmar M (2001) Induction of tumor lymphangiogenesis by VEGF-C promotes breast cancer metastasis. Nat Med 7(2):192–198

Stacker SA, Caesar C, Baldwin ME, Thornton GE, Williams RA, Prevo R, Jackson DG, Nishikawa S, Kubo H, Achen MG (2001) VEGF-D promotes the metastatic spread of tumor cells via the lymphatics. Nat Med 7(2):186–191

Uehara H, Cho Y, Simonis J, Cahoon J, Archer B, Luo L, Das SK, Singh N, Ambati J, Ambati BK (2013) Dual suppression of hemangiogenesis and lymphangiogenesis by splice-shifting morpholinos targeting vascular endothelial growth factor receptor 2 (KDR). FASEB J 27(1):76–85. doi:10.1096/fj.12-213835. Epub 2012 Sep 20. Source: Moran Eye Center, University of Utah, Salt Lake City, UT 84132, USA

Vorlova S, Rocco G, Lefave CV, Jodelka FM, Hess K, Hastings ML, Henke E, Cartegni L (2011) Induction of antagonistic soluble decoy receptor tyrosine kinases by intronic polyA activation. Mol Cell 43(6):927–939

Westermann F, Schwab M (2002) Genetic parameters of neuroblastomas. Cancer Lett 184(2):127–147

Hyperinsulinemia Tends to Induce Growth Without Growth Hormone in Children with Brain Tumors After Neurosurgery

7

Norishi Ueda and Hideyuki Iwayama

Contents

N. Ueda (✉)
Department of Pediatrics, Public Central Hospital of Matto Ishikawa, 3-8 Kuramitsu, Hakusan, Ishikawa 924-8588, Japan
e-mail: nueda@mattohp.com

H. Iwayama
Department of Pediatrics, Neonatology and Congenital Disorders, Nagoya City University, 1 Kawasumi, Mizuho-cho, Mizho-ku, Nagoya 467-8602, Aichi, Japan

Abstract

Hypothalamo-pituitary dysfunction is commonly seen in children with brain tumors after neurosurgery, resulting in endocrine disorders, including growth hormone deficiency (GHD). GHD causes growth failure, and thus the majority of the patients need GH replacement therapy. Despite GHD, some patients grow normally or excessively, which has been recognized as growth without GH (GWGH). Since hyperinsulinemia is highly associated with the patients with GWGH, it has been considered to play an important role for promoting linear growth. However, the causes of hyperinsulinemia associated with GWGH and the mechanisms of GWGH remain elusive. The data to date collectively suggest that the location of brain tumors and/or the mode of surgery, insulin resistance associated with obesity, insulin-like growth factor (IGF)-I, IGF binding protein (IGFBP)-1 and −3, leptin and prolactin (PRL) may contribute to the regulation of insulin secretion in patients with GWGH. Besides its metabolic effects, insulin exerts the diverse effects as a growth factor, including proliferation and differentiation of

M.A. Hayat (ed.), *Tumors of the Central Nervous System, Volume 12*,
DOI 10.1007/978-94-007-7217-5_7,

osteoblasts, leading to acceleration of linear growth. Interaction between insulin- and IGF-I-induced signaling pathways and of insulin with other hormonal factors such as leptin or PRL may play a crucial role for promoting linear growth in patients with GWGH. Despite normal or excessive linear growth, patients with GWGH still have metabolic abnormalities and retarded bone maturation. It remains elusive whether GH replacement therapy solves these problems and enables the patients to reach normal height in adulthood. Better understanding for the mechanisms of GWGH is essential to improve the quality of life of patients with GWGH. Because of a lack of accumulating data, further studies would be necessary to clarify the clinical characteristics and the mechanisms of GWGH in more detail in the future.

Introduction

Hypothalamo-pituitary (HP) dysfunction occurs in the majority of children with brain tumors after neurosurgery. The most common HP dysfunction includes growth hormone deficiency (GHD) and diabetes insipidus (Carmel et al. 1982; Di Battista et al. 2006). GHD causes growth failure, and thus GH replacement therapy is necessary in the majority of patients with brain tumors after neurosurgery.

In 1964, it was first reported that despite GHD, some patients with brain tumors after neurosurgery grew normally or excessively (Matson 1964). This phenomenon has been recognized as growth without GH (GWGH). The mechanisms of GWGH remain elusive. However, hyperinsulinemia is often associated with the patients with GWGH, and thus it has been considered to play a crucial role for promoting linear growth in these patients. In this chapter, we will focus on a role of hyperinsulinemia for GWGH by reviewing the auxological and endocrinological data of the children with GWGH after neurosurgery of brain tumors reported in the literature. In addition, we will discuss the possible causes of hyperinsulinemia associated with GWGH and the proposed mechanisms of GWGH, including a role of insulin-induced cell signaling and of interaction between insulin and other hormonal factors for promoting linear growth in patients with GWGH.

Growth Hormone Deficiency (GHD) and Growth Failure in Craniopharyngiomas Before and After Neurosurgery

Craniopharyngiomas (CPs) are the most common brain tumors, affecting the HP region, and account for approximately 10 % of primary intracranial tumors in children (DeVile et al. 1996; Srinivasan et al. 2004). HP dysfunction is commonly associated with the pediatric patients with CPs even before neurosurgery (Thomsett et al. 1980; Blethen and Weldon 1986; Sorva 1988; DeVile et al. 1996; Pinto et al. 2000; Di Battista et al. 2006; Trivin et al. 2009). GHD occurs in 62–90 % of the patients with CPs (Thomsett et al. 1980; Lyen and Grant 1982; Tiulpakov et al. 1998), and growth failure caused by GHD is seen in 15–90 % of these patients before neurosurgery (Costin et al. 1976; Thomsett et al. 1980; Carmel et al. 1982; Lyen and Grant 1982; Stahnke et al. 1984; Sorva 1988; DeVile et al. 1996; Pinto et al. 2000; Di Battista et al. 2006). Since the brain lesion itself causes the damage to the cells in the HP region and/or to the vessels that transfer the hypothalamic hormones to the pituitary, the incidence and severity of HP dysfunction may depend on the location of brain lesions. The majority of the patients with CPs have a suprasellar lesion (~95 %); purely suprasellar, 20–46 %; both supra- and intrasellar, 39–75 %, and purely intrasellar, 1.5–15 % (Stahnke et al. 1984).

The treatment of the brain lesion by surgery may be a determinant for the incidence and severity of HP dysfunction. HP dysfunction is significantly increased and becomes almost universal in patients with CPs after neurosurgery (Matson 1964; DeVile et al. 1996; Pinto et al. 2000). In fact, severe GHD is more frequently found in patients with CPs after neurosurgery, ranging from 73 % to 100 % of the patients reported (Thomsett et al. 1980; Lyen and Grant 1982; Tiulpakov et al. 1998;

Gonc et al. 2004). In patients with CPs, total resection of tumors has been suggested to significantly increase the incidence and severity of HP dysfunction compared to subtotal resection alone and/or radiotherapy (Matson 1964; Thomsett et al. 1980), although it was challenged (Gonc et al. 2004; Di Battista et al. 2006; Trivin et al. 2009).

Overview of Growth Without Growth Hormone (GWGH)

Since Matson (1964) has first reported the cases of CPs with normal growth despite GHD, at least 180 cases of GWGH with CPs or other brain tumors after neurosurgery have been reported in the literature (Table 7.1). Approximately 39 % of the patients with brain tumors after neurosurgery grow normally or excessively. The majority of the patients with GWGH have CPs, and only a few case reports of GWGH with other sellar tumors have been documented, including astrocytoma and pinealoma (Finkelstein et al. 1972; Schoenle et al. 1995), chordoma (Saenger et al. 1974), glioma and tuberculoma (Gluckman and Holdaway 1976), teratoma (Araki et al. 2000), Langerhans cell histiocytosis (Nagasaki et al. 2010), or germinoma (Iwayama et al. 2011).

The location of brain tumors and the mode of surgery may affect the incidence of GWGH. GWGH has been more frequently found in the patients with suprasellar tumors (Bucher et al. 1983; Blethen and Weldon 1986; Tiulpakov et al. 1998). On the other hand, it was reported that 5 (42 %) of the 12 children with GWGH underwent a total resection of the tumors (Carmel et al. 1982). Thomsett et al. (1980) have shown that 4 (57 %) and 3 (43 %) of the 7 children with GWGH received total and partial resection of the tumors. Similarly, other investigators have suggested that the severity of HP dysfunction in the patients with GWGH was not related to the total or subtotal resection of the brain tumors (Di Battista et al. 2006). However, because of a limited data, it remains inconclusive whether the mode of surgery affects the incidence of GWGH among children with brain tumors after neurosurgery.

In patients with GWGH, the "catch-up" growth spurt is usually seen within the first 2 years after neurosurgery, which is often paralleled with weight gain (Holmes et al. 1968; Thomsett et al. 1980; Bucher et al. 1983; Sorva 1988; Tiulpakov et al. 1998). However, an unusual case of GWGH with teratoma has been reported (Araki et al. 2000), in which the linear growth was poor until 4 years without GH replacement therapy, but accelerated 5 years after neurosurgery despite before puberty. The "catch-up" growth spurt may be self-limited. It was reported that the linear growth was decelerated in older children with GWGH and that the final adult height for 3 (30 %) of the 10 patients with GWGH was more than −2.5 SD below the mean adult height for gender 1.5–6 years after neurosurgery (Blethen and Weldon 1986). In this study, all surviving patients with GWGH, who grew excessively, continued to grow at a relatively high or normal growth rate until the adult height was reached. Similar trend has been reported by other study (Bucher et al. 1983). Sorva (1988) has reported that of the 5 patients with CPs and GWGH, the growth rate declined in 1 with tumor recurrence, 1 subsequently needed the GH replacement therapy, and the remaining 3 (60 %) patients reached the final height with height SDS, ranging from +0.2 to −2.4 during 1.7–8.2 years after neurosurgery. In other series (Thomsett et al. 1980; Bucher et al. 1983; Schoenle et al. 1995; Tiulpakov et al. 1998), 57–100 % of the patients with GWGH achieved a relatively high or normal linear growth rate during 2–14 years after neurosurgery. These data suggest that some patients with GWGH do decelerate the linear growth 2 or more years after neurosurgery. Because of a lack of the long-term follow-up data, it remains unknown what is the frequency of the patients with GWGH who maintain normal or excessive linear growth till a final normal height is reached in adulthood.

GWGH and Puberty

Sex steroids, secreted by the control of gonadotropins (luteinizing hormone, LH, and follicle stimulation hormone, FSH), induce growth spurt

Table 7.1 Auxological and endocrinological data in children with GWGH after surgical resection of brain tumors

Reference	No. of patients with BT	No. of GWGH patients	No. of obese GWGH	Serum insulin at baseline			Insulin secretion after loading			Serum IGF-I			Serum IGFBP-3			Serum leptin			Serum prolactin		
				High	Normal	Low	High	Normal	Low	High	Normal	Low	High	Normal	Low	High	Normal	Low	High	Normal	Low
Holmes et al. (1968)	9	9	8	2	4	–	2	3	1		ND			ND			ND			ND	
Kenny et al. (1968)	10	3	3	–	1	–	1	–	–		ND			ND			ND		1	–	–
Finkelstein et al. (1972)	3	3	3	–	3	–	–	3	–	–	3	–		ND			ND			ND	
Saenger et al. (1974)	1	1	1	–	1	–		ND		–	1	–		ND			ND		–	1	–
Costin et al. (1976)	8	7	2	1	6	–	2	5	–	–	5	–		ND			ND		–	5	–
Gluckman and Holdaway (1976)	3	3	1	1	1	1		ND		–	3	–		ND			ND		2	1	–
Thomsett et al. (1980)	42	7	7		ND			ND			ND			ND			ND		1	4	–
Carmel et al. (1982)	43	12	NA		ND			ND			ND			ND			ND			ND	
Lyen and Grant (1982)	59	14	8		ND			ND			ND			ND			ND			ND	
Bucher et al. (1983)	19	13	9		NA		7	6	–	–	11	2		ND			ND		8	4	1
Stahnke et al. (1984)	28	10	8		ND		10	–	–	–	3	3		ND			ND		–	10	–
Blethen and Weldon (1986)	10	10	9	1	4	–	4	1	–	4	1	–		ND			ND		1	3	1
Sorva (1988)	22	5	3	–	4	–	3	1	–	–	1	3		ND			ND			ND	
Schoenle et al. (1995)	6	6	2	2	4	–		ND		–	–	6	–	1	5		ND			ND	
DeVile et al. (1996)	75	32	NA		ND			ND			ND			ND			ND			ND	
Tiulpakov et al. (1998)	25	4	NA		NA			NA			NA			NA			ND			NA	
Araki et al. (2000)	1	1	1	1	–	–		ND		–	–	1	–	–	1		ND		–	1	–
Pinto et al. (2000)	17	11	NA		NA			ND			ND			NA			NA			NA	
Pavlou et al. (2001)	1	1	1	1	–	–	1	–	–	–	–	1	–	–	1		ND		1	–	–
Srinivasan et al. (2004)	15	10	NA	–	4	–		NA		–	–	4		ND		4	–	–		ND	
Di Battista et al. (2006)	32	8	NA	6	2	–		ND		–	3	5		ND			ND			NA	
Nagasaki et al. (2010)	2	2	1	1	1	–		ND		–	–	2		ND		2	–	–		ND	
Simoneau-Roy et al. (2010)	15	5	NA		NA			NA			NA			ND		–	5	–		ND	
Iwayama et al. (2011)	14	3	2	3	–	–		ND		–	–	3	–	–	3	1	2	–	–	2	1
Total	460	180	69/98	19	35	1	30	19	1	4	31	30	0	1	10	7	7	0	14	31	3
(%)		(39)	(70)	(34)	(64)	(2)	(60)	(38)	(2)	(6)	(48)	(46)	(0)	(9)	(91)	(50)	(50)	(0)	(29)	(65)	(6)

BT brain tumors, *GWGH* growth without growth hormone, *IGF* insulin-like growth factor, *IGFBP* IGF binding protein, *NA* not available, *ND* not done

during puberty. Approximately 71–95 % of the patients with CPs have gonadotropin deficiency after neurosurgery (Thomsett et al. 1980; Lyen and Grant 1982; Stahnke et al. 1984; Schoenle et al. 1995; DeVile et al. 1996; Gonc et al. 2004; Srinivasan et al. 2004; Di Battista et al. 2006; Iwayama et al. 2011). Only 1 (5 %) boy of the 20 patients with CPs and gonadotropin deficiency, older than 12 years of age, has been shown to develop precocious puberty 6 years after neurosurgery (Di Battista et al. 2006). In other study, of the 48 patients with CPs, only 3 (6 %) boys had precocious puberty and 1 (2 %) girl showed full adult sexual maturation 6.7 years after neurosurgery (DeVile et al. 1996).

Because of hypogonadotropic-hypogonadism, the patients with GWGH also lack sex steroids, resulting in failure or delay of growth spurt during puberty. It was shown that 14 of the 15 patients, including the patients with GWGH, had abnormal serum levels of LH and FSH, which did not differ between the patients with GWGH and those without (Bucher et al. 1983). Holmes et al. (1968) have found that all 4 patients with GWGH, more than 15 years of age, remained sexually immature with no detectable gonadotropin excretion. It was reported that of the 14 patients with GWGH, only 1 boy (7 %) and 2 girls (14 %) had precocious puberty and pubertal development, respectively, 1–6 years after neurosurgery (Lyen and Grant 1982). Schoenle et al. (1995) have found that 4 of the 6 patients with GWGH had no puberty and that only 2 (33 %) patients, including one of each boy and girl, developed puberty. The replacement therapy with sex steroids or gonadotropin was necessary to induce the onset of puberty in the majority of the patients with CPs after neurosurgery, including the patients with GWGH (DeVile et al. 1996). These data suggest that hypogonadotropic-hypogonadism, resulting in delayed puberty, is associated with the majority of the patients with GWGH and that hormone replacement therapy is necessary to induce pubertal growth spurt in these patients.

Recently, serum levels of insulin and insulin-like growth factor (IGF)-I have been shown to be higher in girls with precocious puberty than healthy controls (Sorensen et al. 2012). Thus, increased serum levels of insulin and/or IGF-I may play a role for the development of "catch-up" growth spurt, especially in girls with GWGH. However, because of a lack of data, it remains elusive whether puberty may develop more frequently in patients with GWGH than those without, and whether insulin- and IGF-I-induced signaling pathways play a role for promoting "catch-up" growth spurt in patients with GWGH.

GWGH and Hyperinsulinemia

Hyperinsulinemia is highly associated with the patients with GWGH compared to those without (Bucher et al. 1983; Iwayama et al. 2011). The incidence of hyperinsulinemia in the patients with GWGH ranges from 11 % to 100 % in some series (Kenny et al. 1968; Costin et al. 1976; Gluckman and Holdaway 1976; Bucher et al. 1983; Stahnke et al. 1984; Blethen and Weldon 1986; Sorva 1988; Tiulpakov et al. 1998; Srinivasan et al. 2004; Di Battista et al. 2006; Simoneau-Roy et al. 2010; Iwayama et al. 2011). Of the 55 patients with GWGH reported, in whom the data for serum insulin levels are available, serum levels of insulin are increased in 19 (34 %), within normal range in 35 (64 %), and decreased in only 1 (2 %) (Table 7.1). Of the 50 patients with GWGH, in whom the data for insulin secretion after loading are available, the insulin secretion is increased in 30 (60 %), normal in 19 (38 %), and decreased in only 1 (2 %). These data, although limited, suggest that approximately one thirds of the patients with GWGH have hyperinsulinemia and that the ability of insulin secretion is well preserved in almost all of these patients. It is noteworthy that only 2 patients with GWGH who had low serum insulin levels and/or insulin secretion have been reported (Holmes et al. 1968; Gluckman and Holdaway 1976).

The peak serum levels of insulin in response to pharmacological loading have been shown to be higher in the CPs patients with GWGH than in those without (Bucher et al. 1983; Stahnke et al. 1984), and significantly correlated with linear growth, including the patients with GWGH (Stahnke et al. 1984). In addition, we have previously shown that some patients without GWGH

maintained normal linear growth within the first year postoperatively while hyperinsulinemia was present, whereas the subsequent linear growth was decelerated with a decrease in serum levels of insulin (Iwayama et al. 2011). Taken together, these data suggest a crucial role of insulin for promoting linear growth in patients with GWGH.

Hyperinsulinemia and Other Hormonal Factors in Obesity Associated with GWGH

GHD leads to increased fat mass, which is associated with metabolic derangements, including insulin resistance (Kreitschmann-Andermahr et al. 2010). Hyperphagia and obesity are commonly seen in children with CPs after neurosurgery (Sorva 1988; Roth et al. 1998; Srinivasan et al. 2004). The body mass index (BMI) in children with suprasellar CPs has been shown to be greater than that in those with intrasellar tumors (Tiulpakov et al. 1998). A positive correlation between plasma fasting insulin levels and BMI, IGF-I and IGF-II has been found in the patients with CPs before neurosurgery (Pinto et al. 2000). Similarly, serum fasting insulin levels and/or insulin secretion after loading have been shown to be positively correlated with BMI and weight gain in the CPs patients after neurosurgery (Tiulpakov et al. 1998). These data suggest that the location of brain tumor may affect the metabolism and body weight gain and that insulin and IGFs play an important role for the regulation of body weight gain and/or obesity in patients with CPs after neurosurgery.

Obesity is found in 70 % of the patients with GWGH reported in the literature (Table 7.1). It is commonly seen in the patients with GWGH who have suprasellar lesions, excessive growth, and associated hyperinsulinemia (Thomsett et al. 1980; Bucher et al. 1983; Sorva 1988; DeVile et al. 1996; Tiulpakov et al. 1998; Pavlou et al. 2001). The patients with GWGH and excessive growth have been found to be more obese than those with normal growth or without GWGH (Thomsett et al. 1980; Lyen and Grant 1982; Bucher et al. 1983). Similarly, the patients with GWGH have been shown to be more obese than those without before neurosurgery, and this trend becomes more profound after neurosurgery (Stahnke et al. 1984). Hyperphagia and obesity are commonly seen during the initial period of the "catch-up" growth spurt in the patients with GWGH after neurosurgery (Holmes et al. 1968; Stahnke et al. 1984; Sorva 1988; DeVile et al. 1996). In addition, some patients with GWGH but no obesity have normal serum levels of insulin and subnormal levels of IGF-I (Sorva 1988). In obesity, insulin resistance and associated hyperinsulinemia to overcome insulin resistance play an important role in the regulation of metabolism of glucose, free fatty acids and amino acids (Kreitschmann-Andermahr et al. 2010). In fact, the altered composition of the fatty acids in the subcutaneous adipose tissue has been found in the obese patients with GWGH and associated hyperinsulinemia (Holmes et al. 1968). These lines of clinical evidence suggest a crucial role of hyperinsulinemia in the regulation of energy balance and metabolism, leading to obesity, and that there is a positive relationship between body weight gain and/or obesity and serum levels of insulin and normal or excessive growth in patients with GWGH.

GH increases hepatic synthesis of IGF-I (Giustina et al. 2008). Under the conditions of GHD, GH-independent IGF-I secretion is an additional important metabolic regulator. Interaction between insulin and IGF-I through their own receptors regulates metabolism in obesity (Kreitschmann-Andermahr et al. 2010). In addition, the biological actions of IGF-I are regulated by IGF binding proteins (IGFBPs) (Giustina et al. 2008; Kreitschmann-Andermahr et al. 2010).

A positive correlation between BMI and serum levels of IGF-I, IGF-II and IGFBP-3 has been shown in the patients with CPs before or after neurosurgery (Tiulpakov et al. 1998; Pinto et al. 2000). In contrast, a negative correlation between BMI and serum levels of IGFBP-1 has been found in these patients (Tiulpakov et al. 1998). Obesity, hyperinsulinemia and/or high insulin secretion after loading as well as low serum levels of IGFBP-3 are associated with the majority of the patients with GWGH (Table 7.1). In addition, more than a half of the patients with GWGH have normal or high levels of IGF-I, suggesting that BMI may be positively correlated with serum

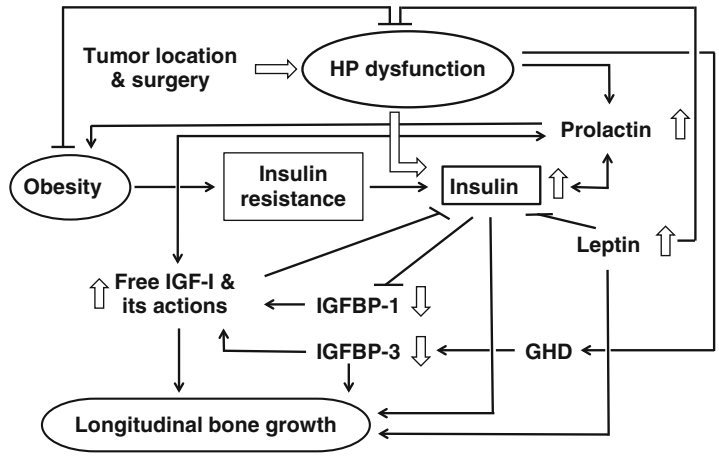

Fig. 7.1 The possible mechanisms of hyperinsulinemia and growth without growth hormone (GWGH). The location of brain tumors and/or the mode of surgery may affect serum levels of insulin and/or insulin secretion probably through an axis between hypothalamo-pituitary and pancreas. Insulin resistance associated with obesity increases insulin secretion. Insulin-like growth factor (IGF)-I suppresses insulin secretion, but plays a minor role for the regulation of insulin secretion. Leptin inhibits insulin secretion from the pancreas directly or by improving insulin resistance associated with obesity through inhibition of hypothalamic neuropeptide, resulting in reduced appetite. However, hyperinsulinemia cannot be corrected by hyperleptinemia. Hyperprolactinemia, resulting from disturbed secretion of the prolactin (PRL) inhibiting factor due to hypothalamic damage, increases food intake and body weight gain. Insulin and IGF-I stimulate PRL release from extrapituitary sites, including adipose tissue. Conversely, PRL stimulates insulin secretion and hepatic synthesis of IGF-I. Interaction between insulin/insulin receptors (IRs)- and IGF-I/IGFIR-induced signaling pathways stimulates proliferation of osteoblasts, resulting in acceleration of longitudinal bone growth. Insulin and growth hormone deficiency (GHD) reduce IGF binding protein (IGFBP)-1 and −3, respectively. Reduced serum levels of IGFBP-1 and -3 increase free fraction of IGF-I and its biological actions, including proliferation of osteoblasts. Decreased concentrations of IGFBP-3 by itself and leptin stimulate proliferation of osteoblasts. PRL may promote linear growth by increasing insulin secretion and IGF-I, resulting in activation of insulin/IRs- and IGF-I/IGFIR-induced signaling pathways. See in the text. →; stimulation, ┤; inhibition, =>; regulation (stimulation or inhibition)

levels of insulin and/or insulin secretion and IGF-I in patients with GWGH. On the contrary, BMI is likely to be negatively correlated with serum levels of IGFBP-3 in the patients with GWGH. This finding is in contrast to previous studies using the patients without GWGH (Tiulpakov et al. 1998; Pinto et al. 2000), in which a positive correlation was found between BMI and serum levels of IGFBP-3. A regulatory role of IGF-I for weight gain is controversial in the patients with GHD (Kreitschmann-Andermahr et al. 2010). However, these data suggest a role of IGF-I and IGFBP-3 and of interaction between insulin and these factors for the regulation of metabolism associated with obesity in patients with GWGH.

Leptin, secreted by adipose tissue, plays a major role for the regulation of fat metabolism (Roth et al. 1998; Mantzoros et al. 2011; Su et al. 2011). Congenital leptin deficiency results in marked obesity due to hyperphagia and failure to reach puberty without growth spurt (Mantzoros et al. 2011). Leptin reduces appetite by inhibiting hypothalamic neuropeptide Y, resulting in controlled food intake (Roth et al. 1998; Mantzoros et al. 2011). Hyperleptinemia associated with low insulin sensitivity has been found in the obese patients with CPs after neurosurgery (Srinivasan et al. 2004; Trivin et al. 2009; Simoneau-Roy et al. 2010). Serum levels of leptin have been shown to be increased in the obese patients with suprasellar CPs after neurosurgery, and positively correlated with BMI (Roth et al. 1998), suggesting a role of leptin for the regulation of weight gain and/or obesity and that the location of brain tumors and/or surgery may affect serum levels of leptin (Fig. 7.1). Of the 14 obese patients with GWGH reported, in whom the data for serum leptin levels are available, serum levels of leptin

are increased in 7 (50 %) and normal in the remaining 7 (50 %) patients, but none of the patients have low serum levels (Table 7.1). The studies in humans have shown that serum leptin levels are positively correlated with the percentage of body fat. Thus, normal or increased serum levels of leptin found in the patients with GWGH may represent the status of weight gain and/or obesity.

Leptin may synergize with IGF-I to affect body fat composition (Su et al. 2011). It was shown that serum levels of leptin were positively correlated with those of insulin and IGF-I in the obese patients with CPs but without GWGH after neurosurgery (Trivin et al. 2009). In contrast, no significant correlation has been found between BMI and insulin secretion or leptin in the patients with CPs after neurosurgery, including a small number of the patients with GWGH (Simoneau-Roy et al. 2010). In the 9 obese patients with GWGH reported, in whom the data for serum levels of insulin, IGF-I and leptin are available, serum levels of IGF-I are decreased despite normal or high serum levels of insulin and leptin (Table 7.1). These data may suggest that BMI is positively correlated with serum levels of insulin and leptin and negatively correlated with those of IGF-I in obese patients with GWGH, and that leptin and insulin rather than IGF-I play an important role for the regulation of body weight gain and/or obesity in some cases of GWGH with low serum levels of IGF-I. Because of a lack of enough data, it remains to be elucidated whether interaction between leptin and insulin or IGF-I plays a role for the regulation of body weight gain and/or obesity in patients with GWGH.

Prolactin (PRL) affects the regulation of body weight, differentiation of adipocytes, lipid metabolism, and adipogenesis (Ben-Jonathan et al. 2008). Hyperprolactinemia is associated with an increase in food intake and body weight gain (Ben-Jonathan et al. 2008). The basal serum levels of PRL have been shown to be significantly higher in the patients with GWGH than in those without or healthy children, and the patients with GWGH were highly associated with obesity, particularly during the first year postoperatively (Bucher et al. 1983), suggesting a role of PRL for obesity. However, of the 48 patients with GWGH reported, in whom the data for serum levels of PRL are available, only 14 (29 %) patients show hyperprolactinemia, whereas 31 (65 %) and 3 (6 %) patients have normal or low serum levels of PRL (Table 7.1). Obesity is associated with almost all of these patients. Similar observation has been reported by other study, in which mild hyperprolactinemia was only found in 20 % of the patients with CPs after neurosurgery and serum PRL levels were not significantly correlated with BMI (Tiulpakov et al. 1998). In addition, serum levels of PRL have been shown to be normal in both obese and non-obese patients with GWGH (Costin et al. 1976; Blethen and Weldon 1986; Araki et al. 2000; Iwayama et al. 2011). Furthermore, low serum levels of PRL have been found in the obese patients with GWGH (Schoenle et al. 1995). Thus, it remains inconclusive whether PRL plays a role for the regulation of weight gain and/or obesity in patients with GWGH.

Other Hormonal Factors Promoting Linear Growth in GWGH

IGFs/IGFBPs

Neither hyperinsulinemia nor increased insulin secretion after loading is associated with some patients with GWGH. Although such patients have normal serum levels of insulin and/or insulin secretion, other hormonal factors should be responsible for promoting linear growth. These hormonal factors include IGFs (IGF-I and -II) and IGFBP-3, which play a crucial role for the regulation of skeletal growth and bone metabolism (Giustina et al. 2008). It is little doubt that they contribute to normal growth in patients with GWGH, regardless of the presence or absence of hyperinsulinemia and/or high insulin secretion.

Little information is available about an alteration of serum IGF-I levels in patients with GWGH. Bucher et al. (1983) have shown that serum IGF-I levels were normal in all 7 patients with GWGH and excessive growth and that only 2 of the 6 patients with GWGH with normal

growth had low serum IGF-I levels. They have found that serum IGF-I levels were within normal range but significantly higher in patients with GWGH than in those without GWGH. Other investigators have reported similar finding that serum levels of somatomedin C (SMC; IGF-I) were higher in patients with GWGH than in those without, and, in addition, that some children with GWGH had marked reduction in serum levels of SMC when their growth rates were decelerated (Blethen and Weldon 1986). The patients with GWGH who already had abnormal low IGF-I levels during the first year postoperatively did the growth rate decelerate slowly, and the GH replacement therapy was subsequently initiated (Bucher et al. 1983). In addition, serum levels of IGF-I have been shown to be positively correlated with linear growth in the patients with CPs after neurosurgery, which was the most important predictor of linear growth rate (Tiulpakov et al. 1998). These data suggest a crucial role of IGF-I for promoting linear growth in patients with GWGH.

Of the 65 patients with GWGH reported, in whom the data for serum levels of IGF-I are available, 4 (6 %), 31 (48 %), and 30 (46 %) patients have high, normal, or low serum levels of IGF-I (Table 7.1). These data suggest that more than a half of the patients with GWGH have high or normal serum levels of IGF-I and that nearly half of those have low levels. Hyperinsulinemia and/or high insulin secretion after loading is found in almost all of the GWGH patients with low serum levels of IGF-I. In such patients, insulin-induced cell signaling may promote linear growth despite relatively low biological functions of IGF-I. In fact, we have found that serum levels of IGF-I were decreased in all 3 patients with GWGH and 7 of the 9 patients without GWGH and that the former but not the latter had hyperinsulinemia (Iwayama et al. 2011). These data suggest an important role of IGF-I and of interaction between insulin and IGF-I for the regulation of linear growth in patients with GWGH.

There is only one study showing an alteration of serum IGF-II levels in patients with GWGH, in which serum levels of IGF-II were within normal range, independent of the presence or absence of GWGH (Bucher et al. 1983), suggesting a minor role of IGF-II for linear growth in patients with GWGH. However, because of a lack of enough data, a role of IGF-II in the regulation of linear growth remains to be elucidated in patients with GWGH.

The biological functions of IGFs are regulated by IGFBPs (IGFBP-1-6) in the local cellular environment (Giustina et al. 2008). IGFBP-3 is a major component of the circulating IGF complex, and interacts with IGF-I receptor (IGFIR), leading to inhibition of the binding of IGF-I to IGFIR in a competitive manner. In addition, low concentrations of IGFBP-3 by itself stimulate bone growth in vivo (Giustina et al. 2008).

Serum levels of IGFBP-3 have been shown to be normal in 12 of 31 measurements, and a positive correlation was found between serum IGFBP-3 levels and linear growth in the CPs patients without GWGH after neurosurgery (Tiulpakov et al. 1998). Although this study included a small number of the patients with GWGH, the data for serum levels of IGFBP-3 in these patients are not available. Regarding an alteration of serum levels of IGFBP-3, 10 (91 %) patients with GWGH reported have low serum levels of IGFBP-3, whereas only 1 patient shows normal levels (Table 7.1). Serum IGFBP-3 levels are decreased in these patients because of a lack of GH-induced increase in IGFBP-3 concentrations (Giustina et al. 2008). Seven (70 %) of these 10 patients with GWGH and low serum levels of IGFBP-3 have hyperinsulinemia, suggesting a negative correlation between serum levels of IGFBP-3 and insulin in patients with GWGH. However, these GWGH patients with low serum levels of IGFBP-3 have low serum IGF-I levels. Despite low serum levels of IGF-I, low serum levels of IGFBP-3 may increase free fraction of IGF-I and its biological activity, and in addition, low serum levels of IGFBP-3 by itself can stimulate bone growth (Giustina et al. 2008). Thus, hyperinsulinemia and/or high insulin secretion, together with low serum levels of IGFBP-3, may account for normal linear growth in some cases of GWGH with low serum levels of IGF-I. Nonetheless, interaction between insulin, IGF-I

and IGFBP-3 plays a crucial role for the regulation of linear growth in patients with GWGH.

Leptin

Leptin has mitogenic effects on various cell types, and stimulate linear growth by regulating the energy balance, bone remodeling and proliferation of chondrocytes of the epiphyseal growth plate (Mantzoros et al. 2011). In addition, leptin stimulates IGF-I receptor gene expression and acts as a growth factor (Su et al. 2011).

Little information is available on the data for serum levels of leptin in patients with GWGH. All 14 patients with GWGH reported have normal or high serum levels of leptin (Table 7.1). In these patients, serum IGF-I levels are low, but serum insulin levels are normal or increased. These data, although limited, may suggest that serum levels of leptin are positively correlated with those of insulin, but negatively correlated with those of IGF-I. This finding is somewhat different from that in a previous study, in which serum levels of leptin were positively correlated with those of insulin and IGF-I in the patients with CPs without GWGH after neurosurgery (Trivin et al. 2009). The data from the patients with GWGH suggest that leptin by itself, or together with normal or high serum insulin levels, may contribute to linear growth. Because of a lack of enough data, it cannot be excluded that leptin stimulates bone growth through IGF-I actions (Mantzoros et al. 2011; Su et al. 2011).

Prolactin (PRL)

Hyperprolactinemia is found in 5–21 % of the patients with CPs after neurosurgery (Gonc et al. 2004), and often associated with hyperinsulinemia and insulin resistance (Ben-Jonathan et al. 2008). Serum levels of PRL are increased or normal in the majority of the patients with GWGH reported (Table 7.1). In these patients, serum levels of IGF-I are normal and those of insulin and/or insulin secretion are normal or high, suggesting a positive relationship between serum levels of PRL and IGF-I and insulin in patients with GWGH. In support of this finding, serum levels of PRL have been shown to be higher in the patients with GWGH than those without, and they were positively correlated with serum levels of IGF-I in the patients with GWGH during prepubertal period (Bucher et al. 1983). Normally, synthesis of IGF-I is stimulated by GH. However, under GHD conditions, hyperprolactinemia may be responsible for the generation of normal amounts of IGF-I in patients with GWGH (Bucher et al. 1983). This is further supported by the fact that an association of hyperprolactinemia and increased serum IGF-I levels has been found in hypopituitarism (reference in Bucher et al. 1983). In addition, experimental data suggest that PRL stimulates hepatic synthesis of IGF-I (Bole-Feysot et al. 1998). Although there is no evidence for a direct role of PRL for promoting linear growth, PRL might promote linear growth through activation of insulin secretion and/or its interaction with IGF-I in patients with GWGH.

Discussion

Why Does Hyperinsulinemia Occur in Patients with GWGH?

The possible mechanisms of hyperinsulinemia associated with GWGH are illustrated in Fig. 7.1. An association of hyperinsulinemia with GWGH has been found not only in patients with neurosurgery of brain tumors but also in those with other HP lesions, suggesting the existence of an axis between HP and pancreas. This is further supported by the observation that the CPs patients with hypothalamic involvement had higher serum levels of insulin than those without after neurosurgery (Trivin et al. 2009). Hyperinsulinemia is highly associated with patients with GWGH after neurosurgery, and GWGH is commonly seen in patients with suprasellar tumor (Bucher et al. 1983; Blethen and Weldon 1986; Tiulpakov et al. 1998). Serum levels of insulin and/or insulin secretion have been shown to be greater in the patients with suprasellar CPs than in those with intrasellar

tumors, including a small number of the patients with GWGH (Tiulpakov et al. 1998). In addition, CPs by itself and neurosurgery have been suggested to modulate insulin secretion (Pinto et al. 2000). Although enough data are lacking, these observations suggest that the location of brain tumors and the mode of surgery may affect serum levels of insulin and/or the ability of insulin secretion, probably through an axis between HP and pancreas, in patients with GWGH.

Insulin increases free IGF-I by inhibiting IGFBP-1 (Kreitschmann-Andermahr et al. 2010). Conversely, IGF-I suppresses insulin secretion from β-cells of the pancreas and restore insulin sensitivity (Kreitschmann-Andermahr et al. 2010). The GWGH patients with high serum levels of IGF-I have high serum levels of insulin and/or insulin secretion (Table 7.1). In addition, despite that almost all of the patients with GWGH have high or normal serum levels of insulin and/or insulin secretion, only a half of these patients show normal or high serum IGF-I levels. This is in contrast to a previous study showing a positive correlation between serum levels of IGF-I and insulin secretion in the patients without GWGH after neurosurgery (Tiulpakov et al. 1998). These data from the patients with GWGH reported suggest that hyperinsulinemia and/or high insulin secretion cannot be corrected by IGF-I and that the inhibitory effect of IGF-I on insulin secretion plays a minor role for the regulation of serum levels of insulin and/or insulin secretion in patients with GWGH.

Insulin resistance, a state of reduced sensitivity of insulin-responsive tissues to insulin, is commonly associated with obese patients with CPs after neurosurgery (Srinivasan et al. 2004; Simoneau-Roy et al. 2010). Insulin secretion is increased to overcome insulin resistance, affecting glucose metabolism and cell differentiation and proliferation. Thus, insulin resistance might induce hyperinsulinemia in patients with GWGH, particularly in those associated with obesity. So far, there is no study examining a role of insulin resistance in patients with GWGH and those without.

In vitro and in vivo studies suggest that leptin reduces insulin release from β-cells of the pancreas under physiological conditions, and restore the insulin sensitivity (Mantzoros et al. 2011). However, serum leptin levels have been shown to be positively correlated with those of insulin in the obese patients with CPs after neurosurgery (Trivin et al. 2009). Despite hyperleptinemia, hyperinsulinemia and low insulin sensitivity are often associated with the patients with GWGH (Simoneau-Roy et al. 2010). All GWGH patients with normal or increased serum levels of leptin have normal or high serum levels of insulin (Table 7.1), suggesting a positive correlation between serum levels of leptin and insulin. These clinical observations suggest that hyperinsulinemia cannot be corrected by hyperleptinemia and that the inhibitory effect of leptin on insulin secretion plays a minor role for the regulation of insulin secretion in patients with GWGH.

PRL is released not only from lactotrophs of pituitary cells, which is regulated by hypothalamic dopaminergic neurons, but also from extrapituitary sites, including adipose tissue (Ben-Jonathan et al. 2008). The stimulatory factors for extrapituitary PRL release include insulin and IGF-I. PRL is more potent and has longer-lasting action than GH to increase glucose-stimulated insulin secretion, insulin synthesis, and proliferation of pancreatic β-cells (Ben-Jonathan et al. 2008). Normal or high serum levels of insulin and/or insulin secretion after loading are found in almost all of the GWGH patients with normal or high serum levels of PRL (Table 7.1). These data suggest a positive correlation between serum levels of PRL and insulin and that PRL may be a determinant of hyperinsulinemia in patients with GWGH (Bucher et al. 1983).

A Role of Insulin and Interaction Between Insulin and Other Factors for Promoting Linear Growth in GWGH

A number of possible mechanisms of GWGH have been proposed, including hyperinsulinemia, IGF-I and possively IGF-II, hyperprolactinemia, GH variants and structurally similar lactogenic

hormones as well as other possible and unidentified growth factors. In this section, we will discuss a role of insulin and of its interaction with other hormonal factors, including IGF-I, leptin and PRL, for promoting linear growth in patients with GWGH (Fig. 7.1).

A role of Insulin for Promoting Linear Growth

Insulin-induced cell signaling may promote linear growth in patients with GWGH. In fact, a role of insulin as a growth factor has been suggested in other clinical setting. For example, children with diabetes mellitus show growth retardation, and insulin treatment can induce catch-up growth (Laron 2008). A genetically determined low response of insulin secretion has been associated with some children with idiopathic short stature (Laron 2008).

The diverse effects of insulin are mediated by its binding to cell-surface insulin receptors (IRs), which belongs to a family of transmembrane receptor tyrosine kinases, consisting of two isoforms, IR-A and IR-B (Siddle 2011). Insulin binds to both isoforms with similar affinity. IGF-I exclusively binds to its receptor, IGFIR, but IGF-II have greater affinity for IR-A than IR-B, and thus IR-A is a significant mediator of IGF-II action at physiological concentrations (Siddle 2011). Insulin binds to both IRs and IGF receptors (IGFRs), leading to activation of phosphoinositide 3-kinase (PI3K), which, in turn, activates the serine/threonine kinase Akt, a major downstream effector of PI3K. Activation of PI3K/Akt plays a crucial role for insulin-mediated biological effects, including insulin-induced metabolic processes such as stimulation of glucose uptake, activation of glycogen synthase, and inhibition of hepatic gluconeogenesis. On the other hand, the binding of insulin to IRs and IGFRs results in activation of the Ras/Raf-1/MEK/ERK signaling pathway, which mediates insulin-induced cellular growth and differentiation, including osteoblasts (Giustina et al. 2008; Laron 2008; Kawai and Rosen 2009), leading to promotion of linear growth.

IRs have a high homology with IGFRs, and, in addition, there is a 40–50 % homology between the entire molecule of insulin and that of IGF-I (Laron 2008). Thus, insulin may exert its biological effects, including growth promoting actions, directly or through interaction with IGF-I-induced signaling system. Both IR isoforms can form hybrids with IGFRs (Laron 2008; Siddle 2011). Hetero-dimerisation of pro-receptors, generating insulin/IGF hybrid receptors, occurs with similar efficiency to homo-dimerisation (Laron 2008). IGFs can bind to these hybrid receptors with similar affinity to IGFRs, and insulin can bind to the hybrid receptors with lower affinity than IRs. To date, the physiological role of insulin/IGF hybrid receptors remains unknown in humans.

Insulin and Bone Metabolism

In pre-pubertal children, bone age is predominantly influenced by GH and thyroxine (Giustina et al. 2008). Despite normal or excessive linear growth, the bone age has been shown to be delayed in some patients with CPs and GWGH after neurosurgery (Holmes et al. 1968; Gluckman and Holdaway 1976; Bucher et al. 1983; Sorva 1988; Pavlou et al. 2001), indicative of poor skeletal maturation. In contrast, no delayed or even increased bone age has been reported in the patients with GWGH (Finkelstein et al. 1972; Thomsett et al. 1980). The fact that patients with GWGH achieve normal or excessive linear growth despite retarded bone maturation suggests that GH-independent growth-promoting mitogenic activity in bone may be well preserved in these patients despite a lack of GH/IGF-I axis activity.

Insulin markedly stimulates differentiation of pre-cartilage cells to chondroblasts and chondrocytes in vitro (Laron 2008). A recent in vitro study has shown that insulin/IRs-induced signaling in osteoblasts regulates bone acquisition, suggesting the presence of a bone-pancreas axis through which insulin signaling in the osteoblasts ensures differentiation of osteoblasts and stimulates osteocalcin production, which, in turn, regulates insulin

sensitivity and pancreatic insulin secretion (Fulzele et al. 2010). The insulin/IRs-induced signaling pathway, which is implicated in the regulation of proliferation of osteoblasts and bone metabolism, may contribute to promotion of linear growth in patients with GWGH.

Interaction Between Insulin and IGFs/IGFBPs

Longitudinal bone growth is determined by proliferation and differentiation of chondrocytes in the epiphyseal growth plate. From postnatal to puberty, GH and IGF-I play a critical role for the regulation of not only skeletal growth but also bone modeling and remodeling (Giustina et al. 2008). Systemic IGF-I is synthesized predominantly by the liver in GH-dependent manner, but IGF-I is also synthesized in extrahepatic tissues in GH-independent manner, where it acts as a local growth factor (Giustina et al. 2008). In circulation, IGF-I forms a complex with IGFBPs or the acid labile subunit. IGF-I exerts growth-promoting properties through its binding to the receptor, IGFIR. The availability and biological activity of IGF-I are regulated by IGFBPs, particularly IGFBP-3, and less than 1 % of total serum IGF-I exists as a free hormone (Kawai and Rosen 2009). Reduced concentrations of IGFBP-3 caused by GHD (Giustina et al. 2008) enhance the biological actions of IGF-I through a decrease in its inhibitory effect on the binding of IGF-I to IGFIR. Insulin increases free fraction of IGF-I by inhibiting hepatic synthesis of IGFBP-1 (Giustina et al. 2008; Kreitschmann-Andermahr et al. 2010). Although IGF-II shares similar biological properties to IGF-I, it is much more active during prenatal life, and IGF-I is the predominant regulator of linear growth from postnatal to prepubertal periods (Giustina et al. 2008).

The binding of IGF-I to IGFIR initiates receptor autophosphorylation in the intracellular kinase domain, thereby activating similar cell signaling pathways utilized by insulin/IRs-induced signaling, including PI3K/Akt and Ras/Raf-1/MAP pathways. IGF-I/IGFIR-induced activation of PI3K/Akt pathway plays a critical role for skeletal acquisition and of Ras/Raf-1/MAP pathway stimulates the proliferation of osteoblasts, leading to acceleration of longitudinal bone growth (Kawai and Rosen 2009).

Clinical evidence supports the contention that IGF-I regulates bone growth and metabolism in GH-dependent and -independent ways. Decreased bone mineral density is associated with children with GHD and low serum levels of IGF-I, and the GH replacement therapy improves bone mass, which is accompanied by increased serum levels of IGF-I (Kawai and Rosen 2009). On the other hand, the human recombinant IGF-I therapy increases the linear growth rate in children with short stature, IGF-I deficiency and GH insensitivity (Chernausek et al. 2007), suggesting that IGF accelerates bone growth in GH-independent manner.

Despite a lack of GH/IGF-I axis activity, serum levels of IGF-I have been shown to be greater in the patients with CPs after neurosurgery, and correlated with linear growth and bone age (Tiulpakov et al. 1998). Hyperinsulinemia and normal serum levels of IGF-I have been found most frequently in the patients with CPs who had fast growing despite GHD (Tiulpakov et al. 1998). So far, only 1 case of GWGH with hypoinsulism but normal serum levels of IGF-I has been reported in the literature (Gluckman and Holdaway 1976). In addition, increased insulin secretion has been suggested to maintain nearly normal serum levels of IGF-I in children with CPs (Pinto et al. 2000). This is further supported by the fact that insulin increases free serum IGF-I levels through inhibition of IGFBP-1 (Kreitschmann-Andermahr et al. 2010). Serum levels of IGF-I have been shown to be normal in patients with GWGH, but low in those with decelerated growth (Bucher et al. 1983). Taken together, these data suggest a crucial role of interaction between insulin- and IGF-I-induced signaling pathways for promoting linear growth in patients with GWGH.

GH promotes renal phosphate absorption directly or through IGF-I actions. A patient with GWGH has been reported, in whom the GH-dependent renal retention of phosphate and serum levels of IGF-I were persistently low and

normalized with GH replacement therapy (Pavlou et al. 2001). These observations suggest that the GH-dependent renal retention of phosphate, contributing to skeletal development and bone mineralization, may be impaired in patients with GWGH. IGF-I induces phosphate retention by raising the renal threshold for phosphate, independent of parathyroid hormone (PTH) and vitamin D activity (Giustina et al. 2008). It also mediates anabolic actions of PTH in bone and reproduces selected effects of PTH on proliferation and survival of osteoblasts. IGF-I modulates renal 1α-hydroxylase and 24-hydroxylase activities, with increased production of active 1,25-dihydroxyvitamin D3, contributing to bone mineralization (Giustina et al. 2008). Serum IGF-I levels are normal or high in 54 % of the patients with GWGH reported (Table 7.1). In these patients, these IGF-I-mediated cellular processes may be relatively well preserved, but those with low serum IGF-I levels may develop retarded bone maturation.

Do the diverse effects of hyperinsulinemia on promoting linear growth require normal serum levels of IGF-I in patients with GWGH? Hypoinsulism and low serum levels of IGF-I are uniform features of the CPs patients without GWGH after neurosurgery (Bucher et al. 1983; Iwayama et al. 2011). Hyperinsulinemia associated with normal serum levels of IGF-I have been more frequently found in the patients with GWGH and excessive growth than those with GWGH and normal growth or those without GWGH (Bucher et al. 1983). Increased or normal serum levels of insulin and/or insulin secretion, together with normal IGF-I levels, are most frequent features of the patients with GWGH (Table 7.1), which may explain normal or excessive linear growth in these patients. However, nearly a half of the GWGH patients with increased or normal serum levels of insulin and/or insulin secretion show low serum levels of IGF-I. These data suggest a predominant role of insulin for promoting linear growth in patients with GWGH, regardless of the presence or absence of low serum levels of IGF-I. However, some GWGH patients with normal serum levels of insulin and low IGF-I levels do decelerate the linear growth subsequently (Bucher et al. 1983). To our best knowledge, there is no case of GWGH reported in the literature, in which both serum levels of insulin and/or insulin secretion and IGF-I are decreased. Taken together, these lines of clinical evidence suggest a predominant role of insulin for promoting linear growth but that an alteration of serum levels of both insulin and IGF-I may be a determinant for linear growth in patients with GWGH.

Interaction Between Insulin, Leptin and Prolactin for Linear Growth

Serum levels of leptin have been found to be low and associated with lower bone age in children with GHD (Su et al. 2011). The serum fasting insulin levels have been shown to be positively correlated with IGF-I and leptin in the patients with CPs before or after neurosurgery (Pinto et al. 2000; Trivin et al. 2009). It is likely that serum levels of leptin are positively correlated with serum levels of insulin and/or insulin secretion in the patients with GWGH reported (Table 7.1). In vitro and in vivo studies have shown that leptin increases bone growth by regulating bone marrow stroma cells, proliferation of osteoblasts and osteoclastogenesis (Mantzoros et al. 2011). Although a crosstalk exists between the insulin- and leptin-induced signaling pathways, especially PI3K (Mantzoros et al. 2011), there is no evidence for a role of interaction between insulin and leptin for the regulation of bone growth. Children with congenital leptin deficiency have normal linear growth, but those with the leptin receptor mutation develop early growth delay (Mantzoros et al. 2011). This raises a question as to whether leptin plays a role for linear growth in patients with GWGH. Further studies are needed to clarify a role of leptin-induced signaling, including the leptin receptor mutation, and of interaction between leptin and insulin for promoting linear growth in patients with GWGH.

Hyperprolactinemia, resulting from disturbed secretion of the PRL inhibiting factor due to hypothalamic damage, have been found in children

with GWGH after neurosurgery. PRL enhances pancreatic insulin secretion and hepatic synthesis of IGF-I (Bole-Feysot et al. 1998; Ben-Jonathan et al. 2008), which, in turn, may promote linear growth thorough activation of insulin- and IGF-I-induced signaling pathways. Conversely, insulin and IGF-I stimulate the release of PRL (Bole-Feysot et al. 1998).

As discussed earlier, a positive correlation between serum levels of PRL and insulin has been found in the patients with GWGH reported in the literature. Of the 38 patients with GWGH, in whom the data for both serum levels of PRL and IGF-I are available, 28 (74 %) patients show normal or high serum levels of IGF-I (Table 7.1). In addition, serum levels of PRL are normal or high in the majority of the patients, suggesting a positive correlation between serum levels of PRL and IGF-I. In support of this finding, serum PRL levels have been shown to be higher in patients with GWGH than in those without, and there was a positive correlation between serum levels of PRL and IGF-I in all prepubertal patients with GWGH (Bucher et al. 1983). These data suggest an important role of PRL for the generation of normal amounts of IGF-I and of interaction between insulin, IGF-I and PRL, which may promote linear growth. Further studies are needed to determine whether PRL and its interaction with insulin or IGF-I play a role for the regulation of linear growth in patients with GWGH.

Do Children with GWGH Need GH Replacement Therapy for Their Quality of Life?

Despite normal or excessive linear growth, children with GWGH still have metabolic abnormalities after neurosurgery, including obesity, insulin resistance, dyslipidemia, fatty liver and retarded bone age (Sorva 1988; Schoenle et al. 1995; Pavlou et al. 2001; Srinivasan et al. 2004; Nagasaki et al. 2010; Simoneau-Roy et al. 2010). Recent case reports have shown the beneficial effect of GH replacement therapy on metabolic abnormalities in children with GWGH. The short-term (4-day) GH replacement therapy has been suggested to improve renal retention of phosphate in a patient with GWGH (Pavlou et al. 2001). The long-term (2-year) GH replacement therapy has been shown to accelerate the linear growth in a patient with GWGH, but not in the other patient (Nagasaki et al. 2010). In this study, dyslipidemia was improved in both cases, but the percentage of body fat decreased in 1 patient. The long-term (1-year) GH replacement therapy failed to increase linear growth but decreased BMI in the patients with GWGH (Schoenle et al. 1995). These observations raise an important clinical issue as to whether the patients with GWGH should be treated with GH replacement therapy for improving linear growth and metabolic abnormalities. Further studies would be necessary to address whether GH replacement therapy improves the metabolic abnormalities and enables the patients to reach normal height in adulthood.

In summary, the patients with brain tumors involving HP area develop various endocrine disorders, including GHD, before neurosurgery. The HP dysfunction becomes universal and more profound after neurosurgery, but some patients achieve normal or excessive growth despite GHD, being recognized as GWGH. The patients with GWGH are likely to have suprasellar tumors, hyperinsulinemia and/or high insulin secretion, and obesity. It remains elusive why hyperinsulinemia occurs in patients with GWGH. However, the data to date collectively suggest that the location of brain tumors and/or the mode of surgery, insulin resistance associated with obesity, IGF-I, IGFBP-1 and −3, leptin and PRL may contribute to the regulation of serum levels of insulin and/or insulin secretion in these patients. Despite extensive studies, the mechanism of GWGH remains to be elucidated. Besides its metabolic effects, insulin exerts the diverse effects as a growth factor, including proliferation and differentiation of osteoblasts and bone metabolism, leading to acceleration of linear growth. Interaction between insulin/IRs- and IGF-I/IGFIR-induced signaling pathways and of insulin with other hormonal factors such as leptin or PRL may play a crucial role for promoting linear growth in patients with GWGH.

Despite normal or excessive linear growth, children with GWGH still have metabolic abnormalities and retarded bone maturation. This raises an important clinical issue as to whether GH replacement therapy solves these problems and enables the patients to reach normal height in adulthood. Better understanding for the mechanisms of GWGH is essential to improve the quality of life of patients with GWGH. Further studies would be necessary to address these issues in more detail in the future.

Acknowledgements The authors are grateful to Drs. T. Kamijo and H. Mizuno for their helpful suggestions.

References

Araki K, Koga M, Okada T, Kurashige T, Naruse K, Hiroi M (2000) A boy with normal growth in spite of growth hormone deficiency after resection of a suprasellar teratoma. Endocr J 47(Suppl):S101–S104

Ben-Jonathan N, LaPensee CR, LaPensee EW (2008) What can we learn from rodents about prolactin in humans? Endocr Rev 29:1–41

Blethen SL, Weldon VV (1986) Outcome in children with normal growth following removal of a craniopharyngioma. Am J Med Sci 292:21–24

Bole-Feysot C, Goffin V, Edery M, Binart N, Kelly PA (1998) Prolactin (PRL) and its receptor: actions, signal transduction pathways and phenotypes observed in PRL receptor knockout mice. Endocr Rev 19:225–268

Bucher H, Zapf J, Torresani T, Prader A, Froesch ER, Illig R (1983) Insulin-like growth factors I and II, prolactin, and insulin in 19 growth hormone-deficient children with excessive, normal, or decreased longitudinal growth after operation for craniopharyngioma. N Eng J Med 309:1142–1146

Carmel PW, Antunes JL, Chang CH (1982) Craniopharyngiomas in children. Neurosurgery 11:382–389

Chernausek SD, Backeljauw PF, Frane J, Kuntze J, Underwood LE, GH Insensitivity Syndrome Collaborative Group (2007) Long-term treatment with recombinant insulin-like growth factor (IGF)-I in children with severe IGF-I deficiency due to growth hormone insensitivity. J Clin Endocrinol Metab 92:902–910

Costin G, Kogut MD, Phillips LS, Daughaday WH (1976) Craniopharyngioma: the role of insulin in promoting postoperative growth. J Clin Endocrinol Metab 42:370–379

DeVile CJ, Grant DB, Hayward RD, Stanhope R (1996) Growth and endocrine sequelae of craniopharyngioma. Arch Dis Child 75:108–114

Di Battista E, Naselli A, Queirolo S, Gallarotti F, Garré ML, Milanaccio C, Cama A (2006) Endocrine and growth features in childhood craniopharyngioma: a mono-institutional study. J Pediatr Endocrinol Metab 19(Suppl 1):431–437

Finkelstein JW, Kream J, Ludan A, Hellman L (1972) Sulfation factor (somatomedin): an explanation for continued growth in the absence of immunoassayable growth hormone in patients with hypothalamic tumors. J Clin Endocrinol Metab 35:13–17

Fulzele K, Riddle RC, DiGirolamo DJ, Cao X, Wan C, Chen D, Faugere MC, Aja S, Hussain MA, Brüning JC, Clemens TL (2010) Insulin receptor signaling in osteoblasts regulates postnatal bone acquisition and body composition. Cell 142:309–319

Giustina A, Mazziotti G, Canalis E (2008) Growth hormone, insulin-like growth factors, and the skeleton. Endocr Rev 29:535–559

Gluckman PD, Holdaway IM (1976) Prolactin and somatomedin studies in the syndrome of growth hormone-independent growth. Clin Endocrinol (Oxf) 5:545–549

Gonc EN, Yordam N, Ozon A, Alikasifoglu A, Kandemir N (2004) Endocrinological outcome of different treatment options in children with craniopharyngioma: a retrospective analysis of 66 cases. Pediatr Neurosurg 40:112–119

Holmes LB, Frantz AG, Rabkin MT, Soeldner JS, Crawford JD (1968) Normal growth with subnormal growth-hormone levels. N Engl J Med 279:559–566

Iwayama H, Kamijo T, Ueda N (2011) Hyperinsulinemia may promote growth without GH in children after resection of suprasellar brain tumors. Endocrine 40:130–133

Kawai M, Rosen CJ (2009) Insulin-like growth factor-I and bone: lessons from mice and men. Pediatr Nephrol 24:1277–1285

Kenny FM, Iturzaeta NF, Mintz D, Drash A, Garces LY, Susen A, Askari HA (1968) Iatrogenic hypopituitarism in craniopharyngioma: unexplained catch-up growth in three children. J Pediatr 72:766–775

Kreitschmann-Andermahr I, Suarez P, Jennings R, Evers N, Brabant G (2010) GH/IGF-I regulation in obesity-mechanisms and practical consequences in children and adults. Horm Res Paediatr 73:153–160

Laron Z (2008) Insulin-a growth hormone. Arch Physiol Biochem 114:11–16

Lyen KR, Grant DB (1982) Endocrine function, morbidity, and mortality after surgery for craniopharyngioma. Arch Dis Child 57:837–841

Mantzoros CS, Magkos F, Brinkoetter M, Sienkiewicz E, Dardeno TA, Kim SY, Hamnvik OP, Koniaris A (2011) Leptin in human physiology and pathophysiology. Am J Physiol Endocrinol Metab 301:E567–E584

Matson DD (1964) Craniopharyngioma. Clin Neurosurg 10:116–129

Nagasaki K, Tsumanuma I, Yoneoka Y, Jinguji S, Ogawa Y, Kikuchi T, Uchiyama M (2010) Metabolic effects of growth hormone replacement in two pediatric

patients with growth without growth hormone. Endocr J 57:771–775

Pavlou M, Tsatsoulis A, Efstathiadou Z, Bitsis S, Papadopoulou ZL (2001) A study of the growth-promoting and metabolic effects of growth hormone (GH) in a patient with the "growth without GH" syndrome. Growth Horm IGF Res 11:225–230

Pinto G, Bussières L, Recasens C, Souberbielle JC, Zerah M, Brauner R (2000) Hormonal factors influencing weight and growth pattern in craniopharyngioma. Horm Res 53:163–169

Roth C, Wilken B, Hanefeld F, Schröter W, Leonhardt U (1998) Hyperphagia in children with craniopharyngioma is associated with hyperleptinaemia and a failure in the downregulation of appetite. Eur J Endocrinol 138:89–91

Saenger P, Levine LS, Wiedemann E, Schwartz E, New MI (1974) Growth with absent growth hormone by radioimmunoassay. J Pediatr 85:137–138

Schoenle EJ, Zapf J, Prader A, Torresani T, Werder EA, Zachmann M (1995) Replacement of growth hormone (GH) in normally growing GH-deficient patients operated for craniopharyngioma. J Clin Endocrinol Metab 80:374–378

Siddle K (2011) Signalling by insulin and IGF receptors: supporting acts and new players. J Mol Endocrinol 47:R1–R10

Simoneau-Roy J, O'Gorman C, Pencharz P, Adeli K, Daneman D, Hamilton J (2010) Insulin sensitivity and secretion in children and adolescents with hypothalamic obesity following treatment for craniopharyngioma. Clin Endocrinol (Oxf) 72:364–370

Sorensen K, Aksglaede L, Petersen JH, Andersson AM, Juul A (2012) Serum IGFI and insulin levels in girls with normal and precocious puberty. Eur J Endocrinol 166:903–910

Sorva R (1988) Children with craniopharyngioma. Early growth failure and rapid postoperative weight gain. Acta Paediatr Scand 77:587–592

Srinivasan S, Ogle GD, Garnett SP, Briody JN, Lee JW, Cowell CT (2004) Features of the metabolic syndrome after childhood craniopharyngioma. J Clin Endocrinol Metab 89:81–86

Stahnke N, Grubel G, Lagenstein I, Willig RP (1984) Long-term follow-up of children with craniopharyngioma. Eur J Pediatr 142:179–185

Su PH, Chen JY, Yu JS, Chen SJ, Yang SF (2011) Leptin expression and leptin receptor gene polymorphisms in growth hormone deficiency patients. Hum Genet 129:455–462

Thomsett MJ, Conte FA, Kaplan SL, Grumbach MM (1980) Endocrine and neurologic outcome in childhood craniopharyngioma: review of effect of treatment in 42 patients. J Pediatr 97:728–735

Tiulpakov AN, Mazerkina NA, Brook CGD, Hindmarsh PC, Peterkova VA, Gorelyshev SK (1998) Growth in children with craniopharyngioma following surgery. Clin Endocrinol (Oxf) 49:733–738

Trivin C, Busiah K, Mahlaoui N, Recasens C, Souberbielle JC, Zerah M, Sainte-Rose C, Brauner R (2009) Childhood craniopharyngioma: greater hypothalamic involvement before surgery is associated with higher homeostasis model insulin resistance index. BMC Pediatr 9:24

Childhood Brain Tumours: Proton Beam Therapy

8

Yasmin Lassen-Ramshad, Jørgen B. Petersen, Akmal Safwat, Henrik Pagh Schultz, and Morten Høyer

Contents

Y. Lassen-Ramshad (✉) • A. Safwat
H.P. Schultz • M. Høyer
Oncological Department, Aarhus University Hospital, Aarhus, Denmark
e-mail: yasmlass@rm.dk

J.B. Petersen
Department of Medical Physics, Aarhus University Hospital, Aarhus, Denmark

Abstract

There is a long tradition for multidisciplinary therapy which includes surgery, chemotherapy and radiotherapy in the treatment of paediatric malignancies. In most childhood brain tumours radiotherapy is a necessity for the achievement of local control. However, radiation treatment may also lead to serious late side effects that may affect the quality of life of the children who become long time survivors.

The dosimetric advantages of proton beams make them very attractive for paediatric radiotherapy.

There are three main advantages of using protons instead of photons:

1. Protons reduce late side effects by sparing normal tissue,
2. Because of the reduced side effects, it might be possible to escalate the radiation dose resulting in better tumour control and
3. Protons reduce the risk of secondary malignancy

The advantage of protons over photons has been demonstrated in several treatment planning studies, but there are no randomized

M.A. Hayat (ed.), *Tumors of the Central Nervous System, Volume 12,*
DOI 10.1007/978-94-007-7217-5_8, © Springer Science+Business Media Dordrecht 2014

controlled studies proving the superiority of protons. Nevertheless, a large number of hospital based modern proton facilities are currently under construction and in the close future protons will be available for a larger group of cancer patients, especially for children. This chapter describes the basic principles of proton radiotherapy and provides a review of the literature on paediatric brain tumours irradiation with special emphasis on the value of proton radiotherapy.

Introduction

Long Term Outcome in Childhood Malignancies

The incidence of malignancies in children under 15 years in the developed countries is 140 per million. The most common are leukemias, brain tumours and lymphomas. The survival rates are about 80 % after 5 years for the whole group of paediatric cancers, ranging from over 90 % for Hodgkin's lymphoma and retinoblastoma to 60 % for AML and cPNET (Kaatsch 2010). These survival rates are very much in contrast to the survival rates in the 1960s where the 5 year overall survival rate for all paediatric cancer patients was only 30 % (Robison et al. 2009). The increase in survival is a result of improvements in diagnostic methods and therapies such as surgery, radiation therapy, chemotherapy and supportive care, and it is especially due to the introduction of a multidisciplinary approach which now characterizes paediatric oncology.

Although the survival improvement is a success, it appears that cure comes at a high price as survivors are at a high risk for chronic morbidity such as cardiovascular, pulmonary, musculoskeletal, endocrine diseases or heavy neurocognitive impairment. Brain tumours are the second most common childhood cancers and survivors of childhood brain cancer have a high risk for functional and cognitive impairments. These patients often present with multiple morbidities such as seizures, auditory or visual and neurocognitive disturbances or endocrine disorders (Oeffinger et al. 2006). On top of this, these patients have a considerably increased risk for secondary radiation induced cancer. As seen in the studies of the Japanese atomic bomb survivors, children have a higher sensitivity for radiation induced cancer than adults. The lifelong risk of having a radiation induced cancer is age dependent, and varies between children and adults by a factor of 10. Scatter radiation inside the treated patient is also more important in the small body of a child than in a large body of an adult. Some childhood malignancies also have genetical susceptibilities that make them more likely to develop a radiation induced cancer (Hall 2006).

However, by combining radiotherapy with chemotherapy it has become possible to reduce the radiation dose in some patient groups. This has been shown in randomised studies, especially for low risk medulloblastoma where the total dose to the craniospinal axis in some patients could be reduced when RT is combined with chemotherapy. In addition, chemotherapy may be used to postpone RT in small infants. Since the brain in infants less than 3 years old is especially vulnerable to radiation it is of utmost importance, whenever possible, to delay RT until after this age. In intracranial low risk germinoma, chemotherapy has replaced the craniospinal irradiation and radiation is only needed for the periventricular and initial tumour volumes.

Finally, prophylactic brain irradiation is now most often omitted after chemotherapy for childhood leukemia. These changes in treatment policy will lead to a reduction in the long term morbidity after childhood cancer therapy.

Modern Radiotherapy

The present literature on radiation related morbidity following therapy for childhood brain cancer is based on the use of traditional photon therapy. Use of photon radiotherapy inevitably leads to unintended exposure of the surrounding normal tissue. Until recently two to four photon fields were usually used to achieve an acceptable homogeneous dose to the tumour volume. As a

result of these beam arrangements large volumes of normal brain received a dose which potentially leads to radiation induced morbidity. It has been the goal of the technological development in modern radiotherapy to reduce the radiation dose to the normal tissue.

Accurate patient alignments by use of imaging of the patients in the treatment position at the accelerator immediately prior to each treatment session represent a major step forward in radiation therapy. Image guided radiation therapy (IGRT) is based on either mega-voltage X-rays delivered by the accelerator or by kilo-voltage systems that are mounted on the accelerator. Both technologies allow for planar and volumetric imaging. Most sophisticated is the cone-beam CT which allows acquisition of CT images which are matched to the treatment planning scans. From these matched images, errors in positioning can be determined and the patient can be accurately repositioned.

Another technological development has been to conform the dose distribution more precisely to the tumour volume. Intensity modulated radiotherapy (IMRT) is a technique which uses advanced treatment planning algorithms and powerful computers. The use of multiple beams shaped by a multi-leaf collimator enables dose distributions conforming to the shape of the target with a steep dose fall-off outside the target. By volumetric arc therapy (VMAT), the radiation is delivered during one or two perpendicular gantry rotations around the patient. Novel technologies are now being developed with the specific purpose to deliver IMRT under IGRT guidance. The tomotherapy machine is a compact LINAC integrated with a MV single-slice CT scanner which treats the patient slice-by-slice with simultaneous imaging of the treated volume.

IMRT is useful in the therapy of a number of childhood brain tumours. As an example, it has become possible to spare the inner ear in the therapy of posterior fossa medulloblastoma. However, by IMRT or VMAT the radiation dose is being re-distributed from critical normal tissue to less critical normal tissue or over a larger volume with less dose and the total body dose is increased because of leakage radiation by the accelerator equipment. Modelling studies have suggested an increased risk for secondary malignancies when IMRT is used (Hall 2006).

Proton Radiotherapy

William Bragg discovered the deposition of ionization density at the end of the path of alpha particles already in 1905. Protons are charged particles produced by removing an electron from a hydrogen atom. They deposit almost all their energy in a very narrow spot, the Bragg Peak, and there is only a small exit dose. Because of their mass, their penetration in depth can be controlled. They have thus a finite range in the body. This physical characteristic can be used to spare normal tissue beyond the tumour and to keep the irradiated volume and thus late side effects low.

In 1954, the first patient was treated with proton irradiation of the pituitary gland at Berkeley University. Until recently, proton units were mainly operated by physical laboratories that were conducting physical particle research but allowed radiation oncologist clinics to use their accelerators with dedicated time slots for patients. Technical development offering lighter and more comfortable machines has increased the availability of proton therapy for the radiation community in the last years. Although these treatment facilities have a high cost and despite the fact that protons are not the usual standard of care in the therapy of a large number of tumour types, the number of hospital based proton centers under planning or under construction worldwide is increasing considerably. Thirty-five proton treatment units exist today, of which seven have an energy that only permits the treatment of ocular lesions. Nineteen other units are in a planning or construction phase. So far, more than 96,000 patients have been treated with protons worldwide (PTCOG 2012).

The unique dose distribution characteristics of protons allowing a high dose at the end of their path with virtually no exit dose make them particularly attractive in the field of paediatric radiotherapy. The total dose to the body is lower for protons than for photons and might lessen the risk for induction of secondary cancers (Fig. 8.1).

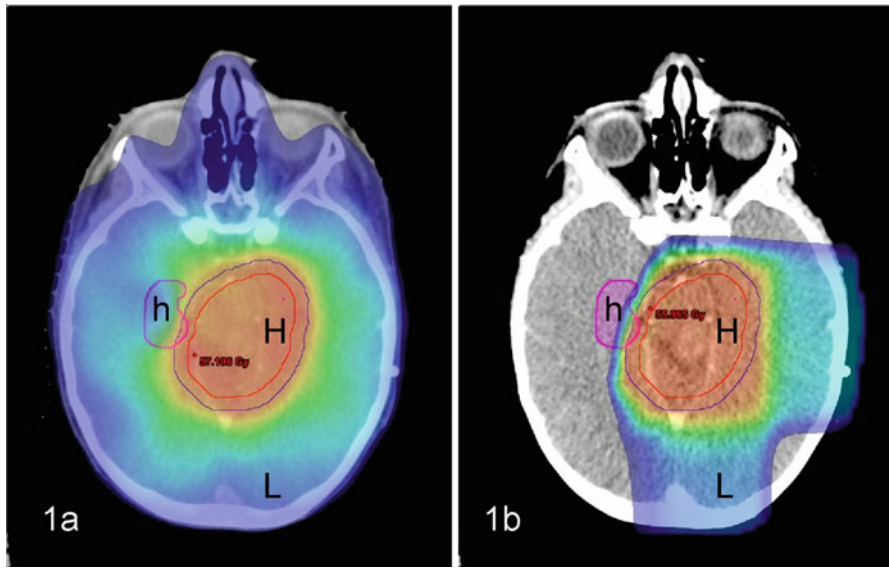

Fig. 8.1 Treatment planning study for a 3 year old child with a glioma. (**a**) Shows a VMAT photon plan and (**b**) a two field proton plan for a treatment with 54 Gy. (The threshold dose of the dose colorwash was set to 7 Gy). The low dose area *L* is spread out over a much larger volume with the VMAT plan, the high dose area *H* is nearly identical for the two techniques and highly conformal to the target. The right hippocampus *h* can be better spared by the proton plan

Although photons and protons differ with respect to the physical dose distribution, they are almost identical in regards to the radiobiological effects. Protons have a very discrete increased radiobiological effectiveness (RBE) with respect to photons. In general, the dose of 1 Gy in protons is equivalent to 1.1 Gy in photons.

The high precision of proton beams is a challenge in treatment delivery. Proton radiation plans are less robust than photon radiation plans. Minor changes in patient anatomy or set up errors can increase or decrease the beam range and dose delivered to the patient and can thus lead to an increase or decrease of dose in the target and the organs at risks. Image guided techniques and firm immobilization are therefore of utmost importance in proton therapy.

As stated above proton treatment can be especially attractive in paediatric radiotherapy as long time survivors are not at risk for developing functional impairments and secondary cancers. However, there is a lack of statistical evidence to demonstrate the clinical superiority of proton treatment. Some studies have shown that local control is comparable to photon treatment, but there are as yet no published studies on late morbidity after proton therapy (Brada et al. 2009). Some caution is also advisable, since the risk of secondary cancer might be higher than theoretically estimated for proton treatment because of neutron contamination with some proton delivery systems. There are no randomized controlled trials comparing the therapies in children and it is controversial whether conduction of such trials would be possible or desirable. Right now there are not enough proton facilities worldwide to meet the needs for treatment of paediatric patients therefore it is not realistic to expect that all children needing radiotherapy will be treated with protons. Accordingly, a case selection is necessary. It must be emphasized that protons are mainly superior to photons when patients are treated for cure. In case of palliative radiotherapy there is no or very little advantage of protons.

As large randomized controlled face-to-face trials comparing modern photon and proton radiotherapy are not expected to be conducted, it is important that all information on children treated on routine basis are collected in databases and evaluated. It is therefore desirable that all

children treated with modern treatment modalities such as photon IMRT or proton radiotherapy are included in large multi-institutional databases for registration of local control, survival and late morbidity outcomes.

The following review will focus mainly on childhood brain tumours with a good prognosis, when proton therapy is expected to have an important impact on the long term outcome compared with modern photon treatment.

Photon Radiotherapy for Common Childhood Brain Tumours

Medulloblastoma

Primitive neuroectodermal tumours (PNET) arise from the neural crest. PNET tumours of the posterior fossa of the brain are referred to as medulloblastoma.

Due to their location adjacent to the fourth ventricle they often cause increased intracranial pressure at the time of diagnosis. They are considered as grade IV tumours in the WHO classification and have an aggressive growth not only locally but also by their potential to disseminate in the whole subarachnoid space.

Radiation therapy to the complete cerebrospinal axis combined with systemic therapy has dramatically improved survival and today medulloblastoma patients have a 5 year survival rate of 60–80 % depending on their risk profile.

Treatment for medulloblastoma includes surgical resection, radiotherapy and chemotherapy. The surgery needs to be as radical as possible. Standard risk patients have no or only residuals following surgery and no dissemination to the cerebrospinal fluid (CSF) or along the surbarachnoidal space. High risk patients have macroscopic residual tumour following surgery or spread of tumour cells to the CSF. Radiotherapy consists of irradiation of the complete cerebrospinal axis and a boost in the posterior fossa. Chemotherapy has allowed reduction of the dose to the craniospinal axis in standard risk patients and the delay of radiotherapy in small infants. A routine prescription for standard risk patients is 23.4 Gy to the craniospinal axis combined with a boost in the posterior fossa to a total dose of 54–55 Gy. High risk patients need a radiation dose to the craniospinal axis of 36 Gy followed by a boost in the posterior fossa to a total dose of 55 Gy. Concomitant single agent chemotherapy is administered along with the radiotherapy and multidrug chemotherapy is continued for several cycles after completion of radiotherapy for all medulloblastoma patients. Newer protocols and studies are aiming to confine the boost volume to the tumour bed with a small margin instead of irradiating the whole posterior fossa.

Traditional irradiation of the craniospinal axis is conducted with photons. The technique consists of two lateral fields to include the whole brain and the upper cervical spine combined with posterior fields to cover the rest of the subarachnoidal space until the sacral roots. Often two to three posterior fields have to be applied depending on the length of the spinal cord. All the fields have to be perfectly matched and it has to be assured that field junctions between the fields are neither under- or overdosed. Although only the spinal cord is the desired target to treat, the beam will exit through the organs anterior to the spinal cord, thus resulting in a considerable dose to the vertebral bodies, the thyroid gland, the heart, the gastrointestinal tract, the lungs, the kidneys and the female reproductive tract, resulting in possible side effects to multiple organs from irradiation. With modern photon based IMRT techniques doses to organs anterior to the craniospinal axis like the mediastinum, the thyroid gland or the heart as well as structures anterior to the posterior fossa like the cochleae or the pituitary gland can be spared to some degree.

Electron irradiation of the spinal axis has been proposed and is practised in some institutions. It has the advantage that with the rapid fall off of dose at depth, tissues anterior to the spinal cord can be better spared. But matching with cranial photon fields and resulting dosimetric uncertainties make electrons difficult to use. Because of insufficient range of the electrons this technique may lead to underdosage of deeply located parts of the spinal subarachnoid space.

Nowadays prospective clinical studies often stratify patients according to immunohistochemical

and histological risk factors, and patients may be allocated to treatments designed according to the risk factors, but the principle of irradiating the whole subarachnoid space and boosting the tumour bed remains for the moment unchanged. Pattern of failure studies have shown that cerebral recurrences often occur in the posterior fossa, the subventricular area and the frontal area and it has been speculated whether the whole brain irradiation could be replaced with subtotal irradiation of the brain which includes these areas (Miralbell et al. 1997a, b).

Radiation remains an integral part of the therapy of medulloblastoma, but the risk for late morbidity for these patients is high because of the large volumes needing irradiation.

Low Grade Glioma

Low grade glioma originate from the glial cells. These tumours present a variety of different histologies and localisations in the brain. They often grow along the midline structures of the brain like the optical pathways, the hypothalamus and the brainstem and can also be found in the supratentorial hemispheres and the cerebellum. Long term survival is favourable in patients treated with macroradical resection. Radical resection can often be achieved in tumours of the supratentorial hemispheres, but more rarely in the cerebellum and in the midline regions where even a biopsy carries a risk of severe morbidity.

Radiotherapy is used for patients with progressing tumours where radical surgery is not possible. The timing of radiotherapy is controversial. Immediate postoperative radiotherapy in the case of residual disease has shown to increase the progression free survival, but not the overall survival. Therefore, radiotherapy is in general deferred in case of asymptomatic patients with slowly progressing low grade glioma. Radiotherapy is advised in the case of symptoms or progressing tumour at the time of recurrence. Trials are investigating the use of chemotherapy at progression of low grade glioma with the primary purpose of deferring radiotherapy as long as possible Radiotherapy is usually applied with conformal techniques with localized irradiation of the lesion and an appropriate margin for microscopic disease. The dose given is usually 45–54 Gy in 25–30 fractions depending on the site of the lesion. Small lesions have been successfully treated by some centers with stereotactic radiosurgery or fractionated stereotactic radiotherapy with favourable local control and morbidity (Kortmann et al. 2003). The overall survival of children with low grade glioma treated with radiotherapy is in the range of 80 % at 10 and 20 years after treatment.

Ependymoma

Ependymoma arise from the neuroepithelial linings of the ventricles. They are graded into grade II ependymoma and grade III anaplastic ependymoma. Two thirds of the tumours are located in the posterior fossa and one third in the hemispheres. It is mainly a neoplasm of children and adolescents, but one third of the patients are small infants (MacDonald and Yock 2010).

The standard treatment for cerebral ependymoma constists in gross tumour resection followed by radiation therapy. Radical surgery is an important prognostic factor and improves survival. If the surgery was not radical, a second look operation is often recommended. Postoperative chemotherapy may be considered in case of residual tumour (MacDonald and Yock 2010; Massimino et al. 2006).

Postoperative radiotherapy consists of involved field irradiation of the tumour bed with an appropriate margin to a total dose of 54 Gy. Radiotherapy yields a local control of up to 80 % if the initial surgery was radical (MacDonald and Yock 2010).

Less than 10 % of cerebral ependymoma disseminate into the subarachnoid space or the CSF. The pattern of failure is mainly locally, and postoperative craniospinal radiotherapy has been abandoned as a standard treatment for non disseminated tumours. In cases with CSF seeding the postoperative radiotherapy should include radiotherapy to the whole craniospinal axis with 36 Gy and a local boost to the spinal metastases and the initial tumour site.

Postoperative chemotherapy may defer radiotherapy in infants younger than 3 years old. Studies on young infants have conflicting results. There are reports on long term survival in infants treated by chemotherapy without radiotherapy. On the other hand several studies have shown that the progression free survival is impaired if radiotherapy is delayed to more than 1 year after surgery (MacDonald and Yock 2010; Koshy et al. 2011).

Craniopharyngioma

Craniopharyngioma are benign tumours arising from embryonic tissue in the pituitary region and often affect the functions of the optic chiasm, the hypothalmus and the pituitary gland. They often contain a mixture of cystic components and solid components.

The primary therapy is surgery, but as the lesions are situated in the area described, in close proximity to important risk organs, radical resection is often not possible. Postoperative radiotherapy is not needed in case of total tumour resection, but salvage radiotherapy is often used in case of progression after primary surgery. The overall survival is good, in most series approximately 80 % at 20 years after diagnosis.

Radiotherapy needs to be applied with a dose of at least 50 Gy (Fitzek et al. 2006). Although this tumour is often curable using combined treatment modalities, the patients often suffer from side effects related to therapy.

Intracranial Germinoma

Intracranial germ cell tumours are rare tumours that arise in the region of the third ventricle. Histologically, they are divided – like germ cell tumours in other locations – into pure germinoma and non-germinomateous germ cell tumours. In this section intracranial pure germ cell tumours will be described. These germ cell tumours may occur in children and in adolescents and have an excellent prognosis. Surgery may be omitted unless a histological confirmation of the diagnosis in addition to serum markers and MRI-scans is needed. These tumours may be cured with radiotherapy alone. Previously, radiotherapy of pure intracranial germ cell tumours included the whole craniospinal axis with a boost in the tumour region. Nowadays, the therapy consists of combined chemo- and radiotherapy where the later is restricted to the periventricular volume and a boost to the tumour volume.

Morbidity After Radiotherapy for Childhood Brain Tumours

In radiation therapy it is important to distinguish between acute, temporary toxicities like headache, nausea or fatigue starting during the course of radiotherapy and late complications. Acute side effects are often due to edema and are usually treated with steroids and disappear in less than 3 months after the treatment. Late toxicity is defined as toxicity appearing later than 3 months after the treatment, these side effects usually do not resolve and may become permanent. Neurocognitive impairments, neuroendocrine deficits, hearing loss, impaired vision, increased risk for vascular insult and secondary cancer are examples of late reactions caused by irradiation of the brain. Impaired thyroid gland-, cardiac- and pulmonary function, growth retardation and infertility may be late manifestations of irradiation of the craniospinal axis. The development of these morbidities is dose and often also volume dependent.

Neurocognitive Problems After Radiotherapy

Varying degrees of neurocognitive changes after cerebral irradiation unfortunately are a frequent occurrence and often result in reduced quality of life. Survivors have a lower chance of getting employed and of getting married (Fossati et al. 2009). The brain tumour itself and the surgical procedure may lead to intellectual deficits. This may be further worsened however by structural changes caused by radiation therapy. Endocrine disturbances and ototoxicity may attribute to the neurocognitive problems as well. Neurocognitive

decline is most pronounced after whole brain irradiation. The mechanism involved is mostly white matter loss, but vascular factors and glial cell atrophy may be responsible as well (Fossati et al. 2009).

Neurocognitive disturbances are more pronounced after irradiation of children than in adolescents or adults. Neurocognitive impairment is dose dependent and reduction of the whole brain irradiation dose from 36 to 23.4 Gy in standard risk medulloblastoma patients has resulted in less neurocognitive decline (Fossati et al. 2009).

The neurocognitive function has been correlated to the dose delivered to the whole brain, supratentoriel brain, and the temporal lobes. Regarding the dose to the supratentorial brain it was shown in a study of childhood ependymoma that the risk of neurocognitive loss was related not only to the irradiation of the high dose volume (> 40 Gy), but also the low dose volume (< 20 Gy) and even the very low dose volume (< 5 Gy). This has to be considered when treating these patients with IMRT because the very low dose and low dose volume will be increased with IMRT (Merchant et al. 2005). Unfortunately the supratentorial brain and temporal lobes, as well as the subventricular and hippocampal areas may often not be spared in the therapy of midline and supratentorial tumours. However, the dose to the brain outside the target should be kept at a minimum.

Neuroendocrine Problems After Radiotherapy

Endocrine effects occur as a consequence of irradiation of the hypothalamic-pituitary axis. Growth hormone deficiency may be caused by irradiation of the hypothalamic region and has an impact not only on growth, but also on metabolism, cardiovascular function and neurocognitive function. The threshold dose for development of neuroendocrine dysfunction is low; when doses > 16 Gy are given to the hypothalamus the patient may develop growth hormone deficiency. The higher the dose to the hypothalamus, the higher is the risk for growth hormone deficiency and the earlier it may appear (Merchant et al. 2011). This condition can be treated by growth hormone substitution. Accordingly it is important that children who have received radiotherapy to the hypothalamic region are screened regularly (Fossati et al. 2009).

Irradiation of the pituitary gland will often result in dysfunction of the gonadotropine axis. This may result in precocious puberty which together with growth hormone deficiency and irradiation of the vertebral bodies during craniospinal irradiation may lead to growth retardation. Patients should also be screened for adrenal cortical hormone deficiency and thyroid hormone deficiency due to a hypopituitarism.

Vascular Problems After Radiotherapy

It has been demonstrated that children treated for brain tumours have a higher risk of vasculopathy like Moyamoya disease and strokes and also for developing vascular malformations and aneurysms. In the childhood cancer survivor study cohort it has been shown that the relative risk of developing stroke after irradiation for childhood brain cancer was 7 % higher for patients than for their siblings, 25 years after radiotherapy. There was proposed a dose effect, with the risk for stroke increasing at doses above 30 Gy and the risk being highest at doses above 50 Gy. Endocrine changes can also attribute to this. Vascular changes after radiotherapy are more often seen in children with neurofibromatosis NF1. Venoocclusive disease and Moyamoya vasculopathy may already develop in the first years after radiotherapy. Mineralizing microangiopathia can already be seen at doses as low as 15 Gy. Some adult survivors are also at increased risk of developing migraine attacks several years after treatment (Morris et al. 2009).

Auditive Problems After Radiotherapy

Ototoxicity results from irradiation of the cochlear region and is a sensorineuronal hearing loss. It is dose dependent and the threshold dose

has been estimated at 35 Gy (Moeller et al. 2011). Hearing loss therefore often occurs if tumours are located in the posterior fossa, as it is the case for medulloblastoma or ependymoma. The risk is increased by addition of chemotherapy such as cisplatinum which is often given with radiotherapy in the treatment of medulloblastoma. New generations of protocols allowing restriction of the irradiated volume to the tumor bed instead of the whole posterior fossa will most likely have an impact on the risk of hearing loss. With modern photon based IMRT techniques the inner ears can often be spared.

Visual Problems After Radiotherapy

Reduced vision due to development of cataract may occur after irradiation of the lens at low doses of 7 Gy. In young children the frontal sinus is not well developed and therefore the cribriform plate is often located at the same level as the lens and the lens may receive some dose during radiation treatment of medulloblastoma. In pattern of failure studies, recurrences appeared at the cribriform plate because of shielding of the lens (Miralbell et al. 1997a, b). However, as cataract is relatively easily treatable, the dose coverage to the cribriform plate should not be compromised. Vision loss due to irradiation of the chiasm and the optical nerves is rare, as the dose of 54 Gy customarily employed for irradiation of childhood brain tumours is generally tolerated by the optic apparatus.

Secondary Cancer After Radiotherapy

Cancer secondary to irradiation is a concept founded mainly on radiobiological models as well as the experience of following the Japanese atomic bomb survivors. The field is filled with uncertainties and conflicting results.

Carcinogenesis is derived partly from the primary irradiation of the radiation field. This risk will probably be reduced in proton treatment as less radiation is necessary to achieve the same coverage of the target. But carcinogenesis is also induced by secondary radiation. In photon treatment secondary radiation is due to leakage from the accelerator head and multileaf-collimator. This stray irradiation is difficult to estimate and is generally not reported by treatment planning systems. With conformal radiotherapy techniques the tumour is irradiated through few portals with a homogenous dose and secondary cancers are expected to arise in the high dose volumes along with the treatment fields. In modern IMRT the high dose volume is reduced at the expense of increased medium and low dose volumes. It is speculated if IMRT techniques increase the risk of secondary cancer induction (Hall 2006).

Among children followed in the childhood cancer survivor study, medulloblastoma patients had the highest risk for death from secondary cancer in comparison to other childhood malignancies. It was concluded that increased risk for secondary cancer was due to the craniospinal irradiation which leads to secondary neoplasms in the brain as well as in the body (Armstrong et al. 2009).

Toxicities After Radiotherapy of the Craniospinal Axis

Irradiation of the entire spinal cord as in therapy for medulloblastoma leads to a considerable dose to organs anterior to the spinal cord resulting in acute as well as late toxicity. As acute toxicity the children often experience nausea which may be reduced with modern antiemetic therapy. The patients may also present with moderate mucositis. Transient haematological toxicity is also often present and haematological parameters need to be followed during treatment and at follow up.

Radiation induced cardiac diseases have been described especially after the treatment of mediastinal targets in Hodgkin's disease. They often develop several decades after the radiation therapy. The risk for cardiac morbidity in patients with Hodgkin's disease is even further increased by the use of anthracycline chemotherapy. Cardiac toxicity after craniospinal radiotherapy is less well studied. In treatment planning studies it has

been shown that the dose to the heart can be reduced by modern IMRT photon technique. Studies from the childhood cancer survivor study cohort show that patients with Hodgkins lymphoma or nephroblastoma are at the highest risk of cardiac mortality and that medulloblastoma patients even after a long period of follow up and treated with conventional photon treatment do not have an increased risk for cardiac mortality. However this cohort has not yet reached a plateau for late toxicity and cardiac toxicity might still arise at a later time in the craniospinal group (Armstrong et al. 2009).

Asymptomatic restrictive lung disease has been described in medulloblastoma patients and is attributed to radiotherapy not because of a high dose nor volume treated, but because of a reduced chest volume due to the reduced growth of the spine (Fossati et al. 2009).

Height and especially sitting height is impaired in medulloblastoma patients after craniospinal radiotherapy. This is due to both neuroendocrinological dysfunction and irradiation of the vertebral bodies. The lumbar spine is often more affected than the thoracic region and the upper cervical region seems to be least affected. The threshold dose for growth retardation seems to be approximately 25 Gy (Fossati et al. 2009).

Ovarian function may suffer after craniospinal irradiation and also after chemotherapy regimens containing especially alkylating agents (Fossati et al. 2009). Preservation of ovarian tissue is therefore advisable before radiotherapy. Likewise in boys sperm conservation is advisable prior to radiotherapy.

Proton Radiotherapy for Common Childhood Brain Tumours

Proton treatments, although already available for several decades have in the past mainly been used for the treatment of ocular melanoma or of skull base tumours. In the last decade proton treatment has gained much more interest in radiation oncology and many treatment planning studies for different tumour histologies and localisations have demonstrated that proton treatment is superior to photon treatment for sparing organs at risk that are not a part of the target region and makes it feasible to decrease the total body dose to the patient necessary to deliver the desired dose in the target.

Proton Radiotherapy for Medulloblastoma

In dose planning studies proton treatment has been shown to be important for decreasing the risk of late toxicities that can develop after craniospinal irradiation with a boost to the posterior fossa. When considering the different components of the treatment, target coverage is generally as good as with photon treatment. The technique for the neuraxis is often the same as with conventional photon treatment, lateral fields for the whole brain part, posterior fields for the spinal cord and often lateral fields for the boost to the posterior fossa.

Considering the whole brain part of the irradiation no normal brain tissue can be spared as the whole brain is the target. It was shown that with two posterior oblique proton fields the lens can be spared more efficiently without compromising coverage of the cribriform plate (Cochran et al. 2008).

Considering the irradiation of the spine, the target is essentially the subarachnoid space. The vertebral bodies are usually included to avoid asymmetrical growth. One treatment planning study showed that the dose to the vertebral body could be reduced to 6 Gy with protons a dose that is considered negligible for growth problems (Miralbell et al. 1997a, b). It is controversial if all the vertebral body has to be included into the target to avoid asymmetric growth. The organs in front of the spinal cord are not considered as targets but cannot be avoided with photon techniques unless modern IMRT techniques are used. Several treatment planning studies have shown that with proton treatment the dose to the heart and lungs is negligible and that the total body dose to the patient is reduced in comparison to modern photon techniques (Lee et al. 2005; St. Clair et al. 2004; Brodin et al. 2011; Miralbell et al. 1997a, b; Yoon et al. 2011). Also the ovaries can be spared (Fig. 8.2).

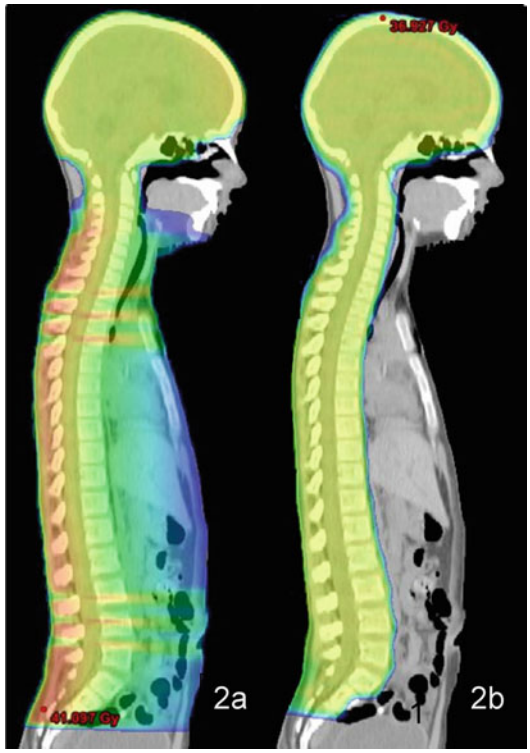

Fig. 8.2 Shows a treatment planning study for a 9 year old boy with a medulloblastoma for a treatment of the craniospinal axis with 35 Gy, (the threshold dose of the colour wash was set to 15 Gy). (**a**) Shows a photon plan and (**b**) shows a proton plan. The dose anterior to the spinal cord is neglectable in the proton plan, whereas in the photon plan a larger low dose area is found anterior to the spine

The boost irradiation to the posterior fossa increases the dose to organs at risk near the posterior fossa like the inner ear and the hippocampus, more distantly also to the pituitary gland, the temporal lobes and parts of the supratentorial brain. With 3 D conformal photon treatment all these structures receive considerable doses by the boost treatment. With intensity modulating techniques the dose to critical structures can be decreased to acceptable levels. With proton treatment the dose to the organs at distance in the supratentorial brain becomes negligible, the dose to the inner ear is reduced substantially and the total dose to the brain is diminished in comparison to modern photon techniques. As the supratentorial brain and the temporal lobes are not receiving as much from the boost dose in protons as in photon treatment, neurocognitive models have shown that the expected decline in intelligence after irradiation for medulloblastoma might be slower after proton radiotherapy than after photon radiotherapy (Merchant et al. 2008).

A clinical study that followed patients treated for medulloblastoma with proton therapy for ototoxicity showed that high grade ototoxicity was found only in 5 % of the patients at 1 year after treatment (Moeller et al. 2011).

Several treatment planning studies have tried to assess the risk for secondary cancer after irradiation of medulloblastoma patients with different techniques. However, it has to be emphasized that several uncertainties have to be accounted for when estimating the risk of radiation induced secondary cancer. Proton therapy decreases the risk of secondary cancer induction because of a lower total body dose to the patient. In proton treatment secondary radiation is due to neutron contamination, which can be higher with passive modulated treatment delivery techniques than with pencil beam scanning techniques. However, the pencil beam scanning techniques are more sophisticated and more challenging and most of the proton centers still employ the passive modulated technique (Hall 2006). Neutrons are important for carcinogenesis, but the amount of neutrons produced by proton treatments is again difficult to estimate and cannot be calculated by a treatment planning system. In general treatment planning studies show that the risk of developing secondary cancer is substantially reduced by protons also when secondary stray irradiation by neutrons is taken into account (Table 8.1).

Although the risk of secondary cancer can be substantially reduced by proton irradiation it will take several decades until this will be demonstrated in the clinical setting.

Proton Radiotherapy for Low Grade Glioma

Low grade glioma requires focal radiation therapy in the area of the brain where the tumour is situated. When the tumour is localised in the optical pathways, the optical nerves or the chiasm can

Table 8.1 Showing several doseplanning studies for development of secondary cancer in medulloblastoma and comparing proton and photon irradiation

Protons (%)	3 D Photons (%)	IMRT/VMAT/Tomo (%)	Endpoint	Reference
7	45	56	2ndary cancer	Brodin et al. (2011)
			Lifetime risk	
			Dose 23.4 Gy	
9	56	71	2ndary cancer	Brodin et al. (2011)
			Lifetime risk	
			Dose 36 Gy	
0.05	0.71	0.43	2ndary cancer	Miralbell et al. (2002)
			Yearly incidence after radiotherapy	
4.4–5.1	54.8	31.4	2ndary cancer	Newhauser et al. (2009)
			Lifelong risk	

be either part of the target volume or very close to it. Similarly, the hypothalamus and the pituitary gland are in close relationship with these structures. Additionally the medial parts of the temporal lobes and sometimes the hippocampal zone as well can be close to the target. When the tumour is localised in the supratentorial hemispheres, sparing of the controlateral hemisphere is very important, a feat that can be difficult to achieve with modern photon IMRT techniques as the volume irradiated with low doses is substantially increased. When the tumour is localised in the cerebellum, the inner ears, the brain stem as well as the hippocampal zones might be near the target volume.

Although stereotactic photon radiotherapy methods spare normal tissue effectively when the target is small, a treatment planning study showed that protons could spare the normal brain better than stereotactic treatment delivered by linacs or gamma knife and that this effect became more pronounced with larger or more irregular shaped lesions (Verhey et al. 1998).

One series of 27 children treated for low grade glioma with protons had comparable local control and survival data compared to photon data and no recurrence was found at the field margins or outside the high dose region. No serious late effects apart from one case of Moyamoya vascular disease in a child with neurofibromatosis were noted after a median follow up of 3.3 years (Hug et al. 2002).

In a treatment planning study of optical pathway low grade glioma comparing irradiation with protons and photons it was shown in a neurocognitive model that the differences in dose to the structures important for neurocognitive function was only small but that it was still expected that this would be clinically significant (Merchant et al. 2008).

Proton Radiotherapy for Ependymoma

Radiotherapy for childhood ependymoma usually consists in focal irradiation to the posterior fossa carrying a risk for late toxicities concerning the auditory, neurocognitive and endocrine function and a risk of vascular disease and secondary malignancies.

A cohort of 17 ependymoma patients were treated with localised radiotherapy with protons. Tumours were located both infra- as supratentorially. The outcome data after a median follow up of 26 months were excellent, the proton treatment did not impair local control or survival. Subtotally resected patients had a worse outcome than radically resected, as expected. No major toxicity was seen in the patients so far at follow up (MacDonald et al. 2008).

A treatment planning study of an ependymoma case with a neurocognitive model analysing the dose to the neurocognitive structures showed that

these structures could be spared better by protons than by photons (Merchant et al. 2008). That could also be confirmed in a second treatment planning study that analysed doses to the same structures (MacDonald et al. 2008). This is noteworthy as the patients are often very young children and neurocognitive late effects can be expected to be worsened when treatment is done at a younger age. In the two studies it was also demonstrated that the dose to the hypothalamus can be decreased significantly by protons in comparison to conventional photons or photon IMRT. The same was true for the dose to the inner ear (MacDonald et al. 2008).

Proton Radiotherapy for Craniopharyngioma

Craniopharyngioma are usually situated in the midbrain area and treated if indicated with local irradiation in this area. This can lead to toxicities from the optical apparatus, the endocrine system, the vascular system and the neurocognitive functions. Two studies have reported outcome and toxicity data of children treated with protons for craniopharyngioma. The outcome data are good and in the same range as for comparative photondata, demonstrating that local control is not impaired by more conformal therapy. In one study, five irradiated children also finished high school, and three of them went to college, all were living independently at follow up. These children did not experience any serious side effects from the radiation treatment after a median follow up of 13 years (Fitzek et al. 2006). In another study three children out of 12 long time survivors experienced serious side effects at a mean follow up of 60 months. One child had developed hypopituitarism, one child an ischemic episode and one child a meningioma. This child had also received photon radiotherapy at an earlier time in the same location (Luu et al. 2006).

A treatment planning study with a neurocognitive model analysed doses to the neurocognitive structures in cranophayngioma patients with protons and photons. The difference in dose to these structures was small but was assumed to be clinically significant (Merchant et al. 2008).

Another treatment planning study in craniopharyngioma patients has shown that the dose to the central vessels could be reduced with protons in comparison to photon IMRT therapy (Boehling et al. 2012).

Craniopharyngioma poses a particular challenge to radiotherapy because the cysts can alter their volume during the several weeks of irradiation. An increase in the size of the cysts especially during the beginning of the treatment has been described, sometimes necessitating an aspiration of the cysts. Studies have demonstrated that regular interfractional scanning of the target volume is necessary to assess the size of the cystical components during treatment and that adaptive replanning often has to be performed. Assessment of the cyst size is critically important as target coverage is very precise with proton therapy (Winkfield et al. 2009).

Proton Radiotherapy for Intracranial Germinoma

As these tumours have an excellent prognosis, the long term survivors are at risk for developing long term sequelae that can be mainly neurocognitive and endocrine as the periventricular area and the tumour is irradiated.

The early outcome data for 22 children treated with proton therapy for germ cell tumours after a median follow up of 28 months showed that the local control was excellent, as expected. One patient had a peritoneal failure attributed to a ventriculoperitoneal shunt. As late complications only growth hormone and thyroid hormone deficiency have been noted. The authors also made a treatment planning study of a periventricular irradiation case comparing protons with intensity modulating photon irradiation. The dose to the temporal lobes and to the whole brain was significantly reduced by proton treatment, although the paraventricular hippocampal zone could not be spared. It was noted that the ocular lenses received

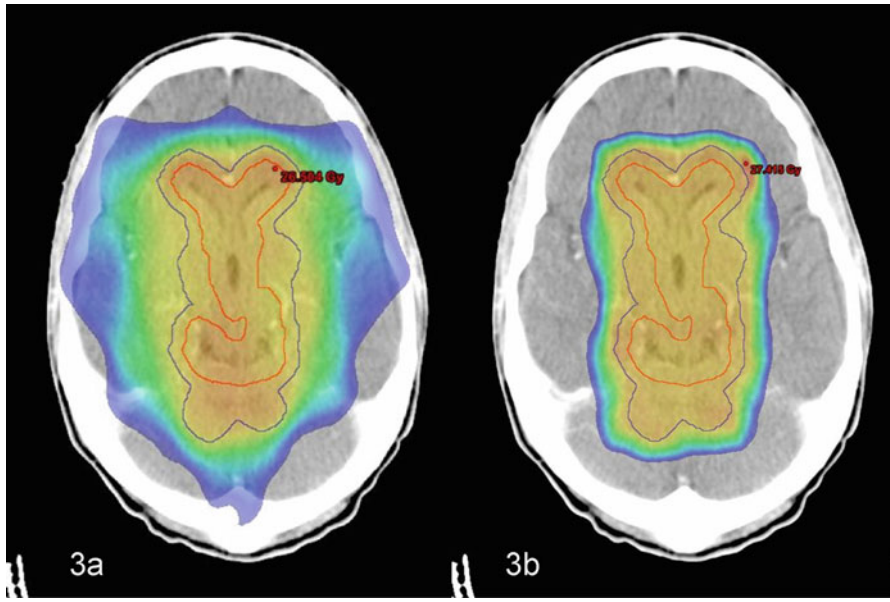

Fig. 8.3 Shows a treatment planning study for a 17 year old adolescent with a cranial germinoma for a treatment with 26 Gy in the ventricular area. (The threshold dose for the colorwash was set to 15 Gy). (**a**) Shows a six field IMRT plan. (**b**) Shows a three field proton plan. The proton plan is highly conformal and the lateral temporal lobes are better spared from low and intermediate dose

radiation doses that could induce a cataract with the photon plan. The lenses could be completely spared by the protons (MacDonald et al. 2011) (Fig. 8.3).

Conclusion

Radiotherapy is an important part in the multidisciplinary treatment of childhood brain tumours. For some tumours chemotherapy has permitted a decrease in the radiation dose or volume necessary for achieving local control. However, in most curable childhood brain tumours radiotherapy cannot be omitted.

With modern radiotherapy techniques doses to organs at risk outside the target volume can be efficiently spared by using intensity modulating photon techniques. The disadvantage of these very efficient techniques is a redistribution of the radiation dose to a larger low dose region and an increase of the total body dose distant to the target, which might lead to an increase in secondary cancer in the future.

Proton radiotherapy has been shown in both dose planning studies as well as in forthcoming clinical studies that organs at risks are efficiently spared by the favourable dose depth characteristics that allow for sparing organs beyond the target. In addition, organs that are relatively close to the target can be better spared than with any photon technique and dose to organs further away can become negligible, simultaneously the total dose to the body is decreased and thus the risk for developing a secondary cancer can be reduced at the same time.

This makes protons especially interesting for the use in paediatric malignancies and it is to be hoped that more proton facilities will soon be available so that children with curable diseases necessitating radiotherapy will have an easy access to proton radiotherapy.

References

Armstrong GT, Liu Q, Yasui Y, Neglia JP, Leisenring W, Robison LL, Mertens AC (2009) Late mortality among 5-year survivors of childhood cancer: a summary from the childhood cancer survivor study. J Clin Oncol 27(14):2328–2338

Boehling NS, Grosshans DR, Bluett JB, Palmer MT, Song X, Amos RA, Sahoo N, Meyer JJ, Mahajan A, Woo SY

(2012) Dosimetric comparison of three-dimensional conformal proton radiotherapy, intensity-modulated proton therapy, and intensity-modulated radiotherapy for treatment of pediatric craniopharyngiomas. Int J Radiat Oncol Biol Phys 82(2):643–652

Brada M, Pijls-Johannesma M, De Ruysscher D (2009) Current clinical evidence for proton therapy. Cancer J 15(4):319–324

Brodin NP, Rosenschold PM, Aznar MC, Kiil-Berthelsen A, Vogelius IR, Nilsson P, Lannering B, Bjork-Eriksson T (2011) Radiobiological risk estimates of adverse events and secondary cancer for proton and photon radiation therapy of pediatric medulloblastoma. Acta Oncol 50(6):806–816

St Clair WH, Adams JA, Bues M, Fullerton BC, La Shell S, Kooy HM, Loeffler JS, Tarbell NJ (2004) Advantage of protons compared to conventional X-ray or IMRT in the treatment of a pediatric patient with medulloblastoma. Int J Radiat Oncol Biol Phys 58(3): 727–734

Cochran DM, Yock TI, Adams JA, Tarbell NJ (2008) Radiation dose to the lens during craniospinal irradiation-an improvement in proton radiotherapy technique. Int J Radiat Oncol Biol Phys 70(5):1336–1342

Fitzek MM, Linggood RM, Adams J, Munzenrider JE (2006) Combined proton and photon irradiation for craniopharyngioma: long-term results of the early cohort of patients treated at Harvard Cyclotron Laboratory and Massachusetts General Hospital. Int J Radiat Oncol Biol Phys 64(5):1348–1354

Fossati P, Ricardi U, Orecchia R (2009) Pediatric medulloblastoma: toxicity of current treatment and potential role of protontherapy. Cancer Treat Rev 35(1):79–96

Hall EJ (2006) Intensity-modulated radiation therapy, protons, and the risk of second cancers. Int J Radiat Oncol Biol Phys 65(1):1–7

Hug EB, Muenter MW, Archambeau JO, DeVries A, Liwnicz B, Loredo LN, Grove RI, Slater JD (2002) Conformal proton radiation therapy for pediatric low-grade astrocytomas. Strahlenther Onkol 178(1):10–17

Kaatsch P (2010) Epidemiology of childhood cancer. Cancer Treat Rev 36(4):277–285

Kortmann RD, Timmermann B, Taylor RE, Scarzello G, Plasswilm L, Paulsen F, Jeremic B, Gnekow AK, Dieckmann K, Kay S, Bamberg M (2003) Current and future strategies in radiotherapy of childhood low-grade glioma of the brain. Part I: treatment modalities of radiation therapy. Strahlenther Onkol 179(8):509–520

Koshy M, Rich S, Merchant TE, Mahmood U, Regine WF, Kwok Y (2011) Post-operative radiation improves survival in children younger than 3 years with intracranial ependymoma. J Neurooncol 105(3): 583–590

Lee CT, Bilton SD, Famiglietti RM, Riley BA, Mahajan A, Chang EL, Maor MH, Woo SY, Cox JD, Smith AR (2005) Treatment planning with protons for pediatric retinoblastoma, medulloblastoma, and pelvic sarcoma: how do protons compare with other conformal techniques? Int J Radiat Oncol Biol Phys 63(2):362–372

Luu QT, Loredo LN, Archambeau JO, Yonemoto LT, Slater JM, Slater JD (2006) Fractionated proton radiation treatment for pediatric craniopharyngioma: preliminary report. Cancer J 12(2):155–159

MacDonald SM, Yock TI (2010) Proton beam therapy following resection for childhood ependymoma. Childs Nerv Syst 26(3):285–291

MacDonald SM, Safai S, Trofimov A, Wolfgang J, Fullerton B, Yeap BY, Bortfeld T, Tarbell NJ, Yock T (2008) Proton radiotherapy for childhood ependymoma: initial clinical outcomes and dose comparisons. Int J Radiat Oncol Biol Phys 71(4):979–986

MacDonald SM, Trofimov A, Safai S, Adams J, Fullerton B, Ebb D, Tarbell TJ, Yock TI (2011) Proton radiotherapy for pediatric central nervous system germ cell tumours: early clinical outcomes. Int J Radiat Oncol Biol Phys 79(1):121–129

Massimino M, Giangaspero F, Garre ML, Genitori L, Perilongo G, Collini P, Riva D, Valentini L, Scarzello G, Poggi G, Spreafico F, Peretta P, Mascarin M, Modena P, Sozzi G, Bedini N, Biassoni V, Urgesi A, Balestrini MR, Finocchiaro G, Sandri A, Gandola L, AIEOP Neuro-oncology group (2006) Salvage treatment for childhood ependymoma after surgery only: pitfalls of omitting "at once" adjuvant treatment. Int J Radiat Oncol Biol Phys 65(5):1440–1445

Merchant TE, Kiehna EN, Li C, Xiong X, Mulhern RK (2005) Radiation dosimetry predicts IQ after conformal radiation therapy in pediatric patients with localized ependymoma. Int J Radiat Oncol Biol Phys 63(5): 1546–1554

Merchant TE, Hua CH, Shukla H, Ying X, Nill S, Oelfke U (2008) Proton versus photon radiotherapy for common pediatric brain tumors: comparison of models of dose characteristics and their relationship to cognitive function. Pediatr Blood Cancer 51(1): 110–117

Merchant TE, Rose SR, Bosley C, Wu S, Xiong X, Lustig RH (2011) Growth hormone secretion after conformal radiation therapy in pediatric patients with localized brain tumors. J Clin Oncol 29(36):4776–4780

Miralbell R, Bleher A, Huguenin P, Ries G, Kann R, Mirimanoff RO, Notter M, Nouet P, Bieri S, Thum P, Toussi H (1997a) Pediatric medulloblastoma: radiation treatment technique and patterns of failure. Int J Radiat Oncol Biol Phys 37(3):523–529

Miralbell R, Lomax A, Russo M (1997b) Potential role of proton therapy in the treatment of pediatric medulloblastoma/primitive neuro-ectodermal tumors: spinal theca irradiation. Int J Radiat Oncol Biol Phys 38(4):805–811

Miralbell R, Lomax A, Cella L, Schneider U (2002) Potential reduction of the incidence of radiation-induced second cancers by using proton beams in the treatment of pediatric tumors. Int J Radiat Oncol Biol Phys 54(3):824–829

Moeller BJ, Chintagumpala M, Philip JJ, Grosshans DR, McAleer MF, Woo SY, Gidley PW, Vats TS, Mahajan A (2011) Low early ototoxicity rates for pediatric medulloblastoma patients treated with proton radiotherapy. Radiat Oncol 6:58

Morris B, Partap S, Yeom K, Gibbs IC, Fisher PG, King AA (2009) Cerebrovascular disease in childhood

cancer survivors: a children's oncology group report. Neurology 73(22):1906–1913

Newhauser WD, Fontenot JD, Mahajan A, Kornguth D, Stovall M, Zheng Y, Taddei PJ, Mirkovic D, Mohan R, Cox JD, Woo S (2009) The risk of developing a second cancer after receiving craniospinal irradiation. Phys Med Biol 54:2277–2291

Oeffinger KC, Mertens AC, Sklar CA, Kawashima T, Hudson MM, Meadows AT, Friedman DL, Marina N, Hobbie W, Kadan-Lottick NS, Schwartz CL, Leisenring W, Robison LL, Study CCS (2006) Chronic health conditions in adult survivors of childhood cancer. N Engl J Med 355(15):1572–1582

PTCOG (2012) Particle therapy facilities in operation. Available at: http://ptcog.web.psi.ch/ptcentres.html. Accessed 2 June 2012

Robison LL, Armstrong GT, Boice JD, Chow EJ, Davies SM, Donaldson SS, Green DM, Hammond S, Meadows AT, Mertens AC, Mulvihill JJ, Nathan PC, Neglia JP, Packer RJ, Rajaraman P, Sklar CA, Stovall M, Strong LC, Yasui Y, Zeltzer LK (2009) The childhood cancer survivor study: a national cancer institute-supported resource for outcome and intervention research. J Clin Oncol 27(14): 2308–2318

Verhey LJ, Smith V, Serago CF (1998) Comparison of radiosurgery treatment modalities based on physical dose distributions. Int J Radiat Oncol Biol Phys 40(2):497–505

Winkfield KM, Linsenmeier C, Yock TI, Grant PE, Yeap BY, Butler WE, Tarbell NJ (2009) Surveillance of craniopharyngioma cyst growth in children treated with proton radiotherapy. Int J Radiat Oncol Biol Phys 73(3):716–721

Yoon M, Shin DH, Kim J, Kim JW, Kim DW, Park SY, Lee SB, Kim JY, Park HJ, Park BK, Shin SH (2011) Craniospinal irradiation techniques: a dosimetric comparison of proton beams with standard and advanced photon radiotherapy. Int J Radiat Oncol Biol Phys 81(3):637–646

Pathogenesis of Medulloblastoma: Role of Molecular Genetic Alterations

9

Mustafa Nadi, Claudia Faria, and James T. Rutka

Contents

Abstract

Medulloblastoma (MB) was first described as a distinct neuropathological entity about a century ago, but it is still responsible for significant morbidity and mortality. Over the last decade, we have entered an era where our understanding of the molecular genetics of MB may soon play a role in directing patients' management and eventually affecting their prognosis and outcome. In this review, we will describe our current knowledge of the presumed cell of origin of MB. We discuss the role of inherited genetic syndromes associated with MB such as Gorlin Syndrome. We review the development of the normal cerebellum in the context of signaling pathways which, if altered, can lead to MB formation. And finally, we will discuss the significance of molecular genetics in the prognosis of MB patients and then summarize the potential areas for further research.

Introduction

Medulloblastoma is a cancer of cerebellum and the most common malignant brain tumor in childhood. It accounts for up to 40 % of all posterior fossa neoplasms and is the cause of many paediatric oncology-related deaths (Sardi et al. 2007). Medulloblastoma is currently diagnosed on histopathological examination of tumor tissue obtained at surgery. However, recent transcriptomic approaches have demonstrated that MB is

M. Nadi • C. Faria • J.T. Rutka, FRCSC (✉)
Division of Neurosurgery, The Hospital for Sick Children, 555 University Avenue, Suite 1503, M5G 1X8 Toronto, ON, Canada

Department of Surgery, University of Toronto, Toronto, ON, Canada
e-mail: James.rutka@sickkids.ca

M.A. Hayat (ed.), *Tumors of the Central Nervous System, Volume 12*,
DOI 10.1007/978-94-007-7217-5_9,

comprised of multiple clinically and molecularly distinct subgroups (Thompson et al. 2006; Kool et al. 2008). At least four subgroups of MB have now been described: WNT, SHH, Group 3, and Group 4 (Northcott et al. 2009). Additionally, there may be other subtypes within these subgroups (Northcott et al. 2012).

Recent advances in molecular biology have led to the development of powerful tools for the study of MB tumorigenesis which have revealed new insights into the molecular underpinnings of this disease (Onvani et al. 2010). Emerging evidence indicates that the different precursor cell populations that form the cerebellum and the cell signaling pathways that regulate its development likely represent distinct compartments from which the various subtypes of MB arise. Definitive characterization of each MB subtype will undoubtedly improve treatment of this disease and provide important insights to the origins of cancer (Gilbertson and Ellison 2008).

Medulloblastoma: Cells of Origin

Medulloblastomas are known to arise from two different cerebellar germinal zones. The cerebellar anlage is established within the roof of the metencephalon (Miale and Sidman 1961). In contrast to most other brain regions, the cells of the cerebellum are derived from two distinct germinal zones.

1. Glutamatergic projection neurons of the deep nuclei arise from the rhombic lip and migrate to their final positions via the nuclear transitory zone, which is located just below the pial surface at the rostral end of the cerebellar plate (Fink et al. 2006).
2. GABAergic neurons that include those of the deep nuclei, Purkinje cells and Golgi neurons, arise sequentially from multipotent precursor cells of the primary germinal epithelium in the roof of the fourth ventricle (Morales and Hatten 2006). Once this neurogenic process is underway, a second germinal zone forms from cells within the rhombic lip. This germinal zone comprises granule neuron precursor cells (GNPCs) that invade rostrally across the cerebellum anlage to produce the external germinal layer (EGL). GNPCs then migrate inward along Bergmann glial fibers, past the Purkinje cell layer, to form the mature granule cell neurons of the internal granular layer. The EGL persists until the second postnatal year in the human.
3. A stem cell population was recently identified within the white matter of the postnatal cerebellum (Di Marcotullio et al. 2006). These cells express the neural stem cell markers CD133 and Nestin; they undergo extensive self-renewal; and they are multipotent, generating astrocytes, oligodendrocytes, and neurons but not granule cell neurons, in vivo. Thus, the cerebellum includes three distinct pools of progenitor cells that might each serve as cells of origin for the MB and its variants. This may explain their histological and molecular heterogeneity.

The ventricular zone gives rise to classic midline MBs, whereas the external granule layer (EGL) gives rise to the lateral cerebellar hemispheric desmoplastic MBs (Onvani et al. 2010). The external granule cell lineage of desmoplastic MBs was demonstrated through expression of the *ZIC1* gene, a marker of the granule cell lineage (Yokota et al. 1996; Behesti and Marino 2009).

Several important developmental signal transduction pathways, including Sonic hedgehog (SHH), Wingless (WNT) and Notch signaling cascades, are implicated in the cellular transition from the EGL to the IGL. Aberrancies in these signaling pathways can promote tumorigenesis.

Medulloblastoma and Hereditary Cancer Syndromes

There are several hereditary cancer syndromes that have been associated with a higher incidence of MB formation. The study of genetic profile of these familial conditions has revealed several pathway abnormalities that are integral in MB pathogenesis. Our understanding of MB molecular pathogenesis has come from examining genetic alterations in these syndromes. However, most MBs develop as a result of sporadic mutations in

these signaling pathways as well as in a number of other growth factor pathways.

1. Gorlin syndrome (nevoid basal-cell carcinoma syndrome) is an autosomal dominant disorder where patients have a germline deletion in the patched homologue 1 (*PTCH1*) gene locus at 9q22. The *PTCH1* gene encodes a transmembrane receptor protein and serves as a negative regulator of the SHH pathway during normal cerebellar development. Mutations in the *PTCH1* gene therefore result in aberrant SHH signaling leading to the development of a transformed phenotype. Consequently, the patients have a predisposition to cancers, including multiple cutaneous basal cell carcinomas, ovarian fibromas and MB. The incidence of MBs in these patients ranges from 5 % to 20 % (Taylor et al. 2000; Friedrich 2007).
2. Turcot syndrome is found in kindred with primary brain tumors and multiple colorectal adenomas/carcinomas. It is further divided into two groups:
   A. Brain Tumor-Polyposis Syndrome 1: (BTPS1) Colorectal cancer associated with gliomas in which kindreds harbor germ-line mutations in the DNA mismatch repair gene *hMLH1*.
   B. Brain Tumor-Polyposis Syndrome 2: (BTPS2) Colorectal cancer associated with MB and related to an autosomal-dominant mutation in the adenomatous polyposis coli (*APC*) tumor suppressor gene. The *APC* gene regulates the WNT signaling pathway, and altered regulation can predispose to tumor formation (Huang et al. 2000).
3. Li–Fraumeni syndrome is a rare familial syndrome associated with germline mutations in the *TP53* tumor suppressor gene. These patients have a predisposition for several malignancies, including sarcomas, leukemia and CNS tumors, such as MBs (Barel et al. 1998).
4. Rubenstein–Taybi is an autosomal dominant condition, also known as broad thumb-hallux syndrome. It is characterized by short stature, moderate to severe learning difficulties, distinctive facial features, broad thumbs and first toes and an increased risk of developing non-cancerous and cancerous tumors, lymphoma and MB.

   This syndrome is due to a genetic mutation in the CREBBP and EP300 genes. CREBBP plays an important role in regulating cell growth and division and is essential for normal fetal development. Mutations in the EP 300 gene are responsible for a small percentage of cases of this syndrome (Taylor et al. 2001).
5. Aicardi syndromes is a rare genetic disease which typically arises from a mutation localized on the distal part of the short arm of the X chromosome, an area that may be of importance for tumor development. It occurs almost exclusively in females. It is defined by the triad of lacunar chorioretinopathy, flexor spasms, and agenesis of the corpus callosum. Clinically the patients have intractable seizures and severe cognitive impairment (Palmer et al. 2004).

Histopathological Classification

The latest (2007) WHO classification of tumors of the CNS lists the classic MB and several variants: desmoplastic, anaplastic, large-cell MBs, and the MB with extensive nodularity (MBEN). Of these variants, the anaplastic and large-cell MBs form a continuum; all large-cell MBs have regions of anaplasia. Large-cell and anaplastic tumors make up between 2–4 % and 10–22 % of MBs, respectively (Ellison 2002; McManamy et al. 2003; Gilbertson and Ellison 2008). Because these two variants form a continuum with a poor prognosis, they have been grouped as large cell/anaplastic (LCA) MBs in several studies.

Desmoplastic MBs encompass the nodular/desmoplastic MB and the MBEN, which contribute approximately 7 % and 3 % of all MBs, respectively (Ellison 2002) (Fig. 9.1). Classic MBs constitute the remainder. Morphological differentiation in MBs can be diverse, but occurs principally along neuronal lines (Ellison 2002; Gilbertson and Ellison 2008). Neuronal differentiation is most common while glial differentiation is rare.

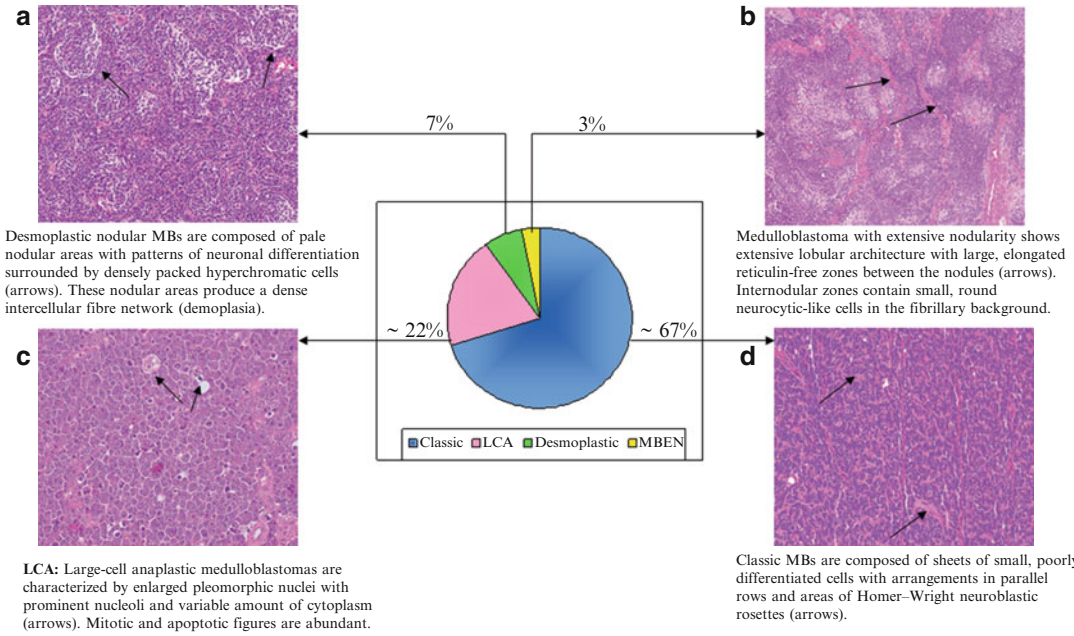

Fig. 9.1 Histology of medulloblastoma (*MB*) subgroups and Pie chart frequency. (**a**) Desmoplastic nodular MBs are composed of pale nodular areas with patterns of neuronal differentiation surrounded by densely packed hyperchromatic cells (*arrows*). These nodular areas produce a dense intercellular fibre network (demoplasia). (**b**) Medulloblastoma with extensive nodularity shows extensive lobular architecture with large, elongated reticulin-free zones between the nodules (*arrows*). Internodular zones contain small, round neurocytic-like cells in the fibrillary background. (**c**) **LCA**: Large-cell anaplastic medulloblastomas are characterized by enlarged pleomorphic nuclei with prominent nucleoli and variable amount of cytoplasm (*arrows*). Mitotic and apoptotic figures are abundant. (**d**) Classic MBs are composed of sheets of small, poorly differentiated cells with arrangements in parallel rows and areas of Homer–Wright neuroblastic rosettes (*arrows*)

Molecular Heterogeneity

The observation that MB encompasses a number of distinct morphologic variants suggests that these tumors represent different entities arising through alternative mechanisms. Studies of gross chromosomal alterations in MB support this notion and have provided the first clues that different molecular processes underlie the development of MB subtypes (Ellison 2002; Gilbertson 2002; Gilbertson and Ellison 2008).

Deletions of 17p and isochromosome 17q (i17q), which combines loss of 17p and gain of 17q, have long been recognized as the most common chromosomal alterations in MB (Griffin et al. 1988). However, these alterations are not distributed equally among the histologic variants. i17q has been observed in 34 % and 36 % of classic and LCA tumors, respectively, but in only 12 % of desmoplastic MBs (Gilbertson et al. 2001; Lamont et al. 2004; Thompson et al. 2006). Furthermore, the presence of i17q in tumors has been associated with a poor clinical outcome, suggesting that this cytogenetic alteration may contribute to the development of aggressive variants of MB (Batra et al. 1995; Gilbertson et al. 2001).

In contrast, monosomy 6 has recently been shown to occur exclusively in favorable prognosis, mainly classic MBs that contain an intact chromosome 17 and activating mutations in the β-catenin gene (Ellison et al. 2005; Clifford et al. 2006; Thompson et al. 2006) Thus, chromosome 6 may harbor a tumor suppressor gene that cooperates with aberrant Wingless (WNT) signaling to generate an especially curable subtype of MB.

The desmoplastic and LCA variants are also associated with specific chromosomal alterations. Deletions of 9q are observed in up to 40 % of

Table 9.1 Key pathway aberrations and inhibitors associated with medulloblastoma

Pathway	Gene	Aberration	Pathway inhibitor
SHH	*PTCH*	Loss of function	Hh-Antag691
	SUFU	Loss of function	Cyclopamine
	SMO	Activation	
	MYC	Amplification, overexpression	
WNT	*APC*	Loss of function	Unavailable
	β-*catenin*	Activation	
	AXIN1	Loss of function	
	GSK3-β	Decreased expression	
NOTCH	*NOTCH2*	Gain	GSI-18
	HES1	Overexpression	DFK-167
EGF	*ERBB2*	Overexpression	Erlotinib
	MAP2K1	Activation	
	MAP2K2	Activation	
	MAPK1/3	Activation	
HGF/cMET	*cMET*	Gain	PHA665752

desmoplastic MBs, but occur rarely in tumors of the classic variant (Schofield et al. 1995), and amplifications of the *MYCC* and *MYCN* oncogenes occur predominantly in LCA tumors (Ellison 2002). Furthermore, a recent study showed that MB cells transduced with *MYCC* adopt a severely anaplastic phenotype when grown as xenografts, suggesting a causative relationship between *MYCC* expression and the LCA phenotype (Stearns et al. 2006).

Aberrations of Genes and Signaling Pathways

Tumor formation is in many ways similar to normal development since both involve processes such as cell proliferation, migration, differentiation and apoptosis. Tumorigenesis is in fact 'development gone wrong', whereby developmental signaling or growth factor pathways involved in normal development become aberrant and drive tumor formation. Table 9.1 summarizes signaling and growth factors pathway aberrations.

SHH Signaling Pathway

This pathway has been implicated in the pathogenesis of the desmoplastic variant of MB (Behesti and Marino 2009). It plays a major role in proliferation of the GNPCs during cerebellar development. During this time, the SHH glycoprotein is predominantly produced by the Purkinje cells ventral to the EGL and secreted to bind with the PTCH1 receptor on EGL precursor cells. This process releases the PTCH1-mediated inhibition of the SHH pathway, which leads to the activation of target genes via the Gli family of transcription factors and promotes GNPCs proliferation (Fig. 9.2) (Rossi et al. 2008). Consequently, mutations of the SHH pathway may induce aberrant pathway activation and uncontrolled GNPCs proliferation, resulting in the formation of MBs. Mutations affecting *PTCH1* and other components of the SHH signaling complex, namely, *SUFU*, *PTCH2* and *SMO,* have been identified in up to 25 % of sporadic cases of MB (Taylor et al. 2002).

Supportive Evidence:

1. The role of *PTCH1* mutations in the genesis of MB has been further supported by murine models, where ~14 % of mice with a heterozygous deletion of *Ptc (Ptc+/−)* develop MB.
2. Overexpression of the polycomb transcription regulator BMI-1 has been reported in a subset of human primary MBs and linked with SHH pathway activation. This gene also regulates GNPCs proliferation during cerebellar development and its correlation with SHH pathway

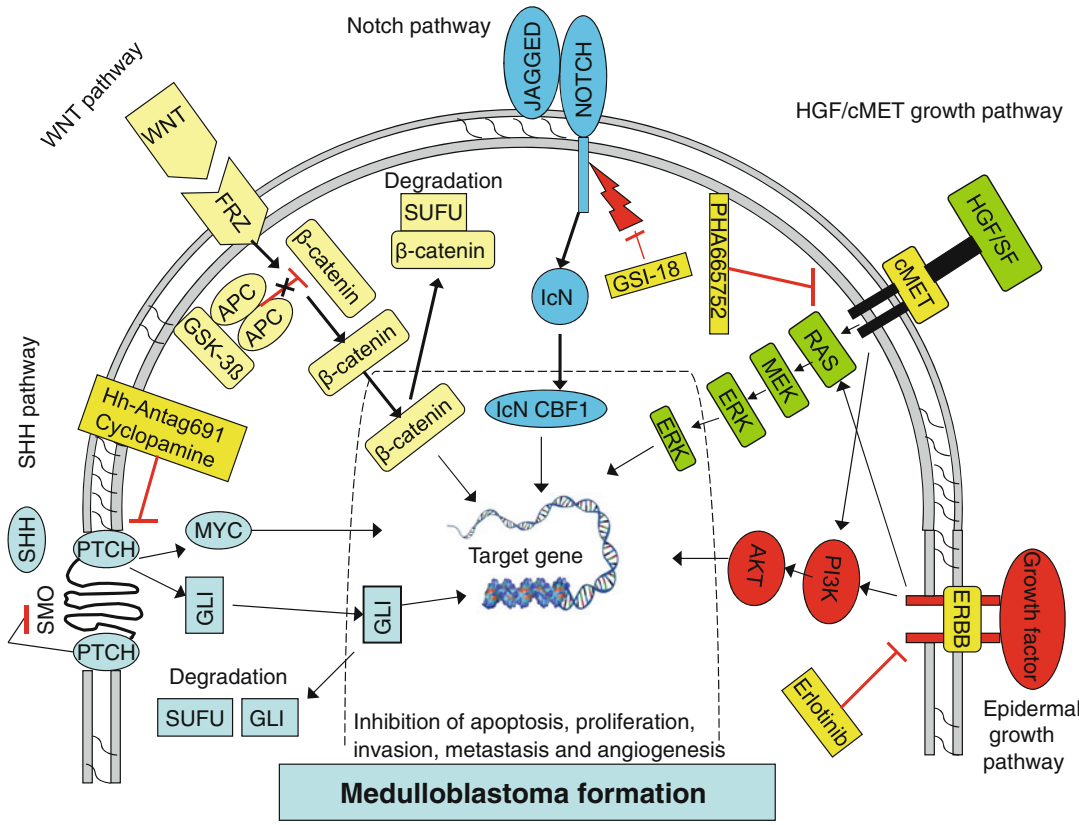

Fig. 9.2 Signaling and growth factor activation pathways implicated in medulloblastoma formation. *Arrows* activators, *bars* repressors

activity suggests an alternative mechanism for SHH signaling in the development of MB.

WNT Signaling Pathway

During normal development, WNT ligands bind with the receptor Frizzled (FRZ) to activate this pathway and relay signals to the nucleus via a multiprotein complex (Fig. 9.2) (Rossi et al. 2008). The APC protein is a regulator of WNT signaling that functions in a complex with AXIN, glycogen synthase kinase-binding protein and glycogen synthase kinase-3b to regulate proliferation and specification of neural progenitor cells during early cerebellar development. APC functions as a tumor suppressor by modulating the levels of cytoplasmic b-catenin, a downstream component of the WNT signaling pathway. Inactivating mutations in *APC* and other WNT signaling cascade members result in an uncontrolled increase in b-catenin levels in the cytoplasm. Consequently, b-catenin translocates to the nucleus where it activates transcription of several oncogenes, including *MYC* and cyclinD1 (*CCND1*), resulting in enhanced cellular proliferation.

Supportive Evidence:

1. Similar observations have also been reported in mutations of *SUFU*, a downstream component of the SHH pathway, which causes ineffective b-catenin nuclear export resulting in an increased b-catenin-mediated gene expression (Taylor et al. 2004).
2. Mutations in the WNT signaling complex, especially activating mutations in b-catenin (*CTNNB1*), account for 15 % of sporadic cases of MBs. In addition, b-catenin mutations and

nuclear localization have been associated with a favorable prognosis, but of unknown molecular mechanisms.

NOTCH Signaling Pathway

Notch promotes proliferation of GNPCs and prevents their differentiation (Behesti and Marino 2009). To date, four highly conserved Notch receptors have been identified (Notch1, -2, -3 and -4) that are single-pass transmembrane proteins. Binding of the Notch receptor by its ligand triggers proteolytic cleavage and activation of the receptor, followed by the release of an intracellular domain of the receptor from the membrane that translocates to the nucleus (Carlotti et al. 2008). In the nucleus this protein forms a complex with the DNA-binding protein CBF1, activating the transcription of effector genes including *Hes1*, *Hes5*, *p21* and *cyclin D1* (Fig. 9.2).

Supportive Evidence:

The Notch pathway has been implicated in medulloblastoma tumorigenesis in a number of studies. For example,

1. Fan et al. 2004 reported increased *Notch2* copy number in 15 % of MBs, consistent with its expression in proliferating GNPCs during normal cerebellar development.
2. Upregulation of the Notch pathway target gene *Hes1* in a subset of MB samples.
3. Hes1 expression also correlated with poor patient survival.

Growth Factors Mutations

In addition to the developmental pathways described earlier, other pathways have been implicated in MB pathogenesis and these have been investigated for a more precise understanding of the molecular basis of this tumor. Abnormalities in the EGF family of receptor tyrosine kinases, for example, have been detected in MBs. Receptor activation through ligand binding leads to its dimerization, autophosphorylation and activation of downstream PI3K and MAPK signaling cascades (Fig. 9.2). This process is essential for normal development of the CNS. Consequently, aberrant activation of this pathway results in upregulation of downstream signaling elements, which leads to increased cell proliferation and altered cell migration through the activation of transcription factor target proteins. In line with this, upregulation of RAS–MAP kinase downstream components, such as *MAP2K1*, *MAP2K2* and *MAPK1/3*, has been correlated with metastatic behavior of MBs (MacDonald et al. 2001; Del Valle et al. 2002; Gilbertson and Clifford 2003). Furthermore, overexpression of the EGF receptor family member ERBB2 has been reported in MBs and linked to metastasis. High levels of expression of this protein co-overexpressed with ERBB4 signifies poor clinical outcome in cases of MB.

The HGF/cMET signaling pathway is also known to contribute to MB formation (Fig. 9.2). HGF signaling through the cMET receptor plays a critical role in cerebellar GNPCs proliferation and survival as they migrate from the EGL inward to form the mature IGL. Overactivation of this pathway can thus promote malignancies via increased cell proliferation and cell cycle dysregulation and lead to metastatic behavior by abnormal cell migration and invasion.

Aberrant signaling of the HGF/cMET pathway due to loss of pathway inhibition, ligand or receptor overexpression and/or activating mutations has been implicated in several human malignancies, including renal, lung, breast and CNS tumors. In MB, *MET* gene copy number gains have been detected by comparative genomic hybridization in 38.5 % of primary tumor samples and the receptor mRNA expression levels have been inversely correlated with patient survival(Tong et al. 2004; Li et al. 2005).

Finally, the amplification of *MYC* and *MYCN* proto-oncogenes has been detected in 5–15 % of primary MBs (Herms et al. 2000; Aldosari et al. 2002). *MYCN* is an early transcriptional target of the SHH pathway and its activation by SHH promotes the expression of the cell cycle proteins CyclinD1 and CyclinD2 leading to GNPCs proliferation. A high expression level of MYC is reported to cause progression of MB to an anaplastic phenotype and has been linked to poor clinical outcome.

DNA Repair Pathways and Medulloblastoma

Genes that have recently emerged as important suppressors of MB tumorigenesis are those that regulate the DNA damage response. The DNA repair pathway includes proteins such as poly-(ADP-ribose) polymerase (PARP-1) that sense DNA damage and proteins that repair the damage. DNA double-strand breaks activate two major repair pathways, homologous recombination repair and nonhomologous end joining.

The breast/ovarian cancer susceptibility protein BRCA2 is a DNA repair protein with a key role in homologous recombination repair. BRCA2 colocalizes with Partner and localizer of BRCA2 (PALB2) protein, which stabilizes BRCA2 within nuclear structures, facilitating DNA repair. Proteins involved in nonhomologous end joining include the nuclear ligase Lig4 and XRCC4.

Inactivating mutations in *BRCA2* and *PALB2* cause Fanconi anemia (FA) types D1 and N, respectively. FA includes a collection of disorders characterized by chromosomal instability, growth retardation, congenital malformations, progressive bone marrow failure, cancer predisposition, and cellular hypersensitivity to DNA cross-linking agents. Mutations in 12 genes have been identified in families with the various forms of the disease. FA-D1 and -N each carry a high risk of childhood solid tumors, including MB. Indeed, at least five of seven childhood brain tumors diagnosed in six FA-D1 kindreds were MBs, and seven patients identified with FAN5 had MB (Offit et al. 2003; Hirsch et al. 2004; Reid et al. 2007).

Although suppression of human MB by other components of the DNA damage response pathway remains to be established, mice null for either *Lig4*, *XRCC4*, or *Parp-1* and *p53* develop MB with high penetrance. Interestingly, most *XRCC4*-null/p53-deficient MBs delete *Ptch1* and, in *Parp-1* deficient mice, develop within the EGL. These tumors also express markers of GNPC and Shh pathway activation. Thus, defects in DNA repair may cooperate with mutations in the Shh pathway to cause MB.

Molecular Genetics Analysis of Medulloblastomas

Similar to what happened in WHO Classifications, MB was re-classified more than once depending on its biologic behavior, recent advances in gene expression profiling techniques have led to the generation of several molecular classification schemes in MBs:

1. Thompson et al. in 2006 were the first to report molecular subgroups of MBs, identifying five distinct clusters of MB (subgroups A to E). They used a combination of FISH and direct sequencing for gene expression analysis. Subgroup-specific abnormalities included mutations in the Wingless (WNT) pathway and deletion of chromosome 6 (subgroup B) and mutations in the Sonic Hedgehog (SHH) pathway (subgroup D) (Thompson et al. 2006).
2. Kool et al. in 2008 corroborated Thompson's molecular subgroup findings by using a combination of gene expression and comparative genomic hybridization (CGH) array. Signature genetic and genomic events within the five molecular subgroups included WNT signaling (group A), SHH signaling (group B), expression of neuronal differentiation genes (groups C and D) and photoreceptor genes (D and E). This study showed that groups C, D and E were genetically related to each other, and clinically associated with metastatic disease, most strongly with group E. Monosomy of chromosome 6 occurred only in type A tumors, loss of 9q mostly occurred in type B tumors, whereas chromosome 17 aberrations, most common in MB, were strongly associated with type C or D tumors. Loss of the inactivated X-chromosome was highly specific for female cases of type C, D and E tumors (Kool et al. 2008).
3. Northcott et al. in 2009 identified four distinct molecular subgroups of MB, including the well-characterized WNT and SHH groups, as well as two independent subgroups (group C and D). They used both mRNA and miRNA microarrays (Northcott et al. 2009). Of interest, miR-17/92, an oncogenic miRNA cluster, was most highly expressed in SHH tumors in

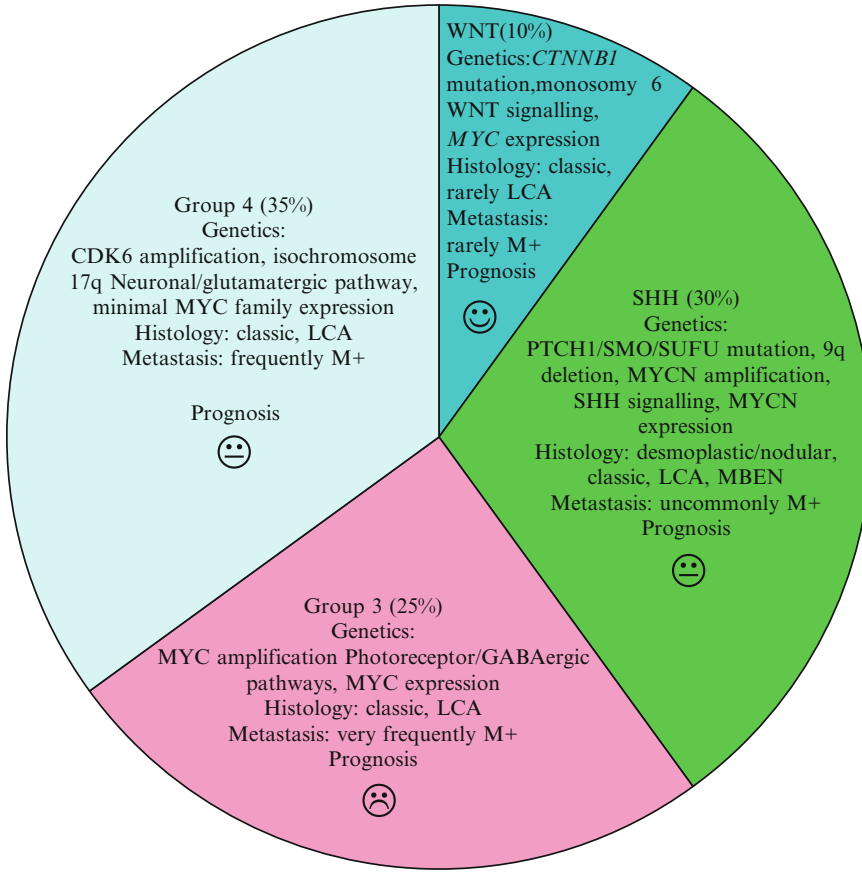

Fig. 9.3 Medulloblastoma subgroups. Pie chart illustrating the frequency, genetics, gene expression of the four subgroups of medulloblastoma. *LCA* large-cell anaplastic, *MBEN* medulloblastoma with extensive nodularity, *M+* positive for metastasis at diagnosis, *SHH* sonic hedgehog

association with *MYCN*, while its expression in group C tumors was found to be correlated with *MYC* (Fig. 9.3).

Clinical correlation of MB molecular subgroups has a significant potential for disease stratification. Kool et al. (2008) demonstrated that groups C, D and E patients demonstrated a higher metastatic potential. Therefore, such patients would require aggressive treatment.

Medulloblastoma in Adults

Adult MB is rare and distinct from pediatric MB in terms of genomic aberrations and their impact on clinical outcomes. The following are some of these differences:

1. Approximately 25 % of adult MB shows no genomic imbalances in comparison to 5 % within the pediatric cohort, suggesting that genomic instability is more critical for tumorigenesis in childhood MB (Korshunov et al. 2010).
2. CDK6 was the frequent focal amplification in adult MB detected to date, whereas focal amplifications of MYC/MYCN are far more common in pediatric tumors.
3. Gain of chromosomes 3q, 4, and 19 are more common in adult MB, whereas gain of chromosomes 1q, 2, 7, and 17q, as well as loss of 16q are more frequent in pediatric MB.
4. All chromosome 6 deletions were monosomy 6 in pediatric tumors, whereas they were mostly partial deletions in adult MB cases.

5. In contrast to pediatric tumors, adult MB cases with CTNNB1 mutation did not always show a monosomy 6.
6. For adult MB, shortened survival was found for tumors with CDK6 amplification, 17q gain, and 10q loss.
7. Adult MB with WNT signaling pathway activation, however, did not share the excellent prognosis seen in childhood MB.

Therefore, adult MBs have their age-specific risk stratification model, a molecular staging system based on DNA copy number status of 10q and 17q (Korshunov et al. 2010; Pfister et al. 2010).

Genetic Divergence of Metastatic Medulloblastoma

It is well known that MB disseminates through the cerebrospinal fluid (CSF) in the leptomeningeal space to coat the brain and spinal cord. Dissemination, a marker of poor prognosis, is found in up to 40 % of children at diagnosis and in most children at the time of recurrence. The mechanisms of dissemination through the CSF are poorly studied, and MB metastases have been assumed to be biologically similar to the primary tumour. The studies revealed that the metastases from an individual are extremely similar to each other but are divergent from the matched primary tumour. Clonal genetic events in the metastases can be demonstrated in a restricted subclone of the primary tumour, suggesting that only rare cells within the primary tumour have the ability to metastasize. Failure to account for the divergent molecular pathology of the metastatic compartment may result in selection of therapeutic targets present in the primary tumour, which is more amenable to surgical control, but not the metastases, which are the more frequent cause of death and this could be a major barrier to the development of effective targeted therapies (Wu et al. 2012).

Prognostication from Genetic/ Molecular Point of View

The following genetic observations have been associated with poor clinical outcome and favorable prognosis.

A. Poor Clinical Outcome
   1. Deletions of 17p and isochromosome 17q (i17q), which combines loss of 17p and gain of 17q, which is the most common chromosomal alterations in MB.
   2. Hes1 expression.
   3. RAS–MAP kinase downstream components upregulation, such as *MAP2K1*, *MAP2K2* and *MAPK1/3*, are associated with metastatic behavior of MB.
   4. Overexpression of the EGF receptor family member ERBB2 has been linked to MB metastasis. High levels of expression of this protein co-overexpressed with ERBB4 signifies poor clinical outcome.
   5. HGF/cMET signaling pathway overactivation and/or mutations has been correlated to metastasis.
   6. *MET* gene copy number gains and the receptor mRNA expression levels have been inversely correlated with patient survival.
   7. A MYC high expression level has been linked to poor clinical outcome.

B. Favorable Clinical Outcome
   1. Monosomy 6 occurs exclusively in favorable prognosis, mainly classic MBs that contain an intact chromosome 17.
   2. β-catenin gene mutations and nuclear localization.
   3. The detection of high mRNA expression levels of neurotrophin-3 receptor.

Current Researches and Future Directions

The challenge for the future will be to identify the patient subgroups who respond well to current treatment, and those who respond poorly and

eventually to improve patients' survival. Multiple lines of evidence suggest that the response to treatment is determined by the biology of the tumor and that treatments targeting cell signaling pathways involved in MB might provide therapeutic alternatives with lower toxicity profiles than the conventional approaches (Gilbertson 2004).

The existing molecular heterogeneity within MBs is considered to be responsible for the observed differences in treatment response and treatment-related toxicities between patients (Kool et al. 2008). This means a single population-based therapeutic approach is inadequate. As a result, the current research focus is conducting multi-inhibitor studies to target multiple factors simultaneously.

In the future, it is possible that MB treatment protocols will include target-specific chemotherapy, minimally invasive surgery and elimination of radiation therapy. It is expected that, individualized patient therapy will offer dramatic changes in cancer treatment that will improve patients' quality of life along with lowering the burden of current treatments and their related toxic side effects.

Conclusions

The myriad of genomic discoveries in MB in the last decade has enriched the field of neuro-oncology enormously. The recent development of precise and sensitive molecular biology techniques has greatly improved knowledge of the basic biology of MB formation. To a certain extent, the enigma of MB heterogeneity has been elucidated. Genetic analysis of some of hereditary syndromes has helped us understand the molecular profile of MB. Evidence has emerged recently supporting the fact that the genetic aberrations have a major role in driving MB formation. These mutations encompass the various signaling pathways, growth factor pathways, and DNA repair mechanisms.

The elucidation of molecular factors that contribute to MB pathogenesis will help in refining disease risk stratification, prognostication and facilitating accurate prediction of treatment outcomes. Progress in the field of personalized medicine will enable the implementation of less toxic and more effective therapeutic approaches, leading to substantial improvements in patient quality of life. This comprehensive detailed understanding of MB molecular genetics allows for the identification of novel therapeutic targets against which patient-specific targeted therapies could be developed.

Acknowledgements Supported by: Canadian Cancer Society, Grant number: 2011-700751; Pediatric Brain Tumor Foundation of the United States, Brain Tumour Foundation of Canada, Wiley Fund at the Hospital for Sick Children and b.r.a.i.nchild. JTR is a Scientist of the CIHR.

References

Aldosari N, Bigner SH, Burger PC, Becker L, Kepner JL, Friedman HS, McLendon RE (2002) MYCC and MYCN oncogene amplification in medulloblastoma. A fluorescence in situ hybridization study on paraffin sections from the Children's Oncology Group. Arch Pathol Lab Med 126:540–544

Barel D, Avigad S, Mor C, Fogel M, Cohen IJ, Zaizov R (1998) A novel germ-line mutation in the noncoding region of the p53 gene in a Li-Fraumeni family. Cancer Genet Cytogenet 103:1–6

Batra SK, McLendon RE, Koo JS, Castelino-Prabhu S, Fuchs HE, Krischer JP, Friedman HS, Bigner DD, Bigner SH (1995) Prognostic implications of chromosome 17p deletions in human medulloblastomas. J Neurooncol 24:39–45

Behesti H, Marino S (2009) Cerebellar granule cells: insights into proliferation, differentiation, and role in medulloblastoma pathogenesis. Int J Biochem Cell Biol 41:435–445

Carlotti CG Jr, Smith C, Rutka JT (2008) The molecular genetics of medulloblastoma: an assessment of new therapeutic targets. Neurosurg Rev 31:359–368, discussion 368–359

Clifford SC, Lusher ME, Lindsey JC, Langdon JA, Gilbertson RJ, Straughton D, Ellison DW (2006) Wnt/Wingless pathway activation and chromosome 6 loss characterize a distinct molecular sub-group of medulloblastomas associated with a favorable prognosis. Cell Cycle 5:2666–2670

Del Valle L, Enam S, Lassak A, Wang JY, Croul S, Khalili K, Reiss K (2002) Insulin-like growth factor I receptor activity in human medulloblastomas. Clin Cancer Res 8:1822–1830

Di Marcotullio L, Ferretti E, Greco A, De Smaele E, Po A, Sico MA, Alimandi M, Giannini G, Maroder M, Screpanti I, Gulino A (2006) Numb is a suppressor of

Hedgehog signalling and targets Gli1 for Itch-dependent ubiquitination. Nat Cell Biol 8:1415–1423
Ellison D (2002) Classifying the medulloblastoma: insights from morphology and molecular genetics. Neuropathol Appl Neurobiol 28:257–282
Ellison DW, Onilude OE, Lindsey JC, Lusher ME, Weston CL, Taylor RE, Pearson AD, Clifford SC (2005) beta-Catenin status predicts a favorable outcome in childhood medulloblastoma: the United Kingdom Children's Cancer Study Group Brain Tumour Committee. J Clin Oncol 23:7951–7957
Fan X, Mikolaenko I, Elhassan I, Ni X, Wang Y, Ball D, Brat DJ, Perry A, Eberhart CG (2004) Notch1 and notch2 have opposite effects on embryonal brain tumor growth. Cancer Res 64:7787–7793
Fink AJ, Englund C, Daza RA, Pham D, Lau C, Nivison M, Kowalczyk T, Hevner RF (2006) Development of the deep cerebellar nuclei: transcription factors and cell migration from the rhombic lip. J Neurosci 26:3066–3076
Friedrich RE (2007) Diagnosis and treatment of patients with nevoid basal cell carcinoma syndrome [Gorlin-Goltz syndrome (GGS)]. Anticancer Res 27:1783–1787
Gilbertson R (2002) Paediatric embryonic brain tumours. Biological and clinical relevance of molecular genetic abnormalities. Eur J Cancer 38:675–685
Gilbertson RJ (2004) Medulloblastoma: signalling a change in treatment. Lancet Oncol 5:209–218
Gilbertson RJ, Clifford SC (2003) PDGFRB is overexpressed in metastatic medulloblastoma. Nat Genet 35:197–198
Gilbertson RJ, Ellison DW (2008) The origins of medulloblastoma subtypes. Annu Rev Pathol 3:341–365
Gilbertson R, Wickramasinghe C, Hernan R, Balaji V, Hunt D, Jones-Wallace D, Crolla J, Perry R, Lunec J, Pearson A, Ellison D (2001) Clinical and molecular stratification of disease risk in medulloblastoma. Br J Cancer 85:705–712
Griffin CA, Hawkins AL, Packer RJ, Rorke LB, Emanuel BS (1988) Chromosome abnormalities in pediatric brain tumors. Cancer Res 48:175–180
Herms J, Neidt I, Luscher B, Sommer A, Schurmann P, Schroder T, Bergmann M, Wilken B, Probst-Cousin S, Hernaiz-Driever P, Behnke J, Hanefeld F, Pietsch T, Kretzschmar HA (2000) C-MYC expression in medulloblastoma and its prognostic value. Int J Cancer 89:395–402
Hirsch B, Shimamura A, Moreau L, Baldinger S, Hagalshiekh M, Bostrom B, Sencer S, D'Andrea AD (2004) Association of biallelic BRCA2/FANCD1 mutations with spontaneous chromosomal instability and solid tumors of childhood. Blood 103:2554–2559
Huang H, Mahler-Araujo BM, Sankila A, Chimelli L, Yonekawa Y, Kleihues P, Ohgaki H (2000) APC mutations in sporadic medulloblastomas. Am J Pathol 156:433–437
Kool M, Koster J, Bunt J, Hasselt NE, Lakeman A, van Sluis P, Troost D, Meeteren NS, Caron HN, Cloos J, Mrsic A, Ylstra B, Grajkowska W, Hartmann W, Pietsch T, Ellison D, Clifford SC, Versteeg R (2008) Integrated genomics identifies five medulloblastoma subtypes with distinct genetic profiles, pathway signatures and clinicopathological features. PLoS One 3:e3088
Korshunov A, Remke M, Werft W, Benner A, Ryzhova M, Witt H, Sturm D, Wittmann A, Schottler A, Felsberg J, Reifenberger G, Rutkowski S, Scheurlen W, Kulozik AE, von Deimling A, Lichter P, Pfister SM (2010) Adult and pediatric medulloblastomas are genetically distinct and require different algorithms for molecular risk stratification. J Clin Oncol 28:3054–3060
Lamont JM, McManamy CS, Pearson AD, Clifford SC, Ellison DW (2004) Combined histopathological and molecular cytogenetic stratification of medulloblastoma patients. Clin Cancer Res 10:5482–5493
Li Y, Lal B, Kwon S, Fan X, Saldanha U, Reznik TE, Kuchner EB, Eberhart C, Laterra J, Abounader R (2005) The scatter factor/hepatocyte growth factor: c-met pathway in human embryonal central nervous system tumor malignancy. Cancer Res 65:9355–9362
MacDonald TJ, Brown KM, LaFleur B, Peterson K, Lawlor C, Chen Y, Packer RJ, Cogen P, Stephan DA (2001) Expression profiling of medulloblastoma: PDGFRA and the RAS/MAPK pathway as therapeutic targets for metastatic disease. Nat Genet 29: 143–152
McManamy CS, Lamont JM, Taylor RE, Cole M, Pearson AD, Clifford SC, Ellison DW (2003) Morphophenotypic variation predicts clinical behavior in childhood non-desmoplastic medulloblastomas. J Neuropathol Exp Neurol 62:627–632
Miale IL, Sidman RL (1961) An autoradiographic analysis of histogenesis in the mouse cerebellum. Exp Neurol 4:277–296
Morales D, Hatten ME (2006) Molecular markers of neuronal progenitors in the embryonic cerebellar anlage. J Neurosci 26:12226–12236
Northcott PA, Fernandez LA, Hagan JP, Ellison DW, Grajkowska W, Gillespie Y, Grundy R, Van Meter T, Rutka JT, Croce CM, Kenney AM, Taylor MD (2009) The miR-17/92 polycistron is up-regulated in sonic hedgehog-driven medulloblastomas and induced by N-myc in sonic hedgehog-treated cerebellar neural precursors. Cancer Res 69:3249–3255
Northcott PA, Korshunov A, Pfister SM, Taylor MD (2012) The clinical implications of medulloblastoma subgroups. Nat Rev Neurol 8:340–351
Offit K, Levran O, Mullaney B, Mah K, Nafa K, Batish SD, Diotti R, Schneider H, Deffenbaugh A, Scholl T, Proud VK, Robson M, Norton L, Ellis N, Hanenberg H, Auerbach AD (2003) Shared genetic susceptibility to breast cancer, brain tumors, and Fanconi anemia. J Natl Cancer Inst 95:1548–1551
Onvani S, Etame AB, Smith CA, Rutka JT (2010) Genetics of medulloblastoma: clues for novel therapies. Expert Rev Neurother 10:811–823
Palmer L, Nordborg C, Steneryd K, Aman P, Kyllerman M (2004) Large-cell medulloblastoma in Aicardi syndrome. Case report and literature review. Neuropediatrics 35:307–311

Pfister SM, Korshunov A, Kool M, Hasselblatt M, Eberhart C, Taylor MD (2010) Molecular diagnostics of CNS embryonal tumors. Acta Neuropathol 120:553–566

Reid S, Schindler D, Hanenberg H, Barker K, Hanks S, Kalb R, Neveling K, Kelly P, Seal S, Freund M, Wurm M, Batish SD, Lach FP, Yetgin S, Neitzel H, Ariffin H, Tischkowitz M, Mathew CG, Auerbach AD, Rahman N (2007) Biallelic mutations in PALB2 cause Fanconi anemia subtype FA-N and predispose to childhood cancer. Nat Genet 39:162–164

Rossi A, Caracciolo V, Russo G, Reiss K, Giordano A (2008) Medulloblastoma: from molecular pathology to therapy. Clin Cancer Res 14:971–976

Sardi I, Cavalieri D, Massimino M (2007) Emerging treatments and gene expression profiling in high-risk medulloblastoma. Paediatr Drugs 9:81–96

Schofield D, West DC, Anthony DC, Marshal R, Sklar J (1995) Correlation of loss of heterozygosity at chromosome 9q with histological subtype in medulloblastomas. Am J Pathol 146:472–480

Stearns D, Chaudhry A, Abel TW, Burger PC, Dang CV, Eberhart CG (2006) c-myc overexpression causes anaplasia in medulloblastoma. Cancer Res 66:673–681

Taylor MD, Mainprize TG, Rutka JT (2000) Molecular insight into medulloblastoma and central nervous system primitive neuroectodermal tumor biology from hereditary syndromes: a review. Neurosurgery 47:888–901

Taylor MD, Mainprize TG, Rutka JT, Becker L, Bayani J, Drake JM (2001) Medulloblastoma in a child with Rubenstein-Taybi syndrome: case report and review of the literature. Pediatr Neurosurg 35:235–238

Taylor MD, Liu L, Raffel C, Hui CC, Mainprize TG, Zhang X, Agatep R, Chiappa S, Gao L, Lowrance A, Hao A, Goldstein AM, Stavrou T, Scherer SW, Dura WT, Wainwright B, Squire JA, Rutka JT, Hogg D (2002) Mutations in SUFU predispose to medulloblastoma. Nat Genet 31:306–310

Taylor MD, Zhang X, Liu L, Hui CC, Mainprize TG, Scherer SW, Wainwright B, Hogg D, Rutka JT (2004) Failure of a medulloblastoma-derived mutant of SUFU to suppress WNT signaling. Oncogene 23:4577–4583

Thompson MC, Fuller C, Hogg TL, Dalton J, Finkelstein D, Lau CC, Chintagumpala M, Adesina A, Ashley DM, Kellie SJ, Taylor MD, Curran T, Gajjar A, Gilbertson RJ (2006) Genomics identifies medulloblastoma subgroups that are enriched for specific genetic alterations. J Clin Oncol 24:1924–1931

Tong CY, Hui AB, Yin XL, Pang JC, Zhu XL, Poon WS, Ng HK (2004) Detection of oncogene amplifications in medulloblastomas by comparative genomic hybridization and array-based comparative genomic hybridization. J Neurosurg 100:187–193

Wu X, Northcott PA, Dubuc A, Dupuy AJ, Shih DJ, Witt H, Croul S, Bouffet E, Fults DW, Eberhart CG, Garzia L, Van Meter T, Zagzag D, Jabado N, Schwartzentruber J, Majewski J, Scheetz TE, Pfister SM, Korshunov A, Li XN, Scherer SW, Cho YJ, Akagi K, MacDonald TJ, Koster J, McCabe MG, Sarver AL, Collins VP, Weiss WA, Largaespada DA, Collier LS, Taylor MD (2012) Clonal selection drives genetic divergence of metastatic medulloblastoma. Nature 482:529–533

Yokota N, Aruga J, Takai S, Yamada K, Hamazaki M, Iwase T, Sugimura H, Mikoshiba K (1996) Predominant expression of human zic in cerebellar granule cell lineage and medulloblastoma. Cancer Res 56:377–383

Medulloblastomas: Survival Differences Between Children and Adults

10

Nicolas Smoll

Contents

Abstract

Age is a very well known prognostic factor in brain tumors. Adults with a medulloblastoma (MB) have a poorer outcome compared to children with a MB. A feature specific to MB's relationship to age when determining survival is the appearance of differences in survival between age groups after a particular follow-up time. Up to 4 years post-diagnosis, the prognosis remains the same, but between 4 and 10 years of follow-up, adults become significantly more likely to die than children.

The relationship between age and survival may be a confounded relationship due to the genetic basis of the tumor, responses and compliance to treatment protocols, and the anatomical location of the tumor. Each of these factors may be the actual "drivers" of these differences, rather than age itself. When measuring the differences across age groups in MBs, there are two important statistical concepts that are key: relative survival and the proportional hazards assumption. Both of these are discussed within this chapter. This chapter focuses on the factors that may be the drivers of the survival differences, such as clinical factors, genetics, treatment response and/or compliance, and progression patterns.

N. Smoll (✉)
Department of Clinical Neurosciences,
Department of Neurosurgery, Faculty of Medicine,
University Hospitals of Geneva,
Rue Gabrielle-Perret-Gentil 4, 1211 Geneva, Switzerland
e-mail: nrsmoll@gmail.com

M.A. Hayat (ed.), *Tumors of the Central Nervous System, Volume 12*,
DOI 10.1007/978-94-007-7217-5_10,

Introduction

Medulloblastomas (MB) originate from primitive embryonal cells, typically with neurectodermal components, which is why this tumor is classified as a primitive neurectodermal tumor (PNET). The incidence of this tumor is just under 2 per million, and children are 10 times more likely to be affected than adults (Smoll and Drummond 2012). Today, MBs are considered to be distinct from PNETs (Pomeroy et al. 2002), and MBs are considered to be made up of four different subgroups: WNT tumors showing wingless pathway activation (excellent prognosis) make up only 11 % of MBs; SHH showing hedgehog pathway activation (worse prognosis, affects infants and adolescents/adults (affects children less), similar to a "bathtub" distribution) form approximately 28 % of all MBs; group 3 tumors (worst prognosis, rarely found in adults) compose 27 % of all MBs; and group 4 tumors are the most common MB subtype (34 % of MB). Therefore, I suggest that age may be surrogate variable associated with outcomes, because its association with survival is really a relationship confounded by several "driver" variables described here.

In 2012 I demonstrated how the differences in survival across age-categories is time-dependant, using a large population-based dataset. This means that the differences in hazard rates (and similarly, survival rates) across the age groups only emerge after 4 years of follow-up, also known as a "fork" type interaction because of it's appearance on Kaplan–Meier curves or similar hazard rate plots. To exemplify this, children and adults had 75 % and 75 % 2-year survival rates, but 57 % and 46 % 10-year survival rates respectively. Thus demonstrating how differences in survival are follow-up time-dependant.

It is suggested that MBs probably develop silently during embryologic phases of development, and mutations after repeated multiplication will accumulate throughout life until a certain combination of mutations (especially those associated with a specific MB subtype) lead to tumor growth (Jones et al. 2012). This is based on the findings that adult MBs have higher frequencies of passenger mutations (Parsons et al. 2010) and confirmed by Jones et al. (2012) finding that the rate of mutations is positively correlated with age.

The question regarding survival differences between adults and children has been a difficult one to answer, as the two patient groups are remarkably different across the entire range of variables. The most obvious example of these important differences is that children and adults get treated in different institutions because of the different requirements of each age group. Since we cannot randomize patients into adult and childhood age groups, the differences across these age groups are best measured using data from observational and/or registry studies. Like all observational/registry studies, there are an infinite number of important variables that cannot be controlled for, and there are probably multiple variables which may confound the relationship. What is important to note, is that age is a variable that is probably confounded by other "driver" variables, which are the variables that are imbalanced across age groups, but are independant factors affecting survival rates.

There are probably several important interactions (effects of an independent variable or predictor which vary across the range of values of another variable) between variables that are known to predict outcomes. Unfortunately, to detect these one must have large sample sizes, or very large effect sizes. For example, a particular type of chemotherapy protocol may show efficacy in children with an MB, but may not show the same efficacy in adults with an MB, revealing an interaction between chemotherapy and age groups (or more precisely, some as yet unknown biological driver variable closely related to age). Interactions are probably (it could be argued certainly) present between genetic subtypes of MBs and their response to chemotherapy and or radiotherapy. While the genetic subtypes of MB are dominating the field of MB research, outcomes are also determined by other factors. There are clinical and/or treatment variables that also impact the differences in survival outcomes between adults and children.

Using relative survival (RS) to remove the effect of expected mortality rates seen in the general population, it appears that adults and children have the same survival outcomes up to 4 years post-diagnosis. After 4 years, adults become significantly more likely to die than children (Smoll 2012). Although recent randomized studies are showing impressive results, with some finding 5-year survival rates in children of up to 95 % (Packer et al. 2006; Rutkowski et al. 2005). Most importantly, this chapter will focus on discussing the drivers of survival differences between children and adults.

Genetic Drivers of Survival Differences Between Children and Adults

The most promising factor in MB research currently is the four genomic subtypes of MB, first discussed by Kool et al. in 2008. Kool et al.'s recent study demonstrated impressive survival rates in patients with metastases positive and metastases negative wingless (WNT) tumors (greater than 95 % 5-year survival for both age categories). Across all age categories, the WNT subtypes were virtually always found in the Classical histology category, which is typically known to have a worse prognosis than the Desmoplastic histology subtype. Nonetheless, this genetic subtype has similarly excellent outcomes in both adults and children (Kool et al. 2012).

The sonic hedgehog (SHH) driven subtype which is more likely to be found in infants and adults similar to a "bathtub"-type age distribution, may be the driver of the differences in survival between adults and children seen after 4 years. This was remarkably different at 10 years post-diagnosis, with survival rates for SHH tumors at 34 % in adults and 51 % in children. Therefore, the differences in survival seen after 5-years post-diagnosis may be because adults are more likely to be affected by the SHH-driven subtype, and the differences in survival in this subtype begins to appear after 5-years post-diagnosis, and are clear by 10 years (Table 10.1).

Treatment Drivers of Survival Differences Between Children and Adults

Investigators must remember that patients are exposed to treatment regimens that are often different for adults when compared to children. Children and adults differ in their ability to withstand different treatment protocols. Greenberg et al. 2001 and Packer et al. 1994 found that 44 % of children were able to complete a multi-agent CDP protocol (to the 8th cycle), while no adult patients in Greenberg et al.'s study were able to complete the CDP protocol (Greenberg et al. 2001; Packer et al. 1994). While the inability to complete therapy may have something to do with the differences in survival, perhaps a more complex mechanism is at work. Adults are typically offered the same post-operative adjuvant therapy protocols as children, but because they are more likely to have SHH-driven tumors, the effect of chemotherapy is less, because SHH-driven tumors may not have the same response as WNT, group 3, and group 4 tumor subtypes. Thus, while we suspect that WNT tumors respond well to typical adjuvant therapies because of their impressive survival rates, the interaction between the latest radiochemotherapy protocols and MB subtypes is unclear when survival or progression-free survival is the measured outcome.

Anatomical Location Drivers of Survival Differences Between Children and Adults

It is well known that adults get more MBs in the cerebellar hemispheres, while children are more likely to have tumors located in the cerebellar vermis. While it is often thought that it is easier to obtain gross-total resection in hemispherically located tumors, there is little evidence that location is associated with survival (Greenberg et al. 2001). Lastly, the effect of anatomical location on survival is probably a relationship confounded by gross-total resection rates or genetic factors.

Table 10.1 Differences between children and adults

Clinical	**Children are more likely to present with midline lesions and adults with hemispheric lesions**. 83 % of children present with midline lesions compared with 49 % of adults (Sarkar et al. 2002)
	Tumors rarely (2 %) present with metastases in adults, while 24 % of tumors appear to have metastases in children (Kool et al. 2012)
Histologic	**Children are more likely to present with the classic histological subtype, while adults are more likely to present with the desmoplastic variant of MBs.** 32 % of adults present with a desmoplastic variant, while only approximately 12 % of children may present with a desmoplastic variant (Bloom and Bessell 1990; Kortmann et al. 2000)
	The relationship of MIB index of tumors to age remains unclear. Some believe adults have lower proliferation indices (Sarkar et al. 2002), and other believe the proliferation index is higher (Giordana et al. 1997). Giordana et al. 1997 found a median MIB-1/PCNA labelling index of 20/25 % in children and 35/50 % in adults
Genetic	**Children have fewer passenger mutations compared to adults, but they have the same amount of driver mutations (probable cancer- causing mutations)** (Parsons et al. 2010)
	There is a positive correlation between genome-wide mutation rates and age, a relationship which is stronger in diploid tumors (Jones et al. 2012)
	WNT (wingless pathway) tumors have excellent survival rates (>90 % 5-year survival) even in the presence of metastatic disease. This is the smallest subgroup of with a peak incidence at 10-12 years of age (Kool et al. 2012)
	SHH showing hedgehog pathway activation (worse prognosis, affects infants and older children/adults, similar to a "bathtub" distribution) make up approximately 28 % of all MBs
	Group 3 tumors have the worst prognosis and are rarely found in adults. They compose 27 % of all MBs
	Group 4 tumors are the most common MB subtype (35% of MB), almost exclusively found in those under the age of 18yrs, and have a similar prognosis to those with an SHH subtype of tumor
Treatment	**Tolerance of treatment protocols may be less in adults, so fewer adults appear to be able to complete chemotherapy protocols**. In 2000, Greenberg et al. noted in a series of 17 adults that adults had higher rates of toxicity from chemotherapy and that all adults were unable to complete their course of treatment compared with 44 % of children were unable to complete the same treatment protocol (Packer Protocol) (Greenberg et al. 2001; Packer et al. 1994)
Outcomes	**Incidence of late relapses is greater in adults, with relapses in children tending to occur before 3 years, as seen in progression-free survival curves plateauing earlier**

To briefly recap: confounding is considered to be the situation in which the study exposure groups (in this case, age-categories) differ in their hazard rates or in relative survival-excess hazard rates for reasons other than the effects of the exposure group variable (Greenland et al. 1999). To relate this to the ideas presented here, if anatomical location was known to have an impact on excess hazard rates, when gross-total resection rates are taken into account (controlled for), the effect of anatomical location on excess hazard rates may disappear. In other words, the anatomical location has a relationship with survival, only because it affects the surgeons ability to achieve a gross-total resection at surgery.

Relapse-Free Survival as a Driver of Survival Differences Between Children and Adults

Incidence of late relapse appears to be greater in adults, with relapses in children tending to occur before 3 years post-diagnosis. Khalil (2008) presents a series of 51 pediatric MBs in which all patients that relapsed (10, or 20 %) relapsed before 2 years. Brandes et al. 2007 demonstrated 17 relapses in 36 adult patients (47 %), with a median recurrence time of 3 years post-diagnosis (Brandes et al. 2007). In addition, when one reviews the progression-free curves of various studies including children, plateaus are noted to

start at or before 4 years for children (Allen et al. 2009; Evans et al. 1990; Rutkowski et al. 2010; Zeltzer et al. 1999). When compared to adults the progression-free curve of adults continues to decrease and reaches a plateau at 10 years (Padovani et al. 2007). While these progression-free curves are consistent with the finding of survival differences between adults and children (because adults appear to progress later than children), although it may seem logical, but we are as yet unclear if later progressions explain the survival difference seen after 4 years.

Relative Survival and Measuring Differences Between Children and Adults

To measure survival differences between adults and children, investigators must take into account that adults, and especially elderly people in the general population are already more likely to die than children. The mortality rate of the general population is called the *expected mortality rate*. Subtracting the expected mortality rate from the hazard rate in a population of cancer patients gives us a measure known as *the excess hazard rate*, and when transformed into the survival scale this gives us the measure known as relative survival (RS). RS is considered to be the gold standard of cause-specific survival estimation because of its robustness and non-reliance on death certificates for correct descriptions of the cause of death.

When one compares the survival rates of children to those of adults, the relationship between the categories changes during follow-up (at least in population-based studies). As mentioned previously, survival rates are virtually identical before 4 years. After 4 years the survival rates begin to differ, with adults faring worse. This concept is known as *non-proportional hazards*, and is key to understanding changing relationships between two groups. As a brief recap, hazard rates are what underpin survival rates. A hazard rate is the instantaneous event per unit of time. In other words, it is the amount of deaths per smallest unit of time. Some might call this the "speed of death" or "speed of mortality". Regression models that present hazard ratios generally present a ratio of two hazard rates. For example, if during a particular month 5 children per 100 children died, and this was compared with 10 adults per 100 died, a hazard ratio of 2 would be present.

Proportional hazards models (such as the Cox proportional hazards model) assume that this difference will be present throughout the entirety of follow-up, and therefore only one estimate is presented, like if it was an average over time. This is unanimously, and I believe erroneously considered to be appropriate for almost all brain tumors and all situations. This is evidenced by most analyses of data published on brain tumors relying on Cox's proportional hazards model to provide regression estimates. The assumption of "proportional hazards" has been found to be violated for MBs and low grade gliomas (Smoll 2012; Smoll et al. 2012). In these studies, the differences in hazard rates changed throughout follow-up. For example, when young adults are compared to the elderly, the excess hazard rates for low-grade gliomas (adjusted for expected mortality) are enormously different (magnitude of 30 times in the first year) for the first 2 years, and as time progresses the excess hazard rates re-approximate for what is termed the "reverse fork-type interaction". For a more extensive discussion of this problem, see the article by Miguel Hernan (2010).

In addition to non-proportionality, adults and children have much different expected mortality rates when all-cause mortality is considered. Adults are simply more likely to die from all causes. Therefore, to truly extract differences in survival between adults and children, the use of relative survival methodology is required. Relative survival is considered the gold-standard of cause-specific survival, because all deaths in a particular population that are above the rate normally seen in the general population can be considered to be due to the tumor, irrespective of the listed cause of death. This is particularly important when we measure the differences between adults and children because it is well known that adults and children have different

expected mortality profiles, and relative survival methods intrinsically control for this factor.

Excess hazard rates of MBs have therefore demonstrated the quality of non-proportionality when adults and children are compared, which means the investigator must beware when using proportional hazards models when modeling MB data. Thus, modelling of age differences requires the use of specialized models such as a discrete-time survival models or Dickman's piecewise constant hazards model for relative survival data to accurately model such data (Dickman et al. 2004; Singer and Willett 1993).

In conclusion, the differences in survival between children and adults with MB/PNETs are clear, but the relationship is complex. We know that the differences in survival become apparent after 4 years and that adults appear to relapse often at later stages, but the difficult part is finding out why. Adults are more likely to be affected by the SHH-subtype which has a worse prognosis. Children may be more likely to complete chemotherapy protocols and their tumors progress/recur earlier. But there are many factors that speak in favor of adult tumors having better prognosis. Therefore, while the relationship is complex, new information on the genomics is emerging. Thus, to find out if there is truly a relationship between age and survival, we must first be able to control for the imbalances in the independant predictors of survival.

References

Allen J, Donahue B, Mehta M, Miller DC et al (2009) A phase II study of preradiotherapy chemotherapy followed by hyperfractionated radiotherapy for newly diagnosed high-risk medulloblastoma/primitive neuroectodermal tumor: a report from the Children's Oncology Group (CCG 9931). Int J Radiat Oncol Biol Phys 74:1006–1011

Bloom HJ, Bessell EM (1990) Medulloblastoma in adults: a review of 47 patients treated between 1952 and 1981. Int J Radiat Oncol Biol Phys 18:763–772

Brandes AA, Franceschi E, Tosoni A, Blatt V et al (2007) Long-term results of a prospective study on the treatment of medulloblastoma in adults. Cancer 110:2035–2041

Dickman PW, Sloggett A, Hills M, Hakulinen T (2004) Regression models for relative survival. Stat Med 23:51–64

Evans AE, Jenkin RD, Sposto R, Ortega JA et al (1990) The treatment of medulloblastoma. Results of a prospective randomized trial of radiation therapy with and without CCNU, vincristine, and prednisone. J Neurosurg 72:572–582

Giordana MT, Cavalla P, Dutto A, Borsotti L et al (1997) Is medulloblastoma the same tumor in children and adults? J Neurooncol 35:169–176

Greenberg HS, Chamberlain MC, Glantz MJ, Wang S (2001) Adult medulloblastoma: multiagent chemotherapy. Neuro Oncol 3:29–34

Greenland S, Pearl J, Robins JM (1999) Causal diagrams for epidemiologic research. Epidemiology 10:37–48

Hernan MA (2010) The hazards of hazard ratios. Epidemiology 21:13–15

Jones DT, Jager N, Kool M, Zichner T et al (2012) Dissecting the genomic complexity underlying medulloblastoma. Nature 488:100–105

Khalil EM (2008) Treatment results of adults and children with medulloblastoma NCI, Cairo University experience. J Egypt Natl Canc Inst 20:175–186

Kool M, Korshunov A, Remke M, Jones DT et al (2012) Molecular subgroups of medulloblastoma: an international meta-analysis of transcriptome, genetic aberrations, and clinical data of WNT, SHH, Group 3, and Group 4 medulloblastomas. Acta Neuropathol 123:473–484

Kortmann RD, Kuhl J, Timmermann B, Mittler U et al (2000) Postoperative neoadjuvant chemotherapy before radiotherapy as compared to immediate radiotherapy followed by maintenance chemotherapy in the treatment of medulloblastoma in childhood: results of the German prospective randomized trial HIT '91. Int J Radiat Oncol Biol Phys 46:269–279

Packer RJ, Sutton LN, Elterman R, Lange B et al (1994) Outcome for children with medulloblastoma treated with radiation and cisplatin, CCNU, and vincristine chemotherapy. J Neurosurg 81:690–698

Packer RJ, Gajjar A, Vezina G, Rorke-Adams L et al (2006) Phase III study of craniospinal radiation therapy followed by adjuvant chemotherapy for newly diagnosed average-risk medulloblastoma. J Clin Oncol 24:4202–4208

Padovani L, Sunyach MP, Perol D, Mercier C et al (2007) Common strategy for adult and pediatric medulloblastoma: a multicenter series of 253 adults. Int J Radiat Oncol Biol Phys 68:433–440

Parsons DW, Li M, Zhang X, Jones S et al (2010) The genetic landscape of the childhood cancer medulloblastoma. Science, pp 435–439

Pomeroy SL, Tamayo P, Gaasenbeek M, Sturla LM et al (2002) Prediction of central nervous system embryonal tumour outcome based on gene expression. Nature 415:436–442

Rutkowski S, Bode U, Deinlein F, Ottensmeier H et al (2005) Treatment of early childhood medulloblastoma by postoperative chemotherapy alone. N Engl J Med 352:978–986

Rutkowski S, von Hoff K, Emser A, Zwiener I et al (2010) Survival and prognostic factors of early childhood medulloblastoma: an international meta-analysis. J Clin Oncol 28:4961–4968

Sarkar C, Pramanik P, Karak AK, Mukhopadhyay P et al (2002) Are childhood and adult medulloblastomas different? A comparative study of clinicopathological features, proliferation index and apoptotic index. J Neurooncol 59:49–61

Singer JD, Willett JB (1993) It's about time: using discrete-time survival analysis to study duration and the timing of events. J Educ Stat 18:40

Smoll NR (2012) Relative survival of childhood and adult medulloblastomas and primitive neuroectodermal tumors (PNETs). Cancer 118:1313–1322

Smoll NR, Drummond KJ (2012) The incidence of medulloblastomas and primitive neurectodermal tumours in adults and children. J Clin Neurosci 19:1541–1544

Smoll NR, Gautschi OP, Schatlo B, Schaller K et al (2012) Relative survival of patients with supratentorial low-grade gliomas. Neuro Oncol 14:1062–1069

Zeltzer PM, Boyett JM, Finlay JL, Albright AL et al (1999) Metastasis stage, adjuvant treatment, and residual tumor are prognostic factors for medulloblastoma in children: conclusions from the Children's Cancer Group 921 randomized phase III study. J Clin Oncol 17:832–845

Survivors of Childhood Cancer: Risk of Glioma and Meningioma Following Radiotherapy

11

Lucie M. Turcotte and Joseph P. Neglia

Contents

Abstract

Pediatric cancer survival rates have improved significantly over the past several decades as advances have been made in both therapies and supportive care. Improved survival rates have been accompanied by increased recognition of therapy-related late effects, such as second neoplasms. Two of the most common classes of pediatric cancers include acute leukemias and tumors of the central nervous system, both of which have historically involved CNS-directed radiation therapy. Through multiple childhood cancer survivor cohorts, it has been recognized that survivors previously treated with radiation to the central nervous system are at increased risk for developing secondary gliomas and meningiomas, both of which have been shown to occur at well-defined time points and in a dose-responsive fashion. Based on these findings, current era treatment protocols have been modified to minimize toxicity and reduce the use of radiation when possible. Long term follow up of cancer survivors remains an imperative part of their ongoing care given the long latency period that has been observed to development of secondary CNS tumors.

L.M. Turcotte • J.P. Neglia (✉)
University of Minnesota, D-557 Mayo Building, MMC 484, 420 Delaware Street SE, Minneapolis, MN 55455, USA
e-mail: jneglia@umn.edu

M.A. Hayat (ed.), *Tumors of the Central Nervous System, Volume 12*,
DOI 10.1007/978-94-007-7217-5_11,

Introduction

Survival of childhood cancer has improved dramatically over the past four decades, predominantly due to improvements in therapies, surgical techniques and supportive care. Two of the most common childhood cancers are the acute leukemias and central nervous system (CNS) tumors. Both leukemias and, to a lesser extent, CNS tumors have traditionally been treated with a combination of chemotherapy and therapeutic radiation, as well as surgery in CNS tumors. Acute lymphoblastic leukemia is the most common childhood cancer, with associated survival rates of >85 % and resultant 2000 new 5-year survivors every year in the United States (Bhatia et al. 2002). Tumors of the CNS represent the second most common class of tumors behind acute leukemias and also represent the second leading cause of cancer-related deaths in children. Overall 5-year survival for primary CNS tumors currently exceeds 70 % in children (Altekruse et al. 2010).

While improved survival from these and other malignancies is widely recognized as success, it may bring with it multiple late effects resulting from the original cancer itself or from therapy. One of the best studied of these late effects is the development of both benign and malignant subsequent neoplasms. Although the leading cause of death among 5-year cancer survivors is recurrence of the original cancer (Mertens et al. 2008), by 20 years from initial cancer diagnosis, the mortality rate from second neoplasms exceeds that of recurrence (Armstrong et al. 2009; Mertens et al. 2008). Despite having utility in the treatment of multiple malignancies, radiation has been implicated in the development of secondary neoplasms including neoplasms of the central nervous system (CNS) (Pui et al. 2003). Secondary CNS tumors can cause significant morbidity with long-lasting health impacts, and in some cases, mortality.

Several large cohort studies have looked at subsequent malignancies in childhood cancer survivors (Mike et al. 1982; Hawkins et al. 1987; Friedman et al. 2010; Taylor et al. 2010). Within all of these cohorts, secondary CNS tumors were noted at frequencies much higher than would be anticipated in the general population. As the studies have become more sophisticated, they have looked at specific risk factors, including chemotherapy and radiation and their roles in second cancers, and confirmed that use of radiation increased risk of second CNS tumors, including gliomas and meningiomas.

Secondary Glioma

Gliomas are a broad class of tumors, typically occurring in the brain, that are more specifically identified by their cell type, histologic grade and location. They can behave as low-grade tumors with relatively good prognosis to more aggressive, high-grade tumors that behave in a malignant fashion. Both low-grade and high-grade gliomas have been identified in childhood cancer survivors; one of the difficulties in this group can be differentiating between recurrence of a primary CNS malignancy and development of a new tumor. Much of the available body of literature likely tends towards more conservative estimates with more stringent exclusion criteria for similar second malignancies. This implies that the actual number of secondary gliomas may be underestimated.

In an analysis of the North American Childhood Cancer Survivor Study (NA-CCSS) cohort of over 14,000 patients, 40 patients were diagnosed with subsequent gliomas (Neglia et al. 2006). The histology of these tumors included ten glioblastomas, nine anaplastic astrocytomas, ten other malignant gliomas, four oligodendrogliomas (two were anaplastic), two juvenile pilocytic astrocytomas, and one each of gliosarcoma, fibrillary astrocytoma, myopapillary ependymoma, ganglioglioma and giant cell astrocytoma. When compared with the general population, the overall standardized incidence ratio was 8.66 (95 % CI 6.24–11.6). More of the cohort leukemia patients went on to develop gliomas as compared to meningiomas. For any patient who received radiation as part of their treatment plan, SIR was 12.9, and primary diagnosis specific SIRs were 16.9 for leukemia and 14.2 for CNS tumors. The majority of gliomas were diagnosed in the first 5 year follow up period (between 5 and 10 years from original cancer diagnosis), with 70 % of patients diagnosed before age 20 years, and only 10 % diagnosed beyond

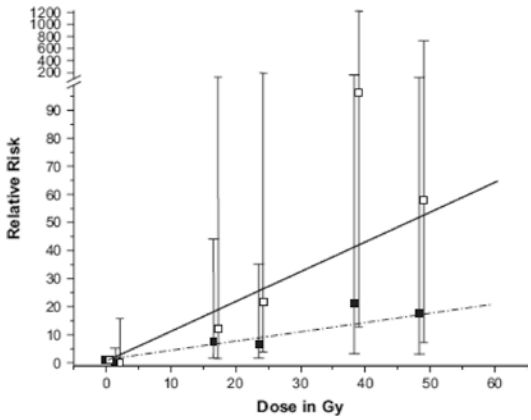

Fig. 11.1 Relative risk of subsequent glioma (*closed boxes*) and meningioma (*open boxes*) within the Childhood Cancer Survivor Study cohort by radiation dose (Printed with permission from Oxford University Press, (Neglia et al. 2006))

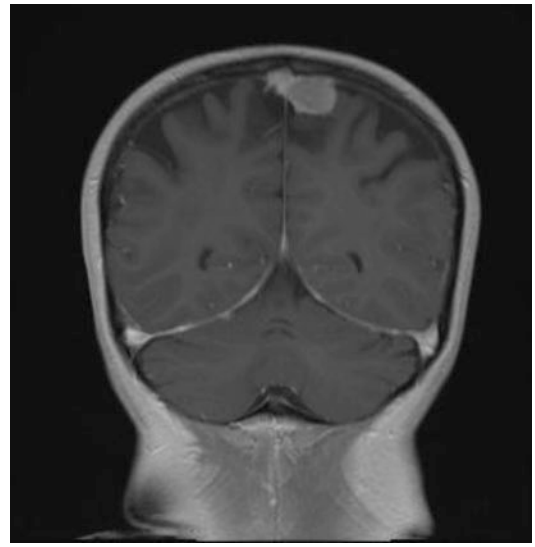

Fig. 11.2 Para-falcine meningioma in a 20+ year survivor of childhood acute lymphoblastic leukemia

15 years of follow up. No sex predilection was observed. While no association was demonstrated between various chemotherapeutic agents and development of a subsequent glioma, there was significant association between radiotherapy and glioma. The risk for developing glioma was highest among children exposed to radiation at less than 5 years of age, with a SIR of 14.5 and an excess absolute risk (EAR) of 31.95 per 10,000 years follow-up. A positive linear dose-response relationship was observed, with increasing risk of glioma with increasing radiation exposure (see Fig. 11.1). Odds ratios peaked at greater than 20-fold at the 30–44.9 Gy dose category, with excess relative risk (ERR) of 0.33 per Gy (Neglia et al. 2006).

In a cohort of ALL survivors followed by St Jude Children's Research Hospital, ten patients of the 1,612 survivors developed subsequent high-grade gliomas (glioblastoma multiforme, n=4, anaplastic astrocytoma, n=2, other high grade glioma, n=4) and one patient developed a low-grade glioma. Of those developing high grade tumors, latency from the time to diagnosis to tumor development ranged from 5.9 to 14.1 years (median 9 years) (Walter et al. 1998). Similar to the NA-CCSS cohort, children less than 6 years at the time of initial cancer diagnosis were more likely to develop high-grade tumors, as were children with CNS disease at the time of diagnosis.

Secondary Meningioma

Meningiomas are typically thought of as benign tumors arising from the dura mater surrounding the brain and spinal cord (see Fig. 11.2). The association with cranial radiation has been understood for quite some time, as these lesions have occurred at higher rates in children treated with radiation for tinea capitis (Ron et al. 1988; Sadetzki et al. 2002).

In the NA-CCSS cohort, meningiomas occurred much later (median 22.9 years, range 15.8–32.7 years) than either subsequent glial tumors or medulloblastomas. This finding was similar to the St. Jude ALL cohort, where meningiomas were diagnosed a median of 19 years from initial cancer diagnosis (Walter et al. 1998), as well as the BCCSS cohort, where meningiomas were diagnosed 23.1 years from initial cancer diagnosis (Taylor et al. 2010).

Among the NA-CCSS cohort, meningioma risk was increased by female sex, younger age at primary diagnosis, radiation therapy exposure and previous treatment for CNS tumor. They occurred at the highest rate among survivors of medulloblastoma, with cumulative incidence of 16.4 % (95 % CI=7.5–25.3 %) (Friedman et al. 2010). Multiple studies have attempted to establish associations between chemotherapy exposure and subsequent meningioma, and for the most part,

no associations have been found; however, Taylor et al. (2010) reported an interesting association between intrathecal methotrexate and risk of meningioma, in an analysis of secondary CNS tumors in the BCCSS. Within the BCCSS cohort, individuals who had received at least 70 mg/m^2 of intrathecal methotrexate had a 36-fold increased risk of meningioma when compared to those unexposed. Within this same cohort, no relationship was observed with systemic methotrexate or other agents. Other studies have failed to find an association between intrathecal chemotherapy and meningioma (Fontana et al. 1987; Walter et al. 1998). In a 2006 analysis of the NA-CCSS patients who had follow-up through 2002, a detailed reconstruction of radiation exposure, including location and dose, was performed to better understand the dose-response relationship between radiotherapy and the development of CNS tumors. Within this cohort, 66 meningiomas were identified, of which three were classified as malignant with other subtypes classified as: meningotheliomatous (5), fibrous (4), and transitional (4) (Neglia et al. 2006). Meningiomas were more common than gliomas in those with secondary CNS tumors. While the overall median time to secondary CNS tumor development was 14 years, it was 17 years for those patients developing meningiomas, with 71 % of patients being diagnosed 15 years or more after their initial cancer diagnosis. The majority of this subset of patients (74 %) was diagnosed after 20 years of age. In children exposed to radiation therapy for their primary malignancy, a positive linear dose-response relationship was observed for development of a meningioma. For survivors treated with 10–20 Gy, the odds of developing meningioma were 12, whereas in those treated with 20–30 Gy the odds increased to 21.6 and, most notably, in survivors who received radiation doses greater than 30 Gy, the odds of developing a meningioma was in the order of 50–100 times that of the general population (see Fig. 11.1).

In an Israeli study of 210 patients treated for acute lymphoblastic leukemia and T-cell non-Hodgkin's lymphoma before 1990, meningiomas were detected in 16 survivors. Median age of detection was 28.7 years and median time from diagnosis was 21 years (10–29 years). Of the 210 patients, 88 had received cranial radiation, and of the 16 identified meningiomas, 15 had received cranial radiation at ages 2–14 years (median 7.6 years); 14 had received 24 Gy and one had received a 18 Gy. This group found the rate of meningiomas increased after 15 years from therapy (Goshen et al. 2007).

In a unique genetic case-control study, a cohort of patients who had been treated with cranial radiation for tinea capitis and then gone on to develop subsequent meningioma was recruited for participation. Their family members, both exposed and not exposed to radiation, were recruited as well. Patients who had been treated with radiation and had not developed subsequent meningioma were recruited, with their family members, as well. Radiation exposure was variable within this group (estimated average dose range to the brain 1.0–6.0 Gy). The patients with radiation-associated meningiomas were more likely to have one or more first-degree relatives develop meningioma as compared to the radiated patients who had not developed meningiomas. These findings suggested the possibility of genetic susceptibility to developing tumors following radiation exposure, although specific candidate genes were not identified and similar studies would be nearly impossible to carry out (Flint-Richter and Sadetzki 2007).

With longer follow-up, meningiomas are now being reported in excess of malignant brain tumors, confirming the longer latency to development (Friedman et al. 2010) and the need for long-term follow up of childhood cancer survivors. There is some evidence that the incidence of meningiomas is underestimated by as much as one-third, since they can often be asymptomatic and routine screening is not part of standard follow-up care (Larjavaara et al. 2008).

Screening

Currently the United Kingdom does not recommend routine imaging or surveillance for childhood cancer survivors previously treated with cranial radiation (CCLG 2005). The North American-based Children's Oncology Group follow-up guidelines recommend screening brain

MRIs beginning 2 years after completion of radiotherapy for survivors with neurofibromatosis (NF) and for symptomatic survivors at high risk of developing second brain tumors (COG 2008). Presently, the majority of subsequent neoplasms of the CNS are identified once they have become symptomatic or incidentally during investigation of another issue.

Survival

There are limited data available on survival following secondary neoplasms of the CNS among childhood cancer survivors. Treatment can be challenging, particularly in higher grade tumors, because of the risks associated with re-irradiation of the CNS. One of the first studies to investigate survival by CNS tumor type was conducted by the BCCSS (Taylor et al. 2009). In their cohort, 13,211 survivors were surveyed and 247 tumors of the brain and spine were identified as secondary neoplasms; of these, 73 were gliomas, 137 meningiomas, and the rest were a variety of other tumors types. Of these 247 second CNS neoplasms, 123 led to death, 62 after glioma and 42 after meningioma; 73 % of the deaths were classified as death from secondary neoplasm. Five year relative survival following meningioma was greater than 80 % for both males and females while for glioma was only 19.5 % with worsening survival paralleling higher tumor grade. Worse outcomes were also observed in patients treated in earlier treatment eras. In a smaller cohort of 1,612 ALL survivors from St. Jude Children's Research Hospital, 22 subsequent CNS tumors were identified; 11 of which were meningiomas, 10 high-grade gliomas, and one low-grade glioma. Overall survival following meningiomas was very good, with all patients alive with up to 10 years of follow-up. Prognosis in the high-grade glioma group was very poor (Walter et al. 1998).

Closing and Future Directions

Exposure to therapeutic radiation for the purpose of treatment of the primary malignancy is the most notable risk factor for the development of subsequent CNS tumors, specifically meningioma and glioma, and evidence is now available to support that a dose-response relationship exists. Children exposed at very young ages appear to be at increased risk for high-grade tumors, emphasizing possible increased susceptibility of the developing brain to radiation effects.

Protocols for chemotherapy and radiation have been modified to minimize toxicity while still maintaining acceptable treatment outcomes (Loning et al. 2000; Bhatia et al. 2002; Hudson et al. 2012). Radiation was first introduced to the treatment of ALL in the late 1960s. Typical radiation dosing at that time was 24 Gy. By the early 1980s, typical prophylactic dosing was 18 Gy for standard risk patients and eventually for patients with high-risk disease as well; although, higher dosing has traditionally been used in the setting of CNS-positive disease (Pui et al. 2003). With the introduction of early intensified intrathecal chemotherapy, patients with standard risk disease were no longer receiving prophylactic cranial radiation and were still able to maintain very low rates of CNS relapse (Pui et al. 1998) and CNS-directed radiation is being given at doses as low as 12 Gy. In the St. Jude cohort, no CNS tumors were observed in patients who were not treated with cranial radiation (Walter et al. 1998).

In the case of primary CNS or head and neck tumors, current radiation modalities such as conformal radiation therapy, intensity-modulated radiation therapy and proton-beam therapy have allowed for more focused therapy with reduced exposure to tissue surrounding the tumor. There are also greater efforts being made to avoid radiation in very young children because of its detrimental effects on the developing central nervous system. In the recent treatment era, the use of chemotherapy has allowed for the reduction of radiotherapy dosing; in the case of average-risk medulloblastoma, Packer et al. (2006) were able to show encouraging event free survival rates in children receiving reduced dosing of craniospinal radiation, consisting of 2,340 cGy versus the standard 3,600 cGy, with the addition of post-radiation adjuvant chemotherapy. Given the long latency that has been observed prior to development of second CNS tumors, particularly in the

case of meningiomas, it will be important to follow patients from the more contemporary treatment protocols to see if decreased rates of second CNS tumors are observed over time.

Ongoing vigilance must be practiced for childhood cancer survivors, as the latency period to development of secondary CNS tumors is often long and symptoms may not be easily identified if primary practitioners are not familiar with late risks. This is particularly important in the context of secondary meningiomas, where the rates have not shown evidence of plateau in the survivor cohorts. As the survivor population ages into adulthood and is no longer following up with their primary pediatric oncology team, continual education of survivors and primary care practitioners, as well as age and personalized, diagnosis- and therapy-specific screening guidelines, are imperative.

Acknowledgement This work was supported by the Children's Cancer Research Fund, Minneapolis, MN and the National Institutes of Health Pediatric Cancer Epidemiology Training Grant T32 CA099936.

References

Altekruse SF, Kosary CL, Krapcho M, Neyman N, Aminou R, Waldron W, Ruhl J, Howlader N, Tatalovich Z, Cho H, Mariotto A, Eisner MP, Lewis DR, Cronin K, Chen HS, Feuer EJ, Stinchcomb DG, Edwards BK (eds) (2010) SEER cancer statistics review, 1975–2007. National Cancer Institute, Bethesda, http://seer.cancer.gov/csr/1975_2007/, based on November 2009 SEER data submission, posted to the SEER web site

Armstrong GT, Liu Q, Yasui Y, Neglia JP, Leisenring W, Robison LL, Mertens AC (2009) Late mortality among 5-year survivors of childhood cancer: a summary from the Childhood Cancer Survivor Study. J Clin Oncol 27:2328–2338

Bhatia S, Sather HN, Pabustan OB, Trigg ME, Gaynon PS, Robison LL (2002) Low incidence of second neoplasms among children diagnosed with acute lymphoblastic leukemia after 1983. Blood 99: 4257–4264

Children's Cancer and Leukaemia Group (CCLG) (2005) Therapy based long term follow up guidelines (Secondary malignancy). www.cclg.org.uk/library/19/PracticeStatement?LTFU-full.pdf

Children's Oncology Group (COG) (2008) Long-term follow-up guidelines for survivors of childhood, adolescent, and young adult cancers. http://www.survivorshipguidelines.org/pdf/LTFUGuidelines.pdf

Flint-Richter P, Sadetzki S (2007) Genetic predisposition for the development of radiation-associated meningioma: an epidemiological study. Lancet Oncol 8: 403–410

Fontana M, Stanton C, Pompili A, Amadori S, Mandelli F, Meloni G, Riccio A, Rubinstein LJ (1987) Late multifocal gliomas in adolescents previously treated for acute lymphoblastic leukemia. Cancer 60: 1510–1518

Friedman DL, Whitton J, Leisenring W, Mertens AC, Hammond S, Stovall M, Donaldson SS, Meadows AT, Robison LL, Neglia JP (2010) Subsequent neoplasms in 5-year survivors of childhood cancer: the Childhood Cancer Survivor Study. J Natl Cancer Inst 102:1083–1095

Goshen Y, Stark B, Kornreich L, Michowiz S, Feinmesser M, Yaniv I (2007) High incidence of meningiomas in cranial irradiated survivors of childhood acute lymphoblastic leukemia. Pediatr Blood Cancer 49:294–297

Hawkins MM, Draper GJ, Kingston JE (1987) Incidence of second primary tumors among childhood cancer survivors. Br J Cancer 56:339–347

Hudson MM, Neglia JP, Woods WG, Sandlund JT, Pui C-H, Kun LE, Robison LL, Green DM (2012) Lessons from the past: opportunities to improve childhood cancer survivor care through outcomes investigations of historical therapeutic approaches for pediatric hematological malignancies. Pediatr Blood Cancer 58:334–343

Larjavaara S, Haapasalo H, Sankila R, Helen P, Auvinen A (2008) Is the incidence of meningiomas underestimated? A regional survey. Br J Cancer 99:182–184

Loning L, Zimmermann M, Reiter A, Kaatsch P, Henzer G, Riehm H, Schrappe M (2000) Secondary neoplasms subsequent to Berlin-Frankfurt-Munster therapy of acute lymphoblastic leukemia in childhood: significantly lower risk without cranial radiotherapy. Blood 95:2770–2775

Mertens AC, Liu Q, Neglia JP, Wasilewski K, Leisenring W, Armstrong GT, Robison LL, Yasui Y (2008) Cause-specific late mortality among 5-year survivors of childhood cancer: the Childhood Cancer Survivor Study. J Natl Cancer Inst 100:1368–1379

Mike V, Meadows AT, D'Angio GT (1982) Incidence of second malignant neoplasms in children: results of an international study. Lancet 320:1326–1331

Neglia JP, Robison LL, Stovall M, Liu Y, Packer RJ, Hammond S, Yasui Y, Kasper CE, Mertens AC, Donaldson SS, Meadows AT, Inskip PD (2006) New primary neoplasms of the central nervous system in survivors of childhood cancer: a report from the Childhood Cancer Survivor Study. J Natl Cancer Inst 98:1528–1537

Packer RJ, Gajjar A, Vezina G, Rorke-Adams L, Burger PC, Robertson PL, Bayer L, LaFond D, Donahue BR, Marymont MH, Muraszko K, Langston J, Sposto R (2006) Phase III study of craniospinal radiation therapy followed by adjuvant chemotherapy for newly diagnosed average-risk medulloblastoma. J Clin Oncol 24:4202–4208

Pui C-H, Mahmoud HH, Rivera GK, Hancock ML, Sandlund JT, Behm FG, Head DR, Relling MV, Ribiero RC, Rubnitz JE, Kun LE, Evans WE (1998) Early intensification of intrathecal chemotherapy virtually eliminates central nervous system relapse in children with acute lymphoblastic leukemia. Blood 92:411–415

Pui C-H, Cheng C, Leung W, Rai SN, Rivera GK, Sandlund JT, Ribiero RC, Relling MV, Kun LE, Evans WE, Hudson MM (2003) Extended follow-up of long-term survivors of childhood acute lymphoblastic leukemia. N Engl J Med 349:640–649

Ron E, Modan B, Boice JD, Alfandary E, Stovall M, Chetrit A, Katz L (1988) Tumors of the brain and nervous system after radiotherapy in childhood. N Engl J Med 319:1033–1039

Sadetzki S, Flint-Richter P, Ben-Tal T, Nass D (2002) Radiation-induced meningioma: a descriptive study of 253 cases. J Neurosurg 97:1078–1082

Taylor AJ, Frobisher C, Ellison DW, Reulen RC, Winter DL, Taylor RE, Stiller CA, Lancashire ER, Tudor ECG, Baggott C, May S, Hawkins MM (2009) Survival after second primary neoplasms of the brain or spinal cord in survivors of childhood cancer: results from the British Childhood Cancer Survivor Study. J Clin Oncol 34:5781–5787

Taylor AJ, Little MP, Winter DL, Sugden E, Ellison DW, Stiller CA, Stovall M, Frobisher C, Lancashire ER, Reulen RC, Hawkins MM (2010) Population-based risks of CNS tumors in survivors of childhood cancer: the British Childhood Cancer Survivor Study. J Clin Oncol 28:5287–5293

Walter AW, Hancock ML, Pui C-H, Hudson MM, Ochs JS, Rivera GK, Pratt CB, Boyett JM, Kun LE (1998) Secondary brain tumors in children treated for acute lymphoblastic leukemia at St. Jude Children's Research Hospital. J Clin Oncol 16:3761–3767

Survivors of Childhood Cancer: Risk of New Primary Neoplasms of the CNS

12

Lucie M. Turcotte and Joseph P. Neglia

Contents

Abstract

Survival following childhood cancer diagnosis has improved dramatically over the past four decades. With this improvement has come increased identification of therapy-related late effects. Among the best studied of these late effects are second neoplasms, and although these can occur at nearly any site, one of the locations often associated with high morbidity and, in some cases mortality, is the central nervous system. Second tumors of the central nervous system most commonly arise in survivors treated for primary CNS tumors or for acute leukemias; this association can be attributed to therapeutic risk factors, most notably prior treatment with radiation therapy. Additional risk factors have been identified, including age at initial cancer diagnosis, as well as underlying genetic predisposition syndromes. Data from multiple childhood cancer survivor cohorts have helped in predicting time to second tumor development and have also helped inform survivor screening and surveillance.

Introduction

There has been dramatic improvement in childhood cancer survival over the past 40 years. These improved outcomes are associated with the use of improved surgical procedures, multi-agent chemotherapy, aggressive supportive care and radiation therapy. As survival has improved, multiple late effects have been identified. Second

L.M. Turcotte • J.P. Neglia (✉)
University of Minnesota, D-557 Mayo Building, MMC 484, 420 Delaware Street SE, Minneapolis, MN 55455, USA
e-mail: jneglia@umn.edu

M.A. Hayat (ed.), *Tumors of the Central Nervous System, Volume 12*,
DOI 10.1007/978-94-007-7217-5_12,

neoplasms have been one of the most widely studied late effects in survivors of childhood cancer, accounting for nearly 20 % of mortality in survivor cohorts (Armstrong et al. 2009a; Mertens et al. 2008). It is noteworthy that by 20 years of follow-up, the death rate from second malignancies exceeds that seen from primary disease recurrence (Mertens et al. 2008). Secondary neoplasms of the central nervous system (CNS) have been well studied and can occur following primary neoplasms both in the CNS as well as in other sites and their occurrences have been associated with characteristics of the treatment of the initial cancer. These tumors may be associated with high rates of morbidity and mortality.

Second tumors of the CNS most commonly arise in survivors previously treated for either a primary CNS tumor or for an acute leukemia. In the cases of primary CNS tumors, second tumors often occur at or near the primary tumor site; at times, these can be difficult to differentiate from recurrence of the primary tumor. The issue can be further complicated by individuals with inherited cancer predisposition syndromes such as neurofibromatosis, in which multiple CNS tumors may occur and appear to be therapy related, when in fact risk is likely in part due to genetics. Behavior of second tumors of the CNS ranges from very benign to highly malignant, and they can be quite devastating; as a result, much has been done to understand risks and modify initial therapies when possible. The strongest known risk factor for is previous cranial radiation. Other risk factors have been investigated through multiple cohort studies and knowledge continues to increase regarding the importance of long-term surveillance for the survivor population.

Epidemiology

The Late Effects Study Group (LESG) conducted one of the earliest studies of second malignant neoplasms in 1982. Records from nearly 15,000 survivors diagnosed between 1950 and 1970 from ten participating centers were analyzed for the occurrence of second malignancies; from this cohort, 113 cases were identified and of these, nine were located in the brain. Histology was not specified. These followed a variety of primary tumor sites (Mike et al. 1982). This was one of the first cohorts with the ability to look at long-term childhood cancer survivors, in part because for the first time survival was long enough to exceed the typical latency period associated with radiation and chemical carcinogenesis. Multiple cohorts have followed, now with more in-depth data collected on primary tumor and type of treatment administered.

The Childhood Cancer Research Group (CCRG) tracked 16,541 cases of 3-year childhood cancer survivors initially diagnosed between 1926 and 1987. There was a fivefold increase in the number of second primary tumors compared with expected numbers (Hawkins et al. 1987). In an early analysis of cohort data, with only 10,106 identified survivors, Hawkins et al. (1987) identified a relative risk of 7 (95 % CI = 4–12) for subsequent CNS tumors. Within the more recent analysis of the cohort, 278(2 %) developed second neoplasms, 44 of which were in the CNS, giving a SIR of 12.4(95 % CI = 9–16.6) for secondary CNS tumors (Jenkinson et al. 2004).

The British Childhood Cancer Survivor Study (BCCSS) has also looked at secondary neoplasms of the CNS in 17,980 5-year British cancer survivors; members within this cohort were diagnosed with cancer between 1940 and 1991, so overlapping with the CCRG study above. Within their cohort, 247 second primary CNS tumors were observed, including 137 meningiomas, 73 gliomas, 16 schwannomas, 9 PNETs and 12 other CNS tumors. The observed mean time to development of glioma from initial cancer diagnosis was 17.4 years (15.5 years for low-grade, 18.7 years for high-grade and 21 years for grade 4), whereas mean time to development of meningioma was 23.1 years (23.5 years for low-grade and 15.9 years for high-grade) (Taylor et al. 2009). The overall standardized incidence ratio (SIR) for glioma was 10.8 (95 % CI = 8.5–13.6) (Taylor et al. 2010).

The North American Childhood Cancer Survivor Study (NA-CCSS) was initiated in 1994 and includes a cohort of 14,361 5-year childhood

cancer survivors who received treatment between 1970 and 1986. Similar to the BCCSS, the NA-CCSS has been able to identify and follow second neoplasms; mean follow up of this population now exceeds 20 years and information regarding tumor histology, cumulative chemotherapeutic and radiation exposures and surgeries are quite complete. Among these individuals, 1,402 developed at least one secondary neoplasm, with a total of 2,703 secondary neoplasms. Of these, 159 nonmalignant meningiomas, 11 malignant meningiomas, 53 glial tumors, 6 medulloblastomas/PNETs and 16 other CNS tumors have been identified (Friedman et al. 2010).

A nested case–control study of the NA-CCSS cohort was performed to more carefully assess new primary neoplasms of the CNS (Neglia et al. 2006). This study allowed for more precise primary and second tumor localization, and calculation of radiation exposure during initial therapy. This was also one of the first analyses to give histology-specific CNS tumor relative risks associated with radiation and chemotherapeutic agents and look at dose–response relationships in regards to patient characteristics. The tumor histologies observed in this study included: 10 glioblastomas, 9 anaplastic astrocytomas, 10 other malignant gliomas, 4 oligodendrogliomas (2 were anaplastic), 2 juvenile pilocytic astrocytomas, and one each of gliosarcoma, fibrillary astrocytoma, myopapillary ependymoma, ganglioglioma and giant cell astrocytoma. This study revealed a standardized incidence ratio (SIR) of 8.66 (95 % CI = 6.24–11.6) of gliomas in cancer survivors when comparing them to the general population.

Within a population of 5,006 survivors treated on the Berlin-Frankfurt-Munster (BFM) ALL protocols between 1979 and 1995, and followed by the German Childhood Cancer Registry (GCCR), 52 second neoplasms were identified, 13 of which were in the CNS. Histologic subtypes included glioblastoma multiforme (n = 4), astrocytoma (n = 4), PNET (n = 3) and meningioma (n = 2). The median time from initiation of primary treatment to diagnosis of a CNS tumor was 7.9 years. By 15 years from initial treatment, cumulative risk of a secondary CNS tumor exceeded that of secondary AML. In comparison with the general population, a 19-fold increase in tumors of the CNS was observed among the ALL survivors (Loning et al. 2000). The longest follow-up reported in this analysis was only 18 years, so likely with a longer follow-up more secondary CNS tumors will be reported.

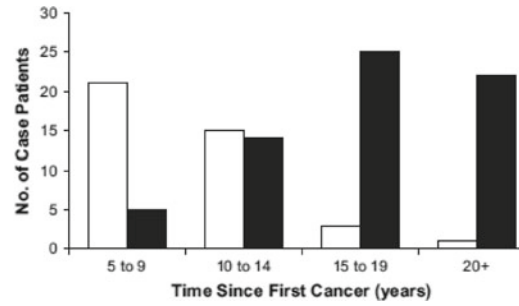

Fig. 12.1 Time to recurrence of subsequent glioma (*open bars*) and meningioma (*closed bars*) in the Childhood Cancer Survivor Study cohort (Printed with permission from Oxford University Press (Neglia et al. 2006))

In terms of time to development of a second CNS neoplasm, the NA-CCSS cohort and the BCCSS investigators found gliomas and medulloblastomas developed after much shorter latency following primary tumor treatment (glial tumor, median = 11.7 years, range = 6–25 years; medulloblastoma, median = 11.6 years, range 8–14.6 years) as compared to malignant meningiomas (median = 22.9 years, range = 15.8–32.7 years) (Friedman et al. 2010). The majority of gliomas occurred in the 5–9 years following initial cancer diagnosis, whereas more than 70 % of meningiomas were diagnosed more than 15 years after initial cancer diagnosis and there is no evidence of decline in the number of new meningiomas with increasing time (see Fig. 12.1) (Neglia et al. 2006). The median age at the time of new CNS tumor diagnosis was 20.5 years; 70 % of gliomas were diagnosed before age 20 and 70 % of meningiomas were diagnosed after 20 years of age. Similar findings were observed in a cohort of ALL survivors from St. Jude Children's Research Hospital (SJCRH); median latency to diagnosis of 12.6 years was reported for all diagnoses combined, with 9.1 years for high-grade gliomas and 19 years for meningiomas (Walter et al. 1998).

There is suggestion that since some tumor types, such as meningioma, can behave in a relatively benign manner, they may be underreported. Estimates have placed incidence as much as one-third higher than reported figures (Larjavaara et al. 2008). This is addressed in an Israeli study of survivors of childhood ALL or T-cell lymphoma in which the survivors were followed with serial cranial imaging (either CT or MRI), every 3–6 years. The patient population included both children who had been treated with cranial radiation (n = 76) and children who had not received radiation (n = 74). The investigators observed 16 meningiomas, with median time of 21 years from initial tumor diagnosis; fifteen of the survivors who developed meningioma had previously received radiation therapy. Of the sixteen meningiomas, only one had clinical symptoms (seizures); the remaining were diagnosed because of screening. Of patients who had received cranial radiation and remained available for screening, cumulative incidence was remarkably high (53.8 %) at 25 years from cranial radiation exposure (Goshen et al. 2007).

Therapeutic Risk Factors

Radiation therapy has been recognized as a risk factor for development of subsequent CNS tumors for quite some time; as a result of this and other considerations, the proportion of children receiving radiotherapy as part of their initial cancer therapy has decreased over time, with 56 % of children receiving it in 1973–1979, to only 28 % in 1995–2002 (Inskip and Curtis 2007). In an analysis of 446 children treated with megavoltage radiation at the University of Minnesota, 37 subsequent neoplasms were identified, including 6 meningiomas and 2 astrocytomas, all of which developed within the initial radiation field. This represented a 4 % (95 % CI = 2–8 %) cumulative risk of developing a brain tumor at 30 years of follow-up (Gold et al. 2003). Goshen and colleagues identified 16 meningiomas in their population of 150 childhood cancer survivors and all but one of those individuals had been previously treated with cranial radiation (Goshen et al. 2007). Similarly, in the SJCRH cohort of 1612 ALL survivors, 21 survivors developed subsequent CNS tumors and all had previously been treated with radiation therapy (Walter et al. 1998). Within the CCSS cohort, second neoplasms were higher among those treated with radiation therapy, with a relative risk of 2.7 (95 % CI = 2.2–3.3) (Friedman et al. 2010). Similarly, within the GCCR cohort of ALL survivors, all secondary CNS tumors except one survivor who developed meningioma had received cranial radiation at some point during therapy. The risk of developing a subsequent CNS tumor was 0.1 % for the non-radiated survivors and 1.3 % for the radiated group and an increased risk was noted with increased radiation dose (Loning et al. 2000).

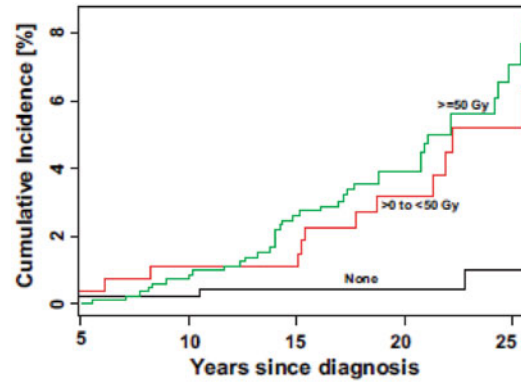

Fig. 12.2 Cumulative incidence of CNS neoplasms by cranial radiation therapy dose (Printed with permission from Oxford University Press (Armstrong et al. 2009b))

Highly significant radiation dose–response relationships have been observed in multiple cohorts (see Fig. 12.2). Within the NA-CCSS cohort, this relationship was observed when all CNS tumors were combined and persisted when individual tumor histologies were examined separately; specifically, the odds of developing glioma rose across radiation categories to a peak of 21 for the 30–44.9 Gy category and the odds of meningioma peaked at 96.3 in the 30–44.9 category (Neglia et al. 2006). The risk of both meningiomas and gliomas was strongly associated with dose of radiation therapy, with an excess relative risk (ERR) of 1.06 per Gy for meningioma and 0.33 per Gy for glioma (Neglia et al. 2006). Similar

linear relationships were described in the BCCSS cohort, although with different effects, both for the development of subsequent gliomas/PNETs (ERR = 0.079 per Gy) and for meningiomas (ERR = 5.1 per Gy). At a cumulative radiation dose of ≥ 40 Gy, the relative risk of developing a subsequent meningioma was 479 times that of non-radiated survivor, whereas the relative risk of subsequent glioma/PNET was 4.4 (Taylor et al. 2010). This is the highest relative risk currently reported for meningioma.

As the use of radiation therapy has decreased over time, the trend has moved in the opposite direction for chemotherapy (Inskip and Curtis 2007). With the advent of improved risk-stratification, high-risk patients are receiving more aggressive chemotherapy regimens (Hudson et al. 2012) and more aggressive intrathecal chemotherapy regimens are being used in place of prophylactic radiation in the case of ALL (Pui et al. 1998). There has been some debate regarding the association of systemic chemotherapy and the development of subsequent neoplasms in the CNS. Multiple cohort studies have looked at this issue and have reported variable results.

Within the NA-CCSS cohort, when adjusting for radiation exposure and original diagnosis, chemotherapy exposure did not appear to significantly increase the risk of second CNS tumor development, even when looking at different chemotherapy classes separately (Neglia et al. 2006; Friedman et al. 2010). Similarly, within the GCCR cohort of ALL survivors and the French-British cohort of non-leukemia childhood cancer survivors, no associations were observed between types or doses of systemic chemotherapy and development of a secondary CNS tumor (Loning et al. 2000; Little et al. 1998). Although no associations were observed between any types of systemic chemotherapy, including methotrexate, and the development of either glioma/PNET or meningioma within the BCCSS, an association between intrathecal methotrexate and subsequent CNS neoplasms has been reported. When adjusting for radiation exposure, a linear relationship was observed with the risk among those exposed to ≥ 70 mg/m^2 was 36 times greater than among those who were not treated with intrathecal methotrexate (Taylor et al. 2010). Associations between intrathecal chemotherapy and risk of subsequent CNS neoplasms have previously been evaluated in the ALL population; however, no other significant associations have been identified to date (Fontana et al. 1987; Walter et al. 1998).

One of the few studies to identify a link between systemic chemotherapy and subsequent CNS tumors was published by Relling et al. (1999) from SJCRH. They identified an increased rate of secondary malignant brain tumors in children receiving therapy on one of their research protocols which gave more intensive antimetabolite therapy before and during radiation therapy. Of the 153 children enrolled, 52 had received cranial radiation, and of those, 6 (12.8 %) developed brain tumors within 7–10 years from the time of radiation. Tumor histologies included: glioblastoma multiforme (3), anaplastic astrocytoma (2) and PNET (1). None of the non-radiated children developed a secondary CNS tumor. Additionally, they determined that 4/6 patients had elevated red blood cell concentrations of thioguanine nucleotide compared to the rest of the irradiated group; furthermore, among the 7 children with a genetic defect in thiopurine methyltransferase (TPMT) activity, cumulative risk of brain tumor development was 42.9 % as compared to 8.3 % in the 45 children with wild-type activity. No other therapy-related associations were identified. These findings raised concern about the possibility of antimetabolites contributing to tumor development when given concurrently with radiation; however, these findings have not been confirmed to date.

The treatment era in which a child was initially diagnosed and treated for their primary cancer has also been associated with risk of second CNS tumors in some cohorts. In the NA-CCSS cohort, survivors treated in 1975–1979 and 1980–1986 had decreased risk of second cancers as compared to those treated in 1970–1974, suggesting that changes are being seen with more conservative radiation, particularly in the ALL treatment protocols, but also recognizing that shorter follow up may be partially responsible for this finding (Friedman et al. 2010). Interestingly, when looking

specifically at gliomas, higher SIR was observed for survivors treated in the most recent period of subject accrual (for diagnosis between 1980 and 1986, SIR = 12.7) (Neglia et al. 2006). Data is not available for patients being treated on contemporary treatment protocols which include more exposure to anthracyclines and cyclophosphamide. Long-term follow up is needed to determine whether risk or type of second cancers has significantly changed.

Host Risk Factors

Available cohort data suggest a role of age in modifying risk for subsequent CNS tumors, although findings have not been completely consistent. Bhatia et al. (2002) found that age at acute leukemia diagnosis did not impact risk of developing subsequent CNS neoplasm; however, Friedman et al. (2010) found that generally, without regard to primary cancer diagnosis, patients who were treated at a younger age (<10 years) had increased risk of developing subsequent CNS tumors. Within the SJCRH cohort of ALL survivors, diagnosis and treatment at less than 6 years of age was not associated with increased risk of secondary brain tumors overall, but was associated with an increased risk of developing a high grade glioma (Walter et al. 1998). Similarly, in the Children's Cancer Study Group, children who were 5 years or younger at the time of diagnosis had a significantly higher risk of developing a secondary brain tumor as compared to those older than 5 years at diagnosis (Neglia et al. 1991).

Loning and colleagues observed that tumors of the CNS were the most common second neoplasm among children who were less than 7 years of age at the time of initial leukemia diagnosis. The cumulative probability of developing a CNS tumor was 1.5 % (95 % CI = 0.2–2.7 %) for this subgroup as compared to risk of 0.1 % (95 % CI = 0–0.3 %) in survivors who were greater than 7 years of age at the time of diagnosis (Loning et al. 2000). Neglia et al. (2006) reported that in the NA-CCSS cohort, when comparing to the general population, standardized incidence ratios for developing glioma was highest among children diagnosed with cancer at less than 5 years of age (SIR = 14.5), and the excess relative risk per Gy was highest for individuals exposed to radiation therapy prior to age 5 years of age (ERR per Gy = 0.64) as compared to those exposed at 5–9 years (ERR per Gy = 0.1) or 10–20 years (ERR per Gy = 0.15). Within the BCCSS cohort, there was a statistically significant decline in the excess relative risk of subsequent glioma/PNET with increasing age of first exposure to radiation. They did not report an effect of age of exposure on developing a subsequent meningioma (Taylor et al. 2010).

Genetic cancer predisposition syndromes, such as Neurofibromatosis 1 and 2, as well as Gorlin's syndrome, tuberous sclerosis and Von Hippel-Lindau syndrome are all associated with increased risk of CNS tumor development (Little et al. 1998). Other host characteristics, such as gender, have not been significantly associated with risk of CNS tumor development.

Role of Primary Cancer Diagnosis

Acute leukemias account for the highest percent of new childhood cancer diagnoses. Acute lymphoblastic leukemia, specifically, is the most common, causing 3–4 cases per 100,000 children annually (Gurney et al. 1995). Five-year survival rates exceed 85 % (Jemal et al. 2010), meaning that there are approximately 2,000 long-term survivors of childhood ALL each year (Bhatia et al. 2002). In ALL survivors treated with cranial irradiation, central nervous system tumors are among the most commonly observed second neoplasms (Neglia et al. 1991; Bhatia et al. 2002; Pui et al. 2003). Within the SJCRH cohort of ALL survivors, CNS leukemia at the time of diagnosis was associated with an increased risk of a subsequent brain tumor and also increased the risk of developing a high-grade tumor; these relationships held, even when radiation dose was controlled for within the analysis (Walter et al. 1998). Cumulative incidence of secondary brain tumors after ALL therapy has been fairly consistent across different cohort studies: 0.47 % at 10

years (Bhatia et al. 2002), 1 % at 15 years (Loning et al. 2000), 1.39 % at 20 years (Walter et al. 1998). These estimates represent an approximate tenfold increased risk of developing a brain tumor as compared to the general population (Bhatia et al. 2002). A variety of CNS tumor histologies have been observed. Bhatia et al. (2002) looked at a cohort of 8,831 children treated for ALL between 1983 and 1995 on Children's Cancer Group (CCG) research protocols. Within the cohort, 63 s malignancies were identified, 19 of which were CNS tumors. Histologies included: glioblastomas multiforme (9), anaplastic astrocytoma (4), primitive neuroectomdermal tumors (PNET) of the brain (3), meningioma (2), and medulloblastoma (1). A study of 856 ALL survivors, treated at SJCRH between 1962–1992, compared survivors treated with radiation (n = 597) and those without (n = 259) (Pui et al. 2003). Of the 44 s neoplasms, 15 occurred in the central nervous system; 10 were meningiomas and 5 were malignant tumors of various types. Among the CCSS cohort, Neglia et al. (2006) found that childhood leukemia survivors were more likely to develop subsequent gliomas as opposed to meningiomas; however, among the SJCRH cohort, primary diagnosis of leukemia was associated with risk of meningioma (Hijaya et al. 2007).

Central nervous system malignancies represent approximately 17 % of all primary childhood malignancies and, as a group, represent the second most common diagnosis in childhood cancer and the most commonly diagnosed solid tumor in childhood (Ries et al. 1999). Survivors of childhood CNS tumors have one of the highest risks for late mortality (Mertens et al. 2008). In the CCSS cohort, 2888 (14 %) were survivors of primary CNS malignancies. Compared to the US population, their risk of death is increased 13-fold, with standardized mortality ratio (SMR) of 12.9 (95 % CI = 11.8–14). Late mortality is highest among survivors of ependymoma or embryonal tumors, followed by medulloblastomas and PNETs. Death attributable to a second neoplasm accounts for 9 % of deaths, and by 30 years after primary cancer diagnosis, death rate from a second neoplasm exceeded that of primary disease recurrence. Incidence of meningioma in this population has steadily increased over time with no evidence of plateau; incidence at 30 years was 3.5 % (95 % CI = 0.9–6.1 %). In patients treated with ≥ 50 Gy of radiation, cumulative incidence of a subsequent CNS neoplasm was 7.1 % (95 % CI = 4.5–9.6 %) at 25 years. In contrast, those treated with less than 50 Gy had an incidence of 5.2 % (95 % CI = 2.1–8.3 %) and in those who had no radiation exposure, the incidence was 1 % (95 % CI = 0–2.3 %) (Armstrong et al. 2009b).

Outcomes and Screening

One of the few studies to date to focus on survival after secondary CNS tumors was published in 2009, from the BCCSS. Five-year relative survival after glioma was 19.5 % (95 % CI = 9.8–33.7 %) in both males and females, with much lower relative survival in those with high-grade tumors (4.9 %, 95 % CI = 0.8–14.6 %) and higher relative survival in those with low-grade tumors (38.9 %, 95 % CI = 22.1–55.4 %). Interestingly, while these survival rates are similar to those observed for gliomas in the general population, most of the cohort patients were diagnosed prior to 30 years of age, a time period in which better survival would be expected. In meningiomas, 5-year relative survival was similar for males (84 %, 95 % CI = 72.6–91.1 %) and females (81.7 %, 95 % CI = 69.9–89.3 %). High-grade meningiomas had decreased survival (57.3 %, 95 % CI 17.2–84 %) as compared to low-grade meningiomas (84.3 %, 95 % CI = 76.5–90 %). Survival was decreased in those treated for their initial childhood cancer prior to 1970 (76.1 %, 95 % CI 61.4–86 %), showed an increase for those initially treated during the 1970s (89.3 %, 95 % CI = 78.5–94.9 %) and then decreased again for those treated between 1980 and 1991 (78.6 %, 95 % CI = 52.2–91.6 %). Five-year relative survival was also significantly decreased in cohort members with underlying genetic syndromes who developed meningiomas (40.1 %, 95 % CI = 5.2–75.4 %) (Taylor et al. 2009). Within the SJCRH ALL cohort, tumor type was strongly linked to survival; all of the patients with low-grade tumors were alive at the time of study

publication, but 80 % of the patients with high-grade gliomas had died (Walter et al. 1998). In the CCG cohort of ALL survivors, mortality was notable, with 11 of 19 patients dead at the time of article publication; although, statistics were not given based on tumor histology (Bhatia et al. 2002).

No current recommendations exist for monitoring for subsequent tumors of the CNS in childhood cancer survivors. As suggested by Goshen and colleagues in their study of childhood ALL and T-cell lymphoma survivors who underwent routine imaging follow-up, significantly higher rates were observed than in non-screened populations (Goshen et al. 2007). Currently, these tumors are identified either once they become symptomatic or incidentally, when imaging is performed for another purpose. Routine MRI screening is typical in patients with a primary CNS tumor and this may facilitate early detection of recurrence or secondary CNS tumors; however, routine MRIs may not extend through the entire latent period prior to development of a new tumor. It is not possible to know whether some of the high-grade tumors reported in the cohort studies had undergone malignant transformation or whether earlier detection may have improved survival. Since the majority of second tumors in the CNS arise after patients have been previously treated with radiotherapy, treatment options are limited; there is limited ability of the CNS to tolerate re-irradiation at the same site.

Closing and Future Directions

As survival has continued to improve for childhood cancers, more is being understood about the occurrence and underlying causes of second neoplasms and other late effects. Based on current studies, exposure to therapeutic radiation for treatment of a primary cancer is by far the most important risk factor for development of a secondary CNS tumor. This is true regardless of primary cancer diagnosis or histology of the second cancer, and the relationship behaves in a dose-responsive fashion. Variable data exists regarding the role of chemotherapy, suggesting the need for further study, particularly as treatment practices evolve over time. Efforts are being made to preserve current outcomes while decreasing toxicity, when possible. Caution must be used when applying current knowledge about survivorship and late effects to patients currently receiving treatment, as treatment regimens have changed over time (Hudson et al. 2012).

Acknowledgement This work was supported by the Children's Cancer Research Fund, Minneapolis, MN and the National Institutes of Health Pediatric Cancer Epidemiology Training Grant T32 CA099936

References

Armstrong GT, Liu Q, Yasui Y, Neglia JP, Leisenring W, Robison LL, Mertens AC (2009a) Late mortality among 5-year survivors of childhood cancer: a summary from the Childhood Cancer Survivor Study. J Clin Oncol 27:2328–2338

Armstrong GT, Liu Q, Yasui Y, Huang S, Ness KK, Leisenring W, Hudson MM, Donaldson SS, King AA, Stovall M, Krull KR, Robison LL, Packer RJ (2009b) Long-term outcomes among adult survivors of childhood central nervous system malignancies in the Childhood Cancer Survivor Study. J Natl Cancer Inst 101:946–958

Bhatia S, Sather HN, Pabustan OB, Trigg ME, Gaynon PS, Robison LL (2002) Low incidence of second neoplasms among children diagnosed with acute lymphoblastic leukemia after 1983. Blood 99:4257–4264

Fontana M, Stanton C, Pompili A, Amadori S, Mandelli F, Meloni G, Riccio A, Rubinstein LJ (1987) Late multifocal gliomas in adolescents previously treated for acute lymphoblastic leukemia. Cancer 60:1510–1518

Friedman DL, Whitton J, Leisenring W, Mertens AC, Hammond S, Stovall M, Donaldson SS, Meadows AT, Robison LL, Neglia JP (2010) Subsequent neoplasms in 5-year survivors of childhood cancer: the Childhood Cancer Survivor Study. J Natl Cancer Inst 102:1083–1095

Gold DG, Neglia JP, Dusenbery KE (2003) Second neoplasms after megavoltage radiation for pediatric tumors. Cancer 97:2588–2596

Goshen Y, Stark B, Kornreich L, Michowiz S, Feinmesser M, Yaniv I (2007) High incidence of meningiomas in cranial irradiated survivors of childhood acute lymphoblastic leukemia. Pediatr Blood Cancer 49:294–297

Gurney JG, Severson RK, Davis S, Robison LL (1995) Incidence of cancer in children in the United States: sex-, race-, and 1-year age-specific rates by histologic type. Cancer 75:2186–2195

Hawkins MM, Draper GJ, Kingston JE (1987) Incidence of second primary tumors among childhood cancer survivors. Brit J Cancer 56:339–347

Hijaya N, Hudson MM, Lensing S, Zacher M, Oneiu M, Behm FG, Razzouk BI, Ribiero RC, Rubnitz JE, Sandlund JT, Rivera GK, Evans WE, Relling MV, Pui C-H (2007) Cumulative incidence of secondary neoplasms as a first event after childhood acute lymphoblastic leukemia. JAMA 297:1207–1215

Hudson MM, Neglia JP, Woods WG, Sandlund JT, Pui C-H, Kun LE, Robison LL, Green DM (2012) Lessons from the past: opportunities to improve childhood cancer survivor care through outcomes investigations of historical therapeutic approaches for pediatric hematological malignancies. Pediatr Blood Cancer 58:334–343

Inskip PD, Curtis RE (2007) New malignancies following childhood cancer in the United States, 1973–2002. Int J Cancer 121:2233–2240

Jemal A, Siegel R, Xu J, Ward E (2010) Cancer statistics, 2010. CA: A Cancer J Clin 60:277–300

Jenkinson HC, Hawkins MM, Stiller CA, Winter DL, Marsden HB, Stevens MCG (2004) Long-term population-based risks of second malignant neoplasms after childhood cancer in Britain. Brit J Cancer 91:1905–1910

Larjavaara S, Haapasalo H, Sankila R, Helen P, Auvinen A (2008) Is the incidence of meningiomas underestimated? A regional survey. Brit J Cancer 99:182–184

Little MP, De Vathaire F, Shamsaldin A, Oberlin O, Campbell S, Grimaud E, Chavaudra J, Haylock RGE, Muirhead CR (1998) Risks of brain tumor following treatment for cancer in childhood: modification by genetic factors, radiotherapy and chemotherapy. Int J Cancer 78:269–275

Loning L, Zimmermann M, Reiter A, Kaatsch P, Henzer G, Riehm H, Schrappe M (2000) Secondary neoplasms subsequent to Berlin-Frankfurt-Munster therapy of acute lymphoblastic leukemia in childhood: significantly lower risk without cranial radiotherapy. Blood 95:2770–2775

Mertens AC, Liu Q, Neglia JP, Wasilewski K, Leisenring W, Armstrong GT, Robison LL, Yasui Y (2008) Cause-specific late mortality among 5-year survivors of childhood cancer: the Childhood Cancer Survivor Study. J Natl Cancer Inst 100:1368–1379

Mike V, Meadows AT, D'Angio GT (1982) Incidence of second malignant neoplasms in children: results of an international study. Lancet 320:1326–1331

Neglia JP, Meadows AT, Robison LL, Kim TH, Newton WA, Ruymann FB, Sather HN, Hammond GD (1991) Second neoplasms after acute lymphoblastic leukemia in childhood. N Engl J Med 325:1330–1336

Neglia JP, Robison LL, Stovall M, Liu Y, Packer RJ, Hammond S, Yasui Y, Kasper CE, Mertens AC, Donaldson SS, Meadows AT, Inskip PD (2006) New primary neoplasms of the central nervous system in survivors of childhood cancer: a report from the Childhood Cancer Survivor Study. J Natl Cancer Inst 98:1528–1537

Pui C-H, Mahmoud HH, Rivera GK, Hancock ML, Sandlund JT, Behm FG, Head DR, Relling MV, Ribiero RC, Rubnitz JE, Kun LE, Evans WE (1998) Early intensification of intrathecal chemotherapy virtually eliminates central nervous system relapse in children with acute lymphoblastic leukemia. Blood 92:411–415

Pui C-H, Cheng C, Leung W, Rai SN, Rivera GK, Sandlund JT, Ribiero RC, Relling MV, Kun LE, Evans WE, Hudson MM (2003) Extended follow-up of long-term survivors of childhood acute lymphoblastic leukemia. N Engl J Med 349:640–649

Relling MV, Rubnitz JE, Rivera GK, Boyett JM, Hancock ML, Felix CA, Kun LE, Walter AW, Evans WE, Pui C-H (1999) High incidence of secondary brain tumors after radiotherapy and antimetabolites. Lancet 354:34–39

Ries LAG, Smith MA, Gurney JG, Linet M, Tamra T, Young JL, Bunin GR (eds) (1999) Cancer Incidence and Survival among Children and Adolescents: United States SEER Program 1975–1995, National Cancer Institute, SEER Program. NIH Pub. No. 99–4649. Bethesda

Taylor AJ, Frobisher C, Ellison DW, Reulen RC, Winter DL, Taylor RE, Stiller CA, Lancashire ER, Tudor ECG, Baggott C, May S, Hawkins MM (2009) Survival after second primary neoplasms of the brain or spinal cord in survivors of childhood cancer: results from the British Childhood Cancer Survivor Study. J Clin Oncol 34:5781–5787

Taylor AJ, Little MP, Winter DL, Sugden E, Ellison DW, Stiller CA, Stovall M, Frobisher C, Lancashire ER, Reulen RC, Hawkins MM (2010) Population- based risks of CNS tumors in survivors of childhood cancer: the British Childhood Cancer Survivor Study. J Clin Oncol 28:5287–5293

Walter AW, Hancock ML, Pui C-H, Hudson MM, Ochs JS, Rivera GK, Pratt CB, Boyett JM, Kun LE (1998) Secondary brain tumors in children treated for acute lymphoblastic leukemia at St. Jude Children's Research Hospital. J Clin Oncol 16:3761–3767

Part III

Treatments

Brain Tumor Typing and Therapy Using Combined Ex Vivo Magnetic Resonance Spectroscopy and Molecular Genomics

13

Loukas G. Astrakas and A. Aria Tzika

Contents

Abstract

A novel approach was developed that combines biomarkers detected with magnetic resonance spectroscopy (MRS) and molecular genomics to improve the typing and prognostication of biospecimens in clinical medicine. Metabolite and genome wide profiles from 55 biopsies from subjects with brain tumors were analyzed with a classification algorithm that produces unique tumor fingerprints. We found that the fusion of 15 gene expressions and 15 MRS metabolites were able to distinguish tumor categories and predict survival better than when either dataset was used alone. Our approach improves the typing and understanding of the complexity of human brain tumors, generates testable hypotheses regarding neoplasia and promises to guide human brain tumor therapy. Our results further elucidate the biology of brain malignancy subtypes in brain tumor patients, and increase the overall potential for success of future studies that combine clinical MRI, MRS and MR imaging of gene expression in vivo.

Introduction

According to the Central Brain Tumor Registry of the United States (www.cbtrus.org) 24,070 malignant and 40,470 non-malignant new cases of primary brain tumors are expected to be diagnosed in 2012. After leukemia, brain tumors are

L.G. Astrakas (✉)
Department of Medical Physics, Medical School, University of Ioannina, 45110 Ioannina, Greece
e-mail: astrakas@uoi.gr

A.A. Tzika, Ph.D
NMR Surgical Laboratory, Department of Surgery, Massachusetts General Hospital and Shriners Burns Institute Harvard Medical School, 02114 MA, Boston

M.A. Hayat (ed.), *Tumors of the Central Nervous System, Volume 12*,
DOI 10.1007/978-94-007-7217-5_13,

the second leading cause of cancer-related deaths in children under age 20 and in males of ages 20–39. Worldwide the incidence rate of primary malignant central nervous system (CNS) tumors is 2.6 in females and 3.7 in males per 100,000 person-years. Generally, primary malignant brain tumors are lethal leaving only 30 % of adult patients alive, 5 years after the initial diagnosis. Therefore, early and accurate diagnosis and grading are extremely important for a successful prognosis and an optimum therapeutic intervention.

Currently, the golden standard for the brain tumor diagnosis, as described by the 2007 WHO classification scheme, is based on histopathological criteria related to morphological changes, growth pattern and molecular profiles of tissue specimens. However, in many cases (e.g., neuroepithelial tumors, subgroups of diffuse large B-cell lymphoma), tumors often do not follow classic histology and the diagnosis becomes challenging and often controversial among clinicians and neuropathologists (Zarbo et al. 2005). New advanced techniques in the fields of radiology, genetics and molecular biology have been developed to provide additional biomarkers for better tumor typing. The diagnostic utility of these biomarkers lies in their biological relevance with different genetic and metabolic pathways implicated in tumor processes, namely differentiation, proliferation, angiogenesis and apoptosis.

Magnetic resonance spectroscopy (MRS) is a powerful tool of biochemical analysis capable to detect and quantify important metabolites implicated in brain tumor pathology. Recent advents in ex-vivo MRS allow subsequent genetic analysis over the entire human transcriptome in the same tissue biopsies. However, highly informative biomarker profiles are difficult to establish, due to current technical limitations and since the small sample sizes of tissue biopsies pose challenges for producing accurate metabolic and transcriptome data. In this chapter it is shown that fusing genomics and MRS results to improved tumor fingerprints that improve typing and prognosis of brain tumors.

MRS

Nuclear magnetic resonance (NMR) spectroscopy is a analytical and diagnostic tool that detects and quantifies multiple tissue-specific metabolites of the tissue of interest. In vitro NMR uses biofluids, (e.g., urine, serum, tissue extracts) and provides high quality spectra with several dozen metabolites, but it has been accused with metabolite degradation and incomplete recovery in processed samples (Duarte and Gil 2012). On the other hand, in vivo NMR, also called magnetic resonance spectroscopy (MRS) is totally noninvasive, but compared to in vitro NMR has low sensitivity and poor spectral resolution (Glunde and Bhujwalla 2011). Ex vivo MRS, also called high resolution magic angle spinning (HRMAS) is an established solid state NMR technique that uses intact tissue specimens, (e.g. biopsies) and provides high resolution quality spectra without the destruction of tissue histopathological structures (DeFeo and Cheng 2010). HRMAS combines the analytical strength of in vitro NMR with the non-destructive nature of MRS and allows the quantitative evaluation of tumor morphology, biochemistry, or genetic profile on the same surgical specimen.

MRS Biomarkers

Proton MRS has identified several biomarkers of tumor growth and apoptosis (Horska and Barker 2010). Studies of brain tumors using proton MRS have demonstrated: (1) edema and necrosis are associated with reduced or absent n-acetylaspartate (NAA) and total creatine (tCr), (2) increased levels of Cho-containing compounds, possibly due to cell membrane disruption and altered phospholipid metabolism and (3) increased lactate due to metabolic acidosis. Reduced NAA is expected in glial tumors, since NAA is primarily localized in neurons. Therefore, NAA detection within glial tumors corresponds to either partial volume averaging with adjacent normal tissue or tumor infiltration of normal tissue. Since NAA is present in

cell cultures of oligodendroglia progenitors, the NAA in childhood tumors may reflect immature oligodendroglia (Urenjak et al. 1992). A reduction in tCr resonance may indicate cell loss due to necrosis and correspond to exhausted energy reserves resulting from rapid cell proliferation and ischemia. Measurement of tCr may be a valuable independent predictor of tumor response to therapy (Tzika et al. 2001).

The Cho peak consists of water-soluble Cho-containing compounds, such as phosphocholine (PCho), glycerophosphocholine (GPC), and free choline, but contains no membrane-bound phosphatidylcholine (PtdCho). In vivo MRS showed that phosphomonoesters (PME), such as PCho and phosphoethanolamine (PEth), are elevated in tumors and rapidly proliferating tissues (Daly and Cohen 1989). Furthermore, PCho and PEth elevation were correlated with increased cell growth or degradation in tumors in humans and animal models and in cell lines. Especially PCho, which can be measured with either phosphorous or proton MRS, is elevated in actively proliferating cells. In vivo proton MRS studies suggest that the Cho peak reflects proliferative activity in gliomas. The PCho concentration was shown to correlate with the number of S-phase cells, and the PCho/GPC ratio correlated with oncogenic transformation. The PCho-produced Cho signal has also been proposed to depend on local cellularity (Chang et al. 1995). Recently, using an HRMAS proton MRS technique, we found that PCho levels correlated with the percentage of highly cellular malignant glioma in glioblastoma multiforme patients (Cheng et al. 2000). PCho and GPC accumulation reflected early stages of growth arrest or apoptosis (Cheng et al. 2000). In addition, GPC levels increased in cultured mammalian cells that exhibited perturbed energetic metabolism during acidosis. Tissues with a high proliferative potential and tissues that were oncogenically transformed are typically highly cellular when compensating apoptotic mechanisms are absent and there are no limitations in the vascular supply. An elevated Cho peak, detected by in vivo MRS, may indicate that the tissue of interest is highly cellular, has an increased proliferative potential, or includes oncogenically transformed cells.

Cancer cells are apoptotic, and thus typically die upon treatment with conventional chemotherapy, radiation antiangiogenic drugs and ganciclovir. In vivo proton MRS detected a substantial accumulation of polyunsaturated fatty acids during gene therapy-induced apoptosis, and PCho depletion coincides with growth arrest. Prior to volume loss, the treatment response was associated with an increase in tissue water diffusion and T2 relaxation time, which suggested that water content and bulk diffusibility increased. Gliomas undergoing apoptosis exhibited reduced diffusion of Cho-containing compounds. These observations imply an increased viscosity and restriction within cells, perhaps via cell shrinkage. Flow-cytometric studies demonstrated that gene therapy-induced apoptosis is preceded by an irreversible arrest in the late S or G2 phase of the cell cycle. MRS-detected lipids not only correlated with necrosis or apoptosis , but also with the proportion of cells in the S and G2 stages (Wei et al. 1998). Finally, the ceramide resonance region has been associated with the differential diagnosis of brain gliomas with high or low malignancy. This observation deserves further investigation, since apoptotic stimuli such as ceramide, a second messenger related to apoptosis, disrupts electron transport in mitochondria and acts as an important site for apoptosis initiation.

Classification and Statistical Analysis of MRS

Many studies on classification and statistical analysis for both in vivo, ex vivo and in vitro NMR spectra have been reported. Variability of the spectra even in samples of the same type is a major difficulty in such analyses along with the large number of detected metabolites. Another difficulty appears in the cases of extensive heterogeneity of the sample where for example infiltrative tumor tissue might coexist with normal tissue and necrotic areas. Nonetheless, MRS based classification according to histological type and grade has been performed using a variety of supervised or unsupervised methods of

statistical analysis, pattern recognition and machine learning. Examples are the linear discriminant analysis (LDA) after feature extraction with independent components analysis (ICA) in a Bayesian framework (Huang et al. 2003). correlation analysis and stepwise LDA (Tate et al. 2003), belief networks (Reynolds et al. 2007) and support vector machines (Andronesi et al. 2008).

For in vivo MRS multivariate analysis techniques have been applied with so far limited clinical use primarily due to the low spectral resolution. The INTERPRET (International Network for Pattern Recognition of Tumours Using Magnetic Resonance) consortium provides a helpful decision support system based on large database of single voxel spectra. For the richer in vitro or ex vivo spectra the tumor type or grade classification results are better especially when they are combined with the in vivo MR spectroscopic or imaging findings.

Genomics

Gene Expression Profiling in Cancer

Cancer is a genetic disease resulting from mutation in genes regulating cell growth and proliferation. Many times histologically similar tumors present different clinical manifestation resulting from different upstream processes due to diverse gene expression patterns. Therefore, understanding of the genetic substrate in tumors could greatly improve their diagnosis and treatment. Projects like the NCI's Cancer Genome Anatomy Project (CGAP) or the Cancer Genome Characterization Initiative (CGCI) try to better understand the underlying genetic changes leading to cancer, leading eventually to improved detection, diagnosis, and treatment for the patient.

DNA-microarray technology allows us to to examine the expression of thousands of genes at once and has found great utility in tumor typing and grading. The most common microarray technologies are divided, according to the type of probe used, to oligonucleotide microarrays and complementary DNA (cDNA) arrays, each one with advantages and disadvantages (Schulze and Downward 2001). Oligonucleotide microarrays can be used for gene expression, rapid mutation analysis, single nucleotide polymorphism and genotyping analyses. They have also been used in the diagnosis of genetic diseases and gene polymorphism studies. On the other hand cDNA arrays provide a less specific but easier method for large scale screening and expression studies.

The application of photolithography techniques in situ on glass wafers by Affymetrix® resulted to GeneChip® containing in an area of 1.6 cm^2more than 65,000 different oligonucleotides. Non specific cross-hybridization is eliminated by pairs of probes, one that is perfectly complementary to a target sequence (Perfect Match, PM) and one that is identical except for a single base mismatch in its center (Mismatch, MM). The GeneChip Human Genome U133 Plus® 2.0 array, contains 1.3 million distinct oligonucleotides and can be used to analyze the expression levels of over 47,000 transcripts as well as variants, including over 30,000 well-characterized human genes. It can utilize al low as 50 ng of total RNA, minimizing sample extraction requirements. Small samples also avoid contamination of the solid tumor sample from infiltrating tissue, such as stroma, endothelial or lymphoid cells. Other advantages of the GeneChip® DNA microarray platform are the access to probe sequences, probe redundancy (11 sequences per gene) to optimize fidelity of the signal-to noise ratio, ready commercial availability, washing, staining and scanning processes, quality control built into the manufacturing processes, available technical support, and a relatively low cost per investigated gene.

Analysis of Microarray-Based Gene Expression Data

Organization, storage, and especially analysis of gene expression data are challenging (Ermolaeva et al. 1998). The use of DNA microarrays to measure genome-wide RNA expression levels has become an established research methodology in genomics to simultaneously measure the expression of tens of thousands of genes from a single sample (Quackenbush 2001). Cancer research, in particular, has benefited enormously from the use

of high-throughput gene expression studies. Much effort has been devoted to developing data analysis techniques, including application of different pattern recognition algorithms to classify cancers (Macgregor and Squire 2002). Many methods have been used to identify genes that are differentially expressed in transformed cells. To improve the accuracy of cancer diagnosis and prediction of patient response to different treatment options, research has focused on the use of gene expression profile databases collected from different cancer types (Golub et al. 1999).

Unsupervised learning can be used to gather gene expression data from a collection of tumor samples, and cluster the samples into groups. Clustering can be based on aggregate expression profile similarity, or genes can be clustered that share similar expression patterns in different biological contexts. Supervised learning techniques based on linear Support Vector Machines (SVMs) have also proven to be both popular and accurate; however, this learning is dependent on accurate sample labels, which are limited by histopathology. An important concern for use of either learning approach is that microarray experiments typically yield expression data for thousands of genes from a relatively small number of samples. Thus, gene-class correlations can arise by chance alone. This issue can be addressed by collecting more samples, although this is often difficult with clinical cancer samples. Another approach is to perform exploratory analysis on an initial data set and apply the results to an independent data set. Confirmed findings will be less likely to reflect chance. Permutation testing, which involves randomly permuting class labels and determining gene-class correlations, can also be used to determine statistical significance. Observed gene-class correlations are considered statistically significant, if they are stronger than those seen in permuted data (Golub et al. 1999).

Combining MRS and Genomics

Previous studies have shown that the combination of different techniques that provide complementary information enhance the specificity of cancer diagnosis in clinical medicine (Garzon et al. 2011). Along this line PET-CT and MRI-PET scanners have already beeen produced whereas new hybtid schemes are currently in the developing process. HRMAS spectroscopy is an ideal candidate for a multiparametric approach on the tumor typing problem, because it leaves the sample intact for subsequent analysis with other techniques. To this end we have combined ex vivo MRS and whole genome expression profiling in order to produce superior biomarkers which provide unique tumor fingerprints (Astrakas et al. 2011).

Experimental Design

We carried out experiments on a dataset of 55 gene expression profiles derived from normal (9 cases) and tumor (46 cases) classes from subjects ranged in age from 17 to 54 years. The tumor class samples belonged to three categories: high grade (H) [20 cases: 12 glioblastoma multiforme (GBM); 8 anaplastic astrocytoma (AA)], low grade (L) (17 cases: 7 meningioma; 7 schwanoma; 7 pylocitic astrocytoma) and metastasized (M) (11 cases: 5 adenocarcinoma; 3 breast cancer metastasis; 3 other metastasis).

Ex vivo 2D TOBSY HRMAS spectra were acquired on a Bruker BioSpin Avance NMR spectrometer (600.13 MHz) using a 4-mm triple resonance (1H, 13C, 2H) HRMAS probe (Bruker) at −8 °C with 3 kHz MAS speed to minimize tissue degradation (Fig. 13.1). Specimens were preweighed and transferred to a ZrO2 rotor tube (4 mm diameter, 50 μl), containing an external standard [trimethylsilyl propionic-2,2,3,3-d4 acid (TSP), Mw = 172, d = 0.00 ppm] that functioned as a reference both for resonance chemical shift and quantification. TOBSY spectra of intact specimens were analyzed using the XWINNMR 3.5 software package (Bruker Biospin Corp, Billerica, MA). Following the standard procedures of fourier transformation, phasing, apodization, baseline correction and peak fitting. Relative quantification of the brain metabolites, we calculated by dividing the ratio of the cross peak volumes of the metabolites to the TSP diagonal peak volume by the biopsy weight. The impacts of each the following 15 NMR features on the tumor classification were examined: choline (Cho),

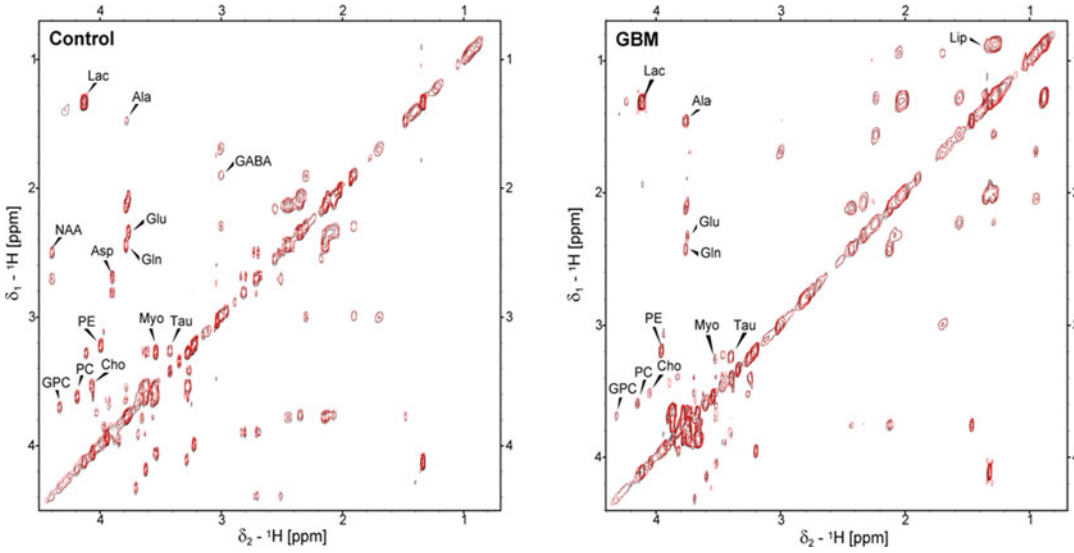

Fig. 13.1 2D [^{1}H,^{1}H] HRMAS spectra from controls (*left*) and GBM (*right*) tumor biopsies, acquired with a 600 MHz (1H) NMR spectrometer at an MAS rate of 3 kHz and at −8 °C. Assigned: Alanine (*Ala*), γ-amino-butyric acid (*GABA*), Choline (*Cho*), Glutamine (*Gln*), Glutamate (*Glu*), Glycerophosphocholine (*GPC*), Lipids (*Lip*), Myoinositol (*Myo*), Phosphocholine (*PC*), Phosphorylethanolamine (*PE*), N-acetyl-aspartate (*NAA*), and Taurine (*Tau*)

phosphocholine (PC), glycerophosphocholine (GPC), phosphoethanolamine (PE), ethanolamine (Etn) γ-amino-butyric acid (GABA), n-acetyl-aspartate (NAA), aspartate (Asp), alanine (Ala), polyunsaturated fatty acids (PUFA), glutamine (Gnl), glutamate (Glu), lactate (Lac), taurine (Tau) and lipids (Lip).

The microscale genome array studies were performed with the commercially available Affymetrix U133Plus® array (Santa Clara, CA). Total experimental RNA were isolated using the modified protocol of the RNeasy purification kit (Qiagen). The Ribo-SPIA protocol (www.nugeninc.com) was used for mRNA labeling and amplification. We used 20 ng total RNA for first strand cDNA synthesis, and the entire procedure for amplification, fragmentation and labeling was performed in 1 day. Normalization and analysis of the expression values was performed using both dChip (http://biosun1.harvard.edu/complab/dchip/) and GC-RMA. Comparison of the expression profiles between tumor biopsies and control tissue microarrays was performed using significant analysis of microarrays (SAMs) (http://www-stat.stanford.edu/~tibs/SAM/) to obtain a list of differentially expressed genes with a false discovery rate (q-value) <0.05 and to properly take into account the substantial multiple comparison problem.

The architecture of our classification system is shown in Fig. 13.2. We first performed a feature selection process by which the high dimensionality of the feature space (consisting of 54,675 genes) was reduced by selecting only the most relevant genes for the classification task. Then, a Support vector machine (SVM) classifier was constructed to these reduced feature vectors in order to optimally partition the space according to class. Finally, the constructed reduced feature space from the gene expression values was combined with the NMR features in order to examine their impact on the classifier.

Feature selection methods typically rank genes according to their differential expressions among phenotypes and pick the top-ranked genes. There are two general schemes for feature selection: filters and wrappers (Inza et al. 2004). We used the minimum redundancy – maximum relevance (MRMR) method (Hanchuan et al. 2005), because it is a powerful framework for selecting features that capture class characteristics in a broad spectrum by reducing mutual

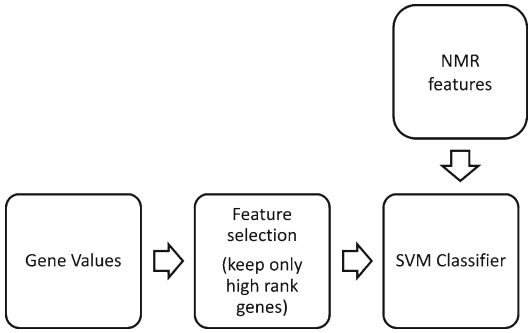

Fig. 13.2 Classification system architecture

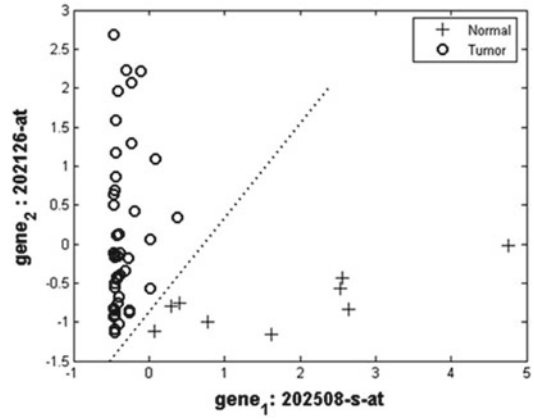

Fig. 13.3 Two genes give 100 % accuracy in normal versus tumor classification

redundancy within the feature set. Thus, it offers greater robustness and generalization properties to the reducing feature space of samples which can significantly improve classification accuracy.

Support vector machine (SVM) is a very powerful classification method that draws hyperplanes in the feature vector space by maximizing the margin between data samples of different classes. SMV is built upon the use of kernels to construct nonlinear decision boundaries. Here, we used linear kernels and the LIBSVM environment for multi-class SVMs (Hsu and Lin 2002). It should be noted that during all experiments with the SVM, we adopted the standard leave-one-out training/testing scheme. That is, one element of the data was used as a training set, and the left-out element was used for testing the predictive performance of the resulting classifier. The SVM soft-margin constant C was set to 10, chosen based on the results of a few runs on one training set. The results indicated that the value of this parameter was not crucial for our experimental dataset.

Two classification problems were studied: Problem (I) distinguish between normal and tumor classes. All 46 samples of the three tumor categories belonged to the same parent-class, tumor (*two-class problem*); Problem (II) study the different tumor categories (H, L and M) and subtypes i.e., GBM, AA, meningioma etc. Experiments were designed for the 55−9 = 46 samples in an attempt to distinguish among the different types of tumor (*multiple-class problem*).

Results

Problem I: In the two-class problem, the performance of the SVM classifier using gene values was perfect. In particular, we obtained 100 % accuracy using only the first two features (genes 202126-at and 202508-s-at) that were selected by the MRMR feature selection method (Fig. 13.3). Their discriminative ability was highy significant as they established a feature space, which could be easily divided into normal and tumor sub-regions. Adding more genes improved further the discriminate between tumor (either high grade or low grade) and metastasis. Among them, gene 1552797_s_at is relevant to a stem cell marker for malignant brain tumors.

Problem II (tumor type and subtype classification): As expected, this classification scheme was more difficult. The classifier had near excellent behavior using the first 9–25 features selected by the MRMR method. Using the first 15 genes, the classifier reached 100 % best accuracy. Specifically, after adding gene 209771_x_at to the feature vectors, the classification performance was 80.4 %; adding gene 229851_s_at increased the performance to 91.3 %; adding gene 225491_at increased it to 95.6 %; adding genes 211991_s_at, 1552797_s_at, 224209_s_at, 206349_at, 204131_s_at and 241938_at increased it to 97.8 %. Finally, the addition of

gene 204501_at increased the classification performance to 100 % for anaplastic astrocytoma and menignioma. We also tested the impact of combining selected NMR features (isolated or combined) with the gene values. Using all 15 NMR features and selected genes (obtained from the MRMR genes selection method) increased the classification performance from 95.6 % to 97.8 % for the high grade typing (11 genes and 15 NMR features), from 95.6 % to 100 % for schwanoma subtyping (1 gene 209169_at and 15 NMR features) and from 95.6 % to 97.8 % for metastasis subtyping (12 genes and 15 NMR features).

Using logistic regression we have also investigated how the 15 metabolite values from HRMAS MRS data, the 15 best genes, or their combination predict survival using 49 available binary clinical outcomes (33 survived vs. 16 deceased). We found that gene data alone result to excellent predictivity sensitivity 94 %, specificity 97 %, and accuracy 96 %. HRMAS MRS data had inferior performance with sensitivity 69 %, specificity 85 % and accuracy 80 %. However the combination of genomics and HRMAS MRS data achieved a perfect 100 % classification for all indices. Due to our small sample size we consider these promising results not as a definite proof of the strength of the fusion approach of MRS and genomics but rather as an positive indication of its potential.

Discussion

Previous studies applied MRS succesfuly to answer important clinically question related with treatment response and survival of patients with CNS tumors. Similarly, gene profiling studies have shown greater accuracy than histology in outcome and survival prediction. Here we introduced a novel approach that combines MRS and molecular genomic biomarkers in order to develop a useful tool that allows accurate tumor fingerprinting. This would facilitate diagnosis and treatment course decisions, but also it would enhance our understanding the underlying biological processes, an important step for novel drug development. Our approach demonstrated the potential of HRMAS and its combination with gene expression profiles to offer better tumor classification and survival prediction than each methodology alone.

It is interesting that gene 1552797_s_at is relevant to a stem cell marker for malignant brain tumors, cd133 (Sakariassen et al. 2007). This suggests that our work using adult brain tumor biopsies has demonstrated that with appropriate quality control, we are able to produce meaningful data and introduce a novel classification scheme that complements and substantiates the current hypothesis of cancer stem cells as a means of determining brain tumor classification and treatment. We also found that certain genes were useful to subtype brain tumors (FOXG1, UCP2, RARRES2, LPIN1, FYN, STK38L, STX7, MSL-1, MUC1, SUB1, FLJ20273, NAP1L2, GDA, FKBP5, PILRB, CLDN11, SALL1, DOCK5, EPPK1, GLT8D4, QKI) and certain other genes were useful for survival classification (NFIB, LOC100129015, SH3KBP1, ITIH2, VCAN, FAM155A, GBP2, MEST, GOLIM4, BBOX1, MFN1, TOMM22, CSNK2A2, AIF1, HERC1). These genes have been reported for other cancers or diseases but the majority of them are novel to brain tumors. This indicates common genetic mechanisms across different tumor types and underlines the potential of our approach for production of new knowledge.

Our approach requires biopsy collection which is a risky invasive procedure not always available. However it provides MRS and genetic biomarkers of tumor typing which in principle are useful in the clinical setting using in vivo MRS and targeted molecular imaging technologies. Already, at the research level, in vivo 2D MRS has developed as a means to type inoperable tumors in the absence of biopsies or gene expression data. Previous studies have shown an agreement between in vivo and ex vivo MRS measurements allowing the utilization of the results of our approach for analysis of in vivo data. Also knowing the important genes for tumor classification specific complimentary reporter probes can be developed that couple to them, accumulated at the tumor area and be detected

noninvasively with in vivo molecular-genetic imaging techniques.

The strength of our approach lies in the combination of complementary metabolic and genetic information. Despite the genetic substrate of tumors, in many cases proteins and therefore metabolites concentration does not depend on gene expression but it is determined by their rate of degradation, or their activity is controlled by allosteric effects or post translational modification. In principle MRS metabolites are more directly related to tumor phenotype than gene expression data and their fusion with the genomic data is meaningful. Unfortunately, proton MRS can detects only a tiny amount of tumor metabolic profile and further studies employing phosphorus or carbon-13 MRS appear promising, although not yet widely available at the clinical setting.

References

Andronesi OC, Blekas KD, Mintzopoulos D, Astrakas L, Black PM, Tzika AA (2008) Molecular classification of brain tumor biopsies using solid-state magic angle spinning proton magnetic resonance spectroscopy and robust classifiers. Int J Oncol 33:1017–1025

Astrakas L, Blekas KD, Constantinou C, Andronesi OC, Mindrinos MN, Likas AC, Rahme LG, Black PM, Marcus KJ, Tzika AA (2011) Combining magnetic resonance spectroscopy and molecular genomics offers better accuracy in brain tumor typing and prediction of survival than either methodology alone. Int J Oncol 38:1113–1127

Chang L, McBride D, Miller BL, Cornford M, Booth RA, Buchthal SD, Ernst TM, Jenden D (1995) Localized in vivo 1H magnetic resonance spectroscopy and in vitro analyses of heterogeneous brain tumors. J Neuroimaging 5:157–163

Cheng LL, Anthony DC, Comite AR, Black PM, Tzika AA, Gonzalez RG (2000) Quantification of microheterogeneity in glioblastoma multiforme with ex vivo high-resolution magic-angle spinning (HRMAS) proton magnetic resonance spectroscopy. Neuro Oncol 2:87–95

Daly PF, Cohen JS (1989) Magnetic resonance spectroscopy of tumors and potential in vivo clinical applications: a review. Cancer Res 49:770–779

DeFeo EM, Cheng LL (2010) Characterizing human cancer metabolomics with ex vivo 1H HRMAS MRS. Technol Cancer Res Treat 9:381–391

Duarte IF, Gil AM (2012) Metabolic signatures of cancer unveiled by NMR spectroscopy of human biofluids. Prog Nucl Magn Reson Spectrosc 62:51–74

Ermolaeva O, Rastogi M, Pruitt KD, Schuler GD, Bittner ML, Chen Y, Simon R, Meltzer P, Trent JM, Boguski MS (1998) Data management and analysis for gene expression arrays. Nat Genet 20:19–23

Garzon B, Emblem KE, Mouridsen K, Nedregaard B, Due-Tonnessen P, Nome T, Hald JK, Bjornerud A, Haberg AK, Kvinnsland Y (2011) Multiparametric analysis of magnetic resonance images for glioma grading and patient survival time prediction. Acta Radiol 52:1052–1060

Glunde K, Bhujwalla ZM (2011) Metabolic tumor imaging using magnetic resonance spectroscopy. Semin Oncol 38:26–41

Golub TR, Slonim DK, Tamayo P, Huard C, Gaasenbeek M, Mesirov JP, Coller H, Loh ML, Downing JR, Caligiuri MA et al (1999) Molecular classification of cancer: class discovery and class prediction by gene expression monitoring. Science 286:531–537

Hanchuan P, Fuhui L, Ding C (2005) Feature selection based on mutual information criteria of max-dependency, max-relevance, and min-redundancy. IEEE Trans Pattern Anal Mach Intell 27:1226–1238

Horska A, Barker PB (2010) Imaging of brain tumors: MR spectroscopy and metabolic imaging. Neuroimaging Clin N Am 20:293–310

Hsu CW, Lin CJ (2002) A comparison of methods for multiclass support vector machines. IEEE Trans Neural Netw 13:415–425

Huang Y, Lisboa PJ, El-Deredy W (2003) Tumour grading from magnetic resonance spectroscopy: a comparison of feature extraction with variable selection. Stat Med 22:147–164

Inza I, Larranaga P, Blanco R, Cerrolaza AJ (2004) Filter versus wrapper gene selection approaches in DNA microarray domains. Artif Intell Med 31:91–103

Macgregor PF, Squire JA (2002) Application of microarrays to the analysis of gene expression in cancer. Clin Chem 48:1170–1177

Quackenbush J (2001) Computational analysis of microarray data. Nat Rev Genet 2:418–427

Reynolds GM, Peet AC, Arvanitis TN (2007) Generating prior probabilities for classifiers of brain tumours using belief networks. BMC Med Inform Decis Mak 7:27

Sakariassen PO, Immervoll H, Chekenya M (2007) Cancer stem cells as mediators of treatment resistance in brain tumors: status and controversies. Neoplasia 9:882–892

Schulze A, Downward J (2001) Navigating gene expression using microarrays–a technology review. Nat Cell Biol 3:E190–E195

Tate AR, Majos C, Moreno A, Howe FA, Griffiths JR, Arus C (2003) Automated classification of short echo time in in vivo 1H brain tumor spectra: a multicenter study. Magn Reson Med 49:29–36

Tzika AA, Zurakowski D, Poussaint TY, Goumnerova L, Astrakas LG, Barnes PD, Anthony DC, Billett AL, Tarbell NJ, Scott RM et al (2001) Proton magnetic spectroscopic imaging of the child's brain: the response of tumors to treatment. Neuroradiology 43:169–177

Urenjak J, Williams SR, Gadian DG, Noble M (1992) Specific expression of N-acetylaspartate in neurons, oligodendrocyte-type-2 astrocyte progenitors, and immature oligodendrocytes in vitro. J Neurochem 59:55–61

Wei SJ, Chao Y, Hung YM, Lin WC, Yang DM, Shih YL, Ch'ang LY, Whang-Peng J, Yang WK (1998) S- and G2-phase cell cycle arrests and apoptosis induced by ganciclovir in murine melanoma cells transduced with herpes simplex virus thymidine kinase. Exp Cell Res 241:66–75

Zarbo RJ, Meier FA, Raab SS (2005) Error detection in anatomic pathology. Arch Pathol Lab Med 129:1237–1245

Atlas-Based Segmentation of Tumor-Bearing Brain Images

14

Stefan Bauer, Roland Wiest, Johannes Slotboom, and Mauricio Reyes

Contents

Abstract

In diagnostic neuroradiology as well as in radiation oncology and neurosurgery, there is an increasing demand for accurate segmentation of tumor-bearing brain images. Atlas-based segmentation is an appealing automatic technique thanks to its robustness and versatility. However, atlas-based segmentation of tumor-bearing brain images is challenging due to the confounding effects of the tumor in the patient image. In this article, we provide a brief background on brain tumor imaging and introduce the clinical perspective, before we categorize and review the state of the art in the current literature on atlas-based segmentation for tumor-bearing brain images. We also present selected methods and results from our own research in more detail. Finally, we conclude with a short summary and look at new developments in the field, including requirements for future routine clinical use.

Introduction

Brain Tumors and Clinical Brain Tumor Imaging

Although brain tumors are not frequent (with an incidence of about 1‰ in the western population), they are among the most fatal cancers (DeAngelis 2001). Due to their different characteristics they are categorized into different classes. The most widely used grading scheme

S. Bauer (✉) • M. Reyes
Institute for Surgical Technology and Biomechanics, University of Bern, Stauffacherstrasse 78, CH-3014 Bern, Switzerland
e-mail: Stefan.bauer@istb.unibe.ch

R. Wiest • J. Slotboom
SCAN, University Institute of Diagnostic and Interventional Neuroradiology, Inselspital, Bern University Hospital, Freiburgerstrasse, CH-3010 Bern, Switzerland

M.A. Hayat (ed.), *Tumors of the Central Nervous System, Volume 12*,
DOI 10.1007/978-94-007-7217-5_14,

was suggested by the World Health Organization (WHO), classifying brain tumors into grades from I to IV with increasing malignancy. Treatment for brain tumors strongly depends on the tumor classification and the rate of progression, with treatment options ranging from surgical resection to radiation therapy, chemotherapy and/or anti-angiogenic therapy.

Brain tumors are commonly diagnosed by neuro-imaging procedures, ideally by magnetic resonance imaging (MRI) (DeAngelis 2001). There is a variety of imaging sequences that provide the possibility to vary tissue contrast, thus highlighting different pathological or healthy tissue compartments. The most relevant MRI sequences in clinical practice of brain tumor imaging incorporate T_1-weighted images, T_1-weighted images with contrast enhancement (usually Gadolinium-DTPA), T_2-weighted images and T_{2Flair} images (Drevelegas and Papanikolaou 2011). Although imaging is very powerful and important in brain tumor diagnosis and treatment planning, even advanced imaging methods may fail in the delineation of the complete extent of the actual tumor.

Medical Image Segmentation

Medical images must be processed and the relevant information has to be extracted in order to provide useful information to the neuroradiologist and the clinician. This information contains tumor location and size, including a precise delineation of the tumor boundaries, but also the location of healthy tissues and subcortical structures surrounding the tumor, which is of relevance for radiotherapy and neurosurgery. Medical image segmentation (Pham et al. 2000) aims at dividing an image into several different compartments. These compartments can be chosen according to structures of interest or tissue types. In today's clinical practice, the most common approach is to perform manual segmentation by drawing the outline of the structure or tissue of interest on the patient image. The drawback of this approach is that it is very time-consuming, especially for 3D images, and it also lacks in reproducibility (Mazzara et al. 2004). Therefore, automatic methods to segment tumor-bearing brain images are promising, because they can significantly reduce segmentation time during post-processing and also offer better reproducibility with respect to their objectiveness.

Automatic segmentation methods for tumor-bearing brain images usually require some pre-processing, which may include skull-stripping (Speier et al. 2011) and the alignment of sequential or multi-modal images in a common frame of reference by image registration (Mang et al. 2008). The current segmentation methods for brain tumor images can be roughly divided into two different categories. On the one hand, there are methods that operate on multi-modal images and on the other hand, there are methods which operate on preselected mono-modal sequences only. Multi-modal approaches are commonly based on classification methods and consider several MRI modalities simultaneously (e.g. Bauer et al. 2011b). They are good at outlining the tumor including its sub-compartments, i.e. necrotic tissue, enhancing lesions and edema. These methods are not further discussed in this article. On the other hand, mono-modal approaches for segmentation of tumor-bearing brain images often rely on atlas registration. These methods, commonly referred to as "atlas-based segmentation", excel at delineating small healthy structures surrounding the tumor. Different approaches for atlas-based segmentation of tumor-bearing brain images will be discussed in more detail in the following sections. We intend to provide a short review and categorization of the state of the art of atlas-based segmentation of tumor-bearing brain images and also discuss some of our own research in more detail.

Atlas-Based Segmentation of Tumor-Bearing Brain Images

Clinical Requirements

Atlas-based segmentation has been shown to be more suitable for delineating healthy tissues and

structures around the tumor than for segmenting the tumor itself. Therefore, its most important application comes from neurosurgical or radiotherapy planning, where manual delineation of the tissues and structures at risk for damage is currently state of the art. To make the transition from the current manual segmentation to a fully automatic atlas-based segmentation in a clinical environment, the methods have to fulfill certain requirements. These include proven accuracy and robustness of the segmentation result, but also a limit on the maximum computation time of the algorithm. Computation time is crucial for the productive use of a method in daily clinical practice. Another important aspect is the user-friendliness of the tool provided: Physicians are unlikely to make routine use of a new method unless it is easy to use and well-understood, to rely on it for making clinical decisions. Additionally, it would be useful if the chosen segmentation method is able to handle a large variety of different brain tumors, including multifocal lesions, without requiring too much user intervention.

The Basics of Atlas-Based Segmentation

Atlas-based segmentation performs implicit segmentation by registering an atlas to the patient image and propagating the atlas labels (Cabezas et al. 2011). In general, the method requires an atlas and a transformation model for the registration. An atlas consists of an anatomical image and the segmentation label map for the structures of interest. There are a number of publicly available single-subject atlases or average atlases derived from multiple subjects; one recent example was described by Rohlfing et al. (2010). The transformation model defines how the atlas is aligned with the patient image. Most authors follow a two-step procedure for this alignment, by first performing a rough registration of both images with an affine transformation model and then doing a refined non-rigid registration for a more precise alignment of both images (Zitova and Flusser 2003). Image alignment is usually performed by using an intensity-based cost function, which is iteratively minimized with a dedicated optimizer. Finally, the atlas label map can be transformed and warped to the patient image to be overlaid on it, using the transformation parameters obtained from the alignment of the anatomical images. This provides an implicit segmentation of the patient image. In the case of image analysis for brain tumor studies, atlas-based segmentation is mostly applied on high-resolution isotropic T_1-weighted or T_1-contrast-enhanced (CE) MR images.

The major challenge in atlas-based segmentation of tumor-bearing brain images is the missing correspondence between healthy atlas image and pathological patient image. A number of approaches have been suggested to circumvent this problem. They can be broadly separated into approaches which are purely registration-based and approaches that employ a biomechanical tumor-growth model for establishing initial correspondence between both images, before a final non-rigid registration step performs a refined alignment of brain structures.

Purely Registration-Based Approaches for Atlas-Based Segmentation

The simplest solution is to use standard registration methods without considering the fact that the patient image has been distorted by the presence of a tumor. Isambert et al. (2008) delineated organs at risk in a clinical radiotherapy context by registering a standard brain atlas to the patient image using multi-affine block-matching. Figure 14.1 shows an example of their automatic delineation in green of the optic nerves, eyes, brain stem and cerebellum for one patient, together with a manually defined ground truth in red. Deeley et al. (2011) combined multi-affine and non-rigid registration with a final level-set refinement for the segmentation of brain structures in the presence of space-occupying lesions.

Brett et al. (2001) were among the first to explicitly address the problem of missing correspondence in registration of tumor images. They suggested masking the cost function of a combined affine and non-rigid registration method.

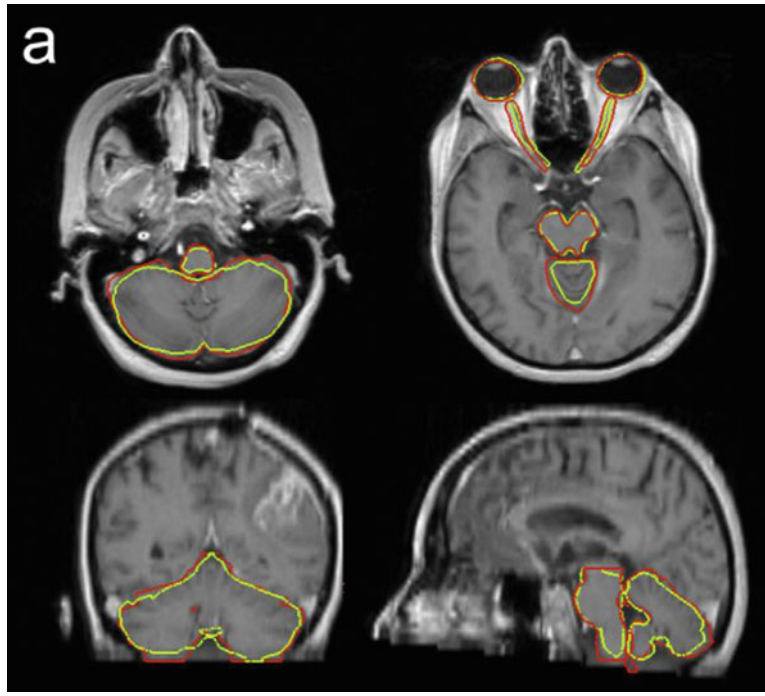

Fig. 14.1 Automatic (in *green*) and manual (in *red*) delineation of brain organs at risk in radiotherapy. The segmented structures include optic nerves, eyes, brain stem and cerebellum (From Isambert et al. (2008))

For this, a manual pre-segmentation of the lesion was required and could be used as a mask for the similarity criterion during the registration. A similar approach was chosen by Stefanescu et al. (2004). A confidence map with zero confidence for all voxels inside the pre-segmented tumor mask was used for the similarity metric during the registration process. Additionally, adaptive regularization was allowed in different tissue regions.

Dawant et al. (2002) placed small tumor seeds in the atlas at the patient's approximate tumor location. Then, a non-rigid registration was performed, which simultaneously deformed the seeds in the atlas to approximately match the pre-segmented patient tumor. Commowick et al. (2005) employed statistical measures of anatomical variability for guiding the regularization during the registration process, where regions of low variability were more strongly regularized and regions of high variability, like tumor regions, could deform more. Chitphakdithai and Duncan (2010) used an indicator map to model different correspondence assumptions for various tissue classes. Registration was regarded as a maximum a posteriori (MAP) problem and solved in an expectation maximization (EM) framework, whereas the probability term of the transformation could be seen as a similarity metric.

A different idea is to incorporate a lesion model directly into the registration method, which allows for a decoupling of the deformations due to tumor growth and inter-subject variations. In this direction, Bach-Cuadra et al. (2004) suggested a model of lesion growth for atlas-based segmentation of tumor-bearing brain images. To this end, a simplistic radial lesion growth model was incorporated into a Demons-based non-rigid registration method. The lesion growth model modified a healthy atlas and adapted it to the tumor-bearing patient image. Despite having two distinct deformation models, this method relied on registration models only and did not include any kind of bio-mechanical

tumor-growth simulation. Later, Bach-Cuadra et al. (2006) from the same group improved their previous method by replacing the SSD-based Demons registration algorithm with an optical flow method employing the more robust mutual information similarity metric, which allowed them to drop the assumption of a linear intensity correspondence relation between the two images. Niethammer et al. (2011) proposed a metamorphosis model, which combined two distinct deformations in order to jointly estimate a deformation in space and a change in image appearance. A global geometric deformation was employed to model changes in image appearance and local matching for considering the tumor was based on an image composition model in an LDDMM framework.

Methods Combining Tumor Growth Modeling with Registration for Atlas-Based Segmentation

Another idea to circumvent the problem of a missing correspondence between the atlas image of healthy individuals and the pathological patient image is to seed the atlas with a tumor before applying the non-rigid registration. Most of the underlying approaches make use of a bio-mechanical tumor-growth model that simulates patient-specific tumor growth in the atlas image, and they finally apply a standard non-rigid registration method to the modified atlas image.

Kyriacou et al. (1999), the first ones to suggest this type of approach, assumed a uniform strain of the tumor and non-linear elastic behavior of the surrounding tissues. In a first step, they shrank the tumor in the patient image to obtain a simulated healthy patient image. Then, the tumor shrinkage process was inverted by performing tumor growth on the registered atlas using a regression method. This allowed them to obtain a patient-adapted atlas including pathology in a final step. Mohamed et al. (2006) grew the tumor in the atlas according to the pathological patient image, instead of shrinking the tumor first. The final adaptation of the modified atlas to the patient image was achieved with a non-rigid registration method. To handle the significant computational cost of the tumor growth modeling in 3D, they employed an approach based on a statistical model using principal component analysis (PCA). For each available case, they estimated the most likely parameters and applied the deformation using the pre-built statistical model. Zacharaki et al. (2008) improved this approach by implementing a multi-resolution framework for registration of brain tumor images. In their so-called ORBIT method, they also used a statistical model of tumor-induced deformation, but they embedded it into a hierarchical framework for parameter optimization. Local information was incorporated into the tumor growth model and the registration methodology was improved. In a further step, the same group improved their tumor growth model compared to the previous method (Zacharaki et al. 2009). They dropped the need for a simplified PCA-based tumor growth model while still achieving computational efficiency. To this end, they employed a piecewise Eulerian tumor mass-effect simulator with a uniform outward-pushing pressure model for the bulk tumor. Parameter optimization was parallelized for further speed improvements.

Recently, researchers from the same group built upon the previous methods by making improvements to the tumor growth model. Instead of considering only bio-mechanical mass effects with a simplified pressure model, they proposed a more sophisticated coupled physio-mechanical model. In GLISTR, Gooya et al. (2011a), employed a diffusion–reaction model for tumor growth, which was coupled with an Eulerian finite element method (FEM) for simulating the mass effect. They operated on multi-sequence images to obtain a probability map of the different tissue classes using classification techniques. In the atlas, a patient-specific tumor was grown and a Demons-like algorithm was finally used for the atlas-to-patient transformation. For this, the tissue probability map output from the classifier was used in the cost function. The process was formulated as an EM problem, which jointly estimated tumor growth parameters and the spatial transformations to adapt the atlas to the patient image. This resulted in a large

optimization problem, which had to be solved. In a next step, Gooya et al. (2011b) dropped the requirement for pre-classification and proposed a joint segmentation and registration model, which also included tumor growth. This was again formulated in an EM framework for joint estimation of tumor growth parameters and the deformation field for registration. The posterior tissue probabilities, which had been derived from the deformed atlas, yielded the segmentation of the patient image.

Our own research was inspired by methods which suggested combining tumor-growth modeling for the tumor mass effect and the establishment of initial correspondence between atlas and patient image with advanced non-rigid registration. In our method for atlas-based segmentation of tumor-bearing brain images, we explored two different lines of research: On the one hand, we worked on a simplistic but fast method for atlas-based segmentation, and on the other hand, we explored a more sophisticated but computationally more demanding approach.

For the simplistic but fast approach, in Bauer et al. (2011a), we developed a method, that segmented the healthy tissues surrounding the tumor in a brain image by atlas-based segmentation. These tissues included cerebrospinal fluid (CSF), gray matter (GM) and white matter (WM). The method used a simplistic but computationally fast bio-mechanical tumor growth method to first grow a patient-specific tumor in the atlas and then deform the modified atlas to match the patient image using a non-rigid Demons registration method. We relied on a pre-segmentation of the tumor as an input and performed automatic skull-stripping in a pre-processing step. Then, we aligned the atlas to the patient image using an affine transformation model. From there, we defined a tumor seed in the atlas which was located in the center of mass of the patient tumor. Subsequently, a mesh-free method based on Markov Random Fields (MRF) was used for modeling the tumor-mass effect. We chose a radial expansion model which was propagated by an MRF on the deformation field and which was bio-mechanically justified because it considered the Young's modulus of different brain tissues during tumor expansion. Tumor expansion was formulated as an energy minimization problem in an MRF context which was solved using the iterated conditional modes (ICM) algorithm. The ICM algorithm had the advantage that it could be parallelized very easily and it was implemented on a massively parallel graphics processing unit (GPU); this led to significant speed improvements. After tumor growth modeling, the final adaptation of the modified atlas to the patient image was done using an ITK implementation (Ibanez et al. 2005) of the Diffeomorphic Demons non-rigid registration method (Vercauteren et al. 2009). Figure 14.2 illustrates the pipeline. A tumor seed was automatically selected in the center of mass of the patient tumor and the tumor was grown in the atlas, deforming the surrounding tissues, before the final non-rigid registration was applied. The results were analyzed on four T_1-weighted images from the ContraCancrum database (Marias et al. 2011) and four synthetically generated brain tumor images with a well-defined ground truth (Prastawa et al. 2009). Quantitative evaluation was performed using the Dice similarity coefficient, which measures the overlap with the ground-truth segmentation. The Dice coefficient can range from 0 to 1, with 0 indicating no overlap and 1 indicating perfect overlap. The algorithm achieved Dice coefficients between 0.7 and 0.82 for the relevant tissue CSF, GM and WM within a total computation time of less than 30 min on a GPU.

For the biophysically more realistic approach, in Bauer et al. (2012), we explored a computationally more demanding method for multi-scale tumor growth modeling in atlas-based segmentation of tumor-bearing brain images. We chose the same pipeline as in the previous method that included automatic skull-stripping of the patient image, affine registration of the atlas, seeding the atlas with a physically realistic tumor seed in the center of mass of the patient tumor, tumor growth simulation to model the tumor mass effect, and final non-rigid registration. The difference was that, in this case, we replaced the simplified purely bio-mechanical tumor growth model with a more sophisticated tumor growth model which considered multiple scales ranging from the

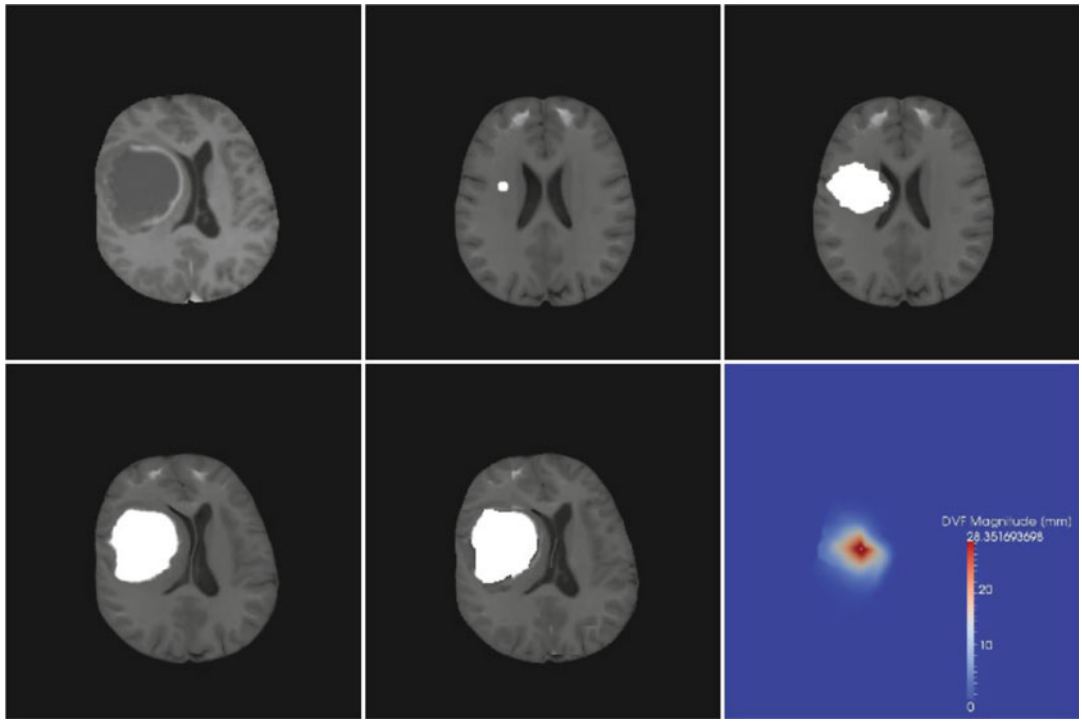

Fig. 14.2 Results of atlas-based tissue segmentation illustrated on one axial slice of a patient image. *Top row left* to *right*: patient image, seeded atlas after affine registration, deformed atlas after tumor growth. *Bottom row left* to *right*: modified atlas after final non-rigid registration, tissue checkerboard of final result and the magnitude of the displacement field resulting from the tumor mass effect simulation (From Bauer et al. (2011a))

microscopic cellular level up to the macroscopic bio-mechanical level. To this end, a discrete-entity, discrete-event cellular-level based oncosimulator (Stamatakos et al. 2010) focusing on biological phenomena like cell-cycling and apoptosis was coupled with a bio-mechanical stress/strain simulation (May et al. 2011) which could provide pressure gradient information. Since the limit of applicability of the standard Lagrangian formulation of structural mechanics was reached under large tumor-induced deformations, the linear-elastic model was solved in an Eulerian implementation of FEM. Thus, the calculation was performed on a fixed geometrical mesh and material properties were advected to neighboring elements upon deformation. Furthermore, this allowed for operating directly on the voxel mesh obtained from the image, eliminating the need for complex mesh generation procedures. The cell simulator required information on the direction into which new tumor cells would spread. This direction could be decided based on the pressure of the surrounding tissues. The pressure was obtained from the mechanical simulator which in turn required information about the expansion of each geometrical cell. This was calculated from the cellular proliferation model. The direction of least pressure $\mathbf{d}$ was calculated based on the negative gradient

$$\mathbf{d} = -\frac{\nabla p}{\|\nabla p\|}$$

whereas the pressure p was given in terms of the trace of the stress tensor $\boldsymbol{\sigma}$. A linear elastic model with Young's modulus E and Poisson ratio υ served as the governing physical law for the non-uniform stress distribution. With this approach, the tumor was grown in the atlas until the approximate volume of the patient tumor was reached, and the

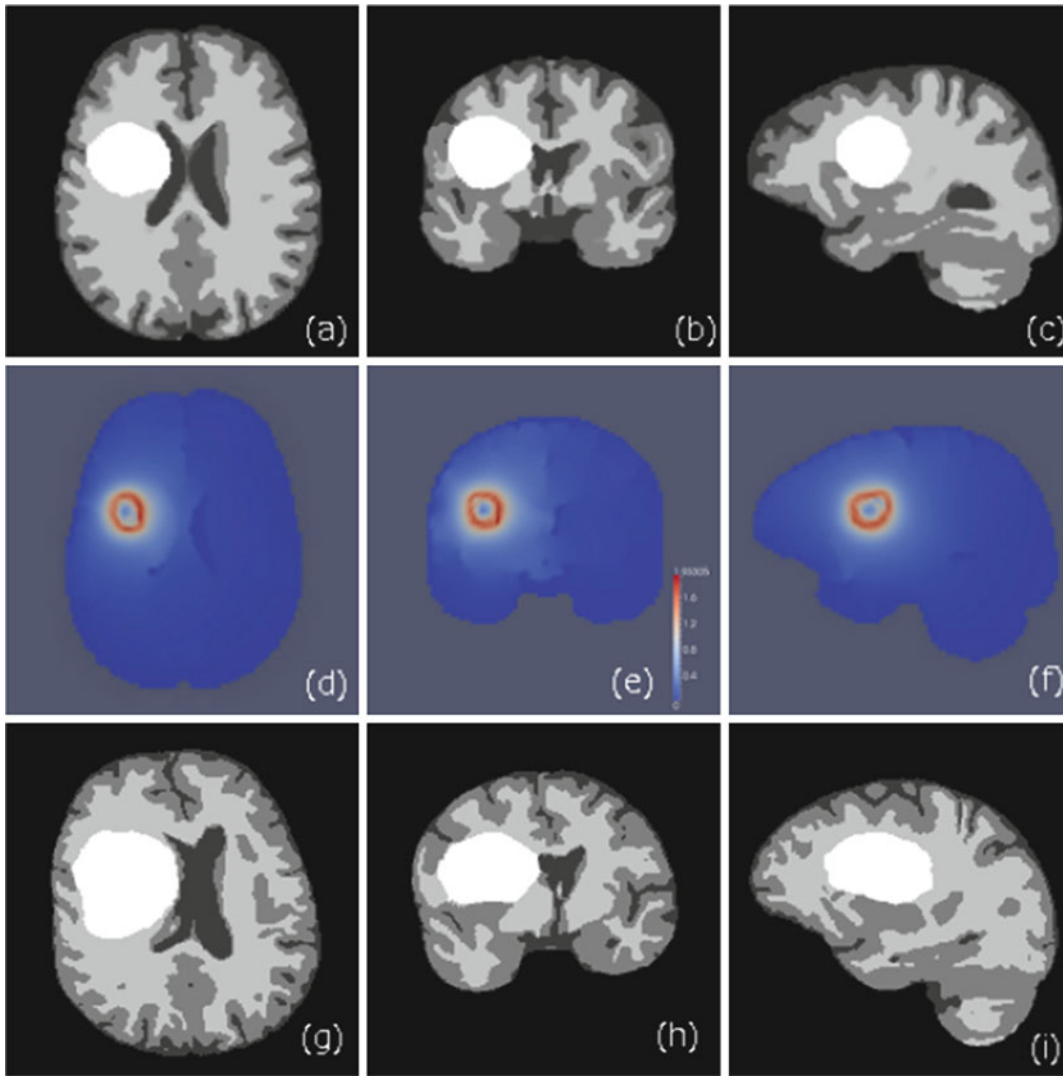

Fig. 14.3 Results of atlas-based segmentation on one slice of a patient image. *Top row*: deformed atlas label map (CSF, GM, WM, tumor) after the final tumor growth modeling step. *Center row*: magnitude of the displacement field in the final tumor growth simulation step. *Last row*: atlas label image after tumor growth and non-rigid registration. This label map forms the segmentation of the patient image. All images are shown in axial, coronal and sagittal view (From Bauer et al. (2012))

final non-rigid Diffeomorphic Demons registration (Vercauteren et al. 2009) was applied subsequently. Due to the enormous computational requirements of the multi-scale tumor growth model, simulation was performed on a coarse version of the atlas only. Figure 14.3 shows results for this approach on one patient image, including the magnitude of the displacement field. It can be inferred from the displacement field that this approach was able to account for the effect of necrosis which occurred in the tumor center. This was achieved thanks to the coupling of a cellular proliferation model with a bio-mechanical mass effect model. The method was evaluated on four synthetic datasets (Prastawa et al. 2009) and four real patient T_1-weighted datasets (Marias et al. 2011) with Dice

similarity coefficients ranging from 0.56 to 0.8 for the relevant tissues. Computation time was between 10 and 36 h depending on the size of the patient tumor.

Currently, we are exploring ways to integrate all the information available from clinical multimodal image acquisition protocols for further improving and automatizing atlas-based segmentation of tumor-bearing brain images Bauer et al. (2013). To this end, we are first performing a fully automatic segmentation of the tumor and its different layers based on the multimodal classification method presented in Bauer et al. (2011b). This serves as prior information for an atlas-based segmentation approach similar to the one presented in Bauer et al. (2012). The method allows us to segment not only tissues, but also subcortical structures. This could have important implications for planning in radiotherapy or neurosurgery.

Discussion and Outlook

Atlas-based methods for segmentation of tumor-bearing brain images usually operate on monomodal high-resolution isotropic T_1-weighted magnetic resonance images. They can be broadly classified into methods employing standard registration models and methods which combine standard registration with patient specific tumor-growth modeling. Both approaches have their advantages and disadvantages: While pure registration methods are in general faster and more versatile, integrated simulation and registration methods are generally more realistic and accurate. After having moved from purely bio-mechanical tumor-growth simulation models for establishing initial correspondence between atlas and patient image to more sophisticated coupled diffusion-bio-mechanics or coupled cellular-bio-mechanics models, an obvious next step would be to integrate all three levels of complexity to model tumor behavior. These levels would include the microscopic level for modeling cell proliferation, the macroscopic level for modeling the diffusion of cancer cells along the fiber directions in the brain and finally the bio-mechanical level modeling the tumor mass-effect, as initially proposed in Marias et al. (2011). Additionally, it would be interesting to see if additional prior knowledge from multimodal structural images could be incorporated in a meaningful way in order to allow for better segmentations and more accurate predictions. Another option would be to rely on crisp multi-channel atlases similar to (Prastawa et al. 2009) to increase the amount of prior information obtained from the atlas.

However, from the clinical perspective, a major problem of most current approaches is still the tremendous computational requirements, which are mostly due to the multi-scale tumor growth models employed in atlas-based segmentation. This is also the main reason why most of the current methods are in favor of pure research explorations so far and will not reach routine clinical use before significant improvements in computational speed are being made. In daily practice, computation times on the order of a few minutes at most are required.

Validation is another critical issue. It is doubtful whether the currently used global evaluation schemes that mostly measure volumetric overlap of individual structures, are the best choice. Especially in neurosurgery and radiotherapy, it is of utmost importance to accurately delineate healthy tissues and subcortical structures in close proximity of the tumor tissue instead of more distant tissues and structures; but so far there exists no well-accepted evaluation method to make this distinction.

Acknowledgements This work was partially funded by the European Union within the framework of the ContraCancrum project (FP7 – IST-223979).

References

Bach-Cuadra M, Pollo C, Bardera A, Cuisenaire O, Villemure JG, Thiran JP (2004) Atlas-based segmentation of pathological MR brain images using a model of lesion growth. IEEE Trans Med Imaging 23:1301–1314

Bach-Cuadra M, De Craene M, Duay V, Macq B, Pollo C, Thiran JP (2006) Dense deformation field estimation for atlas-based segmentation of pathological MR brain images. Comput Meth Progr Biomed 84:66–75

Bauer S, Nolte LP, Reyes M (2011a) Segmentation of brain tumor images based on atlas-registration combined with a Markov-Random-Field lesion growth model. Int Symp Biomed Imaging 8:2018–2021

Bauer S, Nolte LP, Reyes M (2011b) Fully automatic segmentation of brain tumor images using support vector machine classification in combination with hierarchical conditional random field regularization. Lect Notes Comput Sci 6893:354–361

Bauer S, May C, Dionysiou D, Stamatakos G, Büchler P, Reyes M (2012) Multi-scale modeling for image analysis of brain tumor studies. IEEE Trans Biomed-Eng 59:25–29

Bauer S, Lu H, May CP, Nolte L-P, Büchler P, Reyes M (2013) Integrated segmentation of brain tumor images for radiotherapy and neurosurgery. Int J Imaging Syst Technol 23(1):59–63

Brett M, Leff AP, Rorden C, Ashburner J (2001) Spatial normalization of brain images with focal lesions using cost function masking. Neuroimage 14:486–500

Cabezas M, Oliver A, Lladó X, Freixenet J, Bach-Cuadra M (2011) A review of atlas-based segmentation for magnetic resonance brain images. Comput Meth Progr Biomed 104:58–77

Chitphakdithai N, Duncan JS (2010) Non-rigid registration with missing correspondences in preoperative and postresection brain images. Lect Notes Comput Sci 6361:367–374

Commowick O, Stefanescu R, Fillard P, Arsigny V, Ayache N, Pennec X, Malandain G (2005) Incorporating statistical measures of anatomical variability in atlas-to-subject registration for conformal brain radiotherapy. Lect Notes Comput Sci 3750:927–934

Dawant BM, Hartmann SL, Pan S, Gadamsetty S (2002) Brain atlas deformation in the presence of small and large space-occupying tumors. Comput Aided Surg 7:1–10

DeAngelis LM (2001) Brain tumors. N Engl J Med 344:114–123

Deeley MA, Chen A, Datteri R, Noble JH, Cmelak AJ, Donnelly EF, Malcolm AW, Moretti L, Jaboin J, Niermann K, Yang ES, Yu DS, Yei F, Koyama T, Ding GX, Dawant BM (2011) Comparison of manual and automatic segmentation methods for brain structures in the presence of space-occupying lesions: a multi-expert study. Phys Med Biol 56:4557–4577

Drevelegas A, Papanikolaou N (2011) Imaging modalities in brain tumors. Imag Brain Tumors Histol Corr 13–34

Gooya A, Biros G, Davatzikos C (2011a) Deformable registration of glioma images using EM algorithm and diffusion reaction modeling. IEEE Trans Med Imaging 30:375–390

Gooya A, Pohl K, Bilello M, Biros G, Davatzikos C (2011b) Joint segmentation and deformable registration of brain scans guided by a tumor growth model. Lect Notes Comput Sci 6892:532–540

Ibanez L, Schroeder W, Ng L, Cates J (2005) The ITK software guide 2nd ed., Kitware

Isambert A, Dhermain F, Bidault F, Commowick O, Bondiau PY, Malandain G, Lefkopoulos D (2008) Evaluation of an atlas-based automatic segmentation software for the delineation of brain organs at risk in a radiation therapy clinical context. Radiother Oncol 87:93–99

Kyriacou SK, Davatzikos C, Zinreich SJ, Bryan RN (1999) Nonlinear elastic registration of brain images with tumor pathology using a biomechanical model. IEEE Trans Med Imaging 18:580–592

Mang A, Schnabel JA, Crum WR, Modat M, Camara-Rey O, Palm C, Caseiras GB, Jäger HR, Ourselin S, Buzug T, Hawkes DJ (2008) Consistency of parametric registration in serial MRI studies of brain tumor progression. Int J Comput Ass Radiol Surg 3:201–211

Marias K, Dionysiou D, Sakkalis V, Graf N, Bohle RM, Coveney PV, Wan S, Folarin A, Büchler P, Reyes M, Clapworthy G, Liu E, Sabczynski J, Bily T, Roniotis A, Tsiknakis M, Kolokotroni E, Giatili S, Veith C, Meese E, Stenzhorn H, Kim YJ, Zasada S, Haidar AN, May C, Bauer S, Zhao Y, Karasek M, Grewer R, Franz A, Stamatakos G (2011) Clinically driven design of multi-scale cancer models: the ContraCancrum project paradigm. J R Soc Interface Focus 1:450–461

May CP, Kolokotroni E, Stamatakos GS, Büchler P (2011) Coupling biomechanics to a cellular level model: an approach to patient-specific image driven multi-scale and multi-physics tumor simulation. Prog Biophys Mol Biol 107:193–199

Mazzara GP, Velthuizen RP, Pearlman JL, Greenberg HM, Wagner H (2004) Brain tumor target volume determination for radiation treatment planning through automated MRI segmentation. Int J Radiat Oncol 59:300–312

Mohamed A, Zacharaki EI, Shen D, Davatzikos C (2006) Deformable registration of brain tumor images via a statistical model of tumor-induced deformation. Med Image Anal 10:752–763

Niethammer M, Hart GL, Pace DF, Vespa PM, Irimia A, van Horn JD, Aylward SR (2011) Geometric metamorphosis. Lect Notes Comput Sci 6892:639–646

Pham DL, Xu C, Prince JL (2000) Current methods in medical image segmentation. Annu Rev Biomed Eng 2:315–337

Prastawa M, Bullitt E, Gerig G (2009) Simulation of brain tumors in MR images for evaluation of segmentation efficacy. Med Image Anal 13:297–311

Rohlfing T, Zahr NM, Sullivan EV, Pfefferbaum A (2010) The SRI24 multichannel atlas of normal adult human brain structure. Hum Brain Mapp 31:798–819

Speier W, Iglesias J, El-Kara L, Tu Z, Arnold C (2011) Robust skull stripping of clinical glioblastoma multiforme data. Lect Notes Comput Sci 6893: 659–666

Stamatakos GS, Kolokotroni E, Dionysiou D, Georgiadi E, Desmedt C (2010) An advanced discrete state-discrete event multiscale simulation model of the

response of a solid tumor to chemotherapy: mimicking a clinical study. J Theor Biol 266:124–139

Stefanescu R, Commowick O, Malandain G, Bondiau PY, Ayache N, Pennec X (2004) Non-rigid atlas to subject registration with pathologies for conformal brain radiotherapy. Lect Notes Comput Sci 3216: 704–711

Vercauteren T, Pennec X, Perchant A, Ayache N (2009) Diffeomorphic demons: efficient non-parametric image registration. Neuroimage 45:S61–S72

Zacharaki EI, Shen D, Lee SK, Davatzikos C (2008) ORBIT: a multiresolution framework for deformable registration of brain tumor images. IEEE Trans Med Imaging 27:1003–1017

Zacharaki EI, Hogea CS, Shen D, Biros G, Davatzikos C (2009) Non-diffeomorphic registration of brain tumor images by simulating tissue loss and tumor growth. Neuroimage 46:762–774

Zitova B, Flusser J (2003) Image registration methods: a survey. Image Vision Comput 21:977–1000

Nonthermal Irreversible Electroporation as a Focal Ablation Treatment for Brain Cancer

15

Paulo A. Garcia, John H. Rossmeisl Jr., Thomas L. Ellis, and Rafael V. Davalos

Contents

Abstract

Irreversible Electroporation (IRE) is a new focal tissue ablation technique that has shown great promise as a treatment for a variety of soft-tissue neoplasms. The therapy uses pulsed electric fields to destabilize cell membranes and achieve tissue death in a non-thermal manner. The procedure is minimally invasive and is performed through small electrodes inserted into the tissue with treatment duration of about 1 min. In this chapter we describe the first systematic in vivo studies of IRE in canine brain tissue. We confirmed that the procedure can be applied safely in the brain and was well tolerated clinically in normal dogs. The necrotic lesions created with IRE were sub-millimeter in resolution, sharply delineated from normal brain, and spared the major blood vessels. In addition, our preliminary results in a rodent study indicate that IRE transiently disrupts the BBB adjacent to the

P.A. Garcia (✉)
School of Biomedical Engineering and Sciences,
Virginia Tech – Wake Forest University,
330 ICTAS Building, Stanger Street,
Blacksburg, VA 24061, USA
e-mail: pgarcia@vt.edu

J.H. Rossmeisl Jr.
Department of Small Animal Clinical Sciences,
Virginia-Maryland Regional College of Veterinary Medicine, 205 Duck Pond Drive,
Blacksburg, VA 24061, USA

T.L. Ellis
Department of Neurosurgery, Wake Forest University School of Medicine, 1 Medical Center Blvd,
Winston-Salem, NC 27157, USA

R.V. Davalos
School of Biomedical Engineering and Sciences,
Virginia Tech – Wake Forest Universitye,
329 ICTAS Building, Stanger Street,
Blacksburg, VA 24061, USA

M.A. Hayat (ed.), *Tumors of the Central Nervous System, Volume 12*,
DOI 10.1007/978-94-007-7217-5_15,

ablated area in a voltage-dependent manner with implications for enhanced delivery of cytotoxic agents to regions with infiltrative tumor cells. Finally, we present representative case examples demonstrating therapeutic planning aspects, clinical applications, and results of IRE ablation of spontaneous malignant intracranial gliomas in canine patients. Our group has demonstrated that IRE ablation can be performed safely, and is effective at reducing the tumor volume and associated intracranial hypertension, and allows for improvement in tumor-associated neurologic dysfunction. Our work illustrates the potential benefits of IRE for in vivo ablation of neoplastic brain tissue, especially when traditional methods of cytoreductive surgery are not possible or ideal.

Introduction

High-grade gliomas, most notably glioblastoma multiforme (GBM), are among the most aggressive of all malignancies in humans and dogs. High-grade variants of gliomas are difficult to treat and generally considered incurable with singular or multimodal therapies (Stupp et al. 2005; La Rocca and Mehdorn 2009). Many patients with GBM die within 1 year of diagnosis, and the 5-year survival rate in people is approximately 10 % (Stupp et al. 2005). Despite extensive research and advancement in diagnostic and therapeutic technologies, very few therapeutic developments have emerged that have significantly improved survival for humans with GBM over the last seven decades (Stupp et al. 2005).

Considering the therapeutic challenge that neurosurgeons are faced with when managing patients with malignant glioma (MG), many recent efforts have been directed into the development of minimally invasive techniques that can be used for focal neoplastic tissue ablation as alternatives to traditional surgical approaches. Thermal-dependent tissue ablation techniques, such as cryoablation (Tacke 2001), laser interstitial thermotherapy (Atsumi et al. 2001), and radiofrequency lesioning (Cosman et al. 1983) have been developed, but with limited success or applicability in the brain primarily due to the heat sink effect associated with the vascular brain parenchyma.

Irreversible electroporation (IRE) is a new technique for the focal ablation of undesirable tissue with pulsed electric fields (Al-Sakere et al. 2007). One of the main advantages of IRE over other focal ablation techniques is that the therapy does not rely on temperature changes to kill the cells (Garcia et al. 2011b), a process which is also referred to as non-thermal irreversible electroporation (N-TIRE). The thermal sparing effect of IRE is advantageous compared to previously described methods of tissue destruction that are dependent on local tissue temperature changes and results in sparing of major blood vessels, extracellular matrix, and other critical structures within the treated tissue (Al-Sakere et al. 2007).

An IRE treatment involves placing minimally invasive electrodes within the region of interest and delivering a series of electric pulses that are microseconds in duration (Lee et al. 2007). The pulses create an electric field that induces an increase in the resting transmembrane potential (TMP) of the cells in the tissue (Davalos et al. 2005). The induced increase in the TMP is dependent on the electric pulse (e.g. strength, duration, repetition rate, shape, and number), impedance distribution of the tissue as well as the tissue type, and physical configuration of the electrodes used to deliver the pulses. Depending on the magnitude of the induced TMP, as well as its duration and repetition rate for induction, the electric pulses can have no effect, transiently increase membrane permeability, or cause cell death. Spatially, for a given set of conditions, the TMP and therefore the degree of electroporation is dependent on the local electric field and the tissue type to which the cells are exposed. Because the transitions in cellular response to the electric pulses are sudden, the treated regions are sharply delineated. Consequently, numerical models that simulate the electric field distributions in tissue can be used to predict the treated region (Miklavcic et al. 2000; Edd and Davalos 2007).

Recently, IRE has shown promise as a therapy for soft-tissue neoplasms, using minimally invasive instrumentation and allowing for treatment

monitoring with routine clinical procedures (Ball et al. 2010; Neal et al. 2011; Thomson et al. 2011). Studies of focal IRE ablations in mammalian liver and prostate have shown that therapeutic protocols are safe and can be implemented to preserve the integrity of sensitive tissues, such as the major vasculature and ductal frameworks within treated parenchymal volumes (Lee et al. 2007; Onik et al. 2007; Rubinsky et al. 2007; Appelbaum et al. 2012; Ben-David et al. 2012). We believe that the IRE technology possesses other inherent properties that make it well suited for the treatment of brain lesions in which the therapeutic intent is focal and highly controlled tissue destruction.

This chapter presents results on the first in vivo experimental use of IRE to ablate normal brain (Ellis et al. 2011) demonstrating the safety, vascular sparing, and other focal ablative characteristics of intracranial IRE procedures. We also present preliminary data on the duration and extent of blood–brain-barrier (BBB) disruption surrounding an IRE-induced zone of ablation in rodents (Garcia et al. 2012). Finally, we describe applications of IRE for the in vivo treatment of inoperable spontaneous canine intracranial MGs, highlighting its potential for more widespread clinical usage for the ablation of neoplastic brain tissue (Garcia et al. 2011a). Our studies have demonstrated the ability of IRE to safely ablate pathologically heterogeneous brain tissue while preserving vascular integrity and patient neurological functions. We illustrate the minimally invasive nature of IRE and the ability to plan and execute IRE therapy using procedures routinely used in clinical evaluation of neurosurgical patients.

Safety Study

Treatment Parameters

The safety study was approved by the Virginia Tech Institutional Animal Care and Use Committee (IACUC). The dogs were systemically healthy and neurologically intact prior to the study, based on normal physical and neurologic examinations, results of complete blood counts, and serum biochemistry profiles. No abnormalities were detected on scalp-recorded electroencephalograms (EEG) and baseline magnetic resonance imaging (MRI) examinations of the brain. After administration of general anesthesia, neuromuscular blockade, and an anti-convulsant (phenobarbital 6 mg/kg IV), routine craniectomies were performed to expose the right parietotemporal region of the brain of each dog. Focal ablative IRE lesions were created in the ectosylvian gyrus using a NanoKnife™ pulse generator and blunt tip electrodes (AngioDynamics®, Queensbury, NY USA).

For dog 1, a single probe (1.65 mm diameter) with both an energized and ground contact was used at a depth of 2 mm below the gyral surface. For the remaining test dogs smaller dual probes (1.0 mm diameter) were used at a depth of 7 mm below the cortex, where one probe was energized and the other grounded. IRE lesions were created by administering nine sets of ten 50-μs pulses at a rate of 4 pulses per second. The pulses were configured with alternating polarity between each set to minimize total charge delivered to the brain. The strength of the electric field is dependent on the applied voltage and electrode configuration which are given in Table 15.1. The voltage and

Table 15.1 Pulse parameters used in safety study of intracranial IRE in normal canine brain (Adapted from Ellis et al. (2011))

Dog	Blunt tip electrodes	Electrode exposure [mm]	Separation distance [mm]	Voltage [V]	Total pulses
1	Single	7 and 5.3	8	1,600	9×10
2	Dual	5	5	1,000	9×10
3	Dual	5	5	500	9×10
4 – Control	Dual	5	5	1,000	9×10
	Dual	5	10	2,000	9×10
5 – Control	Dual	5	5	0	0

pulse parameters were determined from the literature and from ex vivo experiments on canine brain (Al-Sakere et al. 2007; Lee et al. 2007; Onik et al. 2007). The animals were treated with 1,600, 1,000, and 500 V, respectively in order to assess whether lower voltages could still produce ablations.

One control animal (Dog 4) was treated at a higher voltage to evaluate the upper safety limit of the procedure by delivering ~4.5× more energy than in Dog 2 (Ellis et al. 2011). In this animal, two lesions were created using the dual electrode configuration at applied voltages of 1,000 and 2,000 V. The last animal was used as a sham control to examine the physical effects of electrode insertion without pulse delivery. Non-energized electrodes were advanced into the brain and maintained in place for approximately 30 s, the time required to deliver the IRE pulses in the other animals.

Neurologic, Imaging, and Histopathological Evaluation

After the IRE procedure, the animals were evaluated and treated in the standard fashion for post-craniectomy canine patients. There was no significant deterioration in neurologic ability or coma scale scores from baseline evaluations. The animals were able to ambulate and eat within 10 h of the procedure. No seizures were observed. Analysis of the intra-operative ultrasound obtained for each animal revealed a clearly demarcated hypoechoic zone with hyperechoic rim within the targeted brain parenchyma which was consistent with results in other organs (Lee et al. 2007; Appelbaum et al. 2012; Schmidt et al. 2012).

MRI examinations performed immediately post-operatively revealed fluid accumulation within the ablation sites and a focal disruption of the BBB (Fig. 15.1). These images also show that the IRE ablation zones were sharply demarcated and iso- to hypointense on T1-weighted sequences, hyperintense on T2-weigthed sequences, and markedly and contrast enhancing following intravenous administration of gadolinium.

The IRE lesion in the brain of Dog 1 was more superficial than the lesions in the other animals, due to the depth of insertion of the electrodes. In this animal, a single probe was inserted parallel to the surface of the brain at a depth of 2 mm. Grossly visible brain edema and surface blanching of the gyrus overlying the inserted electrode were observed within 2 min of completion of the IRE procedure. This edema resolved completely following intravenous administration of 1.0 g/kg of 20 % mannitol. Because of these effects, the subsequent animals were treated with a smaller dual probe configuration with electrodes inserted perpendicular to the brain surface at a 7-mm depth. Brain edema and surface blanching were not observed during treatment of the remaining dogs.

The microscopic lesions from the histopathology correlated well with the gross appearance and MRI sequences in dogs 1–3. A histological comparison between the sham control and dog 3 revealed that the isolated effect of electrode insertion was limited when compared to the IRE lesion. Histopathologic sections also demonstrated that the IRE lesions have a sub-millimeter line of demarcation between areas of necrosis and normal brain. The areas of treatment were represented by foci of malacia and dissociation of white and grey matter. Small perivascular hemorrhages were present although there was sparing of major blood vessels. High-voltage pulses in dog 4 were associated with non-selective coagulative necrosis of all tissues within the treatment field, resulting in lacunar infarction secondary to arterial thrombosis. Moderate diffuse perivascular and intraglial edema, reactive gliosis, as well as death of neuronal and glial cells were also observed. The treatment area was moderately infiltrated with mixed inflammatory cells, including neutrophils, macrophages, plasma cells, and small lymphocytes. Smaller lesions were observed when decreasing the voltage between dogs. As a result, customizing the pulse parameters should allow the ablation of volumes with varying sizes and shapes.

The ablations were confirmed with histopathological analysis, revealing a sub-millimeter boundary between the necrotic and normal brain. Reconstructed lesion volumes of 1.655, 0.599, and 0.258 cm^3 were calculated from the post-operative T2W MRIs using open source image

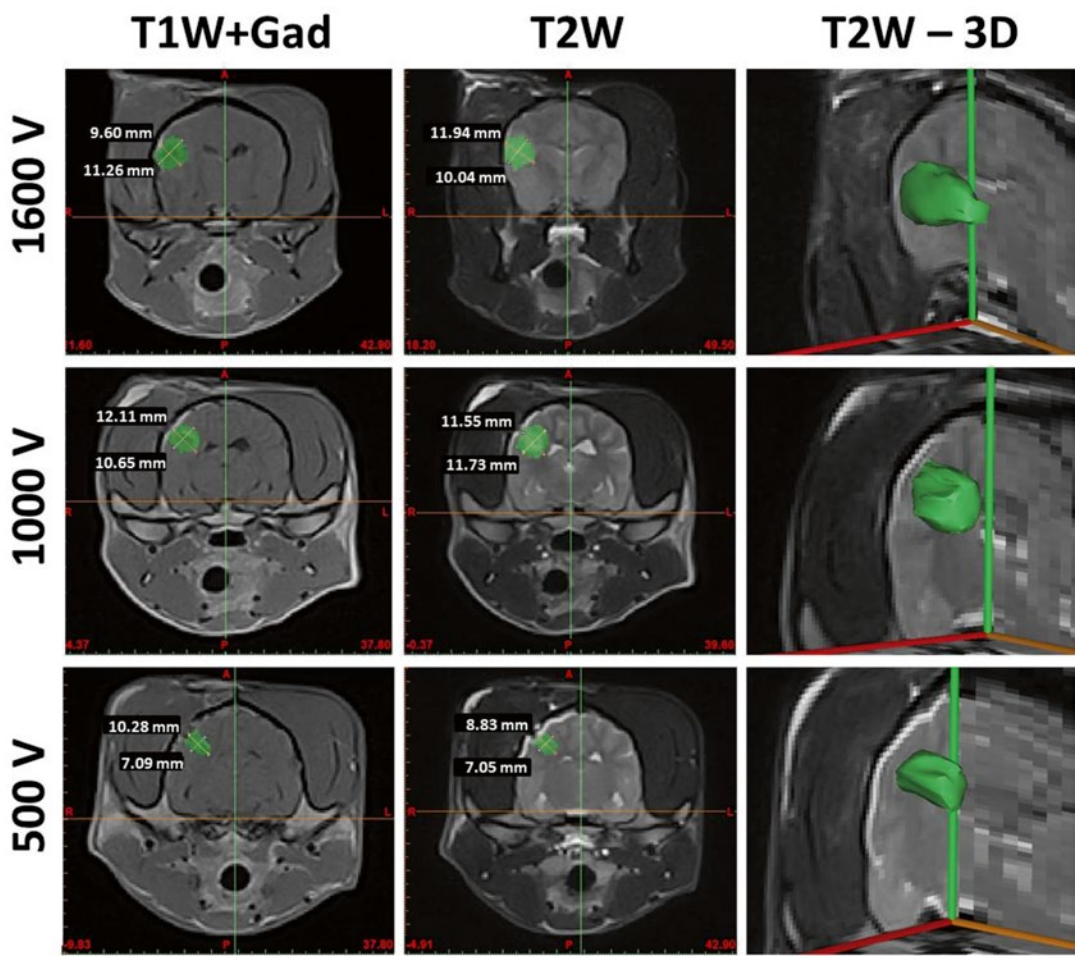

Fig. 15.1 MRI characteristics of focal brain ablations induced by IRE. Lesions (*green shading*) are well demarcated from surrounding brain parenchyma, homogenously T2 hyperintense, and markedly enhanced on TIW post-contrast images. There is a positive correlation between lesion size and the applied voltages

analysis software (OsiriX, Geneva, Switzerland). The accuracy of the computed lesion volumes was limited to the interval between the MRI scans (2.5–3.0 mm). It is important to note that the volumes of the lesions were reconstructed from MRIs taken within 60 min after pulse administration, so the observed ablation volume is likely to be that resulting from immediate IRE induced cellular necrosis (Garcia et al. 2011b). This means that any additional cellular death resulting from late-onset apoptosis may not be taken into account in the electric field correlation (Garcia et al. 2011b). Our results support the hypothesis that IRE can be used safely in the brain and that lesion volume can be correlated with applied voltage. In this canine study, as in other studies of soft-tissue organs, IRE associated edema developed following treatment. Although the vasogenic edema observed on the MRI of dogs in this study was not associated with any clinical deterioration, it is a cause of concern. Brain edema after IRE should be anticipated and treated with perioperative corticosteroids.

IRE may offer advantages over surgical resection for selected brain tumors. The small electrode size makes the procedure minimally invasive and adaptable to virtually any neuroanatomic location

with existing stereotactic guidance systems. IRE creates a sharply delineated volume of ablated tissue with sub-millimeter resolution that may make it suitable for treating deep-seated, well-circumscribed brain tumors. The minimal heat generation during treatment and sparing of major blood vessels may also make it appropriate for tumors adjacent to, or enveloping critical vascular structures. The following two sections in the chapter describe representative treatment planning procedures and clinical applications of IRE for the treatment of canine patients with spontaneous brain cancer.

Treatment Planning

Some of the advantages of IRE over other focal ablation techniques are that the treated regions are highly predictable and the technique does not depend on thermal changes to achieve tissue death (Al-Sakere et al. 2007; Ahmed et al. 2011). The extent of IRE is determined by the impedance distribution of the tissue as well as the tissue type, electrode-tissue geometry, and pulse parameters including strength, duration, number, shape, and repetition rate. However, for a given set of pulse conditions, the primary parameters affecting the degree of electroporation are the tissue type and the local electric field distribution (Edd and Davalos 2007). Therefore, the electric field distribution must be determined in order to design effective protocols for IRE procedures. Furthermore, to verify that specific protocols do not induce thermal damage due to excessive Joule heating, the temperature distribution can also be calculated from the electric field distribution and the thermal properties of the tissue. Knowledge of the electric field and temperature distribution enables researchers and physicians to reliably predict the results of an IRE procedure and minimize damage to surrounding healthy tissue. This insight enables surgeons to plan and optimize the electrode configuration and pulse parameters to:

1. Perform IRE treatment planning using medical images
2. Minimize applied voltages in order to reduce charge delivered
3. Avoid inducing thermal damage due to excessive Joule heating
4. Reduce treatment time, invasiveness, and number of procedures
5. Ensure coverage of the entire tumor, especially when multiple applications are needed

In this section we outline the IRE treatment planning procedures for canine patients with brain cancer. Specifically we describe the tissue segmentation, volumetric meshing, and finite element modeling used for therapeutic planning prior to surgical procedures.

Segmentation and Meshing of Tissue Components

Mimics 14.1 image analysis software (Materialise, Leuven, BG) is used to segment the brain tumor geometry from normal brain tissue components including the ventricles and the white and gray matter. The tumor is traced in each of the two-dimensional (2-D) diagnostic MRI, CT, or any other DICOM format imaging modalities according to intensity values. A three-dimensional (3-D) solid representation of the tumor volume, the ventricles, and the brain tissue is then refined and exported to 3-matic version 6.1 (Materialise, Leuven, BG) in order to generate a volumetric mesh for the computational models. The refined volumetric meshes are then imported into a finite element modeling (Comsol Multiphysics, v.4.2a, Stockholm, Sweden) software in order to simulate the physical effects of the electric pulses in the tumor and surrounding normal brain tissue.

Finite Element Modeling of Electric Field Distribution

The methods used to generate the electric field distributions in tissue are similar to the ones described by Edd and Davalos (2007). The electric field distribution associated with the electric pulse is given by solving the Laplace equation:

$$\nabla \cdot (\sigma \nabla \varphi) = 0 \tag{15.1}$$

where σ is the electrical conductivity of the tissue and φ is the electrical potential (Edd and Davalos 2007). Boundary conditions most often include surfaces where electric potential is specified, as in the case of a source or sink electrode, or surfaces that are electrically insulating, as on the free surfaces of the tissue, for example. The electrical boundary condition along the tissue that is in contact with the energized electrode is $\varphi = V_o$. The electrical boundary condition at the interface of the other electrode is set to ground. The remaining boundaries are treated as electrically insulating:

$$\frac{\partial \varphi}{\partial n} = 0 \tag{15.2}$$

The models are fully defined and readily solvable using numerical methods once an appropriate set of boundary conditions, initial conditions, and physical properties of the tissue are defined. The computations are performed with a commercial finite element package (Comsol Multiphysics 4.2a, Stockholm, Sweden). The analyzed domain extends far enough from the area of interest (i.e. the area near the electrodes) that the electrically insulating boundaries at the edges of the domain do not significantly influence the results in the treatment zone.

The numerical models have been adapted to account for a dynamic non-linear tissue conductivity that occurs as a result of electroporation and redistributes the electric field during the treatment (Garcia et al. 2010, 2011a, b; Neal et al. 2012). The significant non-linear changes in the electrical conductivity of treated tissues occur because of cell membrane defects that facilitate the flow of ions and current through cells and are necessary in order to accurately represent IRE treatments. The dynamic conductivity, $\sigma(E,T)$, is a function of the electric field (E) and temperature (T) of the tissue during the IRE treatment. In tissue and tumors, this increase in conductivity is approximately 3×–6× the baseline conductivity when fully electroporated (Ivorra et al. 2009; Neal et al. 2012) and needs to be determined for normal and pathologic brain tissue components.

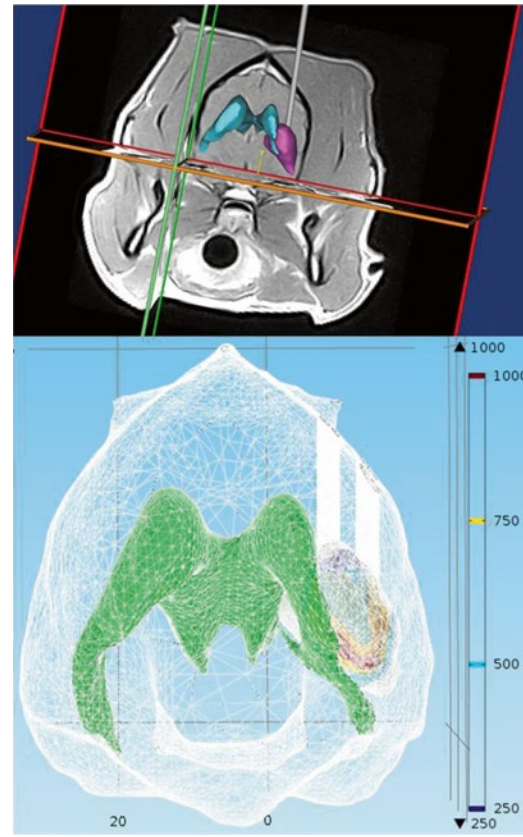

Fig. 15.2 Imaging-based computational models for treatment planning and optimization of IRE procedures in canine patients with brain cancer with (*top*) 3D reconstructed tissue components and the (*bottom*) simulated electric field distribution [V/cm]

Based on the tumor dimensions and computational simulations, IRE pulse parameters are determined to ensure coverage of the entire tumors and minimize damage to the surrounding healthy tissue. The resulting electric field distributions from these parameters can be visualized in Fig. 15.2. We are currently evaluating the electric field threshold in a clinical IRE study of canine patients with MG and are using the method proposed by Neal et al. (2012) to determine the non-linear conductivity function used in the finite element simulations. The promising clinical results that we have achieved in these patients suggest that our simulations are correct and that the electric field threshold used is capable of killing the tumor tissue.

Therapeutic Application

Dogs with spontaneous brain tumors have been shown to be excellent translational models of human disease. Canine malignant gliomas exhibit similar clinical, biologic, pathologic, molecular, and genetic properties as their human counterparts (Stoica et al. 2004; Dickinson et al. 2006; Rossmeisl et al. 2007). Here we illustrate the therapeutic application of IRE for treatment of MG using canines with spontaneous supratentorial gliomas. These canine patients are typically referred to our academic veterinary neurosurgical service for evaluation of tumor associated-seizures and interictal motor, sensory, and/or behavioral dysfunction referable to a focal intracranial neuroanatomic lesion following documentation of solitary intra-axial mass lesions with MR imaging characteristics consistent with gliomas (Fig. 15.3a-top panels); (Garcia et al. 2011a; Young et al. 2011). Prior to IRE therapy, peritumoral edema is treated with diuretics and corticosteroids, and anticonvulsants are administered as indicated.

Irreversible Electroporation Therapy

We use two general techniques to deliver IRE to canine MG, with the technique selection based on patient specific factors such as the volume and neuroanatomic location of the tumor, and the type and severity of any tumor-related complications (peritumoral edema, intratumoral hemorrhage, brain herniation, etc.). The first technique uses routine craniectomy approaches, similar to that described in our safety study (Fig. 15.3a-middle panels). The second is a minimally invasive, stereotactic approach in which a customized polymeric array is fabricated to accommodate the optimal electrode trajectory and configuration to a patient's specific tumor. The polymeric array is then implanted into the skull and the electrodes passed through the array into the tumor target during treatment (Fig. 15.3b-top panels). The polymeric array also provides a readily accessible and minimally invasive means for objective pathological evaluation of the tumor response through serial biopsy (Fig. 15.3b-bottom panels).

Total intravenous general anesthesia is induced and maintained with propofol and fentanyl constant rate infusions. Following biopsy of the tumor, neuromuscular blocking agents are administered to effect. The tumor is then ablated according to patient-specific treatment planning protocols (Table 15.2) using the NanoKnife™ (AngioDynamics®, Queensbury, NY USA), and blunt tip electrodes (1.0 mm diameter). Pulse delivery is synchronized with the electrocardiogram (ECG) signal to prevent ventricular fibrillation or other cardiac arrhythmias (Ivy Cardiac Trigger Monitor 3000, Branford, CT, USA). Pulse sets are delivered with alternating polarity between the sets to reduce charge build-up on the surface of individual electrodes. In addition, shorter pulse durations than those used in IRE studies (Al-Sakere et al. 2007; Onik et al. 2007; Rubinsky et al. 2007) outside the central nervous system (CNS) are used in order to reduce the charge delivered to the tissue and decrease resistive heating during the procedure. Our calculations and temperature measurements from previous intracranial IRE procedures ensure that no thermal damage is induced (Garcia et al. 2011b).

Post-IRE Evaluations

Objective tumor responses are evaluated using serial clinical neurologic examinations, brain MRI, and neuropathological studies. As illustrated in the acute post-treatment MR images (Fig. 15.3a-middle panels and Fig. 15.3b-bottom left panel), IRE therapy results in rapid reduction in contrast-enhancing tumor volumes and intracranial pressure without causing or exacerbating intratumoral hemorrhage or peritumoral edema. Neuropathological examinations of IRE treated MG (Fig. 15.3b-right panels) reveal near uniform neoplastic cell death and obliteration of tumor architecture. The scarce neoplastic cells with identifiable individual features within IRE ablated regions demonstrate apoptotic features

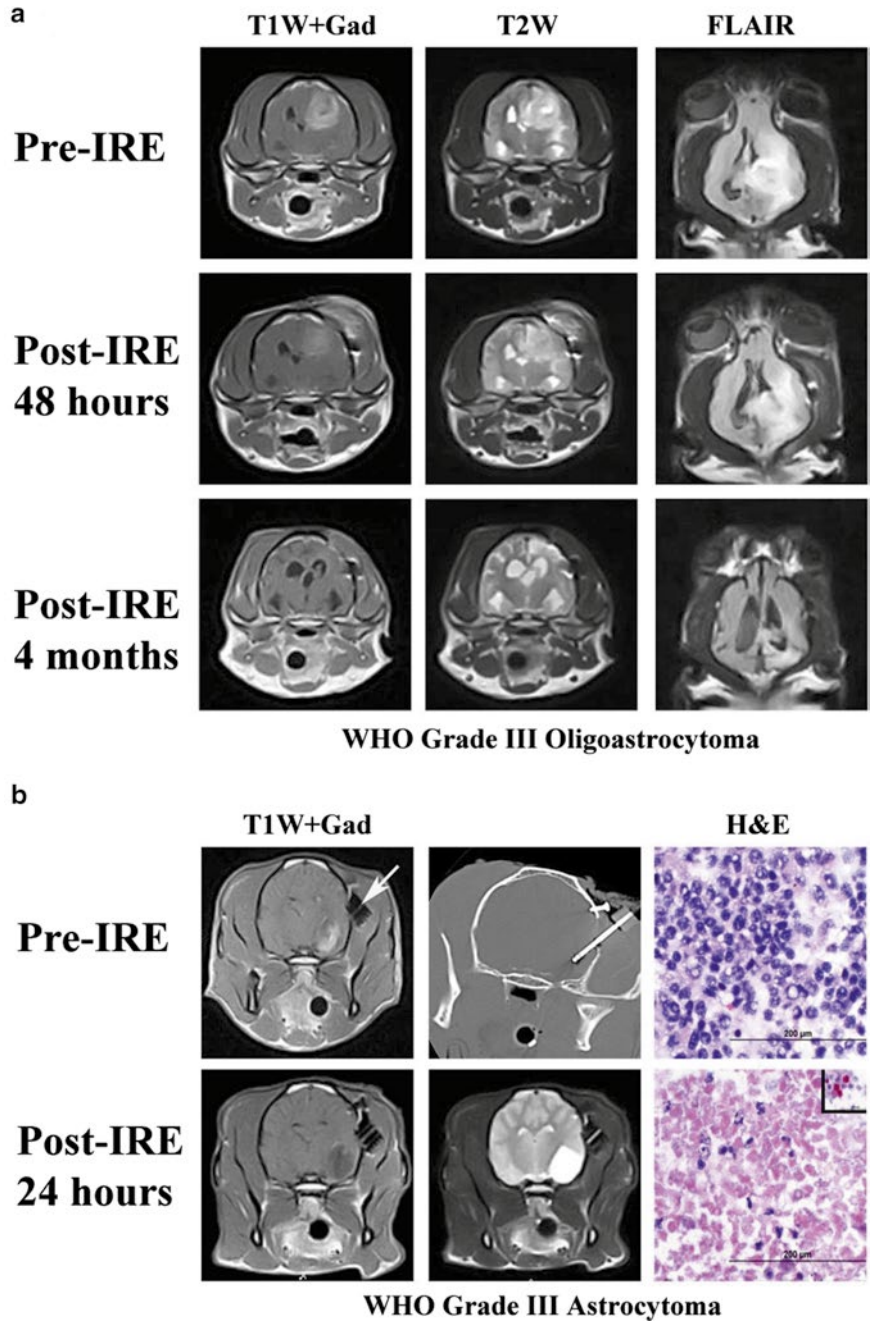

Fig. 15.3 MRI (**a**) and histologic (**b**) characteristics of focal tumor ablation before and after IRE treatment in canine patients with spontaneous malignant gliomas

(Fig. 15.3b, bottom right panel), and caspase-3 immunoreactivity (Fig. 15.3b, bottom right panel inset). These objective tumor responses are associated with acute post-operative improvements in neurological functions and overall clinical performance scores. The initial canine patient with MG treated with IRE and adjunctive radiation therapy at our institution experienced complete remission

Table 15.2 Representative IRE treatment protocol for canine patients with malignant glioma patient (Adapted from Garcia et al. (2011a))

Voltage (V)	Electrode gap (cm)	Electrode exposure (cm)	Volt-to-dist ratio (V/cm)	Pulse duration (μs)	Number of pulses	Frequency
500	0.5	0.5	1,000	50	2×20	ECG synchronized
625	0.5	0.5	1,250	50	4×20	ECG synchronized

(Fig. 15.3a-bottom panels), but did ultimately succumb to complications associated with radiation encephalopathy (Garcia et al. 2011a).

Discussion

Despite advances in cancer treatment, MG remains highly resistant to therapy. By nature of their neuroinvasiveness, MG are often not amenable to curative surgery and recur with high frequency (Stoica et al. 2004; Stupp et al. 2005; La Rocca and Mehdorn 2009). Even with aggressive multimodal treatment most patients succumb to the disease within 1 year. The 5-year survival rate for human patients with GBM is 10 % and this statistic has remained nearly unchanged over the last 70 years (Stupp et al. 2005). Although much less is known regarding the effects of single or multimodal therapies on the survival of dogs with gliomas, the prognosis is considered poor for dogs with MG, with one study reporting a median survival of 9 days for all dogs with non-meningeal origin neoplasms (Heidner et al. 1991).

IRE is a new minimally invasive technique to focally ablate undesired tissue using low energy electric pulses (Al-Sakere et al. 2007). These pulses permanently destabilize the membranes of the tumor cells, achieving death without inducing thermal damage in a precise and controllable manner with sub-millimeter resolution (Al-Sakere et al. 2007; Garcia et al. 2011a). The application of IRE requires minimal time and can be performed at the time of surgery or using stereotactic image (i.e. CT or MRI) guidance (Garcia et al. 2011b). This is an ideal treatment strategy for brain cancer patients where either tumor volumes are often sufficiently large to preclude safe traditional surgical excision without associated significant perioperative morbidity; or excision is not possible due to the neuroanatomic location of the tumor. We believe that, in addition to the ability to effectively ablate tissue in a non-thermal manner, a major advantage of IRE treatment is the very sharp transition between treated and non-treated tissue, which allows for sparing of sensitive neuroanatomic structures in proximity to the treatment field.

This chapter described the first systematic in vivo study of IRE for intracranial surgery (Ellis et al. 2011). We also presented the therapeutic planning aspect and implementation of IRE for treating canine patients with spontaneous brain tumors (Garcia et al. 2011a). Our results support the hypothesis that IRE can be used safely in the brain and that lesion volume can be correlated with applied voltage (Garcia et al. 2010; Ellis et al. 2011). IRE is a non-thermal ablation technique that kills tissue in a focal manner depicted by MR imaging and transiently disrupts the BBB adjacent to the ablated area in a voltage-dependent manner. In a rodent study in the brain we have also determined the extent and duration of the BBB disruption (Garcia et al. 2012) which will be critical for enhanced delivery of cytotoxic agents to regions with infiltrative tumor cells, especially high grade gliomas.

In conclusion, we have successfully shown that IRE is safe for use within the sensitive intracranial environment. The advantages of IRE over other focal ablation techniques lay within its ability to ablate tissue through a non-thermal mechanism. This method preserves the extracellular matrix, major blood vessels, and other sensitive tissues, enhancing treatment outcome. The IRE treatment is rapid, minimally invasive, and can be monitored using ultrasound, CT, and MRI. In addition, the lesions are sharply delineated between treated and non-treated tissue and are

sub-millimeter in resolution. Using a canine spontaneous model of MG, our group has developed and continues to refine IRE treatment planning and delivery methods that are effective for focal ablation of normal and neoplastic brain tissue.

Acknowledgments The work highlighted in this chapter was supported by the Coulter Foundation, the Golfer's Against Cancer, and by the CBET-0933335 and CAREER CBET-1055913 awards from the National Science Foundation (NSF) in the United States of America. The authors would also like to thank AngioDynamics® Inc. for loan of their equipment and for technical support of these studies.

References

Ahmed M, Brace CL, Lee FT Jr, Goldberg SN (2011) Principles of and advances in percutaneous ablation. Radiology 258(2):351–369

Al-Sakere B, Andre F, Bernat C, Connault E, Opolon P, Davalos RV, Rubinsky B, Mir LM (2007) Tumor ablation with irreversible electroporation. PLoS One 2(11):e1135

Appelbaum L, Ben-David E, Sosna J, Nissenbaum Y, Goldberg SN (2012) Us findings after irreversible electroporation ablation: radiologic-pathologic correlation. Radiology 262(1):117–125

Atsumi H, Matsumae M, Kaneda M, Muro I, Mamata Y, Komiya T, Tsugu A, Tsugane R (2001) Novel laser system and laser irradiation method reduced the risk of carbonization during laser interstitial thermotherapy: assessed by MR temperature measurement. Lasers Surg Med 29(2):108–117

Ball C, Thomson KR, Kavnoudias H (2010) Irreversible electroporation: a new challenge in "out of operating theater" anesthesia. Anesth Analg 110(5):1305–1309

Ben-David E, Appelbaum L, Sosna J, Nissenbaum I, Goldberg SN (2012) Characterization of irreversible electroporation ablation in in vivo porcine liver. Am J Roentgenol 198(1):W62–W68

Cosman ER, Nashold BS, Bedenbaugh P (1983) Stereotactic radiofrequency lesion making. Appl Neurophysiol 46(1–4):160–166

Davalos RV, Mir LM, Rubinsky B (2005) Tissue ablation with irreversible electroporation. Ann Biomed Eng 33(2):223–231

Dickinson PJ, Roberts BN, Higgins RJ, Leutenegger CM, Bollen AW, Kass PH, LeCouteur RA (2006) Expression of receptor tyrosine kinases vegfr-1 (flt-1), vegfr-2 (kdr), egfr-1, pdgfra and c-met in canine primary brain tumours. Vet Comp Oncol 4(3):132–140

Edd JF, Davalos RV (2007) Mathematical modeling of irreversible electroporation for treatment planning. Technol Cancer Res Treat 6:275–286

Ellis TL, Garcia PA, Rossmeisl JH Jr, Henao-Guerrero N, Robertson J, Davalos RV (2011) Nonthermal irreversible electroporation for intracranial surgical applications. Laboratory investigation. J Neurosurg 114(3):681–688

Garcia PA, Pancotto T, Rossmeisl JH, Henao-Guerrero N, Gustafson NR, Daniel GB, Robertson JL, Ellis TL, Davalos RV (2011a) Non-thermal irreversible electroporation (N-TIRE) and adjuvant fractionated radiotherapeutic multimodal therapy for intracranial malignant glioma in a canine patient. Technol Cancer Res Treat 10(1):73–83

Garcia PA, Rossmeisl JH Jr, Neal RE 2nd, Ellis TL, Davalos RV (2011b) A parametric study delineating irreversible electroporation from thermal damage based on a minimally invasive intracranial procedure. Biomed Eng Online 10(1):34

Garcia PA, Rossmeisl JH, Neal RE II, Ellis TL, Olson J, Henao-Guerrero N, Robertson J, Davalos RV (2010) Intracranial nonthermal irreversible electroporation: in vivo analysis. J Membr Biol 236(1):127–136

Garcia PA, Rossmeisl JH Jr, Robertson JL, Olson JD, Johnson AJ, Ellis TL, Davalos RV (2012) 7.0-T Magnetic resonance imaging characterization of acute blood–brain-barrier disruption achieved with intracranial irreversible electroporation. PLoS ONE 7(11):e50482

Heidner GL, Kornegay JN, Page RL, Dodge RK, Thrall DE (1991) Analysis of survival in a retrospective study of 86 dogs with brain tumors. J Vet Intern Med 5(4):219–226

Ivorra A, Al-Sakere B, Rubinsky B, Mir LM (2009) In vivo electrical conductivity measurements during and after tumor electroporation: conductivity changes reflect the treatment outcome. Phys Med Biol 54(19):5949–5963

La Rocca RV, Mehdorn HM (2009) Localized BCNU chemotherapy and the multimodal management of malignant glioma. Curr Med Res Opin 25(1):149–160

Lee EW, Loh CT, Kee ST (2007) Imaging guided percutaneous irreversible electroporation: ultrasound and immunohistological correlation. Technol Cancer Res Treat 6(4):287–294

Miklavcic D, Semrov D, Mekid H, Mir LM (2000) A validated model of in vivo electric field distribution in tissues for electrochemotherapy and for DNA electrotransfer for gene therapy. Biochim Biophys Acta 1523(1):73–83

Neal R II, Garcia P, Robertson J, Davalos R (2012) Experimental characterization and numerical modeling of tissue electrical conductivity during pulsed electric fields for irreversible electroporation treatment planning. IEEE Trans Biomed Eng 99:1

Neal RE II, Rossmeisl J, Garcia PA, Lanz O, Henao-Guerrero N, Davalos RV (2011) A case report on the successful treatment of a large soft-tissue sarcoma with irreversible electroporation. J Clin Oncol 29:1–6

Onik G, Mikus P, Rubinsky B (2007) Irreversible electroporation: implications for prostate ablation. Technol Cancer Res Treat 6(4):295–300

Rossmeisl JH, Duncan RB, Huckle WR, Troy GC (2007) Expression of vascular endothelial growth factor in tumors and plasma from dogs with primary intracranial neoplasms. Am J Vet Res 68(11):1239–1245

Rubinsky B, Onik G, Mikus P (2007) Irreversible electroporation: a new ablation modality–clinical implications. Technol Cancer Res Treat 6(1):37–48

Schmidt CR, Shires P, Mootoo M (2012) Real-time ultrasound imaging of irreversible electroporation in a porcine liver model adequately characterizes the zone of cellular necrosis. HPB 14(2):98–102

Stoica G, Kim HT, Hall DG, Coates JR (2004) Morphology, immunohistochemistry, and genetic alterations in dog astrocytomas. Vet Pathol 41(1):10–19

Stupp R, Mason WP, van den Bent MJ, Weller M, Fisher B, Taphoorn MJ, Belanger K, Brandes AA, Marosi C, Bogdahn U, Curschmann J, Janzer RC, Ludwin SK, Gorlia T, Allgeier A, Lacombe D, Cairncross JG, Eisenhauer E, Mirimanoff RO (2005) Radiotherapy plus concomitant and adjuvant temozolomide for glioblastoma. N Engl J Med 352(10):987–996

Tacke J (2001) Thermal therapies in interventional mr imaging Cryotherapy. Neuroimaging Clin N Am 11(4):759–765

Thomson KR, Cheung W, Ellis SJ, Federman D, Kavnoudias H, Loader-Oliver D, Roberts S, Evans P, Ball C, Haydon A (2011) Investigation of the safety of irreversible electroporation in humans. J Vasc Interv Radiol 22(5):611–621

Young BD, Levine JM, Porter BF, Chen-Allen AV, Rossmeisl JH, Platt SR, Kent M, Fosgate GT, Schatzberg SJ (2011) Magnetic resonance imaging features of intracranial astrocytomas and oligodendrogliomas in dogs. Vet Radiol Ultrasound 52(2):132–141

The Role of Whole Brain Radiation Therapy for Metastatic Brain Tumors

16

Melvin Omodon and Steven Kalkanis

Contents

Abstract

Whole brain radiation therapy (WBRT) has long served as an important treatment modality for patients diagnosed with metastatic brain tumors, both alone and in combination with other therapies including surgical resection. The recently published multidisciplinary treatment guideline by Gaspar and Kalkanis for brain metastases evaluates the evidence for the continued use of WBRT, with recommendations for specific clinical scenarios. We will address the subject of the role of WBRT in brain metastases throughout this chapter.

Introduction

Approximately 1.4 million people in the US are diagnosed with cancer every year according to the American Cancer Society. About 20–40 % of cancer patients will go on to develop brain metastases. The incidence of these secondary brain tumors is about four to five times that of primary brain tumors (American Cancer Society 2006; Gavrilovic and Posner 2005; Linskey and Kalkanis 2010). The mode of spread is primarily hematogenous with local extension also possible. In 11 % of patients with no known cancer history, cerebral metastasis was the presenting symptom (Voorhies et al. 1980). The most common primary sites for brain metastases are lungs and breast. 85 % of brain metastases are found in the cerebral hemispheres, 10–15 % in the cerebellum and 1–3 % in the brainstem.

M. Omodon • S. Kalkanis (✉)
Department of Neurosurgery, Henry Ford Center for Cancer Surgery, 2799 West Grand Blvd., 48202 Detroit, MI, USA
e-mail: skalkan1@hfhs.org

M.A. Hayat (ed.), *Tumors of the Central Nervous System, Volume 12*,
DOI 10.1007/978-94-007-7217-5_16,

Typically the signs and symptoms of brain metastasis are usually slowly progressive. These include headache, focal weakness, mental disturbances, gait ataxia, seizures, speech difficulty, visual disturbance, sensory disturbance and limb ataxia.

Whole brain radiation therapy (WBRT) typically had been the mainstay for treatment for metastatic brain tumor until the 1990s when surgical resection and stereotactic radiosurgery (SRS) became more popular. WBRT has been shown to prolong survival to about 3–6 months compared to the 1–2 months in patients who did not receive any treatment (Patchell et al. 1998; Kondziolka et al. 1999). In 1954, Chao et al. (1954) showed that WBRT increased the median survival of patients with metastatic brain tumors by up to 3–6 months. Other studies (Posner 1977; Zimm et al. 1981) have shown similar improvement in overall survival in these patients. Response rate to WBRT ranges from 50 % to 85 % (Katz 1981).

Tumors that are more sensitive to WBRT are small cell lung ca, germ cell tumors, lymphoma, leukemia, multiple myeloma (Patchell et al. 1990). Highly resistant tumors are thyroid, renal cell, malignant melanoma, sarcoma, adenocarcinoma (Nieder et al. 1997). Patients with metastatic brain tumors who are candidates for WBRT usually receive steroids to decrease the peritumoral edema and WBRT over the course of 2 weeks. Mortality from metastatic brain tumors is mostly due to complications of extracranial tumor activity.

The Role of Surgery Combined with WBRT

Guidelines pertaining to the role of surgery combined with WBRT have been published (Gaspar et al. 2010). Class I evidence supports combined treatment with surgical resection plus postoperative WBRT, compared to WBRT alone or surgical resection alone, in patients who are functionally independent, who spend less than 50 % of time in bed and who have limited extra-cranial disease. There is no unified recommendation for patients with poor performance scores, advanced systemic disease, or multiple brain metastases.

The randomized control trial by Patchell et al. (1998) involved 48 patients with systemic cancer, evidence of single metastasis to the brain and Karnofsky performance scores (KPS) of 70 or greater who had received either needle biopsy and WBRT (radiation group), or complete surgical resection and WBRT (surgical group). Both groups received the same total radiation dose of 36 Gy given in 12 daily fractions of 3 Gy each. Patients with acute neurologic deterioration and radiosensitive tumors (SCLC, germ-cell, lymphoma, leukemia and multiple myeloma) were excluded. Patients in the surgical group were reported to have had complete resection verified by postoperative computerized tomography (CT) scanning. Compared to the radiation group, the surgical group had an increase in the overall length of survival (median 40 weeks vs. 15 weeks; $P<0.01$), increased duration of functional independence and quality of life, and decreased frequency of recurrence of the original tumor. There was no extra mortality noted in the surgical group.

A multi-centered trial in the Netherlands of patients who had a single brain metastasis randomized 63 patients into surgical resection and WBRT versus WBRT alone (Vecht et al. 1993). Patients in this study were generally ambulatory and did not require continuous nursing care. Patients who received the combined treatment had significantly longer median survivals (10 vs. 6 months) and longer functional independent survival (7.5 vs. 3.5 months). There was no difference in the median survival (5 months) between treatment regimens in patients with poorly controlled systemic disease. The study showed that this benefit was only seen in patients less than 60 years old and without progressive systemic disease who were within 3 months of diagnosis. Three patients were excluded from analysis. Two patients were lost to follow up.

A RCT by Mintz and Cairncross (1998) on 84 patients with a single brain metastasis was published in 1996. Forty-three patients were allocated to undergo radiation alone and 41 patients received

surgery plus radiation. The authors concluded that combined surgery and WBRT is as efficacious as WBRT alone in terms of overall survival, or quality of life. Patients were excluded if they had leukemia, lymphoma, or SCLC.

There have been possible explanations put forth to suggest why the data from this study is different from the other two studies. Most of the patients in this study had either uncontrolled primary or extracranial metastasis which is a relative contraindication to surgery. Also since most of the neurosurgically treated patients died of progression of systemic disease it is likely that there will be difference in outcomes because progressive disease has the same median survival (5 months) irrespective of combined surgery and WBRT versus WBRT alone. Also of note, this trial included patients less than 80 years old and with Karnofsky scores (KPS) of at least 50. This differs from the previous trials in that these patients could spend greater than 50 % of their day in bed. Another reason for this difference could be the lack of mandatory MRI scans in patients included in the study giving rise to the possibility that additional lesions were not seen in pre operative CT scans.

Ampil et al. (1996) retrospectively studied 45 patients at a single institution who had cerebellar metastasis and who received either surgery plus WBRT (11 patients) or WBRT alone (34 patients). Most of the patients who received WBRT alone had additional supratentorial brain metastases. The authors found that patients who received combined treatment had a median survival of 15 months compared to 3 months for patients who received WBRT alone. They concluded that the outcome of patients with metastasis to the cerebellum was significantly improved when the metastatic lesion was resected and when its origin was not from the lung.

WBRT Dosing

Radiation dosages are expressed as tumor response biologically effective dose (BED) to account for total dose of radiation, fraction size, overall time to deliver the radiation, and presumed repair of irradiated tissue. This is calculated with equation: $BED = nd\left[1 + d/(\alpha/\beta)\right]$ where n = number of treatments, d = dose per fraction; and $\alpha/\beta = 10$ Gy for tumor effects of each schedule. The standard WBRT dose is 30 Gy in 10 fractions given over 2 weeks (Gaspar et al. 2010).

In an effort to increase the duration of overall survival and to improve the morbidity from WBRT several randomized controlled trials (RCTs) were conducted to identify the optimal dose of radiation. There is no additional benefit in overall survival, neurologic function or symptom control with altered dose-fractionation schedules compared to the standard (Gaspar et al. 2010; Kalkanis et al. 2010).

In two RCTs by Borgelt et al. (1980), patients were randomly selected to receive one of five WBRT schedules that ranged from 40 Gy for a 4 week duration to 20 Gy for a 1 week duration. The following year, Borgelt et al. (1981) conducted two RCTs where patients were treated with 10 Gy in 1 fraction versus 30–40 Gy in 10–20 fractions, and also 12 Gy in 2 fractions versus 20 Gy in 5 fractions. The authors concluded that there was no statistically significant difference in the overall median survival of patients who received different radiation schedules.

Other RCTs (Harwood and Simson 1977; Chatani et al. 1994) and a Cochrane review (Tsao et al. 2012) did not find any statistically significant difference in the outcomes of patients who received varying WBRT schedules. Also, no difference in symptom control, or improvement in neurological function was observed in patients who received doses higher than 30 Gy over 10 fractions (Gaspar et al. 2010). Patients who received lower than that dose fared worse ($p = 0.03$) (Tsao et al. 2012). A RCT study conducted in the UK compared 30 Gy in 10 fractions over 2 weeks versus 12 Gy in 2 fractions on 2 days showed that patients who received 30 Gy in 10 fractions had an improved median survival of 84 days compared to 77 days ($p = 0.04$) (Priestman et al. 1996) with fewer adverse effects.

Whole Brain Radiation Therapy Combined with Other Therapies

Role of WBRT and SRS

A multi-centered RCT (Andrews et al. 2004) by the Radiation Therapy Oncology Group (RTOG) compared patients with one to three solid brain metastases, less than 4 cm in maximum diameter, and KPS > 70 who received WBRT (133 patients) and those who received both WBRT and SRS (139 patients). This study found that patients who received both WBRT and SRS had statistically significant longer survival (6.5 vs. 5.7 months, $p = 0.04$), decreased progression of disease (71 % vs. 82 %), and a higher rate of improved KPS (43 % vs. 27 %, $p = 0.03$) compared to patients who received only WBRT.

Another RCT (Kondziolka et al. 1999) randomized patients with two to four brain metastases no more than 25 mm diameter and KPS scores less than 70 to WBRT alone (14 patients) versus WBRT and SRS (13 patients) evaluating for radiological evidence of local tumor control. They found that patients who received both radiation therapies had longer median time to local failure (36 vs. 6 months, $p = 0.0005$), and longer survival (11 vs. 7.5 months) compared to patients with WBRT alone. This study did not report any neurologic or systemic morbidity related to additional stereotactic radiosurgery. Retrospective studies have also shown improved outcomes in patients who received both single dose SRS and WBRT compared to WBRT alone (Li et al. 2000; Sanghavi et al. 2001; Wang et al. 2002).

WBRT Plus SRS Versus SRS Alone

Aoyama et al. (2006) conducted a multicentered RCT of patients in Japan with no more than four metastastic brain lesions each smaller than 3 cm in diameter and KPS > 70 to compare especially for overall survival, and also brain tumor recurrence. 65 randomly selected patients received both WBRT and single dose SRS and 67 patients received SRS alone. The SRS dose in the combined group arm was reduced by 30 % compared to the SRS only group. It was noted that there was no statistically significant difference in the median survival time between patients who received WBRT and SRS compared to SRS alone. The combined treatment group had a median survival time of 7.5 months compared to 8.0 months for SRS alone. The 1 year distant brain site recurrence rate was significantly higher in the SRS alone group (76.4 % for SRS vs. 46.8 % in the combined group; $p < 0.001$). Also the SRS only group was more likely to require salvage brain therapy of either WBRT or SRS (43.3 % vs. 15.4 %).

Chang et al. (2009) found that patients who received combined SRS and WBRT had a more severe decline in learning and memory function compared to the SRS only group. This trial randomized 30 patients with one to three brain metastases to receive SRS alone, and 28 to receive combined SRS and WBRT but was stopped early because it was noted that the combined group were significantly more likely to show a decline in learning and memory function. It was also noted that the combined group patients had more patients free of recurrence of distant brain metastasis (73 % compared to 27 %, $p = 0.0003$).

Li et al. (2000) conducted a study to compare WBRT, SRS, and WBRT + SRS in terms of local response, survival, and quality of life in patients with squamous cell and non squamous cell lung cancer with single brain metastases < 4.5 cm in diameter and KPS > 60. This study found that both SRS alone and SRS + WBRT were statistically better in terms of prolonging life and improving quality of life than WBRT alone. When the combined treatment arm was compared with the SRS only arm, there was no statistically significant advantage in survival, tumor control, or enhance quality of life except for improved freedom from new brain metastasis in the combined arm.

A European trial (Kocher et al. 2011) was conducted to evaluate if patients with brain metastasis who were post-surgery or post-SRS had increased length of functional independence after adjuvant WBRT. The patients included in this

study had one to three brain metastases and WHO performance status (PS) of zero to two. Patients who had prior treatment with surgery or SRS were randomized to receive adjuvant WBRT or placebo. There was no difference observed in the overall survival between both groups. WBRT reduced the 2-year relapse rate both at initial metastasis site (surgery: 59–27 %, P < .001; radiosurgery: 31–19 %, P = .040) and at new sites (surgery: 42–23 %, P = .008; radiosurgery: 48–33 %, P = .023). The adjuvant WBRT had reduced relapse rate and less salvage therapies.

Role of Sensitizers

Sensitizers are agents that in conjunction with radiotherapy increase the cytotoxic effects and improve the therapeutic ratio. Motexafin gadolinium is a metallotexaphrin that accumulates within tumors in significantly higher concentration than in normal tissue. Efaproxiral is thought to cause a modification of the 3D structure of hemoglobin decreasing its oxygen binding capacity hence allowing more free oxygen to be available to tumor cells. Increased oxygen is thought to be destructive to the tumors. Several RCTs (Eyre et al. 1984; DeAngelis et al. 1989; Komarnicky et al. 1991; Phillips et al. 1995; Mehta et al. 2003; Suh et al. 2006) investigated outcomes in terms of overall survival, KPS and neurologic function involving the use of radiosensitizers such as motexafin, RSR13 (efaproxiral), lonidamide, metronidazole, misonidazole, gadolinium, and bromodeoxyuridine (BrdU). When used in conjunction with WBRT, these radiosensitizersdid not provide any added survival benefits andin fact, there were increased side effects.

WBRT and Chemotherapy

There have been studies (Eyre et al. 1984; DeAngelis et al. 1989; Komarnicky et al. 1991; Phillips et al. 1995; Postmus et al. 2000; Mehta et al. 2003; Suh et al. 2006) that evaluated outcomes of patients with brain metastasis who had WBRT and chemotherapeutic agents for changes in survival. These studies failed to demonstrate any improvement in median survival duration when chemotherapy was given in addition to WBRT.

WBRT Treatment Outcome by Histopathology

A retrospective study (Sundstrom et al. 1998) evaluated 75 patients with brain metastases from solid tumors, who received 25 Gy WBRT, for differences in outcomes based on histopathology. The primary cancers included 35 cases of lung cancer, 19 cases of breast cancer, 9 cases of renal-cell cancer, 6 cases of melanoma and 6 cases of other primary sites. In general, patients with breast cancer had better survival than patients with other primary cancers. There are however no formal recommendations concerning the effectiveness of WBRT for one histopathological type versus another (Kalkanis et al. 2010) due to the low number of studies addressing this topic.

Discussion

Surgical resection plus post-operative WBRT has been shown to produce better outcomes compared to WBRT alone in patients with limited extra-cranial disease and with good functional status. Surgical resection and WBRT also produces better local and distant brain control when compared to surgical resection alone. This recommendation however does not apply to relatively radiosensitive tumors histologies such as small cell lung cancer, leukemia, lymphoma, germ cell tumors and multiple myeloma (Gaspar et al. 2010; Kalkanis et al. 2010). The standard dose/fractionation scheme for WBRT is 30 Gy in 10 fractions. Other doses and fractionation schedules have not shown improved local control, neurocognitive outcomes or median survival.

WBRT combined with single dose SRS results in improved local tumor control, functional status, and longer survival, compared with WBRT alone for patients with one to four metastatic lesions

who have KPS scores greater than 70. Single dose SRS with WBRT may be just as efficacious as single dose SRS alone as long as there is regular surveillance for local and distant recurrence so salvage therapy could be initiated promptly. Adjuvant chemotherapy after WBRT has not been shown to increase survival. Radiation sensitizers have not been shown to improve outcomes in patients receiving WBRT. Also due to the relative paucity of data there are no recommendations to be made regarding the efficacy of WBRT for different tumor histology. Further investigation is required for future recommendations.

References

American Cancer Society (2006) Cancer facts & figures. The Society, Atlanta

Ampil FL, Nanda A, Willis BK, Nandy I, Meehan R (1996) Metastatic disease in the cerebellum. The LSU experience in 1981–1993. Am J Clin Oncol 19:509–511

Andrews DW, Scott CB, Sperduto PW, Flanders AE, Gaspar LE, Schell MC, Werner-Wasik M, Demas W, Ryu J, Bahary JP, Souhami L, Rotman M, Mehta MP, Curran WJ Jr (2004) Whole brain radiation therapy with or without stereotactic radiosurgery boost for patients with one to three brain metastases: phase III results of the RTOG 9508 randomised trial. Lancet 363:1665–1672

Aoyama H, Shirato H, Tago M, Nakagawa K, Toyoda T, Hatano K, Kenjyo M, Oya N, Hirota S, Shioura H, Kunieda E, Inomata T, Hayakawa K, Katoh N, Kobashi G (2006) Stereotactic radiosurgery plus whole-brain radiation therapy vs. stereotactic radiosurgery alone for treatment of brain metastases: a randomized controlled trial. JAMA 295:2483–2491

Borgelt B, Gelber R, Kramer S, Brady LW, Chang CH, Davis LW, Perez CA, Hendrickson FR (1980) The palliation of brain metastases: final results of the first two studies by the radiation therapy oncology group. Int J Radiat Oncol Biol Phys 6:1–9

Borgelt B, Gelber R, Larson M, Hendrickson F, Griffin T, Roth R (1981) Ultra-rapid high dose irradiation schedules for the palliation of brain metastases: final results of the first two studies by the radiation therapy oncology group. Int J Radiat Oncol Biol Phys 7:1633–1638

Chang EL, Wefel JS, Hess KR, Allen PK, Lang FF, Kornguth DG, Arbuckle RB, Swint JM, Shiu AS, Maor MH, Meyers CA (2009) Neurocognition in patients with brain metastases treated with radiosurgery or radiosurgery plus whole-brain irradiation: a randomised controlled trial. Lancet Oncol 10:1037–1044

Chao JH, Phillips R, Nickson JJ (1954) Roentgen-ray therapy of cerebral metastases. Cancer 7:682–689

Chatani M, Matayoshi Y, Masaki N, Inoue T (1994) Radiation therapy for brain metastases from lung carcinoma. Prospective randomized trial according to the level of lactate dehydrogenase. Strahlenther Onkol 170:155–161

DeAngelis LM, Currie VE, Kim JH, Krol G, O'Hehir MA, Farag FM, Young CW, Posner JB (1989) The combined use of radiation therapy and lonidamine in the treatment of brain metastases. J Neurooncol 7:241–247

Eyre HJ, Ohlsen JD, Frank J, LoBuglio AF, McCracken JD, Weatherall TJ, Mansfield CM (1984) Randomized trial of radiotherapy versus radiotherapy plus metronidazole for the treatment metastatic cancer to brain. A southwest oncology group study. J Neurooncol 2:325–330

Gaspar LE, Mehta MP, Patchell RA, Burri SH, Robinson PD, Morris RE, Ammirati M, Andrews DW, Asher AL, Cobbs CS, Kondziolka D, Linskey ME, Loeffler JS, McDermott M, Mikkelsen T, Olson JJ, Paleologos NA, Ryken TC, Kalkanis SN (2010) The role of whole brain radiation therapy in the management of newly diagnosed brain metastases: a systematic review and evidence-based clinical practice guideline. J Neurooncol 96:17–32

Gavrilovic IT, Posner JB (2005) Brain metastases: epidemiology and pathophysiology. J Neurooncol 75:5–14

Harwood AR, Simson WJ (1977) Radiation therapy of cerebral metastases: a randomized prospective clinical trial. Int J Radiat Oncol Biol Phys 2:1091–1094

Kalkanis SN, Kondziolka D, Gaspar LE, Burri SH, Asher AL, Cobbs CS, Ammirati M, Robinson PD, Andrews DW, Loeffler JS, McDermott M, Mehta MP, Mikkelsen T, Olson JJ, Paleologos NA, Patchell RA, Ryken TC, Linskey ME (2010) The role of surgical resection in the management of newly diagnosed brain metastases: a systematic review and evidence-based clinical practice guideline. J Neurooncol 96:33–43

Katz HR (1981) The relative effectiveness of radiation therapy, corticosteroids, and surgery in the management of melanoma metastatic to the central nervous system. Int J Radiat Oncol Biol Phys 7:897–906

Kocher M, Soffietti R, Abacioglu U, Villa S, Fauchon F, Baumert BG, Fariselli L, Tzuk-Shina T, Kortmann RD, Carrie C, Ben Hassel M, Kouri M, Valeinis E, van den Berge D, Collette S, Collette L, Mueller RP (2011) Adjuvant whole-brain radiotherapy versus observation after radiosurgery or surgical resection of one to three cerebral metastases: results of the EORTC 22952-26001 study. J Clin Oncol 29:134–141

Komarnicky LT, Phillips TL, Martz K, Asbell S, Isaacson S, Urtasun R (1991) A randomized phase III protocol for the evaluation of misonidazole combined with radiation in the treatment of patients with brain metastases (RTOG-7916). Int J Radiat Oncol Biol Phys 20:53–58

Kondziolka D, Patel A, Lunsford LD, Kassam A, Flickinger JC (1999) Stereotactic radiosurgery plus whole brain radiotherapy versus radiotherapy alone for patients with multiple brain metastases. Int J Radiat Oncol Biol Phys 45:427–434

Li B, Yu J, Suntharalingam M, Kennedy AS, Amin PP, Chen Z, Yin R, Guo S, Han T, Wang Y, Yu N, Song G, Wang L (2000) Comparison of three treatment options for single brain metastasis from lung cancer. Int J Cancer 90:37–45

Linskey ME, Kalkanis SN (2010) Evidence-linked, clinical practice guidelines-getting serious; getting professional. J Neurooncol 96:1–5

Mehta MP, Rodrigus P, Terhaard CH, Rao A, Suh J, Roa W, Souhami L, Bezjak A, Leibenhaut M, Komaki R, Schultz C, Timmerman R, Curran W, Smith J, Phan SC, Miller RA, Renschler MF (2003) Survival and neurologic outcomes in a randomized trial of motexafin gadolinium and whole-brain radiation therapy in brain metastases. J Clin Oncol 21:2529–2536

Mintz AP, Cairncross JG (1998) Treatment of a single brain metastasis: the role of radiation following surgical resection. JAMA 280:1527–1529

Nieder C, Berberich W, Schnabel K (1997) Tumor-related prognostic factors for remission of brain metastases after radiotherapy. Int J Radiat Oncol Biol Phys 39:25–30

Patchell RA, Tibbs PA, Walsh JW, Dempsey RJ, Maruyama Y, Kryscio RJ, Markesbery WR, Macdonald JS, Young B (1990) A randomized trial of surgery in the treatment of single metastases to the brain. N Engl J Med 322:494–500

Patchell RA, Tibbs PA, Regine WF, Dempsey RJ, Mohiuddin M, Kryscio RJ, Markesbery WR, Foon KA, Young B (1998) Postoperative radiotherapy in the treatment of single metastases to the brain: a randomized trial. JAMA 280:1485–1489

Phillips TL, Scott CB, Leibel SA, Rotman M, Weigensberg IJ (1995) Results of a randomized comparison of radiotherapy and bromodeoxyuridine with radiotherapy alone for brain metastases: report of RTOG trial 89-05. Int J Radiat Oncol Biol Phys 33:339–348

Posner JB (1977) Management of central nervous system metastases. Semin Oncol 4:81–91

Postmus PE, Haaxma-Reiche H, Smit EF, Groen HJ, Karnicka H, Lewinski T, van Meerbeeck J, Clerico M, Gregor A, Curran D, Sahmoud T, Kirkpatrick A, Giaccone G (2000) Treatment of brain metastases of small-cell lung cancer: comparing teniposide and teniposide with whole-brain radiotherapy–a phase III study of the European organization for the research and treatment of cancer lung cancer cooperative group. J Clin Oncol 18:3400–3408

Priestman TJ, Dunn J, Brada M, Rampling R, Baker PG (1996) Final results of the royal college of radiologists' trial comparing two different radiotherapy schedules in the treatment of cerebral metastases. Clin Oncol (R Coll Radiol) 8:308–315

Sanghavi SN, Miranpuri SS, Chappell R, Buatti JM, Sneed PK, Suh JH, Regine WF, Weltman E, King VJ, Goetsch SJ, Breneman JC, Sperduto PW, Scott C, Mabanta S, Mehta MP (2001) Radiosurgery for patients with brain metastases: a multi-institutional analysis, stratified by the RTOG recursive partitioning analysis method. Int J Radiat Oncol Biol Phys 51:426–434

Suh JH, Stea B, Nabid A, Kresl JJ, Fortin A, Mercier JP, Senzer N, Chang EL, Boyd AP, Cagnoni PJ, Shaw E (2006) Phase III study of efaproxiral as an adjunct to whole-brain radiation therapy for brain metastases. J Clin Oncol 24:106–114

Sundstrom JT, Minn H, Lertola KK, Nordman E (1998) Prognosis of patients treated for intracranial metastases with whole-brain irradiation. Ann Med 30:296–299

Tsao MN, Lloyd N, Wong RK, Chow E, Rakovitch E, Laperriere N, Xu W, Sahgal A (2012) Whole brain radiotherapy for the treatment of newly diagnosed multiple brain metastases. Cochrane Database Syst Rev 4:CD003869

Vecht CJ, Haaxma-Reiche H, Noordijk EM, Padberg GW, Voormolen JH, Hoekstra FH, Tans JT, Lambooij N, Metsaars JA, Wattendorff AR et al (1993) Treatment of single brain metastasis: radiotherapy alone or combined with neurosurgery? Ann Neurol 33:583–590

Voorhies RM, Sundaresan N, Thaler HT (1980) The single supratentorial lesion. An evaluation of preoperative diagnostic tests. J Neurosurg 53:364–368

Wang LG, Guo Y, Zhang X, Song SJ, Xia JL, Fan FY, Shi M, Wei LC (2002) Brain metastasis: experience of the Xi-Jing hospital. Stereotact Funct Neurosurg 78:70–83

Zimm S, Wampler GL, Stablein D, Hazra T, Young HF (1981) Intracerebral metastases in solid-tumor patients: natural history and results of treatment. Cancer 48:384–394

Craniotomy for Intracranial Tumors: Role of Postoperative Hematoma in Surgical Mortality

17

Torstein R. Meling, Benjamin Lassen, and Eirik Helseth

Contents

Abstract

Radical surgery within safe limits is the cornerstone of brain tumor treatment, not only to provide symptom relief, improved quality of life, smaller tumor burden for other treatment modalities and improved survival, but also to establish an exact tissue diagnosis. However, craniotomies are not without inherent risks, be it surgical mortality, postoperative hematomas or infections. With respect to intracranial hematomas, the consequences are often devastating, with reported mortality rates of 30 % and a significant neurological morbidity rate. In a recent large series, the surgical mortality, defined as death within 30 days of surgery, was 2.3 % (n = 60) and the cause of death was postoperative hematomas in 21 cases (35.0 %). Independent risk factors were age > 60 (OR 2.43 95 % CI (1.35, 4.39), $p < 0.001$), whereas neither sex, resection versus biopsy, primary versus secondary craniotomy, nor tumor type were significantly associated with risk of developing postoperative hematoma.

Introduction

According to The Central Brain Tumor Registry of the United States (CBTRUS), the incidence rate of all primary brain and central nervous system (CNS) tumors is 16.5 cases per 100,000 person–years (9.2 per 100,000 person–years for

T.R. Meling (✉) • B. Lassen • E. Helseth
Department of Neurosuregry, Oslo University Hospital, 0027 Oslo, Norway
e-mail: torevmel@online.no

M.A. Hayat (ed.), *Tumors of the Central Nervous System, Volume 12*,
DOI 10.1007/978-94-007-7217-5_17,

non–malignant tumors and 7.3 per 100,000 person–years for malignant tumors) (CTBRUS 2008). The prevalence rate for all primary brain and central nervous system tumors was estimated to be 130.8 per 100,000 inhabitants (CTBRUS 2008). Metastatic brain tumors are thought to have a higher incidence than primary brain tumors (Percy et al. 1972).

The cornerstone of brain tumor treatment is surgery. The objective of surgery is not only to provide symptom relief, improved quality of life, smaller tumor burden for other treatment modalities and improved survival, but also to establish an exact tissue diagnosis (Claus et al. 2005; Hart et al. 2005; Keles et al. 2006; McGirt et al. 2009; Mirimanoff et al. 1985; Nitta and Sato 1995; Vecht et al. 1990).

However, craniotomies are not without inherent risks, be it surgical mortality (Barker 2004; Fadul et al. 1988; Lassen et al. 2011), postoperative hematomas (Gerlach et al. 2004; Kalfas and Little 1988; Lassen et al. 2011) or infection (Lassen et al. 2011; Mahaley et al. 1989). With respect to surgical mortality, the reported series are often of limited size (Sawaya et al. 1998) and based on a selected patient group (Paek et al. 2005). Furthermore, to ascertain surgical deaths, either death before discharge (in-hospital mortality) or within 30 days of surgery is used, with the former missing more than 25 % of surgery-related deaths and creates potential for bias across institutions (John D. Birkmeyer, personal communication). With respect to intracranial hematomas, the consequences are often devastating, with a mortality rate of 30 % and a significant morbidity rate (Palmer et al. 1994).

The Oslo University Hospital Experience

A recent study by Lassen et al. (2011) of 2,630 consecutive craniotomies is the largest prospective series with regard to postoperative hematomas after craniotomies for brain tumors. All adult patients who underwent craniotomy for an intracranial tumor at Oslo University Hospital in the time period 2003–2008 were reported and the strengths of this study lie in the setting, design and follow-up. The data were restricted to one health centre, thereby reducing the possible confounding effect of differences in the access to health care services between health centers and avoiding the selection bias inherently present in large multi-center studies. Furthermore, the data were prospectively registered and included all craniotomies performed for a histologically verifiable brain tumor, leaving no selection bias. The study is contemporary, thereby reflecting current neurosurgical practice and was performed within a relatively short time span, thereby reducing confounding factors as changes in antibiotic prophylaxis regimen or operating theatres. With respect to data, only easily verifiable end points (i.e., mortality, reoperation for hematomas) were used. Lastly, follow-up was 100 %.

Clinical Setting

The defined neurosurgical catchment area for Oslo University Hospital (OUH) is the south and eastern health region of Norway. It has 2.7 million inhabitants (56 % of the Norwegian population) and OUH treat approximately 99 % of the neurosurgical tumor patients within this region (The Norwegian Cancer Registry, unpublished data). A total of 2,630 consecutive craniotomies at the Oslo University Hospital in the time period 2003–2008 were included in this study (Table 17.1). The mean age at surgery was 56 years (range 18–89 years), with a male-to-female ratio of 1:1.06. Follow-up was 100 %.

Perioperative Craniotomy Routines

A consultant anesthetist should see all craniotomy patients preoperatively. Elderly patients (>70 years) and patients on multiple medications should routinely also seen by consultant internist, to optimize the general medical condition and medications. At our institution, patients with a known heart condition are referred to cardiologist for cardiac ultrasound and ECG stress test.

Table 17.1 Patients' characteristics (n = 2630)

	N	%
Patients	2,630	100
Sex		
Male	1,275	48.5
Female	1,355	51.5
Age (years)		
18–29.9	141	5.4
30–39.9	300	11.4
40–49.9	437	16.6
50–59.9	604	23.0
60–69.9	649	24.7
70–79.9	411	15.6
>80	88	3.3
Type of surgery		
Primary	2,141	81.4
Second	489	18.6
Craniotomy		
Resection	2,556	97.2
Open biopsy	74	2.8
Main histology		
High-grade glioma (HGG)	830	31.6
Meningioma	693	26.3
Metastases	449	17.1
Low-grade glioma (LGG)	289	11.0
Schwannoma	73	2.8
Primary CNS-lymphoma	51	1.9
CNS hemangioblastoma	39	1.5
Cavernous hemangioma	38	1.4
Pituitary adenoma	8	0.3
Others	160	6.1

Patients with a past hematological history are referred to a consultant hematologist. Aspirin, dipyridamole and clopidogrel are stopped at least 10 days prior to surgery and when on anticoagulation, the INR should be below 1.5. All patients receive compressive stockings the day before surgery and keep them until fully mobilized. Postoperatively, the patients are observed in the recovery for 3–6 h, whereafter they are transferred to a level 2 bed. After a craniotomy for a supratentorial tumor, the patients are generally observed for 24 h. For infratentorial tumors, the length of observation is minimum 48 h Low-molecularweight heparin is given the first postoperative day. The patients are mobilized either in the afternoon at the day of surgery or on the first postoperative day.

Incidence of Craniotomies

First-time craniotomies with primary resection were performed in 2,073 cases, 483 cases were reoperations with repeated resection, and 74 cases were open biopsies. Thus, the incidence of first-time craniotomy for a brain tumor was 12.8/100,000 inhabitants per year and for a repeat resection 3.0/100,000 inhabitants per year.

Surgical Mortality

The surgical mortality, defined as death within 30 days of surgery, was 2.3 % (n = 60). In 21 cases, the cause of death was postoperative hematomas (35.0 %). In the remaining patients, the cause of death was either tumor progression (35.0 %), infectious diseases (13.3 %), postoperative edema and subsequent herniation (6.7 %), and other causes in 10 % (Table 17.2). Using multivariate Cox regression analyses, age > 60 (Odds ratio (OR) 1.84, 95 % CI (1.05, 3.22), $p < 0.05$) and biopsy compared to resection (OR 4.67, 95 % CI (1.80, 12.14) $p < 0.01$) were shown to be significantly associated with increased surgical mortality (Table 17.3).

Postoperative Hematomas Requiring Recraniotomy

A postoperative hematoma was surgically evacuated in 54 patients (2.1 %) (Table 17.4). Of these, 23 (42.6 %) were intra-cerebral (ICH), 13 (24.1 %) were acute epidural (EDH), 2 (3.7 %) were acute subdural (aSDH), 4 (7.4 %) were intracerebellar, 1 (1.9 %) was in the brain stem, 8 (14.8 %) were chronic subdural hematomas (cSDH), and 3 (5.6 %) were subcutaneous (SC) (Table 17.4).

Risk Factors for Reoperation for Postoperative Hematomas

Using multivariate Cox regression analyses, age > 60 was shown to be significantly associated with increased risk of developing postoperative hematoma (OR 2.43 95 % CI (1.35,4.39),

Table 17.2 Surgical mortality: patients who died within 30 days of tumor surgery (n = 60)

Age	Sex	Histology[a]	Op.type[b]	Time[c]	Comments
43	M	Hemangioblastoma	R	3	Postop. hematoma
29	F	HGG	R	17	Tumor progression
41	M	HGG	R	13	Postop. brain edema/herniation
41	F	HGG	R	3	Postop. hematoma
48	M	HGG	B	10	Pneumonia
49	F	HGG	R	11	Tumor progression
54	F	HGG	R	2	Tumor progression
56	F	HGG	B	8	Postop. hematoma
60	M	HGG	R	30	Postop. hematoma
64	M	HGG	R	17	Tumor progression
64	F	HGG	R	4	Postop. brain edema/herniation
65	F	HGG	R	22	Postop. hematoma
66	F	HGG	R	24	Tumor progression
67	F	HGG	R	5	Tumor progression
67	M	HGG	R	19	Tumor progression
69	M	HGG	B	29	Tumor progression
74	F	HGG	R	30	Tumor progression
75	M	HGG	R	11	Postop. hematoma
75	M	HGG	R	22	Tumor progression
76	M	HGG	R	15	Postop. hematoma
76	F	HGG	R	4	Postop. hematoma
77	F	HGG	R	8	Postop. hematoma
81	F	HGG	B	28	Tumor progression
82	M	HGG	R	21	Pulmonary embolism
84	F	HGG	R	14	Postop. brain edema/herniation
32	F	LGG	R	17	Shunt failure
48	M	LGG	R	18	Pneumonia
68	M	LGG	R	24	Postop. hematoma
62	M	Lymphoma	B	12	Tumor progression
75	F	Lymphoma	B	13	Tumor progression
78	M	Lymphoma	B	26	Tumor progression
31	F	Melanocytoma	R	11	Tumor progression
55	F	Meningioma	R	6	Postop. brain edema/herniation
73	M	Meningioma	R	11	Postop. hematoma
77	M	Meningioma	R	4	Postop. hematoma
79	F	Meningioma	R	12	Postop. hematoma
83	M	Meningioma	R	15	Pneumonia
83	M	Meningioma	R	29	Cardiac arrest
35	M	Metastasis	R	12	Tumor progression
40	M	Metastasis	R	27	Pneumonia
45	F	Metastasis	R	4	Postop. hematoma
46	F	Metastasis	R	9	Hydrocephalus
49	F	Metastasis	R	25	Postop. hematoma
49	F	Metastasis	R	26	Postop. hematoma
52	M	Metastasis	R	6	Postop. hematoma
53	F	Metastasis	R	5	Tumor progression

(continued)

Table 17.2 (continued)

Age	Sex	Histology[a]	Op.type[b]	Time[c]	Comments
56	M	Metastasis	R	3	Cardiac arrest
60	M	Metastasis	R	1	Postop. hematoma
61	M	Metastasis	R	30	Postop. hematoma
61	F	Metastasis	R	12	Pneumonia
62	M	Metastasis	R	19	Tumor progression
62	M	Metastasis	R	29	Postop. hematoma
65	F	Metastasis	R	22	Sepsis
71	F	Metastasis	R	25	Tumor progression
73	M	Metastasis	R	24	Sepsis
77	F	Metastasis	R	19	Tumor progression
78	M	Metastasis	R	29	Subdural empyema
81	F	Metastasis	R	25	Tumor progression
48	M	Pituitary adenoma	R	16	Cerebral infarction
69	M	Pituitary adenoma	R	9	Postop. hematoma

M male, *F* female
[a]Histology: *HGG* high-grade glioma, *LGG* low-grade glioma
[b]Op. type = resection (*R*) or biopsy (*B*)
[c]Time = time to death in days after primary surgery

Table 17.3 Univariate and multivariate analysis of factors possibly associated with surgical mortality and surgery for postoperative hematoma

	30 day mortality		Postop hematoma	
	Univariate	Multivariate	Univariate	Multivariate
	Odds ratio (95 % CI)	Odds ratio (95 % CI)	Odds ratio (95 % CI)	Odds ratio (95 % CI)
Age > 60	2.27**	1.84*	2.42**	2.43**
No/Yes	[1.34,3.86]	[1.05,3.22]	[1.38,4.26]	[1.35,4.39]
Sex	0.94	1.09	0.94	0.94
Male/Female	[0.56,1.57]	[0.64,1.84]	[0.55,1.61]	[0.54,1.64]
Primary Op	0.77	1.01	0.99	1.14
Primary/secondary	[0.38,1.57]	[0.48,2.13]	[0.50,1.99]	[0.56,2.31]
Operation	4.93***	4.67**	[a]	[a]
Resection/Biopsy	[2.16,11.26]	[1.80,12.14]		
Observations		2,557		2,523
Pseudo-R^2		0,064		0,025
H-L test		$p = 0.66$		$p = 0.78$

HGG high grade glioma, *LGG* low grade glioma, *H-L* hosmer-lemeshow
*$p < 0.05$; **$p < 0.01$; ***$p < 0.001$
[a]Insufficient events in one of the contrasting categories to calculate odds ratio

$p < 0.001$) (Table 17.3). Neither sex, resection versus biopsy, primary versus secondary craniotomy, nor tumor type were significantly associated with risk of developing postoperative hematoma.

Time to Reoperation for Postoperative Hematomas

The surgically evacuated hematomas were reoperated within 6 h. in 11 cases (20.4 %), within 12 h in 14 cases (25.9 %), within 24 h in

Table 17.4 Patients reoperated for postoperative hematoma (n = 54)

Age	Sex	Histology[a]	Location[b]	Time to reop. (hh:mm)[c]	Outcome[d]	Time to death (days)[e]
63	F	Carcinoma	SC	19:45	NAD	
65	M	Carcinoma	EDH	69:53	Minor	
43	M	Hemangioblastoma	Brain stem	28:35	Death	3
77	M	Hemangioblastoma	Cerebellum	47:04	NAD	
31	M	HGG	ICH	14:15	NAD	
33	M	HGG	cSDH	107 days	NAD	
34	M	HGG	Cerebellum	152:57	Minor	
46	F	HGG	EDH	26:22	NAD	
48	F	HGG	ICH	01:36	Minor	
55	F	HGG	ICH	06:20	Minor	
57	M	HGG	cSDH	43 days	NAD	
58	M	HGG	ICH	44:10	NA	
65	F	HGG	ICH	16:58	Death	22
70	F	HGG	EDH	74:25	NAD	
72	F	HGG	EDH	02:50	Minor	
75	M	HGG	ICH	01:35	Death	11
76	M	HGG	SC	03:15	NAD	
76	F	HGG	ICH	30:38	Minor	
76	F	HGG	ICH	04:12	Death	4
77	F	HGG	EDH	07:57	Death	8
81	M	HGG	EDH	30:17	Minor	
51	M	LGG	EDH	46:06	Minor	
60	F	LGG	ICH	27:35	NAD	
52	M	Melanocytoma	EDH	42:45	NAD	
51	M	Meningioma	EDH	48:50	NAD	
52	F	Meningioma	aSDH	10 days	NAD	
54	F	Meningioma	ICH	93:35	Major	
60	F	Meningioma	ICH	02:20	Minor	
67	F	Meningioma	ICH	14:20	Minor	
69	F	Meningioma	ICH	01:45	NAD	
69	F	Meningioma	cSDH	47 days	NAD	
69	F	Meningioma	ICH	22:00	Minor	
70	M	Meningioma	SC	06:20	NAD	
70	M	Meningioma	cSDH	73 days	NAD	
71	F	Meningioma	Cerebellum	22:20	Major	
75	F	Meningioma	ICH	167:45	NA	
76	M	Meningioma	ICH	03:27	Major	
78	M	Meningioma	ICH	03:40	Minor	
78	F	Meningioma	cSDH	383 days	Death	390
80	F	Meningioma	cSDH	13 days	Minor	
45	F	Metastasis	ICH	45:20	Death	4
49	F	Metastasis	ICH	26 days	Death	26
52	M	Metastasis	EDH	17:41	Death	6
54	M	Metastasis	EDH	53:07	NAD	
61	M	Metastasis	Cerebellum	38:05	Death	30
63	F	Metastasis	ICH	32:40	Minor	
68	M	Metastasis	ICH	03:40	Minor	

(continued)

Table 17.4 (continued)

Age	Sex	Histology[a]	Location[b]	Time to reop. (hh:mm)[c]	Outcome[d]	Time to death (days)[e]
72	F	Metastasis	EDH	04:15	NAD	
73	F	Metastasis	cSDH	68 days	NAD	
73	M	Metastasis	ICH	47:17	Death	54
62	M	Pituitary adenoma	ICH	58:10	Major	
69	M	Pituitary adenoma	aSDH	45:15	Death	9
69	M	Pituitary adenoma	cSDH	107 days	Minor	
46	M	Schwannoma	EDH	61:08	NAD	

M male, *F* female
[a]Histology: *HGG* high-grade glioma, *LGG* low-grade glioma
[b]Location of hematoma: *SC* subcutaneous hematoma, *EDH* epidural hematoma, *aSDH* acute subdural hematoma, *cSDH* chronic subdural hematoma, *ICH* intracerebral hematoma
[c]Time = time of reoperation in hours and minutes after primary surgery
[d]Outcome = hematoma-inflicted disability: *NAD* no additional disability, *Minor* minor additional disability, *Major* major additional disability, *NA* no information available
[e]Time to death = time from tumor surgery to death, when caused by the hematoma

21 cases (38.9 %), within 48 h in 35 cases (64.8 %), and within 72 h in 40 cases (74.1 %) (Table 17.4). Four patients were operated between day 3 and day 7 after surgery, three patients were operated between day 7 and day 30, and seven patients after 30 days of surgery. All seven in the latter group were cSDH. Excluding the cSDHs, the median time from tumor surgery to reoperation for hematoma was 1 day (mean 2.2 days, range 0–26).

Consequences of Postoperative Hematoma

Twenty patients (37.0 %) had no additional disability, 16 (29.6 %) had minor additional disability, 4 (7.4 %) had major additional disability, and 12 (22.2 %) died due to their hematoma. Long-term data are inconclusive for two patients (3.7 %). Six out of twenty-three (26.1 %) patients with ICH died, while 2/13 (15.4 %) patients with EDH died ($p > 0.05$) (Table 17.4).

Discussion

The incidence of surgical mortality after craniotomy for tumors is reported to be between 0 % and 9.6 %, varying with the diagnosis (Barker 2004; Barker et al. 2005; Boviatsis et al. 2007; Brell et al. 2000; Chang et al. 2003; Cowan et al. 2003; Curry et al. 2005; Lassen et al. 2011; Long et al. 2003; Morokoff et al. 2008; Sawaya et al. 1998; Stark et al. 2005). Long et al. (2003) reported a mortality rate at high-volume hospitals (>50 craniotomies/year) of 2.5 % after craniotomy for various intracranial tumors, both benign and malignant. Barker et al. (2005) reported in their series of primary supratentorial brain tumors a mortality rate of 2.9 %. However, both these studies were in-hospital mortality rates, whereas Lassen et al. (2011) reported a 30-day mortality rate of 2.3 %.

The causes of surgical mortality include complications to surgery and factors not directly related to surgery, as well as other factors, like tumor progression or other morbidity. Several risk factors are associated with increased hazard of death, e.g. advanced age (Barker 2004; Barker et al. 2005; Cowan et al. 2003; Lassen et al. 2011; Sawaya et al. 1998), a low preoperative KPS score (Sawaya et al. 1998), and comorbidity (Barker 2004; Barker et al. 2005). Several of the complications are avoidable, and should be paid close attention to.

Postoperative hematomas carry a high mortality rate (Palmer et al. 1994). Lassen et al. (2011) suspected hematomas to be the cause of, or significant contributor to, 35 % of the deaths within 30 days of surgery. Consequently, avoiding hematomas is the single most important factor to reduce surgical mortality.

Pulmonary embolism (PE) has an incidence rate of between 1.5 % and 3 %, and a mortality rate between 9 % and 50 %, and is a frequent cause of death among neurosurgical patients (Danish et al. 2004). In our study, one patient died from a PE postoperatively. The prevention of PE in neurosurgical patients is contentious, as the commonly used medical prophylaxis, i.e., unfractioned or low-molecular-weight heparin, may increase the rate of intracranial bleeding, with its deleterious effects (Danish et al. 2005). Danish et al. showed that mechanical prophylaxis yields outcomes in craniotomy patients superior of those of heparin (Danish et al. 2005), but the field remains controversial. Patients with a past hematological history should be referred to a consultant hematologist for a preoperative assessment. All patients should have compressive stockings the day before surgery and keep them until fully mobilized. Low-molecular-weight heparin can be administered the first postoperative day. Importantly, the patients should be mobilized very early, either the same afternoon or on the first postoperative day (Lassen et al. 2011). Age is an independent risk factor for surgical mortality. Still, age should not be used as a selection criterion for surgery for intracranial tumors alone (Rogne et al. 2009). A careful selection among patients with a low preoperative KPS score and with comorbidity should be carried out to lower operative mortality rates.

Postoperative Hematomas Requiring Reoperation

In our series, we found a rate of postoperative hematomas of 2.1 % (Lassen et al. 2011). This includes three subcutaneous hematomas and eight cSDH. Other studies have reported a hematoma rate of 0.6–4.0 % (Barker et al. 2005; Boviatsis et al. 2007; Brell et al. 2000; Chang et al. 2003; Curry et al. 2005; Morokoff et al. 2008; Rabadan et al. 2007; Rogne et al. 2009; Sawaya et al. 1998; Stark et al. 2005).

Risk Factors

Advanced age is significantly associated with development of postoperative hematoma, in both uni- and multivariate analyses (Lassen et al. 2011). This finding is supported by other studies (Boviatsis et al. 2007; Gerlach et al. 2004; Palmer et al. 1994) and has been attributed to tissue fragility observed in the elderly (Danish et al. 2005). Palmer et al. (1994) showed in their series of 6,668 intracranial procedures an increased risk of postoperative hematoma for meningiomas compared with intrinsic tumors.

In the aforementioned series, Palmer et al. (1994) identified several risk factors associated with postoperative hematoma, including thrombocytopenia, anticoagulants, a history of heavy alcohol intake, coagulopathy, malignancy outside the central nervous system, and the administration of antiplatelet agents during the 2 weeks preceding surgery. Administration of antiplatelet agents was the most frequent risk factor, being used by 43 % of those reoperated for hematoma (Palmer et al. 1994).

Mortality Rate of Postoperative Hematomas

The reported mortality rate of postoperative hematomas is 18–32 % (Basali et al. 2000; Palmer et al. 1994; Taylor et al. 1995). In our prospective study, we found a mortality rate of 22 %, with an additional 2 % being severely disabled due to the hematoma (Lassen et al. 2011). Consequently, postoperative hematomas may have deleterious consequences and it is utmost important to reduce or eliminate as many risk factors as possible, and thereby reducing the incidence of postoperative hematomas. Vassilouthis et al. (1999) indicated in their series of 526 patients undergoing craniotomy, that the incidence of postoperative intracranial hematoma should become negligible, provided that necessary modifications regarding anesthesia are adopted. Their strict anesthesiological protocol included a deep opioid analgesia to eliminate any acute elevations of the arterial pressure during and immediately after craniotomy. Furthermore, emergence from anaesthesia was delayed for an average of 1 1/2–2 h following the neurosurgical procedure. Even though postoperative hematomas occur rarely, more studies on how to avoid them are needed, as the consequences of them are often devastating.

Timing of Postoperative Intracranial Hematoma Development

Taylor et al. (1995) reported a 2.2 % rate of postoperative hematomas in their series of 2,305 patients undergoing intracranial surgery of miscellaneous reasons. Clinical deterioration as a result of postoperative hematoma occurred within 6 h. of surgery in 88 % of the cases and < 24 h after surgery in the remaining 12 % hematoma cases. They concluded that a 6-h observation period in the recovery area/intensive care unit after craniotomy before transfer to further nursing on a neurosurgical ward should be sufficient for most patients, but they recommended longer observation times after emergency craniotomies and posterior fossa surgery. In our series, only 11 patients (25 %) were reoperated within 6 h, indicating that a 6 h. observation period in recovery may be insufficient to sift out the majority of the patients in need of emergency surgery for a postoperative hematoma. However, close observation on a specialized neurosurgical ward may overcome this problem. Furthermore, our results indicate that a patient undergoing a craniotomy should be observed closely for a total of at least 48 h postoperatively, as 80 % of our patients that needed a recraniotomy for postoperative hematoma are operated within 2 days.

In conclusion, the mortality rate, rate of postoperative hematomas and infections were low. Although advanced age was significantly associated with a higher 30-day surgical mortality and risk of postoperative hematomas, surgery in selected elderly patients is worthwhile and not futile. The single most important way to reduce surgical mortality is avoidance of postoperative hematomas.

References

Barker FG 2nd (2004) Craniotomy for the resection of metastatic brain tumors in the U.S., 1988–2000: decreasing mortality and the effect of provider caseload. Cancer 100(5):999–1007

Barker FG 2nd, Curry WT Jr, Carter BS (2005) Surgery for primary supratentorial brain tumors in the United States, 1988 to 2000: the effect of provider caseload and centralization of care. Neuro Oncol 7(1):49–63

Basali A, Mascha EJ, Kalfas I, Schubert A (2000) Relation between perioperative hypertension and intracranial hemorrhage after craniotomy. Anesthesiology 93(1):48–54

Boviatsis EJ, Bouras TI, Kouyialis AT, Themistocleous MS, Sakas DE (2007) Impact of age on complications and outcome in meningioma surgery. Surg Neurol 68(4):407–411

Brell M, Ibanez J, Caral L, Ferrer E (2000) Factors influencing surgical complications of intra-axial brain tumours. Acta Neurochir (Wien) 142(7):739–750

Chang SM, Parney IF, McDermott M, Barker FG 2nd, Schmidt MH, Huang W, Laws ER Jr, Lillehei KO, Bernstein M, Brem H, Sloan AE, Berger M (2003) Perioperative complications and neurological outcomes of first and second craniotomies among patients enrolled in the Glioma Outcome Project. J Neurosurg 98(6):1175–1181

Claus EB, Horlacher A, Hsu L, Schwartz RB, Dello-Iacono D, Talos F, Jolesz FA, Black PM (2005) Survival rates in patients with low-grade glioma after intraoperative magnetic resonance image guidance. Cancer 103(6):1227–1233

Cowan JA Jr, Dimick JB, Leveque JC, Thompson BG, Upchurch GR Jr, Hoff JT (2003) The impact of provider volume on mortality after intracranial tumor resection. Neurosurgery 52(1):48–53

CTBRUS (2008) Statistical report: primary brain tumors in the United States, 2000–2004. http://www.cbtrus.org/reports//2007-2008/2007report.pdf

Curry WT, McDermott MW, Carter BS, Barker FG 2nd (2005) Craniotomy for meningioma in the United States between 1988 and 2000: decreasing rate of mortality and the effect of provider caseload. J Neurosurg 102(6):977–986

Danish SF, Burnett MG, Stein SC (2004) Prophylaxis for deep venous thrombosis in patients with craniotomies: a review. Neurosurg Focus 17(4):E2

Danish SF, Burnett MG, Ong JG, Sonnad SS, Maloney-Wilensky E, Stein SC (2005) Prophylaxis for deep venous thrombosis in craniotomy patients: a decision analysis. Neurosurgery 56(6):1286–1292

Fadul C, Wood J, Thaler H, Galicich J, Patterson RH Jr, Posner JB (1988) Morbidity and mortality of craniotomy for excision of supratentorial gliomas. Neurology 38(9):1374–1379

Gerlach R, Raabe A, Scharrer I, Meixensberger J, Seifert V (2004) Post-operative hematoma after surgery for intracranial meningiomas: causes, avoidable risk factors and clinical outcome. Neurol Res 26(1):61–66

Hart MG, Grant R, Walker M, Dickinson H (2005) Surgical resection and whole brain radiation therapy versus whole brain radiation therapy alone for single brain metastases. Cochrane Database Syst Rev 1:CD003292

Kalfas IH, Little JR (1988) Postoperative hemorrhage: a survey of 4992 intracranial procedures. Neurosurgery 23(3):343–347

Keles GE, Chang EF, Lamborn KR, Tihan T, Chang CJ, Chang SM, Berger MS (2006) Volumetric extent of

resection and residual contrast enhancement on initial surgery as predictors of outcome in adult patients with hemispheric anaplastic astrocytoma. J Neurosurg 105(1):34–40

Lassen B, Helseth E, Ronning P, Scheie D, Johannesen TB, Maehlen J, Langmoen IA, Meling TR (2011) Surgical mortality at 30 days and complications leading to recraniotomy in 2630 consecutive craniotomies for intracranial tumors. Neurosurgery 68(5): 1259–1269

Long DM, Gordon T, Bowman H, Etzel A, Burleyson G, Betchen S, Garonzik IM, Brem H (2003) Outcome and cost of craniotomy performed to treat tumors in regional academic referral centers. Neurosurgery 52(5):1056–1063

Mahaley MS Jr, Mettlin C, Natarajan N, Laws ER Jr, Peace BB (1989) National survey of patterns of care for brain-tumor patients. J Neurosurg 71(6):826–836

McGirt MJ, Chaichana KL, Gathinji M, Attenello FJ, Than K, Olivi A, Weingart JD, Brem H, Quinones-Hinojosa AR (2009) Independent association of extent of resection with survival in patients with malignant brain astrocytoma. J Neurosurg 110(1):156–162

Mirimanoff RO, Dosoretz DE, Linggood RM, Ojemann RG, Martuza RL (1985) Meningioma: analysis of recurrence and progression following neurosurgical resection. J Neurosurg 62(1):18–24

Morokoff AP, Zauberman J, Black PM (2008) Surgery for convexity meningiomas. Neurosurgery 63(3): 427–433

Nitta T, Sato K (1995) Prognostic implications of the extent of surgical resection in patients with intracranial malignant gliomas. Cancer 75(11):2727–2731

Paek SH, Audu PB, Sperling MR, Cho J, Andrews DW (2005) Reevaluation of surgery for the treatment of brain metastases: review of 208 patients with single or multiple brain metastases treated at one institution with modern neurosurgical techniques. Neurosurgery 56(5):1021–1034, discussion 1021–1034

Palmer JD, Sparrow OC, Iannotti F (1994) Postoperative hematoma: a 5-year survey and identification of avoidable risk factors. Neurosurgery 35(6):1061–1064

Percy AK, Elveback LR, Okazaki H, Kurland LT (1972) Neoplasms of the central nervous system. Epidemiologic considerations. Neurology 22(1):40–48

Rabadan AT, Hernandez D, Eleta M, Pietrani M, Baccanelli M, Christiansen S, Teijido C (2007) Factors related to surgical complications and their impact on the functional status in 236 open surgeries for malignant tumors in a Latino-American hospital. Surg Neurol 68(4):412–420, discussion 420

Rogne SG, Konglund A, Meling TR, Scheie D, Johannesen TB, Ronning P, Helseth E (2009) Intracranial tumor surgery in patients >70 years of age: is clinical practice worthwhile or futile? Acta Neurol Scand 120:288–294

Sawaya R, Hammoud M, Schoppa D, Hess KR, Wu SZ, Shi WM, Wildrick DM (1998) Neurosurgical outcomes in a modern series of 400 craniotomies for treatment of parenchymal tumors. Neurosurgery 42(5):1044–1055

Stark AM, Tscheslog H, Buhl R, Held-Feindt J, Mehdorn HM (2005) Surgical treatment for brain metastases: prognostic factors and survival in 177 patients. Neurosurg Rev 28(2):115–119

Taylor WA, Thomas NW, Wellings JA, Bell BA (1995) Timing of postoperative intracranial hematoma development and implications for the best use of neurosurgical intensive care. J Neurosurg 82(1):48–50

Vassilouthis J, Anagnostaras S, Papandreou A, Dourdounas E (1999) Is postoperative haematoma an avoidable complication of intracranial surgery? Br J Neurosurg 13(2):154–157

Vecht CJ, Avezaat CJ, van Putten WL, Eijkenboom WM, Stefanko SZ (1990) The influence of the extent of surgery on the neurological function and survival in malignant glioma. A retrospective analysis in 243 patients. J Neurol Neurosurg Psychiatry 53(6):466–471

Pituitary Adenomas: Treatment Using the Endonasal Approach

18

Leo F.S. Ditzel Filho, Nancy McLaughlin, Domenico Solari, Daniel M. Prevedello, Amin B. Kassam, Ricardo L. Carrau, and Daniel F. Kelly

Contents

Abstract

Pituitary adenomas are the most common sellar pathology. They can be classified according to size (micro vs. macroadenomas) and according to endocrine function (active vs. inactive). Indications for surgical removal include macroadenomas causing compression of neighboring structures and endocrine-active adenomas that cause detrimental systemic effects, as seen in acromegaly and Cushing's disease. The majority of pituitary tumors can be safely and effectively removed through an endonasal, transsphenoidal route. Historically, this procedure has been performed under microscopic visualization; however, the recent emergence and evolution of endoscopic techniques have gained acceptance among skull base surgeons managing these lesions. The endoscope may be used as the sole source

L.F.S. Ditzel Filho • D.M. Prevedello
Department of Neurosurgery, The Ohio State University Wexner Medical Center, 410 W 10th Avenue, Columbus, OH 43215, USA

N. McLaughlin
Department of Neurosurgery, University of California, Los Angeles, 300 UCLA Medical Plaza, Suite B200, Los Angeles, CA 90095, USA

D. Solari
Department of Neurosurgery, Università degli Studi di Napoli Federico II, Via S. Pansini 5, 80131 Naples, Italy

A.B. Kassam
Division of Neurosurgery, University of Ottawa, 1053, Carling Avenue, Ottawa, Ontario, K1Y 4E9, Canada

R.L. Carrau
Department of Otolaryngology – Head & Neck Surgery, The Ohio State University Wexner Medical Center, 410 W 10th Avenue, Columbus, OH 43215, USA

D.F. Kelly (✉)
Brain Tumor Center, John Wayne Cancer Institute at Saint John's Health Center, 2200, Santa Monica Blvd., Santa Monica, CA 90404, USA
e-mail: kellyd@jwci.org

M.A. Hayat (ed.), *Tumors of the Central Nervous System, Volume 12*,
DOI 10.1007/978-94-007-7217-5_18,

of visualization or as an adjunct in the microscopic approach. Its increased luminosity and angled profile grants the surgeon the possibility of visualization of lateral and posterior components of the sellar compartment, a feature particularly useful in macroadenomas invading the cavernous sinuses. In this chapter we describe the surgical technique, indications and complication avoidance strategies of the microscopic, endoscope-assisted transsphenoidal removal of pituitary adenomas.

Introduction

Pituitary adenomas are among the most common intracranial neoplasms. Their surgical resection is reserved for those cases in which the tumor is endocrine active and not responsive to primary drug therapy, as seen in acromegaly (Hardy and Somma 1979; Jane et al. 2001) and Cushing's Disease (Cushing 1912; Laws et al. 2002; Kelly 2007); as well as endocrine inactive tumors that have reached significant size (macroadenomas, larger than 10 mm in diameter) and are causing compression of neighboring structures, especially the optic chiasm.

The most common surgical route utilized in the resection of pituitary tumors, regardless of their size, is the transsphenoidal approach (Wilson and Dempsey 1978; McDonald and Laws 1982; Liu et al. 2001; Jane et al. 2002; Prevedello et al. 2007). Through the nasal corridor and the sphenoid sinus, the surgeon has ample access to the sella turcica, the suprasellar region, the parasellar cavernous sinuses and the infrasellar clivus. This approach can be performed under microscopic (Fatemi et al. 2008a) or endoscopic visualization (Jho and Carrau 1997), or even a combination of both (Kawamata et al. 2002a, b; Powell 2009). Although most neurosurgeons are more familiar with the microscope, recent technology advances have popularized the use of the endoscope in endonasal skull base surgery (Kassam et al. 2004, 2005a, b), particularly in pituitary surgery. As a technical adjunct to the microscope, the endoscope's angled view is particularly useful in following extensions of tumor into the parasellar cavernous sinuses (Frank and Pasquini 2002, 2006) and the suprasellar space; its increased luminosity is also superb during sellar inspection and to confirm total removal of the pituitary tumor (Spencer et al. 1999; Catapano et al. 2006; Frank et al. 2006; Dehdashti et al. 2008; Rotenberg et al. 2010). Although the use of the microscopic endonasal approach for pituitary adenomas clearly appears to be on the decline given the increased success and popularity of the fully endoscopic approach, it remains a viable approach for pituitary tumors with a long track record of safety and success. Based on our recent experience, the microscopic approach is greatly enhanced with the use of endoscopic visualization (McLaughlin et al. 2012). In this chapter, we describe the surgical technique for the microscopic, endoscope-assisted transsphenoidal resection of pituitary adenomas.

Patient Selection

Virtually every pituitary adenoma can be surgically treated through the transsphenoidal route; transcranial approaches are reserved for removal of extra-sellar masses in giant multi-compartment adenomas.

Surgical Technique

Patient Positioning and Preparation

The patient is positioned supine after general anesthesia, with the head resting on a horseshoe head-holder. The surgeon takes position along the patient's right side; hence, the endotracheal tube is secured towards the left side of the mouth so as to prevent any obstacle to the insertion of instruments in the patient's nostrils. The head is tilted slightly to the left with no neck extension. The patient receives preoperative intravenous prophylactic antibiotics, typically a first generation cephalosporin, during anesthetic induction. Glucocorticoids are only used in patients with adrenal insufficiency. The patient's face and abdo-

men (in case a fat graft is required) are prepped and covered with sterile fields; only the nasal aperture is exposed. Although the face receives a topical antibiotic, no solutions are used in the nasal cavity.

The entire procedure takes place under frameless stereotactic navigation, with merged Computed Tomography (CT) and Magnetic Ressonance Imaging (MRI) studies. This tool is particularly useful in patients with previous transnasal operations (Lasio et al. 2002) and in tumors with extensive cavernous sinus invasion and internal carotid artery (ICA) involvement.

Microscopic Transsphenoidal Approach

The initial transnasal approach to the sphenoid sinus takes place under direct microscopic visualization. Given the surgeon's position along the patient's right side, typically the right nostril is utilized for the approach. However, either nostril can be used; the patient's nasal anatomy (presence of a hypertrophic turbinate, septum deviation) and tumor features (size, cavernous sinus invasion) will ultimately dictate this choice. Pituitary adenomas that project towards a specific side of the sella and ipsilateral cavernous sinus may be more easily accessed through the contralateral nostril, across the midline.

During the initial approach, the surgeon inserts a hand-held speculum into the nostril; the inferior and middle turbinates are visualized, as well as the choana and the floor of the nasal cavity. Although the local anatomy may vary greatly among patients, the relation between the head of the middle turbinate and the apex of the choana as landmarks to the rostrum of the sphenoid sinus is particularly constant. The middle turbinate is out-fractured and laterally displaced. The blades of the speculum are moved posteriorly until the junction of the septum and the rostrum of the sphenoid sinus is reached; the mucosa along this junction is cauterized and the keel of the sphenoid is exposed. A Cottle dissector is used to elevate the mucosa from the keel and separate the posterior septum from it; the tips of the speculum blades are then pushed toward the contralateral nasal cavity to displace the proximal septum off the midline, thus exposing the contralateral sphenoid keel. The speculum is reopened providing a view of the entire sphenoid keel and ostia, which should be seen at approximately the 10 and 2 o'clock positions.

At this point, the hand-held speculum is replaced by a self-retaining short trapezoidal speculum (Fatemi et al. 2008b) and the angle of the trajectory to the sella is confirmed by navigation. Next, an ample bilateral sphenoidotomy is performed with Kerrison roungers until the sella, tuberculum sellae, bilateral carotid impressions and clivus can be visualized. We recommend that bone removal of the sphenoid rostrum be extended superiorly to the ethmoid cells and inferiorly to the floor of the sphenoid sinus to ensure adequate exposure and to facilitate instrument placement and movement throughout the procedure. Furthermore, Mattozo et al. (2006) have found that insufficient sphenoid removal and sellar exposure are directly related to incomplete tumor removal and should, therefore, be avoided (Mattozo et al. 2006). Finally, sphenoid septations must be removed to complete the sellar exposure. As Fernandez-Miranda et al. (2009) demonstrated, the majority of these septations are inserted into the bony prominences of the paraclival and parasellar portions of the ICA (Fernandez-Miranda et al. 2009); for this reason we find that drilling is safer than their blunt removal with Kerrison roungers.

The mucosa overlying the sellar anterior surface is removed; the remaining mucosa along the sphenoid sinus walls can be spared to prevent excessive crusting in the postoperative period. The sellar bone is then carefully drilled down to egg-shell thickness and removed until the dark colored dura of both cavernous sinuses and of the superior and inferior circular sinuses can be seen. In patients with macroadenomas with suprasellar extension the tuberculum sellae is also removed. Any drilling performed close to the optic nerves and chiasm impressions is accompanied by copious irrigation to prevent heat damage to these structures.

Once the dura is fully exposed, Doppler probes are utilized to safely recognize the position and

course of both ICAs (Dusick et al. 2007). Typically, the point of greater risk of injury to the ICAs is located at their medial course from the parasellar cavernous portion into the intracranial compartment, at the height of the tuberculum sellae. If the Doppler probe does not satisfactorily detect the ICAs, further bone removal is performed until so.

The dura is opened in "U" shape, with special care not to transgress the tumor's pseudo-capsule or the normal pituitary tissue. The dura is then detached from the sellar contents with microdissectors and the opening enlarged in any direction that may facilitate tumor removal, avoiding transgression of the cavernous sinuses and of the superiorly located sellar diaphragm.

Tumor Removal

Initial tumor removal is also performed under microscopic visualization. Whenever possible and especially in microadenomas, an attempt is made to locate and dissect the plane between the tumor's pseudo-capsule and the surrounding healthy pituitary tissue (Oldfield and Vortmeyer 2006); this will help ensure gross total tumor removal; an essential goal in endocrine active tumors (Jagannathan et al. 2009).

In large macroadenomas this technique may not be feasible; the tumor is subsequently incised and debulked inferiorly initially. By removing the inferior pole of tumor first, the superior-lateral gland-tumor interface can often be better preserved. If invasion of the cavernous sinus is present, debulking of the sellar component is performed before the endoscope-assisted portion of the procedure begins and the lateral segment of the tumor is pursued. If the tumor presents with significant suprasellar extension, further opening of the dura cranially across the region of the tuberculum sellae may be necessary, especially if the tumor is of fibrous consistency. On occasion, excessive venous bleeding from the superior circular sinus may be present, requiring coagulation or hemostasis with Surgifoam. Soft tumors, however, will usually deliver themselves, pushed by the brain's pulsation, into the sellar compartment once their caudal segment has been resected. Nevertheless, care must be taken not to address the most cranial segment of the lesion early during tumor removal, as this will cause the sellar diaphragm to collapse over the surgical field, increasing the difficulty of the dissection and the likelihood of a cerebrospinal fluid (CSF) leak.

Endoscope Assistance

Once a thorough tumor removal has been accomplished with the microscope, the endoscope is introduced to help visualize residual tumor not seen with the microscope. Although the endoscope is generally more useful for larger macroadenomas, our experience suggests that in up to 20 % of microadenomas, residual tumor that can be removed may be seen (McLaughlin et al. 2012). To take full advantage of endoscopic visualization and allow two-hand microscopic dissection, an assistant should control the endoscope. Although a fixed endoscope holder can be used, it does not allow rapid and dynamic alterations in view to be accomplished and can be quite limiting. The speculum may be kept in place or removed to facilitate endoscope and instrument maneuverability; if a bi-nostril approach is desired, however, the laterally displaced mucosa that once covered the sphenoid rostrum must be incised to allow passage into the sinus.

Initially, the 0° endoscope is introduced and the sellar cavity is inspected for tumor remnants. The 30° and 45° endoscopes are then used and rotated laterally to allow direct visualization of the medial cavernous sinus wall and of the area directly posterior to it, a common site of invasion and where residual tumor can often be found. Tumor invading the cavernous sinus wall can be removed; the ensuing venous bleeding will signal that the majority of tumor tissue has been resected and can be controlled by direct application of Surgifoam. Furthermore, one must be cautious while entering the cavernous sinus since complete removal in the setting of extensive cavernous invasion is unlikely while posing significant risk of injury to the cranial nerves that are lateral to the cavernous carotid. The endoscope is also rotated upward to examine the sellar diaphragm

and the suprasellar cistern; when the diaphragm is collapsing into the sella a simple q-tip or cottonoid can be used as a retractor to suspend the arachnoid layer and allow inspection (Prevedello et al. 2010). Resection of residual tumor is accomplished by a combination of suction and dedicated endonasal instruments, including angled dissectors and micro-forceps.

Hemostasis

After tumor removal is achieved to satisfaction, the endoscope is removed and the microscope is reintroduced. The nasal cavity is irrigated with copious amounts of warm saline to clear any debris and to stimulate local coagulation factors. The cavernous sinuses are inspected for bleeding and the sellar diaphragm is checked for CSF leakage. Venous bleeding from the sinus and sellar cavity can be controlled through direct Surgifoam application or use of other similar hemostatic agents. Full-strength hydrogen peroxide can also be irrigated into the sella 30–60 s for hemostasis provided there is not a large diaphragmatic defect. We have found this to be effective and safe in terms of pituitary gland function (Fatemi et al. 2008c). Persistent bleeding from sources other than the sinuses may indicate residual tumor and must be carefully evaluated (Kassam et al. 2005a, b).

Skull Base Closure and CSF Leak Repair

As recently described (Esposito et al. 2007), skull base reconstruction and CSF leak repair can be tailored to the size of the CSF leak and bony and dural defects. Prior to reconstruction, an assessment of the size of the diaphragmatic defect is performed. If no obvious defect is seen, a Valsalva maneuver is induced to help visualize an occult or small (Grade 1) CSF leak emanating through a small diaphragmatic defect.

All repairs involve use of collagen sponge (Duragen, Integra Corp., Plainsboro, NJ; Helistat, Integra Corp., Plainsboro, NJ or Instat, Ethicon Inc., Somerville, NJ), as part of the repair, which acts as a scaffolding for fibroblast in-growth, and a vascularized dural replacement(Kleinman et al. 1981; Narotam et al. 1993, 1995; Kelly et al. 2001). In patients with no CSF leak (Grade 0), a single layer of minimally moistened collagen sponge placed over the exposed diaphragma sellae, pituitary gland and sellar dura, is typically used as the only repair material. For most small (Grade 1) CSF leaks, the repair includes intrasellar collagen sponge with a second outer layer of collagen sponge that extends out along the parasellar bone. In some cases, an intrasellar, extradural buttress of septal bone, titanium mesh or synthetic plate (Lactosorb, Biomet, Jacksonville, FL, or Medpor TSI Implant, Porex Corp., Fairburn, GA) is also used. The repair is typically held in position with a small amount of tissue glue. For medium (Grade 2) CSF leaks or Grade 1 leaks with a large intrasellar dead space, the repair includes an intrasellar abdominal fat graft and a layer of collagen sponge typically followed by a buttress as described above, placed in the intrasellar extradural space. Additional fat is typically placed over the sella followed by another layer of collagen; the construct is held in position with tissue glue. In some recent cases of Grade 1 and 2 leaks, no buttress has been used and instead the repair with collagen sponge with or without a fat graft has been reinforced only with tissue glue. Such patients are also placed on Diamox (acetazolamide) 250 mg, every 8 h for 48 h after surgery to diminish CSF production. Although this is anecdotal, to date, this simplified repair method without a rigid buttress appears to have a high success rate in select cases. To further assess the adequacy of the repair, prior to placing tissue glue, the anesthesiologist is asked to perform a Valsalva maneuver to raise the patient's intracranial pressure; should there be CSF streaming around the repair or movement of the buttress, the repair should be revised.

For the large (Grade 3) defects, typically seen with extended suprasellar or trans-clival approaches, the repair construct is similar to the Grade 2 repair, and a lumbar drain for CSF diversion is often also placed for 48 h. Grade 3 leaks, however, are uncommon after adenoma

Illustrative Cases

Case 1

A 51 year-old man presented with headaches, low energy and visual loss. Upon examination he was noted to have a mild bitemporal hemianopsia. Sellar MRI revealed a 3×4 cm invasive macroadenoma with extension into the sphenoid sinus and chiasmal compression (Fig. 18.1a, b, c). Hormonal testing revealed mild hyperprolactinemia (25.7 ng/mL, reference 3–19 ng/mL), hypothyroidism and low testosterone (30 ng/dL, reference 47–244 ng/dL). He underwent endonasal microscopic adenoma resection with endoscopic assistance (Fig. 18.2). After maximal tumor removal under microscopic visualization, the endonasal speculum was removed and using a 0° and then a 45° endoscope, additional small remnants of tumor along the undersurface of the compressed pituitary gland were removed. His post-operative MRI confirmed a gross total tumor resection. Post-operatively, his headaches resolved, vision normalized and his hypogonadism and hypothyroidism resolved (Fig. 18.1d, e, f).

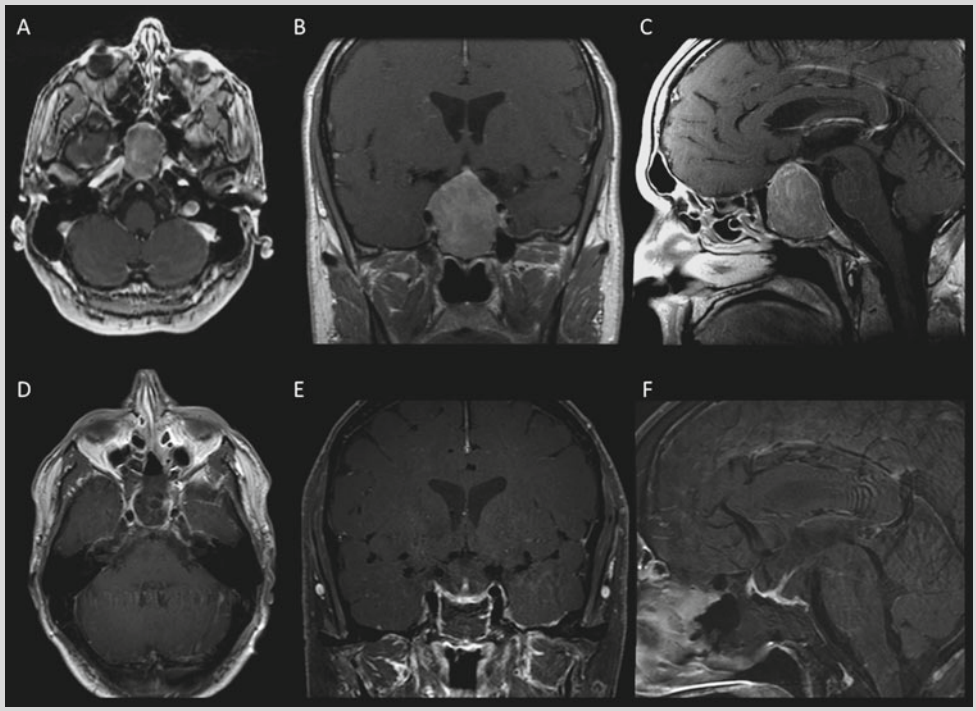

Fig. 18.1 Case 1 (**a**–**f**): Preoperative axial (**a**), coronal (**b**) and sagittal (**c**) T1 weighted contrast MRI showing a giant adenoma with moderate suprasellar extension and almost complete filling of the sphenoid sinus. Postoperative day #1 axial (**d**), coronal (**e**) and sagittal (**f**) T1 weighted post-contrast MRI shows gross total tumor removal and pituitary gland re-expansion

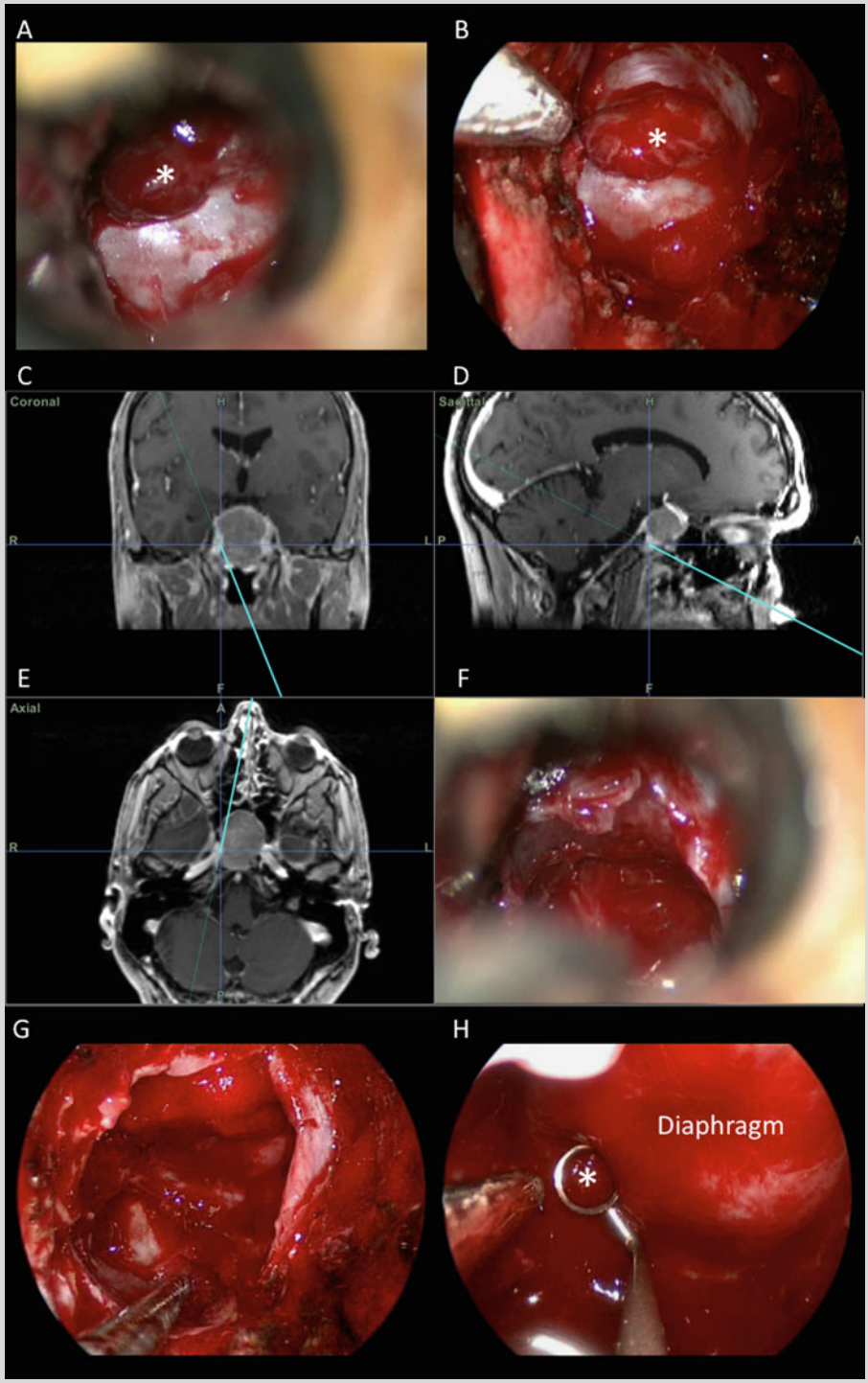

Fig. 18.2 (**a**–**h**): Intraoperative images of the endonasal tumor removal described in case 1. Microscopic (**a**) and endoscopic (**b**) views of the sellar dura, with superior tumor eroding through dura (*). Navigational images (**c**, **d** and **e**) with pointer along right cavernous sinus wall as seen with microscopic view (**f**). A 0° endoscopic view after further tumor removal (**g**) and a 45° endoscopic view of postero-superior sellar cavity (**h**), where tumor remnants were removed from below compressed gland (*)

Case 2

A 19 year-old woman with infrequent menses since adolescence was found to have an elevated prolactin of 171 ng/ml (normal range 5–23 ng/ml). Pituitary MRI revealed a 15 mm predominantly cystic sellar mass with severe gland compression and evidence of subacute and chronic hemorrhagic changes (Fig. 18.3a, b). Given the hemorrhagic nature of this presumed macroprolactinoma, she underwent endonasal tumor removal (Fig. 18.4). After maximal tumor removal with the microscope, the endoscope revealed no obvious residual adenoma. Her prolactin level decreased to 21 ng/ml on post-operative day #1 and no residual tumor was seen on postoperative MRI. At 13 months after surgery, her menstrual periods were normal, she had no galactorrhea and her MRI showed no obvious adenoma (Fig. 18.3c, d). However, her prolactin level had gradually increased to 43 ng/ml. She was consequently started on a low dose of cabergoline (0.25 mg twice weekly) and continues to do well.

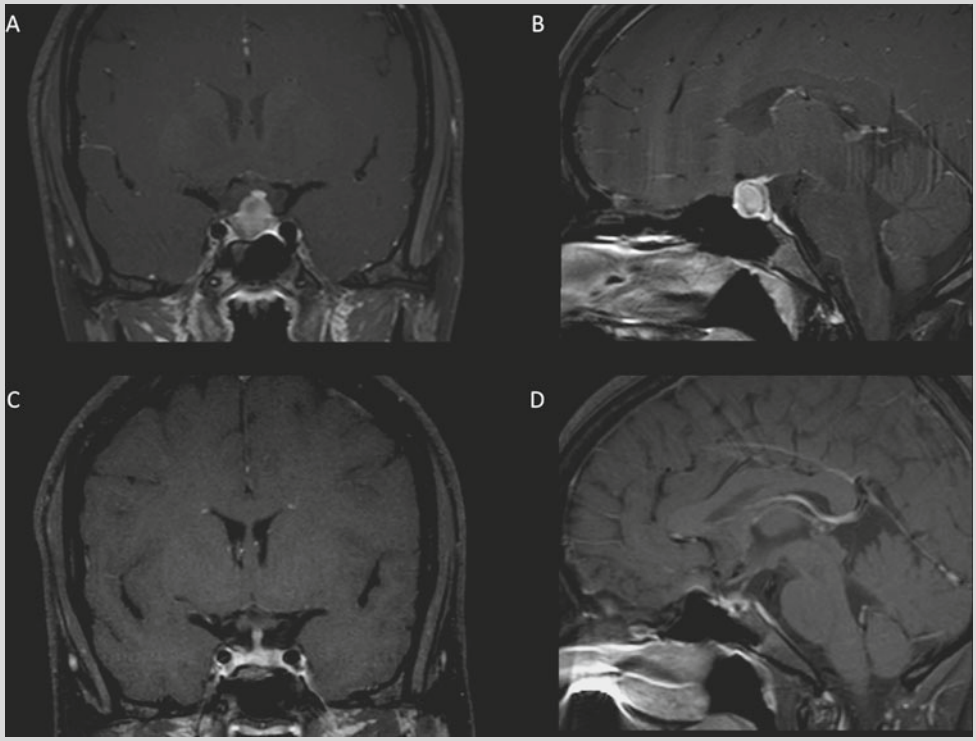

Fig. 18.3 Case 2 (**a**–**d**): Preoperative coronal (**a**) and sagittal (**b**) T1 weighted post-contrast MRI showing a hemorrhagic pituitary adenoma with leftward pituitary stalk deviation and the normal pituitary gland pushed superiorly and posteriorly. Postoperative coronal (**c**) and sagittal (**d**) T1 weighted contrast MRI showing gross total tumor removal with midline pituitary stalk

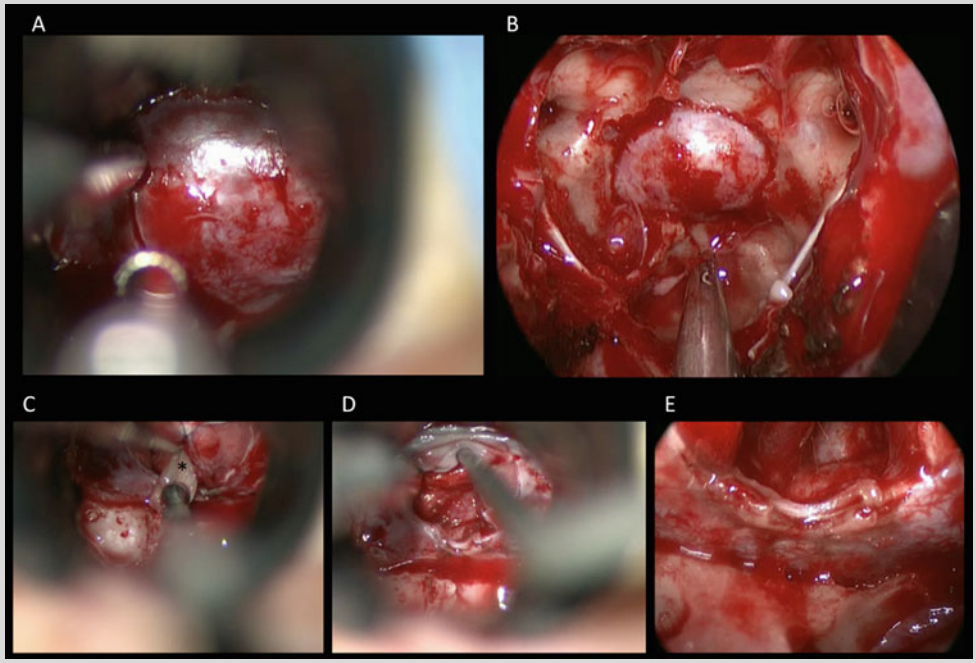

Fig. 18.4 (**a**–**e**): Intraoperative images of the endonasal removal or hemorrhagic prolactinoma described in case 2. Microscopic (**a**) and endoscopic (**b**) views of the bone window and sellar dura on the posterior surface of the sphenoid sinus. Observe the panoramic view afforded by the 0° endoscope (**b**). Once the dura is incised under microscopic visualization (**c**), tumor tissue (*) is removed. The dural opening is then widened to facilitate complete tumor removal (**d**). The 30° endoscope is brought in at the end of the procedure (**e**) to inspect the sellar cavity and the areas posterior to the ICAs and lateral sellar compartments, towards the cavernous sinuses. No residual tumor was seen with endoscopic inspection

removal unless they are extensively invasive above the diaphragma sellae. It is important to note that use of tissue glue in this repair paradigm is not for stopping egress of CSF per se but more to prevent migration of the construct materials (fat and collagen) away from the sella.

After skull base reconstruction, the self-retaining speculum is removed and the hand-held speculum is brought back into place. The middle turbinate is medialized and the septum is returned to the midline. Both nostrils are inspected for mucosal bleeding, which is easily cauterized. No nasal packing is used. Care is taking during extubation to prevent coughing and gagging, which can displace the sellar closure and cause mucosal bleeding.

References

Catapano D, Sloffer CA, Frank G, Pasquini E, D'Angelo VA, Lanzino G (2006) Comparison between the microscope and endoscope in the direct endonasal extended transsphenoidal approach: anatomical study. J Neurosurg 104(3):419–425

Cushing H (1912) The Pituitary body and its disorders: clinical states produced by disorders of the hypophysis cerebri. J.B. Lippincott, Philadelphia, pp 296–305

Dehdashti AR, Ganna A, Karabatsou K, Gentili F (2008) Pure endoscopic endonasal approach for pituitary adenomas: early surgical results in 200 patients and comparison with previous microsurgical series. Neurosurgery 62(5):1006–1015, discussion 1015–1007

Dusick JR, Esposito F, Malkasian D, Kelly DF (2007) Avoidance of carotid artery injuries in transsphenoidal surgery with the Doppler probe and micro-hook blades. Neurosurgery 60(4 Suppl 2):322–328, discussion 328–329

Esposito F, Dusick JR, Fatemi N, Kelly DF (2007) Graded repair of cranial base defects and cerebrospinal fluid leaks in transsphenoidal surgery. Neurosurgery 60(4 Suppl 2):295–303, discussion 303–294

Fatemi N, Dusick JR, de Paiva Neto MA, Kelly DF (2008a) The endonasal microscopic approach for pituitary adenomas and other parasellar tumors: a 10-year experience. Neurosurgery 63(4 Suppl 2):244–256, discussion 256

Fatemi N, Dusick JR, Malkasian D, McArthur DL, Emerson J, Schad W, Kelly DF (2008b) A short trapezoidal speculum for suprasellar and infrasellar exposure in endonasal transsphenoidal surgery. Neurosurgery 62(5 Suppl 2):ONS325–ONS329, discussion ONS329-330

Fatemi N, Dusick JR, Mattozo C, McArthur DL, Cohan P, Boscardin J, Wang C, Swerdloff RS, Kelly DF (2008c) Pituitary hormonal loss and recovery after transsphenoidal adenoma removal. Neurosurgery 63(4):709–718, discussion 718–709

Fernandez-Miranda JC, Prevedello DM, Madhok R, Morera V, Barges-Coll J, Reineman K, Snyderman CH, Gardner P, Carrau R, Kassam AB (2009) Sphenoid septations and their relationship with internal carotid arteries: anatomical and radiological study. Laryngoscope 119(10):1893–1896

Frank G, Pasquini E (2002) Endoscopic endonasal approaches to the cavernous sinus: surgical approaches. Neurosurgery 50(3):675

Frank G, Pasquini E (2006) Endoscopic endonasal cavernous sinus surgery, with special reference to pituitary adenomas. Front Horm Res 34:64–82

Frank G, Pasquini E, Farneti G, Mazzatenta D, Sciarretta V, Grasso V, Faustini Fustini M (2006) The endoscopic versus the traditional approach in pituitary surgery. Neuroendocrinology 83(3–4):240–248

Hardy J, Somma M (1979) Acromegaly. Surgical treatment by transsphenoidal microsurgical removal of the pituitary adenoma. In: Collins WF, Tindall GT (eds) Clinical management of pituitary disorders. Raven, New York, pp 209–217

Jagannathan J, Smith R, DeVroom HL, Vortmeyer AO, Stratakis CA, Nieman LK, Oldfield EH (2009) Outcome of using the histological pseudocapsule as a surgical capsule in cushing disease. J Neurosurg 111(3):531–539

Jane JA Jr, Thapar K, Laws ER Jr (2001) Acromegaly: historical perspectives and current therapy. J Neurooncol 54(2):129–137

Jane JA Jr, Thapar K, Kaptain GJ, Maartens N, Laws ER Jr (2002) Pituitary surgery: transsphenoidal approach. Neurosurgery 51(2):435–442, discussion 442–434

Jho HD, Carrau RL (1997) Endoscopic endonasal transsphenoidal surgery: experience with 50 patients. J Neurosurg 87(1):44–51

Kassam A, Snyderman C, Carrau R (2004) An evolving paradigm to the ventral skull base. Skull Base 14(suppl 1)

Kassam A, Snyderman CH, Carrau RL, Gardner P, Mintz A (2005a) Endoneurosurgical hemostasis techniques: lessons learned from 400 cases. Neurosurg Focus 19(1):E7

Kassam A, Snyderman CH, Mintz A, Gardner P, Carrau RL (2005b) Expanded endonasal approach: the rostrocaudal axis. Part I. Crista galli to the sella turcica. Neurosurg Focus 19(1):E3

Kawamata T, Iseki H, Ishizaki R, Hori T (2002a) Minimally invasive endoscope-assisted endonasal trans-sphenoidal microsurgery for pituitary tumors: experience with 215 cases comparing with sublabial trans-sphenoidal approach. Neurol Res 24(3):259–265

Kawamata T, Kamikawa S, Iseki H, Hori T (2002b) Flexible endoscope-assisted endonasal transsphenoidal surgery for pituitary tumors. Minim Invasive Neurosurg 45(4):208–210

Kelly DF (2007) Transsphenoidal surgery for cushing's disease: a review of success rates, remission predictors, management of failed surgery, and Nelson's syndrome. Neurosurg Focus 23(3):E5

Kelly DF, Oskouian RJ, Fineman I (2001) Collagen sponge repair of small cerebrospinal fluid leaks obviates tissue grafts and cerebrospinal fluid diversion after pituitary surgery. Neurosurgery 49(4):885–889, discussion 889–890

Kleinman HK, Klebe RJ, Martin GR (1981) Role of collagenous matrices in the adhesion and growth of cells. J Cell Biol 88(3):473–485

Lasio G, Ferroli P, Felisati G, Broggi G (2002) Image-guided endoscopic transnasal removal of recurrent pituitary adenomas. Neurosurgery 51(1):132–136, discussion 136–137

Laws ER, Reitmeyer M, Thapar K, Vance ML (2002) Cushing's disease resulting from pituitary corticotrophic microadenoma. Treatment results from transsphenoidal microsurgery and gamma knife radiosurgery. Neurochirurgie 48(2–3 Pt 2):294–299

Liu JK, Das K, Weiss MH, Laws ER Jr, Couldwell WT (2001) The history and evolution of transsphenoidal surgery. J Neurosurg 95(6):1083–1096

Mattozo CA, Dusick JR, Esposito F, Mora H, Cohan P, Malkasian D, Kelly DF (2006) Suboptimal sphenoid and sellar exposure: a consistent finding in patients treated with repeat transsphenoidal surgery for residual endocrine-inactive macroadenomas. Neurosurgery 58(5):857–865, discussion 857–865

McDonald TJ, Laws ER Jr (1982) Historical aspects of the management of pituitary disorders with emphasis on transsphenoidal surgery. In: Laws ER Jr, Randall RV, Kern EB, Abboud CF (eds) The management of pituitary adenomas and related lesions with emphasis on transsphenoidal microsurgery. Appleton, New York, pp 1–13

McLaughlin N, Eisenberg A, Cohan P, Chaloner C, Kelly DF (2012) The value of endoscopy for maximizing tumor removal in endonasal transsphenoidal pituitary adenoma surgery. J Neurosurg 118:613–620

Narotam PK, Van Dellen JR, Bhoola K, Raidoo D (1993) Experimental evaluation of collagen sponge as a dural graft. Br J Neurosurg 7(6):635–641

Narotam PK, van Dellen JR, Bhoola KD (1995) A clinicopathological study of collagen sponge as a dural graft in neurosurgery. J Neurosurg 82(3):406–412

Oldfield EH, Vortmeyer AO (2006) Development of a histological pseudocapsule and its use as a surgical cap-

sule in the excision of pituitary tumors. J Neurosurg 104(1):7–19

Powell M (2009) Microscope and endoscopic pituitary surgery. Acta Neurochir 151(7):723–728

Prevedello DM, Doglietto F, Jane JA Jr, Jagannathan J, Han J, Laws ER Jr (2007) History of endoscopic skull base surgery: its evolution and current reality. J Neurosurg 107(1):206–213

Prevedello DM, Kassam AB, Gardner P, Zanation A, Snyderman CH, Carrau RL (2010) "Q-tip" retractor in endoscopic cranial base surgery. Neurosurgery 66(2):363–366, discussion 366–367

Rotenberg B, Tam S, Ryu WH, Duggal N (2010) Microscopic versus endoscopic pituitary surgery: a systematic review. Laryngoscope 120(7): 1292–1297

Spencer WR, Das K, Nwagu C, Wenk E, Schaefer SD, Moscatello A, Couldwell WT (1999) Approaches to the sellar and parasellar region: anatomic comparison of the microscope versus endoscope. Laryngoscope 109(5):791–794

Wilson CB, Dempsey LC (1978) Transsphenoidal microsurgical removal of 250 pituitary adenomas. J Neurosurg 48(1):13–22

Intracranial Tumors: Treatment with Endoscopic Neurosurgery

19

Giuseppe Talamonti, Giuseppe D'Aliberti, and Alberto Debernardi

Contents

Abstract

Neuroendoscopy is presently a routine procedure in most neurosurgical services. It was originally developed to deal with obstructive hydrocephalus, but modern technical advancements have made possible to face also other neurological diseases including brain tumors. Presently, small endoscopes with exquisite detail visualization, high resolution screens, 3D cameras, dedicated ultrasonic aspirators and laser beams offer therapeutic options which could be just dreamed a few years ago. The friendly interface with image-guided systems further improves the technique. Nowadays, the golden standard treatment of ventricular tumors includes biopsy under endoscopic control and (if necessary) treatment of the associated hydrocephalus during the same procedure. Endoscopic biopsy may be followed (if indicated) by traditional microsurgery, but it may also remain the only surgical procedure needed since several midline tumors either do not require surgical excision or may be managed by radiosurgery, chemotherapy, and/or radiation-therapy. Another endoscopic option is the fenestration/aspiration of cystic space occupying lesions. This technique may result very useful in selected cases of craniopharyngioma, metastases, abscesses and cystic tumors in general. This treatment aims to the endoscopic cyst shrinkage followed by radiosurgery or other adjunctive therapies. Moreover, there are particular expansive lesions which may be even endoscopically excised.

G. Talamonti (✉) • G. D'Aliberti • A. Debernardi
Department of Neurosurgery, Niguarda Ca'Granda Hospital, Milan, Italy
e-mail: giuseppe.talamonti@ospedaleniguarda.it

M.A. Hayat (ed.), *Tumors of the Central Nervous System, Volume 12*,
DOI 10.1007/978-94-007-7217-5_19,

This is especially the case of 3rd ventricle colloid cysts, for which endoscopy has become the first choice treatment in a lot of neurosurgical units. Finally, most CSF-cysts (arachnoid, choroid, ependymal, post-surgical, post-hemorrhagic) may be endoscopically treated thus avoiding open surgery or cysto-peritoneal shunting.

Introduction

The modern armamentarium to manage cerebral tumors cannot prescind from Neuroendoscopy. Following the pioneer attempts of the first decades of the past century, neuroendoscopy received a new boost in 1978 thanks to the paper by Fukushima (1978) who first reported biopsy of intraventricular tumors under direct endoscopic visualization. In the meantime, the endoscopic third ventriculostomy (ETV) progressively became the method of choice to face with obstructive hydrocephalus. Precedent management of intraventricular tumors with hydrocephalus included CSF diversion, stereotactical biopsy and/or microsurgical excision often followed by ventriculoperitoneal shunting. However, this approach resulted often problematic because multiple procedures were needed, the risks of infection and shunt malfunction were not negligible, and there was the possibility of extracranial tumor dissemination through the shunt. Therefore, neuroendoscopy became very popular since it allows tumor biopsy and hydrocephalus management during the same procedure with virtually no risk of infection. The availability of frameless image-guided techniques to be interfaced with the neuroendoscope further refined the technique. The recent technological improvements are providing *via via* thinner endoscopes with better quality of visualization (the 3D endoscope is already reality); sophisticated endoscopic tools and instruments (such as dedicated laser beam and ultrasonic aspirators) are now available to handle any type of tumors; more precise, versatile and friendly neuronavigators permit multiple safe trajectories and easy instant-by-instant localization.

Accordingly, today indications to neuroendoscopy go beyond the simple biopsy of intraventricular tumors and ETV: small endoventricular tumors may be now even completely excised, colloid cysts may be emptied or even removed, intraventricular and paraventricular cysts (regardless they are tumor or not) may be fenestrated, emptied, stented, and so on; moreover, endoscope may be used also to manage space occupying lesions which are located or emerge into the subarachnoid spaces; finally, endoscopy may enhance the common microsurgical techniques by providing different angles of view (the socalled "endoscopic assisted microsurgery"), and, in a lot clinical contests, endoscopic surgery is going to completely replace microsurgery in the trans-nasal approach to sellar and parasellar tumors. Since the endoscopic assisted microsurgery and the trans-nasal endoscopy represent quite different items, they will be not discussed in this chapter.

Endoscopic Biopsy of Intraventricular Tumors

Intraventricular tumors represent about 2 % of cerebral tumors, and neuroendoscopy is now widely used to obtain biopsy material of tumors within the ventricular system. There is even a subset of tumors which either do not require aggressive surgical removal or this is contraindicated. In these cases, endoscopy may remain the only tumor surgery needed (Depreitere et al. 2007). Depending on tumor location and local anatomical situation, most endoscopic biopsies may be performed without any image guided system, basing just on anatomical landmarks. However, modern neuronavigators are easy to use and are not time consuming. Furthermore, in our experience, they increase the biopsy success rate. Accordingly, since the routine combination of neuronavigator/neuroendoscope, we usually prefer rigid lens-endoscopes rather than flexible or steerable fibroscopes.

The biopsy procedure is usually performed trough a single burr hole, preferentially on the

non-dominant side. The trajectory is chosen to enter the ventricular cavity in front of the tumor, so that the biopsy can be performed at the interface CSF-tumor under direct visual control. The modern operative neuroendoscopes, in spite of external diameters of 4–5 mm to minimize cerebral trauma, have large working channels to obtain adequate tissue sampling. In case of hydrocephalus, an attempt is made to obtain biopsy and to perform ETV or septostomy through the same burr hole just changing the endoscope angulations. Sometimes, particular tumor locations preclude the use of the same burr hole. For instance, in case of pineal tumors causing obstructive hydrocephalus, it is quite difficult to perform both biopsy and ETV using a rigid endoscope through a single access. In these cases, the ETV can be made through the classical precoronal burr hole and the biopsy through a second more anterior hole; otherwise, a flexible fibroscope may be used to perform the ETV through the classic approach, then the endoscope may be angled backward to obtain the biopsy. Each time a double procedure is needed, we prefer to perform first the procedure with minor bleeding risk. This means the ETV is usually performed before the biopsy so that, if the procedure has to be interrupted due to hemorrhage, at least the hydrocephalus has been already treated (Depreitere et al. 2007). The biopsy starts with the inspection of the tumor bulging looking for a relatively avascular zone. Then, the selected point for biopsy is usually coagulated using monopolar, bipolar, or laser beam. In our experience, this seems to decrease the hemorrhagic risk without interfering with sample adequacy. Subsequently, the biopsy is performed at different depths using apposite forceps. Each sampling is often followed by more or less bleeding. In the vast majority of cases, such hemorrhage results not conspicuous and self limited. Sometimes, more important bleeding may be arrested by delicate compression using a fogarty balloon into the biopsy groove. In these circumstances, we do not like blindly coagulation which probably would result not effective and even dangerous. Unfortunately, in neuroendoscopy, in general, when bleeding occurs, the surgeon cannot do a lot except remaining patient, keeping on washing and…hoping! Sometimes, in case of bleeding, an external ventricular drain may be useful (Oppido et al. 2011).

The main problems of endoscopic biopsy are the risk of bleeding and the sampling adequacy in comparison with traditional stereotactic biopsy. Stereotaxis offers 91 % of diagnostic accuracy which decreases in midline lesions that are also the more dangerous to biopsy with overall mortality and morbidity rates of 0.7 % and 3.5 % (Oppido et al. 2011). On the other hand, endoscopic biopsy has low or no mortality, in spite of 2–3 % of significant hemorrhage (Luther et al. 2005; Oppido et al. 2011; Macarthur et al. 2002). The rate of effective and reliable tissue diagnosis with endoscopic biopsy has been variously reported, but may arrive up to 100 % particularly using frameless guidance tools (Depreitere et al. 2007; Macarthur et al. 2002; Pople et al. 2001; Souweidane 2005; Yamini et al. 2004). Also the efficacy of endoscopy for the treatment of hydrocephalus when combined with endoscopic biopsy has been variously reported but it may arrive up to 96 % (Depreitere et al. 2007; Souweidane 2005; Yamini et al. 2004).

Our series is reported in Table 19.1. A total of 51 patients underwent endoscopic biopsy for newly diagnosed tumors. There was no mortality and 1 case of permanent morbidity (1.9 %). Complications with transitory morbidities were observed in 4 patients (7.8 %). Significant hemorrhages occurred in 6 patients (11.7 %): in 1 case (1.9 %) the procedure had to be abandoned and the diagnosis remained not conclusive; in the remaining 5 cases the hemorrhage was uneventful. In 1 case of pineal germinoma, the endoscopy was followed by dissemination into the lateral ventricles and along the endoscope passage. In 38 cases, obstructive hydrocephalus was managed during the same procedure. This resulted effective in 36 cases (94.7 %) while 2 patients required ventriculoperitoneal shunts. The series consists of 9 tumors of the lateral ventricles, 41 tumors of the 3rd ventricle and 1 of the 4th

Table 19.1 Biopsy of newly diagnosed intraventricular tumors (1997–2012)

		No	Significant hemorrhage	Other complications	Subsequent microsurgical excision	Subsequent adjunctive therapies
High grades gliomas	VL	1	1			1
	3rd V	4	1			3
Low grades gliomas	VL	2			2	
	3rd V	5		Diabetes insipidus[a]	1	3
	4th V	1				1
Germinomas	VL	–				
	3rd V	6		Dissemination		6
Pineocytoma	VL	–				
	3rd V	7	1	Parinaud	7	
Malignant pineal tumors	VL	–				
	3rd V	4		Parinaud	1	3
Metastases	VL	1			1	1
	3rd V	4				4
Lymphomas	VL	2				2
	3rd V	2	1			2
Craniopharyngiomas	VL	–				
	3rd V	6		3rd nerve palsy	5	3
PNETs	VL	2	1		2	2
	3rd V	–				
Meningiomas	VL	1			1	
	3rd V	1			1	
Sarcoidosis	VL	–				
	3rd V	1				1
Not conclusive	VL	–				
	3rd V	1	1			
Total		51	6 (11.7 %)	5 (9.8 %)	20 (39.2 %)	32 (62.7 %)

[a]Permanent complication

ventricle. Moreover, 6 of 9 patients with lateral ventricle tumors underwent subsequent microsurgical excision, while this occurred just in 14 of 41 (34.1 %) tumors of the 3rd ventricle (the vast majority of the operated tumors were pineocytomas and craniopharyngiomas). These figures undoubtedly reflect our policy which tendentially indicated direct surgical excision for lateral ventricle tumors and preliminary biopsy for 3rd ventricle lesions. It is our opinion that the endoscopic era provoked a few changes in the global management of lateral ventricle tumors, while it radically changed the strategies in 3rd ventricle tumors where endoscopic biopsy often remains the only surgical procedure.

Endoscopic Aspiration of Cystic Brain Tumors

Several brain tumors may present cystic aspect. Cystic components are relatively typical for craniopahryngiomas, hemangioblastomas, and pilocytic astrocytomas, but may be present also in malignant gliomas, metastases and so on. Attempts at cyst aspiration belong to the history of neurosurgery, but simple aspiration represented just palliation and remained not popular till recently when modern adjunctive therapies became available. In particular, the advent of frameless stereotaxis, endoscopy and radiosurgery offers new tools to face with selected cases of cystic brain tumor. In fact, now the cyst aspiration

has the purpose to decrease the cyst volume and improve the patient's suitability for radiosurgery, by transforming the remaining cystic mass is an adequately small solid mass (Park et al. 2011). The cyst aspiration with or without subsequent radiosurgical treatment have been reported for various types of cerebral tumors (Hadjipanayis et al. 2002; Miki et al. 2008; Pan et al. 1998; Reda et al. 2002) but this treatment seems more properly suitable for craniopharyngiomas (Barajas et al. 2002; Joki et al. 2002; Nicolato et al. 2004; Park et al. 2011). In these particular tumors, the cystic component often represents even 80–90 % of the total mass (Nicolato et al. 2004). It is well known that the best treatment option for craniopharyngioma is radical microsurgical removal. However, in many cases, radical excision may be problematic and dangerous owing to the very tight adhesions to the optic pathways, the hypothalamus and the pituitary stalk. In fact, visual deterioration, endocrine disturbance, and hypothalamic dysfunction are not unusual following radical surgery. Furthermore, the rate of 5-year recurrences following radical resection has been reported in the order of 50 % (Puget et al. 2007). An alternative treatment strategy may be the subtotal resection followed by radiation therapy or radiosurgery on the residual tumor, integrated in selected cases by endoscopic cyst aspiration, cyst marsupialisation. A permanent catheter with an Ommaya reservoir may be also placed to repeat cyst aspiration and/or to deliver intracystic chemotherapy or radioactive drugs. A further less invasive management may consist of direct neuroendoscopy combined with stereotactic radiosurgery used as primary treatment in a multimodal strategy (Barajas et al. 2002; Joki et al. 2002; Reda et al. 2002). Of course, less invasive is the management, lower is the rate of complications but higher is the rate of recurrences and shorter is the disease-free interval (Park et al. 2011). However, since their mini-invasivity, endoscopic procedures may be repeated without major problems (Fig. 19.1).

In our clinical practice, the first treatment option for craniopharyngioma usually consists of an attempt at gross total removal. In this regard, endoscopic assisted microsurgery may be very useful; sometimes a transventricular endoscopic approach may provide the view from above, while the tumor is resected through the pterional or the inter-emispheric/subfrontal approaches. Depending on tumor size and local anatomical conditions, the planned gross total removal often has to be converted in subtotal excision. The tumor parts which are more tightly joined to the hypothalamus or the cranial nerves are usually deliberately left in place. We think, the present availability of powerful alternative therapies should prevent the neurosurgeon from feeling forced to pursue radical solutions at any cost. Therefore, postsurgery, the solid tumor rests are treated by gamma-knife, while the cystic residual lesions are endoscopically managed. Endoscopic treatment usually consists of an image-guided procedure with trans-ventricular trajectories that are selected to approach the cysts from above. We think intracystic bleomicine has no role owing to the high risk of toxicity in case of intraventricular diffusion. Accordingly, we try to create the widest possible communications between the ventricles and the cysts and between the cysts and the subarachnoid spaces. Suprasellar cysts are fenestrated both on the superior and inferior walls so that the ventricles can communicate with the subarachnoid space through the cyst itself. Therefore, a sort 3rd ventriculostomy is created through the cyst (Fig. 19.1). This would maintain washed the cyst in the hope that the risk of cyst recurrence could be decreased or at least delayed. In our experience there was no case of chemical ventriculitis due to the diffusion of the cyst content. Theoretically, cyst aspiration and fenestration could be also obtained by stereotaxis (Park et al. 2011). However, the wall of these cysts is often calcified and thick, and the endoscope has the undoubted advantage that the wall may be handled under direct visual control and using the various endoscopic instruments. Usually, a ventricular catheter is placed through the fenestrations as a sort of stent, and anchored to a subcutaneous Ommaya reservoir. This may be useful for subsequent cyst aspiration.

At our Institution, during the last 15 years, a total of 11 patients with recurrent or residual craniopharyngioma underwent endoscopic cyst

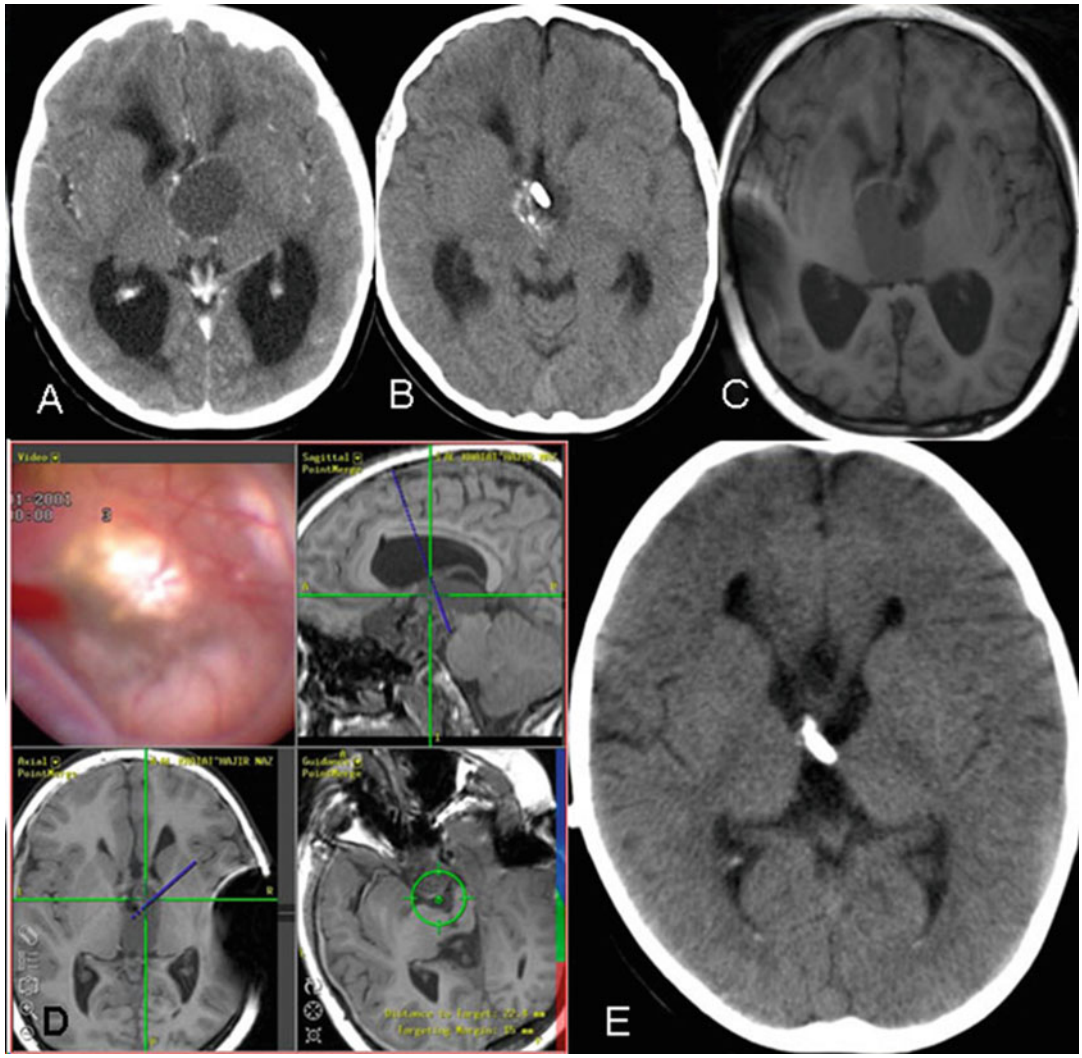

Fig. 19.1 Cystic craniopharyngioma recurring 2 years after subtotal microsurgical excision. (**a**) CT-scan showing a cystic mass inside the 3rd ventricle. (**b**) Postoperative CT-scan following transventricular endoscopic access with cyst aspiration and placement of an intracystic catheter with an Ommaya reservoir. Note the typical calcification inside the 3rd ventricle close to the catheter tip. (**c**) RMN obtained 1 year later showing a new cyst completely filling the 3rd ventricle. (**d**) Snapshot of the neuronavigator screen showing the endoscopic view of the cyst wall at level of the Monro Foramen; the planned trajectory is also shown: the tumor cyst is being to be fenestrated on the superior dome towards the lateral ventricles and on the inferior floor toward the brainstem cisterns. A sort of ETV is being created through the cyst in order to maintain it washed away. Three months after surgery, the patient will undergo gamma-knife. (**e**) Follow-up CT scan obtained 2 years later: no cyst is evident: note the new catheter coming from the Ommaya reservoir cruising through the right Monro Foramen towards the cisterns

fenestration and subsequent radiotherapy (6 patients before 2008) or radiosurgery (the last 5 patients). Multiple repeated endoscopic procedures were needed in 8 of 11 patients owing to cyst recurrence. Two patients required subsequent adjunctive microsurgical removal. Endoscopy associated with conventional radiotherapy represented just a palliation and had scarce efficacy on the global disease control. Conversely, the preliminary experience with endoscopy plus radiosurgery seems more satisfactory but the follow-up period is too short to draw any definitive conclusion.

Recently, a small number of large cystic metastatic lesions, which were initially deemed not amenable for radiosurgery, have been treated by endoscopic cyst aspiration and subsequent gamma-knife on the shrunk rest. These results seem encouraging.

Endoscopic Resection of Brain Tumors

Since the beginning of neuroendoscopy, endoscopic tumor resection was one of the main ambitions. Indeed, cases of endoscopically removed brain tumors remain sporadic (Sood et al. 2011; Souweidane et al. 2006). Bi-portal approaches, single large port using multiple instruments by two hands, dedicated ultrasonic aspirators, laser, and myriad tumor resection devices have been developed, but, to date, the only tumor which is currently endoscopically resected is the colloid cyst. This is a benign tumor, which accounts for less than 1 % of brain tumors and typically originates from the roof of the 3rd ventricle being closely associated with the velum interpositum and the choroid plexus near the foramen of Monro (Boogaarts et al. 2011; Levine et al. 2007). It may be occasionally found and may even remain asymptomatic, but obliteration of the Monro foramina and acute hydrocephalus are possible with severe clinical manifestations and even sudden death. While there are few doubts about the surgical treatment of symptomatic cases, indications of occasionally found cysts are sometimes debated (Boogaarts et al. 2011; Greenlee et al. 2008; Levine et al. 2007). Surgical treatment ranges from simple ventricular drainage to radical cyst resection. During the past decades, microsurgical excision through the transcortical/transventricular or the transcallosal approaches became the treatment of choice. However, despite morbidity and mortality progressively declined, their rates remained not negligible (Boogaarts et al. 2011; Mathiesen et al. 1997). Postoperative epilepsy, venous infarction, and damage to the fornices were not uncommon. Therefore, neuroendoscopy progressively gained wide acceptance for the treatment of colloid cysts (Boogaarts et al. 2011; Greenlee et al. 2008; Hellwig et al. 2003; Levine et al. 2007; Longatti et al. 2006a). The mini-invasivity of endoscopy would warrant lower complication rates above all for what concerns postoperative seizures and fornices damage (Boogaarts et al. 2011; Greenlee et al. 2008). Indeed, memory disturbances are not uncommon even following endoscopy, but they would be more often transitory than following microsurgery (Greenlee et al. 2008). The better neurological results would be counterbalanced by higher rates of cyst recurrence due to the endoscopic difficulty to achieve complete cyst wall removal (Levine et al. 2007). However, the question about the real importance of complete cyst removal still remains unsettled (Levine et al. 2007). Very long disease-free periods have been reported following partial excision while cyst recurrence is possible even following apparently total cyst removal (Boogaarts et al. 2011). Of course, in these cases, owing to the peculiar pathology of the colloid cysts, it is reasonable to think that the removal is just apparently total, and cyst recurs originating from small remnants which are seen neither during surgery nor on postoperative MRI. The MRI features have been analyzed to predict the cyst behaviour: hyperintensity on T2-weighted images would indicate higher probability of cyst growing, while hypointensity on the same images would predict difficulty in endoscopic cyst aspiration and proper removal (Boogaarts et al. 2011). Anyway, over the last few years, the rates of endoscopic total or nearly total removal improved from 65 % to 90 % (Boogaarts et al. 2011; Hellwig et al. 2003; Longatti et al. 2006a), but probably less radicality remains justified by lower complication rates. Moreover, in case of cyst recurrence, a new endoscopic treatment is not only possible but it may result even easier (Boogaarts et al. 2011).

In our experience, the endoscopic management of the colloid cysts may be performed without the neuronavigator owing to the constant cyst location and the local anatomy. The procedure starts with the placement of the endoscope into the lateral ventricle where the cyst almost always overlooks at the Monro Foramen (Fig. 19.2). The

Table 19.2 Endoscopic management of newly diagnosed colloid cysts (2001–2011)

Intraoperative surgeons' impression		Trans-choroidal approach	No visible remnants on postoperative MRI	Clinical complications	Recurrence/reoperation	Final outcome: neurologically intact
Total removal	9	4	7	2[a]	1/1	9
Cyst wall remnants	6	–	4	1[b]	1/–	6
Total	15	4	11	3	2/1	15

[a]Transitory memory impairment
[b]CSF leak

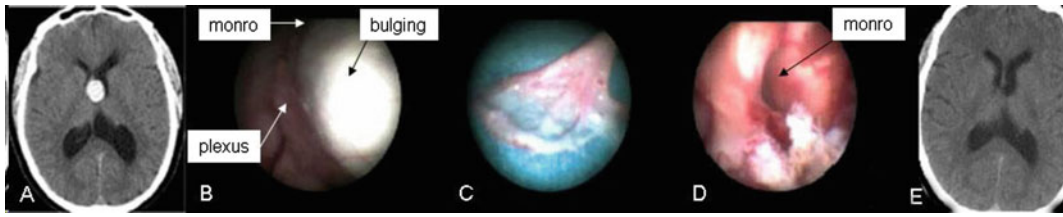

Fig. 19.2 Colloid cyst of the 3rd ventricle. (**a**) Preoperative CT-scan showing an hyperdense mass at the level of the Monro Foramina. (**b**) Initial endoscopic view from the right lateral ventricle: the tumoral bulging is occupying the whole right Monro Foramen and the choroid plexus is displaced backward. (**c**) The cyst wall has been completely excised. (**d**) Final endoscopic view from the right lateral ventricle: the patency of the Monro Foramina has been restored and pellucidostomy is evident. (**e**) Follow-up CT-scan obtained 3 years later: neither residual tumor nor hydrocephalus are evident.

access to the contralateral ventricle can be draped in all cases, but, we found out that the biportal access is rarely indispensable. Wide pellucidostomy is usually performed to gain the access to the contralateral foramen for simple inspection or adjunctive removal. Then, the cyst wall is taped and the cyst content aspirated. Sometimes, particularly dense and gelatinous contents prevent from complete aspiration. In these cases, the cyst wall is widely incised and the content is either piecemeal removed or washed away. In our experience, the CSF dissemination of this material never represented a problem as described by others (Levine et al. 2007). In most cases, the cyst may be completely emptied through the Monro Foramen without any adjunctive neural incision, but large cysts with posterior extension may also require more extended approaches. When this occurs, we prefer to enter the 3rd ventricle through the choroidal fissure by a small incision along the tenia fornicis, while we never used the transforniceal or the interforniceal approaches. Following the cyst emptying, the cyst attachment on the roof of 3rd ventricle is carefully inspected. Flexible or rigid endoscopes with angled views may result particular useful for bilateral Monro inspection. A gentle attempt at cyst wall dissection and total removal is usually attempted. Cases of thick adhesions or tight relationships with vascular structures may often advise against radical excision. In these cases, the cyst wall remnant is extensively coagulated and shrunk. Cases of endoscopic surgery which had to be converted into open surgery (Greenlee et al. 2008; Levine et al. 2007) were never encountered.

Our recent series is summarized in Table 19.2. It consists of 15 newly diagnosed colloid cysts which were endoscopically managed during the last 10 years. Monoportal access through the non-dominant site was adequate in 13 cases (Fig. 19.2), while 2 patients (early in the series) required a biportal approach. In 14 cases, the ventricles were more or less enlarged and the endoscope could be easily inserted and manoeuvred.

In one case, both lateral ventricles were small: therefore, a ventricular catheter was placed on the right site and the ventricles were gently, progressively and very slowly filled by lactated ringer's solution under continuous intracranial pressure monitoring. Eventually, adequate working room was gained in this case too. Eleven patients could be managed just through the Monro foramina, while 4 patients required a trans-choroidal approach too. Intraoperatively, the excision was considered radical in 9 of 15 cases (Fig. 19.2): postoperative MRI showed small remnants in 2 of these cases. It's interesting that no remnants were visible in the postoperative MRI of 4 out of 6 patients in whom the excision had been considered incomplete at surgery. Three patients with partial cyst removal also underwent ETV during the same procedure. There was neither mortality nor permanent morbidity. Complications consisted of 2 cases of transient memory disturbances with subsequent complete recovery, 1 case of CSF leak which could be conservatively managed, 2 cases of mild ventricular hemorrhages which remained completely uneventful. During a mean follow-up was 4.2 years, there were 2 cases of asymptomatic cyst re-growing: one patient was successfully managed by redo endoscopy, whereas the other patient refused the reoperation but remained asymptomatic with stable cyst during the following 2 years.

In conclusion, it's our opinion that neuroendoscopy now represents the treatment of choice for colloid cysts. It warrants good disease control with low invasivity, no mortality and minimal morbidity.

Endoscopic Management of Brain Abscesses

Brain abscesses usually behave like tumors and are often difficult to differentiate despite modern neuroimaging. The most common clinical presentation consists of neurological focality with or without intracranial hypertension, whereas local or general infective signs are often mild or even absent (Longatti et al. 2006b). Common treatment strategies contemplate surgery only in case of lesions with marked mass effect, great size, or antibiotic inefficacy. Surgical treatment ranges from simple cyst aspiration to radical abscess and capsule removal (Yadav et al. 2008). On the one hand, image guided aspiration is really mini-invasive and has proved effective and safe in a lot of cases; on the other hand, abscess excision is undoubtedly more invasive but provides higher and faster rates of cure (Yadav et al. 2008). In fact, following aspiration, the residual shrunk capsule needs to be followed for relatively long period. Conversely, following radical capsule excision, the healing times are usually those of a common craniotomy. However, these differences in healing times have been not confirmed by others (Longatti et al. 2006a).

In our clinical practice, patients whose abscesses are located in easily and safely accessible areas usually undergo open surgery. Patients with lesions in eloquent or deep areas and those with multiple lesions are endoscopically managed. In ours and others' opinion (Longatti et al. 2006a), endoscope provides some advantages in comparison with stereotactic aspiration: the manoeuvre is not blind; sometimes the capsule is hard and thick and may be perforate only using the endoscopic instruments; following aspiration the capsule may collapse and a stereotactically placed catheter may slip out of the abscess cavity; the abscess can be septated and residual purulent cavities may be avoided only using an endoscope. Moreover, the endoscope can manage also intraventricular and subdural collections. Finally, postoperative bleeding is quite more frequent in blind aspiration (Yadav et al. 2008).

Our recent series consists of 7 patients during the last 10 years: in 2 cases, the abscesses were multiple, and in other 2 cases the lesions were intraventricular; multiloculated abscesses were seen in 2 cases. In all cases, the procedure was image guided, the capsule was perforated, the purulent collection was aspirated, the residual cavity abundantly irrigated. Real time CT or ultrasound-guided operative procedures may be sometimes useful, but in our experience the direct endoscopic visualization of the abscessual cavity makes these techniques of limited utility. Of course, multiple lesions required multiple accesses

while multiloculated lesions could be handled through a single access by selecting the proper trajectory on the neuronavigator. Pyogenic infection was documented in all cases. We never encountered parasitic or yeast abscesses. A catheter was always left in place and local antibiotic therapy was administered for about 1 week. All patients eventually healed despite times for complete cure were longer than 4 weeks in 4 cases.

Endoscopic Management of Cerebrospinal Fluid-Cysts

Intracranial cysts containing CSF-like fluid may be acquired or developmental. The former may originate when CSF compartments remain isolated owing to adhesions and scar following hemorrhage, injury, or surgery; the latter evolve from developmental aberrations such as splitting of the arachnoid membrane, sequestration of primitive ependymal layer, aberrant growing of the choroid plexus (Talamonti et al. 2011). Both acquired and developmental CSF-cysts represent sequestration of CSF lakes, both have the potential for mass effect, and both may be treated by cyst drainage or cyst fenestration thus normalizing the CSF dynamics between cyst and ventricle/cisterns (Talamonti et al. 2011). Above all, both cysts have the tendency to remain benign and asymptomatic throughout the life, thus usually requiring no treatment. Nevertheless, some cysts may behave aggressively: CSF may accumulate inside the cyst because of active secretion or valve mechanism; the intracystic pressure may increase and the cyst may enlarge and/or compress the surrounding brain; otherwise, the cyst may rupture or bleed either spontaneously or following even trivial head injuries. The inability to predict the natural history of a given CSF-cyst accounts for the constellation of different indications and different treatment modalities which have been proposed (Talamonti et al. 2011). There is vast consensus that symptomatic cysts deserve some type of treatment, but some debate exists about the definition of symptomatic cysts: for instance, simple headache is not a good indicator for treatment. The doubts markedly increase in asymptomatic cysts: while adults are generally non-operatively treated, some Authors think that infants with progressively enlarging cysts or babies with huge cysts (>50 cm^3) can have chances of cyst reduction following surgical treatment (Talamonti et al. 2011).

The modality of surgical treatment is another discussed item (Gangemi et al. 2011; Oertel et al. 2010; Talamonti et al. 2011): surgery ranges from cysto-peritoneal shunting to cyst fenestration which aims to create wide communications towards the ventricles and/or the cisterns. Such fenestration may be performed either by open microsurgery or by endoscopic techniques (Gangemi et al. 2011; Oertel et al. 2010; Talamonti et al. 2011). The cyst location may influence the choice of the surgical modality: while endoscopy now warrants highest success rates in ventricular and paraventricular cysts, indeed the results in temporal cysts are a little bit less satisfactory (Gangemi et al. 2011; Oertel et al. 2010). Nothwithstanding that, papers with endoscopy as the first treatment option for any type of CSF-cysts are progressively increasing (Oertel et al. 2010; Talamonti et al. 2011).

The endoscopic fenestration is usually conducted under the neuronavigator control by selecting trajectories which trespass the lees possible brain and allow multiple and wide fenestrations towards the CSF pathways. The use of the neuronavigator is sometimes questioned since, during the procedure, CSF leakage may lead to cyst collapse with alteration of the spatial parameters (the socalled shift effect). Indeed, this problem should not be overemphasized: first, the neuronavigator is used to drive close to the target but undoubtedly the final step is not to be travelled with "instrumental navigation" but rather with "sailing by sight"; second, the shift effect can be obviated by selecting deep landmarks with fixed position such as the main arterial trunks or bone structures so that the space anatomical orientation may be maintained; third, the shift effect can be limited by entering the cyst through a very small access, just the diameter of the endoscope, that prevents from excessive CSF leakage and by maintaining adequate perfusion throughout the procedure thus preventing cyst collapse. Indeed,

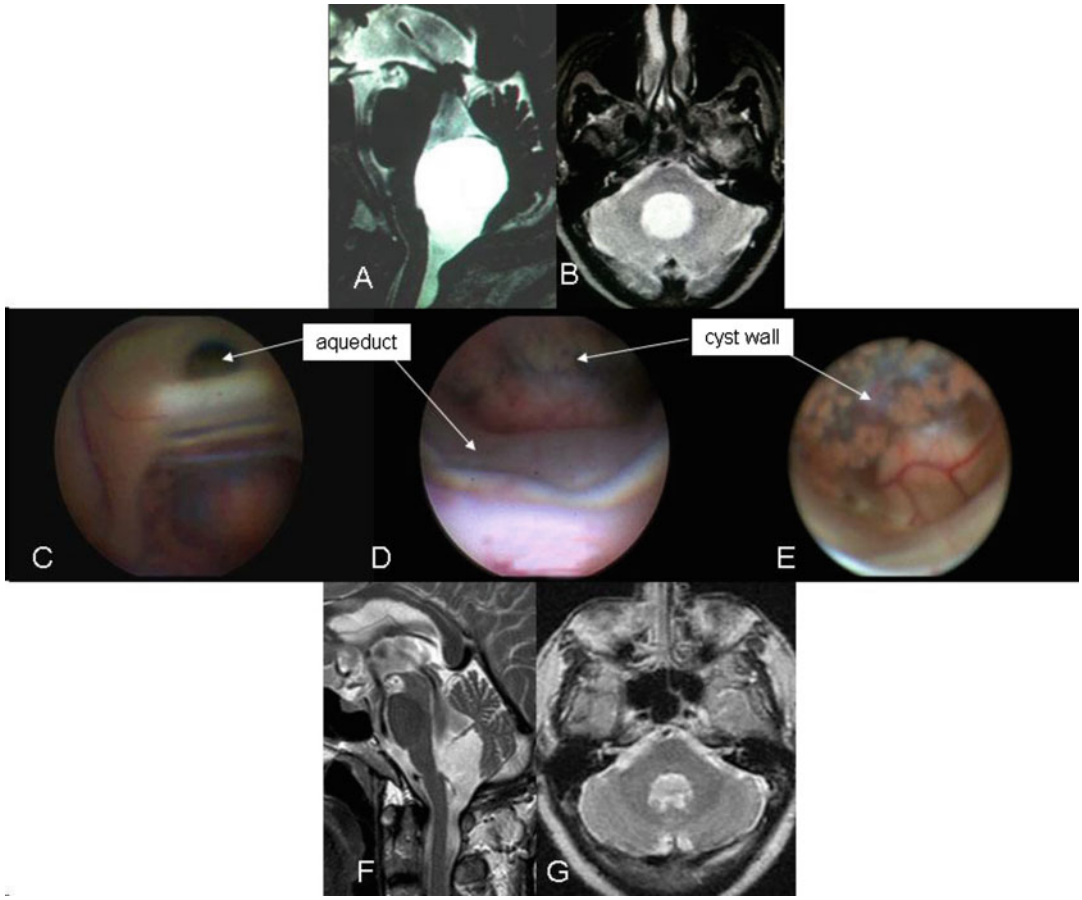

Fig. 19.3 CSF cyst of the 4th ventricle. (**a-b**) Preoperative MRI (sagittal and axial views) showing a CSF cyst inside the 4th ventricle with obstructive hydrocephalus. (**c**) Endoscopic view of the posterior part of the 3rd ventricle. (**d**) Close-up view of the aqueduct access with the cyst wall becoming visible. (**e**) Endoscopic view of the 4th ventricle following aqueduct cannulation. The cyst wall is going to be fenestrated. (**f-g**) Follow-up MRI (sagittal and axial views), obtained 1 year later, showing the CSF cyst collapsed. Note the flow artifacts inside the aqueduct

in our experience, most cyst walls were transparent so the neuronavigator resulted useful but not indispensable.

The cyst wall fenestration is fashioned using the common endoscopic instruments: fogarty balloons, coagulators, forceps, scissors and so on. Recently, there are laser beams which can be used in immersion, such as the thulium-laser. Anyway, the widest possible fenestration should be created. The ideal fenestration should be at least 8–15 mm of diameter and should allow free and abundant CSF flow through the cyst: for instance, in a suprasellar cyst which is fenestrated towards both the 3rd ventricle (ventriculo-cystostomy) and the basal cisterns (cysto-cisternostomy). However, cases may exist in which the wall is very thick and hard; otherwise, the ideal area to perform the fenestration (that is where the cyst wall faces the CSF pathways) is narrow or crowded by delicate neuro-vascular structures. In these cases, the fenestration diameter may be less than desired and a stent cruising through the cyst wall may be left in place to maintain the communication.

Our series of CSF-cysts consists of 16 patients with acquired cysts and 55 with developmental cysts. There were patients of any age and cysts of any locations (Fig. 19.3). Treatment consisted of endoscopic cyst-wall fenestration in all cases.

Significant intraoperative bleeding was reported in one case but it was uneventful. In 2 patients, a very thick and hard cyst wall prevented from the planned endoscopic cyst fenestration. In both these cases, the burr hole of the endoscope was converted in a key-hole craniotomy and the patients underwent traditional microsurgery. A total of 11 patients required a ventriculoperitoneal shunt to manage not the cyst but the associated hydrocephalus, while 5 cases of hydrocephalus could be resolved during the same endoscopic procedure for the cyst. Six patients experienced transitory morbidity which always completely resolved in a few months. Clinical improvement and cyst reduction were achieved in all cases of acquired cysts. As to the developmental cysts, there was no case of postoperative clinical worsening or cyst increase, 90 % of patients clinically improved, and 75 % obtained cyst reduction on follow-up neuroimaging (Fig. 19.3). Accordingly, about 15 % of patients clinically improved but their cysts remained unchanged. This is a well known phenomenon: it is possible that cyst fenestration was able to remove the tension on the cyst wall, but the surrounding brain was unable to re-expand because of structural transformation from elasticity to plasticity (Talamonti et al. 2011). Three patients experienced cyst recurrence during the follow-up: two were successfully treated by redo endoscopy, one underwent microsurgery.

Although the results were undoubtedly better in very young patients and in paraventricular cysts, our series demonstrates that endoscopic treatment may be a valid option in all cases of cysts regardless age and location.

Conclusion

In conclusion, presently, Neuroendoscopy represents a powerful tool which cannot lack in the neurosurgical armamentarium. The vast majority of recent papers report no mortality and very low morbidity. The possibility to manage associated hydrocephalus and intracranial mass during the same procedure cannot be overemphasized.

To date, Neuroendoscopy represents the first line of treatment for endoventricular tumors, colloid cysts, and intra- and paraventricular CSF cysts, and the second line of treatment for cystic craniopharyngiomas. This treatment may be particularly suitable for cystic tumors in general, for abscesses and for most CSF cysts.

The continuous technical improvement of the present days will probably enlarge the future endoscopic indications also to lesions which are now classically managed.

References

Barajas MA, Ramírez Guzmán G, Rodríguez Vázquez C, Toledo Buenrostro V, Velásquez Santana H, del Robles RV, Cuevas Solórzano A, Rodríguez Hernández G (2002) Multimodal management of craniopharyngiomas: neuroendoscopy, microsurgery, and radiosurgery. J Neurosurg 97(5 Suppl):607–609

Boogaarts HD, Decq P, Grotenhuis JA, Le Guerinel C, Nseir R, Jarraya B, Djindjian M, Beems T (2011) Long-term results of the neuroendoscopic management of colloid cysts of the third ventricle: a series of 90 cases. Neurosurgery 68:179–187

Depreitere B, Dasi N, Rutka J, Dirks P, Drake J (2007) Endoscopic biopsy for intraventricular tumors in children. J Neurosurg 106(5 Suppl Pediatrics):340–346

Fukushima T (1978) Endoscopic biopsy of intraventricular tumors with the use of a ventriculofiberscope. Neurosurgery 2:110–113

Gangemi M, Seneca V, Colella G, Cioffi V, Imperato A, Maiuri F (2011) Endoscopy versus microsurgical cyst excision and shunting for treating intracranial arachnoid cysts. J Neurosurg Pediatr 8:158–164

Greenlee JDW, Teo C, Ghahreman A, Kwok B (2008) Purely endoscopic resection of colloid cysts. Neurosurgery 62(ONS Suppl 1):ONS51–ONS56

Hadjipanayis CG, Kondziolka D, Gardner P, Niranjan A, Dagam S, Flickinger JC, Lunsford LD (2002) Stereotactic radiosurgery for pilocytic astrocytomas when multimodal therapy is necessary. J Neurosurg 97:56–64

Hellwig D, Bauer BL, Schulte M, Gatscher S, Riegel T, Bertalanffy H (2003) Neuroendoscopic treatment for colloid cysts of the third ventricle: the experience of a decade. Neurosurgery 52:525–533

Joki T, Oi S, Babapour B, Kaito N, Ohashi K, Ebara M, Kato M, Abe T (2002) Neuroendoscopic placement of Ommaya reservoir into a cystic craniopharyngioma. Childs Nerv Syst 18:629–633

Levine NB, Miller MN, Crone KR (2007) Endoscopic resection of colloid cysts: indications, technique, and results during a 13-year period. Minim Invasive Neurosurg 50:313–317

Longatti P, Godano U, Gangemi M, Delitala A, Morace E, Genitori L, Alafaci C, Benvenuti L, Brunori A, Cereda C, Cipri S, Fiorindi A, Giordano F, Mascari C, Oppido PA,

Perin A, Tripodi M (2006a) Cooperative study by the Italian neuroendoscopy group on the treatment of 61 colloid cysts. Childs Nerv Syst 22:1263–1267

Longatti P, Perin A, Ettorre F, Fiorindi A, Baratto V (2006b) Endoscopic treatment of brain abscesses. Childs Nerv Syst 22:1447–1450

Luther N, Cohen A, Souweidane MM (2005) Hemorrhagic sequelae from intracranial neuroendoscopic procedures for intraventricular tumors. Neurosurg Focus 19:E9

Macarthur DC, Buxton N, Punt J, Vloeberghs M, Robertson IJ (2002) The role of neuroendoscopy in the management of brain tumors. Br J Neurosurg 16:465–470

Mathiesen T, Grane P, Lindgren L, Lindquist C (1997) Third ventricle colloid cysts: a consecutive 12-year series. J Neurosurg 86:5–12

Miki T, Nakajima N, Akimoto J, Wada J, Haraoka J (2008) Neuroendoscopic trans-third ventricle approach for lesions of the ventral brainstem surface. Minim Invasive Neurosurg 51:313–318

Nicolato A, Foroni R, Rosta L, Gerosa M, Bricolo A (2004) Multimodality stereotactic approach to the treatment of cystic craniopharyngiomas. Minim Invasive Neurosurg 47:32–40

Oertel JMK, Wagner W, Mondorf Y, Baldauf J, Schroeder HDS, Gaab MR (2010) Endoscopic treatment of arachnoid cysts: a detailed account of surgical techniques and results. Neurosurgery 67:824–836

Oppido PA, Fiorindi A, Benvenuti L, Cattani F, Cipri S, Gangemi M, Godano U, Longatti P, Mascari C, Morace E, Tosatto L (2011) Neuroendoscopic biopsy of ventricular tumors: a multicentric experience. Neurosurg Focus 30:E2

Pan L, Wang EM, Wang BJ, Zhou LF, Zhang N, Cai PW, Da JZ (1998) Gamma knife radiosurgery for hemangioblastomas. Stereotact Funct Neurosurg 70(Suppl 1): 179–186

Park YS, Chang JH, Park YG, Kim DS (2011) Recurrence rates after neuroendoscopic fenestration and gamma knife surgery in comparison with subtotal resection and gamma knife surgery for the treatment of cystic craniopharyngiomas. J Neurosurg 114:1360–1368

Pople IK, Athanasiou TC, Sandeman DR, Coakham HB (2001) The role of endoscopic biopsy and third ventriculostomy in the management of pineal region tumors. Br J Neurosurg 15:305–311

Puget S, Garnett M, Wray A, Grill J, Habrand JL, Bodaert N, Zerah M, Bezerra M, Renier D, Pierre-Kahn A, Sainte-Rose C (2007) Pediatric craniopharyngiomas: classification and treatment according to the degree of hypothalamic involvement. J Neurosurg 106(1 Suppl):3–12

Reda WA, Hay AA, Ganz JC (2002) A planned combined stereotactic approach for cystic intracranial tumors. Report of two cases. J Neurosurg 97(5 Suppl):610–612

Sood S, Nundkumar N, Ham SD (2011) Interhemispheric endoscopic resection of large intraventricular and thalamic tumors. Technical note. J Neurosurg Pediatr 7:596–599

Souweidane MM (2005) Endoscopic management of pediatric brain tumors. Neurosurg Focus 18(6A):E1

Souweidane MM, Luther N (2006) Endoscopic resection of solid intraventricular brain tumors. J Neurosurg 105:271–278

Talamonti G, D'Aliberti G, Picano M, Debernardi A, Collice M (2011) Intracranial cysts containing cerebrospinal fluid-like fluid: results of endoscopic neurosurgery in a series of 64 consecutive cases. Neurosurgery 68:788–803

Yadav YR, Sinha M, Neha, Parihar V (2008) Endoscopic management of brain abscesses. Neurol India 56:13–16

Yamini B, Refai D, Rubin CM, Frim DM (2004) Initial endoscopic management of pineal region tumors and associated hydrocephalus: clinical series and literature review. J Neurosurg 100(5 Suppl Pediatrics): 437–441

Incidence of Recraniotomy for Postoperative Infections After Surgery for Intracranial Tumors

20

Torstein R. Meling, Benjamin Lassen, and Eirik Helseth

Contents

Abstract

The prevalence rate for all primary brain and central nervous system tumors is estimated to be 130.8 per 100,000 inhabitants (CTBRUS (2008) Statistical report: primary brain tumors in the United States, 2000–2004. http://www.cbtrus.org/reports//2007-2008/2007report.pdf). The cornerstone of brain tumor treatment is surgery, where the objective is radical surgery within safe limits and to establish an exact tissue diagnosis. However, craniotomies are not without inherent risks, be it surgical mortality, postoperative hematomas or infections. Infections after neurosurgical procedures often present as meningitis, subdural empyema, or cerebral abscess. Although meningitis can often be treated with intravenous antibiotics, cases that involve a bone flap infection, subdural empyema, or cerebral abscess usually require a repeated operation. In a recent large series, 1.5 % of the patients were reoperated for postoperative infection. Of these infections, 59.0 % were extradural. Independent risk factors were male sex and meningioma histopathology. The vast majority of reoperations occurred within 3 months of tumor surgery. The consequences of postoperative infections were generally minor, as 85 % had a good outcome with no or only a mild disability, but within the group of patients reoperated for infection, the mortality rate was 5 %.

T.R. Meling (✉) • B. Lassen • E. Helseth
Department of Neurosuregry, Oslo University Hospital, 0027 Oslo, Norway
e-mail: torevmel@online.no

M.A. Hayat (ed.), *Tumors of the Central Nervous System, Volume 12*,
DOI 10.1007/978-94-007-7217-5_20, © Springer Science+Business Media Dordrecht 2014

Introduction

Primary brain and central nervous system (CNS) tumors occur with an incidence of about 16.5 cases per 100,000 person–years (9.2 per 100,000 person–years for non–malignant tumors and 7.3 per 100,000 person–years for malignant tumors), whereas the prevalence rate for all primary brain and central nervous system tumors is estimated to be 130.8 per 100,000 inhabitants (CTBRUS 2008). Metastatic brain tumors are thought to have a higher incidence than primary brain tumors (Percy et al. 1972).

The cornerstone of brain tumor treatment is surgery. The objective of surgery is to remove as much tumor as possible, as well as to establish an exact tissue diagnosis. The possible benefits of tumor removal include symptom relief, improved quality of life, smaller tumor burden for other treatment modalities and improved survival (Claus et al. 2005; Hart et al. 2005; Keles et al. 2006; McGirt et al. 2009; Mirimanoff et al. 1985; Nitta and Sato 1995; Vecht et al. 1990). However, craniotomies are not without inherent risks, be it surgical mortality (Barker 2004; Fadul et al. 1988), postoperative hematomas (Gerlach et al. 2004; Kalfas and Little 1988) or infection (Mahaley et al. 1989). Infections after neurosurgical procedures often present as meningitis, subdural empyema, or cerebral abscess. Although meningitis can often be treated with intravenous antibiotics, cases that involve a bone flap infection, subdural empyema, or cerebral abscess usually require a repeated operation.

The Oslo University Hospital Experience

A recent prospective study by Lassen et al. (2011), is the largest published series with regard to postoperative infections within 30 days of craniotomy for brain tumors. All patients >18 years who underwent craniotomy for an intracranial tumor at Oslo University Hospital in the time period 2003–2008 were reported and the strengths of this study lie in the setting, design and follow-up. The data were restricted to one health centre, thereby reducing the possible confounding effect of differences in the access to health care services between health centers and avoiding the selection bias inherently present in large multi-center studies. Furthermore, the data were prospectively registered and included all craniotomies performed for a histologically verifiable brain tumor, leaving no selection bias. The study is contemporary, thereby reflecting current neurosurgical practice and was performed within a relatively short time span, thereby reducing confounding factors as changes in antibiotic prophylaxis regimen or operating theatres. With respect to data, only easily verifiable end points (i.e. reoperations for infections) were used. Lastly, follow-up was 100 %.

Clinical Setting

The defined neurosurgical catchment area for Oslo University Hospital (OUH) is the south and eastern health region of Norway. It has 2.7 million inhabitants (56 % of the Norwegian population) and OUH treat approximately 99 % of the neurosurgical tumor patients within this region (The Norwegian Cancer Registry, unpublished data). A total of 2,630 consecutive craniotomies at the Oslo University Hospital in the time period 2003–2008 were included in this study (Table 20.1). The mean age at surgery was 56 years (range 18–89 years), with a male-to-female ratio of 1:1.06. Follow-up was 100 %.

Perioperative Craniotomy Routines

A consultant anesthetist should see all craniotomy patients preoperatively. Elderly patients (>70 years) and patients on multiple medications should routinely also seen by consultant internist, to optimize the general medical condition and medications. At our institution, a second-generation cephalosporin is administered intravenously at initiation of surgery and continued every 90 min until the case is completed or the maximum daily dose of 8 g is reached. For long

Table 20.1 Patients' characteristics (n = 2,630)

	N	%
Patients	2,630	100
Sex		
Male	1,275	48.5
Female	1,355	51.5
Age (years)		
18–29.9	141	5.4
30–39.9	300	11.4
40–49.9	437	16.6
50–59.9	604	23.0
60–69.9	649	24.7
70–79.9	411	15.6
>80	88	3.3
Type of surgery		
Primary	2,141	81.4
Second	489	18.6
Craniotomy		
Resection	2,556	97.2
Open biopsy	74	2.8
Main histology		
High-grade glioma (HGG)	830	31.6
Meningioma	693	26.3
Metastases	449	17.1
Low-grade glioma (LGG)	289	11.0
Schwannoma	73	2.8
Primary CNS-lymphoma	51	1.9
CNS hemangioblastoma	39	1.5
Cavernous hemangioma	38	1.4
Pituitary adenoma	8	0.3
Others	160	6.1

cases, erythromycin or a third-generation cephalosporin is started after the maximum daily dose of a second-generation cephalosporin is reached and continued until completion of the case. Antibiotics are not routinely used in the postoperative phase.

Incidence of Craniotomies

First-time craniotomies with primary resection were performed in 2,073 cases, 483 cases were reoperations with repeated resection, and 74 cases were open biopsies. Thus, the incidence of first-time craniotomy for a brain tumor was 12.8/100,000 inhabitants per year and for a repeat resection 3.0/100,000 inhabitants per year.

Postoperative Infection Requiring Recraniotomy

A total of 39 patients (1.5 %) were reoperated for deep postoperative infection (Table 20.2). Of these infections, 23 (59.0 %) were extradural (ED), 6 (15.4 %) intradural (ID), and 10 (25.6 %) were both intra- and extradural.

Risk Factors of Reoperation for Postoperative Infection

Multivariate Cox regression analysis demonstrated that meningiomas had an increased risk of infection compared to gliomas (odds ratio 5.88, 95 % CI (2.47, 13.87), $p < 0.001$) (Table 20.3). Men also had an increased risk of infections ($p < 0.01$). Neither resection vs. biopsy, nor primary vs. secondary craniotomy were significantly associated with risk of developing postoperative deep infection. The postoperative infection rate was 1.0 % (n = 8) for HGG, 0.0 % (n = 0) for LGG, 3.2 % (n = 22) for meningiomas, and 1.1 % (n = 5) for metastases.

Time to Reoperation for Postoperative Infection

The median time from tumor surgery to reoperation for infection was 42 days (mean 95.7 days, range 16–667 days). The number of patients who were reoperated within 1, 2, 3, 6 and 12 months, were 11 (28.2 %), 27 (69.2 %), 29 (74.4 %), 32 (82.1 %) and 37 (94.9 %), respectively.

Consequences of Postoperative Infection

Of the 39 patients with deep infection, 29 (74.4 %) had no additional disability, 5 (12.8 %) had minor additional disability, 3 (7.7 %) had major additional disability, 2 (5.1 %) died due to the infection.

Discussion

The rate of postoperative infections after a craniotomy for an intracranial tumor requiring surgical treatment was 1.5 % in our series, thus

Table 20.2 Patients reoperated for postoperative infection (n = 39)

Age	Sex	ASA	ECOG	Immune compromise	Histology[a]	Location[b]	Time to reop. (days)[c]	Outcome[d]
18	M	2	2	–	HGG	ED	16	NAD
40	M	2	3	–	HGG	ED	46	NAD
57	M	NA	1	–	HGG	ED	20	NAD
59	M	3	3	–	HGG	ED	307	NAD
64	M	3	3	–	HGG	ED	49	Death
69	M	3	3	Diabetes	HGG	ED	80	Major
70	M	2	1	–	HGG	ED	20	NAD
70	F	2	1	–	HGG	ID	25	NAD
34	M	2	2	HIV	Lymfoma	ED	667	NAD
26	F	1	1	–	Meningioma	ED	71	NAD
33	F	2	1	–	Meningioma	ED	119	NAD
38	M	2	1	–	Meningioma	ED	248	NAD
40	F	1	1	–	Meningioma	ED	270	NAD
42	F	1	1	–	Meningioma	ED/ID	25	Minor
49	M	2	1	–	Meningioma	ED/ID	29	NAD
51	M	3	1	–	Meningioma	ID	31	NAD
53	F	2	1	–	Meningioma	ED	42	NAD
55	M	2	1	–	Meningioma	ED	18	NAD
56	M	3	1	Diabetes	Meningioma	ID	45	NAD
56	F	NA	1	–	Meningioma	ED/ID	38	Minor
56	M	2	1	–	Meningioma	ED	35	NAD
58	M	3	1	–	Meningioma	ED	59	NAD
64	M	2	1	–	Meningioma	ID	59	NAD
66	M	2	1	Diabetes	Meningioma	ED/ID	40	NAD
71	M	3	2	–	Meningioma	ED/ID	37	NAD
72	M	3	1	Cortison	Meningioma	ED	37	NAD
74	F	2	3	–	Meningioma	ED	190	Minor
74	M	3	1	–	Meningioma	ID	36	NA
75	M	2	3	–	Meningioma	ED/ID	38	NAD
76	M	2	1	–	Meningioma	ED/ID	56	NAD
78	F	3	3	–	Meningioma	ED	17	Minor
45	M	2	0	–	Metastasis	ED/ID	25	NAD
59	F	3	3	–	Metastasis	ED/ID	116	Minor
63	M	2	1	–	Metastasis	ED	25	NAD
71	M	2	1	–	Metastasis	ED/ID	109	Major
78	M	4	2	Diabetes	Metastasis	ID	20	Death
66	F	1	1	–	Other	ED	393	NAD
62	M	1	1	Cortisone	Pituitary adenoma	ED	232	Major
40	F	2	1	–	Schwannoma	ED	43	NAD

M male, *F* female, *ASA* American Society of Anesthesiologists' classification of physical status, *ECOG* Eastern cooperative oncology group's classification of physical status

[a]Histology: *HGG* high-grade glioma, *LGG* low-grade glioma

[b]Location = location of infection: *ED* extradural infection, *ID* intradural infection, *ED/ID* both intradural and extradural infection

[c]Time = time of reoperation in days after primary surgery

[d]Outcome = clinical outcome after postoperative infection: *NAD* no additional disability, *Minor* minor additional disability, *Major* major additional disability

Table 20.3 Univariate and multivariate analysis of factors possibly associated with surgery for postoperative infection using Cox regression

	Infection	
	Univariate	Multivariate
	Odds ratio (95 % CI)	Odds ratio (95 % CI)
Age > 60	1.11	0.97
No/yes	[0.59, 2.09]	[0.50, 1.86]
Sex	0.47*	0.33**
Male/female	[0.24, 0.91]	[0.16, 0.66]
Primary Op	1.74	2.01
Primary/secondary	[0.86, 3.51]	[0.97, 4.17]
Operation	[a]	[a]
Resection/biopsy		
Histology		
HGG	1	1
LGG	[a]	[a]
Meningioma	3.70***	4.61***
	[1.95, 7.02]	[1.98, 10.73]
Metastasis	0.71	1.34
	[0.28, 1.83]	[0.43, 4.21]
Lymphoma	1.34	3.43
	[0.18, 9.94]	[0.41, 28.80]
Capillary hemangioblastoma	[a]	[a]
Schwannoma	0.43	0.75
	[0.10, 1.79]	[0.16, 3.56]
Others	0.92	1.61
	[0.12, 6.80]	[0.20, 13.19]
Observations		2,286
Pseudo-R^2		0.069
H-L test		$p = 0.85$

HGG High grade glioma
LGG Low grade glioma
H-L Hosmer-Lemeshow
*$p < 0.05$; **$p < 0.01$; ***$p < 0.001$
[a]Insufficient events in one of the contrasting categories to calculate odds ratio

being in the lower end of the scale as contemporary neurosurgical series have reported an incidence of postoperative infections after craniotomy of 0.6–6.6 % (Chang et al. 2003; Dashti et al. 2008; Korinek et al. 2005; McClelland and Hall 2007; Morokoff et al. 2008; Rabadan et al. 2007), although some of these series have included non-operative cases as well.

Risk Factors for Postoperative Infections

We observed a statistically significant association between male gender and postoperative infections. This has not been noted in other large neurosurgical series (Korinek 1997; Lietard et al. 2008; Mollman and Haines 1986), but Korinek et al. (2006) observed an increased risk of nosocomial meningitis after craniotomy in males. At present, we have no explanation for our finding.

Meningioma surgery was significantly associated with development of postoperative infection in both uni- and multivariate analyses. This was also shown by Korinek et al. (2005), although only in univariate analysis. They attributed this to hemostasis and closure difficulties in meningioma surgery. They also showed an association between infection and surgery duration over 4 h, a finding that also has been demonstrated by others (Idali et al. 2004; Korinek 1997). As meningioma operations are often time-consuming procedures, this might be a contributing factor to the higher incidence of infections after meningioma surgery.

Korinek et al. (2005) studied the effect of antibiotic prophylaxis (ABP) on neurosurgical site infections after craniotomy for various reasons, e.g. tumor surgery, vascular surgery, and trauma surgery. Among the 4,578 patients studied, 77 (1.7 %) developed bone flap osteitis, and 126 (2.7 %) developed brain abscess or subdural empyema, for a total of 4.4 %. As patients with both osteitis and abscess/empyema were counted once in each group, the number of patients with infections was a bit lower. ABP significantly reduced the incidence of bone flap osteitis (3.1 % in patients with no ABP and 1.3 % in patients with ABP, $p < 0.0002$) and abscess/empyema (5.6 % vs. 2.0 %, $p < 0.0001$). In our practice, we use a second-generation cephalosporin i.v. at initiation of surgery and continued every 90 min until the case is completed or the maximum daily dose of 8 g is reached, whereafter erythromycin or a third-generation cephalosporin is started and continued until completion of the case.

Timing of Postoperative Infection Development

In our series, almost 75 % of the patients with infection were reoperated within 3 months of tumor surgery. Korinek et al. (2005) showed a mean time between surgery and onset of infection of 118 ± 157 days for bone flap osteitis, and 25 ± 27 days for brain abscesses or subdural empyema. Dashti et al. (2008) reported a median duration between craniotomy and presentation of postoperative infection of 1.5 months (range 4 days–5 years). In our series, most postoperative infections requiring reoperation occur within 3 months of surgery, but some infections, in particular bone flap osteitis, may occur later than 1 year after surgery, reportedly as late as 5 years later (Blomstedt 1985; Korinek 1997).

Consequences of Postoperative Infection

The consequences of postoperative infection are not at all as severe as the consequences of postoperative hematoma. In our series, 2 patients (5 %) died due to the infection, while 33 (85 %) had a good outcome, with no or only a mild disability. It is important to point out that we did not include patients with meningitis.

In conclusion, the rate of postoperative infections was low as only 1.5 % of the patients were reoperated for postoperative infection. Of these infections, 59.0 % were extradural. Independent risk factors were male sex and meningioma histopathology. The vast majority of reoperations occurred within 3 months of tumor surgery. The consequences of postoperative infections were generally minor, as 85 % had a good outcome with no or only a mild disability, but within the group of patients reoperated for infection, the mortality rate was 5 %.

References

Barker FG 2nd (2004) Craniotomy for the resection of metastatic brain tumors in the U.S., 1988–2000: decreasing mortality and the effect of provider caseload. Cancer 100(5):999–1007

Blomstedt GC (1985) Infections in neurosurgery: a retrospective study of 1143 patients and 1517 operations. Acta Neurochir (Wien) 78(3–4):81–90

Chang SM, Parney IF, McDermott M, Barker FG 2nd, Schmidt MH, Huang W, Laws ER Jr, Lillehei KO, Bernstein M, Brem H, Sloan AE, Berger M (2003) Perioperative complications and neurological outcomes of first and second craniotomies among patients enrolled in the Glioma Outcome Project. J Neurosurg 98(6):1175–1181

Claus EB, Horlacher A, Hsu L, Schwartz RB, Dello-Iacono D, Talos F, Jolesz FA, Black PM (2005) Survival rates in patients with low-grade glioma after intraoperative magnetic resonance image guidance. Cancer 103(6):1227–1233

CTBRUS (2008) Statistical report: primary brain tumors in the United States, 2000–2004. http://www.cbtrus.org/reports//2007-2008/2007report.pdf

Dashti SR, Baharvahdat H, Spetzler RF, Sauvageau E, Chang SW, Stiefel MF, Park MS, Bambakidis NC (2008) Operative intracranial infection following craniotomy. Neurosurg Focus 24(6):E10

Fadul C, Wood J, Thaler H, Galicich J, Patterson RH Jr, Posner JB (1988) Morbidity and mortality of craniotomy for excision of supratentorial gliomas. Neurology 38(9):1374–1379

Gerlach R, Raabe A, Scharrer I, Meixensberger J, Seifert V (2004) Post-operative hematoma after surgery for intracranial meningiomas: causes, avoidable risk factors and clinical outcome. Neurol Res 26(1):61–66

Hart MG, Grant R, Walker M, Dickinson H (2005) Surgical resection and whole brain radiation therapy versus whole brain radiation therapy alone for single brain metastases. Cochrane Database Syst Rev 1, CD003292

Idali B, Lahyat B, Khaleq K, Ibahioin K, El Azhari A, Barrou L (2004) Postoperative infection following craniotomy in adults. Med Mal Infect 34(5):221–224

Kalfas IH, Little JR (1988) Postoperative hemorrhage: a survey of 4992 intracranial procedures. Neurosurgery 23(3):343–347

Keles GE, Chang EF, Lamborn KR, Tihan T, Chang CJ, Chang SM, Berger MS (2006) Volumetric extent of resection and residual contrast enhancement on initial surgery as predictors of outcome in adult patients with hemispheric anaplastic astrocytoma. J Neurosurg 105(1):34–40

Korinek AM (1997) Risk factors for neurosurgical site infections after craniotomy: a prospective multicenter study of 2944 patients. The French Study Group of Neurosurgical Infections, the SEHP, and the C-CLIN Paris-Nord. Service Epidemiologie Hygiene et Prevention. Neurosurgery 41(5):1073–1079

Korinek AM, Golmard JL, Elcheick A, Bismuth R, van Effenterre R, Coriat P, Puybasset L (2005) Risk factors for neurosurgical site infections after craniotomy: a critical reappraisal of antibiotic prophylaxis on 4,578 patients. Br J Neurosurg 19(2):155–162

Korinek AM, Baugnon T, Golmard JL, van Effenterre R, Coriat P, Puybasset L (2006) Risk factors for adult

nosocomial meningitis after craniotomy: role of antibiotic prophylaxis. Neurosurgery 59(1):126–133

Lassen B, Helseth E, Ronning P, Scheie D, Johannesen TB, Maehlen J, Langmoen IA, Meling TR (2011) Surgical mortality at 30 days and complications leading to recraniotomy in 2630 consecutive craniotomies for intracranial tumors. Neurosurgery 68(5):1259–1268, discussion 1268–9

Lietard C, Thebaud V, Besson G, Lejeune B (2008) Risk factors for neurosurgical site infections: an 18-month prospective survey. J Neurosurg 109(4):729–734

Mahaley MS Jr, Mettlin C, Natarajan N, Laws ER Jr, Peace BB (1989) National survey of patterns of care for brain-tumor patients. J Neurosurg 71(6):826–836

McClelland S 3rd, Hall WA (2007) Postoperative central nervous system infection: incidence and associated factors in 2111 neurosurgical procedures. Clin Infect Dis 45(1):55–59

McGirt MJ, Chaichana KL, Gathinji M, Attenello FJ, Than K, Olivi A, Weingart JD, Brem H, Quinones-Hinojosa AR (2009) Independent association of extent of resection with survival in patients with malignant brain astrocytoma. J Neurosurg 110(1):156–162

Mirimanoff RO, Dosoretz DE, Linggood RM, Ojemann RG, Martuza RL (1985) Meningioma: analysis of recurrence and progression following neurosurgical resection. J Neurosurg 62(1):18–24

Mollman HD, Haines SJ (1986) Risk factors for postoperative neurosurgical wound infection. A case–control study. J Neurosurg 64(6):902–906

Morokoff AP, Zauberman J, Black PM (2008) Surgery for convexity meningiomas. Neurosurgery 63(3):427–433

Nitta T, Sato K (1995) Prognostic implications of the extent of surgical resection in patients with intracranial malignant gliomas. Cancer 75(11):2727–2731

Percy AK, Elveback LR, Okazaki H, Kurland LT (1972) Neoplasms of the central nervous system. Epidemiologic considerations. Neurology 22(1):40–48

Rabadan AT, Hernandez D, Eleta M, Pietrani M, Baccanelli M, Christiansen S, Teijido C (2007) Factors related to surgical complications and their impact on the functional status in 236 open surgeries for malignant tumors in a Latino-American hospital. Surg Neurol 68(4):412–420, discussion 420

Vecht CJ, Avezaat CJ, van Putten WL, Eijkenboom WM, Stefanko SZ (1990) The influence of the extent of surgery on the neurological function and survival in malignant glioma. A retrospective analysis in 243 patients. J Neurol Neurosurg Psychiatry 53(6):466–471

Transsphenoidal Surgery for Non-Adenomatous Tumors: Effect on Pituitary Function

21

Garni Barkhoudarian, Aaron Cutler, and Daniel F. Kelly

Contents

Abstract

Pituitary adenomas are the most common intrasellar tumor. However, a wide variety of non-adenomatous lesions also arises in the sellar and parasellar region and can impact pituitary gland function. The lesions most commonly associated with pituitary hormonal disturbance include craniopharyngiomas, Rathke's cleft cysts, arachnoid cysts and sellar metastases while meningiomas and clival chordomas less commonly affect gland function. Depending on the specific lesion and location, surgical resection can result in improvement or worsening of endocrinopathy. Thorough pre-operative hormonal evaluation, sellar imaging with attention to gland and infundibulum location as well as intra-operative dissection techniques aimed at preserving the hypothalamic-pituitary axis are essential to minimize the risk of new hormonal dysfunction. This chapter discusses the surgical management of these lesions and characterizes the presenting and post-operative pituitary hormonal outcomes related to the specific lesion pathology.

Introduction

The transsphenoidal approach to the sella for removal of pituitary adenomas has been in practice for a century. Since the late 1960s, the operating microscope has allowed selective removal of adenomas with a goal of preserving gland function as

G. Barkhoudarian • A. Cutler
John Wayne Cancer Institute at Saint John's Health Center, 2200 Santa Monica Blvd., Santa Monica, CA 90404, USA

D.F. Kelly (✉)
Brain Tumor Center, John Wayne Cancer Institute at Saint John's Health Center, 2200, Santa Monica Blvd., Santa Monica, CA 90404, USA
e-mail: kellyd@jwci.org

M.A. Hayat (ed.), *Tumors of the Central Nervous System, Volume 12*,
DOI 10.1007/978-94-007-7217-5_21,

originally described by Hardy. The extended transsphenoidal microscopic approach for non-adenomatous lesions such as craniopharyngiomas was first described by Weiss in 1987 and then others. Since then, the concept of minimally invasive endonasal removal of anterior skull base pathology has evolved dramatically in large part due to increasing use of the endoscope and a transition away from the microscope (Cappabianca and de Divitiis 2004; Jho et al. 1997; Prevedello et al. 2007). The enhanced panoramic high-definition endoscopic view has become an essential feature of this approach. Still, whether using the microscope or endoscope, paramount among the surgical objectives is preservation of the parasellar neurovascular and when possible, preservation of the pituitary gland and infundibulum. The aim of this chapter is to review the neuroendocrine presentation and outcomes for surgical removal of non-adenomatous lesions of the sellar and parasellar region, as well as the surgical techniques to maximize chances of pituitary hormonal functional preservation.

Pituitary Imaging and Hormonal Testing for Non-Adenomatous Lesions

The most common sellar and parasellar lesion is the pituitary adenoma. Depending on the clinical presentation, anatomic location and imaging characteristics, a wide range of pathology can exist in this region. Modern imaging techniques utilize high-resolution CT imaging and MR imaging with various sequences to differentiate between these pathologies. The ideal imaging sequence is a "Pituitary Protocol" MRI of the brain that, in addition to whole brain sequences, includes magnified pre- and post-contrast sequences acquired in the sagittal and coronal planes centered around the parasellar region. Adjunct imaging modalities can include thin-cut CT to evaluate for intralesional calcifications and bony changes. Cerebral angiography is helpful to rule out a parasellar aneurysm and can help identify critical vascular structures in more complex lesions. PET imaging may be helpful in the overall staging of metastatic disease with possible parasellar dissemination. It is important to note that pituitary adenomas and other hypermetabolic lesions can have high signal on PET imaging as well. It is essential to identify the possible location of the normal gland on imaging to help prevent post-operative pituitary dysfunction. Identification of the infundibulum, posterior pituitary gland (via the T1 "bright spot"), and cavernous sinuses can be helpful aids to pituitary gland localization.

A thorough pre-operative endocrinological work-up is necessary for all parasellar lesions that impinge upon or otherwise distort the hypothalamic-pituitary axis and sella. All anterior gland axes should be evaluated to diagnose possible pituitary dysfunction, including: TSH, T4, free T4, ACTH, cortisol, LH, FSH, prolactin, total and free testosterone in men, estrogen in women, GH and IGF-1. Should the lesion potentially be a pituitary adenoma, screening for functional adenomas (acromegaly, Cushing's disease, prolactinoma, thyrotropinoma) should be pursued in collaboration with an endocrinologist. If there is a suspicion of diabetes insipidus (DI) either clinically or due to suspected pathology (e.g., craniopharyngioma or RCC), urine specific gravity, serum and urine osmolarity should be assessed. A water deprivation trial may be necessary to fully elucidate the diagnosis of DI.

Hormonal Dysfunction Associated with Non-Adenomatous Parasellar Lesions

Anterior and posterior pituitary dysfunction is frequently seen with non-adenomatous lesions and can sometimes be the presenting finding leading to their diagnosis. The most common lesions affecting gland function are craniopharyngiomas, Rathke's cleft cysts, arachnoid cysts, and sellar metastases while chordomas and parasellar meningiomas infrequently affect gland function (Table 21.1). Other relatively rare entities such as epidermoid cysts, dermoid cysts and germ cell tumors can also occasionally impact gland function. Lymphocytic hypophysitis also frequently impacts pituitary gland function but is rarely treated surgically and will not be discussed.

Table 21.1 Presenting pituitary dysfunction

Lesion	Overall endocrinopathy	Diabetes insipidus	Panhypopituitarism
Craniopharyngioma	56–83 %	4–37 %	24–42 %
Rathke's cleft cyst	66–70 %	0–13 %	0–11 %
Arachnoid cyst	50–60 %	Case reports	Case reports
Tuberculum sella meningioma	2–39 %	4.5 %	4.5 %
Chordoma	Case reports	Insufficient data	Insufficient data
Metastases/Lymphoma	23–100 %	45–100 %	23–25 %

Table 21.2 Post-operative pituitary outcome

Lesion	New anterior pituitary dysfunction	New diabetes insipidus	Improvement of pre-operative pituitary dysfunction
Craniopharyngioma	17–80 %	23–69 %	0–35 %
Rathke's cleft cyst	1.7–6 %	2–19 %	22–41 %
Arachnoid cyst	0 %	0 %	25–100 %
Tuberculum sella meningioma	0–23 %	0 %	0 %
Chordoma	Case reports	Case reports	Insufficient data
Metastases/Lymphoma	Insufficient data	Insufficient data	Insufficient data

Following surgical resection of non-adenomatous sellar lesions, anterior pituitary gland function can improve, as is commonly seen with Rathke's cleft cysts and sellar arachnoid cysts. However, it is extremely uncommon for diabetes insipidus to resolve post-operatively (Table 21.2). New post-operative anterior and/or posterior gland dysfunction is most commonly seen with craniopharyngiomas and occasionally with Rathke's cleft cysts (particularly supraglandular cysts adherent to the infundibulum), but rarely with parasellar meningiomas and clival chordomas. The relevant surgical anatomy and imaging, surgical nuances for preserving gland function and hormonal outcomes for each of these lesion types is discussed below.

Endonasal Transsphenoidal Approach with Attention to Gland Identification and Preservation

The endonasal transsphenoidal approach, enhanced with neuroendoscopy, offers a safe surgical trajectory for the great majority of parasellar lesions. In terms of preserving gland function, a careful review of the preoperative sellar MRI allows one to anticipate gland location and the course of the infundibulum relative to the tumor. While most pituitary adenomas distort the gland by pushing it laterally, posteriorly and or superiorly, non-adenomatous lesions can push the gland anteriorly (as is often the case with Rathke's cleft cysts and sellar arachnoid cysts) or inferiorly (as is often the case with craniopharyngiomas and tuberculum sella and dorsum sellae meningiomas). While craniopharyngiomas are the most variable in their location, they are the tumor that most commonly engulfs the infundibulum and extends into the retro-chiasmal space.

In patients with fully or partially intact pituitary gland function, in whom functional preservation is a goal, the gland should be gently manipulated. To access a tumor or cyst behind the gland, it is generally safe to make a low vertical gland incision and even to remove a small window of attenuated gland as a working corridor (Dusick et al. 2008, Table). This approach is preferred over putting excessive traction on the gland which can compromise gland and infundibulum neurovasculature. An alternative and technically more demanding approach for working in

the retro-glandular space is pituitary gland transposition as described by Kassam et al. (2008) for some lesions such as craniopharyngiomas, chordomas and meningiomas. For lesions that extend into the suprasellar and supra-diaphragmatic space, particularly for retrochisamal craniopharyngiomas and tuberculum sellae meningiomas, it is also critical to visualize and preserve the superior hypophyseal arteries which typically course from laterally to medially to the infundibulum in 2 or 3 branches and then bifurcate superiorly to the undersurface of the chiasm and inferiorly to the gland . Injury to these delicate arteries can contribute to gland dysfunction as well as visual field loss from chiasmal ischemia (Kassam et al. 2008).

Specific Sellar Lesions: Approach and Hormonal Outcomes

Craniopharyngioma

Relevant Anatomy and Imaging: Craniopharyngiomas typically have their epicenter around the infundibulum but can extend into various locations including intrasellar, suprasellar, intraventricular, or a combination of these areas as well as into the frontal and middle fossas. However, the most common location for craniopharyngiomas is in the sellar, suprasellar and retrochiasmal space.

Clinical Presentation and Hormonal Outcomes: In addition to the common presentation of visual loss and headaches, craniopharyngiomas lead to pituitary hormonal dysfunction in 56–83 % of patients. The most common hypothalamic pituitary axes affected are the gonadotrope and somatotrope systems. The incidence of panhypopituitarism is approximately 24–42 %. Diabetes insipidus is a less common presenting finding (4–37 %) (Honegger et al. 1999, Table; Shin et al. 1999, Table). Following surgery, the incidence of new panhypopituitarism is 17–80 %. This is dependent on the tumor location, the surgical approach, the degree of tumor resection, and the preservation of the normal pituitary gland and infundibulum. The incidence of post-operative prolonged diabetes insipidus is 23–69 % (Honegger et al. 1999; Shin et al. 1999). With more extensive tumors involving the hypothalamus, the incidence of adipsic DI, temperature dysregulation and hypothalamic obesity can occur. These syndromes are very difficult to manage as the thirst and satiety nuclei of the hypothalamus are affected and hormone replacement alone does not suffice (Crowley et al. 2010). With tumors that significantly involve the infundibulum, deliberate pituitary stalk sectioning may be necessary, resulting in DI and pan-hypopituitarism. In tumors where there is apparent anatomic preservation of the pituitary gland, the incidence of pituitary dysfunction remains elevated regardless of surgical approach (Honegger et al. 1999). Even with stalk preservation, post-operative DI still occurs in 52–64 % of patients. Post-operative hypocortisolism occurs in up to 40 % of patients.

Surgical Nuances for Maximizing Gland Preservation: Given that the majority of craniopharyngiomas are in the sellar, suprasellar and retrochiasmal space, an endonasal transsphenoidal approach with endoscopy or endoscopic assistance is recommended for the majority of such tumors. In some tumors with predominantly pre-chiasmal or lateral suprasellar extensions, the supraorbital or pterional approach may be preferred (Fatemi et al. 2009). For lesions predominantly within the third ventricle, a transventricular approach may be utilized.

If preoperative pituitary gland function is largely intact, an attempt is made to identify the pituitary stalk and its site of insertion to the pituitary gland early in the dissection and to avoid traction on the stalk during tumor removal. However, when pre-operative diabetes insipidus or multiple anterior gland deficiencies are present and/or the pituitary stalk is engulfed by tumor on the pre-operative MRI, persevering gland function is less likely and thus less of a priority although an effort should be made in every case to identify and preserve the infundibulum. While total resection of craniopharyngiomas has been advocated by some, it is associated with a higher morbidity and mortality (Zhou and Shi 2004). Consequently, the goal should be safe maximal resection and settling for subtotal removal if

dense adhesions to neurovascular structures are present (Puget et al. 2007; Van Effenterre and Boch 2002). In recent reports, total removal rates have ranged from 7 % to 89 % in transsphenoidal series with the microscope and/or endoscope (Chakrabarti et al. 2005; Czirjak and Szeifert 2006; Laws et al. 2005), 40–74 % in supra-orbital series (Czirjak and Szeifert 2006; Jallo et al. 2005) and 6–100 % by the subfrontal or pterional routes (Fahlbusch and Schott 2002, Table; Puget et al. 2007; Van Effenterre and Boch 2002).

Rathke's Cleft Cyst

Relevant Anatomy and Imaging: Rathke's cleft cysts are the most common non-adenomatous symptomatic lesions affecting the pituitary gland (Dusick et al. 2005, Table). They most commonly are intrasellar with or without suprasellar extension causing anterior displacement of the anterior gland and posterior displacement of the posterior lobe. Less commonly they can be entirely supraglandular in location often adherent to infundibulum and extending into the suprasellar space (Potts et al. 2011) (Fig. 21.1).

Clinical Presentation and Hormonal Outcomes: These lesions are most commonly associated with headaches (70–85 %), typically frontal or retro-orbital in location. Hypopituitarism can also occur, though more frequent in children (Aho et al. 2005, Table; Madhok et al. 2010, Table; Potts et al. 2011, Table). In a large series of symptomatic patients with RCC, pituitary dysfunction was present in 66–70 % of patients, with 0–13 % presenting with DI (Aho et al. 2005). Pre-operative anterior hormonal deficits frequently improve as shown in our recent report with a 41 % rate of resolved anterior axis deficiencies and a 67 % rate of resolved stalk hyperprolactinemia (Dusick et al. 2008). Resolution of diabetes insipidus however is extremely rare (Frank et al. 2005).

Surgical Nuances for Maximizing Gland Preservation: For intrasellar RCCs, since such cysts are typically located behind the anterior lobe, their removal involves an approach through the anterior gland via a low midline vertical glandular incision or as described by Madhok et al. (2010) using an infrasellar approach to the cyst contents with minimal gland incision. Through this small low anterior or inferior corridor, the cyst contents are removed with suction, curettes and irrigation. Given that the resection cavity is generally formed by the anterior and posterior pituitary lobes and the cyst lining is generally adherent to these normal structures no attempt should be made to vigorously strip the cyst wall off of the normal gland, since this approach has been associated with a higher rate of post-operative pituitary gland dysfunction including diabetes insipidus (Aho et al. 2005). However, this less aggressive approach is also associated with a higher rate of cyst recurrence (Kim et al. 2004). A detailed endoscopic visualization of the cyst wall and normal pituitary structures may improve surgical outcomes and decrease the incidence of DI. Although occasionally utilized, instilling caustic agents such as ethanol or hydrogen peroxide does not appear to decrease the recurrence rate of these cysts, and may increase pituitary gland dysfunction (Benveniste et al. 2004).

Sellar Arachnoid Cysts

Relevant Anatomy and Imaging: Arachnoid cysts of the sellar and parasellar region are generally thought to be congenital and/or developmental in origin. Pre-operative imaging demonstrates a cyst with signal characteristics similar to CSF (hyperintense on T2, hypointense on T1, no diffusion restriction on DWI). Unlike sellar Rathke's cleft cysts which consistently reside between the anterior and posterior lobes of the pituitary, sellar arachnoid cysts have a much more variable relationship to the gland and infundibulum. The gland may be pushed anteriorly or splayed bilaterally, superiorly or posteriorly by the cyst (McLaughlin et al. 2012, Table).

Clinical Presentation and Hormonal Outcomes: Pre-operative anterior pituitary dysfunction can be seen with sellar arachnoid cysts ranging from 50–60 % (Shin et al. 1999), while DI is rarely

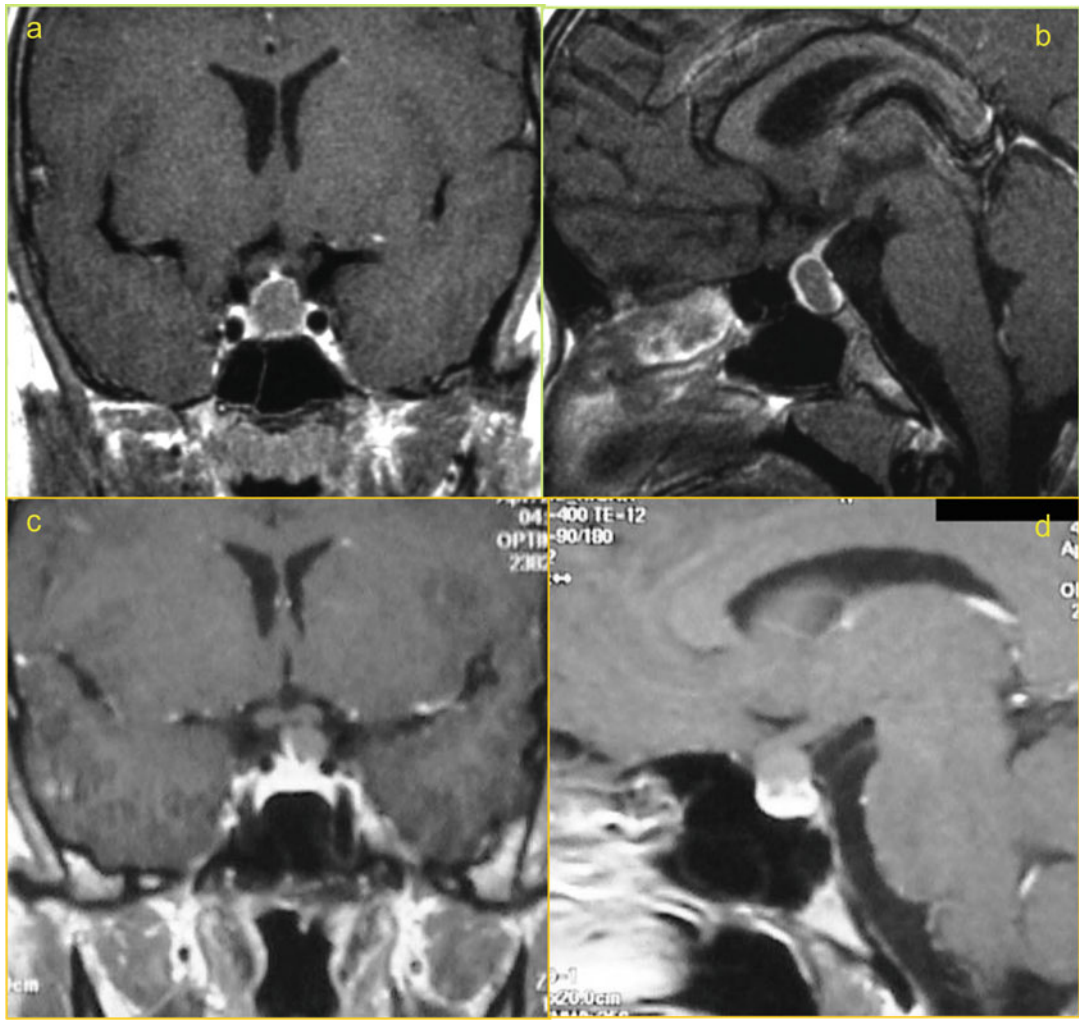

Fig. 21.1 Coronal and Sagittal MRI post-contrast images of Intrasellar (**a**, **b**) and supraglandular (**c**, **d**) Rathke's Cleft Cyst

seen (McLaughlin et al. 2012). Following surgical fenestration and cyst obliteration occlusion, pituitary dysfunction can improve in 0–100 % of patients, being rare to improve in those presenting with panhypopituitarism and common to improve in those with partial deficiencies (Table 21.2).

Surgical Nuances for Maximizing Gland Preservation: As we recently described, our technique for sellar arachnoid cyst obliteration involves a relatively small dural opening and cyst cavity obliteration with an abdominal fat graft and sellar floor reconstruction (McLaughlin et al. 2012). The dural opening should be large enough to pass a 4 mm rigid endoscope but not so large as to increase the complexity of the skull base closure. The anterior arachnoid cyst membrane is opened sharply with a microblade with return of clear cerebrospinal fluid. An inspection of the AC cavity is performed making sure the lesion is not a cystic tumor, and looking for potential diaphragmatic defects or arachnoid diverticula. Widening or dissection through the diaphragmatic defect in order to establish a larger communication to the suprasellar SAS is specifically avoided. Additionally, the cyst wall is not dissected off of the pituitary gland which is typically thinned and attenuated, given the risk of worsening pituitary dysfunction. Subsequently, the defect is obliterated with a fat graft that has enough volume

to fill the cavity without excess pressure on the surrounding normal pituitary gland which is typically thinned. The fat graft is supported with a buttress, collagen sponges, and tissue glue.

Meningioma

Relevant Anatomy and Imaging: Meningiomas involving the sella and pituitary gland can arise from the diaphragm sella, the tuberculum sella, the cavernous sinus or the sphenoid wing. When indicated, the extended transsphenoidal approach can offer a safe alternative for tumor resection as well as pituitary gland preservation especially for tumors under 3–3.5 cms in maximal diameter without large lateral extensions (Fatemi et al. 2009; Laws and Thapar 2000).

Clinical Presentation and Hormonal Outcomes: As these tumors originate from the skull-base dura, the frequency of pituitary gland involvement is much lower than other parasellar lesions. The incidence of pre-operative pituitary dysfunction is 2–39 % (Dusick et al. 2005; Fahlbusch and Schott 2002). Meningioma locations that can affect pituitary function include tuberculum sella and cavernous sinus lesions that extend into the sella itself (Fig. 21.2). The risk of new pituitary dysfunction following surgery for these lesions has been reported to be 0–23 % (Dusick et al. 2008; Fahlbusch and Schott 2002). Conversely, some patients demonstrate improvement of their pre-operative endocrinopathies (Fahlbusch and Schott 2002). Additionally, tumors that involve the posterior clinoid processes or the mesencephalon, necessitating pituitary transposition can affect pituitary function. Following this maneuver, pituitary dysfunction has been reported to be 13 % in a small cohort study (Kassam et al. 2008).

Surgical Nuances for Maximizing Gland Preservation: For tuberculum sellae meningiomas, the tumors arise from the tuberculum sella and often extend onto the diaphragma sella causing downward compression of the normal gland and stretching the infundibulum posteriorly. In these cases, the infundibulum and its insertion site to the gland should be identified after the initial debulking of the more anteriorly located tumor with preservation of these structures and the overlying arachnoid plane as a major goal of the surgery. Careful attention to the superior hypophyseal arteries is also essential to preserve pituitary gland and chiasmal function.

Chordoma and Chondrosarcoma

Relevant Anatomy and Imaging: Clival chordomas are malignant tumors that originate from notochord remnants along the skull base. Chordomas can behave quite aggressively and are often extensively invasive into surrounding skull base structures. A small subset of patients (up to 10 %) may develop metastases to distant sites beyond their site of origin. One of the more common sites from which these originate is at the occipito-sphenoidal suture of the clivus (Colli and Al-Mefty 2001; Henderson et al. 2009). Histological evaluation with special stains identifies some of these lesions as low-grade chondrosarcomas; others have been sub-classified as the chondroid variant of chordoma.

Clinical Presentation and Hormonal Outcomes: Frequently, chordomas may indent or erode the sella and at times may cause some degree of pituitary gland distortion. However, preoperative pituitary hormonal dysfunction is relatively uncommon; the incidence is low and rarely reported. Post-operative pituitary dysfunction after chordoma resection is also low. Sporadic case reports have demonstrated chordomas invading the sella and causing pre-operative pituitary dysfunction complicated by post-operative DI (Galesanu et al. 2007, Table; Wang et al. 2012, Table). Small case series have shown intrasellar chordomas mimicking pituitary adenomas with occasional hyperprolactinemia and pituitary dysfunction (Thodou et al. 2000).

Surgical Nuances for Maximizing Gland Preservation: At surgery, clival chordomas that erode the sella and distort the gland and infundibulum may be found to extend through the sellar dura but more often they only compress

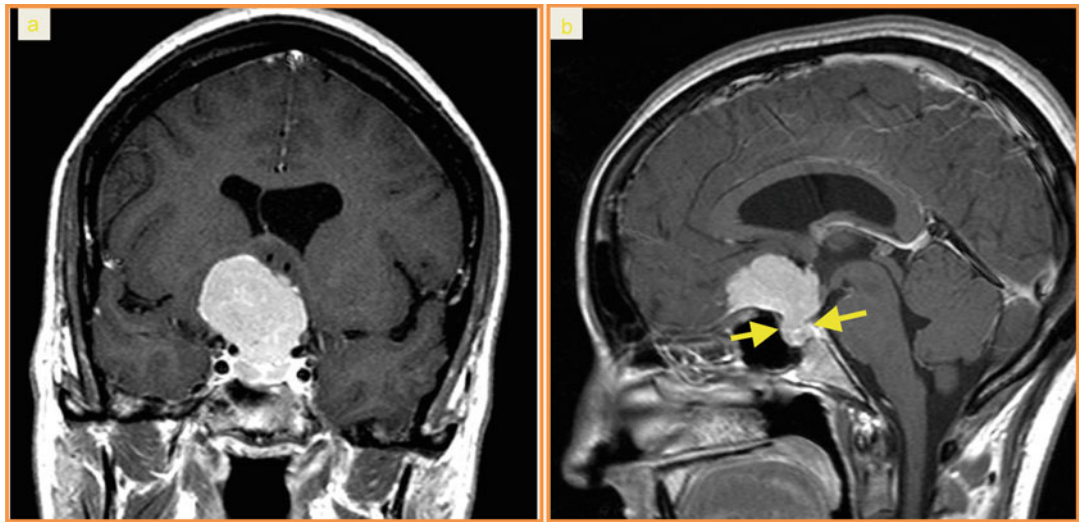

Fig. 21.2 Coronal (**a**) and sagittal (**b**) post-contrast MRI of a large tuberculum sella meningioma causing compression of the brain, optic apparatus, and the pituitary gland. A distinct border can be seen between the tumor and pituitary gland (*arrows*)

sellar dura. Tumor resection in this area must be done cautiously so as not to devascularize the gland or otherwise overly manipulate it.

Metastases and Lymphoma

Relevant Anatomy and Imaging: The pituitary gland is a relatively frequent site of distant metastases for numerous carcinomas. This is likely due to its rich vascular supply and its double capillary bed incorporated into the pituitary portal system. Common cancers metastatic to the pituitary region include: breast, lung, prostate, and renal cell carcinoma (Morita et al. 1998). It is important to note that pituitary adenomas may occur in 10–20 % of the general population and can also be hypermetabolic on PET imaging and can thus mimic metastatic disease (Campeau et al. 2003; Komori et al. 2002; Koo et al. 2006). Hence, isolated pituitary lesions in the setting of a primary carcinoma should warrant a surgical biopsy prior to more aggressive chemotherapy and radiation therapy regimens.

Clinical Presentation and Hormonal Outcomes: The most common finding for symptomatic pituitary metastases is pituitary dysfunction, particularly diabetes insipidus (70–100 %). Anterior pituitary dysfunction is often seen, but to a lesser extent. Other presenting symptoms are those of tumor mass effect, such as headaches, visual field deficits and cranial nerve dysfunction. Although surgical debulking of the tumor offers improvement in quality of life factors such as visual loss and pituitary dysfunction, the overall survival of patients with sellar metastases is poor, averaging 6–7 months. This poor prognosis is primarily due to the systemic tumor burden from the primary carcinoma and the late stage of the disease process (Morita et al. 1998; Sioutos et al. 1996).

Lymphoma of the pituitary gland is a rare but reported entity. Pituitary involvement has been noted in both hematogenous spread of lymphoma and primary CNS lymphoma (PCNSL). In an autopsy review, 23 % of 165 patients with hematological malignancies had hypophyseal lymphoma. Approximately 25 % of a series of 22 patients with PCNSL also had pituitary involvement (Giustina et al. 2001, Table). In patients with pituitary involvement, up to 50 % presented with deficiency in at least one pituitary axis (Giustina et al. 2001; Mathiasen et al. 2000). Systemic lymphoma can also metastasize to the

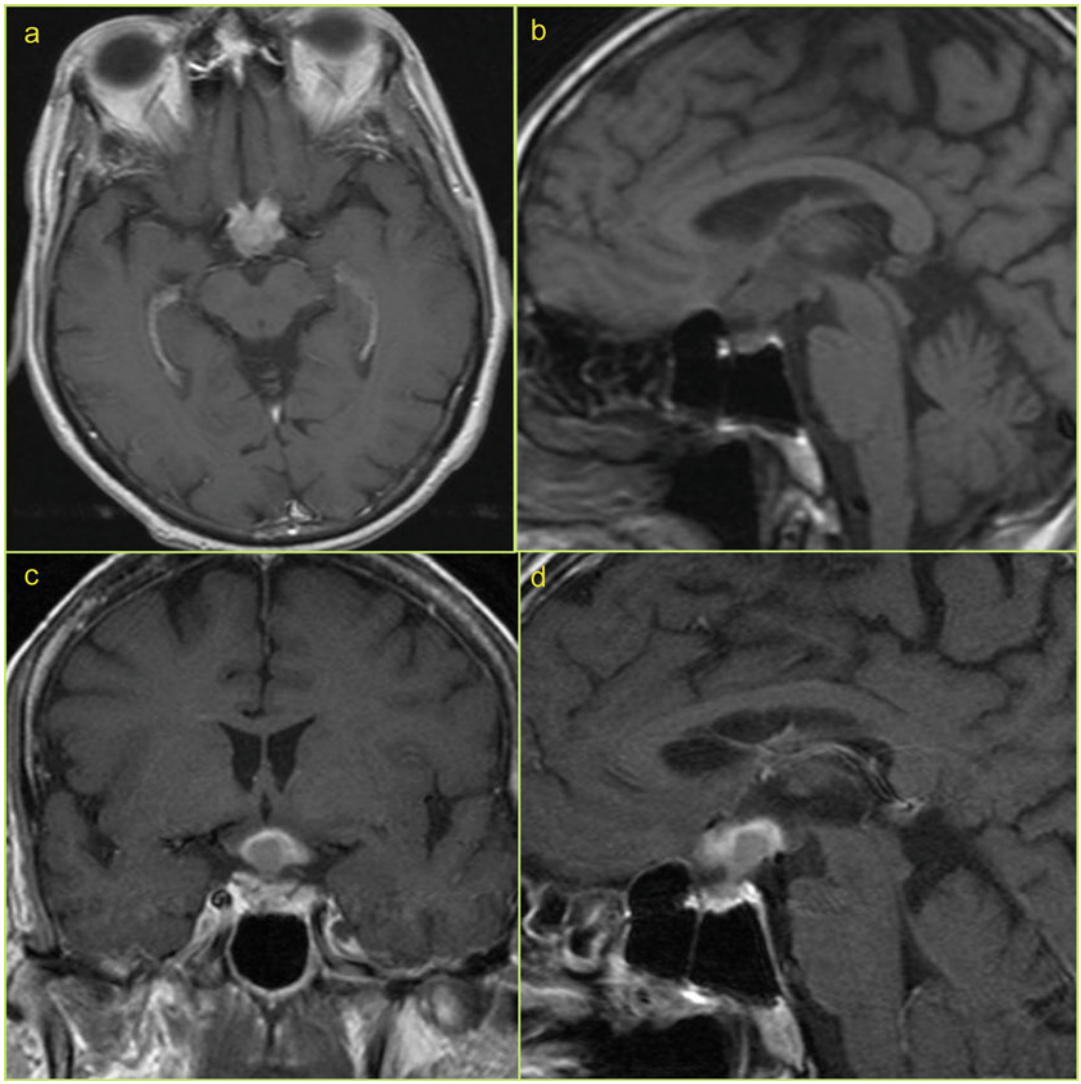

Fig. 21.3 Axial post-contrast (**a**), sagittal pre-contrast (**b**), coronal post-contrast (**c**) and sagittal post-contrast (**d**) MRI of a patient with non-Hodgkin's Lymphoma metastasis to the pituitary gland. Note posterior location of metastasis

pituitary gland, typically associated with anterior and posterior gland dysfunction (Megan et al. 2005; Soussan et al. 2008). Surgical biopsy of these lesions has been reported in selected cases (Landman et al. 2001; Mathiasen et al. 2000). Biopsy secured the initial diagnosis of pituitary lymphoma, allowing for systemic treatment of the disease (Fig. 21.3).

Surgical Nuances for Maximizing Gland Preservation: The primary surgical goal for sellar metastases is to decrease mass effect and obtain diagnostic tissue for tumor staging (when necessary). Metastatic tumors to the pituitary region are often highly invasive and vascular, warranting added caution on the part of the surgeon.

Miscellaneous Lesions

Numerous less common lesions can also be seen in the parasellar region. Some examples include

germ cell tumors, dermoid cysts, epidermoid cysts, lymphocytic hypophysitis and sarcoidosis. A subset of these lesions can present or affect pituitary hormonal function. Germ cell tumors are uncommon lesions that can involve midline intracranial structures, most commonly in the suprasellar and pineal regions. There are various subtypes, germinomas being the most common. Typically, suprasellar germinomas present first with diabetes insipidus (50–86 % in one series), and subsequently may produce visual loss and hypopituitarism (Matsutani et al. 1997). It is important to note that surgical resection of germ cell tumors is not often curative, whereas effective radiation and/or chemotherapy treatment for germinomatous germ-cell tumors may be more effective in achieving disease control (Pashtan and Loeffler 2011).

Although rare entities in the parasellar region, dermoid and epidermoid cysts have been reported (Mamata et al. 1998). Epidermoid tumors can be grossly debulked using mechanical curettage and suction, yet it is often necessary to leave the tumor capsule behind to avoid traction on critical structures. Dermoid cysts, which are often affecting midline structures, can be more intimately involved with the surrounding structures. These tumors rarely present with endocrine dysfunction, although sporadic case reports suggest a syndrome mimicking pituitary apoplexy (Sani et al. 2005; Tuna et al. 2008). The incidence of pituitary dysfunction following surgical removal of these lesions is poorly understood.

In conclusion, the transsphenoidal approach is increasingly used for removal of non-adenomatous sellar and parasellar tumors and its safety and effectiveness appears to have improved with greater use of endoscopy. Many of these lesions are associated with pre-operative pituitary dysfunction. Depending on the lesion, surgical approach and post-operative therapy, pituitary dysfunction can either improve or worsen. Thorough pre-operative evaluation regarding gland function and location, gentle surgical manipulation of the infundibulum, gland and associated vasculature, as well as careful post-operative monitoring are necessary to maximize chances of pituitary hormonal functional preservation and recovery.

References

Aho CJ, Liu C, Zelman V, Couldwell WT, Weiss MH (2005) Surgical outcomes in 118 patients with Rathke cleft cysts. J Neurosurg 102:189–193

Benveniste RJ, King WA, Walsh J, Lee JS, Naidich TP, Post KD (2004) Surgery for Rathke cleft cysts: technical considerations and outcomes. J Neurosurg 101:577–584

Campeau RJ, David O, Dowling AM (2003) Pituitary adenoma detected on FDG positron emission tomography in a patient with mucosa-associated lymphoid tissue lymphoma. Clin Nucl Med 28:296–298

Cappabianca P, de Divitiis E (2004) Endoscopy and transsphenoidal surgery. Neurosurgery 54:1043–1048, discussions 1048–1050

Chakrabarti I, Amar AP, Couldwell W, Weiss MH (2005) Long-term neurological, visual, and endocrine outcomes following transnasal resection of craniopharyngioma. J Neurosurg 102:650–657

Colli BO, Al-Mefty O (2001) Chordomas of the skull base: follow-up review and prognostic factors. Neurosurg Focus 10:E1

Crowley RK, Hamnvik OP, O'Sullivan EP, Behan LA, Smith D, Agha A, Thompson CJ (2010) Morbidity and mortality in patients with craniopharyngioma after surgery. Clin Endocrinol (Oxf) 73:516–521

Czirjak S, Szeifert GT (2006) The role of the superciliary approach in the surgical management of intracranial neoplasms. Neurol Res 28:131–137

Dusick JR, Esposito F, Kelly DF, Cohan P, DeSalles A, Becker DP, Martin NA (2005) The extended direct endonasal transsphenoidal approach for nonadenomatous suprasellar tumors. J Neurosurg 102:832–841

Dusick JR, Fatemi N, Mattozo C, McArthur D, Cohan P, Wang C, Swerdloff RS, Kelly DF (2008) Pituitary function after endonasal surgery for nonadenomatous parasellar tumors: Rathke's cleft cysts, craniopharyngiomas, and meningiomas. Surg Neurol 70:482–490, discussion 490–491

Fahlbusch R, Schott W (2002) Pterional surgery of meningiomas of the tuberculum sellae and planum sphenoidale: surgical results with special consideration of ophthalmological and endocrinological outcomes. J Neurosurg 96:235–243

Fatemi N, Dusick JR, de Paiva Neto MA, Malkasian D, Kelly DF (2009) Endonasal versus supraorbital keyhole removal of craniopharyngiomas and tuberculum sellae meningiomas. Neurosurgery 64:269–284, discussion 284–286

Frank G, Sciarretta V, Mazzatenta D, Farneti G, Modugno GC, Pasquini E (2005) Transsphenoidal endoscopic approach in the treatment of Rathke's cleft cyst. Neurosurgery 56:124–128, discussion 129

Galesanu C, Asiminoaiei I, Saviuc E, Bostaca T, Negru D, Branisteanu D (2007) One case of sellar and suprasellar chordoma. Endocrine Abstracts. p 437

Giustina A, Gola M, Doga M, Rosei EA (2001) Clinical review 136: Primary lymphoma of the pituitary: an emerging clinical entity. J Clin Endocrinol Metab 86:4567–4675

Henderson FC, McCool K, Seigle J, Jean W, Harter W, Gagnon GJ (2009) Treatment of chordomas with CyberKnife: georgetown university experience and treatment recommendations. Neurosurgery 64:A44–A53

Honegger J, Buchfelder M, Fahlbusch R (1999) Surgical treatment of craniopharyngiomas: endocrinological results. J Neurosurg 90:251–257

Jallo GI, Suk I, Bognar L (2005) A superciliary approach for anterior cranial fossa lesions in children. Technical note. J Neurosurg 103:88–93

Jho HD, Carrau RL, Ko Y, Daly MA (1997) Endoscopic pituitary surgery: an early experience. Surg Neurol 47:213–222, discussion 222–223

Kassam AB, Prevedello DM, Thomas A, Gardner P, Mintz A, Snyderman C, Carrau R (2008) Endoscopic endonasal pituitary transposition for a transdorsum sellae approach to the interpeduncular cistern. Neurosurgery 62:57–72, discussion 72–74

Kim JE, Kim JH, Kim OL, Paek SH, Kim DG, Chi JG, Jung HW (2004) Surgical treatment of symptomatic Rathke cleft cysts: clinical features and results with special attention to recurrence. J Neurosurg 100:33–40

Komori T, Martin WH, Graber AL, Delbeke D (2002) Serendipitous detection of Cushing's disease by FDG positron emission tomography and a review of the literature. Clin Nucl Med 27:176–178

Koo CW, Bhargava P, Rajagopalan V, Ghesani M, Sims-Childs H, Kagetsu NJ (2006) Incidental detection of clinically occult pituitary adenoma on whole-body FDG PET imaging. Clin Nucl Med 31:42–43

Landman RE, Wardlaw SL, McConnell RJ, Khandji AG, Bruce JN, Freda PU (2001) Pituitary lymphoma presenting as fever of unknown origin. J Clin Endocrinol Metab 86:1470–1476

Laws ER, Thapar K (2000) Unusual lesions in the sella turcica: intrasellar craniopharyngioma, benign cyst and meningioma. In: Kaye A, Black P (eds) Operative neurosurgery. Churchill Livingstone, London, pp 723–740

Laws ER, Kanter AS, Jane JA Jr, Dumont AS (2005) Extended transsphenoidal approach. J Neurosurg 102:825–827, discussion 827–828

Madhok R, Prevedello DM, Gardner P, Carrau RL, Snyderman CH, Kassam AB (2010) Endoscopic endonasal resection of Rathke cleft cysts: clinical outcomes and surgical nuances. J Neurosurg 112:1333–1339

Mamata H, Matsumae M, Yanagimachi N, Matsuyama S, Takamiya Y, Tsugane R (1998) Parasellar dermoid tumor with intra-tumoral hemorrhage. Eur Radiol 8:1594–1597

Mathiasen RA, Jarrahy R, Cha ST, Kovacs K, Herman VS, Ginsberg E, Shahinian HK (2000) Pituitary lymphoma: a case report and literature review. Pituitary 2:283–287

Matsutani M, Sano K, Takakura K, Fujimaki T, Nakamura O, Funata N, Seto T (1997) Primary intracranial germ cell tumors: a clinical analysis of 153 histologically verified cases. J Neurosurg 86:446–455

McLaughlin N, Vandergrift A, Ditzel Filho LF, Shahlaie K, Eisenberg AA, Carrau RL, Cohan P, Kelly DF (2012) Endonasal management of sellar arachnoid cysts: simple cyst obliteration technique. J Neurosurg 116:728–740

Megan OC, Payne S, Evanson J, Lister T, Grossman A (2005) Lymphoma metastasizing to the pituitary: an unusual presentation of a treatable disease. Pituitary 8:139

Morita A, Meyer FB, Laws ER Jr (1998) Symptomatic pituitary metastases. J Neurosurg 89:69–73

Pashtan I, Oh K, Loeffler J (2011) Radiation therapy. In: Laws ER, Sheehan JM (eds) Sellar and parasellar tumors: diagnosis, treatments, and outcomes. Thieme, New York, pp 206–208

Potts MB, Jahangiri A, Lamborn KR, Blevins LS, Kunwar S, Aghi MK (2011) Suprasellar Rathke cleft cysts: clinical presentation and treatment outcomes. Neurosurgery 69:1058–1068, discussion 1068–1067

Prevedello DM, Doglietto F, Jane JA Jr, Jagannathan J, Han J, Laws ER Jr (2007) History of endoscopic skull base surgery: its evolution and current reality. J Neurosurg 107:206–213

Puget S, Garnett M, Wray A, Grill J, Habrand JL, Bodaert N, Zerah M, Bezerra M, Renier D, Pierre-Kahn A, Sainte-Rose C (2007) Pediatric craniopharyngiomas: classification and treatment according to the degree of hypothalamic involvement. J Neurosurg 106:3–12

Sani S, Smith A, Leppla DC, Ilangovan S, Glick R (2005) Epidermoid cyst of the sphenoid sinus with extension into the sella turcica presenting as pituitary apoplexy: case report. Surg Neurol 63:394–397, discussion 397

Shin JL, Asa SL, Woodhouse LJ, Smyth HS, Ezzat S (1999) Cystic lesions of the pituitary: clinicopathological features distinguishing craniopharyngioma, Rathke's cleft cyst, and arachnoid cyst. J Clin Endocrinol Metab 84:3972–3982

Sioutos P, Yen V, Arbit E (1996) Pituitary gland metastases. Ann Surg Oncol 3:94–99

Soussan M, Wartski M, Ezra J, Glaisner S, Pecking AP, Alberini JL (2008) Non-Hodgkin lymphoma localization in the pituitary gland: diagnosis by FDG-PET/CT. Clin Nucl Med 33:111–112

Thodou E, Kontogeorgos G, Scheithauer BW, Lekka I, Tzanis S, Mariatos P, Laws ER Jr (2000) Intrasellar chordomas mimicking pituitary adenoma. J Neurosurg 92:976–982

Tuna H, Torun F, Torun AN, Erdogan A (2008) Intrasellar epidermoid cyst presenting as pituitary apoplexy. J Clin Neurosci 15:1154–1156

Van Effenterre R, Boch AL (2002) Craniopharyngioma in adults and children: a study of 122 surgical cases. J Neurosurg 97:3–11

Wang HF, Ma HX, Ma CY, Luo YN, Ge PF (2012) Sellar chordoma presenting as pseudo-macroprolactinoma with unilateral third cranial nerve palsy. Chin J Cancer Res 24:167–170

Zhou ZQ, Shi XE (2004) Changes of hypothalamus-pituitary hormones in patients after total removal of craniopharyngiomas. Chin Med J (Engl) 117:357–360

Treatment of Brain Tumors: Electrochemotherapy

22

Mette Linnert, Birgit Agerholm-Larsen, Faisal Mahmood, Helle K. Iversen, and Julie Gehl

Contents

Abstract

There is an increasing clinical challenge in the treatment of primary and secondary brain tumors, mostly because of a rise in the number of patients with brain metastases and the limited treatment results with the standard treatments available today. A novel and promising treatment modality, electrochemotherapy, which is a combination of the technique of electroporation and the chemotherapeutic drug bleomycin, could be a new treatment option for these patients. This chapter elucidates the background and experience with electrochemotherapy and looks into the possibilities for use in the treatment of primary and secondary brain tumors.

Introduction

In this chapter we will outline the clinical challenges regarding brain metastases, and introduce a novel and upcoming treatment in this field: electrochemotherapy.

Brain Metastases

Metastasis to the brain is an increasing problem for cancer patients today, and in Sweden a doubling of hospital admissions for brain metastases was found from 1987 to 2006 (Smedby et al. 2009). One obvious reason is the generally growing proportion of

M. Linnert • B. Agerholm-Larsen • F. Mahmood
H.K. Iversen • J. Gehl (✉)
Department of Oncology, Copenhagen University Hospital Herlev, 54B1, Herlev Ringvej 75, DK-2730, Herlev, Denmark
e-mail: juge@heh.regionh.dk

M.A. Hayat (ed.), *Tumors of the Central Nervous System, Volume 12*,
DOI 10.1007/978-94-007-7217-5_22,

elderly people in the population leading to an increase in the cancer incidence overall, as the risk of cancer increases with age. Another reason is the overall improvement in cancer treatments today, resulting in longer survival. This leads to an increased risk of patients developing brain metastases during the course of the disease. Also, there are more sensitive diagnostic methods available today, such as MRI that detect multiple brain metastases in 75 % versus 50 % of the cases diagnosed with a CT scan (Kuhn et al. 1994), leading to increased detection of the presence of brain metastases. Finally, there is the blood brain barrier, which may limit penetration of anti-cancer drugs, leading to a limited effect in the treatment of brain metastases in both the adjuvant and the palliative setting.

Electrochemotherapy

Patients with brain metastases have an unfavorable prognosis, and there is need for more efficient treatment options. Electrochemotherapy could be a new option in this setting. Electrochemotherapy is a treatment based on the method of electroporation (Fig. 22.1a). Electroporation is a technique that permeabilizes the cell membrane using electric pulses (see section "Electroporation"). The permeabilized state of the membrane can be exploited for various purposes, for example to gain access to the cytosol for a chemotherapeutic drug or even DNA (Fig. 22.1b, c). Electrochemotherapy is a treatment that until now primarily has been used in the treatment of cutaneous metastases in the palliative treatment setting. Treatment response for smaller cutaneous metastases is reported to be consistently high, with complete response rates (CR) after only one treatment of for example 73 % (Marty et al. 2006) and 91 % of the cases (Heller et al. 1998) (Fig. 22.2). So even if electrochemotherapy is only used in the clinic as a palliative treatment, it is in fact eliminating most of the smaller tumors locally (Fig. 22.3a–c). Experience with larger tumors is underway, and a clinical study of electrochemotherapy as a palliative treatment of large chest wall recurrences from breast cancer has shown promising results (Matthiessen et al. 2012).

To perform electrochemotherapy, it is necessary to apply electric pulses to the tissue via electrodes. The electrodes available up until now have primarily been designed to be used on skin (Fig. 22.2a, b). Different groups are now working at developing electrodes for use in internal organs, and we have in corporation with a medical device company developed an electrode suitable for brain tissue. Indeed, for the initial definition of treatment parameters, important data has been obtained by treating cutaneous metastases. This chapter reviews the basis for electrochemotherapy as well as preliminary results on its use in the brain and lists perspectives for the technology.

Clinical Challenges of Brain Metastases

It is a paradox that general improvement of cancer treatment today is both leading to prolonged survival of cancer patients and to an increased number of patients who live long enough to develop brain metastases. The risk of developing brain metastases increases in breast cancer patients, when there are metastases to the liver, lungs and lymph nodes (Ryberg et al. 2005), i.e. with the advancing stage of the cancer. The treatment of brain metastases are, for single or a limited number of metastases, surgery or stereotactic radiosurgery. For multiple brain metastases the evidence based treatment is whole brain radiation therapy (WBRT) and in some cases systemic chemotherapy or other anti-cancer drugs. Still, the overall prognosis is poor with a reported median survival of 10–12 months after treatment with surgery or stereotactic radiosurgery and a reported median survival of 4–6 months after WBRT (Videtic et al. 2009).

The patient's quality of life is related to their neurocognitive function, which is the ability to do daily activities (ADL), such as recognizing safe and unsafe behavior, memory, and

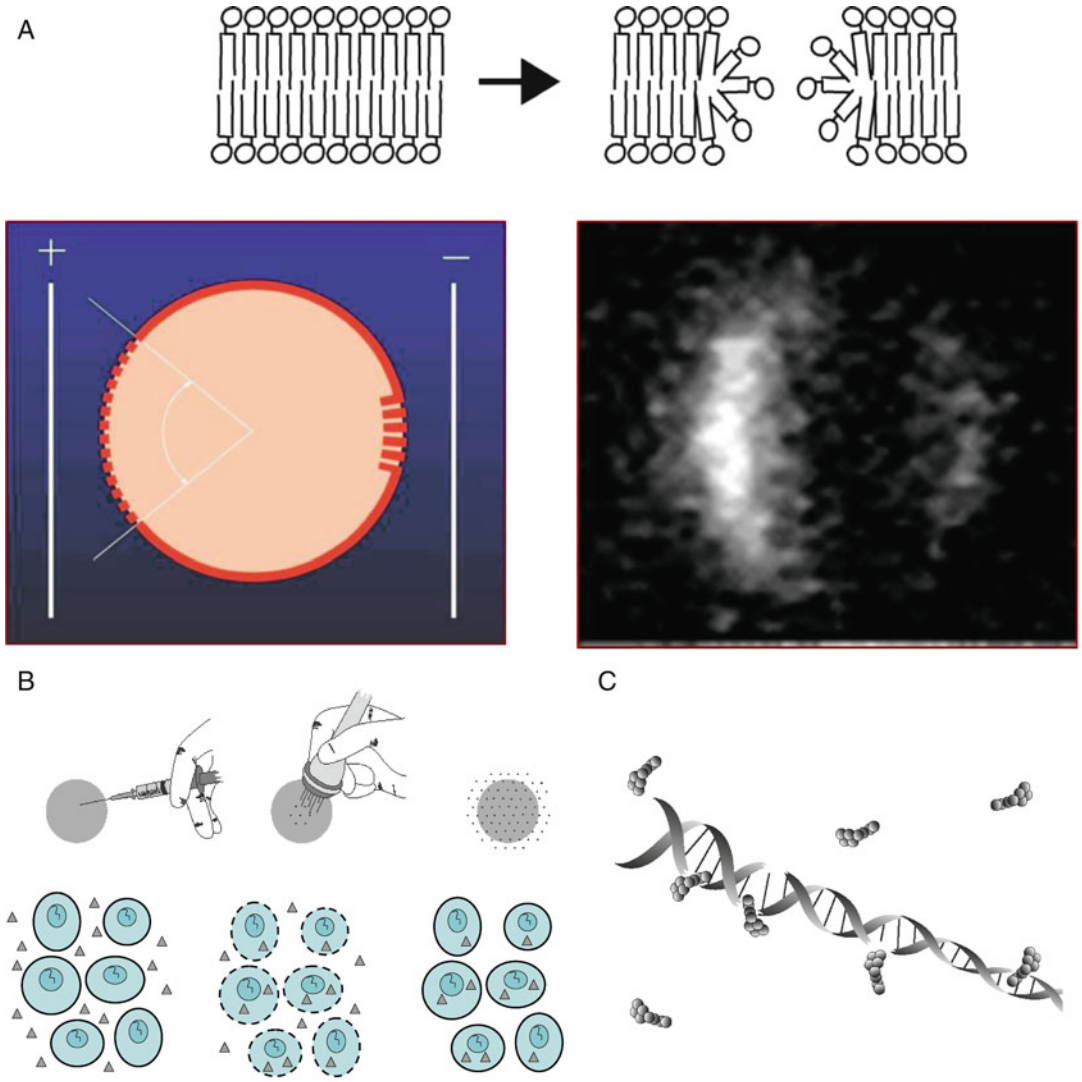

Fig. 22.1 Electroporation (**a**) By application of brief electric pulses it is possible to transiently permeabilise the cell membrane (electroporation). This allows free passage of molecules to the cell cytosol over a matter of minutes. Bleomycin cytotoxicity is augmented over 300-fold when administration is combined with delivery of electric pulses. (**b**) As the electric pulses are subsequently applied, cells are permeabilised and the drug enters. After a few minutes, cells reseal and the extracellular drug is washed out while the internalized molecules remain trapped intracellularly. (**c**) Bleomycin is cytotoxic once in the cytosol and it works by cleaving DNA strands, quantified as 10–15 DNA strand breaks per DNA molecule. Bleomycin induces single-strand and double-strand DNA breaks with a ratio of 10:1

compliance with medical treatments. It has been established, that tumor regression of brain metastases after whole brain radiation therapy (WBRT) is correlated with an increased survival and preservation of neurocognitive function (Li et al. 2007). Another study concluded that the tumor volume before treatment was the only predictor of decreased neurocognitive function (Meyers et al. 2004). Some patients have a better prognosis than others, and several positive prognostic factors have been found, including good performance status, age > 60 years; less than three brain

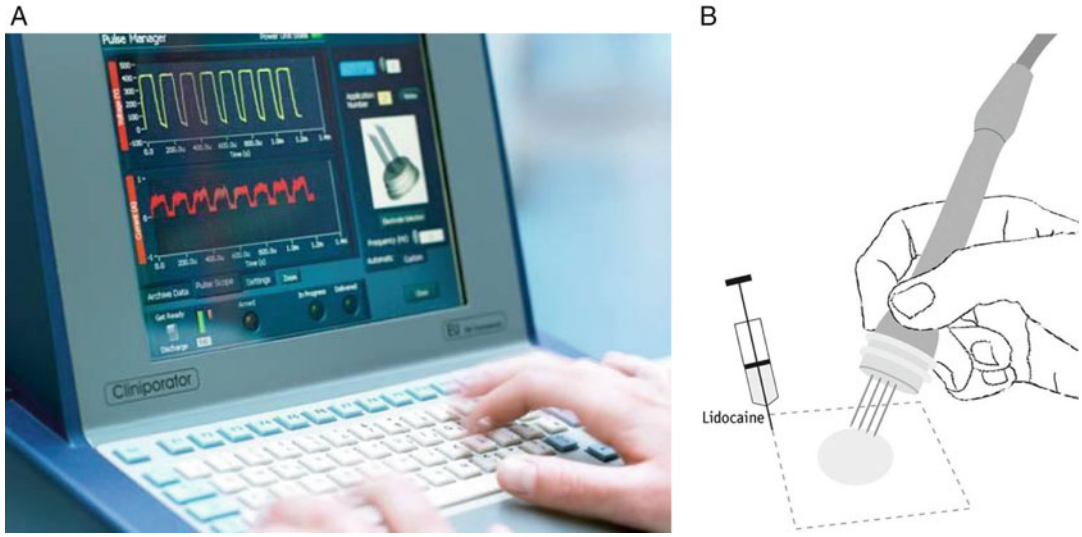

Fig. 22.2 The electrochemotherapy procedure. (**a**) The cliniporator equipment allows monitoring of voltage and current during the pulse. (**b**) The application of pulses to skin tumors must be preceded by local or general anesthesia

metastases and no extracranial metastases (Sperduto et al. 2008). Some cancer histologies also have a better prognosis, for example, in a study of 43 patients with metastatic breast cancer the median survival was 23 months after the diagnosis of brain metastases (Gori et al. 2007). Still, the effect of the available treatments is limited, and when the brain metastases progresses after whole brain radiation therapy, there are no additional standard treatments left to offer for a large number of the patients.

The role of re-irradiation of the whole brain for recurrent/progressive brain metastases is controversial, mainly due to the data on the subject being retrospective and published over a large number of years while the oncological treatments have evolved. These studies of re-irradiation of the brain may therefore have underestimated the toxicity of the treatment and treated different types of patients, with respect to disease status and performance status, which is known to influence patient survival. Response to treatment and median survival differ among the studies, probably reflecting both the difference in radiation doses, patient characteristics and period of time, respectively (AbdelWahab et al. 1997; Cooper et al. 1990; Hazuka and Kinzie 1988; Kurup et al. 1980; Sadikov et al. 2007; Shehata et al. 1974; Wong et al. 1996). The most recent studies indicate that a majority of the patients may benefit from re-irradiation of the brain in the form of complete or partial resolution of symptoms (Cooper et al. 1990; Sadikov et al. 2007; Wong et al. 1996). Opposed to these results is Hazuka et al.'s cohort treated from 1975–1986, where over half the patients failed to respond or deteriorated and 2 patients died from brain necrosis, possibly as a direct consequence of the re-treatment (Hazuka and Kinzie 1988).

Previously, cancer patients died of general disease progression, but today it is not uncommon that the only site of progression is the brain, while the cancer elsewhere in the body is controlled. For example, in the previously mentioned study of 43 breast cancer patients, 60 % of the patients only had disease progression in the brain (Gori et al. 2007). It is therefore increasingly important to prevent brain metastases and explore better treatment options for these patients.

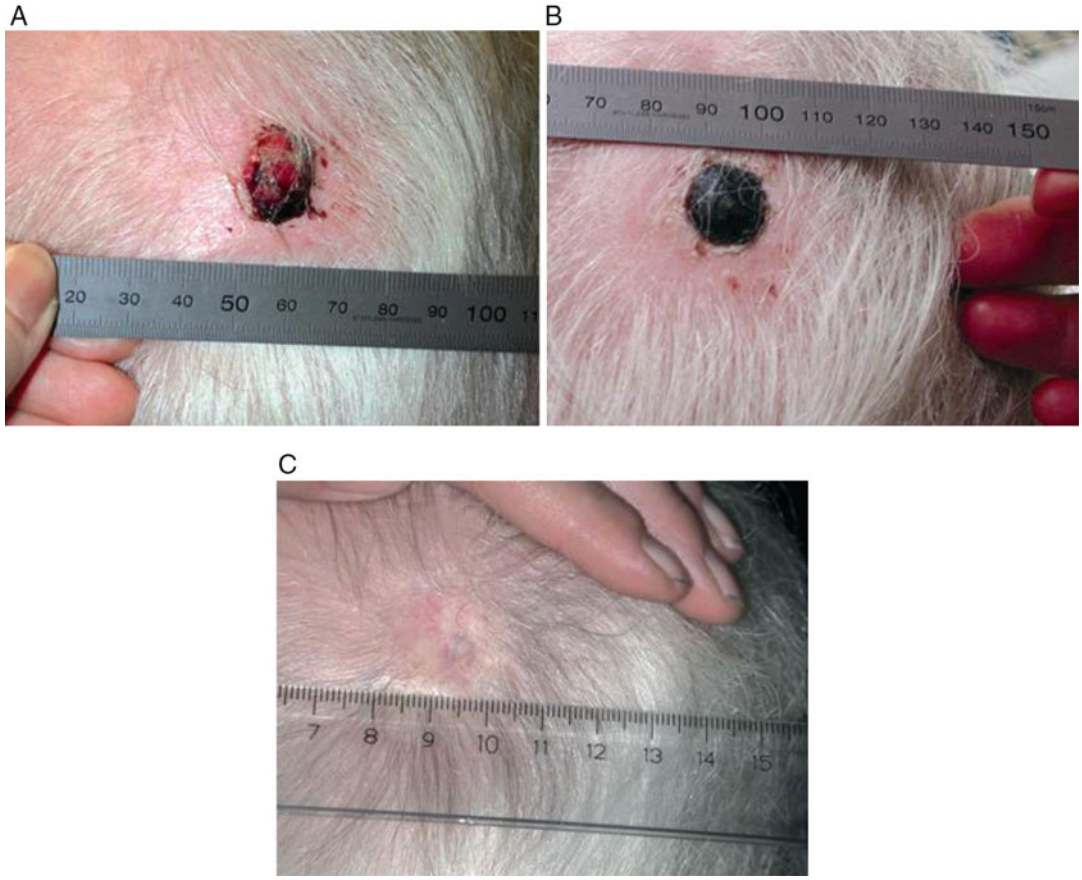

Fig. 22.3 Treatment result of electrochemotherapy in the skin. Course of treatment for patient with malignant melanoma metastases, one of eight treated is shown. The patient was treated with electrochemotherapy in general anaesthesia and intravenous injection of bleomycin. Pictures shows (**a**) Before treatment the metastases was ulcerated and caused haemorrhage, pain and discomfort, (**b**) 1 month after treatment the lesion is covered with a crust, needle marks in normal tis- sue are visible due to treatment of the tumor margin as well. Note that there is no necrosis of normal skin, and (**c**) 6 months after treatment the treated metastases is in CR (complete response) showing normal skin that had healed underneath the nodule (From Gehl, Ugeskrift for laeger, 2005, with permission)

Electroporation

Electroporation (sometimes referred to as electropermeabilization) is basically a technique used to transfer exogenous molecules into cells, by applying a voltage difference across the target tissue. The technique stems from observations made in the 1960s and 1970s showing that cell membranes are made transiently more permeable by the action of voltage pulses thus allowing diffusion of hydrophilic molecules and ions from the extracellular space to the cell cytosol and eventually to the cell nucleus (Gehl 2003). With electroporation a substantial enhancement of transport across cellular membranes can be achieved for certain molecules.

Electroporation and the Transmembrane Potential

The biophysical basis of electroporation is often introduced in terms of the evoked change in the electrical potential across the membrane

(transmembrane potential). The resting transmembrane potential of the cell is mostly between −90 and −70 mV. However, if the cell is exposed to an external voltage difference (electric field), the transmembrane potential is altered. The exact relation between the external electric field and the change in the transmembrane potential is complicated, and for simple practical calculations, approximations are applied.

Two important features need to be emphasized: (1) the transmembrane potential of the cell responds linearly to the electric field strength, e.g. a doubling of the electric field strength doubles the induced change of the transmembrane potential. (2) the change in the transmembrane potential for a given electric field strength, increases linearly with the diameter of (spherical) the cell, implying that it is generally easier to electroporate large cells compared to small cells. Electroporation occurs when the transmembrane potential of the cells in the treated tissue exceeds about 200 mV (Teissie and Rols 1993). If the applied electric field is very strong, producing a transmembrane potential above approximately 1,000 mV, the changes in the membrane phospho-lipid bilayer will be very pronounced, causing what is known as irreversible electroporation, which results in cell death due to prolonged adverse ion concentrations (Hojman et al. 2008). Transient or reversible electroporation is found to last for minutes at physiological temperature, depending on the voltage pulse parameters and tissue type, after which the cells regain their molecular homeostasis (Saulis et al. 1991).

Electroporation Affecting Parameters

The electrode device: To deliver the electric field to the target tissue a mechanical electrode arrangement (electrode device) is used. The size and shape of the electrodes have a large impact on the distribution of the electric field. Two types of electrode devices, the parallel plate electrode device and the needle electrode device, should be mentioned since they are common in clinical applications and commercially available. The parallel plate electrode device consists of two plates (electrodes), typically 1–2 cm^2 each, and delivers the most uniform electric field, however, is applicable only in non-invasive procedures, for example treatment of small prominating tumors. The needle electrode device is available with different numbers of needles (electrodes) arranged in different formations. The needle electrode device, producing a less homogeneous electric field, is typically used to treat subcutaneous tumors because of its ability to penetrate up till about 3 cm tissue at a time.

The pulse parameters: The voltage generator charges the electrodes according to pulse parameters suitable for the particular clinical situation (Fig. 22.2a). The pulse protocols are specified by (1) the number of pulses (in a single treatment), (2) the amplitude of the pulse (voltage), (3) the duration of the pulse and (4) the frequency of the pulses (number of pulses per second). In clinical application only rectangular pulses are considered. In electrochemotherapy a complete treatment session typically consists of 8 pulses delivered as 1 pulse per second (1 Hz), and with pulse duration of 100 milliseconds.

Tissue parameters: Besides the cell diameter, other tissue related parameters may influence electroporation of the target tissue, for example the cellular density of the tissue, the shape of the cells and the general condition of the cells. For example necrotic cells within the treated tissue may distort the electric field distribution, because of local differences in the electric properties (e.g. conductivity) of the tissue. In anisotropic tissue, the efficiency of electroporation may depend on the orientation of the electrodes, since the direction of the electric field is affected by it.

The advantage of electroporation based drug and gene delivery is that by applying the optimal parameters for a given tissue, it is possible to customize delivery of a given drug or gene to a particular region encompassed by the electrodes. In neurological disease, the obvious targets are cancer in the brain (delivery of chemotherapy) and non-viral gene delivery for e.g. Parkinson's disease. Electrodes for use in the brain are described in a subsequent section.

Choice of Chemotherapy

The chemotherapeutic drug of choice in the performance of electrochemotherapy is in our opinion bleomycin. Other chemotherapeutic drugs have been tested regarding the magnitude of enhancement of the cytotoxicity when using electroporation. When testing drugs commonly used in the clinical setting, results show an increase of cytotoxicity by a factor 300–700 for bleomycin (Gehl et al. 1998; Orlowski et al. 1988), a factor 3 and 2.3 for carboplatin and cisplatin, and for the drugs daunorubicin, doxorubicin, etoposide, and paclitaxel no effect of electroporation was found (Gehl et al. 1998). In concordance with this, other results show an enhancement of the cytotoxicity of bleomycin by a factor 5,000, and confirmed a much more limited effect of electroporation when using the drugs carboplatin and cisplatin (Jaroszeski et al. 2000). The next paragraph will clarify the nature of bleomycin, and explain additional reasons why we prefer this drug to others for electrochemotherapy.

Bleomycin

Bleomycin is an antibiotic produced from the fungus Streptomyces verticillus and was discovered by Umezawa et al. in 1966 (Umezawa et al. 1966). It is formed by a mixture of peptides and contains a unique structural component, the bleomycinic acid, and a terminal alkylamine group (Lazo and Chabner 1996). Bleomycin is a hydrophilic and charged molecule with a molecular weight of 1500 Da, and it passes the intact plasma membrane poorly (Poddevin et al. 1991).

Bleomycin is a good chelator of metals and in the presence of oxygen it can bind to ions of iron, cobalt, zinc, and copper. The bleomycin-Fe2+ complex is the most active complex (Gothelf et al. 2003). When bleomycin chelates with iron in the presence of oxygen, a production of free radicals induce DNA breaks and mediate lipid peroxidation (Bokemeyer 2008; Lazo and Chabner 1996). Bleomycin induces single-strand and double-strand DNA breaks with a ratio of 10:1 (Lazo and Chabner 1996). In particular, the double strand breaks and resulting loss of chromosome fragments have a cytotoxic effect. Bleomycin has to be internalized in the cell cytosol to have an effect and the outer cell membrane is the limiting factor (Gothelf et al. 2003). Once in the cell cytosol it will effectuate its toxicity although its way to the cell nucleus is relatively unknown. There are two scenarios depending on how many molecules of bleomycin enter the cell: (i) the cells are arrested in the G2–M phase of the cell cycle and die in approximately three doubling times with low concentration of bleomycin, and (ii) pseudoapoptosis is induced and kills the cell within minutes with high concentrations of bleomycin (Tounekti et al. 2001).

Bleomycin's mechanism of action is effective in all steps of the cell cycle, though cells in G2/M phase are considered more sensitive because the DNA is more accessible in this phase (Mir et al. 1996). Bleomycin is mostly used in the treatment of lymphoma (Hodgkin and non-Hodgkin) and testicular cancer in combination with other antineoplastic drugs (Bokemeyer 2008; Lazo and Chabner 1996). It is also the preferred drug in treating tumors with electrochemotherapy (Gothelf et al. 2003; Heller et al. 1998; Marty et al. 2006). Bleomycin is eliminated from the blood by renal excretion (Mir et al. 1996). The most important toxic reactions affect the lungs and skin, causing pulmonary fibrosis in about 10 %, with a mortality rate of 1 %, and erythema, induration, hyperkeratosis, and peeling of the skin (Lazo and Chabner 1996). The toxicity of bleomycin increases with and is directly related to the cumulative dose received. It should be noted that normally fever occurs 48 h after intravenous drug administration in 25 % of the patients (Lazo and Chabner 1996).

Because electrochemotherapy is a once-only treatment, the doses necessary are not even near the cumulative doses that are reported to cause serious adverse effects. Therefore, the anticipated adverse effects related to bleomycin should be of a mild nature, such as flu-like symptoms and a slight fever. In the treatment of electrochemotherapy bleomycin can be administered both intravenously and intratumorally, and the adverse

effects of course depends on the route of administration. The mentioned adverse effects are seen when bleomycin is administered intravenously. In the next paragraph we will get into the adverse effects seen with intratumoral administration of bleomycin in the brain.

To summarize, bleomycin is the ideal drug for electrochemotherapy as it is very effective once inside the cell, probably because of the ability to induce DNA strand breaks. At the same time bleomycin is a large molecule with less effect on the healthy, non- electroporated cells, where the cell membrane is intact. Bleomycin usually has only few and mild adverse effects in the doses that we use for electrochemotherapy. These facts make bleomycin the drug of choice, when performing a specific and localized cancer treatment with electrochemotherapy.

Clinical Experience with Bleomycin in the Brain

In the preparation for introducing electrochemotherapy to the human brain we have looked in the literature for reported adverse effects of treatment with bleomycin in the brain. Bleomycin has been used in the treatment of brain tumors for more than 30 years. A review of adverse effects of bleomycin as a direct injection into a solid tumor or cyst showed, that only 5 out of 189 patients (3 %) had serious adverse effects and 6 patients (3 %) had moderate adverse effects (Linnert and Gehl 2009). In general, treatment with bleomycin for brain tumors was well tolerated. The most common adverse effects was transient fever in 19 %, headache in 16 %, nausea and vomiting in 10 % and peritumoral edema (swelling and fluid around the tumor) in 4 % of the patients. Fatigue was reported in 5 % of the patients and 3 % (5 patients) had epileptic seizures, out of which two patients already had epilepsy. Five patients had serious adverse effects: 2 patients developed vision loss on one and both eyes respectively; 2 patients had hearing loss and one patient developed generalized brain edema and died. The patient who developed brain edema received an unusually large dose of bleomycin (56 mg) in daily doses over only 8 days. All cases with severe and moderate adverse effects except one were patients with craniopharyngiomas and the adverse effects were probably caused by the tumor localization in the deep brain. In conclusion, bleomycin injection into the brain has been fairly well tolerated at doses much higher than those used for electrochemotherapy.

Concept of Electrochemotherapy

Electrochemotherapy is the electroporation-mediated transfer of antineoplastic drugs to tumors. Electrochemotherapy was invented in the early 1990s proving the potentiation of antitumor effect of chemotherapeutics by applying local electrical pulses. This is a very useful method for delivery of molecules to the cytosol (such as bleomycin) that would otherwise not be able to pass the outer cell membrane. Bleomycin is as mentioned a large, hydrophilic molecule, that passes the cell membrane poorly and there are no cellular uptake mechanisms for bleomycin. Normally the uptake of bleomycin has to depend on diffusion, which limits the efficacy of the drug. However, once inside the cell, bleomycin is a highly effective chemotherapeutic drug that works by inducing DNA strand breakage, quantified as 10–15 DNA strand breaks per DNA molecule (Tounekti et al. 2001). So when bleomycin and electroporation are combined (electrochemotherapy), bleomycin can enter the cell easily, and the cytotoxicity increases over 300-fold (Gehl et al. 1998; Jaroszeski et al. 2000; Orlowski et al. 1988). Because the increase of cytotoxicity is so pronounced, the treatment is successful even in cancer diseases, such as malignant melanoma, where chemotherapy has been abandoned because of a poor response. Electrochemotherapy can also be applied to areas that are previously irradiated (Marty et al. 2006).

Bleomycin can be administered either intravenously or directly into tumor as an injection. The drug enters the cells in sufficient quantities only where the electric pulses are applied and cells are electroporated, hence treatment with electrochemotherapy is always a local treatment

regardless of the method of administration. It has been shown, that electrochemotherapy is very effective in the treatment of cutaneous metastases, where 73–91 % of the tumors show a complete response (CR) after only one treatment (Heller et al. 1998; Marty et al. 2006).

Preclinical Experience with Electrochemotherapy in the Brain

In the early 1990s the first reported initiative was made to explore electrochemotherapy as a treatment modality for brain tumors in a rat model (Salford et al. 1993). Acupuncture needles were used as electrodes to treat rats inoculated with tumor cells with electrochemotherapy, intravenously injected bleomycin being the chemotherapeutic drug. Salford et al. reported an almost double survival time for the electrochemotherapy treated rats than for the bleomycin only treated rats. However, most of the rats given electrochemotherapy (n = 17) had only on average 3–4 days delayed sign of symptoms for late stage tumor growth, and were terminated (n = 15), whereas only a few (n = 2) were without symptoms when terminated, eventually.

Recently electrochemotherapy of primary brain tumors have successfully been performed in an animal model (Agerholm-Larsen et al. 2011). The experimental setup was basically to inoculate rat brains with glial derived tumor cells to obtain primary tumor growth for later once-only electrochemotherapy. The tumor cell line inoculated (Siesjo et al. 1993) was rather potent, and once the tumor appeared at MRI, it would, if untreated, progressively grow for only 2–3 weeks before termination had to be initiated due to tumor size. The tumors, however, in spite of their relative short life time before termination, did show several pathological features similar to human glioblastomas such as palisades and pseudo-palisades.

From the time of initial growth of the primary tumor to the termination of the animal, the tumor size was estimated and/or treatment effects evaluated from in vivo magnetic resonance imaging (MRI). This way, the regression of the tumor could be followed in vivo once the treatment effects (edema and diffuse contrast upload in the target area) had declined within the first week after treatment. The electrochemotherapy was performed with bleomycin, intracranially injected targeting the tumor, and with a newly developed electrode device for electrochemotherapy in soft tissue like the brain, the electrode device being a minor scale of a newly developed electrode device for electrochemotherapy in human brain tissue (Agerholm-Larsen et al. 2011).

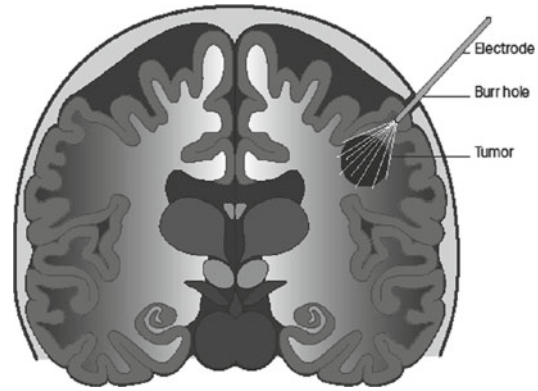

Fig. 22.4 Electrochemotherapy in the human brain. Schematic drawing of the proposed electroporation procedure in the human brain

The results so far have been promising in terms of treatment effect, survival, tolerability of electrochemotherapy and safety issues. For the treatment effect to be 100 % successful the targeted area with the tumor must be permanently eliminated. The preclinical results, however, showed a wide range of steps on the ladder of success, reaching all the way from 50 % to 100 % success of covering the whole tumor leading to either partial or total elimination of the tumor. The data are based on MRI that was used to follow the stages of deterioration of the brain tissue in the targeted area in vivo, and immuno- and histochemical stainings performed in vitro to provide information of necrotic tissue, remains of tumor cells, and effect on neurons and glial cells in the targeted area (Fig. 22.4).

The data in summary were, that necrotic tissue was obtained in brain areas targeted with nce-only electrochemotherapy and clearly distinguishable

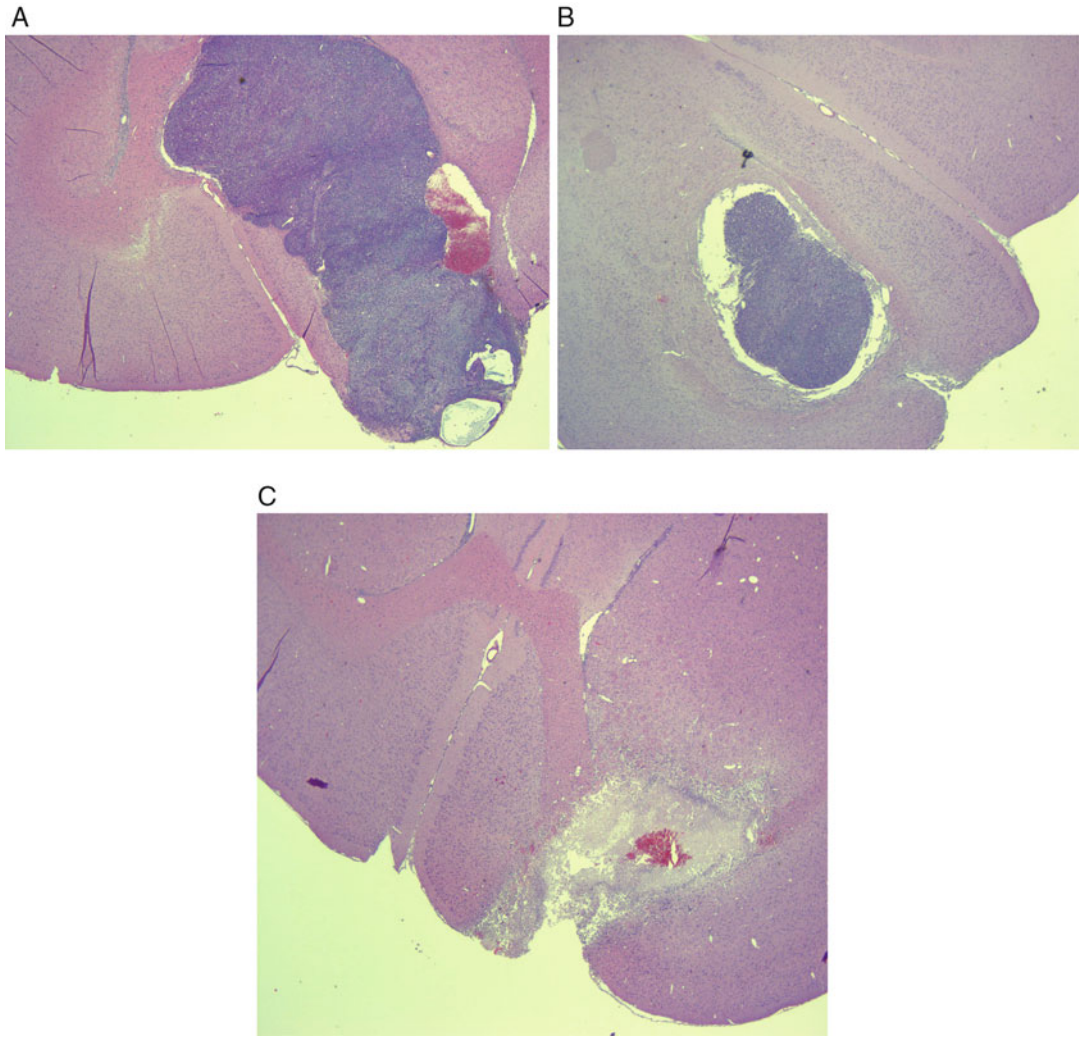

Fig. 22.5 Preclinical treatment results. Rat brain tissue (coronal slices) stained with H&E. All treatment modalities took place 2 weeks after inoculation of tumor cells, and all rats were terminated 1 week after treatment. (**a**) Rat brain treated with electroporation, (**b**) Rat brain treated with bleomycin, (**c**) Rat brain treated with electrochemotherapy

from the controls, where almost no effects were observed in brain areas targeted with bleomycin or electroporation only (Fig. 22.5a–c). These data suggest that bleomycin may be taken up by the tumor cells due to the transient permeabilization of the cell membrane caused by electroporation, and that neither bleomycin nor electroporation alone can cause elimination of a tumor in this animal model. These preclinical data reflect promising preliminary results with the potentials of improvements of success. That is in the animal model the tumor is accessed by electrodes deployed through the burr hole already made for inoculation of the tumor cells. In the clinic brain scans exposing the tumor position will be matched to stereotaxic coordinates to ensure that a burr hole or craniotomy is positioned optimally for treatment. Rats undergoing electrochemotherapy have successfully been followed up until 8 weeks after treatment before termination, showing no obvious sign of basic malfunction either physically or mentally.

Electrochemotherapy in the Human Brain

Electrochemotherapy has been performed in a variety of different tissues, but mostly skin and other easily accessible tissue. Because of advances in electrode technology, it is now possible to pursue this treatment modality in other types of tissue. We have developed an electrode especially suited for use in the brain, which we find to be a suitable target organ for several reasons. Electrochemotherapy is known to be a treatment that is quick, effective, localized and relatively lenient to adjacent healthy tissue. These qualities make electrochemotherapy a new and interesting treatment modality in the brain, where it is very important, that the malignant cells are killed effectively at the same time as the healthy neurons are spared to the greatest extent possible.

In our research group we have run a clinical trial, where brain metastases were treated as a palliative treatment with electrochemotherapy using bleomycin and the novel brain electrode (www.clinicaltrials.gov NTC 01322100). The treatment was performed with the patient in general anesthesia as a once-only procedure (Fig. 22.4). A neurosurgeon was planning the treatment from an MRI of the brain and use stereotactic equipment to guide the brain electrode into the tumor through a burr hole. Endpoints of the study were safety and efficacy evaluated by MRI. The first patient in the study has been treated successfully, and no related adverse events have been observed in the 6 weeks of follow up. Follow up was shortened due to disease progression, so evaluation of response was not possible according to protocol, but we are able to conclude that treatment in the brain with electrochemotherapy is technically feasible. The clinical trial was open for more than 2 years and was closed due to slow patient accrual, so this patient was the only one treated in this protocol.

The Blood–Brain Barrier

The blood brain barrier (BBB) is made of non-fenestrated endothelial cells, which makes it highly impermeable, only allowing passage of small, hydrophobic and uncharged molecules such as water. The endothelial cells are held together by tight junctions in the blood vasculature throughout the brain. Therefore, the BBB often keep anti-cancer drugs from penetrating into the brain tissue. The BBB is disrupted in different degrees by pathological processes, for instance after a stroke, a malignant brain tumor, infection or trauma. After whole brain radiation therapy (WBRT) the BBB is also under continuous break down for weeks to months (De Angelis and Yahalom 1993). The patients in the current trial will have both a pathological process in the form of brain metastases and will have received WBRT as first line treatment, so both factors will influence the BBB integrity. Additionally, deployment of electrodes and electroporation of the brain tissue may lead to increased permeability.

Another perspective of using electrochemotherapy in the brain could be to treat the margins of a primary brain tumor after surgical removal of the bulk of the tumor. Previous studies have pointed out, that it is very important to treat the well-vascularized, actively proliferating, infiltrating edge of the tumor with anti-cancer drugs, but problematic due to the intact BBB. In contrast, it is easier to treat the central, leaky and hypoxic part with anti-cancer drugs. This problem is termed the sink effect and can be the reason for chemotherapy failure in the brain (Neuwelt 2004). Thus, in electrochemotherapy, drug delivery and precision of the expansion of the electric field are key elements. Using electrochemotherapy for treatment of the margins could be suitable for infiltrating tumors such as glioblastoma multiforme and is an important priority in our future research. Lastly, a new perspective of shifting the chemotherapeutic drug for calcium could be a possibility. Recent preclinical research has shown effective tumor kill in mice using intratumoral calcium and electroporation, possibly by triggering apoptotic signals as well as depleting ATP in the tumor cells (Frandsen et al. 2012).

In conclusion, because patients with brain cancer generally have an unfavorable prognosis, there is a need for better treatment options. Electrochemotherapy is a good candidate because

it is a quick, once-only and effective treatment that may also be applied to previously irradiated tissue. Preclinical studies show, that electrochemotherapy can be effective and tolerable in rat brain. Additionally, this treatment modality is relatively lenient to adjacent healthy tissue and should be able to overcome the problems of the blood–brain barrier. Results from our clinical trial showed that the treatment procedure was tehcnically feasible and the patient had no related serious adverse events. Unfortunately, the clinical trial was closed due to slow patient accrual, but more clinical studies may be underway, revealing future implications of electrochemotherapy in the treatment of brain cancer.

References

AbdelWahab MMR, Wolfson AH, Raub W, Landy H, Feun L, Sridhar K, Brandon AH, Mahood S, Markoe AM (1997) The role of hyperfractionated re-irradiation in metastatic brain disease – a single institutional trial. Am J Clin Oncol 20:158–160

Agerholm-Larsen B, Iversen HK, Ibsen P, Moller JM, Mahmood F, Jensen KS, Gehl J (2011) Preclinical validation of electrochemotherapy as an effective treatment for brain tumors. Cancer Res 71:3753–3762

Bokemeyer C (2008) Bleomycin in testicular cancer: will pharmacogenomics improve treatment regimens? J Clin Oncol 26:1783–1785

Cooper JS, Steinfeld AD, Lerch IA (1990) Cerebral metastases – value of reirradiation in selected patients. Radiology 174:883–885

De Angelis LM, Yahalom J (1993) Lymphomas. In: De Vita V, Hellmann S, Rosenberg S (eds) Cancer, principles and practice of oncology, 5th edn. Lippincott-Raven Publishers, Philadelphia, p 2237

Frandsen SK, Gissel H, Hojman P, Tramm T, Eriksen J, Gehl J (2012) Direct therapeutic applications of calcium electroporation to effectively induce tumor necrosis. Cancer Res 72:1336–1341

Gehl J (2003) Electroporation: theory and methods, perspectives for drug delivery, gene therapy and research. Acta Physiol Scand 177:437–447

Gehl J, Skovsgaard T, Mir LM (1998) Enhancement of cytotoxicity by electropermeabilization: an improved method for screening drugs. Anticancer Drugs 9:319–325

Gori S, Rimondini S, De Angelis V, Colozza M, Bisagni G, Moretti G, Sidoni A, Basurto C, Aristei C, Anastasi P, Crino L (2007) Central nervous system metastases in HER-2-positive metastatic breast cancer patients treated with trastuzumab: incidence, survival, and risk factors. Oncologist 12:766–773

Gothelf A, Mir LM, Gehl J (2003) Electrochemotherapy: results of cancer treatment using enhanced delivery of bleomycin by electroporation. Cancer Treat Rev 29:371–387

Hazuka MB, Kinzie JJ (1988) Brain metastases – results and effects of re-irradiation. Int J Radiat Oncol Biol Phys 15:433–437

Heller R, Jaroszeski MJ, Reintgen DS, Puleo CA, DeConti RC, Gilbert RA, Glass LF (1998) Treatment of cutaneous and subcutaneous tumors with electrochemotherapy using intralesional bleomycin. Cancer 83:148–157

Hojman P, Gissel H, Andre FM, Cournil-Henrionnet C, Eriksen J, Gehl J, Mir LM (2008) Physiological effects of high- and Low-voltage pulse combinations for gene electrotransfer in muscle. Hum Gene Ther 19:1249–1260

Jaroszeski MJ, Dang V, Pottinger C, Hickey J, Gilbert R, Heller R (2000) Toxicity of anticancer agents mediated by electroporation in vitro. Anticancer Drugs 11:201–208

Kuhn MJ, Hammer GM, Swenson LC, Youssef HT, Gleason TJ (1994) Mri evaluation Op solitary brain metastases with triple-dose gadoteridol – comparison with contrast-enhanced Ct and conventional-dose gadopentetate dimeglumine Mri studies in the same patients. Comput Med Imaging Graph 18:391–399

Kurup P, Reddy S, Hendrickson FR (1980) Results of re-irradiation for cerebral metastases. Cancer 46:2587–2589

Lazo J, Chabner B (1996) Bleomycin. In: Cancer chemotherapy and biotherapy, 2nd edn. Lippincott-Raven Publishers, Philadelphia, pp 379–393

Li J, Bentzen SM, Renschler M, Mehta MP (2007) Regression after whole-brain radiation therapy for brain metastases correlates with survival and improved neurocognitive function. J Clin Oncol 25:1260–1266

Linnert M, Gehl J (2009) Bleomycin treatment of brain tumors: an evaluation. Anticancer Drugs 20:157–164

Marty M, Sersa G, Garbay JR, Gehl J, Collins CG, Snoj M, Billard V, Geertsen PF, Larkin JO, Miklavcic D, Pavlovic I, Paulin-Kosir SM, Cemazar M, Morsli N, Rudolf Z, Robert C, O'Sullivan GC, Mir LM (2006) Electrochemotherapy – an easy, highly effective and safe treatment of cutaneous and subcutaneous metastases: results of ESOPE (European Standard Operating Procedures of Electrochemotherapy) study. EJC Supplements 4:3–13

Matthiessen LW, Johannesen HH, Hendel HW, Moss T, Kamby C, Gehl J (2012) Electrochemotherapyfor large cutaneous recurrence of breast cancer: a phase II clinical trial. Acta Oncol 51:713–721

Meyers CA, Smith JA, Bezjak A, Mehta MP, Liebmann J, Illidge T, Kunkler I, Caudrelier JM, Eisenberg PD, Meerwaldt J, Siemers R, Carrie C, Gaspar LE, Curran W, Phan SC, Miller RA, Renschler MF (2004) Neurocognitive function and progression in patients with brain metastases treated with whole-brain radiation and motexafin gadolinium: results of a randomized phase III trial. J Clin Oncol 22:157–165

Mir LM, Tounekti O, Orlowski S (1996) Bleomycin: revival of an old drug. Gen Pharmacol 27:745–748

Neuwelt EA (2004) Mechanisms of disease: the blood-brain barrier. Neurosurgery 54:131–140

Orlowski S, Belehradek J Jr, Paoletti C, Mir LM (1988) Transient electropermeabilization of cells in culture. Increase of the cytotoxicity of anticancer drugs. Biochem Pharmacol 37:4727–4733

Poddevin B, Orlowski S, Belehradek J, Mir LM (1991) Very high cytotoxicity of bleomycin introduced into the cytosol of cells in culture. Biochem Pharmacol 42:S67–S75

Ryberg M, Nielsen D, Osterlind K, Andersen PK, Skovsgaard T, Dombernowsky P (2005) Predictors of central nervous system metastasis in patients with metastatic breast cancer. A competing risk analysis of 579 patients treated with epirubicin-based chemotherapy. Breast Cancer Res Treat 91:217–225

Sadikov E, Bezjak A, Yi QL, Wells W, Dawson L, Millar BA, Laperriere N (2007) Value of whole brain re-irradiation for brain metastases – single centre experience. Clin Oncol 19:532–538

Salford LG, Persson BR, Brun A, Ceberg CP, Kongstad PC, Mir LM (1993) A new brain tumour therapy combining bleomycin with in vivo electropermeabilization. Biochem Biophys Res Commun 194:938–943

Saulis G, Venslauskas MS, Naktinis J (1991) Kinetics of pore resealing in cell-membranes after electroporation. Bioelectrochem Bioenerg 26:1–13

Shehata WM, Hendrick FR, Hindo WA (1974) Rapid fractionation technique and retreatment of cerebral metastases by irradiation. Cancer 34:257–261

Siesjo P, Visse E, Lindvall M, Salford L, Sjogren HO (1993) Immunization with mutagen-treated (tum-) cells causes rejection of nonimmunogenic rat glioma isografts. Cancer Immunol Immunother 37:67–74

Smedby KE, Brandt L, Backlund ML, Blomqvist P (2009) Brain metastases admissions in Sweden between 1987 and 2006. Br J Cancer 101:1919–1924

Sperduto PW, Berkey B, Gaspar LE, Mehta M, Curran W (2008) A new prognostic index and comparison to three other indices for patients with brain metastases: an analysis of 1,960 patients in the RTOG database. Int J Radiat Oncol Biol Phys 70:510–514

Teissie J, Rols MP (1993) An experimental evaluation of the critical potential difference inducing cell-membrane electropermeabilization. Biophys J 65:409–413

Tounekti O, Kenani A, Foray N, Orlowski S, Mir LM (2001) The ratio of single- to double-strand DNA breaks and their absolute values determine cell death pathway. Br J Cancer 84:1272–1279

Umezawa H, Maeda K, Takeuchi T, Okami Y (1966) New antibiotics, bleomycin A and B. J Antibiot (Tokyo) 19:200–209

Videtic GM, Gaspar LE, Aref AM, Germano IM, Goldsmith BJ, Imperato JP, Marcus KJ, McDermott MW, McDonald MW, Patchell RA, Robins HI, Rogers CL, Suh JH, Wolfson AH, Wippold FJ (2009) American college of radiology appropriateness criteria on multiple brain metastases. Int J Radiat Oncol Biol Phys 75:961–965

Wong WW, Schild SE, Sawyer TE, Shaw EG (1996) Analysis of outcome in patients reirradiated for brain metastases. Int J Radiat Oncol Biol Phys 34:585–590

Comparison of Navigated Transcranial Magnetic Stimulation to Direct Electrical Stimulation for Mapping the Motor Cortex Prior to Brain Tumor Resection

23

Satoshi Takahashi and Thomas Picht

Contents

Abstract

There are two main indications for mapping of the motor cortex in patients eligible for surgery with rolandic tumors. First, mapping is indicated if the functional anatomy (i.e. the exact spatial relationship between the tumor and the presumed essential motor areas) remains unclear after anatomical imaging. The reasons for this can be the mass effect of the tumor or infiltrative growth. Second, mapping is indicated if there is a discrepancy between the imaging results and the clinical findings (for example, a large tumor within the primary motor cortex but no noticeable motor deficits). In such cases, the functional anatomy may have changed due to tumor-induced plasticity. In either of these two scenarios (which may occur separately or together), motor mapping provides elucidation of the functional anatomy and the state of the motor system. This chapter presents an overview of the possibilities and limitations of transcranial magnetic stimulation (TMS) and direct electrical stimulation (DES) for mapping of the cortical motor topography in the neurosurgical setting. The intriguing feature of TMS is that it is the only painless non-invasive method that allows for direct electrical stimulation of the brain. Findings in basic research have recently been backed up by current studies that TMS is a relevant tool for performing stimulation mapping procedures, which were previously only possible with direct electrical

S. Takahashi • T. Picht (✉)
Department of Neurosurgery, Charite-University Medicine, Campus Virchow Klinikum, Augustenburger Platz 1, Berlin, Germany
e-mail: Thomas.picht@charite.de

M.A. Hayat (ed.), *Tumors of the Central Nervous System, Volume 12*,
DOI 10.1007/978-94-007-7217-5_23, © Springer Science+Business Media Dordrecht 2014

stimulation of the brain during surgery. All relevant studies comparing TMS to DES for mapping of the motor cortex are summarized and commented in this chapter.

Introduction

When a patient has a brain tumor in or near the motor cortex, the neurosurgeon's goal is to maximize the extent of tumor resection, without causing any new functional deficits. Achieving both of these goals simultaneously can be challenging, especially if the tumor is close to essential functional areas of the motor cortex. To achieve both these goals, the surgeon needs precise knowledge of which areas of the brain are functionally essential versus which areas are not essential and can be safely resected. Unfortunately, the functional relevance of tissue in an individual case cannot be predicted from standard anatomical landmarks, not only because of natural anatomical variation between all people, but even more importantly because the tumor mass can displace and/or obscure the familiar anatomical landmarks, and also because the tumor can induce plastic reorganization of the brain's functional areas, especially in the case of slow-growing tumors. So in order to achieve maximal tumor removal without causing functional deficits, it is essential to have case-specific knowledge of the location of functionally essential areas. Intraoperative functional testing of the brain tissue surrounding the tumor is the most accurate and reliable way to obtain this knowledge, but there are many advantages to obtaining such functional maps also *before* the surgery starts.

In the past, intraoperative direct electrical stimulation (DES) of brain tissue was the only modality available for brain mapping. In recent decades, much effort has been spent on developing various technologies for non-invasive pre-operative brain mapping (Picht and Atalay 2012). One of the more promising modalities that has been developed is transcranial magnetic stimulation (TMS). Compared to all other modalities of pre-operative cortical mapping, TMS has the unique advantage that like DES it stimulates the brain and then records the motor output, rather than asking the patient to move, recording the brain activation, and then trying to interpret which cortical areas were essential for that movement. TMS works by holding a wire coil just above the patient's head near the motor cortex and then sending a brief electric current through that wire coil. The electric current generates a corresponding magnetic field, as electricity always does, and this magnetic field passes through the patient's skull. Inside the skull, this magnetic field then again creates an electric flow of ions which can depolarize the patient's neurons and lead to nerve signals in that part of the brain. TMS has been available for more than 20 years already. In the early years of TMS, it was not really possible to accurately know the anatomical location of the stimulus, because the wire stimulation coil was held freehand according to anatomical landmarks, which vary between individuals (Krings et al. 1997). To overcome this problem, TMS has been refined by combining it with neuronavigation systems: "navigated TMS", (nTMS) (Krings et al. 1997; Picht et al. 2009). This has made it possible to electrically stimulate precise areas of the brain with navigational targeting, thus achieving spatially accurate brain mapping pre-operatively (Picht et al. 2011a).

The main purpose of the present book chapter is to review previous reports assessing the spatial accuracy of nTMS by comparing it to the gold standard of DES, and also to summarize the advantages and disadvantages of nTMS. We begin with a general overview of the basic principles of DES and TMS. Next we summarize the literature on the safety and risks of TMS. Then we review the literature on the spatial accuracy of nTMS compared to DES, and we also discuss the limitations of such comparisons. Finally, we will discuss the role of nTMS in pre-operative mapping of motor areas.

Direct Electrical Stimulation: The Gold Standard of Cortical Mapping

For almost a century, applying an electrical current directly to the brain either by means of handheld electrodes or by implanted grids of electrodes

has been the only reliable method for identification of brain areas carrying essential motor function. Clinically, direct electrical stimulation (DES) is still considered to be the "gold standard" for functional mapping of the primary motor cortex (Picht et al. 2011a), since it enables more extensive tumor resection at a lower rate of severe neurological sequela (De Witt Hamer et al. 2012). Current understanding of functional brain topography and connectivity is based on DES findings. And DES is still the only modality that enables cortical and subcortical localization of motor function intra-operatively with absolute spatial accuracy.

The basic principle of DES is to apply an electrical impulse to the brain cortex and record the muscle output. Technically, there are two different ways to do this: monopolar DES and bipolar DES (Kombos and Suss 2009). Comparing bipolar DES to monopolar DES neurophysiologically, it has been demonstrated that stimulation with a bipolar probe was very effective in producing localized current flows; whereas, a monopolar probe at the same stimulation level produced higher current densities and stimulated a larger region of the cortex. The stimulation parameters also differ significantly between the two methods. For monopolar stimulation, the frequency typically varies between 250 and 500 Hz, the pulse width is 0.2–0.7 ms, and the number of pulses in a stimulation train between two and seven, which leads to a stimulation time of 4–28 ms. For bipolar stimulation, the frequency is typically 50 Hz or 60 Hz, the pulse width is 0.2–0.7 ms, and the number of pulses in a train varies between 50 and 200, which leads to a total stimulation time of 1–4 s (Penfield and Boldrey 1937; Taniguchi et al. 1993). These variations lead to marked differences in the net amount of charge applied to the cortex. In addition to these differences of charge applied per time and net amount of charge, several other factors influence the results of the stimulation: the shape of the electrode tips, the type of stimulator used, and the way the electrodes are handled (e.g., pressured onto the cortex/light touch; lots of irrigation/dry field).

In the clinical setting of neurosurgery today, intraoperative DES in patients with brain lesions in or near the motor cortex enables neurosurgeons to identify both cortical and subcortical motor pathways during surgeries (Sanai and Berger 2010). Although many neurosurgeons are aware that DES improves surgeries of brain lesions such as gliomas in or near the motor cortex, there are only a few studies that actually provide scientific evidence of this (De Witt Hamer et al. 2012; Duffau et al. 2005). In 2012, De Witt Hamer et al. reported a meta-analysis of observational studies with 8091 adults patients in an attempt to elucidate the usefulness of intraoperative DES for rolandic infiltrative glioma surgeries (De Witt Hamer et al. 2012). The percentage of gross total resections was higher with intraoperative DES (75 %) than without it (58 %). And the rate of severe neurologic deficits was lower with DES (3.4 %) than without it (8.2 %). That study provides level-one evidence that intraoperative DES make a substantial improvement in outcomes from resecting gliomas in or near the motor cortex, so DES should always be used for such surgeries.

The major drawback of DES is its invasiveness. This restricts its clinical application to the intraoperative situation and largely limits its research usage to mapping that is clinically necessary anyway. The limited understanding of spatial accuracy of the method and evoked current spread into the brain tissue can make interpretation of DES results difficult and in part dependent on the individual team's experience. Induction of epileptic seizures is a possible problem, especially for bipolar DES (Kombos et al. 1999). Yet, the likelihood depends on the exact stimulation parameters and the susceptibility of the individual brain. It is reported that stimulation-associated seizures occur in 1.2 % of patients stimulated with the monopolar technique and in 9.5 % of patients with the bipolar technique (Szelenyi et al. 2007). Bipolar stimulation can also lead to activating several muscles and thus to movement of the patient's extremities; it is therefore unsuitable for monitoring (Kombos et al. 1999). Thus even though DES is the gold standard, its usage is limited to what is clinically necessary during the restricted time period of the operation.

Basic Principles of Navigated Transcranial Magnetic Stimulation

Transcranial magnetic stimulation (TMS) is a technique for noninvasive and painless stimulation of the human brain. The stimulation of the brain is produced by passing a brief electric current through a wire coil held outside the skull. This electric current simultaneously creates a corresponding brief, high-intensity magnetic field, which passes through the skull. The induced electrical field then creates movements of electrically charged ions inside the brain tissue. Depending on the strength of this electrical current and local tissue factors, this can lead to depolarization of neurons, thus to neural signals. If the TMS stimulation coil is placed above the motor cortex, the stimulation can lead to muscle movements, which can be recorded with a standard EMG. The stimulation coil can have different shapes and the parameters of the electric current can also be varied.

TMS was first introduced into clinical practice in 1985 (Barker et al. 1985). But for many years, basic TMS was not much benefit for planning neurosurgery, because the locations stimulated could only be guessed from neuroanatomical landmarks, which was not sufficiently accurate for neurosurgical purposes. In recent years though, neuronavigational systems have been integrated together with TMS. This navigated TMS (nTMS) enables the examiner to see quite precisely on an uploaded MRI where the TMS stimulation is being applied, thus allowing us now to map the motor cortex of patients.

While the basic TMS technology used in neurosurgery is still the same, an important aspect of TMS must be understood to make the method useful: namely, the operator needs to accurately know the location of the maximum electric-field, induced by the magnetic impulse. The best assumption of the location of neuronal activation can be achieved when the electric field evoked by stimulation is displayed in the navigation system. It is important to point out that the primary magnetic field from the coil is not influenced by any tissue variations. In order to calculate the resulting electric field precisely for every intracranial location, several factors must be known: the exact specifications of the coil and the electrical characteristics of the stimulator, the size and shape of the extracranial and intracranial anatomy, and the exact location of the coil with respect to the head in all 6° of freedom (Ruohonen and Karhu 2010). Due to the spherical shape of the head, the absolute value of the electrical conductivity of the respective tissue is of secondary importance when calculating the e-field, when spherical head models are used (Ruohonen and Ilmoniemi 2005).

Yet knowing where the maximum electric field is acting does not necessarily mean that the neuronal activation also takes place at this point. The cortical neuronal structures are most sensitive to depolarization when the induced current is oriented longitudinally to the axons (Day et al. 1989). This means that the threshold for activation of the motor cortex is lowest when the coil is orientated perpendicular to the nearest underlying sulcus, due to the columnar structure of the cortical histological architecture. Thus the initiation of action potentials will most likely appear in the area where the e-field is optimally oriented to the cortex, which is not necessarily where the e-field is at its maximum.

These improvements of the TMS technology in combination with standard EMG recordings have enabled accurate mapping of the motor cortex with delineation of individual muscle representations in healthy subjects (Hannula et al. 2005; Schmidt et al. 2009) and in patients with brain tumors and obscured anatomy (Krieg et al. 2012b; Picht et al. 2011a). Figure 23.1 shows a typical example of a TMS motor mapping in a case of a rolandic tumor and obscured anatomy of the central region. The 3D navigational view shows the results after TMS mapping have been performed. In the left panel of Fig. 23.1 all spots stimulated on the left hemisphere are displayed. The relevant area adjacent to the tumor has been stimulated in a dense raster. The premotor cortices have also been stimulated. In the right panel, the image displays only the spots where a muscle response was observed (MEP > 50 μV peak-to-peak amplitude). Three different hand muscles (abductor pollicis brevis, abductor digiti minimi,

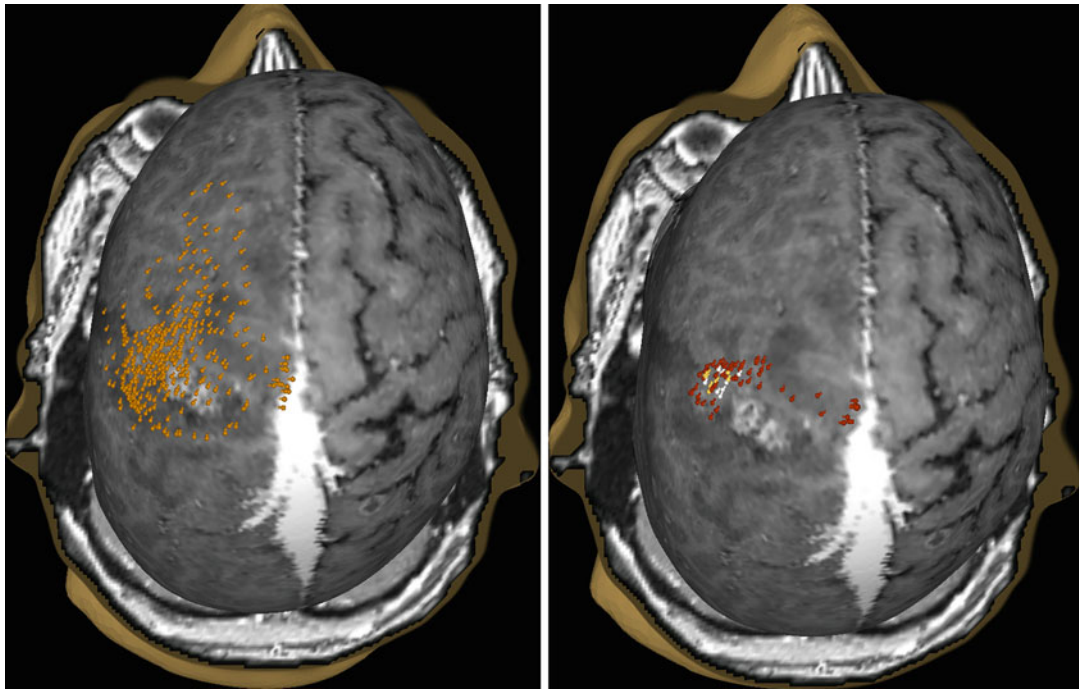

Fig. 23.1 Example of an nTMS mapping, performed on a 63 year-old female patient with a left hemisphere brain tumor, suffering from a mild hemiparesis on her right side. In the *left panel*, all spots stimulated on the left hemisphere are displayed. In the *right panel*, the image displays only the spots where a muscle response was observed (MEP > 50 μV peak-to-peak amplitude). Three different hand muscles (abductor pollicis brevis, abductor digiti minimi, first dorsal interosseus) and one leg muscle (tibialis anterior) were recorded in this case. The color coding corresponds to the intensity of the response, whereby *red* indicates small responses (MEP 50–500 μV), *yellow* indicates medium responses (MEP 500–1,000 μV), and *white* indicates large responses (MEP > 1,000 μV)

first dorsal interosseus) and one leg muscle (tibialis anterior) were recorded in this case. The color coding corresponds to the intensity of the response, whereby red indicates small responses (MEP 50–500 μV), yellow indicates medium responses (MEP 500–1,000 μV), and white indicates large responses (MEP > 1,000 μV). The responses close to the midline are from the leg (TA). This mapping makes it evident that the precentral gyrus has been displaced frontally.

Overview of the Safety and Risks of Transcranial Magnetic Stimulation

When thinking about the safety and risks of transcranial magnetic stimulation, we should recognize that there are different types of TMS: single-pulse TMS, paired-pulse TMS, and repetitive TMS (rTMS). The influence of the magnetic field from these three different types of TMS procedures differs greatly, and thus they have different safety profiles. The modality used for mapping the motor cortex in patients with brain tumors is single-pulse TMS, in which the electro-magnetic influence is the lowest of the three different types of TMS. Generally, single-pulse TMS is considered to have no significant risk from its more than 20 years of clinical experience (Rossi et al. 2009; Groppa et al. 2012). Nonetheless, it is recommended to use a short safety checklist such as a questionnaire developed by "The Safety of TMS Consensus Group" (Rossi et al. 2011) to identify patients with increased risk for performing TMS such as patients with a history of loss of consciousness due to seizures or syncope, brain diseases or medications associated with increased seizure risk, the presence

of implanted metallic devices, and pregnancy (Groppa et al. 2012).

In general, TMS has some direct safety concerns such as heating and magnetic field exposure (Rossi et al. 2009). The heating effects to the brain induced by a single-pulse TMS is estimated to be less than 0.1° Celsius (Ruohonen and Ilmoniemi 2002). As for magnetic field exposure, its exposure to both patients and operators should be taken into account. Magnetic field exposure induced by single-pulse TMS to patients seems not to cause a significant risk, since the total time of exposure is so short, but the potential risk of long-term adverse consequences for TMS operators has not yet been adequately studied (Rossi et al. 2009).

TMS has also several known potential adverse events (Rossi et al. 2009). The adverse events can be divided into two subgroups: (1) adverse events reported both in single-pulse TMS and paired-pulse or rTMS and (2) adverse events reported only in paired-pulse and/or rTMS but not in single-pulse TMS. The former subgroup includes events such as seizure induction, syncope, transient headache, local pain, neck pain, toothache, paresthesia, and transient auditory threshold changes. The latter subgroup contains events such as transient cognitive/neuropsychological changes, induced currents in electrical circuits of medical devices, structural brain changes, histotoxicity, and other transient biological effects such as hormonal change (Rossi et al. 2009). The latter set of adverse events only from paired-pulse or rTMS will not be discussed further here in this chapter about single-pulse TMS.

Induction of seizures is the most severe acute adverse effect for TMS, but most TMS-associated seizures were induced during repetitive TMS (Rossi et al. 2009). Less than 5 % of all the reported TMS-related seizures occurred during single-pulse TMS (Groppa et al. 2012), but this only provides a rough approximation, since it remains unknown what percent of all TMS usage is repetitive TMS. The exact incidence of seizures after single-pulse TMS is not known. Of course this rate should not be underestimated, but it seems to be very low. The question of "what percentage of single-pulse TMS sessions result in a seizure", is a very important issue for patient counseling and safety. Since the literature lacks firm answers, it should be investigated with large-scale multi-institutional studies in the near future. In most cases, single-pulse TMS-related seizures occurred in patients with known structural brain pathology or patients under medication such as amphetamines, lithium, and chlorpromazine, which can lower the seizure threshold (Groppa et al. 2012). Nonetheless, seizures can occur in patients without known risk factors. For example, Kratz et al. (2011) reported on a healthy subject who developed seizure after single-pulse TMS during motor threshold estimation. The risk and benefit balance must always be fully discussed with the patient before TMS is used.

Patients with rolandic tumors frequently suffer from symptomatic seizures and therefore may seem to be a patient group at high-risk of TMS induced seizures. Hufnagel et al. applied TMS to 13 patients with medically intractable complex partial seizures. They found that the epileptic focus was activated by TMS in 12 out of 13 patients, but clinical seizure was induced only in one patient (Hufnagel et al. 1990). Based on a literature review (Schrader et al. 2004), the risk of single-pulse TMS-induced seizure in patients with epilepsy ranges from 0.0 % to 2.8 %. In any case, the TMS examiner should prepare space and medications for managing a seizure, should it occur.

Although TMS-associated syncope is also a rare adverse event, it is more likely to occur than seizure. Because of the lack of systematic studies, the incidence of TMS-associated syncope remains unknown, but many laboratories have experienced it (Groppa et al. 2012). This is an area deserving more attention, and until better reviews have been published, TMS users should be aware of the risk of syncope and proceed with caution in this regards.

As for pain, single-pulse TMS seems to be generally well-tolerated and experienced by most participants as painless (Rossi et al. 2009), but the literature specifically addressing this point also remains scant. As mentioned above though, transient headache, local pain, neck pain, and toothache, as well as paresthesia have all been

reported from single-pulse TMS (Rossi et al. 2009). We would suppose though that these pains were at least transient, if not also mild. As for transient auditory threshold changes, TMS produces a loud clicking sound from the coil, up to 120–130 dB, and all patients should be required to wear earplugs during the procedure to prevent transient auditory threshold changes, so called "noise induced temporary threshold shift" (Groppa et al. 2012).

Three reports have mentioned adverse events from nTMS in patients with rolandic tumors (Paiva et al. 2012; Krieg et al. 2012b; Forster et al. 2011). To summarize these reports, there were two adverse events (unpleasantness in one patient, and headache in one patient) out of 31 nTMS sessions in 30 patients. Although this is too small a sample size to support reliable estimates, provisionally it suggests that about 1 in 15 patients will experience such adverse events. Larger multi-institutional registries would help to better elucidate the frequency of these events, as well as monitor the occurrence of other possible rare adverse events.

Furthermore, we must keep in mind that some neurosurgical patients harbor metals such as titanium skull plates for craniotomy closure or DBS electrodes inside the cranium, both of which present risks in the presence of an electromagnetic field such as TMS. Titanium skull plates may be of greatest concern, since TMS is performed not only pre-operatively, but also post-operatively on these patient populations. Rotenberg et al. assessed the safety of applying rTMS (which has greater electromagnetic influence than single-pulse TMS) to patients with titanium skull plates. They found that small titanium skull plates are not likely to heat sufficiently to injure the surrounding brain tissue during conventional low-frequency rTMS protocols, and they concluded that low-frequency rTMS may be safe for patients with small titanium skull plates that are in the stimulation site (Rotenberg et al. 2007). Besides the problem of heating, one must consider the possibility that the induced currents might displace the titanium skull plates ("Lorentz interaction"). Yet only minimal displacement of loose titanium plates during simulated rTMS has been observed (Rotenberg et al. 2007). As for DBS electrodes, two ex vivo studies have shown that the current and voltages induced by TMS in the deep brain electrodes are smaller than those induced by DBS itself and seemed to be a safe level (Kumar et al. 1999; Kuhn et al. 2004). nTMS is still a quite new technology and further monitoring of its safety is needed from the broader community of clinical users. Clinical users should report any incidents of adverse events that they observe in clinical usage, ideally be sending a brief letter describing the incident to a scientific journal indexed by PubMed.

Review of Studies on the Accuracy of Navigated Transcranial Magnetic Stimulation

To establish the validity of any new method of non-invasive brain mapping, its accuracy must be assessed relative to the gold standard of DES. Several studies have assessed the ability of nTMS to identify the motor cortex and delineate the cortical representation of individual muscles, in order to evaluate its reliability and accuracy for motor mapping. We conducted a review of the literature up to June 2012. The search terms we used on PubMed were: "transcranial magnetic stimulation", "TMS", "direct cortical stimulation", "direct electrical stimulation", "DCS", "DES", "motor cortex", "M1" and "brain tumo(u)r". We reviewed the abstracts of those reports, and if they reported on evaluating patients with rolandic tumors with both nTMS and DES, then we extracted information from the report. A total of eight studies meeting these criteria were identified (Table 23.1).

The first study to compare nTMS to DES for evaluating the motor cortex was by Krings et al. (1997). A mechanical stereotactic arm was used for TMS navigation. They compared areas of motor responses identified by both nTMS and DES in two patients with rolandic tumors. The discrepancy between nTMS and DES maps was never more than 1 cm. The major limitations of this study are that it reported on only two cases, and it used a homemade system that is not commercially available.

Table 23.1 Summary of eight studies comparing nTMS to DCS in terms of motor cortex identification

Reference	N patients with TMS (n comparisons of nTMS and DES)	Histology	Output muscles of nTMS	Method of measurement	Distance between muscle representations identified by nTMS and DCS (mm)	Other modalities compared	Study limitations
Krings et al. (1997)	2	Brain tumors	FCR	Compare single hotspots	<10	None	Small sample size; hotspot method; semi-quantitative
	(2)	Oligoastrocytoma III 3	FDI				
		Oligodendroglioma 1	GG				
Picht et al. (2009)	10	Brain tumors	TM	Compare single hotspots	Mean (SD)	None	Hotspot method; semi-quantitative
	(10)	Glioblastoma 3			3.4 (3.0)		
		Astrocytoma III 3					
		Astrocytoma I 1					
		Metastasis 3					
Kantelhardt et al. (2010)	1	Brain tumor	BR, APB	Compare single hotspots	<5	fMRI (n=6)	Single case; hotspot method; semi-quantitative
	(1)	Meningioma 1	ADM			Unquantitative	
Picht et al. (2011a)	20	Brain tumors	APB n=15	Compare single hotspots	Mean (SE)	None	Hotspot method
	(17: APB n=15 TA n=8)	Glioblastoma 5	TA n=8		APB 7.83 (1.18)		
		Astrocytoma III 3			TA 7.07 (0.88)		
		Metastasis 7					
		Meningioma 3					
		Lymphoma I 1					
Forster et al. (2011)	10	Brain tumors	TM n=5	Compare single hotspots	Overall mean (SD)	fMRI (n=10)	Hotspot method
	(11 sessions in 10 patients)	Glioblastoma 3	TA n=4		10.49 (5.67)	Mean (SD) versus DCS	
		Astrocytoma III 2	FDI, AHB n=3		Median[range]	15.03 (7.59)	
		Astrocytoma II 3	BC, QC n=2		APB		
		Astrocytoma I 1	ADM, OO n=1		12.8 [2.6–27.6]		
		Metastasis 1			ED: 10.6 [7.8–16.4]		
					TA: 11.1 [5.9–15.9]		

Krieg et al. (2012b)	26	Brain tumors	APB	Compare borders between positive and negative stimulation points	Mean (SD)	fMRI(n = 24)	Complicated idiosyncratic measurement method
	(14)	Glioblastoma 13	ADM		4.4 (3.4)	Mean (SD) versus nTMS – upper extremity	
		Astrocytoma III 3	FCR				
		Astrocytoma II 2	BC			9.8 (8.5)	
		Astrocytoma I 1	TA, GN			Lower extremity	
		Metastasis 7				14.7 (12.4)	
Paiva et al. (2012)	6	LGG	Hand and forearm (not specified)	Center-of-gravity approach	Mean	None	Small sample size; statistical methods were not explained sufficiently
	(6)	Astrocytoma II 6			4.16		
Tarapore et al. (2012)	24	Gliomas	ADM	Compare single hotspots	Median (SE)	MEG (n = 23)	Small sample size;
	(8 points in 5 patients)	Glioblastoma 7	APB		2.13 (0.19)	Median (SE) versus nTMS – ADM: 8.98 (1.41)	Hotspot method
		Astrocytoma III 8	OO				
		Astrocytoma II 8				APB: 6.16 (0.73)	
		Treatment effect 1					

Abbreviations: ADM abductor digiti minimi, *AHB* abductor hallucis brevis, *AHB* abductor hallucis brevis,, *BC* biceps, *BR* bracioradialis, *ED* extensor digitorum, *FCR* flexor carpi radialis, *FDI* first dorsal interosseus, *FDIM* first interosseous dorsal, *GG* genioglossus, *GN* gastrocnemius, *LGG* low grade glioma, *MEG* magnetoencephalography, *OO* orbicularis oris, *QC* quadriceps, *TA* tibialis anterior, *TM* thenar muscles

The next study was published more than a decade later (Picht et al. 2009). In this study, the motor cortex of 10 patients with rolandic tumors were evaluated using a homemade nTMS system in which an electromagnetic navigation system was integrated with TMS for the purpose of positioning the TMS coil. The mean (SD) [range] distance between hotspots of the two modalities was 3.4 (3.0) mm [0–7] mm. The limitation of this study was that the preoperative and intraoperative mappings were performed in the same predefined 5-mm raster, so the resulting comparative data were semiquantitative (Picht et al. 2011a). This system is not commercially available, so the applicability of the findings is limited. The next study (Kantelhardt et al. 2010) evaluated hotspots determined by nTMS and DES in two patients with brain tumors. In one patient the distance between hotspots was estimated as less than 5 mm, but in the other case the comparison referred to post-op nTMS. This study is unreliable because of the very small sample size and inadequate reporting.

These first three studies were all semiquantitative and/or had a sample size that was too small. From then on, all but one study (Paiva et al. 2012) have been using the same commercially available system (eXimia "Navigated Brain Stimulation"; Nexstim; Helsinki, Finland). The first and largest of these studies (Picht et al. 2011a) was on 20 patients with rolandic tumors, though only 17 had surgery and thus DES. In this study, DES locations were chosen independently of nTMS, and the distance between nTMS and DES hotspots was determined. The mean (SE) distance between the nTMS and DES hotspots was 7.83 (1.18) mm for the abductor pollicis brevis (APB) muscle (n = 15) and 7.07 (0.88) mm for tibialis anterior (TA) muscle (n = 8). Importantly, the mean (SE) distance decreased to 4.70 (1.09) mm for APB (n = 8), and 5.61 (0.47) mm for TA (n = 5) after exclusion of the patients in which possibly insufficient (<15 stimulations) DES mapping was performed for that muscle. This study also reported comparisons on three other muscles in subsets of the sample.

In the same year, Forster et al. reported their experience with nTMS in 10 patients with rolandic tumors when compared to DES and fMRI (Forster et al. 2011). This study has been of particular interest, despite the small sample size, because it provided a simultaneous comparison of fMRI to DES, thus enabling neurosurgeons to compare their options for pre-operative mapping. The mean (SD) [range] distance between the hotspots evaluated by nTMS and DES was 10.49 (5.67) [2.6–27.6] mm. One problem with this calculation though was that the pairs of nTMS and DES hotspots compared were from nine different muscles. Nonetheless, this result was smaller than the mean (SD) [range] distance between the hotspots of fMRI and DES: 15.03 (7.59) [3.4–22.2] mm. So this study advocated that nTMS is better correlated to DES than fMRI. One major limitation of this study however is that they did not compare responses from the same muscles: five hand/arm muscles, three leg muscles, and one facial muscle were recorded for TMS; whereas, activation areas from the first interosseous dorsal muscle or toe movement were obtained for fMRI. This use of different muscles may have accounted in part for the discrepancy between fMRI and nTMS. Nonetheless, one other interesting finding from this study was that the median [range] distance for the TA muscle relative to DES was larger for nTMS, 11.1 [5.9–15.9] mm, than for fMRI, 9.4 [5.7–19.1] mm. Thus nTMS may be less accurate for deeper lying cortical regions, such as the cortical region corresponding to leg muscles.

Krieg et al. (2012b) reported their experience on using nTMS pre-surgically for the resection of rolandic tumors. They performed preoperative nTMS on 14 patients with lesions located within or adjacent to the precentral gyrus and on 12 patients with lesions in the subcortical white mater motor tract. In the former patient group, they compared the borders between positive and negative stimulation points for nTMS and DES on axial slices by using recalibrated screenshots and BrainLAB iPlan Net Cranial 3.0.1. Although this method of comparing borders may have some advantage of accuracy over the usual hotspot method, it is complicated and idiosyncratic and renders comparisons to other studies problematic. Using this method, the mean (SD)

[range] of the distance between borders for nTMS versus DES was 4.4 (3.4) [1.9–9.2] mm. They also evaluated the difference between borders delineating the primary motor cortex according to BOLD data of fMRI and mapping area identified by nTMS. The mean (SD) [range] deviation between nTMS and fMRI for this method was 9.8 (8.5) [5.3–39.7] mm for the upper extremity and 14.7 (12.4) [8.4–33.5] mm for the lower extremity. They mentioned that their data demonstrate that nTMS correlates well with intraoperative DES, while nTMS and fMRI differed significantly from each other. Regrettably, they did not make any comparison between preoperative fMRI and DES, so it remains difficult to say whether nTMS is more accurate than fMRI on the basis of this study. In particular, the fact that the discrepancy between nTMS and fMRI is greater for the lower extremity than the upper extremity may again, as in the study by Forster et al. (2011) reflect a lesser accuracy of nTMS for the deeper lying cortical representations of leg muscles.

Another study focused on patients with relatively homogeneous brain tumors (i.e. only patients with low grade gliomas with a maximum diameter or 4 cm were included), using an unspecified nTMS system (Paiva et al. 2012). In this study, they used the "center-of-gravity" approach to compare the difference between the two modalities. This method is more time consuming but also more accurate and reliable. They reported a mean [range] distance between nTMS and DES of 4.16 [2.56–5.27] mm. The limitations of this study were its small sample size and inadequate explanation of the statistical methods.

The most recent study identified by our review performed mapping on 24 patients but then made comparisons only in five, because DES revealed a positive motor site in only five patients with the tailored craniotomy they used (Tarapore et al. 2012). They calculated the difference between hotspots identified by nTMS and DES at eight points in five patients as a median (SE) of 2.13 (0.19) mm. An interesting point in this study is that they reported that negative nTMS mapping also correlates with negative DES mapping: in other words, DES mapping did not find any new motor sites where TMS had not. The study also included the result of a comparison between motor areas identified by nTMS and magnetoencephalography (MEG). The median (SE) distance between the two hotspots of 46 sites in 23 patients was reported as 4.71 (1.08) mm. Unfortunately, they did not report a comparison of MEG to DES. Although this study reports some interesting new information, it is otherwise limited by the small number of patients having DES data available.

In summary, all studies reviewed here concluded that nTMS correlated well with the gold standard of DES (Forster et al. 2011; Kantelhardt et al. 2010; Krieg et al. 2012b; Krings et al. 1997; Paiva et al. 2012; Picht et al. 2009, 2011a; Tarapore et al. 2012). A total of 97 attempts in 96 patients to identify the motor cortex using nTMS were described. In only one patient with an infiltrating glioma within the somatosensory cortex, could TMS not identify any motor site (Tarapore et al. 2012).

We have calculated the mean distance between motor cortex identified by nTMS and DES using the mean distance described in five quantitatively evaluated studies (Picht et al. 2011a; Forster et al. 2011; Krieg et al. 2012b; Paiva et al. 2012; Tarapore et al. 2012). We then weighted the mean from each study by the number of patients that mean was derived from. (In one study (Picht et al. 2011a), we used only the data for APB (n = 15) for simplicity.) With the method, we have calculated a weighted mean distance between nTMS and DES in 50 patients as 6.39 mm.

The Accuracy of Transcranial Magnetic Stimulation and Direct Electrical Stimulation

The basic mechanism of neuronal activation is the same for both TMS and DES. An electric field moves electric charges within the target tissue. Wherever the electric field is of adequate strength and direction in relation to the neuronal structures, neurons will be excited and action potentials triggered. Yet, the spread of the electric fields from the electrodes (DES) or the

"virtual electrodes" (TMS) is difficult to predict since the electric current will follow the paths of least impedance in the tissue and is influenced by macroscopic factors (e.g. sulci, CSF) and microscopic factors (e.g. preferred orientation of cells). As a result, the exact extent of the stimulated cortical area remains unclear for both TMS and DES, so spatial discrepancies might reflect methodological differences rather than "inaccuracies" of either method.

For electrical stimulation, it has been established that neurons are excited at lower thresholds when the applied voltage induces currents that are oriented along the axon rather than across it (Day et al. 1989). It has been demonstrated that during bipolar cortical stimulation the current peaks in the region directly below the bipolar electrodes; whereas, current density decreases much less rapidly with depth during monopolar anodal stimulation (Nathan et al. 1993). Consequently, suprathreshold anodic stimulation of the motor cortex leads primarily to direct stimulation of the pyramidal cells. By contrast, single-pulse TMS is likely to involve both tangential cortical fibers and direct corticospinal axonal bundles (Di Lazzaro et al. 2004; Ruohonen and Ilmoniemi 2002). Depending on the e-field direction and the stimulation strength, TMS on the primary motor cortex will preferentially activate the pyramidal cells directly (D-waves) or indirectly (transsynaptically; I-waves) at their axon hillock. In the cerebral cortex, the threshold for TMS excitation is highly sensitive to orientation (Fox et al. 2006). In clinical practice, the coil orientation is adjusted for each stimulated position during the motor mapping, so that the induced electric field is set to be perpendicular to the bank of the gyrus with the help of MRI-based navigation. In sum, it can be hypothesized that suprathreshold anodal monopolar DES and nTMS at 110 % RMT perpendicular to the individual gyral anatomy elicit MEPs through direct axonal depolarization as well as through intracortical transverse connections. This implies that both methods stimulate preferentially the same population of neurons. Nevertheless, the exact stimulation path remains unknown in each individual case, especially around a tumor with possible conductivity changes. So TMS and DES can stimulate via somewhat different paths in any given patient.

In addition to these neurophysiological considerations, one should be aware that the comparison of spatial accuracy of TMS and DCS is also influenced by methodological factors concerning the hardware and study conception which may further inflate the discrepancy between the nTMS and DES results. There are four main reasons why these may cause discrepancy between the nTMS and DES results.

First, the mappings are conducted under different chemical influences and different states of alertness. DES is conducted under general anesthesia, while nTMS is not. Under general anesthesia, MEPs can only be evoked by using a train of stimuli, not by single pulses. This necessity of applying larger electrical charges to evoke muscle responses during DES mapping in comparison to TMS mapping can lead to different stimulation effects of the two methods even if exactly the same area is targeted. In addition, a significant proportion of patients with brain tumors have been using anti-epileptic medications, and we cannot rule out its possible influence.

Second, there are a couple kinds of measurement errors related to the neuronavigation, such as registration error or measurement errors from brain shift (Suess et al. 2007), which could influence the measurement of DES stimulation locations. It can be assumed though that the impact of brain-shift is minimal, because the cortical mapping procedures are all performed before tumor resection begins. The error occurring during coregistration of the 3D MRI dataset and the patient's head is stated to be below 2 mm for nTMS (Ruohonen and Karhu 2010).

Third, the kind of EMG electrodes used by the two methods differ: dermal surface electrodes for nTMS but intramuscular needle electrodes for DES. Cross-talk from adjacent muscles can be picked up by surface electrodes, while this is not the case when using needle electrodes. This also means that dermal electrodes can be more sensitive in picking up very small responses from different muscles as a summation of subliminal responses.

Thus the use of different EMG electrodes may introduce a bias in terms of the recording sensitivity of the muscle output.

Fourth, after all the mapping is done, the most commonly used method for measuring the distance between the muscles representation of the nTMS and DES mappings is to compare the "hotspots": the single point with the largest EMG response for that muscle. This hotspot method is likely to emphasize errors contained by a single response. The "wrong" DES hotspot may have been chosen, if there were multiple foci or a diffuse center for the motor cortex representation of the target muscle or if the true hotspot was never even stimulated. Similarly, the number of stimulation points during DES varies widely depending on the tumor location, craniotomy size, and other factors. Consequently the distance between nTMS and DES hotspots is much greater when there were fewer DES responses (Picht et al. 2011a). Also, in most studies the surgeon was not aware of the exact nTMS locations thus he could not deliberately stimulate them. So in cases where there was a limited number of DES stimulation spots, it was quite possible that the nTMS hotspot and/or the true cortical center of muscle control was never covered, thus leading to a wider discrepancy between nTMS and DES. Using a "center-of-gravity" approach or comparing mapping areas is more accurate, but it is usually restricted by time limitations of surgery, which usually prevent taking enough measurements for such an approach. Altogether, these considerations and findings suggest that DES may not really be a reliable gold standard when a low number of stimulations are performed. Of course DES does tell the surgical team when a spot on the brain is necessary for motor function, but unless extensive freehand mapping is performed, DES will not necessarily reveal the most essential center of cortical control for a muscle. Depending on the tumor location, extensive DES mapping may not be necessary, thus leaving its results unreliable for scientific comparisons to nTMS.

In summary TMS and DES are applying the same basic underlying methodology, namely the electrical stimulation of cortical neurons. In respect to identification of direct corticospinal motor connections differences in the specific neurophysiological details of neuronal activation are of minor relevance. Discrepancies between TMS and DES motor mappings are predominantly caused by system inherent errors (e.g. navigational error) or reflect inadequate surrogate parameters for evaluation of accuracy (e.g., comparison of "hot spots").

The Clinical Role of Navigated Transcranial Magnetic Stimulation

The studies summarized above provide some evidence that nTMS has acceptably good accuracy for identifying cortical representations of individual muscles vis-à-vis the gold standard of DES. Yet preoperative nTMS is not therefore intended as a substitute for intraoperative DES. Instead, it provides complimentary information, derived from its unique features. The overarching strength of nTMS is that it is the only other mapping modality that is analogous to DES (stimulate the brain and record the output), but it can be performed pre-operatively and post-operatively; whereas, DES cannot be. So while DES is still used to guide the actual surgical resection of tumors, nTMS can be used to plan the surgery ahead of time, guide the DES, and assess postoperative or longitudinal changes in cortical motor representation.

Preoperative nTMS can be useful for planning surgeries, while there is still an opportunity to discuss it with the patient. The magnetic stimulation of a precise cortical spot enables the operator to identify cortical areas with direct cortico-spinal motor connections. The synthesis of the patient's clinical status, MRI findings, and TMS mapping can improve the surgical team's ability to better plan the surgical strategy. A prospective study has shown that in about one-fourth of the surgical cases of tumors in presumed motor eloquent location, nTMS brought objective benefit to the surgical team (nTMS changed the surgical indication or the planned extent of resection, or it modified the surgical approach), and in another one-fourth of cases it added critical

awareness of high risk areas, which helped guide the intraoperative DES (Picht et al. 2012).

Several other imaging modalities – such as fMRI, PET, and MEG – have also been used to map the motor cortex preoperatively and plan the surgical resection. Yet nTMS has the advantage over other preoperative mapping methods that nTMS is analogous to DES: nTMS stimulates the brain and records the muscle output, rather than asking the patient to move, recording brain activation, and then trying to interpret which brain areas were essential for the movement versus which ones were merely co-activated. Also, nTMS can be used to evaluate responses from any muscles desired; whereas, functional imaging can only be used to evaluate responses from muscles that can still be moved voluntarily and, ideally, isolated from other muscles. For further comparisons to other preoperative mapping modalities, we refer the reader to a previous book chapter (Picht and Atalay 2012).

It has to be emphasized though that TMS has an entirely different role from DES and is not capable of being a substitute for DES. Surgical resection of brain tumors in eloquent location should be guided by intraoperative mapping and monitoring which nTMS cannot provide, so DES remains essential. Yet nTMS can be useful to plan and guide the DES, and the pre-operative nTMS maps can also serve as a back-up, if intraoperative technical errors or patient seizures make it impossible to continue with intraoperative DES. Also, if the resection will extend to subcortical levels, mapping needs to be carried out on these subcortical levels. nTMS cannot perform mapping of subcortical tracts, so DES remains essential for this function. nTMS can be beneficial by improving diffusion tensor imaging to visualize the subcortical fiber tracts; but the resulting information can only be used for surgical planning and intraoperative guidance of the stimulation probe and not for determining resection margins. In sum, TMS is performed pre-operatively and is used to plan the surgery; whereas DES is used intra-operatively to guide tumor resection. TMS does not have this capability to be performed intra-operatively. Both modalities should be used complementarily, drawing on their respective advantages, to maximize the quality of the surgery.

nTMS has five unique capabilities that supplement the information provided by intraoperative DES: (1) nTMS provides an objective assessment of the possibility of recovery of motor function. For example, in patients who have become plegic, nTMS can show if motor function is still possible (Picht et al. 2011b). (2) nTMS provides pre-operative clarification of detailed cortical functional anatomy, which can resulting in smaller craniotomies and a modification of the surgical approach (Picht et al. 2012; Krieg et al. 2012b), also applicable in small kids (Coburger et al. 2012). (3) nTMS can be performed repeatedly across time, and this can enable visualization of plastic changes, which may influence the timing of surgical interventions (Takahashi et al. 2012). (4) nTMS enables an objective preoperative estimation of the extent of safe cortical tumor resection. In a prospective study, nTMS mapping changed the planned extent of resection in about 8 % of cases (Picht et al. 2012). (5) nTMS can be used to define the accurate "seed-points" for diffusion tensor imaging, to visualize the pathways of the pyramidal fiber tracts. This approach can improve the accuracy of diffusion tensor imaging for fiber tracking (Frey et al. 2012; Krieg et al. 2012a). Altogether, these five unique capabilities of nTMS enable neurosurgeons to improve tumor resection through better advanced planning of the surgery.

Conclusions

The recent addition of neuronavigation to transcranial magnetic stimulation has greatly improved the accuracy and usefulness of this cortical mapping technology. nTMS provides a valuable complement to the gold standard of DES for mapping the motor cortex. Because nTMS can be performed pre-operatively with little risk or discomfort to the patient, it provides the surgical team with important information about each individual patient's functionally essential areas of the motor cortex. Having this information

preoperatively is often quite useful in various ways for planning the surgery. nTMS has the advantage over all other preoperative methods of functional imaging that only nTMS stimulates the brain and records motor output – just like DES. All other forms of preoperative imaging ask the patient to move (if they can and will), record brain activation, and then attempt to interpret which areas of the brain were essential for the movement versus which ones were incidental.

Our literature review here supports the view that the accuracy of TMS is sufficiently high to rely upon its results for surgical planning. The overall weighted mean distance between nTMS from DES in 50 patients was calculated as 6.39 mm. Yet it must be emphasized that nTMS and DES have different roles and are not interchangeable: only nTMS can be used preoperatively and postoperatively, while only DES can be used intraoperatively and subcortically. nTMS also has many unique capacities that make it a promising new technology for better understanding the motor cortex. The neurosurgical community is still just beginning to explore the many capabilities of nTMS and further research is sure to yield many more exciting discoveries from this new technology.

Acknowledgments We would like to thank Michael Hanna, Ph.D., (Mercury Medical Research & Writing) for reviewing and revising the manuscript.

References

Barker AT, Jalinous R, Freeston IL (1985) Non-invasive magnetic stimulation of human motor cortex. Lancet 1:1106–1107

Coburger J, Karhu J, Bittl M, Hopf NJ (2012) First preoperative functional mapping via navigated transcranial magnetic stimulation in a 3-year-old boy. J Neurosurg Pediatr 9:660–664

Day BL, Dressler D, Maertens de Noordhout A, Marsden CD, Nakashima K, Rothwell JC, Thompson PD (1989) Electric and magnetic stimulation of human motor cortex: surface EMG and single motor unit responses. J Physiol 412:449–473

De Witt Hamer PC, Robles SG, Zwinderman AH, Duffau H, Berger MS (2012) Impact of intraoperative stimulation brain mapping on glioma surgery outcome: a meta-analysis. J Clin Oncol 30:2559–2565

Di Lazzaro V, Oliviero A, Pilato F, Saturno E, Dileone M, Mazzone P, Insola A, Tonali PA, Rothwell JC (2004) The physiological basis of transcranial motor cortex stimulation in conscious humans. Clin Neurophysiol 115:255–266

Duffau H, Lopes M, Arthuis F, Bitar A, Sichez JP, Van Effenterre R, Capelle L (2005) Contribution of intraoperative electrical stimulations in surgery of low grade gliomas: a comparative study between two series without (1985–96) and with (1996–2003) functional mapping in the same institution. J Neurol Neurosurg Psychiatry 76:845–851

Forster MT, Hattingen E, Senft C, Gasser T, Seifert V, Szelenyi A (2011) Navigated transcranial magnetic stimulation and functional magnetic resonance imaging: advanced adjuncts in preoperative planning for central region tumors. Neurosurgery 68:1317–1324, discussion 1324–1315

Fox PT, Narayana S, Tandon N, Fox SP, Sandoval H, Kochunov P, Capaday C, Lancaster JL (2006) Intensity modulation of TMS-induced cortical excitation: primary motor cortex. Hum Brain Mapp 27:478–487

Frey D, Strack V, Wiener E, Jussen D, Vajkoczy P, Picht T (2012) A new approach for corticospinal tract reconstruction based on navigated transcranial stimulation and standardized fractional anisotropy values. Neuroimage 62:1600–1609

Groppa S, Oliviero A, Eisen A, Quartarone A, Cohen LG, Mall V, Kaelin-Lang A, Mima T, Rossi S, Thickbroom GW, Rossini PM, Ziemann U, Valls-Sole J, Siebner HR (2012) A practical guide to diagnostic transcranial magnetic stimulation: report of an IFCN committee. Clin Neurophysiol 123:858–882

Hannula H, Ylioja S, Pertovaara A, Korvenoja A, Ruohonen J, Ilmoniemi RJ, Carlson S (2005) Somatotopic blocking of sensation with navigated transcranial magnetic stimulation of the primary somatosensory cortex. Hum Brain Mapp 26:100–109

Hufnagel A, Elger CE, Durwen HF, Boker DK, Entzian W (1990) Activation of the epileptic focus by transcranial magnetic stimulation of the human brain. Ann Neurol 27:49–60

Kantelhardt SR, Fadini T, Finke M, Kallenberg K, Siemerkus J, Bockermann V, Matthaeus L, Paulus W, Schweikard A, Rohde V, Giese A (2010) Robot-assisted image-guided transcranial magnetic stimulation for somatotopic mapping of the motor cortex: a clinical pilot study. Acta Neurochir (Wien) 152: 333–343

Kombos T, Suss O (2009) Neurophysiological basis of direct cortical stimulation and applied neuroanatomy of the motor cortex: a review. Neurosurg Focus 27:E3

Kombos T, Suess O, Kern BC, Funk T, Hoell T, Kopetsch O, Brock M (1999) Comparison between monopolar and bipolar electrical stimulation of the motor cortex. Acta Neurochir (Wien) 141:1295–1301

Kratz O, Studer P, Barth W, Wangler S, Hoegl T, Heinrich H, Moll GH (2011) Seizure in a nonpredisposed individual induced by single-pulse transcranial magnetic stimulation. J ECT 27:48–50

Krieg SM, Buchmann NH, Gempt J, Shiban E, Meyer B, Ringel F (2012a) Diffusion tensor imaging fiber tracking using navigated brain stimulation–a feasibility study. Acta Neurochir (Wien) 154:555–563

Krieg SM, Shiban E, Buchmann N, Gempt J, Foerschler A, Meyer B, Ringel F (2012b) Utility of presurgical navigated transcranial magnetic brain stimulation for the resection of tumors in eloquent motor areas. J Neurosurg 116:994–1001

Krings T, Buchbinder BR, Butler WE, Chiappa KH, Jiang HJ, Rosen BR, Cosgrove GR (1997) Stereotactic transcranial magnetic stimulation: correlation with direct electrical cortical stimulation. Neurosurgery 41:1319–1325, discussion 1325–1316

Kuhn AA, Brandt SA, Kupsch A, Trottenberg T, Brocke J, Irlbacher K, Schneider GH, Meyer BU (2004) Comparison of motor effects following subcortical electrical stimulation through electrodes in the globus pallidus internus and cortical transcranial magnetic stimulation. Exp Brain Res 155:48–55

Kumar R, Chen R, Ashby P (1999) Safety of transcranial magnetic stimulation in patients with implanted deep brain stimulators. Mov Disord 14:157–158

Nathan SS, Sinha SR, Gordon B, Lesser RP, Thakor NV (1993) Determination of current density distributions generated by electrical stimulation of the human cerebral cortex. Electroencephalogr Clin Neurophysiol 86:183–192

Paiva WS, Fonoff ET, Marcolin MA, Cabrera HN, Teixeira MJ (2012) Cortical mapping with navigated transcranial magnetic stimulation in low-grade glioma surgery. Neuropsychiatr Dis Treat 8:197–201

Penfield W, Boldrey E (1937) Somatic motor and sensory representation in the cerebral cortex of man as studied by electrical stimulation. Brain 60:389–443

Picht T, Atalay A (2012) Preoperative motor mapping. In: Hayat MA (ed) Tumors of the central nervous system, vol 4. Springer, Netherlands, pp 289–300. doi:10.1007/978-94-007-1706-0_30

Picht T, Mularski S, Kuehn B, Vajkoczy P, Kombos T, Suess O (2009) Navigated transcranial magnetic stimulation for preoperative functional diagnostics in brain tumor surgery. Neurosurgery 65:93–98, discussion 98–99

Picht T, Schmidt S, Brandt S, Frey D, Hannula H, Neuvonen T, Karhu J, Vajkoczy P, Suess O (2011a) Preoperative functional mapping for rolandic brain tumor surgery: comparison of navigated transcranial magnetic stimulation to direct cortical stimulation. Neurosurgery 69:581–588, discussion 588

Picht T, Schmidt S, Woitzik J, Suess O (2011b) Navigated brain stimulation for preoperative cortical mapping in paretic patients: case report of a hemiplegic patient. Neurosurgery 68:E1475–E1480, discussion E1480

Picht T, Schulz J, Hanna M, Schmidt S, Suess O, Vajkoczy P (2012) Assessment of the influence of navigated transcranial magnetic stimulation on surgical planning for tumors in or near the motor cortex. Neurosurgery 70:1248–1256, discussion 1256–1247

Rossi S, Hallett M, Rossini PM, Pascual-Leone A (2009) Safety, ethical considerations, and application guidelines for the use of transcranial magnetic stimulation in clinical practice and research. Clin Neurophysiol 120:2008–2039

Rossi S, Hallett M, Rossini PM, Pascual-Leone A (2011) Screening questionnaire before TMS: an update. Clin Neurophysiol 122:1686

Rotenberg A, Harrington MG, Birnbaum DS, Madsen JR, Glass IE, Jensen FE, Pascual-Leone A (2007) Minimal heating of titanium skull plates during 1Hz repetitive transcranial magnetic stimulation. Clin Neurophysiol 118:2536–2538

Ruohonen J, Ilmoniemi RJ (2002) Physical principles for transcranial magnetic stimulation. Handbook of transcranial magnetic stimulation. Oxford University Press, New York

Ruohonen J, Ilmoniemi RJ (2005) Basic physics and design of TMS devices and coils. In: Hallet M, Chokroverty S (eds) Magnetic stimulation in clinical neurophysiology. Butterworth, Boston, pp 17–30

Ruohonen J, Karhu J (2010) Navigated transcranial magnetic stimulation. Neurophysiol Clin 40:7–17

Sanai N, Berger MS (2010) Intraoperative stimulation techniques for functional pathway preservation and glioma resection. Neurosurg Focus 28:E1

Schmidt S, Cichy RM, Kraft A, Brocke J, Irlbacher K, Brandt SA (2009) An initial transient-state and reliable measures of corticospinal excitability in TMS studies. Clin Neurophysiol 120:987–993

Schrader LM, Stern JM, Koski L, Nuwer MR, Engel J Jr (2004) Seizure incidence during single- and paired-pulse transcranial magnetic stimulation (TMS) in individuals with epilepsy. Clin Neurophysiol 115:2728–2737

Suess O, Picht T, Kuehn B, Mularski S, Brock M, Kombos T (2007) Neuronavigation without rigid pin fixation of the head in left frontotemporal tumor surgery with intraoperative speech mapping. Neurosurgery 60:330–338, discussion 338

Szelenyi A, Joksimovic B, Seifert V (2007) Intraoperative risk of seizures associated with transient direct cortical stimulation in patients with symptomatic epilepsy. J Clin Neurophysiol 24:39–43

Takahashi S, Jussen D, Vajkoczy P, Picht T (2012) Plastic relocation of motor cortex in a patient with LGG (low grade glioma) confirmed by NBS (navigated brain stimulation). Acta Neurochir (Wien) 154(11):2003–8

Taniguchi M, Cedzich C, Schramm J (1993) Modification of cortical stimulation for motor evoked potentials under general anesthesia: technical description. Neurosurgery 32:219–226

Tarapore PE, Tate MC, Findlay AM, Honma SM, Mizuiri D, Berger MS, Nagarajan SS (2012) Preoperative multimodal motor mapping: a comparison of magnetoencephalography imaging, navigated transcranial magnetic stimulation, and direct cortical stimulation. J Neurosurg 117:354–362

The Role of Glutathione and the Glutathione-Linked Enzyme Systems in Brain Tumor Drug Resistance

24

Donald S. Backos, Robyn L. Poerschke, Christopher C. Franklin, and Philip Reigan

Contents

D.S. Backos • R.L. Poerschke
Department of Pharmaceutical Sciences, Skaggs School of Pharmacy and Pharmaceutical Sciences, University of Colorado Anschutz Medical Campus, 12850 Montview Blvd., Rm V20-2102, Aurora, CO 80045, USA

C.C. Franklin • P. Reigan (✉)
Department of Pharmaceutical Sciences, Skaggs School of Pharmacy and Pharmaceutical Sciences, University of Colorado Anschutz Medical Campus, 12850 Montview Blvd., Rm V20-2102, Aurora, CO 80045, USA

University of Colorado Cancer Center, University of Colorado Anschutz Medical Campus, Aurora, CO 80045, USA
e-mail: philip.reigan@ucdenver.edu

Abstract

The current standard of care for patients diagnosed with primary brain tumors consists of surgical resection, when feasible, followed by radiotherapy with concomitant and/or adjuvant chemotherapy. Unfortunately, complete surgical resection is extremely rare due to the location of these tumors and their diffuse and proliferative nature and radiation therapy can enhance the necrotic environment resulting in further tissue damage and more aggressive tumors. A common problem with chemotherapy, that limits its clinical efficacy for brain tumor treatment, is that high doses are required to circumvent drug resistance mechanisms that result in drug-related and dose-limiting toxicities. Therefore, strategies and approaches that target the mechanisms of drug resistance in brain tumors will allow dose reductions in chemotherapy while maintaining clinical efficacy and limiting drug-related toxicities. The contributions of glutathione (GSH) and the GSH-related enzymes to drug resistance in brain tumors have been largely overlooked. The major components of the GSH-related enzyme system, including glutamate cysteine ligase (GCL), glutathione synthetase (GS), glutathione peroxidase (GPx), glutathione reductase (GR), glutathione-S-transferases (GST), and GSH export transporters (GS-X pumps) are often dysregulated and promote the detoxification of various anticancer agents and confer a more drug resistant phenotype.

M.A. Hayat (ed.), *Tumors of the Central Nervous System, Volume 12*,
DOI 10.1007/978-94-007-7217-5_24,

Improving our understanding of the mechanisms of GSH-mediated drug resistance will be critical to develop targeted therapeutic approaches to chemosensitize brain tumors to treatments and to improve clinical outcomes.

Introduction

Most treatment regimens for human brain tumors include surgical resection, where possible, and the use of chemotherapeutic agents, either as primary agents, as adjuvant therapies, or for use in combination with radiotherapy. However, the development of drug resistance in these tumors is a major contributor to the failure of chemotherapeutic agents to elicit substantial improvements in patient outcome. Although a number of cellular mechanisms may be involved in brain tumor chemoresistance, particularly when examining specific agents and/or tumor types, the glutathione (GSH) antioxidant and detoxification system is a major contributor to drug resistance in most human tumors. The characterization of these pathways in brain tumors, however, has been somewhat neglected. GSH is critical to both supporting the metabolic processes required for the enhanced proliferation of tumor cells and to the detoxification of the cytotoxic agents employed in tumor therapies. This review seeks to summarize the key GSH-associated mechanisms of chemotherapy resistance, their role in conferring clinical non-responsiveness to treatment, and the potential of targeting these pathways as a strategy for enhancing the sensitivity of these tumors to therapy.

Overview of GSH and the GSH-dependent Enzymes

Oxygen (O_2) is essential to the generation of cellular ATP via aerobic mitochondrial respiration, which involves a four electron reduction of O_2 to H_2O. This process of oxidative metabolism results in the generation of reactive oxygen species (ROS), including the superoxide anion radical, the hydroxyl radical, and hydrogen peroxide. ROS can damage cellular proteins, lipids, and DNA, resulting in detrimental effects on cellular function and viability. Left unchecked, ROS accumulation can lead to mitochondrial damage, cytochrome c release, and the activation of caspase-mediated apoptosis. A number of cellular antioxidant defense mechanisms are employed to prevent this oxidative damage induced by the endogenous production and accumulation of ROS. Of these, GSH constitutes one of the most abundant and important cellular antioxidants to suppress oxidative stress and maintain redox homeostasis (Lu 2009).

GSH is a tripeptide consisting of glutamate, cysteine, and glycine with the capacity to directly scavenge ROS in a non-enzymatic manner. GSH also serves as a co-factor for glutathione peroxidase (GPx) in the detoxification of hydrogen peroxide (Fig. 24.1), as well as lipid and phospholipid peroxides resulting from ROS-mediated lipid peroxidation reactions. Both non-enzymatic and enzyme-mediated mechanisms result in the oxidation of GSH to glutathione disulfide (GSSG) and the ratio of reduced to oxidized GSH (GSH:GSSG) can serve as an indicator of cellular redox homeostasis and oxidative stress. Glutathione reductase (GR) can recycle GSSG back to GSH by utilizing NADPH as an electron donor. GR activity is generally sufficient to reduce the basal levels of GSSG in non-stressed cells but, during periods of oxidative stress, GR activity can be limiting. This can result in the accumulation of GSSG, a dramatic shift in the GSH:GSSG ratio, and a loss of cellular redox homeostasis, even though the levels of total cellular GSH may be normal. Under these conditions, the GSH:GSSG ratio can be restored via the receptor-mediated efflux of GSSG mediated by multi-drug resistant proteins (MRPs), leading to a reduction in total cellular GSH levels (Dringen and Hirrlinger 2003).

Although maintaining cellular redox homeostasis is critical to protect against oxidative damage, GSH is also closely involved in the detoxification of a number of xenobiotic compounds and toxicants. The family of glutathione-S-transferase (GST) enzymes employs GSH as a co-factor in the Phase II metabolism of a number

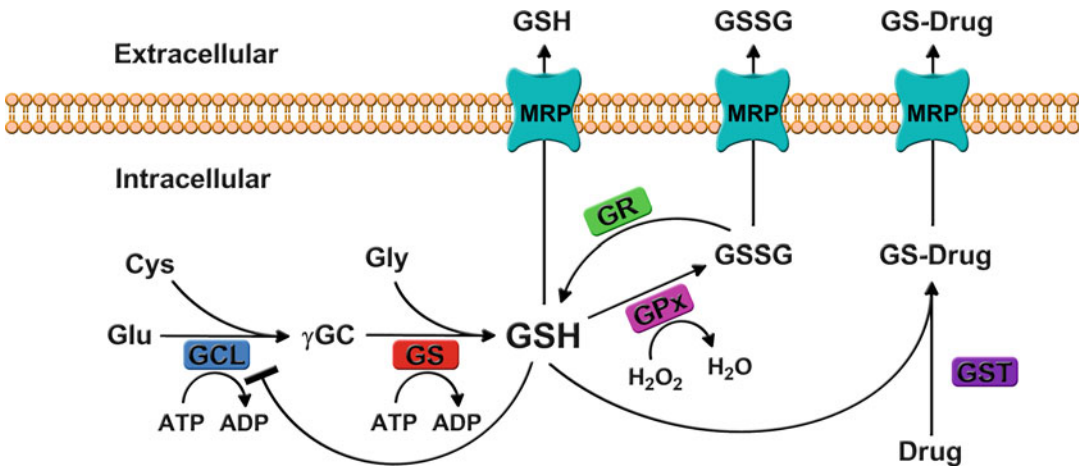

Fig. 24.1 General schematic of cellular GSH biosynthesis, utilization, export, and salvage. Glutathione (*GSH*) biosynthesis requires two ATP-dependent reactions: the glutamate cysteine ligase (*GCL*)-mediated formation of γ-glutamylcysteine (*γGC*) from glutamate (*Glu*) and cysteine (*Cys*) and the glutathione synthetase (*GS*)-mediated formation of GSH from γGC and glycine (*Gly*). GSH functions as a feedback inhibitor of GCL, but not GS. Cellular peroxides are detoxified through the actions of GSH peroxidase (*GPx*) resulting in the formation of oxidized GSH (*GSSG*) that can be salvaged by GSH reductase (*GR*). GSH also serves as a cofactor in glutathione-S-transferase (*GST*)-mediated detoxification of xenobiotics resulting in the formation of GSH conjugates (GS-Drug). Multidrug resistance protein (*MRP*) transporters are capable of effluxing GSH, GSSG, and GS-Drug conjugates into the extracellular space

of chemotherapeutics, resulting in the formation of a covalent linkage between GSH and the drug (Fig. 24.1). GST-mediated GSH conjugation usually leads to the inactivation of the parent compound, while enhancing its water solubility and facilitating the transporter-dependent efflux of the GSH-conjugate from the cell (Townsend and Tew 2003). This leads to the depletion of cellular GSH stores. Cells are unable to effectively uptake intact extracellular GSH so replenishment of cellular GSH requires de novo GSH biosynthesis.

GSH is synthesized via two successive ATP-dependent reactions catalyzed by glutamate cysteine ligase (GCL) and glutathione synthetase (GS). GCL catalyzes the first and rate-limiting step in the process: the formation of γ-glutamyl cysteine (γ-GC) from glutamate and cysteine (Fig. 24.1). GCL is a heterodimeric holoenzyme complex consisting of two subunits. The catalytic subunit (GCLC) contributes all of the enzymatic activity and contains all of the substrate and cofactor binding sites. The modifier subunit (GCLM) possesses no enzymatic activity alone, but formation of GCL holoenzyme by heterodimerization of the two subunits dramatically increases GCL specific activity and affinity for glutamate and ATP while simultaneously lowering affinity for GSH, which functions as a feedback inhibitor of GCL (Franklin et al. 2009). Although GS expression levels and activity do play a role in GSH biosynthesis, GCL enzymatic activity generally dictates cellular GSH levels and GSH biosynthetic capacity. The major determinants of cellular GCL activity are the relative expression of the GCL subunits, availability of the amino acid substrates (particularly cysteine), and the degree of negative feedback inhibition by GSH (Franklin et al. 2009).

The GSH System in the Brain

The brain is composed of a diverse panoply of morphologically and functionally distinct cell populations, constituting a rather unique model of cell-cell interaction. Two major cell types,

neuronal and glial cells, are present in the brain. Neurons are the electrically excitable cells responsible for the generation of action potentials that constitute the mechanism by which the central nervous system (CNS) signals to the rest of the body. Glial cells include oligodendrocytes, which are responsible for the formation and maintenance of the myelin sheath insulating neuronal axons, and astrocytes, which provide structural and metabolic support to neurons. Astrocytes play a critical role in maintaining neuronal GSH levels by providing neurons with lactate for ATP production, cysteine for GSH synthesis, and assist with the removal of glutamate from the synaptic cleft of glutamatergic neurons (Anderson and Swanson 2000). The inability of most cell types to effectively import intact GSH underscores the importance of substrate availability and uptake, as well as de novo GSH biosynthesis, to the maintenance of neuronal GSH homeostasis. Substrate availability is a major determinant of GSH content in the brain and cysteine is typically the rate-limiting substrate for neuronal GSH biosynthesis (Dringen and Hirrlinger 2003). The majority of the cysteine utilized for neuronal GSH synthesis is derived from GSH that is exported from astrocytes and broken down into its constituent amino acids (Fig. 24.2) (Dringen and Hirrlinger 2003). The γ-glutamyl moiety is released by γ-glutamyltranspeptidase (γGT) activity and cysteine and glycine are released from the remnant CysGly dipeptide by the actions of membrane-bound neuronal dipeptidases (Dringen and Hirrlinger 2003). The Na^+-dependent excitatory amino acid transporter (EAAT) family is responsible for the majority of cysteine uptake, with glial cells expressing EAAT1 and EAAT2 isoforms and neurons expressing EAAT 3 and EAAT4 (Anderson and Swanson 2000). Cysteine is rapidly oxidized in the extracellular environment to the dipeptide cystine so the majority of dietary cysteine is packaged into GSH by the liver for systemic transport (Lu 2009). Interestingly, while neuronal cells utilize cysteine for GSH biosynthesis, glial cells have the capacity to use either cysteine or cystine, which is imported via the Na^+-independent glutamate-cysteine antiporter (X_c^-). Although cysteine can also be derived from methionine via the trans-sulfuration pathway for astrocytic GSH synthesis, it does not appear to be a major source of cysteine for neuronal GSH biosynthesis (McBean 2012).

GSH efflux from astrocytes provides cysteine for neuronal GSH biosynthesis and the export of GSH conjugates from neurons and astrocytes is critical in the ultimate removal of conjugated cytotoxic xenobiotics. The multidrug resistance-associated proteins (MRPs) mediate the ATP-dependent export of GSH, GSSG, and GSH conjugates from the cell (Dallas et al. 2006). MRP-mediated efflux of GSH-drug conjugates is thought to play an important role in the development of resistance to various chemotherapeutics in most human CNS tumors (Bredel and Zentner 2002), with MRP overexpression directly correlating with drug resistance in gliomas and inversely with clinical outcome in neuroblastoma (Backos et al. 2012).

The expulsion of GSH-drug conjugates can lead to the depletion of intracellular GSH and a disruption of the GSH:GSSG ratio and cellular antioxidant capacity. These conditions promote the inducible expression of enzymes involved in the de novo GSH synthesis and GSH salvage pathways. The GCL subunits are regulated at the transcriptional, post-transcriptional, and post-translational levels in response to oxidative stress (Backos et al. 2011; Franklin et al. 2009), with the Nrf1/2, AP-1, and NF-κB transcription factors regulating the inducible and constitutive expression of both subunits (Lu 2009). The Nrf2 transcription factor mediates the induction of multiple cytoprotective enzymes involved in GSH biosynthesis, utilization, and export, including GCLC, GCLM, GR, γGT, GPx, GSTs, and MRPs (Lu 2009). Interestingly, Nrf2-dependent upregulation of glial cell GSH biosynthesis is both necessary and sufficient to protect neurons from oxidative stress by providing cysteine for neuronal GSH biosynthesis. Nrf2 activation may also coordinate astrocyte release of GSH and neuronal GSH biosynthesis via transcriptional upregulation of astrocyte GCL and neuronal EAAT3 expression, respectively (Escartin et al. 2011). Although the GCL subunits are often coordinately induced, enhanced GCLM

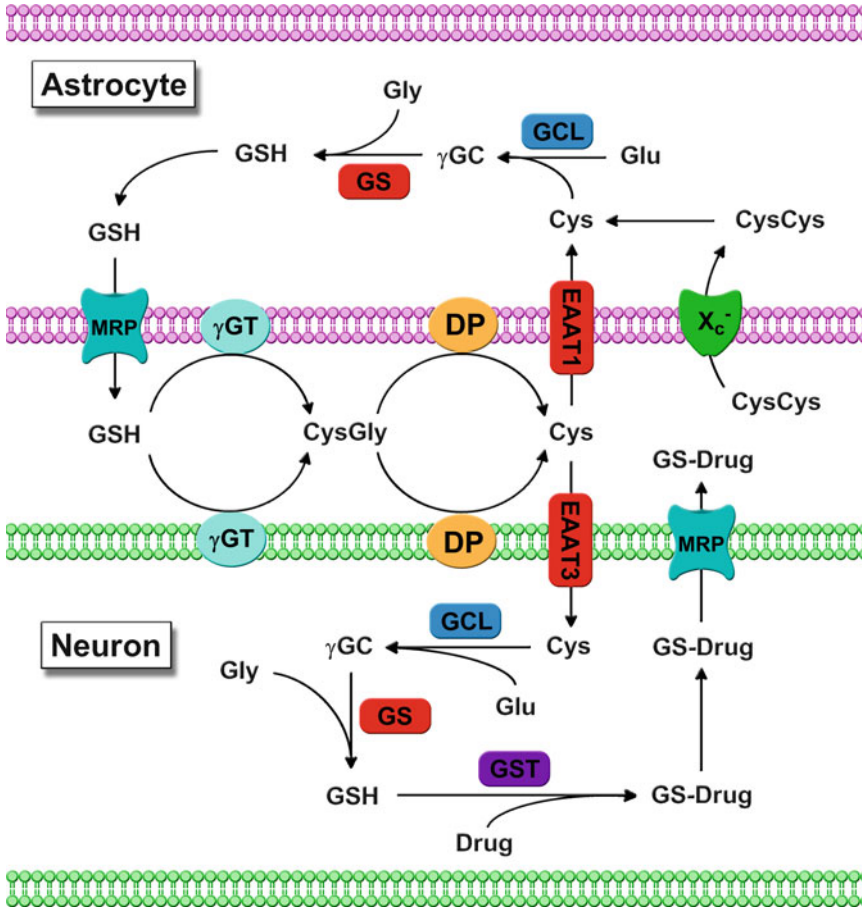

Fig. 24.2 Schematic of GSH-mediated interactions between astrocytes and neurons. Multidrug resistance protein (*MRP*)-mediated GSH efflux into the extracellular space by astrocytes is processed by γ-glutamyl transpeptidase (*γGT*) into glutamate (*Glu*) and cysteinylglycine (*CysGly*). CysGly is further hydrolyzed by cellular dipeptidases (*DP*) followed by excitatory amino acid transporter (*EAAT*)-mediated uptake of the constituent amino acids that can serve as substrates for either protein synthesis or cellular GSH production via the glutamate cysteine ligase (*GCL*)-catalyzed formation of γ-glutamylcysteine (*γGC*) from cysteine (*Cys*) and Glu and the glutathione synthetase (*GS*)-catalyzed formation of GSH from γGC and glycine (*Gly*). GSH is utilized as a cofactor in the glutathione-S-transferase (*GST*)-mediated formation of GSH-drug conjugates (GS-Drug) that are removed from the cell via MRP-mediated efflux. Additional Cys for GSH biosynthesis in astrocytes may also be obtained via the glutamate-cystine antiporter (X_c^-)-mediated uptake of extracellular cystine (CysCys) which is rapidly reduced to Cys within the intracellular compartment

expression has the potential to contribute more significantly to the inducible increase in GCL activity due to the massive increase in activity resulting from heterodimerization with GCLC. However, both GCL subunits are essential for the viability of cultured primary cortical neurons and overexpression of GCLC protects against glutamate- and NO-induced apoptosis (Diaz-Hernandez et al. 2005). Like other GSH metabolic enzymes, the GCL subunits are overexpressed in many tumor cell types and may play a central role in the development of chemoresistance (Lu 2009).

Human Brain Tumors

Tumors of the brain and CNS are among some of the fastest growing, most drug resistant, and most lethal human cancers. In contrast to most other

human cancers, malignant brain tumors do not distally metastasize to other organs or tissues, generally remaining limited to the brain and CNS. The blood–brain barrier (BBB) is an additional hurdle unique to brain tumors which limits the number of chemotherapeutic options to those capable of significant partitioning into the neural compartment. Most studies from the literature examining drug resistance in CNS neoplasms have focused on those tumors with the highest incidence: gliomas in adults and medulloblastomas in children. Consequently, the discussion will focus mainly on these tumor types.

Gliomas

Malignant gliomas, including glioblastoma (GBM), anaplastic astrocytoma, and anaplastic oligodendroglioma, are the most common type of CNS malignancy in adults and comprise approximately 35 % of the total number CNS tumors diagnosed in the United States (Kohler et al. 2011). Standard of care for malignant gliomas usually involves surgical resection followed by radiation and concomitant chemotherapy (Stupp et al. 2009). However, in spite of these intensive therapies, the prognosis for patients diagnosed with malignant glioma is poor. The overall 5-year survival for adults ranges from about 30 % for anaplastic astrocytoma to about 8 % for GBM, while the median survival time after GBM diagnosis is typically 12–14 months, or <3 months without treatment (Kohler et al. 2011). Tumor relapse after an initially successful course of treatment is a common occurrence in gliomas and typically results in greater overall tumor resistance to subsequent therapy. Nullification of this resistance often requires intensifying the chemotherapeutic dosage regimen or incorporating adjuvant and/or experimental therapeutics. Both intrinsic and acquired drug resistance mechanisms have been implicated in the poor response of both primary and recurrent glial tumors to chemotherapy (Bredel and Zentner 2002).

The originating cell type of a brain tumor generally has a substantial impact on the behavior and relative susceptibility of tumors to chemotherapy. GBM and anaplastic astrocytoma are thought to arise from mature astrocytes or from astrocyte and/or glial cell precursors (Fig. 24.3) (Huse and Holland 2010). Astrocytes possess significantly higher levels of GSH compared to neurons and, in keeping with their role in protecting neurons from both oxidative damage and xenobiotic toxicity, astrocytes have a robust GSH biosynthetic and efflux capacity (Dringen and Hirrlinger 2003). Xenobiotic detoxification enzymes are also enriched in astrocytes as these cells are involved in the initial uptake and metabolism of compounds capable of crossing the blood–brain barrier. This characteristic cellular GSH machinery is likely to survive neoplastic transformation and may play a role in the inherent resistance of GBM and astrocytomas to chemotherapy and radiation (Backos et al. 2012).

Oligodendrogliomas, the third most common type of glioma, are diffusely infiltrating brain tumors arising from oligodendrocytes or oligodendrocyte precursors (Fig. 24.3) and represent 3–5 % of primary brain tumors (Kohler et al. 2011). The majority (60–90 %) of oligodendrogliomas exhibit combined chromosome loss of 1p and 19q, which predicts a less aggressive tumor phenotype and enhanced sensitivity to chemotherapy (Backos et al. 2012). Cultured oligodendrocyte precursors have high levels of iron, lower levels of cellular GSH, and higher levels of baseline oxidative stress compared with astrocytes or neurons. In addition, oligodendrocyte precursors are more sensitive to oxidative stress-induced apoptosis in response to GSH depletion than their mature counterparts (Back et al. 1998). Interestingly, while mature oligodendrocytes also contain elevated iron levels and diminished levels of intracellular GSH, they exhibit enhanced hydrogen peroxide metabolic capacity due to increased enzymatic activity of GPx, GR, and catalase (Butts et al. 2008). The low level of cellular GSH in these cells likely plays a central role in the enhanced susceptibility of oligodendrogliomas to chemotherapy due to decreased GSH availability for non-enzymatic and/or GST-mediated detoxification. The abundance of intracellular iron contained in these cells, which has the capacity to participate in metal-catalyzed

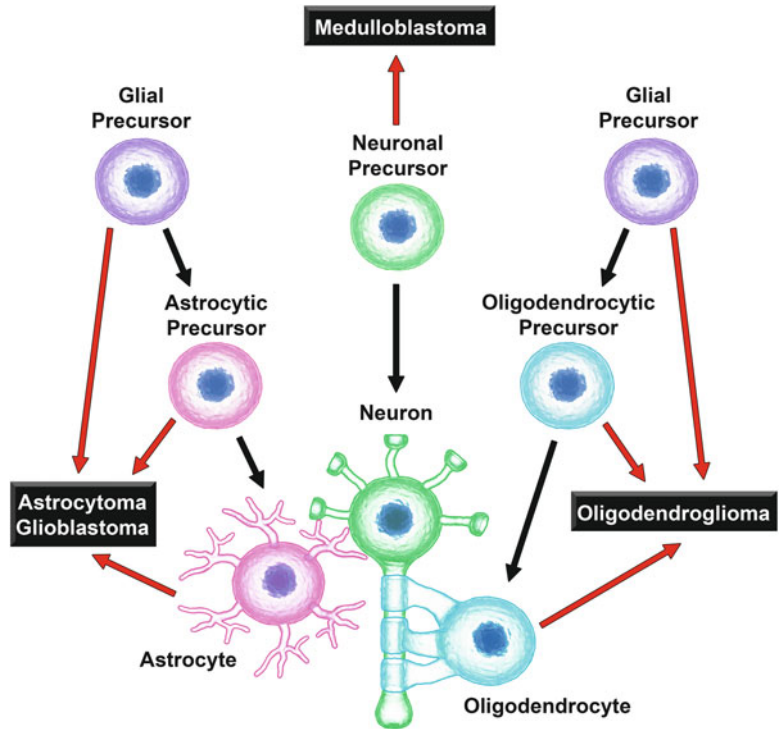

Fig. 24.3 Origins of the major cell populations in normal brain and the proposed origins of the most common types of malignant brain tumors. *Black arrows* indicate the developmental origins of astrocytes (*magenta*), neurons (*green*), and oligodendrocytes (*cyan*), the three major cell types present in normal brain tissue. *Red arrows* indicate the proposed originating cells giving rise to the indicated types of human brain neoplasms (Huse and Holland 2010)

oxidation reactions leading to the formation of highly reactive free radical species, also vastly enhances their sensitivity to the chemotherapeutic-mediated generation of ROS (Backos et al. 2012).

Medulloblastoma

While pediatric gliomas, including astrocytoma, glioblastoma, and oligodendroglioma, make up a sizable percentage of brain tumors diagnosed in children under 20 years of age, medulloblastoma is the most common type of childhood CNS malignancy and is the second leading cause of cancer-related death in this age group (Kohler et al. 2011). Medulloblastoma is a rapidly growing and highly invasive brain tumor that arises from the posterior fossa, typically the cerebellum, capable of metastasis to the spinal column and cerebrospinal fluid (CSF) (Gilbertson and Ellison 2008). Currently, 5-year survival stands at roughly 60 % although clinical outcomes vary with age, histological subtype, and metastatic status (Kohler et al. 2011). In contrast to the gliomas, medulloblastomas are thought to originate from immature neuronal progenitors (Fig. 24.3) (Huse and Holland 2010), with tumor cells exhibiting less differentiated and more stem cell-like characteristics, including robust drug resistance (Backos et al. 2012). The GSH detoxification system has been implicated in the resistance of medulloblastoma to alkylating agents. Treatment with GSH or the GSH precursor substrate N-acetylcysteine (NAC) protects medulloblastoma cells against camptothecin (CPT)-induced apoptosis and medulloblastoma cells resistant to cyclophosphamide (CPA) and 4-hydroperoxy-CPA (4-HC) exhibit enhanced cellular GSH levels and γGT expression (Backos et al. 2012). The expression of catalytically inactive polymorphisms of the

GST isozymes in a tumor would be expected to result in impaired metabolism of some cytotoxic drugs, rendering these tumors vulnerable to treatment. However, medulloblastoma patients with somatic inactive GST null polymorphisms have an increased risk of adverse events during therapy, including myelosuppression, ototoxicity, nephrotoxicity, and cognitive impairment, as well as lower rates of survival due to the fact that the null phenotype is not strictly limited to the tumor and results in enhanced chemotherapy-associated toxicity to normal tissues (Backos et al. 2012).

Brain Metastases

Distal metastasis to the brain is the final stage of a variety of human neoplasms, including lung cancer, malignant melanoma, renal-cell carcinoma, and breast cancer (Barnholtz-Sloan et al. 2004), and is often responsible for the ultimate fatality of these diseases. Metastases to the brain generally occur due to the colonization of cancer cells separated from the tumor and transported through the bloodstream. The first step in the initiation of metastasis involves the direct contact between tumor cells and the capillary endothelial cells lining the microvasculature. This results in the release of pro-inflammatory cytokines and increased ROS production, which is generally lethal to the metastatic cells (Estrela et al. 2006). However, elevated cellular GSH levels protect against the cytotoxic effects of this initial burst of ROS, with GSH levels directly correlating with tumor cell metastatic potential and pharmacological depletion of GSH substantially reducing metastatic invasiveness (Estrela et al. 2006). Interaction of the tumor with the host cells of the brain microenvironment, the astrocyte population in particular, also plays a significant role in protection from chemotherapy-induced toxicity (Fidler 2011). Astrocytes form direct contacts with melanoma cells in vitro and these interactions result in the upregulation of survival genes, including GSTs, and heightened resistance to chemotherapeutic agents (Kim et al. 2011). This enhancement of tumor cell drug resistance by astrocytes has also been demonstrated in lung and breast cancer cells (Fidler 2011). Upregulation of γGT protein expression has also been observed in many brain tumors and this is associated with enhanced drug resistance due to the increased availability of substrates necessary for GSH synthesis. Thus, metastatic cell populations may be able to exploit the supportive nature of astrocytes and utilize their chemoprotective resources, such as GSH, to support the growth of the tumor and confer greater resistance to therapy.

GSH and GSH-linked Enzyme Contributions to Chemoresistance

Role of GSH as an Antioxidant

Increased ROS production, and the resulting dysregulation of cellular redox homeostasis, plays an integral role in the cytotoxicity of various chemotherapeutic compounds towards tumor cells, many of which are not known to involve formation of free radical species (Wondrak 2009). Numerous studies have demonstrated that the generation of ROS is an underlying mediator of tumor cell apoptosis induced by many chemotherapeutics, including cisplatin, paclitaxel, bleomycin, and etoposide (Wondrak 2009). Although depletion of cellular GSH due to metabolic detoxification of chemotherapeutic compounds can result in the disruption of cellular redox balance and the induction of apoptosis, chemotherapy-induced ROS production is not necessarily related to the loss of GSH per se. For example, cisplatin-induced apoptosis has been shown to be associated with enhanced generation of ROS and not with the induction of nuclear DNA damage, which suggests that oxidative stress may be the central mechanism responsible for cisplatin-induced tumor cell death (Wondrak 2009). Similarly, temozolomide (TMZ), an alkylating agent currently comprising the standard of care for the treatment of adult gliomas (Stupp et al. 2009), is also known to induce ROS production in glioma cells and the acquisition of a TMZ-resistant phenotype in these cells involves a decrease in endogenous ROS production due to an increase in mitochondrial coupling (Oliva

et al. 2011). This remodeling of the mitochondrial electron transport chain serves to conserve cellular GSH pools which can then be employed to suppress TMZ-induced ROS production. Thus, the chemoprotective role of GSH in drug-resistant tumor cells is not limited to its functions as a cofactor in the GSH conjugation-mediated metabolism and detoxification of chemotherapeutics, but also includes detoxification of ROS generated by chemotherapeutic agents.

Role of Enhanced GSH Biosynthesis

Many human cancers overexpress one or both of the GCL subunits to enhance cellular GSH biosynthetic capacity in order to protect against the excess of ROS production resulting from enhanced proliferation and energy metabolism. The overexpression of GSH biosynthetic pathway enzymes, particularly GCL, leads to increased cellular GSH concentrations and enhanced tumor drug resistance in brain malignancies. GSH levels are inversely related to nitrogen mustard sensitivity in brain neoplasms and CPT-resistant glioma cells have increased levels of intracellular GSH compared with CPT-sensitive glioma cells (Backos et al. 2012). Increased levels of GSH are also associated with significant inactivation of BCNU and relative chemoresistance to BCNU directly correlates with cellular GSH levels in human brain tumor cell lines (Ali-Osman et al. 1990). BCNU, in addition to its activity as a DNA alkylating agent, is also a potent inhibitor of GR activity and can disrupt cellular antioxidant status by substantially reducing or eliminating GSH salvage from GSSG (Pastore and Piemonte 2012). Thus, BCNU resistance requires enhanced GSH biosynthesis to maintain cellular levels of reduced GSH, suggesting that inhibition of cellular GSH biosynthesis to deplete cellular GSH stores would reverse the resistant phenotype. In this regard, L-buthionine-*S,R*-sulfoximine (BSO), a specific inhibitor of GCL enzymatic activity, was found to enhance BCNU cytotoxicity in glioma cells (Backos et al. 2012).

Enhanced cellular GSH biosynthetic capacity can be accomplished via both constitutive and inducible mechanisms. Constitutive expression of GCLC, for example, is influenced by genetic polymorphisms in a GAG/CTC tri-nucleotide repeat present within the 5′ untranslated region of GCLC, with copy number of this repeat significantly influencing both cellular GSH levels and drug sensitivities in a plethora of human tumor cell lines (Franklin et al. 2009). In contrast, oxidative signaling mechanisms, such as oxidative stress induced by the chemotherapeutic-mediated generation of ROS, are involved in the inducible expression of enzymes involved in GSH biosynthesis. Multiple regulatory elements have been implicated in the transcriptional induction of the GCL subunits, including Nrf2, AP-1, AP-2, and NF-κB response elements. As changes in GCL subunit mRNA largely equate to changes in subunit protein expression, these transcriptional events lead to increased protein translation, with concomitant increases in cellular GCL activity, GSH biosynthetic capacity, and cellular GSH levels (Lu 2009). This constitutes an effective adaptive response for tumor cells to enhance drug resistance when confronted with anticancer regimens. In addition, posttranslational modification of one or both of the existing GCL subunits in response to a variety of oxidative insults can also have a dramatic effect on GCL protein function and activity without requiring the transcription and translation of the subunits and represents an additional mechanism involved in the regulation of GSH biosynthesis (Backos et al. 2011; Franklin et al. 2009).

Most studies seeking to elucidate the role of GSH biosynthesis in tumor drug resistance have focused on GCL since it is usually the rate-limiting step in the process. However, GS, the second enzyme in the GSH biosynthetic pathway mediating the ATP-dependent coupling of γ-GC to glycine, has also been found to play a role. Expression of GS is correlated with cisplatin resistance in human ovarian cancer cells (Backos et al. 2012) and expression was found to be elevated in drug-resistant liver tumors (Lu 2009). GS is transcriptionally regulated and can be coordinately induced with the GCL subunits under certain conditions. While GS activity has been measured in the brain, little is known concerning

its potential role in regulating brain GSH levels or its expression in human brain tumors. However, most pharmacological approaches to inhibiting the GSH biosynthetic pathway have targeted GCL since deficiencies in GS lead to the accumulation of γ-GC which is metabolized to 5-oxoproline and can ultimately cause the induction of metabolic acidosis, hemolytic anemia and nervous system dysfunction (Lu 2009).

Role of Glutathione S-transferases

Glutathione S-transferases (GSTs) are Phase II metabolic enzymes that detoxify a wide array of drugs and other xenobiotics via conjugation with reduced GSH (Townsend and Tew 2003). It is generally thought that GSTs play an important role in cancer development, chemoresistance, and clinical outcome due to their ability to metabolize both carcinogens and cancer chemotherapeutics. The GSH conjugates of chloroethylnitrosoureas (CENUs), platinum compounds and a number of other alkylating agents, including melphalan, cyclophosphamide, chlorambucil, doxorubicin and nitrogen mustards, are more polar and less cytotoxic than their parent compounds and are substrates for transporter-mediated export from the cell (Townsend and Tew 2003). Therefore, cellular GSH conjugation capacity, as dictated by GST enzymatic expression and activity, can be a contributing factor to a drug-resistant phenotype and clinical non-responsiveness of brain tumors to alkylating agent-based therapy.

The GST superfamily is a group of widely distributed and heterogeneous cellular enzymes encoded by separate genes located on different chromosomes. Seven cytosolic GST family members have been identified, with four major isoforms present in the brain: α, μ, π and θ, all of which display distinct substrate specificities and expression profiles (Bredel and Zentner 2002). Studies examining the expression of GSTs in both normal brain parenchyma and brain tumors have identified the GST π isoform as the major contributor to GST activity in both normal brain tissue and tumor tissue (Backos et al. 2012; Bredel and Zentner 2002). The GST π class is also the most highly expressed in human cancers and appears to be the most relevant isoform in brain tumor drug resistance (Bredel and Zentner 2002). Elevated GST π expression is associated with a significantly shorter patient survival time in GBMs and GST π expression levels also directly correlate with tumor grade and inversely correlate with patient survival (Backos et al. 2012). These findings suggest that elevated expression of GST π in brain tumors predicts more aggressive and/or chemoresistant tumors with poorer prognosis. Chemotherapeutic treatment can also induce the expression of GST in human brain tumors. While the GST π gene is overexpressed in about 40 % of human brain tumors, the expression and activity of GST π and μ is increased after treatment with nimustine hydrochloride (ACNU) (Backos et al. 2012). The elevated expression of GST π in brain tumors after treatment suggests that GST-mediated drug resistance can also be an acquired phenomenon that may play a role in the enhanced drug resistance of recurrent brain tumors as well as cross-resistance to other anticancer agents detoxified by GSTs.

Immunohistochemical studies have further established GST π as the predominant isoform in both normal and neoplastic brain tissues. In the normal brain, GST π is present in astrocytes and endothelial cells, but not in neurons or oligodendrocytes (Grant and Ironside 1995). Studies assessing GST π expression in human gliomas demonstrate GST π is expressed in both low and high grade tumors and this expression correlates with increasing malignancy grade (Backos et al. 2012). GST π activity has been shown to correlate with GST π protein expression and mRNA levels, suggesting that transcriptional upregulation of GST may be primarily responsible for the elevated activity of this enzyme in human brain tumors (Townsend and Tew 2003). GST π mRNA and protein levels in ACNU-resistant glioma cells are up to threefold higher than that of their sensitive counterparts and a direct correlation exists between GST π expression and BCNU resistance in malignant glioma cell lines (Backos et al. 2012).

The expression of distinct gene variants of individual GST classes has a substantial impact on the capability of tumor cells to detoxify anticancer agents as well as their susceptibility to chemotherapeutics. Genetic polymorphisms of human GST μ (GST-M1*A, GST-M1*B, and GST-M1*0) and GST θ (GST-T1*0) have been identified that result in catalytically active enzymes with altered charge and kinetic properties compared with their wild-type counterparts (Townsend and Tew 2003). Three closely related full-length GST π cDNA variants (GSTP1*A, GSTP1*B, and GSTP1*C) have been isolated, with the hGSTP1*C variant selectively expressed at greater levels in gliomas than in normal cells (Lo and Ali-Osman 2007). Despite advances in understanding the molecular nature of the GST π gene in human cells, the role of individual variants in xenobiotic metabolism in brain tumors has yet to be established. In addition, the importance of polymorphisms of enzymes involved in de novo GSH synthesis or GSH salvage pathways in drug resistance is currently unknown.

In addition to their role in GSH-conjugation reactions, GSTs can also regulate pro-apoptotic signaling pathways via direct protein-protein interactions (Townsend and Tew 2003). GSTP1 and GSTM1 bind and prevent JNK and ASK1 protein kinase activation, respectively. This regulatory mechanism may play a role in drug resistance as dissociation of the GSTP1-JNK complex and polymerization of GSTP1 is required for optimal etoposide-induced apoptosis in etoposide-resistant human neuroblastoma cells (Lo and Ali-Osman 2007). GSTP1 is also activated via post-translational phosphorylation by protein kinase A (PKA), protein kinase C (PKC), and the epithelial growth factor receptor tyrosine kinase (EGFR-TK), which results in increased metabolism and resistance against cisplatin in human glioblastoma cells (Tew and Townsend 2011). Inhibition of EGFR-TK activity reverses this EGF-induced cisplatin resistance, suggesting that combined therapy may prove to be an effective strategy for treating EGFR positive tumors with elevated GSTP1 expression.

The Role of GSH as a Signaling Molecule

Although disruption of GSH homeostasis, such as GSH depletion or shifts in the GSH:GSSG ratio, results in signaling cascades inducing transcriptional activation of GSH biosynthetic and salvage enzymes, GSH itself can function as a regulator of various cellular signaling processes via its ability to promote post-translational modification of proteins via S-glutathionylation. Glutathionylation is a reversible covalent modification that occurs under oxidative and nitrosative conditions, resulting in the formation of a mixed protein disulfide linkage between GSH and the sulfhydryl group of Cys residue(s). These reactions can be non-enzymatic, via direct thiol/disulfide exchange reactions or the formation of protein cysteinyl or GSH thiyl radicals, or catalyzed by GST π or glutaredoxin (Grx) (Hill and Bhatnagar 2012; Xiong et al. 2011). As human brain tumors overexpress the GST π isoform, GST π -catalyzed glutathionylation is likely elevated in these tumor types. Glutathionylation typically results in a loss of protein activity, often via modification of an active site Cys residue, and can alter protein-protein interactions, ligand binding, or target proteins for proteasome-mediated degradation (Hill and Bhatnagar 2012; Xiong et al. 2011). Glutathionylation may also preserve protein function by preventing the irreversible oxidative inactivation of critical Cys residues. Given the number of redox-sensitive proteins involved in a variety of cellular processes, glutathionylation has the potential to regulate multiple pathways associated with chemoresistance.

The reversible nature of glutathionylation provides the cell with an inducible redox-dependent molecular switch to regulate protein function. Deglutathionylation reactions can be enzymatically mediated, with the predominant function of Grx likely being deglutathionylation (Xiong et al. 2011). Sulfiredoxin (Srx), protein-disulfide isomerase, and thioredoxin have also been reported to exhibit deglutathionylation activity (Hill and Bhatnagar 2012). While Grx and Srx expression levels have yet to be characterized in human brain tumors, these enzymes have been shown to be

differentially expressed in several other tumor types relative to normal tissue. Deglutathionylation reactions can also occur in a spontaneous, non-enzymatic manner through thiol/disulfide exchange in the presence of reduced GSH. Thus, reestablishment of GSH redox homeostasis can also result in the non-enzymatic reversal of these post-translational modifications and restoration of protein function.

There is a clear correlation between the GSH system and brain tumor drug resistance, however the role of glutathionylation in the development of drug resistance is not clear. Studies directly examining the relationship between glutathionylation and cell survival have resulted in contradictory findings. For instance, glutathionylation of p53 following treatment with DNA damaging agents inhibits its activity in U87 malignant glioma cells (Hill and Bhatnagar 2012). Glutathionylation has also been reported to inhibit caspase-3 processing and activation leading to reduced apoptotic cell death (Xiong et al. 2011). In contrast, nitrosoglutathione-induced glutathionylation enhances doxorubicin sensitivity in a resistant cell line (de Luca et al. 2011) and Grx1 overexpression is associated with adriamycin-resistance in breast cancer cells (Wells et al. 1995). These conflicting findings are likely due to the ability of glutathionylation to affect intermediates in multiple signal transduction pathways that influence cell survival, including the Ras-MEK-ERK, NFκB, JNK-c-Jun, and PTEN-PI3K-Akt-p53 pathways (for a more in-depth review, see (Xiong et al. 2011)). In this regard, global glutathionylation may not be a good biomarker for chemosensitivity as the differential glutathionylation of distinct subsets of proteins likely dictates the cellular response.

Interestingly, multiple GSH metabolic enzymes have also been shown to be regulated via glutathionylation. For instance, glutathionylation of GSTP1 promotes the dissociation of the GSTP1-JNK complex and subsequent JNK activation that is required for chemosensitization of etoposide-resistant neuroblastoma cells (Xiong et al. 2011). We have also shown that glutathionylation of the GCL subunits can inhibit GCL holoenzyme formation and activity, which could serve to enhance chemosensitivity via reduced de novo GSH biosynthesis [Poerschke et al., in preparation]. Alternatively, glutathionylation and inhibition of Keap1, the inhibitory regulator of the Nrf2 transcription factor, is thought to increase the expression of a battery of antioxidant and detoxifying enzymes that are regulated by Nrf2 (Pastore and Piemonte 2012), including various GSH metabolic enzymes. By regulating the levels and activities of such antioxidant and detoxification enzymes, glutathionylation likely affects brain tumor chemosensitivity. The identification of specific proteins that are targets for glutathionylation, the conditions that regulate their glutathionylation status, and the downstream effects of such modifications is an ongoing process that will continue to add to our understanding of the role of glutathionylation in brain tumor drug resistance.

Although oxidative stress leads to the production of GSSG, it is unlikely that GSSG would be maintained at levels necessary for direct, non-enzymatic protein glutathionylation. However, conditions that inhibit GR activity could lead to an accumulation of GSSG that is sufficient to promote glutathionylation and cytotoxicity. In fact, this likely occurs with the use of chemotherapeutic nitrosoureas such as BCNU. While BCNU induces protein glutathionylation (Rinna et al. 2006), the role of glutathionylation in mediating the cytotoxicity of BCNU and other nitrosoureas has yet to be established and represents an area of future study.

There are currently several glutathionylation-inducing compounds under investigation for use in cancer chemotherapy. NOV-002 is a GSSG mimetic that promotes glutathionylation but is not cytotoxic as a single agent. NOV-002 has been used in clinical trials in combination with standard therapy, but demonstrates variable benefits (Tew and Townsend 2011). PABA-NO is a GST π-activated pro-drug that releases NO, which promotes nitrosylation and glutathionylation. PABA-NO displays strong anti-proliferative effects as a single agent in U87 malignant glioma cells and exhibits synergistic effects in combination with TMZ, but not carboplatin (Kogias et al. 2012). Interestingly, despite the known role of GST π in the development drug resistance, acquired

resistance to PABA-NO has been described in human leukemia cells, which can be attributed to suppression of GST π expression and reduced NO release (Tew and Townsend 2011). Another GST π-activated NO-releasing pro-drug JS-K also exhibits anti-proliferative effects in U87 glioma cells in vitro and in vivo (Weyerbrock et al. 2012). The continued development of these and other GST π-activated pro-drugs to exploit the overexpression of GST π in brain tumors appears to be a promising approach to overcome GST π-mediated brain tumor drug resistance.

Conclusions

In summary, cellular GSH levels and the expression and activity of the various GSH-dependent enzymes can be a determining factor governing the sensitivity of brain tumors to various chemotherapeutic agents. The differential expression and activity of the GST π isoform among different histopathological groups of brain neoplasms, as well as among individual tumors within a given tumor class, may prove to be a useful biomarker for identifying tumors with the potential to respond to a particular treatment regimen. The interactions between cellular GSH biosynthetic capacity, GSH/GST-mediated drug detoxification, and the MRP-facilitated efflux of GSH-drug conjugates has an important role in conferring drug resistance in primary brain tumors and these three pathways represent excellent targets for novel therapeutic compounds aimed at reducing brain tumor drug resistance. Moreover, the upregulation of enzymes involved in the GSH biosynthetic, conjugation, and export pathways is a common tumor cell response to many chemotherapeutic treatments and targeting these pathways in parallel with the administration of cytotoxic drugs may be a viable method to attenuate or prevent the development of drug resistance in naïve tumors. Pharmacological approaches employing BSO to inhibit cellular GSH biosynthesis and induce GSH depletion as a means of enhancing the efficacy of chemotherapy have shown some promise. However, a major disadvantage to the clinical use of BSO is its potential to enhance toxicity in normal tissue due to a lack of selectivity for tumor cells. It is intriguing to speculate on the feasibility of developing GST π-activated prodrugs that result in the release of inhibitors of GCL, GSTs, MRPs, or other GSH-dependent enzymes directly to the tumor cells as a means to selectively chemosensitize these tumors. Additionally, the role of glutathionylation in mediating tumor chemoresistance is just beginning to be elucidated and future studies on glutathionylation may possibly uncover additional targets for pharmacological intervention to enhance chemotherapy response. In any event, the critical role that GSH and the GSH-linked enzymes play in brain tumor drug resistance should not be overlooked and targeting these pathways with novel small molecule inhibitors may represent a viable method of sensitizing brain tumors to therapy.

Acknowledgements We would like to acknowledge our colleagues in the field who we have not referenced due to the limitations set by the journal guidelines.

References

Ali-Osman F, Stein DE, Renwick A (1990) Glutathione content and glutathione-S-transferase expression in 1,3-bis(2-chloroethyl)-1-nitrosourea-resistant human malignant astrocytoma cell lines. Cancer Res 50(21): 6976–6980

Anderson CM, Swanson RA (2000) Astrocyte glutamate transport: review of properties, regulation, and physiological functions. Glia 32(1):1–14

Back SA, Gan X, Li Y, Rosenberg PA, Volpe JJ (1998) Maturation-dependent vulnerability of oligodendrocytes to oxidative stress-induced death caused by glutathione depletion. J Neurosci 18(16):6241–6253

Backos DS, Fritz KS, Roede JR, Petersen DR, Franklin CC (2011) Posttranslational modification and regulation of glutamate-cysteine ligase by the alpha, beta-unsaturated aldehyde 4-hydroxy-2-nonenal. Free Radic Biol Med 50(1):14–26

Backos DS, Franklin CC, Reigan P (2012) The role of glutathione in brain tumor drug resistance. Biochem Pharmacol 83(8):1005–1012

Barnholtz-Sloan JS, Sloan AE, Davis FG, Vigneau FD, Lai P, Sawaya RE (2004) Incidence proportions of brain metastases in patients diagnosed (1973 to 2001) in the Metropolitan Detroit Cancer Surveillance System. J Clin Oncol 22(14):2865–2872

Bredel M, Zentner J (2002) Brain-tumour drug resistance: the bare essentials. Lancet Oncol 3(7):397–406

Butts BD, Houde C, Mehmet H (2008) Maturation-dependent sensitivity of oligodendrocyte lineage cells to apoptosis: implications for normal development and disease. Cell Death Differ 15(7):1178–1186

Dallas S, Miller DS, Bendayan R (2006) Multidrug resistance-associated proteins: expression and function in the central nervous system. Pharmacol Rev 58(2):140–161

de Luca A, Moroni N, Serafino A, Primavera A, Pastore A, Pedersen JZ, Petruzzelli R, Farrace MG, Pierimarchi P, Moroni G, Federici G, Sinibaldi Vallebona P, Lo Bello M (2011) Treatment of doxorubicin-resistant MCF7/Dx cells with nitric oxide causes histone glutathionylation and reversal of drug resistance. Biochem J 440(2):175–183

Diaz-Hernandez JI, Almeida A, Delgado-Esteban M, Fernandez E, Bolanos JP (2005) Knockdown of glutamate-cysteine ligase by small hairpin RNA reveals that both catalytic and modulatory subunits are essential for the survival of primary neurons. J Biol Chem 280(47):38992–39001

Dringen R, Hirrlinger J (2003) Glutathione pathways in the brain. Biol Chem 384(4):505–516

Escartin C, Won SJ, Malgorn C, Auregan G, Berman AE, Chen PC, Deglon N, Johnson JA, Suh SW, Swanson RA (2011) Nuclear factor erythroid 2-related factor 2 facilitates neuronal glutathione synthesis by upregulating neuronal excitatory amino acid transporter 3 expression. J Neurosci 31(20):7392–7401

Estrela JM, Ortega A, Obrador E (2006) Glutathione in cancer biology and therapy. Crit Rev Clin Lab Sci 43(2):143–181

Fidler IJ (2011) The role of the organ microenvironment in brain metastasis. Semin Cancer Biol 21(2):107–112

Franklin CC, Backos DS, Mohar I, White CC, Forman HJ, Kavanagh TJ (2009) Structure, function, and post-translational regulation of the catalytic and modifier subunits of glutamate cysteine ligase. Mol Aspects Med 30(1–2):86–98

Gilbertson RJ, Ellison DW (2008) The origins of medulloblastoma subtypes. Annu Rev Pathol 3:341–365

Grant R, Ironside JW (1995) Glutathione S-transferases and cytochrome P450 detoxifying enzyme distribution in human cerebral glioma. J Neurooncol 25(1):1–7

Hill BG, Bhatnagar A (2012) Protein S-glutathiolation: redox-sensitive regulation of protein function. J Mol Cell Cardiol 52(3):559–567

Huse JT, Holland EC (2010) Targeting brain cancer: advances in the molecular pathology of malignant glioma and medulloblastoma. Nat Rev Cancer 10(5):319–331

Kim SJ, Kim JS, Park ES, Lee JS, Lin Q, Langley RR, Maya M, He J, Kim SW, Weihua Z, Balasubramanian K, Fan D, Mills GB, Hung MC, Fidler IJ (2011) Astrocytes upregulate survival genes in tumor cells and induce protection from chemotherapy. Neoplasia 13(3):286–298

Kogias E, Osterberg N, Baumer B, Psarras N, Koentges C, Papazoglou A, Saavedra JE, Keefer LK, Weyerbrock A (2012) Growth-inhibitory and chemosensitizing effects of the glutathione-S-transferase-pi-activated nitric oxide donor PABA/NO in malignant gliomas. Int J Cancer (Journal International du Cancer) 130(5):1184–1194

Kohler BA, Ward E, McCarthy BJ, Schymura MJ, Ries LA, Eheman C, Jemal A, Anderson RN, Ajani UA, Edwards BK (2011) Annual report to the nation on the status of cancer, 1975–2007, featuring tumors of the brain and other nervous system. J Natl Cancer Inst 103(9):714–736

Lo HW, Ali-Osman F (2007) Genetic polymorphism and function of glutathione S-transferases in tumor drug resistance. Curr Opin Pharmacol 7(4):367–374

Lu SC (2009) Regulation of glutathione synthesis. Mol Aspects Med 30(1–2):42–59

McBean GJ (2012) The transsulfuration pathway: a source of cysteine for glutathione in astrocytes. Amino Acids 42(1):199–205

Oliva CR, Moellering DR, Gillespie GY, Griguer CE (2011) Acquisition of chemoresistance in gliomas is associated with increased mitochondrial coupling and decreased ROS production. PLoS One 6(9):e24665

Pastore A, Piemonte F (2012) S-Glutathionylation signaling in cell biology: progress and prospects. Eur J Pharm Sci 46(5):279–292

Rinna A, Torres M, Forman HJ (2006) Stimulation of the alveolar macrophage respiratory burst by ADP causes selective glutathionylation of protein tyrosine phosphatase 1B. Free Radic Biol Med 41(1):86–91

Stupp R, Hegi ME, Mason WP, van den Bent MJ, Taphoorn MJ, Janzer RC, Ludwin SK, Allgeier A, Fisher B, Belanger K, Hau P, Brandes AA, Gijtenbeek J, Marosi C, Vecht CJ, Mokhtari K, Wesseling P, Villa S, Eisenhauer E, Gorlia T, Weller M, Lacombe D, Cairncross JG, Mirimanoff RO (2009) Effects of radiotherapy with concomitant and adjuvant temozolomide versus radiotherapy alone on survival in glioblastoma in a randomised phase III study: 5-year analysis of the EORTC-NCIC trial. Lancet Oncol 10(5):459–466

Tew KD, Townsend DM (2011) Regulatory functions of glutathione S-transferase P1-1 unrelated to detoxification. Drug Metab Rev 43(2):179–193

Townsend DM, Tew KD (2003) The role of glutathione-S-transferase in anti-cancer drug resistance. Oncogene 22(47):7369–7375

Wells WW, Rocque PA, Xu DP, Meyer EB, Charamella LJ, Dimitrov NV (1995) Ascorbic acid and cell survival of adriamycin resistant and sensitive MCF-7 breast tumor cells. Free Radic Biol Med 18(4):699–708

Weyerbrock A, Osterberg N, Psarras N, Baumer B, Kogias E, Werres A, Bette S, Saavedra JE, Keefer LK, Papazoglou A (2012) JS-K, a glutathione S-transferase-activated nitric oxide donor with antineoplastic activity in malignant gliomas. Neurosurgery 70(2): 497–510, discussion 510

Wondrak GT (2009) Redox-directed cancer therapeutics: molecular mechanisms and opportunities. Antioxid Redox Signal 11(12):3013–3069

Xiong Y, Uys JD, Tew KD, Townsend DM (2011) S-glutathionylation: from molecular mechanisms to health outcomes. Antioxid Redox Signal 15(1):233–270

Drugs for Primary Brain Tumors: An Update

25

Lauren Nye, Timothy Huyck, and Jeffrey Raizer

Contents

L. Nye • T. Huyck
Department of Medicine, Section Hematology/ Oncology, Northwestern University, 251 East Huron Street, Galter Suite 3-150, Chicago, IL 60611, USA

J. Raizer (✉)
Department of Medicine, Medical Neuro-Oncology, Northwestern University, 710 North Lake Shore Dr. Abbott Hall, Room 1123, Chicago, IL 60611, USA
e-mail: jraizer@nmff.org

Abstract

Primary brain tumors are a heterogeneous mix of tumors that can arise from structures within the cranium. This review will focus on tumors of glial origin. The best first approach to a primary brain tumor is maximal safe surgical resection. If the tumor is not amenable to resection, a biopsy is needed for tissue diagnosis. Despite maximal resection of the tumor, there always remains residual disease due to the infiltrative nature of the tumor. This has led to development of various chemotherapeutic regimens which have been developed for use in the neo-adjuvant, adjuvant and recurrent setting. The most significant development of these tumors is for high grade gliomas. Anaplastic astrocytomas and glioblastoma multiforme are frequently diagnosed tumors that continue to have a poor prognosis and short survival. Historically, chemotherapy has been demonstrated to provide a marginal survival benefit in patients with anaplastic astrocytoma and glioblastoma multiforme when used after surgical resection and radiation therapy. Modest improvement in overall survival was initially seen with the use of nitrosurea drugs, such as BCNU and CCNU, as well as some platinum compounds. More recent data suggests the use of temozolomide (TMZ) leads to an improved overall survival when given concurrently with radiation following resection of these aggressive tumors. Data on the vascular endothelial growth factor

M.A. Hayat (ed.), *Tumors of the Central Nervous System, Volume 12*,
DOI 10.1007/978-94-007-7217-5_25,

(VEGF) inhibitor, bevacizumab, has also been available and will be presented in the preceding text. Chemotherapeutic agents had a less pivotal role in the setting of low grade astrocytomas and other primary brain tumors.

Introduction

In 2010, an estimated 22,020 new cases of primary brain tumors and other nervous system neoplasms were diagnosed in the United States. These tumors were responsible for approximately 12,140 deaths. The number of newly diagnosed primary brain tumors has been increasing in the last 30 years, a number which is particularly appreciated in the elderly population (Jemal et al. 2010). CNS tumors are associated with a wide range of symptoms and complications such as edema, seizures, endocrinopathy, fatigue, psychiatric disorders, venous thromboembolism all of which can negatively impact quality of life of patients. The involvement of an interdisciplinary team, including neurosurgeons, radiation therapists, neuro and medical oncologists, neuroradiologists and neuropathologists optimizes the management of these patients. In the recent past there have been a few proven chemotherapeutic agents which have expanded the role of the oncologist in caring for patients with primary brain tumors.

Historical Overview of Chemotherapy in Maligant Gliomas

Malignant gliomas (MGs) account for almost half of all gliomas. The most common MGs are glioblastoma (GBMs), or rarely gliosarcomas, which account for 60 % of these tumors. Anaplastic gliomas (AG) are composed of astrocytomas (AAs: 10–15 %), anaplastic oligodendrogliomas (AOs: 8–10 %) and anaplastic oligoastrocytomas (AOAs: 8–10 %) (Stern and Raizer 2006). The most common form of initial treatment for MGs is surgical intervention. Indications for surgery include histologic diagnosis, reducing tumor burden and alleviating mass effect. External beam fractionated therapy is an appropriate form of treatment for MGs with numerous randomized controlled clinical trials showing a survival benefit for patients receiving surgical resection and irradiation versus resection alone (Walker et al. 1978). Irradiation is typically performed over 6–7 weeks, with patient receiving treatment 5 days per week (18–200 cGy fractions to a total dose of 6,000–6,140 cGy). In the 1960s and 1970s, surgical resection and postoperative external beam radiation therapy were established as the standard treatment approach for patients with GBM and AG (Laperriere et al. 2002).

In the late 1970s, investigators began to evaluate the role of chemotherapy when it became obvious that surgical resection and radiation were not curative. Early trials identified two nitrosurea drugs (CCNU and BCNU) as having a positive effect in treating patients with high-grade gliomas. In the late 1970s the first large scale multi-center trial for brain cancer was BTCG 7201, Walker et al. (1980) looked at the use of nitrosureas in combination with radiotherapy following surgery. Results of this study suggested a trend toward improved survival in the subjects randomized to receive chemotherapy, however the results were not statistically significant. Multiple other studies followed evaluating the role of chemotherapy in conjunction with irradiation, all of which showed either minimal or modest benefit from chemotherapy. The results of these studies were pooled for analysis for three large in meta-analyses.

The first of these meta-analyses was performed by Fine et al. (1993), with a review of 16 randomized trials that included more than 3,000 patients, to compare survival rates of patients that had received radiation therapy and chemotherapy versus radiation alone. The application of chemotherapy was associated with an absolute increase in survival of 10.1 % at 1 year and 8.6 % at 2 years. This improvement translated to a relative increase in overall survival of 23.4 % at 1 year and 52.4 % improvement at 2 years (Fine et al. 1993). A second meta-analysis by Stewart (2002), looked at individual survival data from 3,004 patients from 12 randomized trials to compare survival after radiation plus

chemotherapy versus irradiation alone. This analysis demonstrated a significant prolongation of survival from the use of chemotherapy with a hazard ration of 0.85 ($p<0.0001$) and a 15 % relative decrease in the risk of death. This effect translated to an absolute increase in 1-year survival of 6 % with a 2-month increase in median survival time. This survival advantage was independent of differences in histology (anaplastic astrocytomas verses glioblastoma multiforme), age, sex, performance status or extent of resection. The combination of these early trials and meta-analyses identified chemotherapy with radiation therapy as a standard of care in patients with malignant gliomas in the US. A third analysis, evaluating patients in the temozolomide era confirmed these observations but had greater responses with longer duration of clinically significant benefit from temozolomide (Chamberlain and Chalmers 2007).

Concomitant Chemotherapy and Radiation

Radiation is an effective therapy for most MGs. Intensive research has led to improved understanding of cellular and molecular basis for radiation sensitivity and radioresistance. This work has led investigators to evaluate agents with the ability to enhance the therapeutic effect of radiation while minimizing additional toxicity. Although numerous compounds have been tested for a radiation sensitizing effect, chemotherapy drugs have been the most effective and form the basis of the evolving discipline of chemoradiation. Chemoradiation has been applied to MGs, initially with the nitrosureas (BCNU and CCNU). Other agents were also explored including cisplatin, fluorouracil, hydroxyurea, irinotecan, etoposide and paclitaxel. Several of the above regimens when dosed concurrently with radiation showed modest improvement in overall and progression-free survival in phase I and II trials, none however were effective enough to warrant a phase III trial (Colevas et al. 2003).

Temozolomide had pre-clinical data demonstrating benefit when given in conjunction to radiation therapy and was the impetus for a small phase II trial by Stupp et al. (2005) that showed a median overall survival of 16 months. This led to the larger trial from EORTC and NCIC that was published in 2005 (Stupp et al. 2005). Their phase III multi-center, randomized controlled trial randomly assigned 573 patients with histologically confirmed MG to receive radiotherapy alone or radiotherapy plus continuous daily temozolomide (75 mg/m2×42 days) while undergoing radiotherapy followed by six cycles of adjuvant temozolomide 150–200 mg/m^2 days 1–5 of a 28 day cycle. The median age of patients enrolled was 56 years, with 84 % of patients having undergone debulking surgery. The median survival was 14.6 months with radiotherapy plus temozolomide and 12.1 months with radiotherapy alone. The 2-year survival rate was 26.5 % with radiotherapy plus temozolomide and 10.4 % with radiotherapy alone. The concomitant treatment with radiotherapy plus temozolomide resulted in higher toxicities in 7 % of the patients (Stupp et al. 2005). The above study has led this regimen to become the standard of care for patients with GBM and also to FDA approval for the treatment of newly diagnosed GBM. Although the results do not necessarily hold true for AG, many of these histologies are treated in a similar fashion. Follow up data suggests that the RT + TMZ group have maintained response out to 5 years (Stupp et al. 2005).

Multiple phase II trials have looked at the addition of compounds to the current standard of care utilizing temozolomide and concurrent radiation therapy, followed by adjuvant chemotherapy. Grossman et al. (2010) outlined three such compounds, talampanel, poly-ICLC, or cilengitide, given in addition to the standard temozolomide and radiation dosing for MG. This study found that the addition of a novel agent to radiation therapy and temozolomide resulted in a longer survival than similar patients treated only with the standard of care. The authors of this study are careful to warn that until the reasons for the varied survival rates are clarified, comparisons should be interpreted with caution, and that further phase III clinical trials are necessary to assess the benefit of additional compounds to

temozolomide and radiation therapy (Grossman et al. 2010). One reason for improvement might be optimization of patient care from surgery, RT and chemotherapy and not that each agent added several months of benefit. This was borne out by RTOG 0525 where the median overall survival (OS) was approaching 16 months (Gilbert et al. 2011).

Chemotherapeutic Limitations

While chemotherapy in various forms has been effective in prolonging survival in MGs, by no means have they been curative, as resistance develops. Limitations of chemotherapy, when given either in the adjuvant or recurrent setting, are significant. Tumor penetration by chemotherapy can be limited due to tissue hypoxia, decreased perfusion into the mass due to a lack of blood supply and increased intra-tumoral pressure. With disruption of blood–brain barrier, specifically with MGs, many drugs can penetrate into the tumor but concentrations may not reach a therapeutic level especially in areas where the barrier remains intact. Another important limitation of chemotherapy is the interaction of chemotherapeutic agents with other medications used in brain tumor patients. Steroids are often utilized to control vasogenic edema, but in the process, they repair the blood–brain barrier thereby decreasing penetration and can interact with therapeutic agents. Older anticonvulsants often used either prophylactically or in the treatment associated with seizures related to MGs are hepatically metabolized and can have a significant drug-drug interaction with multiple chemotherapeutic agents which are typically utilized in the recurrent setting, like paclitaxel and irinotecan (Fetell et al. 1997).

Cellular mechanisms of resistance, intrinsic or acquired, may account for a lack of chemotherapeutic response. Mechanisms of resistance include overexpression of the repair enzyme O-6 alkylguanine-DNA-alkyltransferase (AGAT), also known as methylguanine methyl transferase (MGMT). High levels of MGMT correlate with increased resistance to cytotoxic effects of these agents and inversely correlate with response rates (Friedman et al. 1998; Jaeckle et al. 1998). Hegi et al. (2005) found that methylation status of MGMT gene promoter correlated with survival for patients treated with temozolomide. Methylation of the promoter led to an increase in median survival from 15.3 to 21.7 months for patients treated with radiation plus temozolomide compared with radiation alone. When the MGMT gene promoter is methylated, this acts as a silencing effect on the promoter, thereby not allowing for repair of the damage done by temozolomide and concurrent radiation (Esteller et al. 2000).

This MGMT silencing phenomenon has led to a phase III clinical trial (RTOG 0525) which stratified patients following initial concurrent treatment with temozolomide and radiation based upon methylation status to receive standard post-radiation temozolomide therapy (150–200 mg/m^2 days 1–5 of a 28 day cycle) versus dose-dense temozolomide (75–100 mg/m^2 days 1–21 of a 28 day cycle). This study showed no statistical significance between the two arms of therapy for median overall survival (16.6 monthsvs. 14.9 months, $p=0.63$) or median progression free survival (5.5 months vs. 6.7 months, $p=0.06$). The study did confirm the prognostic significance of MGMT methylation in GBM for newly diagnosed GBM regardless of methylation status (Gilbert et al. 2011).

Most of this data revolves around GBM. The optimal treatment for AG is more difficult in that some AGs are of oligodendroglial lineage and have better outcomes and no standard exists, only physician bias. For AAs, there is no standard recommendation for therapy after surgical resection. Historical data suggested PCV was better than BCNU but this turned out not to be the case (Prados et al. 1999). Data from the NOA 04 trial recently indicates that survival based on using radiation or chemotherapy with PCV or TMZ after surgery leads to similar outcomes when patients are then salvaged with the alternative treatment plan (Wick et al. 2009). Currently the CATNON trial is looking to define standard of care for patients with uni or non-deleted AGs.

Chemotherapy for Recurrent Malignant Gliomas

The path to follow at time of recurrence is less clear. Surgery should be explored if clinically appropriate and logistically feasible and safe. Re-irradiation can also be explored as an option in the recurrent setting, particularly if no further options exist and if there is a small volume of recurrence. Other options include re-challenging with temozolomide, use of another second line chemotherapy or targeted therapy, or the combination.

There had been no consensus as to the optimal second line therapy for patients with recurrent MG, although BCNU or CCNU, procarbazine, etoposide, carboplatin, tamoxifen and irinotecan were all commonly considered and utilized (Butowski et al. 2006). In a phase II trial looking at re-exposure to temozolomide following standard adjuvant TMZ therapy, investigators found that patients who had recurrence of GBM early in initial therapy or after treatment free period, demonstrated benefit from continuous dose dense TMZ (50 mg/m^2/day) with 6 month progression free survival of 27.3 % and 35.7 %, respectively. One-year survival was also increased in these groups (27.3 % and 28.6 % respectively). There was less benefit noted in patients who had progression of disease after receiving six standard cycles of TMZ but before completion of adjuvant therapy (Perry et al. 2010).

Multiple studies have been performed looking at the appropriate chemotherapy in the second line setting. In the mid-2000s, two phase II trials looked at single agent irinotecan (CPT-11) administered every 3 weeks to adults with progressive MG independent of the use of epileptic therapy. Irinotecan was dosed at 350 mg/m^2 IV q 3 weeks in patients not on epileptic therapy and 750 mg/m2 IV q 3 weeks in patients on epileptic therapy. Progression free survival at 6 months was found to be 17.6 % and it was concluded that single agent inrinotecan, independent of the use of epileptic therapy, was ineffective with this schedule (Prados et al. 2006). Other earlier trials also looked at various other schedules of single agent irinotecan but failed to show significant progression free survival (Batchelor et al. 2004).

Friedman et al. (2009) presented data demonstrating bevacizumab as an active antitumor agent without significant increase in adverse events or side effects compared to standard therapy at the time. Patients with progression of disease after treatment with standard TMZ therapy were included in the study and were randomized to receive either bevacizumab (10 mg/kg) alone or in combination with irinotecan (340 mg/m^2 or 125 mg/m^2, dose depending upon use of enzyme-inducing antiepileptic agents). One of the primary outcomes of the study was 6-month progression free survival rates, which were 42.6 % for the bevacizumab-alone group and 50.3 % for the bevacizumab and ironotecan group. The most common side effects in the bevacizumab-alone group were hypertension (8.3 %) and convulsion (6.0 %). In Kreisl et al. (2009) also looked at the combination of bevacizumab and irinotecan. Patients with recurrent glioblastoma were initially treated with bevacizumab (10 mg/kg IV q 2 weeks). After tumor progression on single agent bevacizumab, patients were immediately treated with combination bevacizumab and irinotecan (340 mg/m^2 or 125 mg/m^2 IV q 2weeks, with the dose depending upon the use of enzyme-inducing antiepileptic drug). Forty-eight patients were enrolled. The most common drug-associated adverse events were thromboembolic events (12.5 %), hypertension (12.5 %), hypophosphatemia (6 %) and thrombocytopenia (6 %). Six patients were removed from study for drug-associated toxicity (five for thromboembolic events, one bowel perforation). Median progression free survival was 16 weeks, with median overall survival being 31 weeks. Six-month progression free survival was 29 %, with the 6-month overall survival being 57 % (Kreisl et al. 2009). Based upon the Friedman and Kreisl studies Bevacizumab attained accelerated FDA approval in the US as a single agent based on high response rates. Many trials have added agents to Bevacizumab, including low dose TMZ, Etoposide, Erlotinib, Carboplatin, with similar outcomes (Desjardins et al. 2012; Reardon et al. 2009, 2012; Sathornsumetee et al. 2010).

Other drug delivery systems, particularly implantation of a biodegradable drug-impregnated polymer (Gliadel Wafer) at the tumor site at time of surgical management for recurrent GM, have been explored. In a multi-center trial, 222 patients with recurrent malignant brain tumors requiring re-operations were randomly assigned to receive surgically implanted biodegradable polymer discs with or without BCNU. Median overall survival of the 110 patients who received BCNU polymers was 31 weeks compared with 23 weeks for the 112 patients who received placebo only polymers ($p=0.006$). Six month survival in those treated with BCNU-polymer disc was 50 % greater than in those treated with placebo. There were no reported clinically important adverse reactions related to the BCNU polymer, either in the brain, or systemically (Brem et al. 1995). Westphal et al. (2006) have also evaluated the placement of BCNU wafers at time of initial diagnosis of GBM in conjunction with surgery and irradiation. This multicenter control trial demonstrated increased median survival (13.8 months vs. 11.6 months in placebo group) and increased survival advantage in patients receiving the BCNU wafer; the marginal benefit has limited wide spread acceptance of these wafers.

Special Consideration for Anaplastic Oligodendroglioma

AOs are sufficiently different to warrant their own discussion as they have been found to show more chemosensitivity than other MGs. Cairncross and Macdonald (1988) were first to demonstrate that AOs, unlike other MGs, were chemosensitive when all eight relapsed patients treated with procarbazine, BCNU or diaziquone had a radiographic response to therapy. The chemosensitivity of these tumors led to the design of a trial using high-dose chemotherapy and autologus stem cell rescue. Updated data on newly diagnosed AO treated in this fashion found a median progression free survival of 78 months; the median overall survival has not been reached (Abrey et al. 2006). Cairncross et al. (2006) showed the combined deletion of 1p and 19q led to a greater increase in progression free survival and overall survival than for patients with only 1p deletion. This co-deletion was found to vary from 50 % to 80 % of all AOs depending upon the purity of lesion for oligodendroglial cells (Smith et al. 2000). The optimal approach to treating AOs remains to be determined and studies are limited by relative rarity of the tumor. The standard of care currently recommended by the National Comprehensive Cancer Network is tumor resection followed by radiation therapy with or without adjuvant chemotherapy. However, a survey-based study conducted by Abrey et al. (2007) demonstrated that treatment regimens vary among neuro-oncologist and the chosen therapeutic regimen is often based on molecular genetics even thought data is limited to guide decision making. Recently the Co-Del trial for co-deleted AG was halted due to data showing that chemotherapy with PCV before or after RT treatment lead to significantly longer survivals that RT alone based on re-analysis of more mature data initially presented in 2005 (Cairncross et al. 2006; van den Bent et al. 2006). Data in the RTOG trial showed a 14-year survival for patients with co-deleted anaplastic oligodendrogliomas who received intensive PCV follow by RT compared to RT alone where survival was 7 years (Cairncross et al. 2012; Van Den Bent et al. 2012). Discussions are underway to determine how the trial should be re-designed as the RT only arm is no longer an ethical option.

Conclusion

Over the past 40 years, options for patients following tumor debulking and radiation therapy have been investigated widely but little effect on patient survival has been appreciated. The introduction of temozolomide offered a new treatment option with decreased toxicity related to other adjuvant therapies with modest improvement in overall survival. Over the past decade, drugs that target receptor driven and signal transduction pathways have been looked at in synergy with temozolomide and in the recurrent setting. Among these are the faresyltransferase inhibitors,

PDGFR, VEGF, mTOR, and EGFR inhibitors. The majority of these agents have been looked at only in phase II clinical trials and have shown little or no improvement on the current standard of care. Ultimately, the optimal treatment strategy for MGs will likely come from combining target specific agents with systemic chemotherapy. It remains of utmost importance to enroll patients on clinical trials.

References

Abrey LE, Childs BH, Paleologos N, Kaminer L, Rosenfeld S, Salzman D, Finlay JL, Gardner S, Peterson K, Hu W, Swinnen L, Bayer R, Forsyth P, Stewart D, Smith AM, Macdonald DR, Weaver S, Ramsay DA, Nimer SD, DeAngelis LM, Cairncross JG (2006) High-dose chemotherapy with stem cell rescue as initial therapy for anaplastic oligodendroglioma: long-term follow-up. Neuro Oncol 8:183–188

Abrey LE, Louis DN, Paleologos N, Lassman AB, Raizer JJ, Mason W, Finlay J, MacDonald DR, DeAngelis LM, Cairncross JG (2007) Survey of treatment recommendations for anaplastic oligodendroglioma. Neuro Oncol 9:314–318

Batchelor TT, Gilbert MR, Supko JG, Carson KA, Nabors LB, Grossman SA, Lesser GJ, Mikkelsen T, Phuphanich S (2004) Phase 2 study of weekly irinotecan in adults with recurrent malignant glioma: final report of NABTT 97–11. Neuro Oncol 6:21–27

Brem H, Piantadosi S, Burger PC, Walker M, Selker R, Vick NA, Black K, Sisti M, Brem S, Mohr G, Muller P, Morawetz R, Schold SC (1995) Placebo-controlled trial of safety and efficacy of intraoperative controlled delivery by biodegradable polymers of chemotherapy for recurrent gliomas. The Polymer-brain Tumor Treatment Group. Lancet 345:1008–1012

Butowski NA, Sneed PK, Chang SM (2006) Diagnosis and treatment of recurrent high-grade astrocytoma. J Clin Oncol 24:1273–1280

Cairncross JG, Macdonald DR (1988) Successful chemotherapy for recurrent malignant oligodendroglioma. Ann Neurol 23:360–364

Cairncross G, Berkey B, Shaw E, Jenkins R, Scheithauer B, Brachman D, Buckner J, Fink K, Souhami L, Laperierre N, Mehta M, Curran W (2006) Phase III trial of chemotherapy plus radiotherapy compared with radiotherapy alone for pure and mixed anaplastic oligodendroglioma: Intergroup Radiation Therapy Oncology Group Trial 9402. J Clin Oncol 18:2707–2714

Cairncross JG, Wang M, Edward S, Jenkins R, Scheithauer BW, Brachman D, Buckner JC, Fink KL, Souhami L, Laperriere N, Walter WJ, Mehta MP (2012) Chemotherapy plus radiotherapy (CT-RT) versus RT alone for patients with anaplstic oligodendroglioma: long term results of RTOG 9402 phase III study. J Clin Oncol 31(3):337–343

Chamberlain MC, Chalmers L (2007) A pilot study of primary temozolomide chemotherapy and deferred radiotherapy in elderly patients with glioblastoma. J Neurooncol 82:207–209

Colevas AD, Brown JM, Hahn S, Mitchell J, Camphausen K, Coleman CN (2003) Development of investigational radiation modifiers. J Natl Cancer Inst 95:646–651

Desjardins A, Reardon DA, Coan A, Macello J, Herndon JE, Bailey L, Peters KB, Friedman HD, Vredenburgh JJ (2012) Bevacizumab and daily temozolomide for recurrent glioblastoma. Cancer 118:1302–1312

Esteller M, Garcia-Foncillas J, Andion E, Goodman SN, Hidalgo OF, Vanaclocha V, Baylin SB, Herman JG (2000) Inactivation of the DNA-repair gene MGMT and the clinical response of gliomas to alkylating agents. N Engl J Med 343:1350–1354

Fetell MR, Grossman SA, Fisher JD, Erlanger B, Rowinsky E, Stockel J, Piantadosi S (1997) Preirradiation paclitaxel in glioblastoma multiforme: efficacy, pharmacology, and drug interactions. New Approaches to Brain Tumor Therapy Central Nervous System Consortium. J Clin Oncol 15:3121–3128

Fine HA, Dear KB, Loeffler JS, Black PM, Canellos GP (1993) Meta-analysis of radiation therapy with and without adjuvant chemotherapy for malignant gliomas in adults. Cancer 71:2585–2597

Friedman HS, McLendon RE, Kerby T, Dugan M, Bigner SH, Henry AJ, Ashley DM, Krischer J, Lovell S, Rasheed K, Marchev F, Seman AJ, Cokgor I, Rich J, Stewart E, Colvin OM, Provenzale JM, Bigner DD, Haglund MM, Friedman AH, Modrich PL (1998) DNA mismatch repair and O6-alkylguanine-DNA alkyltransferase analysis and response to Temodal in newly diagnosed malignant glioma. J Clin Oncol 16:3851–3857

Friedman HS, Prados MD, Wen PY, Mikkelsen T, Schiff D, Abrey LE, Yung WK, Paleologos N, Nicholas MK, Jensen R, Vredenburgh J, Huang J, Zheng M, Cloughesy T (2009) Bevacizumab alone and in combination with irinotecan in recurrent glioblastoma. J Clin Oncol 27:4733–4740

Gilbert MR, Wang M, Aldape KD, Stupp R, Hegi M, Jaeckle KA, Armstrong TS, Wefel JS, Won M, Blumenthal DT, Mahajan A, Schultz CJ, Erridge SC, Brown PD, Chakravarti A, Curran WJ, Mehta MP (2011) RTOG 0525: a randomized phase III trial comparing standard adjuvant temozolomide (TMZ) with a dose-dense (dd) schedule in newly diagnosed glioblastoma (GBM). J Clin Oncol 29(suppl; abstr 2006)

Grossman SA, Ye X, Piantadosi S, Desideri S, Nabors LB, Rosenfeld M, Fisher J (2010) Survival of patients with newly diagnosed glioblastoma treated with radiation and temozolomide in research studies in the United States. Clin Cancer Res 16:2443–2449

Hegi ME, Diserens AC, Gorlia T, Hamou MF, de Tribolet N, Weller M, Kros JM, Hainfellner JA, Mason W,

Mariani L, Bromberg JE, Hau P, Mirimanoff RO, Cairncross JG, Janzer RC, Stupp R (2005) MGMT gene silencing and benefit from temozolomide in glioblastoma. N Engl J Med 352:997–1003

Jaeckle KA, Eyre HJ, Townsend JJ, Schulman S, Knudson HM, Belanich M, Yarosh DB, Bearman SI, Giroux DJ, Schold SC (1998) Correlation of tumor O6 methylguanine-DNA methyltransferase levels with survival of malignant astrocytoma patients treated with bis-chloroethylnitrosourea: a Southwest Oncology Group study. J Clin Oncol 16:3310–3315

Jemal A, Siegel R, Xu J, Ward E (2010) Cancer statistics, 2010. CA Cancer J Clin 60:277–300

Kreisl TN, Kim L, Moore K, Duic P, Royce C, Stroud I, Garren N, Mackey M, Butman JA, Camphausen K, Park J, Albert PS, Fine HA (2009) Phase II trial of single-agent bevacizumab followed by bevacizumab plus irinotecan at tumor progression in recurrent glioblastoma. J Clin Oncol 27:740–745

Laperriere N, Zuraw L, Cairncross G (2002) Radiotherapy for newly diagnosed malignant glioma in adults: a systematic review. Radiother Oncol 64:259–273

Perry JR, Belanger K, Mason WP, Fulton D, Kavan P, Easaw J, Shields C, Kirby S, Macdonald DR, Eisenstat DD, Thiessen B, Forsyth P, Pouliot JF (2010) Phase II trial of continuous dose-intense temozolomide in recurrent malignant glioma: RESCUE study. J Clin Oncol 28:2051–2057

Prados MD, Scott C, Curran WJ, Nelson DF, Leibel S, Kramer S (1999) Procarbazine, lomustine, and vincristine (PCV) chemotherapy for anaplastic astrocytoma: a retrospective review of radiation therapy oncology group protocols comparing survival with carmustine or PCV adjuvant chemotherapy. J Clin Oncol 17(11)):3389–3395

Prados MD, Lamborn K, Yung WK, Jaeckle K, Robins HI, Mehta M, Fine HA, Wen PY, Cloughesy T, Chang S, Nicholas MK, Schiff D, Greenberg H, Junck L, Fink K, Hess K, Kuhn J (2006) A phase 2 trial of irinotecan (CPT-11) in patients with recurrent malignant glioma: a North American Brain Tumor Consortium study. Neuro Oncol 8:189–193

Reardon DA, Desjardins A, Vredenburgh JJ, Gururangan S, Sampson JH, Sathornsumetee S, McLendon RE, Marcello JE, Norfleet J, Friedman AH, Bigner DD, Friedman HS (2009) Metronomic chemotherapy with daily, oral etoposide plus bevacizumab for recurrent malignant glioma: a phase II study. Br J Cancer 101:1986–1994

Reardon DA, Desjardins A, Peters KB, Guruangan S, Sampson JH, McLendon RE, Herndon JE, Bulusu A, Threatt S, Friedman AH, Vredenburgh JJ, Friedman HS (2012) Phase II study of carboplatin, irinotecan, and bevacizumab for bevacizumab naive, recurrent glioblastoma. J Neurooncol 107:155–164

Sathornsumetee S, Desjardins A, Vredenburgh JJ, McLendon RE, Marcello J, Herndon JE, Mathe A, Hamilton M, Rich JN, Norfleet JA, Gururangan S, Friedman HS, Reardon DA (2010) Phase II trial of bevacizumab and erlotinib in patients with recurrent malignant glioma. Neuro Oncol 12:1300–1310

Smith JS, Perry A, Borell TJ, Lee HK, O'Fallon J, Hosek SM, Kimmel D, Yates A, Burger PC, Scheithauer BW, Jenkins RB (2000) Alterations of chromosome arms 1p and 19q as predictors of survival in oligodendrogliomas, astrocytomas, and mixed oligoastrocytomas. J Clin Oncol 18:636–645

Stern JI, Raizer JJ (2006) Chemotherapy in the treatment of malignant gliomas. Expert Rev Anticancer Ther 6:755–767

Stewart LA (2002) Chemotherapy in adult high-grade glioma: a systematic review and meta-analysis of individual patient data from 12 randomised trials. Lancet 359:1011–1018

Stupp R, Mason WP, van den Bent MJ, Weller M, Fisher B, Taphoorn MJ, Belanger K, Brandes AA, Marosi C, Bogdahn U, Curschmann J, Janzer RC, Ludwin SK, Gorlia T, Allgeier A, Lacombe D, Cairncross JG, Eisenhauer E, Mirimanoff RO (2005) Radiotherapy plus concomitant and adjuvant temozolomide for glioblastoma. N Engl J Med 352:987–996

van den Bent MJ, Carpentier AF, Brandes AA, Sanson M, Taphoorn MJ, Bernsen HJ, Frenay M, Tijssen CC, Grisold W, Sipos L, Haaxma-Reiche H, Kros JM, van Kouwenhoven MC, Vecht CJ, Allgeier A, Lacombe D, Gorlia T (2006) Adjuvant prcarbacine, lomustine, and vincristine improves progression-free survival but not overall survivial in newly diagnosed anaplastic oligodendrogliomas and oligoastrocytomas: a randomized European Organization for Research and Treatment of Cancer phase III trial. J Clin Oncol 18:2715–2722

van den Bent MJ, Hoang-Xuan K, Brandes AA, Kros J, Kouwenhoven M, Taphoorn M, Delattre JY, Bernsen H, Frenay M, Tijssen C, Grisold W, Sipos L, Enting R, Dinjens W, French P, Vecht C, Allgeier A, Lacombe D, Gorlia T (2012) Long-term follow-up results of EORTC 26951: a randomized phase III study on adjuvant PCV chemotherapy in anaplstic oligodendroglial tumors (AOD). J Clin Oncol 30:344–350

Walker MD, Alexander J, Hunt WE, MacCarty CS, Mahaley MS, Mealey J, Norrell HA, Owens G, Ransohoff J, Wilson CB, Gehan EA, Strike TA (1978) Evaluation of BCNU and/or radiotherapy in the treatment of anaplastic gliomas: a cooperative clinical trial. J Neurosurg 49:333–343

Walker MD, Green SB, Byar DP, Alexander E Jr, Batzdorf U, Brooks WH, Hunt WE, MacCarty CS, Mahaley MS Jr, Mealey J Jr, Owens G, Ransohoff J, Robertson JT, Shapiro WR, Smith KR Jr, Wilson CB, Strike TA (1980) Randomized comparisons of radiotherapy and nitrosoureas for the treatment of malignant glioma after surgery. N Engl J Med 303:1323–1329

Westphal M, Ram Z, Riddle V, Hilt D, Bortey E (2006) Gliadel wafer in initial surgery for malignant glioma: long-term follow-up of a multicenter controlled trial. Acta Neurochir (Wien) 148:269–275, discussion 275

Wick W, Hartmann C, Engel C, Stoffels M, Felsberg J, Stockhammer F, Sabel MC, Koeppen S, Ketter R, Meyermann R, Rapp M, Meisner C, Kortmann RD, Pietsch T, Wiestler OD, Ernemann U, Bamberg M, Reifenberger G, von Diemling A, Weller M (2009) NOA-04 randomized phase III trial of sequential radiochemotherapy of anaplstic glioma with procarbazine, lomustine, and vincristine or temozolomide. J Clin Oncol 35:5874–5880

Neurosurgical Treatment for Brain Metastases: Clinical Features, Operative Strategies, Recurrence and Survival

26

Andreas M. Stark

Contents

Abstract

Brain metastases are a frequent complication of cancer arising in up to 15 % of patients with systemic malignancies. Symptoms and findings are highly dependent on the location and size of the lesion. The diagnostic method of choice is magnetic resonance imaging before and after the administration of contrast material. The initial and essential therapeutic step is complete surgical resection of the lesion in order to (1) erase intracranial space-occupying lesions and (2) gain adequate tissue for histological diagnosis. Resection is usually followed by whole brain radiation therapy and/or radiosurgery.

Bone metastases are far less common than brain metastases. They may affect the calvaria or the skull base. The standard treatment is also surgical resection followed by bone plasty.

Dural metastases are also infrequent. They are an important differential diagnosis of meningioma when they arise as a solid mass. When they manifest as subdural fluid collection, they can mimick chronic subdural hematoma.

Introduction

The Incidence of Metastasis

Distant metastasis is the leading cause of death in cancer patients. The property to form distant metastases is a characteristic feature of malignant tumors. Distant metastasis requires a specialized subset of tumor cells that can migrate from the

A.M. Stark (✉)
Department of Neurosurgery, Schleswig Holstein University Medical Center, Campus Kiel, Arnold Heller Str3, Building 41, D24105 Kiel, Germany
e-mail: starka@nch.uni-kiel.de

M.A. Hayat (ed.), *Tumors of the Central Nervous System, Volume 12*,
DOI 10.1007/978-94-007-7217-5_26,

primary site, invade the bloodstream, survive in the blood vessel, extrude the vessel and migrate to the distant site and, finally, proliferate at the distant site. This multistep process has been named the metastatic cascade (Mina and Sledge 2011).

It is more than 120 years ago that Stephen Paget (1889) showed, based on autopsy findings, that "the distribution of secondary growths is not a matter of chance" (Paget 1889). Today we know that the type of cancer spread is influenced by vascular anatomy and molecular properties of the metastatic cells as well as the host tissue (Liotta and Kohn 2001). As a result, specific cancer types show a predilection to metastazise to certain organs.

The Brain as a Special Environment

The brain is an organ where unwanted movement, namely metastatic cell movement, is highly restricted. The brain lacks significant diffusion channels, it has no significant extracellular matrix and no lymphatic system. The brain tissue contains an extensive capillary bed and it is separated from the blood stream via the blood–brain barrier – hereby excluding many chemotherapeutic agents from targeting cancer cells inside the brain parenchyma (Puduvalli 2001). Thus, cells which are able to migrate to and proliferate into the brain parenchyma must have specific abilities which should also be "visible" in their genetic expression profile (Beasley and Toms 2011).

Following this hypothesis, Yoneda and colleages have inserted human breast cancer cells into mice. As a result, multiple metastases to different organs were formed. The study group then harvested only the brain metastases and inoculated them again into other mice. After several passages these cells exclusively formed brain metastases (Yoneda et al. 2001). Based on this model, we have shown that these "trained" cells have acquired specific molecular properties different from the original "parental" cells, namely overexpression of matrix-metallo-proteinases 1 and 9. Functionally, these factors were associated with cell invasion and migration (Stark et al. 2007). Further factors being differentially expressed in brain-seeking breast cancer cells are vascular factors as TIE-1 and endoglin as well as members of the metastasis-suppressor gene family (Stark et al. 2010).

Maybe due to the fact that the brain is a "special, uncomfortable place" for distant metastases, it is usually affected in an advanced stage of disease. This is also true for other sites of metastastic growths in the neurocranium: bone and dural metastases. Both sites are far less common than intraparenchymal (brain) metastases and are discussed at the end of this chapter.

Brain Metastases

Epidemiology and Definitions

Intraparenchymal "brain" metastases are a common complication of cancer arising in approximately 15 % of all patients with malignancies (Sperduto et al. 2010). The incidence is rising due to the increasing senescence of the population, higher detection rates, and improved treatment of primary tumors (Al-Shamy and Sawaya 2009; Siu et al. 2011). The three most common solid tumors of the human body that cause brain metastases are lung cancer, breast cancer and malignant melanoma. Further frequent primary lesions are colorectal and renal cancer. Among our surgical series of 309 patients with solid cancer brain metastases, the tumor origin was as followed: lung cancer: 49.8 %, breast cancer: 15.2 %, urogenital cancer: 11.0 %, colorectal cancer: 8.4 %, malignant melanoma: 7.1 %, others: 8.4 % (Stark et al. 2011).

When brain metastases are diagnosed, most patients are in an advanced stage of disease. However, in 15 % of patients brain metastases are detected as the first sign of malignant disease and in up to 10 % of patients no primary tumor is found at initial presentation (Al-Shamy and Sawaya 2009; Wesseling et al. 2007). This is especially the case in lung cancer patients. According to our experience in 309 patients, the rate of patients where cancer was detected by the occurrence of brain metastases depending on the primary tumor was as followed: non small

cell lung cancer 50.4 %; malignant melanoma 15.0 %, renal cancer 5.9 %; breast cancer 2.1 %; colorectal cancer 0 % (Stark et al. 2011).

By definition, the term "solitary" brain metastasis refers to one single intracranial lesion without evidence of extracranial metastases. "Singular" brain metastasis refers to one single brain lesion in the presence of extracranial metastases. Usually, the term "multiple" brain metastases refers to a number of at least three intracranial metastases.

Patient History and Physical Examination

Symptoms and findings are highly dependent on the location of the lesion and its size. They may be specific for the location (hemiparesis, aphasia, cranial nerve involvement, visual disturbance) or unspecific (headache/nausea/vomiting, vertigo). According to our experience, the most common initial symptoms in patients with brain metastases are hemiparesis (21 %), headache/nausea/vomiting (17 %), ataxia (16 %), cranial nerve impairement (10 %), aphasia (9 %), vertigo (9 %), and seizures (7 %) (Stark et al. 2011).

According to the expendable growths of brain metastases, Neurological deficits may originate from tumor-caused compression of neural structures and/or from the peritumoral edema. This, mostly finger-like edema, is a characteristic feature of brain metastases and may be significant even in patients with small metastases. Deficits may exclusively being caused by the edema, which can be reduced by corticosteroids and decreases significantly after resection of the lesion.

In most cases, symptoms evolve over days to weeks. However, intratumoral bleeding may lead to stroke-like appearance of symptoms. Metastases from melanoma and renal cancer show a predominance to bleed.

According to the fact that brain metastases compress the adjacent brain instead of infiltrating it, the vast majority of patients shows improvement of performance after surgical removal of the lesion (Stark et al. 2011). This is in contrast to patients with primary brain tumors, namely glioblastoma, where infiltration and destruction of the neighbouring brain is present.

Clinical examination should also evaluate the extent of the primary tumor and extracranial metastases, if known. The overall patient performance is a reliable prognostic factor and should therefore be noticed, mostly according to the Karnofsky Performance Score (KPS) (Karnofsky and Burchenal 1949).

Diagnostic Workup

Magnetic resonance imaging (MRI) before and after the administration of contrast material is the diagnostic method of choice when brain metastases are suspected. MRI can (1) accurately show the anatomical location of the lesion, most often at the gray-/white matter interface, (2) differentiate between the lesion itself and the peritumoral edema, (3) estimate the number of metastases down to a diameter of less than one millimeter and (4) detect complications of metastases such as intratumoral bleeding, ifiltration of the dura, hydrocephalus due to compression of CSF pathways and meningeosis carcinomatosa (Osborn et al. 2010).

Brain metastases appear in MRI studies mostly as circumscribed, contrast enhancing solid, cystic or mixed solid/cystic lesions. The peritumoral edema can be well shown in T2 images and in fluid attenuated inversion recovery (FLAIR), where the cerebrospinal fluid signal is suppressed and interstitial edema is pronounced. Figure 26.1 shows characteristic appearance of an exemplary brain metastasis in MRI and CT.

In cases of tumor location in or adjacent to eloquent neural structures, additional diagnostic workup can be useful. Functional MRI can visualize brain regions with increased metabolism during patient action, such as speech or movement. As a consequence, in tumors located closely to speech or motor areas, functional MRI may give additional information of the functional localization of eleoquent brain areas. This is also very useful in left-handed patients where the functional speech area may be on the left or on

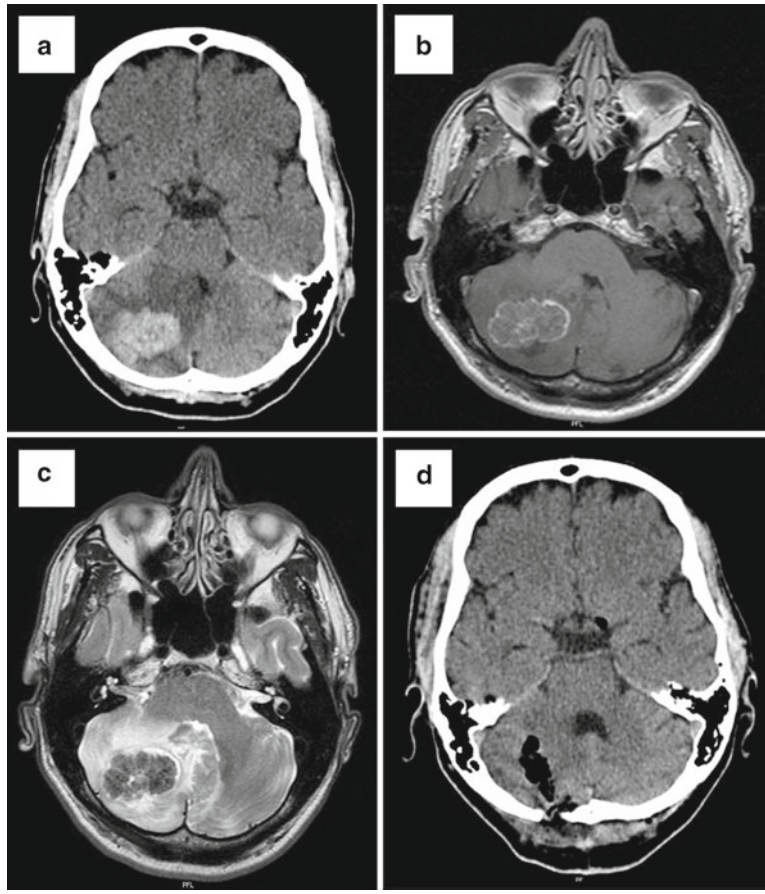

Fig. 26.1 66-year old patient with the history of colorectal cancer who presented with vertigo and dysarthry. (**a**) native CT shows a dense mass in the right cerebellar hemisphere with surrounding edema towards the fourth ventricle (*arrow*). (**b**) T1-weighted MRI after contrast administration shows the same lesion as solid, contrastenhancing mass. (**c**) T2-weighted MRI shows the lesion and highlights the hyperintense peritumoral edema (*arrows*). (**d**) Post-operative CT shows the resection cavity while the fourth ventricle is now, after the removal of the space-occupying lesion, expanded to normal size (*arrow*).

the right or on both sides of the cerebrum. Fiber tracking MRI detects diffusion movement in neural tracts. It is useful in patients with metastases located nearby or even compressing the pyramidal tract or other white matter tracts.

The most important differential diagnoses of brain metastases are glioblastoma and brain abscess. Notably, both lesions can also be multiple. Even in patients with known cancer establishment of a histological diagnosis is often advisable in order to apply adequate treatment. In contrast to brain abscess, brain metastases usually show no restriction on diffusion weighted images. Further differential diagnoses are demyelinating diseases and cerebral infarction (Osborn et al. 2010).

In case of emergency presentation, often a computed tomography scan (CT) is performed. In native CT, the lesion may be hyper-, iso- or hypodense to the brain parenchyma depending on the solid, cystic, necrotic or hemorrhagic nature. More or less surrounding edema is noticed and mass effect may be identified. The patient history of cancer usually is the key to diagnosis. MRI should be followed to adequately approximate the nature of the lesion and show anatomical details.

CT might also be useful in addition to MRI when involvement of the bone is suspected. It is essential in metastases of the skull base. Additionally, CT of the cervical spine is advisable in patients with suspected bone metastasis in order to prevent positioning damage during the operation.

Treatment of Brain Metastasis

The decision whether patients should undergo surgical resection always needs careful evaluation of the individual case and informed consent of the patient. If possible, the patient`s family should be included in the decision process.

The mainstay of treatment for patients with brain metastases is complete surgical excision of the lesion. Surgery is able to (1) erase the space-occupying lesion and therefore relief the patients symptoms and, in most of the cases, improve neurological function (Stark et al. 2011). (2) Surgery enables histological examination of the tumor tissue which is essentially required for adequate adjuvant treatment. According to advances in operative techniques and neuroanesthesia, surgical complications nowadays can be reduced to a minimum and surgical procedures can be applied to a rising amount of patients including patients of advanced age (Al-Shamy and Sawaya 2009; Siu et al. 2011).

The Indication for Surgery

To date, surgery is generally warranted under the following conditions assuming that the metastases are accessible and the primary tumor is under control or unknown.

1. In solitary or singular brain metastasis, either symptomatic or not, surgical treatment is regarded as the standard treatment option. The benefitial role of resection in addition to whole brain radiation therapy has been well documented since the early 1990s (Patchell et al. 1990; Vecht et al. 1993).
2. Life threatening lesions require immediate surgery. This is the case in large lesions causing mass effect, finally leading to tentorial herniation. It is also an important issue in infratentorial tumors causing obstruction of the aqueduct resulting in acute, life-threatening hydrocephalus.
3. The diagnosis is uncertain (cancer of unkown primary, CUP). Tumor resection, or biopsy in cases where tumor removal would cause unacceptable neurological deficits, enables accurate histopathological diagnosis. Remarkably, the rate of histopathological "surprises" in cases with suspected brain metastases based on clinical observations is in the range of 11 % (Al-Shamy and Sawaya 2009).

In contrast to patients with singular metastases, prospective randomized trials are lacking for the treatment of patients with multiple metastases. However, according to the recent literature and our own experience it seems appropriate to resect all lesions if technically feasible (Al-Shamy and Sawaya 2009; Siu et al. 2011). We tend to remove up to 3, maybe 4 lesions in 1–2 operations during one anesthesia in these cases. If needed, the patients head position is changed in between.

As a consequence of increasing senescence of the population, the amount of elderly patients with brain metastases is rising. There is actually no reason to generally exclude elderly patients from surgical treatment. In a systematic review, we have found that survival in patients over the age of 65, in contrast to younger individuals, is affected by the number of metastases (<=3 vs. >3) and the presence of co-morbidities. In younger patients the presence of extracranial metastases was significantly associated with reduced survival. In both groups, as expected, favorable patient performance was associated with prolonged survival (Stark et al. 2011).

The role of histopathological diagnosis in neurooncology cannot be overestimated. Modern imaging techniques can approximate the diagnosis but they can, at least up to now, not prove it. Only histopathological examination based on paraffin sections can. It is essential to obtain enough tissue for diagnosis and store it adequately. Further material might be stored in liquid nitrogen or −80° freezers for genetic testing.

Surgical Technique

Pre-operative preparation for craniotomy requires patient consent to operation and anesthesia as well as MRI before and after contrast administration. CT might be added if bone erosion is suspected, it is essential in cases with skull base involvement. MRI or CT slides are prepared for neuronavigation. Besides laboratory blood examination, we perform chest X-ray and electrocardiogram in every patient over the age of 40 years on a routine basis.

Intraoperatively, rigid head fixation is needed to prevent patient movement during the operation. All intracranial tumor operations are carried out under the microscope with a magnification of 6–40 fold. Neuronavigation is routinely applied for minimizing the access to the tumor and for resection control in large metastatic lesions which, in the end, is benefitial for the patient (Tan and Black 2007). Neuronavigation represents a 3D-computer model based on a pre-operative CT or MRI scan that is intraoperatively available. The surgeon can check the position of a pointer held to (for craniotomy planning) or into (for detection of small lesions and resection control) the patient`s head in reference to the computer model. A limitation of this technique is the fact that the intracranial structures move after opening of the skull and resection of intracranial tissue. This incidence is called brain shift.

After craniotomy, the bone flap and the dura can be inspected for possible tumor infiltration. Superficial lesions are sometimes, though not always, visible through the cortex. In deep-seated small lesions neuronavigation is extremely helpful in minimizing the access through the sulcus or the brain parenchyma. After the lesion is accessed, it is debulked before the border can be dissected in order to prevent damage to the adjacent brain. Cyst fluid can be punctured, leading to additional reduction of space-occupation. The first tumor tissue removed can be used for frozen sections for further approximation of the diagnosis. After dissection of the tumor/brain interface the metastasis is removed, either in toto, or piece by piece. Resection should be complete to reduce the risk of local recurrence. After meticulous hemostasis of the resection cavity, the dura is closed in a watertight fashion. This is important since post-operative CSF fistula is a major source of peri-operative morbidity and a significant risk factor for infection. Following dural closure, the bone flap is replaced and fixed and the wound is closed. To our experience, a wound drainage can be omitted in most of the cases. Figure 26.2 shows pre-operative MRI and intra-operative microscopic images of a superficially located brain metastasis.

Post-operative care

It is essential to mobilize the patient early after the operation in order to prevent thrombosis and pneumonia. In this situation, specially trained physiotherapists can effectively contribute to favorable patient performance and outcome. Depending on the medical system, the hospital stay is usually in the range of 3–7 days. The sutures are removed the 7th–10th postoperative day. Patients can wash their hair 24 h thereafter.

After obtaining the definite histopathological diagnosis based on paraffin sections further therapeutic steps can be planned (radiotherapy, chemotherapy, combined approaches).

Medical and Adjuvant Treatment

Medical treatment for brain metastases constitutes in the application of corticosteroids which can stabilize the blood–brain barrier and therefore reduced peritumoral edema. Corticosteroids are mandatory in the perioperative phase in order to prevent further brain swelling. Postoperatively, the peritumoral edema decreases and corticosteroids can be reduced.

Whole Brain Radiation Therapy

Whole brain radiation therapy in addition to surgical excision has been shown to reduce local and distant recurrence but it does not prolong survival (Al-Shamy and Sawaya 2009).

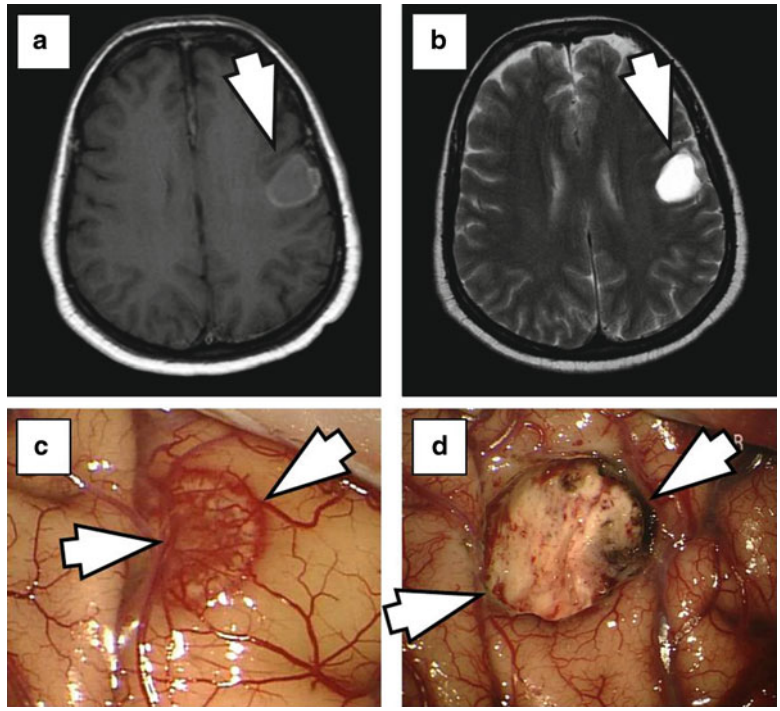

Fig. 26.2 55-year old patient with known breast cancer who presented with aphasia. (**a**) T1-weighted MRI after contrast administration shows a cystic ring-like contrast enhancing left temporo-parietal lesion (*arrow*). (**b**) T2-weighted MRI demonstrates cyst fluid inside the lesion (*arrow*). (**c**) Intra-operatively, after opening the dura, the lesion is visible through the cortex (*arrows*). (**d**) Intra-operative imaging after microsurgical resection shows the resection cavity.

The combination of whole brain radiation therapy and stereotactic radiosurgery can also not prolong survival but again improve local control when compared to radiosurgery alone. This observation has been made in a series including 132 patients with 1–4 metastases (Aoyama et al. 2006).

Stereotactic Radiosurgery

Stereotactic radiosurgery (SRS) refers to the (usually) single time application of small collimated beams of ionizing radiation to an ill-defined intracranial mass. The most often used techniques are Gamma Knife Surgery (multiple cobalt sources) or LINAC (linear accelerator). SRS can be applied on an ambulatory basis. The technique is limited by the size of metastases of up to only 3 cm diameter.

The role of SRS as adjuvant treatment following open resection is currently under examination. In a retrospective study including 47 patients who underwent stereotactic radiosurgery (Gammy Knife) to the resection cavity after complete removal of brain metastases as well as to synchronous or metachronous metastases, Jagannathan et al. saw effective local tumor control. Herein, whole brain radiation was reserved for patients with small numbers of metastases and favorable performance, finally applied in 10/47 patients (Jagannathan et al. 2009).

SRS has also been evaluated as single treatment option for small metastases (<=3 cm in diameter) instead of surgical resection. Overall, there is a growing body of evidence that surgery is superior to SRS in these circumstances (Al-Shamy and Sawaya 2009).

Procedure in Patients with Cancer of Unkown Primary

In cases of cancer of unknown primary (CUP) gaining tumor tissue is essential for histopathological diagnosis. Histopathology can give first information concerning the underlying tumor (adenocarcinoma versus squamous cell carcinoma). Using special immunohistochemical markers, such as certain cytokeratins, the primary tumor can be targeted more precisely (Drlicek et al. 2004). In our series, 93 patients (30.1 %) presented with brain metastases as first sign of malignant disease (the far most of the patients suffered from lung cancer, see above). In a total of 8 patients (2.6 %) the primary tumor remained unknown even after diagnostic workup during the perioperative period (Stark et al. 2011).

Valuable clinical diagnostic steps are chest X-ray, computed tomography of the thorax and abdomen, ultrasound of the abdomen, and endoscopy of the gastrointestinal tract. In women, gynecological examination may give valuable clues as well as examination of the skin for detection of melanoma. In cases where melanoma is suspected and examination of the skin is normal, ophthalmological examination might be useful for detection of choroid melanoma of the orbit.

Chemotherapy

Brain metastases in general are hard to treat by systemic chemotherapy due to the presence of the blood–brain barrier. So, chemotherapy in patients with brain metastases is usually directed to the primary tumor as well as systemic metastases. As an exception, it is the standard initial treatment in certain tumor types as choriocarcinoma and gern cell tumors (Al-Shamy and Sawaya 2009).

Post-operative Follow-Up and Survival

We recommend an observation interval of clinical re-examination and MRI before and after contrast material application every 3 months. This time interval seems adequate in the light of brain metastases progression and helps identify recurrence before it gets clinically symptomatic in most cases.

Median survival of patients with brain metastases overall is less than 1 year. However, recent evidence suggests a complex relationship between prognosis and tumor type as well as prognosis and patient age. In a retrospective database analysis including over 4,000 patients treated during a 22-year interval, Sperduto and colleages have found prognostic factors specific for the primary tumor. Herein, patient age had only prognostic impact in lung cancer whereas patient performance had prognostic impact in lung cancer, melanoma, renal cell cancer and breast cancer. The number of brain metastases was relevant in lung cancer, melanoma and renal cancer but not in breast cancer patients (Sperduto et al. 2010).

In our retrospective series of 309 patients, we found age-dependent impact of prognostic factors. Herein, the incidence of extracranial metastases, complete resection of all metastases and re-craniotomy was only significantly associated to survival in patients >= 65 years. In contrast, co-morbidities and the number of brain metastases <=3 was exclusively associated to survival in patients >65 years (Stark et al. 2011).

Brain Metastases Recurrence

Brain metastases recurrence is traditionally defined as re-manifestation at the site of resection or elsewhere in the brain. In older series, its occurrence is reported in the range of 50 % of patients. According to technical advances (surgical techniques, WBRT, SRS), this incidence might be lower today. According to new data, the recurrence rate at the site of resection can be estimated to 10–15 % and is hereby comparable with the local control rate of stereotactic radiosurgery (Siu et al. 2011).

Re-craniotomy has been shown to prolong survival and improve quality of life in younger patients with favorable performance (Arbit et al.

1995; Al-Shamy and Sawaya 2009; Bindal et al. 1995). Surgery furthermore enables histological examination hereby differentiating between tumor recurrence and radiation necrosis.

In our own series, we performed re-craniotomy for recurrence in 43/309 patients (13.9 %). Herein, re-craniotomy was an independent prognostic factor in patients <= 65 years of age (Stark et al. 2011).

Leptomeningeal Metastasis

Leptomeningeal metastasis (leptomeningeal carcinomatosis, neoplastic meningitis) refers to the metastatic dissemination of tumor cells to the subarachnoid space and the leptomeninges. Its incidence is in the range of 5–15 % of all cancer patients (Walbert and Groves 2010). It might occur along with solid brain metastases or without it. Leptomeningeal carcinomatosis almost always occurs in an advanced stage of disease and it is associated with a poor prognosis. MRI shows contrast-enhancing thickening of the dura, cytology of the subarachnoid space shows malignant cells. Leptomeningeal dissemination is most common in patients with lung and breast cancer, melanoma and lymphoma. Treatment options include intrathecal chemotherapy via a CSF reservoir. The reservoir can also be punctured when hydrocephalus is present which is a common complication of leptomeningeal metastasis (Grewal et al. 2012).

Dural Metastases

Hematogenous metastatic spread to the intracranial dura is found in up to 9 % of cancer autopsies. Although, it is rarely clinically diagnosed (Nayak et al. 2009). Dural metastasis may manifest as solid dura-based lesions mimicking meningioma or as a subdural fluid accumulation mimicking subdural hematoma. Therefore, in patients with subdural fluid collection and the history of cancer, subdural fluid should be sent for cytological examination (Stark and Mehdorn 2004).

In patients with solid growing dural metastases, CT is essential to show erosion of the calvaria or skull base. Only surgical resection has been shown to improve survival. Intraoperatively, the skin and the bone flap must be large enough to enable dural plasty and, if the bone is infiltrated, cranioplasty. In some cases the tumor growths through the bone. Then, the galea aponeurotica may be infiltrated and must then be excised. The brain tissue is infiltrated in as many as 34 % of the cases (Nayak et al. 2009).

Bone Metastases

Hematogenous bone metastases might involve the calvaria or the skull base. Despite the fact that bone metastases can be caused by virtually all malignant primary tumors, breast cancer is the far most common malignancy to cause hematogenous metastasis to the skull (Bontoux et al. 1998). Most lesions stay asymptomatic. Symptomatic lesions cause local swelling, sometimes accompanied by local pain. Rarely, neurological deficits are present at the time of diagnosis of bone lesions. Large lesions may compress the dural sinuses. Skull base metastases may cause cranial nerve impairment and/or exophthalmia when the orbit is involved (Constans and Donzelli 1981; Stark et al. 2003).

Bone erosion is best visualized on CT scan while MRI is superior to CT in detecting dural invasion which is important for operative planning. Surgery is indicated in case of (1) a neurological deficit and/or (2) massive destruction of the bone, (3) a painful mass, (4) solitary metastasis or (5) confirmation of the diagnosis is requested (Stark et al. 2003).

The operative strategy in hematogenous metastases of the calvaria is to resect the lesion leaving an intact bony rim. The defect is replaced by bone cement. The dura, if affected, is excised and replaced, too. A wound drain is mandatory.

In skull base lesions, complete removal can seldomly be achieved without damaging cranial nerves or vascular structures. In cases of large skull base metastases, combined approaches with

tumor biopsy/partial removal followed by radiotherapy should be discussed. Post-operative follow-up is identical to patients with brain metastases. Bone metastases grow very slowly, although, these patients are at high risk for developing intraparenchymal metastases.

Conclusion

In conclusion, intraparenchymal "brain" metastases are a frequent complication of systemic cancer. Surgery should be considered anytime if possible. Far less frequently symptomatic metastatic locations at the neurocranium are the dura and the bone. Both are also treated by surgery. Adjuvant treatment consists in radiotherapy whereas chemotherapy is limited and if applied, it is directed mainly to the systemic manifestation of the disease. Leptomeningeal carcinomatosis is a diffuse tumor cell dissemination along the leptomeninges occurring exclusively in late-stage cancer patients. The placement of a burr hole reservoir enables intrathecal chemotherapy, and, if indicated, CSF release for the treatment of hydrocephalus.

References

Al-Shamy G, Sawaya R (2009) Management of brain metastases: the indispensable role of surgery. J Neurooncol 92:275–282

Aoyama H, Shirato H, Tago M, Nakagawa K, Toyoda T, Hatano K, Kenjyo M, Oya N, Hirota S, Shioura H, Kunieda E, Inomata T, Hayakawa K, Katoh N, Kobashi G (2006) Stereotactic radiosurgery plus whole-brain radiation therapy vs stereotactic radiosurgery alone for treatment of brain metastases: a randomized controlled trial. JAMA 295:2483–2491

Arbit E, Wroński M, Burt M, Galicich JH (1995) The treatment of patients with recurrent brain metastases. A retrospective analysis of 109 patients with nonsmall cell lung cancer. Cancer 76:765–773

Beasley KD, Toms SA (2011) The molecular pathobiology of metastasis to the brain: a review. Neurosurg Clin N Am 22:7–14

Bindal RK, Sawaya R, Leavens ME, Hess KR, Taylor SH (1995) Reoperation for recurrent metastatic brain tumors. J Neurosurg 83:600–604

Bontoux D, Plazanet F, Azais I (1998) Distribution of bone metastases of cancers. A scintigraphic study of 376 cases. Bull Acad Natl Med 182:997–1008

Constans JP, Donzelli R (1981) Surgical features of cranial metastases. Surg Neurol 15:35–38

Drlicek M, Bodenteich A, Urbanits S, Grisold W (2004) Immunohistochemical panel of antibodies in the diagnosis of brain metastases of the unknown primary. Pathol Res Pract 200:727–734

Grewal J, Saria MG, Kesari S (2012) Novel approaches to treating leptomeningeal metastases. J Neurooncol 106:225–234

Jagannathan J, Yen CP, Ray DK, Schlesinger D, Oskouian RJ, Pouratian N, Shaffrey ME, Larner J, Sheehan JP (2009) Gamma Knife radiosurgery to the surgical cavity following resection of brain metastases. J Neurosurg 111:431–438

Karnofsky DA, Burchenal JH (1949) Evaluation of chemotherapeutic agents. In: Macleod CM (ed) Columbia Press, New York, pp 191–205

Liotta LA, Kohn EC (2001) The microenvironment of the tumour-host interface. Nature 411:375–379

Mina LA, Sledge GW Jr (2011) Rethinking the metastatic cascade as a therapeutic target. Nat Rev Clin Oncol 8:325–332

Nayak L, Abrey LE, Iwamoto FM (2009) Intracranial dural metastases. Cancer 115:1947–1953

Osborn AG, Salzman KL, Barkovich AJ (eds) (2010) Salt Lake City. Diagnostic imaging: brain, 2nd edn. Amirsys

Paget S (1889) The distribution of secondary growths in cancer of the breast. Lancet 1:571–573

Patchell RA, Tibbs PA, Walsh JW, Dempsey RJ, Maruyama Y, Kryscio RJ, Markesbery WR, Macdonald JS, Young B (1990) A randomized trial of surgery in the treatment of single metastases to the brain. N Engl J Med 322:494–500

Puduvalli VK (2001) Brain metastases: biology and the role of the brain microenvironment. Curr Oncol Rep 3:467–475

Siu TL, Jeffree RL, Fuller JW (2011) Current strategies in the surgical management of cerebral metastases: an evidence-based review. J Clin Neurosci 18:1429–1434

Sperduto PW, Chao ST, Sneed PK, Luo X, Suh J, Roberge D, Bhatt A, Jensen AW, Brown PD, Shih H, Kirkpatrick J, Schwer A, Gaspar LE, Fiveash JB, Chiang V, Knisely J, Sperduto CM, Mehta M (2010) Diagnosis-specific prognostic factors, indexes, and treatment outcomes for patients with newly diagnosed brain metastases: a multi-institutional analysis of 4,259 patients. Int J Radiat Oncol Biol Phys 77:655–661

Stark AM, Mehdorn HM (2004) Images in neuro-oncology: dural metastases. J Neurooncol 68:11

Stark AM, Eichmann T, Mehdorn HM (2003) Skull metastases – clinical features, differential diagnosis and review of the literature. Surg Neurol 60:219–225

Stark AM, Anuszkiewicz B, Mentlein R, Yoneda T, Mehdorn HM, Held-Feindt J (2007) Differential expression of matrix metalloproteinases in brain- and bone-seeking clones of metastatic MDA-MB-231 breast cancer cells. J Neurooncol 81:39–48

Stark AM, Mentlein R, Mehdorn HM, Held-Feindt J (2010) Genetisches Profil von Hirn- und Knochen-selektiven MDA-MB-231 Klonen. Chirurg Forum 39:19–21

Stark AM, Stöhring C, Hedderich J, Held-Feindt J, Mehdorn HM (2011) Surgical treatment for brain metastases: prognostic factors and survival in 309 patients with regard to patient age. J Clin Neurosci 18:34–38

Tan TC, Black PM (2007) Image-guided craniotomy for cerebral metastases: techniques and outcomes. Neurosurgery 61(1 Suppl):349–356

Vecht CJ, Haaxma-Reiche H, Noordijk EM, Padberg GW, Voormolen JH, Hoekstra FH, Tans JT, Lambooij N, Metsaars JA, Wattendorff AR (1993) Treatment of single brain metastasis: radiotherapy alone or combined with neurosurgery? Ann Neurol 33:583–590

Walbert T, Groves MD (2010) Known and emerging biomarkers of leptomeningeal metastasis and its response to treatment. Future Oncol 6:287–297

Wesseling P, von Deimling A, Aldape KD (2007) Metastatic tumours of the CNS. In: Louis DN, Ohgaki H, Wiestler OD, Cavenee WK (eds) WHO classification of tumours of the central nervous system. IARC Press, Lyon, pp 248–251

Yoneda T, Williams PJ, Hiraga T, Niewolna M, Nishimura R (2001) A bone-seeking clone exhibits different biological properties from the MDA-MB-231 parental human breast cancer cells and a brain-seeking clone in vivo and in vitro. J Bone Miner Res 16:1486–1495

Part IV

Radiosurgery

Image-Guided Radiosurgery for Hypothalamic Hamartomas

27

Karen Huscher and Pantaleo Romanelli

Contents

Abstract

Epileptogenesis is sometimes a distinctive feature of brain tumors, often predating the onset of neurological deficits and/or intracranial hypertension. Hypothalamic hamartomas (HH) are the most exquisite case of brain tumor leading to a severe epileptic disorder. HH are developmental malformations arising from the the hypothalamic area and characterized by an intrinsic epileptogenicity. They can lead to a wide spectrum of epileptic conditions, ranging from a mild form reported as an "urge to laugh" without cognitive impairment up to a catastrophic encephalopathy with early onset of gelastic seizures (GS), precocious puberty and mental retardation. Several studies demonstrated that antiepileptic drugs (AED) are ineffective and moreover cannot prevent the onset of cognitive and behavioural deterioration. Large lesions are associated with mass effect and related intracranial hypertension. Microsurgical resection solves seizures and mass effect but it's associated with significant risk. Stereotactic radiosurgery (SRS) has been explored to minimize the surgical risk in small to medium size HH. SRS is a good option in selected cases such as highly functioning young teenagers and adults where it is important to minimize memory deficits which are more likely following open surgery. This said, here we review the pathologic and clinical features of HH as well as the treatment options available, highlighting the role of SRS.

K. Huscher
Department of Neurosurgery, Kantonsspital St. Gallen, San Gallen, Swiss

P. Romanelli (✉)
Cyberknife Center, Via Saint Bon 20, 20147 Milan, Italy
e-mail: Radiosurgery2000@yahoo.com

M.A. Hayat (ed.), *Tumors of the Central Nervous System, Volume 12*,
DOI 10.1007/978-94-007-7217-5_27,

Introduction

Hypothalamic hamartomas (HH) are developmental malformations involving the hypothalamic area located between the infundibular stalk and the mammillary bodies. HH may be associated with a range of neurologic or endocrine manifestations. Brain magnetic resonance imaging (MRI) shows HH as an abnormality in the region of tuber cinereum and third ventricle. It appears isointense to the gray matter in T1-weighted images and either iso- or hyperintense in T2-weighted sequences. The prevalence of HH is about 1–2 per 100,000, which could be an underestimate of the true prevalence of the disease. Concerning their anathomical features, HHs have been classified as sessile or pedunculate, depending on the breadth of their attachment to the tuber cinereum, and extrahypothalamic or parahypothalamic depending on the pattern of the growth inside the hypothalamus (with contralateral shift of the third ventricle) or expansion toward the interpenduncular space. Sessile hamartomas can be further divided into type 1 (midline), type II (lateral), type III (intraventricular), type IV (giant, > 20 mm in diameter). A further classification divides HH into types Ia and Ib (pedunculated) and types IIa and IIb (sessile), depending on their size, hypothalamic displacement, origin and site of attachement (Valdueza et al. 1994). Type II lesions correspond to medium/large sessile HHs that are broadly attached to the tuber cinereum of mammillary bodies, with (type IIb) or without (type IIa) hypothalamic compression. Several studies have sought to correlate the structural characteristics of HH with clinical features, with type II being more frequently associated with neurological impairment. Pedunculated (parahypothalamic) HHs are occasional findings or may be related to endocrinological disturbances, whereas intrahypothalamic hamartomas are mainly associated with gelastic seizurs (GS) and cognitive, behavioural and psychiatric disorders (Valdueza et al. 1994; Arita et al. 1999; Maixner 2006).

Hypothalamic hamartoma is usually sporadic, but in rare cases it is associated with the autosomal dominant Pallister-Hall syndrome (PHS) due to mutations in the zinc-finger transcription factor gene GLI3 on chromosome 7p13. Somatic mutations in GLI3 gene have been shown to be linked with sporadic cases of HH (Craig et al. 2008). PHS also includes additional congenital malformations, such as insertional polydactyly, imperforated anus and bifid epiglottis or laryngeal cleft. However, epilepsy in PHS is not the rule. Pathologic studies reveal that HH consist of gray matter with small and large neurons, diffusely distributed or clustered, and interspersed glial nuclei. Interestingly, these neurons do not display dysplastic features (Fenoglio et al. 2007). Myelinated nerve fibres and haphazardly arranged myelinated and unmyelinated fibres are present, contributing to the difference in the T2-weighted and proton-density signal on MRI. HH with a few neurons has also been described and may easily be misdiagnosed as pilocytic astrocytomas or subependymomas. Two distinct populations of neurons have been foundsmall clustered GABA-expressing neurons, displaying spontaneous rhythmic firing and large, quiescent pyramidal-like neurons with more extensive dendritic and axonal arborization. These small, spontaneously firing GABAergic neurons project synaptic connections to both large and other small HH neurons: they constitute the basis of the intrinsic epileptogenicity of HH (Fenoglio et al. 2007), as they act as a pacemaker that might synchronize numerous output neurons. Thus, seizure genesis may be the consequence of this pacemaker-like activity, with an increase in network synchrony due to the increase in GABAergic interneurons or of the immature phenotype displayed by these neurons that act as excitatory cells (Maixner 2006).

Epilepsy Syndromes Related to HH

GS-HH syndrome can manifest as a spectrum of conditions with various degrees of severity (Striano et al. 2009). The most severe form is characterized by early onset in previously normal children, with GS evolving toward a catastrophic symptomatic generalized epilepsy, with

cognitive impairment and behavioural disorders. Later onsets are associated with GS evolving toward a severe partial epilepsy with cognitive and behavioural disturbances. Milder syndromes where only a "pressure to laugh" is appreciated have been described in adult patients with small HH. Gelastic seizures (GS) are the distinctive seizure type of HH and the presenting symptom in almost all cases. Gelastic seizures are identified as a "seizure type" in Engel's proposed classification (2001). Trousseau first recognized that compulsive bursts of laughter could be of epileptic nature: "… he (an epileptic boy) experienced episodes characterized by bursts of laughter; seizure lasted only a few seconds and the patient, rapidly recovering, seemed very surprised…; he was not aware it had happened" (Trousseau 1956).

The authors noted the presence of accompanying ictal symptoms such as facial flushing, dilated pupils, motor signs, and staring or complex behaviour; ictal bradycardia or running is also rarely described. Ictal hormonal changes have also been reported, attributed to an abrupt dysfunction of the hypothalamo-pituitary axis with an ictal pulse of gonadotropins, 17beta-estradiol and growth hormone. Gelastic seizures are rarely found in symptomatic frontal or temporal lobe epilepsy, but they characterize epilepsy associated with HH (Striano et al. 2009). More rarely the etiology remains unknown ("cryptogenic" cases) (Striano et al. 1999). In GS related to frontal lobe epilepsy (FLE), laughter is described as unnatural and not associated with feelings of mirth. In TLE, laughter may be natural or forced, unmotivated or associated with a pleasant sensation or feeling, and usually with a loss of contact (Tassinari et al. 1997).

The onset of HH is usually in the first years of life, and their frequency is generally high; sometimes they occur in clusters. The seizures are usually brief and stereotyped; laughter is usually "mechanical", without a sense of mirth and without or with little loss of consciousness. Gelastic seizures may appear in some cases later in life and sometimes may consist only of a "pressure to laugh" in patients with small HH (Striano et al. 2002; Sturm et al. 2000).

Several EEG features may be observed in patients with GS-HH. Slowing of background activity, interictal focal or mutifocal (mostly temporal or frontal), generalized (more frequently slow spike-and-wave complexes) paroxysmal activity, and various patterns of ictal activity are found. Interestingly, "pure" GS may present little or no epileptiform abnormalities on scalp EEG but may show a diffuse flattening of cerebral activity, likely related to "only diencephalic" discharges (Striano et al. 2005). Children with GS-HH usually have no history of abnormal cognitive development before the onset of epilepsy. Subsequently, most children show a cognitive stagnation and deterioration and frequently major behavioural problems with a pervasive developmental and attention deficit disorder. A wide spectrum of severity of cognitive deficits has been described in children and in adults in relation to the severity of the epileptic syndrome and to the size and the characteristics of the HH. Late onset cases and patients with small HHs may not display clear cognitive deficits or behavioural disturbances (Frattali et al. 2001; Quiske et al. 2006; Prigatano 2007; Veendrick-Meekes et al. 2007).

Treatment

Anticonvulsivant medications are poorly effective for GS and other seizure types related to HH, including gelastic status. Poor seizure control in children is often associated with cognitive and behavioural deterioration. On the other hand, microsurgical or endoscopic resection of HH as well as radiosurgical ablation are highly effective to control GS and other seizure types, leading also to reversal of cognitive and behavioral decline (Romanelli et al. 2008). Several surgical approaches have been proposed including microsurgical resection following the transcallosal interforniceal route, the pterional or the subfrontal trans-lamina-terminalis route (Polkey 2003; Rosenfeld and Feiz-Erfan 2007; Frazier et al. 2009). Because of neurological, endocrine or vascular morbidity associated with open surgery, endoscopic resection has also been

performed (Ng et al. 2008). Post-surgical residuals, typically located within the unresectable hypothalamic parenchyma, are common and, with time, associated with seizure recurrence. Stereotactic radiosurgery is an emerging, method to treat small to medium size intrahypothalamic hamartoma and residues of an incomplete surgical excision (Regis et al. 2006).

SRS is based on the combination of stereotactic localization with multiple cross-fired beams from a highly collimated radiation source. This non-invasive method is an effective alternative to conventional neurosurgery, cranial irradiation, and brachytherapy for selected patients affected by several neurological pathologies. Radiosurgery is also an interesting treatment option for refractory focal epilepsy, especially when the seizure focus is located in an eloquent or surgically challenging brain region, locations for which open surgery is associated with an unacceptably high incidence of complications.

The exact mechanism of seizure abolition after radiosurgery is unknown. Depending on the target volume, radiosurgery can induce necrosis and consequent destruction of the epileptic focus and its pathways of spread. Alternatively, suppression of epileptic activity by a neuromodulatory effect at non-necrotising doses has been proposed as a possible mechanism of action (Regis et al. 1996). Doses of 20 Gy or less delivered to volumes less than 7 cm^3 do not seem to produce necrosis, but reduced neuronal density and perivascular sclerosis have been noted on hippocampal specimens resected because of poor clinical efficacy (Srikijvilaikul et al. 2004).

Radiosurgery techniques such as Gamma Knife or Cyberknife ablation have been shown to be safe and effective treatment options for HH, including small children (Unger et al. 2002; Selch et al. 2005; Regis et al. 2000, 2007; Romanelli et al. 2008). Frameless radiosurgery using the CyberKnife may further facilitate the use of radiosurgery in children, offering a totally non-invasive option devoid of major complications (Romanelli and Anschel 2006; Romanelli et al. 2008). Figure 27.1 illustrates a frameless Cyberknife treatment performed uneventfully and with full seizure resolution over time in a 9 year old child. The main limit of radiosurgery is its delayed effect, as seizures start to decrease 3–6 months after the procedure in most patients and with great variability in the timing of response (Téllez-Zenteno et al. 2008). Occasionally, seizure severity may temporarily increase after radiosurgery to subside and then disappear during the following months. Several studies employing different SRS techniques or stereotactically implanted iodine-125 seeds have demonstrated the efficacy of radiation in stopping the spread of epileptic discharges from the hypothalamus to the cortex (Arita et al. 1998; Regis et al. 2004; Rosenfeld 2011; Schulze-Bonhage et al. 2004; Selch et al. 2005). The efficacy of SRS for the treatment of HH has been demonstrated to be highly correlated with the delivered dose, with the best results using a marginal dose > 17 Gy. The post-operative course may include a short interval (2 months) of worsening epilepsy, followed by a gradual overall improvement (Regis et al. 2007; Romanelli et al. 2008). There may be a waiting period of greater than 1 year to obtain the full effect of SRS for epilepsy. So far, no major neurological side effects have been reported. A dramatic improvement of sleep quality, behaviour and learning performance in treated children as well as the preliminary observation that younger patients show an excellent outcome with lower doses, should encourage the further investigation of this therapeutic option in controlled trials. Surgical and radiosurgical treatments can be easily integrated in patients harboring large HH. In such cases, a surgical debulking procedure can be followed by radiosurgery delivered to the unresectable epileptogenic intrahypothalamic component. A combined approach can also be used to treat large epileptogenic lesions (such as low grade gliomas and arteriovenous malformations) involving eloquent cortex (Friehs et al. 2007). In the authors' experience, microsurgical debulking followed by radiosurgical ablation of the lesional component involving eloquent cortex provides seizure control while minimizing the risk of neurological deficits.

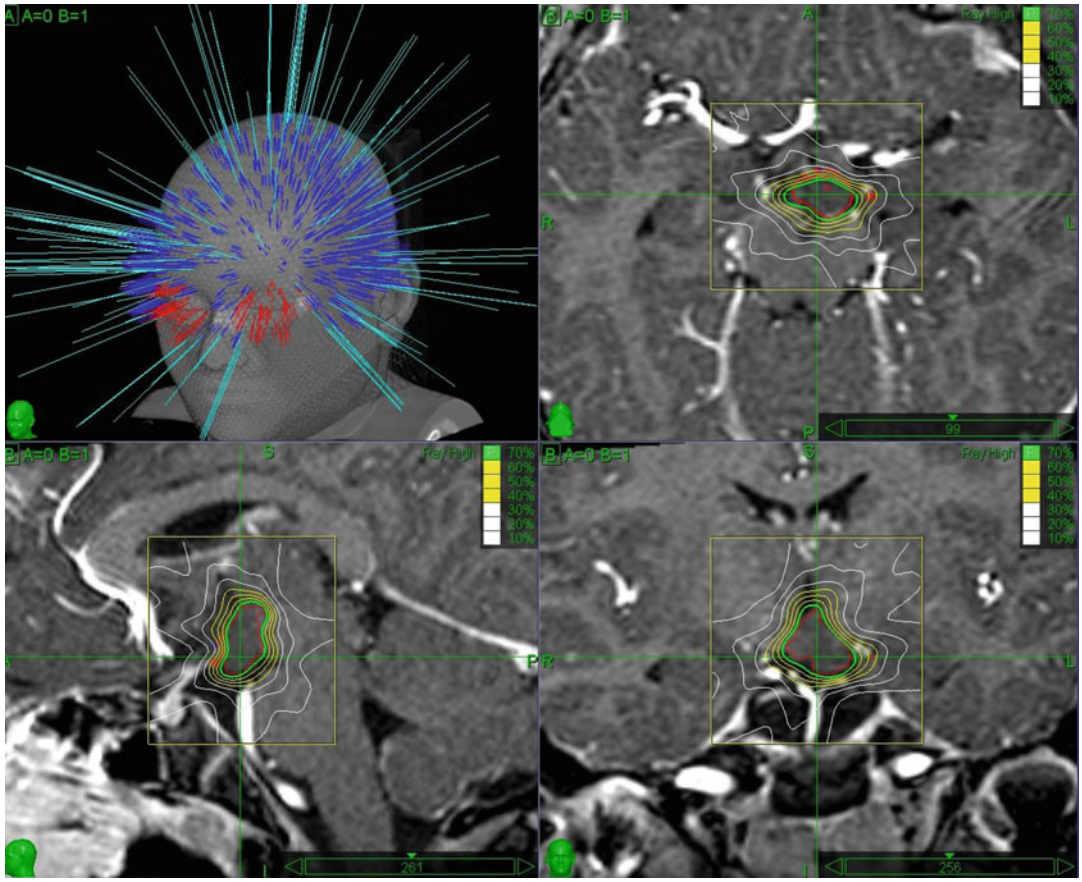

Fig. 27.1 Treatment planning of a left sessile HH extending into the interpeduncular cystern near the optic chiasm. This case was treated with frameless image-guided robotic radiosurgery (Cyberknife) delivering 151 beams carrying a total dose of 16 Gy prescribed to the 70 % isodose (Maximum dose: 22.85 Gy)

Further prospective studies are necessary to evaluate the frequency of complications or possibility of transient seizure worsening after these procedures, as well as delayed seizure remission, all in relation to delivered doses (Romanelli et al. 2008).

In conclusion, HH are brain tumors causing a severe epileptic disorder. Conventional surgical resection is an effective treatment for epilepsy and mass effect but carries a high risk of major neurological deficits and complications. SRS provides an efficacious and low-risk non invasive treatment option for small to medium size HH and for post-surgical residuals.

References

Arita K, Ikawa F, Kurisu K, Sumida M, Harada K, Ouzumi T, Monden S, Yoshida J, Nishi Y (1999) The relationship between magnetic resonance imaging findings and clinical manifestations of hypothalamic hamartoma. J Neurosurg 91(2):212–220

Arita K, Kurisu K, Iida K, Hanaya R, Akimitsu T, Hibino S, Pant B, Hamasaki M, Shinagawa S (1998) Subsidence of seizure induced by stereotactic radiation in a patient with hypothalamic hamartoma. Case report. J Neurosurg 89:645–648

Craig DW, Itty A, Panganiban C, Szelinger S, Krurer MC, Sekar A, Reiman D, Navarayan V, Stephan DA, Kerrigan JF (2008) Identification of somatic chromosomal abnormalities in hypothalamic hamartoma tissue at the GLI3 locus. Am J Hum Genet 82(10):366–374

Fenoglio FA, Wu J, Kim DY, Simeone TA, Coons SW, Retake H, Rho JM, Kerrigan JF (2007) Hypothalamic hamartoma: basic mechanism of intrinsic epileptogenesis. Semin Pediatr Neurol 14(2):51–59

Frattali CM, Liow K, Craig GH, Korenman LM, Makhlouf F, Sato S, Biesecker LG, Theodore WH (2001) Cognitive deficits in children with gelastic seizures and hypothalamic hamartoma. Neurology 57(1):43–46

Frazier JL, Godwin CR, Han ES, Jal JI (2009) A review on the managment of epilepsy associated with hyportalamic hamartomas. Childs Nerv Syst 25(4):423–432

Friehs GM, Park MC, Goldman MA, Zerris VA, Norén G, Sampath P (2007) Stereotactic radiosurgery for functional disorders. Neurosurg Focus 23:E3

Maixner W (2006) Hypothalamic hamartoma: clinical neuropathological and surgical aspects. Childs Nerv Syst 22(8):867–873

Ng YT, Rekate HL, Prenger EC, Wang NC, Chung SS, Feiz-Erfan I, Johnsonbaugh RE, Varland MR, Kerrigan JF (2008) Endoscopic resection of hypotalamic hamartoma for refractory symptomatic epilepsy. Neurology 70(17):1543–1548

Polkey CE (2003) Resective surgery for hypothalamic hamartoma. Epileptic Disord 5(4):281–286

Prigatano GP (2007) Cognitive and behavioral dysfunction in childrenwith hypothalamic hamartoma and epilepsy. Semin Pediatr Neurol 14(2):65–72

Quiske A, Frings L, Wagner K, Unterrainer J, Schulze-Bonhage A (2006) Cognitive functions in juvenile and adults patients with gelastic epilepsy due to hypothalamic hamartoma. Epilepsia 47(1):153–158

Regis J, Bartolomei F, De Toffol B, Genton P, Kobayashi T, Mori Y, Takakura K, Hori T, Inoue H, Schroettner O, Pendl G, Wolf A, Arita K, Chauvel P (2000) Gamma knife surgery for epilepsy related to hypotalamic hamartomas. Neurosurgery 47:1943–1952

Regis J, Kerkerian-Legoff L, Rey M, Vial M, Porcheron D, Nieoullon A, Peraqut JC (1996) First biomechanical evidence of differential functional effects following gamma knife surgery. Stereotact Funct Neurosurg 66:29–38

Regis J, Scavarda D, Tamura M, Nagayi M, Villeneuve N, Bartolomei F, Brue T, Dafonseca D, Chauvel P (2006) Epilepsy related to hypothalamic hamartomas: surgical managment with special reference to gamma knife surgery. Childs Nerv Syst 22(8):881–895

Regis J, Scavarda D, Tamura M, Villeneuve N, Bartolomei F, Brue T, Morange I, Dafonseca D, Chauvel P (2007) Gamma knife surgery for epilepsy related to hypothalamic hamartoma. Semin Pediatr Neurol 14(2):73–77

Regis J, Hayashi M, Eupierre LP, Villeneuve N, Bartolomei F, Brue T, Chauvel P (2004) Gamma knife surgery for epilepsy related to hypothalamic hamartomas. Acta Neurochir Suppl 91:33–50

Romanelli P, Anschel DJ (2006) Radiosurgery for epilepsy. Lancet Neurol 24(5):613–620

Romanelli P, Muacevic A, Striano S (2008) Radiosurgery for hypothalamic hamartoma. Neurosurg Focus 24(5):E9

Rosenfeld JV, Feiz-Erfan I (2007) Hypothalamic hamartoma treatment: surgical resection with the transcallosal approach. Semin Pediatr Neurol 14(2):88–98

Rosenfeld JV (2011) The evolution of treatment for hypothalamic hamartoma: a personal odyssey. Neurosurg Focus 30:E1

Schulze-Bonhage A, Homberg V, Trippel M, Keimer R, Elger CE, Warnke PC, Ostertag C (2004) Interstitial radiosurgery in the treatment of gelastic epilepsy due to hypothalamic hamartomas. Neurology 62:644–647

Selch MT, Gorgulho A, Mattozo C, Solberg TD, Cabatan-Awang C, De Salles AA (2005) Linear accelerator stereotactitc radiosurgery for the treatment of gelastic seizures due to hypothalamic hamartoma. Minim Invasive Neurosurg 48:310–314

Srikijvilaikul T, Najm I, Foldvary-Schaefer N, Lineweaver T, Suh JH, Bingaman WE (2004) Failure of gamma knife radiosurgery for mesial temporal lobe epilepsy: report of five cases. Neurosurgery 54:1395–1404

Striano S, Meo R, Bilo L, Cirillo S, Nocerino C, Rousi P, Striano P, Estraneo A (1999) Gelastic epilepsy. Symptomatic and cryptogenic cases. Epilepsia 40(3): 294–302

Striano S, Striano P, Cirillo S, Nocerino C, Bilo L, Meo R, Ruosi P, Boccella P, Briganti F (2002) Small hypothalamic hamartomas and gelastic seizures. Epileptic Disord 4(2):129–133

Striano S, Striano P, Coppola A, Romanelli P (2009) The syndrome gelastic epilepsy-hypothalamic hamartoma: severe, potentially reversible encephalopathy. Epilepsia 50(suppl 5):62–65

Striano S, Striano P, Sarappa C, Boccela C (2005) The clinical spectrum and and natural hystory of gelastic epilepsy-hypothalamic hamartoma syndrome. Seizure 14(4):232–239

Sturm JW, Andremann F, Berkovic SF (2000) Pressure to laugh: an unusual epileptic syndrome associated wuth hyothalamic hamartomas. Neurology 54(4): 971–973

Tassinari CA, Riguzzi P, Rizzi R, Volpi L (1997) Gelastic seizures. Paediatric epilepsy syndromes and their surgical treatment. John Libbely et Co Ltd, London pp 429–446

Téllez-Zenteno JF, Serrano-Almeida C, Moien-Afshari F (2008) Gelastic seizures associated with hypothalamic hamatromas. An update in the clinical presentation, diagnosis and tratment. Neuropsychiatr Dis Treat 4(6):1021–1031

Trousseau (1956) De l'epilepsie. Lecons cliniques faites a l'Hotel-Dieu, 2nd ed. J.Viat, Paris

Unger F, Schrottner O, Feichtinger M, Bone G, Haselsberger K, Sutter B (2002) Stereotactitc radiosurgery for hypothalamic hamartomas. Acta Neurochir Suppl 84:57–63

Valdueza JM, Cristante L, Dammann O, Bentele K, Vortmeyer A, Saeger W, Padberg B, Freitag J, Herrmann HD (1994) Hypothalamic hamartoma: with special reference to gelastic epilepsy and surgery. Neurosurgery 34(6):949–958

Veendrick-Meekes MJ, Verhoven WM, van Erp MG, van Blarikom W, Tuinier S (2007) Neuropsychiatric aspects of patients with hypothalamic hamartomas. Epilepsy Behav 11(2):218–221

Image-Guided Stereotactic Radiosurgery for Spinal Pathology

28

Pantaleo Romanelli and Alfredo Conti

Contents

Abstract

Radiosurgery is the delivery, in a single or a few fractions, of a concentrated dose of radiation to diseased tissue with a steep dose fall-off outside the treatment volume. Traditionally, radiosurgery is delivered to intracranial targets using a rigid frame to immobilize the target and provide external reference points for target localization. The development of image-guided radiosurgery has allowed the principles of radiosurgery to be applied to the treatment of extracranial pathologies including spinal lesions. Image guidance is the use of imaging to locate the tumor before and during a treatment session and redirect the radiation source or reposition the patient based on these measurements. In this manner dose delivery accuracy comparable to frame-based radiosurgery can be achieved. Furthermore, frameless stereotactic radiosurgery allows treatments to be delivered in more than one fraction, which has the potential to reduce toxicity to healthy tissue and organs at risk such as the spinal cord, an organ that is among the most sensitive to radiation.

Spinal radiosurgery has resulted in excellent rates of tumor control with a relatively low risk of radiation-induced myelopathy. Here we review currently available image-guided stereotactic radiosurgery devices that can be used to treat the spine, summarize clinical data showing the efficacy of these systems, and discuss dose and volume limits to avoid radiation toxicity induced by spinal radiosurgery for malignant and benign pathologies.

P. Romanelli (✉)
Cyber knife Center, Via Saint Bon 20,
20147 Milano, Italy
e-mail: Radiosurgery2000@yahoo.com

A. Conti
Department of Neurosurgery, Cyber Knife Center,
University of Messina, Messina, Italy

M.A. Hayat (ed.), *Tumors of the Central Nervous System, Volume 12*,
DOI 10.1007/978-94-007-7217-5_28,

Introduction

Stereotactic radiosurgery (SRS) was introduced by the Swedish neurosurgeon Lars Leksell in 1951 (Leksell 1951). With this technique, precisely delivered high-dose radiation is used to ablate or control the growth of pathologic targets. SRS has achieved its high spatial accuracy by the use of a rigid frame fixed with screws to the patient's skull, which immobilizes the patient's head during the procedure and provides the coordinate system in which the position of the planning target volume can be accurately defined. To keep the correct position of the target volume in the stereotactic space, the frame cannot be removed during the treatment. The radiosurgery devices (linear accelerators or gamma units) generate dose volumes characterized by a very steep fall-off outside the target's boundaries. This allows the delivery of much higher radiation doses to the target than conventional radiotherapy. SRS has been used in the treatment of several intracranial pathologies such as tumors, vascular malformations, and trigeminal neuralgia. Thus, SRS has progressively become a fundamental therapeutic alternative in the neurosurgical armamentarium and is routinely used to manage a broad spectrum of intracranial disorders.

In the last decade, a great step forward has been taken with the introduction of the image-guided SRS. With image-guided SRS the stereotactic frame is discarded, and instead intraoperative imaging is used to locate the tumor prior to and during a treatment session and redirect the radiation source or reposition the patient based on these measurements. The accuracy of dose delivery of image-guided radiosurgery is comparable to that of radiosurgery performed with a stereotactic frame. The development of this technique allowed the principles of radiosurgery to be applied to the treatment of extracranial pathologies, including spinal lesions.

Investigators at Stanford University published the first clinical description of image-guided spinal radiosurgery in 2001. This preliminary study demonstrated the safety and short-term efficacy of radiosurgery for a variety of neoplastic and vascular spinal lesions (Ryu et al. 2001). Several subsequent reports have confirmed the efficacy and safety of spinal radiosurgery using the robotic CyberKnife® system (Accuray Incorporated, Sunnyvale, CA) (Gerszten et al. 2004, 2007), the Novalis® system (BrainLAB, Heimstetten, Germany) (De Salles et al. 2004), and intensity-modulated radiotherapy (IMRT) (Bilsky et al. 2004; Yamada et al. 2005). Even though spinal radiosurgery is in its infancy, this technique offers an effective and well-tolerated option to many patients suffering from selected spinal lesions. A large study of spinal SRS in 393 patients demonstrated long-term pain control (86 %), long-term tumor control (88 %), and not a single instance of radiation-induced neurological injury (Gerszten et al. 2007).

Devices for Spinal Radiosurgery

The first technical challenge for extension of the concepts of radiosurgery to the extracranial organs was the necessity to define a stereotactic space around organs different from the brain. The first attempts to deliver ablative doses of radiation to spinal lesions were made using a stereotactic frame firmly attached to the spinous processes by means of a series of small incisions made under anesthesia (Hamilton et al. 1995). Although this system provided a mechanism to deliver radiation accurately to spinal targets by use of a LINAC, frame fixation was cumbersome, required a long procedure, and made treatment in more than one fraction impractical.

The introduction of frameless radiosurgical technology overcame the limitations associated with frame-based radiosurgery. The first such system, the CyberKnife® System (Fig. 28.1), was developed by a neurosurgeon whose goal was to eliminate the stereotactic frame for intracranial radiosurgery (Adler et al. 1997). Frameless targeting was made possible by advanced image-guidance based on digital scans acquired through amorphous silicon detectors. X-ray images acquired from either side of the patient were registered to digitally reconstructed radiographs derived from pretreatment planning

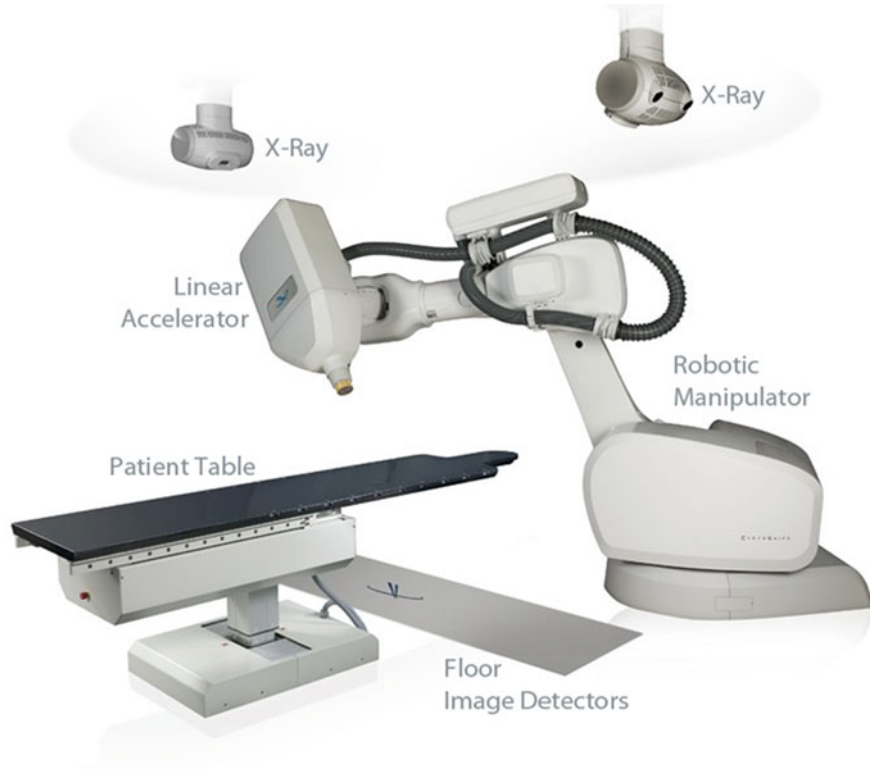

Fig. 28.1 The CyberKnife®. A robotic arm points the lightweight 6 MV LINAC to the target. Real-time image guidance based on X-ray imaging (cameras mounted on ceiling, detectors to either side of treatment couch) provides the aiming for this frameless radiosurgery system. Dose conformality and normal tissue protection is provided by firing thin beams from hundreds of different directions, towards the patient

CT scans. This registration process allows the position of the skeletal anatomy to be translated into the coordinate frame of the robot-mounted LINAC. A control loop between the imaging system and the robotic arm adjusts the position of the LINAC therapeutic beam to the observed position of the treatment target. If the patient moves even slightly, the change is detected during the next imaging cycle and the beam is realigned with the target. A CyberKnife treatment involves usually 100–200 beams delivered from unique beam orientations, followed by an equivalent number of imaging cycles confirming the target position before the next beam is delivered. The Novalis® system uses a similar setup and tracking approach. In this system, the LINAC is mounted on a gantry and treatment is delivered in five to nine beams (Ryu et al. 2003).

With the CyberKnife system, spinal and paraspinal lesions were initially targeted and tracked on the basis of fiducial markers implanted in vertebrae adjacent to the lesion; this form of targeting has been shown to be accurate to within a mean of 0. 7 mm. A targeting and tracking system based on skeletal features, the Xsight® spine tracking system (Accuray Incorporated, Sunnyvale, CA), has been developed and showed to have a total clinical accuracy to 0. 5–0. 6 mm (Ho et al. 2007). Xsight® employs an X-ray-image-enhancement technique to increase the amount of information provided by the bony anatomy surrounding spinal lesions such that lesions can be targeted and tracked on the basis of spinal anatomy itself, without implanted fiducials. Xsight® registers images taken during treatment to pretreatment (synthetic) images by use of a hierarchical mesh

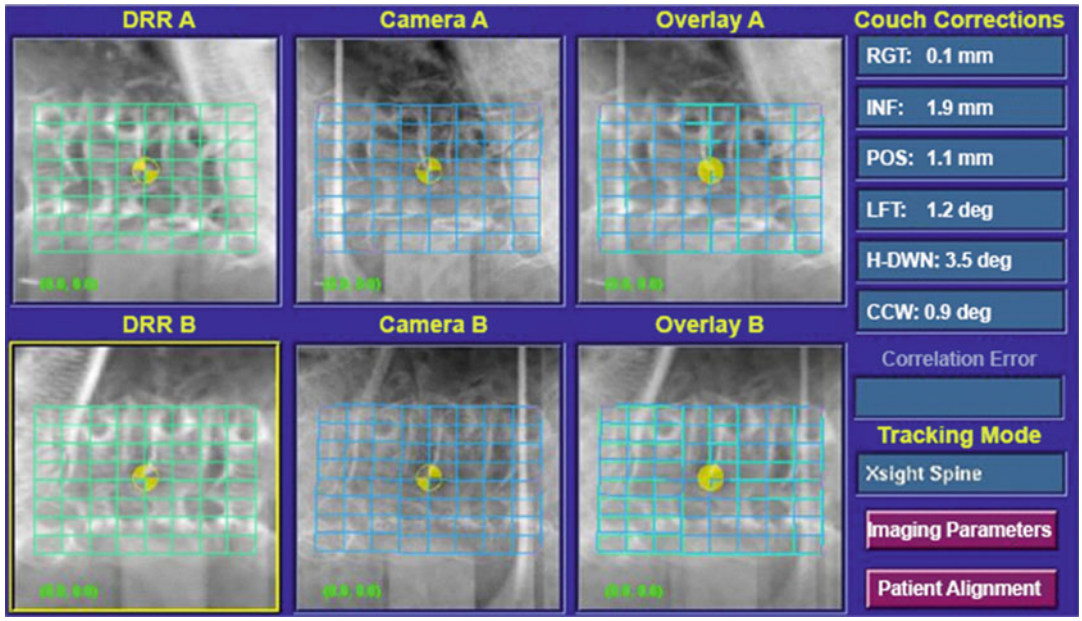

Fig. 28.2 Xsight® spine software registers intra-treatment to pretreatment images by use of a hierarchical mesh technique. In the *left* column of images, two orthogonal synthetic images obtained from the planning CT scan are displayed. Corresponding live images, taken repeatedly during a session, can be seen in the *middle* row. Offsets are calculated at a series of discrete points within the region of interest. The result is a deformable registration model that accounts for nonrigid changes in the patient position and between pretreatment and intratreatment imaging. The deformation can be seen in the *right* column of images. The software calculates errors of patient position in each of the six degrees of motion

technique, where the calculation is made at a series of discrete points within the region of interest. The result is a deformable registration model that accounts for nonrigid changes in the target position throughout treatment. The deformation can be seen in the middle row of images (under camera image A and B) (Fig. 28.2). Eliminating an invasive procedure (fiducial implantation) from what would otherwise be a noninvasive one significantly improves the patient experience without compromising clinical efficacy.

Both the CyberKnife and the Novalis® unit emit photons generated by a 6-MV LINAC. The CyberKnife LINAC is mounted on a robotic arm (KUKA® Roboter GmbH, Augsburg, Germany) that can move and point the LINAC with six degrees of freedom. Photons generated by the LINAC pass through circular collimators ranging from 5 to 60 mm in diameter. Recently a dynamic collimator whose diameter may be changed during treatment has been introduced into the clinical practice. The Novalis® LINAC is mounted on a gantry and is equipped with a micromultileaf collimator with 26 leaf pairs. Radiation can be delivered through circular cone arcs or fixed-shape conformal beams via the micromultileaf collimator.

Other technologies have been developed in order to deliver image-guided radiation therapy, which is characterized by enhanced conformality in comparison to conventional radiotherapy (although the treatments are still performed using conventional fractionation protocols). Such systems (Varian® Trilogy, Varian Medical Systems, Palo Alto, CA; Elekta Synergy®, Elekta AB, Stockholm, Sweden; and TomoTherapy®, TomoTherapy Incorporated, Madison, WI) include integrated onboard X-ray imaging, and even CT acquisition, for use during initial patient set-up.

Frameless radiosurgical technology is characterized by the ability to perform hypofractionated treatments. Hypofractionation allows the

delivery of ablative, radiosurgical doses to the treated lesion, but allows enhanced protection of the adjacent tissues by delivering the total dose in 2–5 lower-dose fractions and at a lower dose rate (which allows precious time for normal tissues to recover between fractions). Frameless hypofractionated radiosurgery of lesions affecting the cranial nerves and spinal cord substantially enhances treatment safety and prevention of dreaded neurological complications (Romanelli et al. 2006). Frameless systems are not limited to delivering spherical dose distributions (i.e., treatment planning and delivery can be nonisocentric). Early radiosurgical systems treated nonspherical targets by delivering radiation to multiple isocenters packed inside the treated volume. Nonisocentric planning provides a straightforward approach for the treatment of irregularly shaped lesions, and can result in a more homogeneous radiation distribution that is usually very conformal to the shape of the target lesion.

Clinical Applications of Spinal Radiosurgery

Since the initial description of image-guided spinal radiosurgery, a steady increase in published reports has occurred. Selection criteria for spinal radiosurgery are evolving rapidly. In addition, there are reports showing that spinal radiosurgery is a safe treatment for target volumes as large as 200 cm^3 (Gerszten et al. 2007); multisession treatments allow the application of SRS to lesions that exceed conventional volume limits. The primary indication for spinal radiosurgery is metastatic cancer in patients who are experiencing pain either owing to disease in vertebrae or because lesions are compressing the spinal cord or nerve roots. Neoplastic lesions (either benign or malignant) are usually quite sensitive to radiation and if proper doses are used, their local growth is arrested. Non-neoplastic lesions such as arteriovenous malformations (AVMs) can also be treated with radiosurgery; such lesions often shrink after irradiation. Radiosurgery does not cause quick decompression of the spinal cord or improve spinal instability and is, therefore, generally contraindicated in the presence of these conditions, although radiosurgical treatment after spinal fixation by kyphoplasty has proven effective (Gerszten et al. 2005b). Of particular note is the fact that radiosurgery can often still be used when conventional radiotherapy has failed (Romanelli and Adler 2008; Romanelli et al. 2006). The available clinical results of spinal radiosurgery are here summarized, paying particular attention to the safety and efficacy of this treatment in relation to specific clinical indications.

Spinal Metastases

Spine is the third most common site of metastatic localization after lung and liver. Spinal metastases are, therefore, a rather common finding in oncological patients, posing a serious challenge to patients and physicians for their tendency to cause severe pain, vertebral instability and spinal cord injuries. The occurrence of spinal metastases in patients with cancer is typically associated with significant morbidity and reduced life expectancy.

Surgery remains the treatment of choice for metastases requiring decompression and vertebral stabilization. Open surgery may achieve the goals of spinal cord decompression, stabilization, pain control, local growth control and histological diagnosis. A posterior approach with laminectomy, however, is sufficient only when the lesion is limited to the posterior elements of the vertebra. In most cases, the massive involvement of the vertebral body would require a full vertebrectomy with instrumented fusion, a complex and bloody procedure, which is offered usually only to a limited number of patients; patients of advanced age, with poor medical condition and disseminated cancer are unable to withstand such surgery.

Image-guided radiosurgery, as well as fractionated conformal radiotherapy, are efficient alternative options for pain relief, neurological function preservation or recovery and control of tumor growth. Radiosurgery, however, as opposed to

conventional radiation therapy, provides a fast and highly effective treatment.

Several studies have demonstrated that radiosurgery is safe and effective for the palliation of spinal metastases. CyberKnife image-guided robotic radiosurgery has been widely used to treat spinal metastases, often as the primary treatment modality. At the University of Pittsburgh Medical Center, the largest clinical series to date has been treated with single-fraction radiosurgery (Gerszten et al. 2007). The study involved over 500 lesions in 393 patients with metastases of various (often moderately or highly radioresistant) histologies. Goals of therapy included tumor control, palliation of symptoms, and restoration of neurological function. The average maximum dose to the tumor was 19 Gy delivered in a single session. Sixty-seven patients had not been previously irradiated. In 48 of these cases, a significant decrease in pain was observed during the follow-up period of 6–48 months (median 16 months). Authors reported long-term radiographic control in 88 % of all cases. A remarkable rate of local growth control (up to 100 %) was reported for breast, lung and renal cell carcinoma when radiosurgery was the primary treatment. An overall long-term improvement in pain was obtained in 290 of the 336 cases that presented with pain as a primary indication (86 %).

Similar local control results were found in a series of 58 patients treated at the Georgetown University Hospital for various metastatic lesions with a dose of 21.2 Gy in 3.6 fractions on average (Degen et al. 2005), Most patients were treated for pain rather than other symptoms. Authors reported a rapid and durable pain relief in short-term follow-up. A more extensive cohort of 200 patients was studied by this group (Gagnon et al. 2009). Using a visual analog scale of pain and the SF-12 to assess quality of life (QOL), they found a significant decrease in pain scores over a 4-year follow-up period, no significant change in physical QOL and improvements in the mental component of QOL. Mild and self-limited side effects and no late radiation toxicity were observed.

The CyberKnife was used by Gibbs et al. (2007) for radiosurgery of 74 patients with 102 metastatic lesions. Doses ranged between 16 and 25 Gy in 1–5 fractions. Two-thirds of the patients had been previously irradiated. Symptoms, including pain and neurological deficits, improved in 84 % of cases. Severe myelopathy occurred in three patients after a mean of 7 months from treatment. Two of these patients had received prior irradiation to doses of 50.4 and 39.6 Gy in 1.8-Gy fractions, at 70 and 81 months, respectively, prior to radiosurgery.

Gerszten and coworkers have reported equally good results treating lesions considered as radioresistant, such as renal cell carcinoma (Gerszten et al. 2005a) and melanoma (Gerszten et al. 2006) metastasizing to the spine. In addition, they have advocated a new minimally invasive treatment paradigm for spinal metastatic compression fractures using a combination of kyphoplasty and radiosurgery (Gerszten et al. 2005b). The combination of these two minimally invasive procedures–likely to be a welcome approach for patients dealing with the long-term effects of primary cancer treatment–proved to be safe and effective on short-term (7–20 months) follow-up.

In two papers describing the largest clinical series of metastatic spine lesions treated with the Novalis® system, Ryu et al. (2007) and Jin et al. (2007) reported outcomes of single-fraction radiosurgery in nearly 200 patients. Doses ranged from 8 to 18 Gy, with lower doses chosen when lesions were nearer the spinal cord. Seven-to-nine-beam plans were sufficient to cover tumor volumes while maintaining dose constraints of 10 Gy to less than 10 % of the spinal cord near the lesion. Pain relief was obtained within 4 weeks in 85 % of the 49 patients presenting with pain (Ryu et al. 2007). The duration of pain relief was not reported. A single case of radiation-induced myelopathy was noted in a patient treated 13 months earlier for a breast cancer metastasis to the clivus and C1 (Jin et al. 2007). The patient had been treated with doses that approximated those used to treat patients who suffered no long-term complications. The cervical location of the lesion and prior and post-treatment chemotherapy may have increased the sensitivity of the cord to damage in this patient.

At least one study has shown a relationship between dose and outcome. Pain recurred most commonly in patients receiving less than 14 Gy in a single session (Ryu et al. 2004). Another question that has not been sufficiently answered is whether the two regimens, single versus hypofractionated treatments, differ in terms of efficacy and toxicity. In this context it is noteworthy that the available studies have failed to demonstrate a significant difference in pain control between single and multiple fraction schemes for external beam radiation therapy. For SRS, a retrospective review of the treatment records of 348 metastatic lesions to the spine in 228 consecutive patients treated at University of Pittsburgh and University of Georgetown between January 2000 and 2008 compared single-session to hypofractionated SRS (Heron et al. 2012). One hundred ninety-five lesions were treated using a single-fraction regimen (mean 16.3 Gy), whereas 153 lesions were treated in 3–5 fractions (mean doses of 20.6 Gy in 3 fractions, 23.8 Gy in 4 fractions, and 24.5 Gy in 5 fractions). The primary end point was pain control. Secondary end points included neurological deficit improvement, toxicity, local tumor control, need for retreatment, and overall survival.

Results were interesting and somewhat surprising. Pain control was significantly improved in the single-fraction group for all measured time points up to 1 year post-treatment (100 % vs. 88 %). Rates of toxicity and improvements in neurological deficits were not statistically different. Local tumor control, on the other hand, was significantly better in the hypofractionation group (96 % vs. 70 %, $p=0.001$). Similarly, the need for retreatment was significantly lower in this group (1 % vs. 13 %, $p<0.001$). One-year overall survival was significantly greater in the hypofractionation than the single-fraction group (63 % vs. 46 %, $p=0.002$). Although the retrospective nature of the study precludes strong conclusions, these data suggest that single-fraction radiosurgery provides greater early pain control and equivalent toxicity, whereas hypofractionated treatments achieve greater tumor control lowering the chances of local growth-control failure and consequent need for retreatment in long-term survivors.

Another debated issue is the definition of the target volume in cases where tumor invasion involves only a portion of the vertebra. Patel et al. (2012) retrospectively evaluated differences in clinical outcomes for 154 metastatic lesions in 117 patients with metastatic spine disease treated with a whole versus partial vertebral body contouring approach. Contouring the whole vertebral body reduced the risk of recurrence, improved symptomatic relief and provided improved local tumor control. With the CyberKnife, it is also possible to plan a SRS treatment with two different target volumes (Fig. 28.3), one including the whole vertebra receiving a lower dose (e.g. 8–10 Gy) and a second one including the tumor mass receiving a higher dose (e.g. 16 Gy). This may offer the advantage of treating the whole vertebra, without the necessity to reduce the dose to the tumor.

Therefore, available data provide clear answers to important issues, including the efficacy and safety of high conformal radiation to metastatic spine. On the other hand, there are several open questions regarding dose, fractionation, and volume delineation. Radiosurgery can be utilized as a salvage treatment for those with persistent symptoms or radiological progression and who have already undergone external beam radiotherapy. Patients with limited spinal disease, favorable overall performance status, and focal neurological symptoms also benefit from SRS. Control of tumor progression and palliation of symptoms are different goals of treatment, applicable to different degrees in patients with more or less extensive disease. These are issues that must be addressed in a randomized phase III study to ultimately determine whether radiosurgery can be the primary treatment modality for spinal metastases. However the clinical evidence so far available is clearly favorable to the use of spinal radiosurgery to achieve pain relief and local growth control in patients not requiring surgical decompression and/or stabilization or otherwise too sick to be able to tolerate invasive procedures.

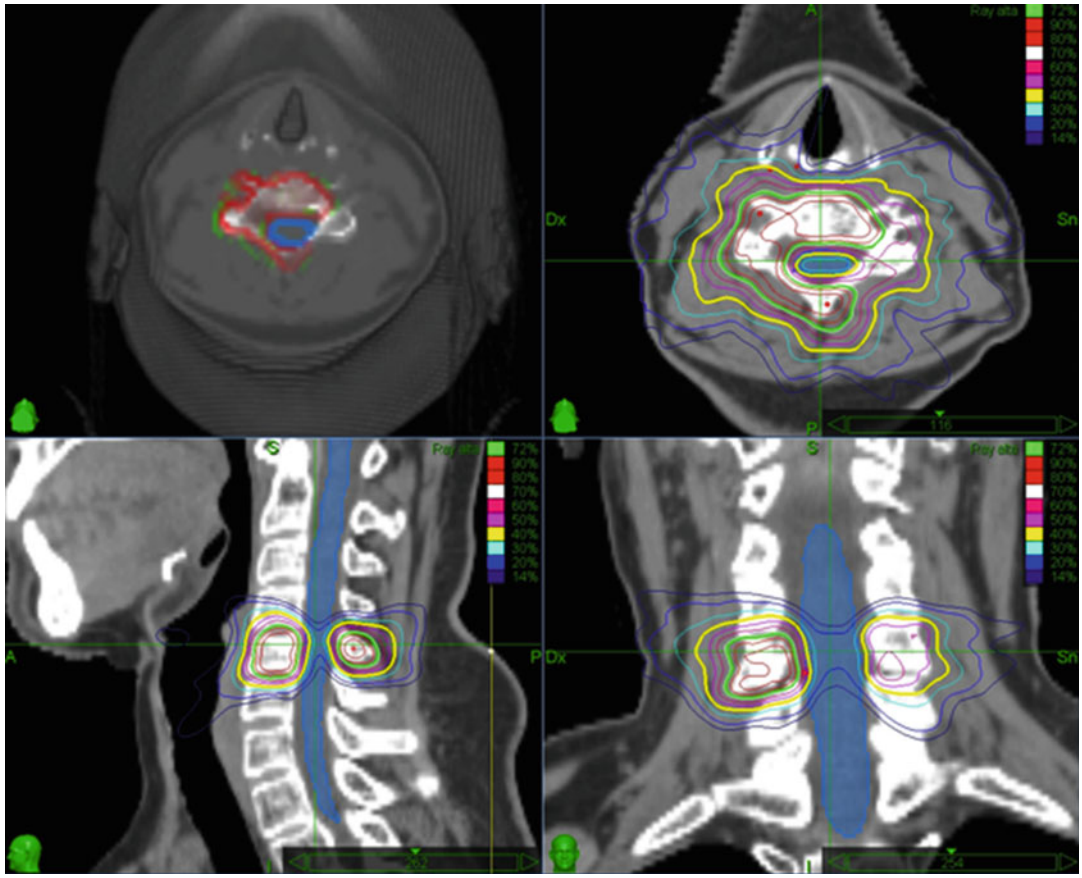

Fig. 28.3 Contours of the entire vertebral body for SRS of metastatic spinal lesions. With the CyberKnife one can plan an SRS treatment with two different target volumes and two different prescribed doses (*upper right*). One volume, incorporating the whole vertebra, is given a lower dose (the *yellow* isodose line represents 10 Gy) and a second one, containing only the tumor mass, receives a higher dose (the *green* isodose line represents 16 Gy). In this manner the whole vertebra can be treated with a dose that can be tolerated by the spinal cord (the *light blue* line represents the 8 Gy isodose line), while the dose to the tumor remains high

Benign Spinal Tumors

Some of the studies that have reported the effects of single-stage or hypofractionated radiosurgery for the treatment of spinal metastases have also examined the effects of radiosurgery on benign spinal tumors (Ryu et al. 2001; De Salles et al. 2004). SRS for benign lesions was first reported by Murphy et al. (2000). The same group later reported clinical outcomes in 16 patients treated with CyberKnife radiosurgery using a dose range of 11–25 Gy delivered in 1–5 fractions (Ryu et al. 2001). Among these patients, six were treated for benign spinal tumors while the rest were treated for spinal AVMs or spinal metastases. No neurological changes were observed over a follow-up period of 3–48 months. Treatment accuracy was based on intraoperative detection of four fiducials implanted on the spine.

The Stanford University group updated the outcomes of CyberKnife radiosurgery in a cohort of 51 patients with 55 intradural extramedullary lesions (30 schwannomas, 9 neurofibromas, and 16 meningiomas) in 2006 (Dodd et al. 2006). Control of lesion growth was analyzed in a subset of 28 patients with a minimum clinical and radiographic follow-up of 24 months (mean follow-up 36 months). Lesion size was found to be stable in

61 % of patients while it decreased in 39 %. None of the lesions increased in size over the follow-up period. Nevertheless, growth control was not sufficient to induce remission of pre-existing myelopathy caused by mass effect: three patients required surgical intervention within a year to reduce spinal-cord compression and improve the myelopathy. The myelopathy might have been reduced if the procedure had reduced the size of the lesions in these cases. Nevertheless, during surgery, no obvious alterations of local anatomy owing to the previous irradiation was found. Radiation-induced myelopathy was observed in one patient 8 months after the treatment, and one patient died of respiratory failure 7 months after irradiation of a C1 meningioma. Postmortem histopathological analysis of the irradiated tumor showed hyalinized tumor vessels and central necrosis.

Recently, the Stanford University group reported on 87 patients with 103 benign intradural extramedullary spinal tumors (32 meningiomas, 24 neurofibromas, and 47 schwannomas) treated with stereotactic radiosurgery from 1999 to 2008 (Sachdev et al. 2011). Twenty-five patients had neurofibromatosis. Treatment was delivered in 1–5 sessions (median 2) with a mean prescription dose of 19.4 Gy (range, 14–30 Gy) to an average tumor volume of 5.24 cm (range, 0.049–54.52 cm). After a mean radiographic follow-up period of 33 months, including 21 lesions followed for $\geq$48 months, 59 % were stable, 40 % decreased in size, and a single tumor (1 %) increased in size. Clinically, 91 %, 67 %, and 86 % of meningiomas, neurofibromas, and schwannomas, respectively, were symptomatically stable or improved at last follow-up. One patient with a meningioma developed a new, transient myelopathy at 9 months, although the tumor was smaller at last follow-up.

Single-stage spinal radiosurgery produced similar results in term of growth control, according to a study from the University of Pittsburgh Medical Center (Gerszten et al. 2008). Seventy-three benign intradural extramedullary spinal tumors, including neurofibromas (25 cases), schwannomas (35 cases), and meningiomas (13 cases), were treated and followed up for 8–71 months (median 37 months). Twenty-one cases were associated with neurofibromatosis Type 1, and nine patients had neurofibromatosis Type 2. The maximum intratumoral dose was 15–25 Gy (mean, 21.6 Gy). Tumor volume ranged from 0.3 to 93.4 cm. Long-term pain improvement occurred in 22 out of 30 cases (73 %). Long-term radiographic tumor control was demonstrated in all cases. Three patients, one with meningioma and two with schwannomas, experienced new symptoms attributed to radiation-induced spinal cord toxicity 5–13 months after treatment. None of these patients had received previous irradiation. All three lesions were located at the level of the cervical spinal column, and all were treated with a tumor marginal dose of 20 Gy in a single fraction.

Recently, Chang et al. (2011) reported the experience of the Korea Cancer Center Hospital in the treatment of 30 benign spinal tumors in 20 patients using the CyberKnife. Authors treated 20 neurogenic tumors (schwannomas and neurofibromas), eight hemangioblastomas, and two meningiomas. Four patients with neurofibromatosis (NF) type 2 and four patients with Von Hippel Lindau disease were also included. Tumor volume ranged from 0.04 to 33.65 cm^3 (mean, 4.52 cm^3). A 14–33 Gy marginal dose was delivered in 1–5 fractions. The mean follow-up period was 35.6 months (range, 12–84 months). On follow-up, most lesions decreased in size (57 %) or remained unchanged (33 %). Authors reported improvement of pain after radiosurgery in most cases (94 %). Motor deficit recovered in two out of five patients and sensory improvement occurred in four out of ten patients. Two patients deteriorated because of tumor enlargement and occurrence of a new lesion.

Overall, these studies demonstrated a remarkable rate of local growth control for benign intradural tumors. Nevertheless, those with myelopathy caused by compression of neural structures did not benefit from radiosurgery and some patients deteriorated. This poses questions regarding the tolerance of the spinal cord to radiation and possible other factors influencing the outcome that will be discussed later.

Arteriovenous Malformations

Intramedullary AVMs pose a formidable treatment challenge. Their location within the spinal cord usually discourages microsurgical dissection of the nidus. Endovascular embolization is feasible in selected cases, but there is a high risk of ischemic damage to the spinal cord. Despite their unfavorable natural history characterized by progressive enlargement, repeated bleeding, and sudden or progressive neurological deterioration, treatment is often deferred because of the high risks of iatrogenic damage associated with these interventions. On the basis of the efficacy of radiosurgery in the treatment of selected brain AVMs (Colombo et al. 2009) the radiosurgery group at Stanford University began to treat intramedullary AVMs with the CyberKnife in 1997. Outcomes of radiosurgical treatment in 15 patients with intramedullary spinal-cord AVMs (nine cervical, three thoracic, and three conus medullaris) were reported by Sinclair et al. in 2006. For the initial 13 patients in this series, target definition was conducted with CT imaging alone. Follow-up studies included MRI and two-dimensional spinal angiography. Three-dimensional rotational spinal angiography has been recently introduced, and allows better identification of the AVM nidus, fusion with the planning CT, and improved identification of the lesion and its spatial relationships to adjacent skeletal landmarks.

Intracranial AVMs require single-session treatments with adequate marginal doses (up to 25 Gy) to obliterate the nidus. The Stanford group was the first to attempt to treat spinal AVMs, beginning with a less aggressive treatment strategy involving hypofractionation (2–5 fractions delivered 24 h apart) with the goal of preventing severe spinal-cord toxicity. The mean target volume for the AVMs in this series was 2.36 cm3 (range 0.79–5.23 cm3). The mean maximum dose was 25 Gy (range 17.7–30.0 Gy). Clinical and MRI follow-up were conducted annually, and spinal angiography was repeated at 3 years. After a mean follow-up of 27.9 months (range 3–59 months), six of the seven patients with more than 3 years' follow-up had significant reductions in AVM volumes on MRI. Postoperative spinal angiography was available in five patients. Complete obliteration of a conus medullaris AVM was observed in one patient 26 months after radiosurgery and substantial reduction of the size of the nidus was observed in three patients, but no visible effect was detected in a patient with a large, incompletely treated lesion. Reduced nidus size on MRI was obtained in the three patients with follow-ups of less than 3 years. No evidence of further hemorrhage or neurologic deterioration following radiosurgery has been detected so far.

Before this preliminary study, the use of radiosurgery to treat spinal-cord lesions had never been reported. Such a task was considered extremely dangerous by most practitioners. The fact that high-dose CyberKnife radiosurgery delivered to intrinsic spinal cord lesions was well tolerated opens a totally new treatment avenue. Data so far indicate that spinal radiosurgery is a safe, accurate and effective tool for the treatment of intramedullary lesions.

Spinal Cord Sensitivity to Radiations

Spinal cord injuries induced by radiation are infrequently encountered in clinical practice and in the literature. When it occurs, however, radiation-induced myelopathy can be very severe ranging from pain, paresthesias, sensory deficits, Brown-Sequard syndrome, loss of control of bowel/bladder, to a complete paralysis. The pathogenesis of such injuries is generally ascribed to vascular damage, glial cell injury, or both.

Clearly the issue of dose limits is of primary importance for spinal radiosurgery; unfortunately precise limits and firm recommendations cannot be drawn simply from patients treated with fractionated radiotherapy owing to the difficulty in translating biologically equivalent dose effects between very different dosing schemes. Relative to conventional radiotherapy, radiosurgery involves a much higher dose per fraction (the biological equivalence of which to radiotherapy is not precisely known), but is

directed to a very limited portion of the spinal cord (again, how this translates into recommendations for dose constraints is not immediately clear). Yet another question deserving attention is the tolerance of the spinal cord to re-irradiation, to which radiosurgery has been shown to be safely applied when larger-field conventional radiotherapy would likely cause radiation-induced complications. Below we review some of the relevant data, noting both the complexity of the problem and tentative recommendations that have been made to date.

Schultheiss (2008) reviewed the literature on external beam radiotherapy and analyzed the incidence of radiation myelopathy in 335 and 1,946 patients receiving radiotherapy to their cervical and thoracic spines, respectively. The risk of myelopathy as a function of dose was estimated using a probability distribution model. A good fit to the combined cervical and thoracic cord data was not possible and separate analyses were performed. For the cervical cord data, at 2-Gy per fraction and assuming α/β of 0.87 Gy, the probability of myelopathy was estimated as 0.03 % at 45 Gy, 0.2 % at 50 Gy, and 50 % at >69 Gy.

The values of Schultheiss (2008) can be used (with caution, Schultheiss stressed) as a reference for calculating the risk of hypofractionated irradiation schemes. To relate the biological effect of a course of radiation to the total dose of radiation administered with the standard fractionation scheme (2 Gy/fraction), the concept of normalized total dose (NTD) can used. The NTD is derived from the linear-quadratic model:

$$\mathrm{NTD} = \mathrm{BED} / (1 + \mathrm{d} / \alpha / \beta)$$

Where BED is the biologically equivalent dose. This can be calculated according to the formula:

$$\mathrm{BED} = \mathrm{nd}\left(1 + \mathrm{d} / \alpha / \beta\right)$$

where n = number of fractions, d = dose/fraction, and nd = total dose.

To establish the equivalence with the standard fractionation scheme (2 Gy/fraction), d would take the value 2 Gy and the α/β could be as slow as 0.55 (Kirkpatrick et al. 2010). This small α/β implies a higher risk of myelopathy for high-dose fractions. Also, although BED calculations seem valid for comparing conventional fractionation regimens, the standard linear quadratic model seems inaccurate when the fractional dose is very high.

Furthermore, unlike conventional radiotherapy during which a full dose is delivered to both the spine and the spinal cord, image-guided radiosurgery systems deliver high doses of radiation to the target region in single or few fractions, while relatively sparing the adjacent spinal cord. Thus, only portions of the spinal cord, rather than the entire spinal cord, are subjected to the prescription dose at the targeted spinal level. A partial-volume dose constraint for spinal cord remains to be determined.

The literature provides an important study on the risk of post-radiosurgery myelopathy. Gibbs et al. (2009) reported six cases of radiation-induced myelopathy among more than 1,000 patients treated for benign and metastatic spinal tumors combining two of the largest CyberKnife spinal radiosurgery series from the University of Stanford and University of Pittsburgh. The volume of spinal cord treated to a dose of more than 8 Gy was less than 1 mL. The normal tissue complication rate using the above-mentioned dose constraint was less than 0.6 %. Despite its importance, few conclusions can be drawn on the basis of the data reported by Gibbs et al. (2009). Indeed, only three of six patients had a maximal dose BED_3 of more than 70 Gy (corresponding to 45 Gy delivered in 2-Gy fractions). For the other three patients the determinants of radiation-induced myelopathy remain undetermined.

A second interesting study was recently published by Daly et al. (2012) from Stanford University. Authors treated 24 spinal hemangioblastomas in 17 patients. Seventeen tumors received a single fraction with a median dose of 20 Gy (range, 18–30 Gy) and 7 received 20–25 Gy in 2 or 3 sessions, with cord maximum doses of 22.7 Gy (range, 17.8–30.9 Gy) and 22.0 Gy (range, 20.2–26.6 Gy), respectively. The Lyman-Kutcher-Burman model was used to calculate the biologically equivalent uniform dose and normal tissue complication probability (NTCP) for each

treatment by using conventional values for α/β, volume parameter n, 50 % complication probability dose TD50, and inverse slope parameter m (Kutcher and Burman 1989). In this study one case (4 %) of myelopathy occurred, but the Lyman-Kutcher-Burman model using radiobiological parameters from Emami (Emami et al. 1991) and the logistic model with parameters from Schultheiss (2008) overestimated complication rates, predicting 13 complications (54 %) and 18 complications (75 %), respectively. Therefore, authors suggested that the spinal cord tolerance for doses common to SRS is higher than predicted by the Lyman-Kutcher-Burman model, and emphasized that radiobiological models traditionally used to estimate spinal cord NTCP may not apply to SRS.

In conclusion image-guided SRS technology has allowed the extension of radiosurgery to the treatment of spinal lesions. Spinal radiosurgery has been shown to safely deliver highly conformal irradiation in a single stage or a limited number of fractions. This technique has been used to treat benign and malignant lesions, resulting in durable pain and local tumor growth control. Even challenging lesions such as intramedullary AVMs have shown good responses to radiosurgery. Furthermore, radiation-induced damage to the spinal cord following radiosurgery is quite rare. Although in its infancy, the role of radiosurgery for the treatment of spinal lesions in selected patients seems to already be quite established.

References

Adler JR, Chang SD, Murphy MJ, Doty J, Geis P, Hancock SL (1997) The Cyberknife: a frameless robotic system for radiosurgery. Stereotact Funct Neurosurg 69:124–128

Bilsky M, Hamada Y, Yenice KM, Lovelock M, Hunt M, Gutin PH, Leibel SA (2004) Intensity-modulated stereotactic radiotherapy of paraspinal tumors: a preliminary report. Neurosurgery 54:823–830

Chang UK, Rhee CH, Youn SM, Lee DH, Park SQ (2011) Radiosurgery using the Cyberknife for benign spinal tumors: Korea cancer center hospital experience. J Neurooncol 101:91–99

Colombo F, Cavedon C, Casentini L, Francescon P, Causin F, Pinna V (2009) Early results of CyberKnife radiosurgery for arteriovenous malformations. J Neurosurg 111:807–819

Daly ME, Luxton G, Choi CY, Gibbs IC, Chang SD, Adler JR, Soltys SG (2012) Normal tissue complication probability estimation by the Lyman-Kutcher-Burman method does not accurately predict spinal cord tolerance to stereotactic radiosurgery. Int J Radiat Oncol Biol Phys 82:2025–2032

De Salles AA, Pedroso AG, Medin P, Agazaryan N, Solberg T, Cabatan-Awang C, Espinosa DM, Ford J, Selch MT (2004) Spinal lesions treated with Novalis shaped beam intensity-modulated radiosurgery and stereotactic radiotherapy. J Neurosurg 101(Suppl 3):S435–S440

Degen JW, Gagnon GJ, Voyadzis JM, McRae DA, Lunsden M, Dieterich S, Molzahn I, Henderson FC (2005) CyberKnife stereotactic radiosurgical treatment of spinal tumors for pain control and quality of life. J Neurosurg Spine 2:540–549

Dodd RL, Ryu MR, Kamnerdsupaphon P, Gibbs IC, Chang SD Jr, Adler JR Jr (2006) CyberKnife radiosurgery for benign intradural extramedullary spinal tumors. Neurosurgery 58:674–685

Emami B, Lyman J, Brown A, Coia L, Goitein M, Munzenrider JE, Shank B, Solin LJ, Wesson M (1991) Tolerance of normal tissue to therapeutic irradiation. Int J Radiat Oncol Biol Phys 21:109–122

Gagnon GJ, Nasr NM, Liao JJ, Molzahn I, Marsh D, McRae D, Henderson FC Sr (2009) Treatment of spinal tumors using cyberknife fractionated stereotactic radiosurgery: pain and quality-of-life assessment after treatment in 200 patients. Neurosurgery 64:297–306

Gerszten PC, Ozhasoglu C, Burton SA, Vogel WJ, Atkins BA, Kalnicki S, Welch WC (2004) CyberKnife frameless stereotactic radiosurgery for spinal lesions: clinical experience in 125 cases. Neurosurgery 55:89–98

Gerszten PC, Burton SA, Ozhasoglu C, Vogel WJ, Welch WC, Baar J, Friedland DM (2005a) Stereotactic radiosurgery for spinal metastases from renal cell carcinoma. J Neurosurg Spine 3:288–295

Gerszten PC, Germanwala A, Burton SA, Welch WC, Ozhasoglu C, Vogel WJ (2005b) Combination kyphoplasty and spinal radiosurgery: a new treatment paradigm for pathological fractures. J Neurosurg Spine 3:296–301

Gerszten PC, Burton SA, Quinn AE, Agarwala SS, Kirkwood JM (2006) Radiosurgery for the treatment of spinal melanoma metastases. Stereotact Funct Neurosurg 83:213–221

Gerszten PC, Burton SA, Ozhasoglu C, Welch WC (2007) Radiosurgery for spinal metastases: clinical experience in 500 cases from a single institution. Spine 32:193–199

Gerszten PC, Burton SA, Ozhasoglu C, McCue KJ, Quinn AE (2008) Radiosurgery for benign intradural spinal tumors. Neurosurgery 62:887–895

Gibbs IC, Kamnerdsupaphon P, Ryu MR, Dodd R, Kiernan M, Chang SD, Adler JR Jr (2007) Image-guided robotic radiosurgery for spinal metastases. Radiother Oncol 82:185–190

Gibbs IC, Patil C, Gerszten PC, Adler JR Jr, Burton SA (2009) Delayed radiation-induced myelopathy after spinal radiosurgery. Neurosurgery 64:A67–A72

Hamilton AJ, Lulu BA, Fosmire H, Stea B, Cassady JR (1995) Preliminary clinical experience with linear accelerator-based spinal stereotactic radiosurgery. Neurosurgery 36:311–319

Heron DE, Rajagopalan MS, Stone B, Burton S, Gerszten PC, Dong X, Gagnon GJ, Quinn A, Henderson F (2012) Single-session and multisession CyberKnife radiosurgery for spine metastases-University of Pittsburgh and Georgetown University experience. J Neurosurg Spine. May 11. [Epub ahead of print]

Ho AK, Fu D, Cotrutz C, Hancock SL, Chang SD, Gibbs IC, Maurer CR Jr, Adler JR Jr (2007) A study of the accuracy of Cyberknife spinal radiosurgery using skeletal structure tracking. Neurosurgery 60:147–156

Jin JY, Chen Q, Jin R, Rock J, Anderson J, Li S, Movsas B, Ryu S (2007) Technical and clinical experience with spine radiosurgery: a new technology for management of localized spine metastases. Technol Cancer Res Treat 6:127–133

Kirkpatrick JP, van der Kogel AJ, Schultheiss TE (2010) Radiation dose-volume effects in the spinal cord. Int J Radiat Oncol Biol Phys 76(3 Suppl):S42–S49

Kutcher GJ, Burman C (1989) Calculation of complication probability factors for non-uniform normal tissue irradiation: the effective volume method. Int J Radiat Oncol Biol Phys 16:1623–1630

Leksell L (1951) The stereotaxic method and radiosurgery of the brain. Acta Chir Scand 102:316–319

Murphy MJ, Adler JR Jr, Bodduluri M, Dooley J, Forster K, Hai J, Le Q, Luxton G, Martin D, Poen J (2000) Image-guided radiosurgery for the spine and pancreas. Comput Aided Surg 5:278–288

Patel VB, Wegner RE, Heron DE, Flickinger JC, Gerszten P, Burton SA (2012) Comparison of whole versus partial vertebral body stereotactic body radiation therapy for spinal metastases. Technol Cancer Res Treat 11:105–115

Romanelli P, Adler JR (2008) Technology insight: image-guided robotic radiosurgery–a new approach for noninvasive ablation of spinal lesions. Nat Clin Pract Oncol 5:405–414

Romanelli P, Schaal DW, Adler JR (2006) Image-guided radiosurgical ablation of intra- and extra-cranial lesions. Technol Cancer Res Treat 5:421–428

Ryu SI, Chang SD, Kim DH, Murphy MJ, Le QT, Martin DP, Adler JR Jr (2001) Image-guided hypo-fractionated stereotactic radiosurgery to spinal lesions. Neurosurgery 49:838–846

Ryu S, Fang YF, Rock J, Zhu J, Chu A, Kagan E, Rogers L, Ajlouni M, Rosenblum M, Kim JH (2003) Image-guided and intensity-modulated radiosurgery for patients with spinal metastasis. Cancer 97:2013–2018

Ryu S, Rock J, Rosenblum M, Kim JH (2004) Patterns of failure after single-dose radiosurgery for spinal metastasis. J Neurosurg 101(Suppl 3):402–405

Ryu S, Jin JY, Jin R, Rock J, Ajlouni M, Movsas B, Rosenblum M, Kim JH (2007) Partial volume tolerance of the spinal cord and complications of single-dose radiosurgery. Cancer 109:628–636

Sachdev S, Dodd RL, Chang SD, Soltys SG, Adler JR, Luxton G, Choi CY, Tupper L, Gibbs IC (2011) Stereotactic radiosurgery yields long-term control for benign intradural, extramedullary spinal tumors. Neurosurgery 69:533–539

Schultheiss TE (2008) The radiation dose–response of the human spinal cord. Int J Radiat Oncol Biol Phys 71:1455–1459

Sinclair J, Chang SD, Gibbs IC, Adler JR Jr (2006) Multisession CyberKnife radiosurgery for intramedullary spinal cord arteriovenous malformations. Neurosurgery 58:1081–1089

Yamada Y, Lovelock DM, Yenice KM, Bilsky MH, Hunt MA, Zatcky J, Leibel SA (2005) Multifractionated image-guided and stereotactic intensity-modulated radiotherapy of paraspinal tumors: a preliminary report. Int J Radiat Oncol Biol Phys 62:53–61

Image-Guided Stereotactic Radiosurgery for Optic Nerve Sheath Meningiomas

29

Pantaleo Romanelli and Alfredo Conti

Contents

Abstract

Optic nerve sheath meningiomas (ONSMs) are benign lesions primarily originating from the dural sheath of the optic nerve. Their progressive growth can lead to gradual loss of vision and exophthalmos. Treatment of these lesions is problematic and depends on the degree of visual impairment and proptosis. In patients with preserved vision and no proptosis, conservative management with frequent ophthalmologic and radiological follow-up is usually preferred. When vision begins to fail surgical intervention can be attempted, but it is often of limited success as far as preserving vision is concerned.

Radiotherapy has gained an increasing role in the management of these lesions. Conventional radiotherapy has been used both pre-operatively and post-operatively for many years. More recently fractionated stereotactic radiotherapy has been employed as an alternative to surgery, and may be superior in terms of vision preservation. Care must be however exercised due to the proximity of other important radiosensitive structures. Highly conformal treatments modality, such as those provided by radiosurgery, may overcome this issue. Frame-based stereotactic radiosurgery has been rarely used because single-fraction high-dose irradiation of the optic nerve may be associated with loss of vision. New frameless radiosurgery devices, such as the robotic CyberKnife, an image-guided radiosurgery system, can provide the extremely tight

P. Romanelli (✉)
Cyberknife Center, Via Saint Bon 20,
20147 Milan, Italy
e-mail: Radiosurgery2000@yahoo.com

A. Conti
Department of Neurosurgery, Cyber Knife Center,
University of Messina, Messina, Italy

M.A. Hayat (ed.), *Tumors of the Central Nervous System, Volume 12*,
DOI 10.1007/978-94-007-7217-5_29,

conformality and submillimetric accuracy of frame-based systems combined with the possibility of delivering radiation in multiple sessions. Here, the authors review the clinical presentation and management of ONSMs, highlighting the emerging use of hypofractionated radiosurgery to treat these challenging lesions.

Introduction

Optic nerve sheath meningiomas (ONSMs) are tumors primarily arising from the intraorbital dural sheath of the optic nerve. They are rare lesions, representing approximately 1–2 % of all intracranial meningiomas, but their origin and location make them one of the most demanding treatment challenges in neurosurgery. Primary ONSMs originate from the meningeal sheath of the orbital or canalicular segment of the optic nerve. Secondary ONSMs have an intracranial origin and invade the orbit, compressing and displacing the optic nerve.

ONSMs are most commonly found in middle-aged women, but may also occur in children with neurofibromatosis type II, in whom they display a more aggressive growth pattern sometimes involving both optic nerves. They are typically detected when patients present with mild proptosis or progressive, painless loss of visual acuity or visual field, most often peripheral constriction. Their growth pattern has classically been viewed as typically circumferential along the optic nerve, although it is not uncommon to find lesions displacing the nerve peripherally (this could be an initial stage of the disease, followed over time by encasement of the nerve). The symptoms are those of a compressive neuropathy and include, in the early stages, dyschromatopsia and afferent pupillary defects. At the time of diagnosis the patients present with more or less marked visual field deficits, reduced visual acuity, and optic disc edema. Over time, ONSMs may extend through the optic canal intracranially. Optic chiasm involvement with bilateral visual deficits may be caused by direct extension or by traction and distortion of the chiasm. In later stages, optociliary shunt vessels and marked proptosis are detected.

Computed tomography (CT) and magnetic resonance imaging (MRI) show typical findings of thickening of the optic nerve, sometimes accompanied by calcification within the tumor. ONSMs appear as contrast-enhancing lesions encasing or compressing and displacing the optic nerve. 3T MRI provides enhanced definition of the nerve allowing better resolution of the nerve-tumor spatial relationship and optimization of the radiosurgical treatment planning (Fig. 29.1).

Because of their intimate relation to the optic nerve and their sharing of a common pial blood supply, ONSMs present a rather unique treatment challenge. Even in very experienced hands, blindness typically follows microsurgical resection of ONSMs (Cristante 1994; Delfini et al. 1996).

This and the typically slow development have encouraged a conservative, watch-and-wait approach reserving the surgical resection for patients with a long history and near-complete or complete loss of vision in the affected eye. Nevertheless, progressive deterioration of vision over time has been reported in approximately 85 % of patients with prolonged follow-up (Dutton and Anderson 1985; Turbin et al. 2002), while long-standing visual deficits are less likely to be reversed by treatment.

Conventional radiotherapy, either as an adjuvant to surgery or alone, has been shown to be moderately effective and reasonably well tolerated. A more conformal technique developed in the last decade, stereotactic fractionated radiation therapy (SFRT) has been successfully applied to the treatment of ONSMs (Jeremic and Pitz 2007; Pitz et al. 2002). Primary use of SFRT has preserved vision in patients with ONSM better than observation alone. Based on its safety and efficacy, and concerns about injury from single-session stereotactic radiosurgery (SRS), SFRT has been proposed as a standard treatment approach for ONSM. Nevertheless, residual dose spillage over the retina and other nearby structures has occasionally led to loss of vision due to radiation retinopathy or vascular occlusion of retinal vessels. Long-term ophthalmic, adnexal and peripheral complications secondary to conventional irradiation or SFRT have been

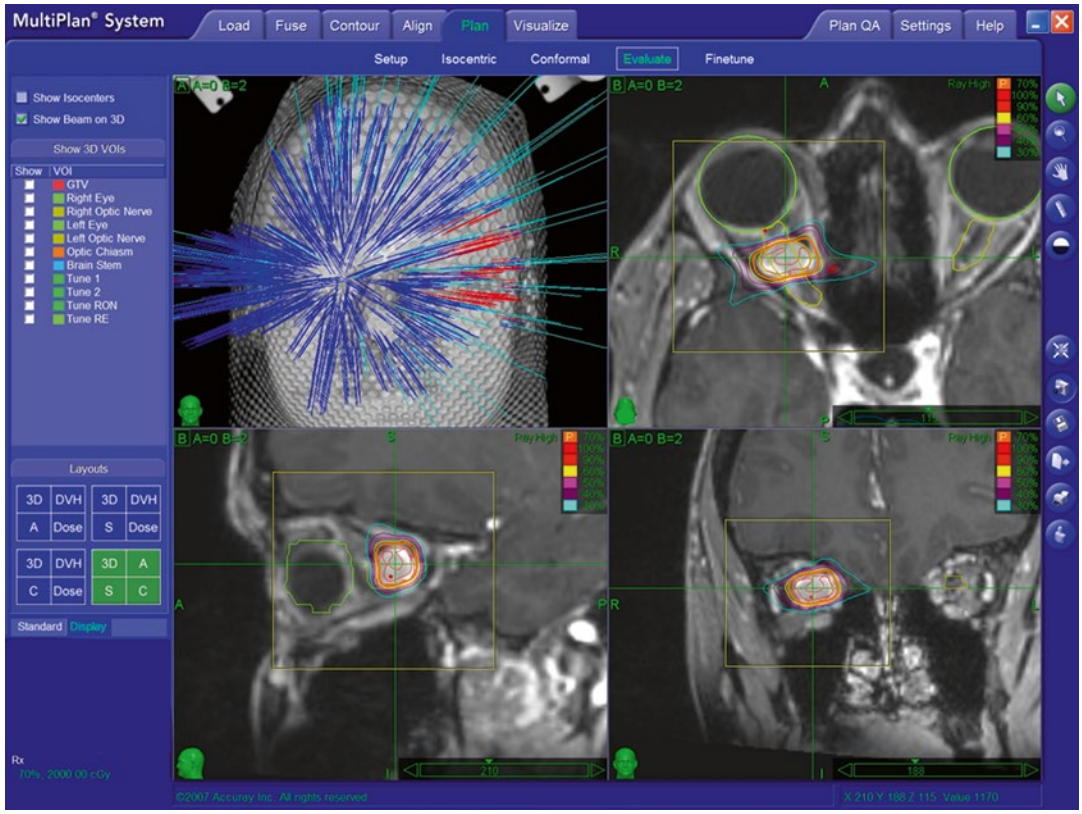

Fig. 29.1 Non isocentric treatment planning delivering staged image-guided radiosurgery using a Cyberknife G4 model to a right ONMS presenting with visual failure in a 28 year old woman. It can be noted the ability of this frameless radiosurgical modality to deliver beams through the basal frontal,orbital and maxillary regions

reported and include iritis, temporal lobe atrophy and endocrine failure (Parsons et al. 1994a, b). Optic neuritis has been also described following SFRT (Andrews et al. 2002).

Stereotactic radiosurgery involves the precise delivery of a very high dose of radiation with the goal of ablating a small-to-medium-sized intracranial target, with sparing of nearby structures. While SFRT relies on a combination of tissue sparing and daily fractionation to protect the optic nerve, radiosurgery provides extremely tight dose distributions and conformality, restricting the irradiation to the tumor and offering the highest degree of perilesional tissue protection, with an unchallenged 80–20 % dose fall-off within 3 mm of the target. Frame-based radiosurgery requires drastic measures for the immobilization of the patient and accurate targeting of the lesion, with the entire treatment being typically delivered in a single session, or stage, of 12–14 Gy, a dose exceeding the tolerance of the optic nerve (Girkin et al. 1997). Nevertheless,it was recently suggested that effective single session radiosurgery may carry an acceptable risk of radioinduced optic neuropathy (Liu et al. 2010).

An emerging radiosurgical technique, frameless image-guided robotic radiosurgery, eliminates the need of a stereotactic frame, introducing multisession (or hypofractionated) radiosurgery as a safe and efficacious new treatment option for ONSM and other lesions affecting radiosensitive structures such as the the cranial nerves or spinal cord (Romanelli and Adler 2008). Hypofractionated SRS delivers high doses of radiations in multiple sessions (usually two to five) while keeping the highest degree of conformality and accuracy, with

consequent sparing of the adjacent critical structures. Staged image-guided robotic radiosurgery has been applied to the treatment of ONSM with promising preliminary results (Romanelli et al. 2007, 2011).

Role of Surgery for ONSM

ONMS confined in the orbit are approached via an orbitotomy. The surgical approach, however, depends on the location of the meningioma in relation to the optic nerve (Boulos et al. 2001). A craniotomy is required in cases of intracranial extension while unroofing of the optic canal is often required to provide decompression (Shimano et al. 2000). En bloc resection of the optic nerve together with the tumor is likely the best strategy in patients in whom functional vision is lost, especially if there is extensive intracranial extension. Orbital exenteratio is performed when the orbit is invaded by tumor beyond the optic nerve (Alper 1981).

Encasement of the optic nerve by an ONSM makes it impossible to obtain a radical resection without causing severe injury to the nerve itself or to its vascular supply, which is peripheral and completely shared by the tumor. As a consequence, vision preservation following microsurgical resection of ONSMs is rare (Alper 1981; Clark et al. 1989). In particular, as a general attitude toward the most common type of ONSMs, a fusiform sheath growing around the optic nerve, most surgeons do not even attempt to dissect the nerve but directly proceed to the resection of the nerve and the tumor together. Surgery is therefore considered in patients with disfiguring exophthalmos and blindness. Young patients with good vision may harbor meningiomas that behave more aggressively and thus carry a poor prognosis. In these cases the risk of chiasmal involvement and bilateral loss of vision should be contemplated and early surgery may be attempted.

Stereotactic Fractionated Radiation Therapy

In 2002 Egan and Lessell published an observational study on 42 patients with ONSM (Egan and Lessell 2002) and reported that, with a 6.2-year follow-up, approximately 50 % of the untreated patients maintained stable visual acuity and 3 out of 16 patients actually showed a slight improvement over time. These results prompted the researchers to warn the neurosurgery community against treating patients with ONSM with stable conditions and thereby subjecting them to unnecessary risk.

On the other hand, a relatively large retrospective study published in 2002 (Turbin et al. 2002) included 64 patients that were either simply observed or treated with surgery only, with radiotherapy only, or with a combination of surgery and radiotherapy. Although the very different patient characteristics and treatment regimens make definitive conclusions difficult, the radiation-only group demonstrated the fewest complications and the smallest degree of deterioration of visual acuity.

SFRT is a technique by which it is possible to use linear accelerators with multiple fields and intensity modulation to obtain radiation dose distributions that are more conformal with relatively sharp dose gradients on the structure surrounding the tumor. This technique produces conformal dose distributions and relatively steep dose gradients with consequent substantial sparing of surrounding normal tissues and is clearly a more sophisticated and safer treatment option than conventional radiotherapy. SFRT has been therefore increasingly used to treat ONSMs. Favorable short-term results have been published (Andrews et al. 2002; Jeremic and Pitz 2007; Moyer et al. 2000; Narayan et al. 2003; Pitz et al. 2002; Turbin et al. 2002), and primary SFRT has been advocated to preserve vision in patients with ONSM rather than undertaking observation alone (Andrews et al. 2002; Turbin et al. 2002). Accordingly, SFRT can be considered a standard treatment approach for ONSM.

However, SFRT cannot reach the extremely tight dose distribution typical of radiosurgery and may still allow radiation doses leaking over the retina and other nearby structures. As a consequence, radiation retinopathy, loss of vision, and endocrine failure may still occur after SFRT for ONSMs (Becker et al. 2002; Subramanian et al. 2004). Radiation optic neuropathy has also been described after low-dose treatment (40–45 Gy delivered at 2 Gy/fraction) of pituitary lesions.

Furthermore, several other long-term ophthalmic and adnexal complications following external-beam radiotherapy and SFRT have been described (Durkin et al. 2007).

Stereotactic Radiosurgery

The optic nerve is one of the most sensitive structures to radiations. Goldsmith et al. (Goldsmith et al. 1992), predicted, based on clinical data, that doses to the optic nerve or chiasm less than or equal to 890 "optic ret" would be safe.

The optic ret is based on the total dose and the number of fractions used:

$$\text{optic ret dose} = D\left(\text{cGy}\right) / N^{0.53} \quad (29.1)$$

where N is the number of fractions used and D is the total physical dose in cGy. Therefore for a particular number of fractions, N, the optic tolerance would be predicted to be total dose D, where

$$D = 890 \times N^{0.53} \quad (29.2)$$

According to this model the maximal dose to the optic nerve should be lower than 890 cGy in single fraction. Even though doses of up to 11 Gy–1 cm^3 of the volume of the nerve are considered safe, at least 13 Gy are necessary to achieve a sufficient probability tumor control of a meningioma. Therefore, it is straightforward that, for ONSMs, it is impossible to achieve a therapeutic ratio between normal tissue complication probability (NTCP) and tumor control probability (TCP).

Despite this widely recognized issue, results on the use of single-session radiosurgery has been recently reported (Liu et al. 2010; Smee et al. 2009). Liu et al. (2010) reported the long-term results of 30 patients who underwent gamma-knife radiosurgery for ONSM. The average dose was 13.3 Gy achieving, at a median follow-up of 56 months, a tumor control in 93 % of patients. Visual acuity improved in 11 patients, remained stable in 13 patients (including 4 patients who were completely blind before GKS), but deteriorated in 6 patients (20 %). These results demonstrates that SRS can reach an high TCP, but carries also carries significant risk of vision impairment and should be reserved mostly to patients who have lost vision already.

Image-Guided Robotic Radiosurgery

The CyberKnife is a frameless 6 MV LINAC system for image-guided robotic radiosurgery (Conti et al. 2012; Romanelli and Adler 2008; Romanelli et al. 2009). Real-time image guidance based on digitally reconstructed skull radiographs is used to localize and treat the targeted site. The robotic arm provides great flexibility and the highest number of noncoplanar penetration trajectories (1,600 with the new G4 model). Radiation is delivered with submillimetric accuracy. The system presumes a fixed relationship between the target and the skull, as with other forms of stereotaxy. A light-weight 6-MV LINAC is accurately positioned by a robotic arm with 6 degrees of freedom.

Two x-ray imaging devices positioned on either side of the patient's anatomy acquire real-time digital radiographs of the skull at repeated intervals during treatment. Amorphous silicon sensors create a high-quality image of the skull or spine with a modest exposure to radiation (10 mA, 75 kV; corresponding to a dose per image of ~25 mrad).

The images acquired during the treatment are automatically registered to digitally reconstructed radiographs derived from the treatment planning CT scans. This registration process allows the position of the skull (and thus the treatment site) to be translated to the coordinate frame of the LINAC. A control loop between the imaging system and the robotic arm adjusts the pointing of the LINAC therapeutic beam to the observed position of the treatment anatomy (target). If the patient moves, the change is detected during the next imaging cycle and the beam is adjusted and realigned.

Frameless radiosurgical technology is characterized by the ability to perform hypofractionated treatments. Hypofractionation allows the delivery of ablative, radiosurgical doses to the treated lesion in association with an enhanced protection of the adjacent tissues receiving lower doses and lower dose rates but also being allowed precious time to recover between fractions. Frameless hypofractionated radiosurgery of lesions affecting the

cranial nerves and spinal cord substantially enhances treatment safety and prevention of dreaded neurological complications (Romanelli and Adler 2008). Furthermore, frameless systems are not limited to delivering spherical dose distributions (i.e., treatment planning and delivery can be nonisocentric). Early radiosurgical systems treated nonspherical targets by delivering radiation to multiple isocenters packed inside the treated volume. Nonisocentric planning provides a straightforward approach for the treatment of irregularly shaped lesions, and can result in a more homogeneous radiation distribution that is usually very conformal to the shape of the target lesion.

The CyberKnife offers a distinct advantages in the treatment of optic pathway lesions due to the absence of a rigid frame placed just under the eyes, banning beam penetration through the lower frontal, orbital, temporal and maxillary fields. Frameless radiosurgery allows the opening of this strategic regions to beam delivery, providing enhanced dose distribution to the tumor and sparing of the optic nerve. By delivering treatment in multiple sessions it is possible to exploit the differential speed of recovery of normal and pathological tissues, thereby limiting or avoiding damage to the visual pathways while controlling tumor growth. Also, inverse planning software is used to optimize target coverage and achieve tightly conformal isodose distributions with substantial sparing of surrounding brain tissue. Nonisocentric beam delivery (as opposed to isocentric multishot technology) also enables a significant measure of dose homogeneity.

According to the optic ret model (Eq. 29.2), the maximal dose tolerated by the optic nerve and chiasm in hypofractionations regimen are: 12.9 Gy in 2 fractions, 15.9 Gy in 3 fractions, 18.6 Gy in 4 fractions, 20.9 Gy in 5 fractions. The optic ret model appears, however, particularly conservative in terms of NTCP.

Alternatively, the linear quadratic (LQ) model can be used to calculate the tolerance of the optic apparatus (Mayo et al. 2010) in hypofractionation regimens.

The biologically effective dose (BED) is an approximate quantity by which different radiotherapy fractionation regimens may be compared. For instance, for an external beam radiotherapy (EBRT) regimen employing *n* equal fractions of conventional size the BED will be:

$$\mathbf{BED} = \mathbf{nD}(\mathbf{1} + \mathbf{D}/\alpha/\beta) \qquad (29.3)$$

where n = number of fractions, D = dose/fraction, and nD = total dose.

To use this model it is necessary to define the α/β of the optic nerve. This can be obtained comparing two treatment regimens with similar results in terms of NTC and NTCP for whom a similar BED is presumed. This is a isoeffect model.

Actually, assuming that the BED_1 of the first treatment is equal to the BED_2 for a tissue of unknown α/β,

$$\mathrm{D1}\left(1+\frac{\mathrm{d1}}{\alpha/\beta}\right)=\mathrm{D2}\left(1+\frac{\mathrm{d2}}{\alpha/\beta}\right) \qquad (29.4)$$

and

$$\alpha/\beta=\frac{D1\times d1-D2\times d2}{D2-D1} \qquad (29.5)$$

Considering isoeffective, in terms of NTCP, a Dmax of 11 Gy in single fraction (Carvounis and Katz 2003; Stafford et al. 2003) and 50 Gy in 25 fractions (5 % at 5 years (Emami et al. 1991)), the α/β of the optic nerve and chiasm turns out to be 0.55 Gy. Using this α/β, the maximal dose values to be delivered to the optic nerve in hypofractionated treatments, having a NTCP similar to that of 50 Gy in 25 fractions are: 15.5 Gy in 2 fractions, 19 Gy in 3 fractions, 22 Gy in 4 fractions, 24 Gy in 5 fractions.

Moving to clinical experiences, multisession treatment protocols involving the CyberKnife to treat lesions close to the optic pathway have been reported to result in excellent rates of tumor control and good preservation of vision. The first series reporting of the use of CyberKnife hypofractionated treatment of perioptic tumors was that of the Stanford University, where the CyberKnife radiosurgery system was developed (Adler et al. 2006; Pham et al. 2004). Adler and coll. treated 49 patients with perioptic tumors, including meningioma (27 pts.), pituitary adenoma (19 pts.), craniopharyngioma (2 pts), or

mixed germ cell tumor (1 pt.). CyberKnife radiosurgery was delivered in 2–5 sessions with a cumulative average marginal dose of 20.3 Gy. At an intermediate-term follow-up of 49 months (range, 6–96 months), vision was unchanged post-radiosurgery in 38 patients, improved in eight (16 %), and worse in three (6 %). In two cases the deterioriation was attributed to tumor progression. In this series use of a more aggressive protocol (21 Gy delivered in three sessions) was associated with loss of vision in one patient. In the largest series on meningiomas treated with the CyberKnife, Colombo and coll. treated 29 perioptic meningiomas using up to 5 fractions and up to 25 Gy (Colombo et al. 2009). Authors recorded a visual worsening in two cases (1 % of the overall series), again this was ascribed to the tumor progression.

Other perioptic tumors have been treated using similar protocols. Killory and coll. treated 20 patients with pituitary adenomas located within 3 mm from the optic chiasm with the CyberKnife. In all cases this team used 25 Gy in 5 fractions under the hypothesis that the optic apparatus may tolerate five consecutive daily fractions of 5 Gy. At a median follow up of 26 months no patient's vision deteriorated. Lee and coll. reported the first treatment of residual craniopharyngiomas situated within 2 mm of the optic apparatus or pituitary gland. Sixteen patients were treated with a mean marginal dose of 21.6 Gy and a mean maximal dose of 29.9 Gy in 3–10 fractions, with 3 patients managed with 27.5 Gy in 5 fractions. No visual deterioration was recorded.

Despite the limited number of patients with sufficient follow up, some considerations can be done on the basis of above-mentioned data. The use of up to 500 cGy per fraction in a 5-session treatment has been adopted, and it is felt safe for the optic nerve. Fundamentally, this is confirmed by clinical data. Considering only mid-term data, no patient deteriorated with 22–25 Gy in 5 fractions, namely with a biologically equivalent dose (BED) ranging 70–87.5 Gy_2. One patient deteriorated with 21 Gy in 3 fractions and a corresponding BED of 94.5 Gy_2.

These clinical results confirm the efficacy of the abovementioned radiobiological models and the limit of 500 cGy per fraction for a maximum of 5 fractions that can be tolerated by the optic nerve.

On the basis of the preliminary experience in the treatment of perioptic tumors lesions reported by the Stanford CyberKnife team led by John Adler, multisession CyberKnife radiosurgery of ONSM was attempted. Our group preliminarily reported staged radiosurgery outcome for the treatment of ONSM in 2007 (Romanelli et al. 2007). A successive paper provided a larger series with prolonged follow-up. Staged radiosurgery was performed with the aim of stopping disease progression and maintaining visual function (Romanelli et al. 2011). Five patients with ONSM presenting with visual field deficits and loss of visual acuity were treated with staged CyberKnife radiosurgery, receiving 20 Gy in four sessions (5 Gy per session). An interval of 24 h was strictly observed between sessions. Treatment planning was based on contrast-enhanced thin-slice CT(1,25 mm slice thickness for the first 3 cases; 0,5 mm for the last two) and volumetric MR imaging (1.5 T for the first three cases, 3 T for the last two). Visual acuity and visual fields were assessed in all patients immediately prior to treatment and at intervals of 6 months thereafter. Follow-up MRIs were performed every 6 months for 2 years, then once per year.

The treatment was well tolerated in all patients. Follow-up ranged from 36 to 74 months. Local growth control was achieved in all patients. Four patients experienced the return to normal vision 6–12 months after the treatment. One patient, who was also affected by diabetic retinopathy, showed a modest improvement after 6 months, remaining stable thereafter.

Return to normal vision in 4/5 of patients was an unexpected gift, most likely related to improved vascular supply to the involved optic nerve following tumor irradiation. The ability to use very tight dose distributions combined with hypofractionation was perhaps associated with the highest degree of protection of the optic nerve that technology has yet made available. In two cases (where a G3 CyberKnife model was used) the optic nerve was included in the 50 % isodose, while in the other two cases (using the G4 CyberKnife model*)

it was kept outside the 30 % isodose. In the first two cases the optic nerve received approximately 2.5 Gy per fraction (for a total dose of 10 Gy in 4 fractions), while in the latter two cases the optic nerve dose per fraction was less than 1.5 Gy (total dose 6 Gy). The tumor received 5Gy per fraction (total dose 20 Gy). Figure 29.1 shows the treatment planning of the latest case,imaged with a 3 T MR allowing the detection of the optic nerve and treated with a nerve-sparing technique using a Cyberknife G4 model.

The patient whose optic nerve was enveloped by the ONSM could not be spared from receiving a similar dose to the nerve and tumor. Nevertheless, this patient showed substantial improvement in visual fields and acuity and maintained this improvement over time (the first patient of this series having had a follow-up of longer than 7 years). This small clinical series demonstrates a promising non-invasive approach to treating ONSM. Patients can be treated in less than a week in comparison with the full month required by conventional radiation techniques, including SFRT. The degree of sparing of the optic nerve, when this is peripherally displaced by the tumor is unmatched: robotic image guided radiosurgery can provide doses effective at halting the tumor progression and restoring visual function, while at the same time the dose received by the optic nerve itself can be less than 1.5 Gy per fraction (as described for the last two cases treated using a Cyberknife G4). Furthermore, when the optic nerve cannot be distinguished from the tumor and a sufficient dose gradient cannot be achieved it is still possible to deliver up to 500 cGy/fraction to the tumor and nerve in up to 5 fraction to achieve a therapeutic NTCP/TCP.

Conclusions

Optic nerve sheath meningiomas are slow-growing tumors causing progressive loss of vision. Optimal management is controversial, but it appears that early intervention using SFRT or staged radiosurgery can achieve growth control and stop the progression of visual deficits. Multisession image-guided robotic radiosurgery is a novel treatment modality that combines the highest degree of conformality and accuracy with the ability to deliver treatment in several sessions and improve the tolerance of the optic nerve to the irradiation. Further studies are required to assess the value of multisession radiosurgery compared with single-session radiosurgery and SFRT. Nonetheless, staged radiosurgery presents a number of potential advantages and can be considered as a candidate to became the first treatment option for selected patients harbouring ONSM.

References

Adler JR Jr, Gibbs IC, Puataweepong P, Chang SD (2006) Visual field preservation after multisession cyberknife radiosurgery for perioptic lesions. Neurosurgery 59:244–254, discussion 244–254

Alper MG (1981) Management of primary optic nerve meningiomas. Current status–therapy in controversy. J Clin Neuroophthalmol 1:101–117

Andrews DW, Faroozan R, Yang BP, Hudes RS, Werner-Wasik M, Kim SM, Sergott RC, Savino PJ, Shields J, Shields C, Downes MB, Simeone FA, Goldman HW, Curran WJ Jr (2002) Fractionated stereotactic radiotherapy for the treatment of optic nerve sheath meningiomas: preliminary observations of 33 optic nerves in 30 patients with historical comparison to observation with or without prior surgery. Neurosurgery 51:890–902, discussion 903–894

Becker G, Jeremic B, Pitz S, Buchgeister M, Wilhelm H, Schiefer U, Paulsen F, Zrenner E, Bamberg M (2002) Stereotactic fractionated radiotherapy in patients with optic nerve sheath meningioma. Int J Radiat Oncol Biol Phys 54:1422–1429

Boulos PT, Dumont AS, Mandell JW, Jane JA Sr (2001) Meningiomas of the orbit: contemporary considerations. Neurosurg Focus 10:E5

Carvounis PE, Katz B (2003) Gamma knife radiosurgery in neuro-ophthalmology. Curr Opin Ophthalmol 14:317–324

Clark WC, Theofilos CS, Fleming JC (1989) Primary optic nerve sheath meningiomas. Report of nine cases. J Neurosurg 70:37–40

Colombo F, Casentini L, Cavedon C, Scalchi P, Cora S, Francescon P (2009) Cyberknife radiosurgery for benign meningiomas: short-term results in 199 patients. Neurosurgery 64:A7–A13

Conti A, Pontoriero A, Arpa D, Siragusa C, Tomasello C, Romanelli P, Cardali S, Granata F, De Renzis C, Tomasello F (2012) Efficacy and toxicity of CyberKnife re-irradiation and “dose dense” temozolomide for recurrent gliomas. Acta Neurochir (Wien) 154:203–209

Cristante L (1994) Surgical treatment of meningiomas of the orbit and optic canal: a retrospective study with particular attention to the visual outcome. Acta Neurochir (Wien) 126:27–32

Delfini R, Missori P, Tarantino R, Ciapetta P, Cantore G (1996) Primary benign tumors of the orbital cavity: comparative data in a series of patients with optic nerve glioma, sheath meningioma, or neurinoma. Surg Neurol 45:147–153, discussion 153–144

Durkin SR, Roos D, Higgs B, Casson RJ, Selva D (2007) Ophthalmic and adnexal complications of radiotherapy. Acta Ophthalmol Scand 85:240–250

Dutton JJ, Anderson RL (1985) Idiopathic inflammatory perioptic neuritis simulating optic nerve sheath meningioma. Am J Ophthalmol 100:424–430

Egan RA, Lessell S (2002) A contribution to the natural history of optic nerve sheath meningiomas. Arch Ophthalmol 120:1505–1508

Emami B, Lyman J, Brown A, Coia L, Goitein M, Munzenrider JE, Shank B, Solin LJ, Wesson M (1991) Tolerance of normal tissue to therapeutic irradiation. Int J Radiat Oncol Biol Phys 21:109–122

Girkin CA, Comey CH, Lunsford LD, Goodman ML, Kline LB (1997) Radiation optic neuropathy after stereotactic radiosurgery. Ophthalmology 104:1634–1643

Goldsmith BJ, Rosenthal SA, Wara WM, Larson DA (1992) Optic neuropathy after irradiation of meningioma. Radiology 185:71–76

Jeremic B, Pitz S (2007) Primary optic nerve sheath meningioma: stereotactic fractionated radiation therapy as an emerging treatment of choice. Cancer 110:714–722

Liu D, Xu D, Zhang Z, Zhang Y, Li Y, Liu X, Jia Q, Zheng L, Song G (2010) Long-term results of gamma knife surgery for optic nerve sheath meningioma. J Neurosurg 113(Suppl):28–33

Mayo C, Martel MK, Marks LB, Flickinger J, Nam J, Kirkpatrick J (2010) Radiation dose-volume effects of optic nerves and chiasm. Int J Radiat Oncol Biol Phys 76:S28–S35

Moyer PD, Golnik KC, Breneman J (2000 May) Treatment of optic nerve sheath meningioma with three-dimensional conformal radiation. Am J Ophthalmol 129(5):694–696

Narayan S, Cornblath WT, Sandler HM, Elner V, Hayman JA (2003) Preliminary visual outcomes after three-dimensional conformal radiation therapy for optic nerve sheath meningioma. Int J Radiat Oncol Biol Phys 56(2):537–543

Parsons JT, Bova FJ, Fitzgerald CR, Mendenhall WM, Million RR (1994a) Radiation optic neuropathy after megavoltage external-beam irradiation: analysis of time-dose factors. Int J Radiat Oncol Biol Phys 30:755–763

Parsons JT, Bova FJ, Fitzgerald CR, Mendenhall WM, Million RR (1994b) Severe dry-eye syndrome following external beam irradiation. Int J Radiat Oncol Biol Phys 30:775–780

Pham CJ, Chang SD, Gibbs IC, Jones P, Heilbrun MP, Adler JR Jr (2004) Preliminary visual field preservation after staged CyberKnife radiosurgery for perioptic lesions. Neurosurgery 54:799–810, discussion 810–792

Pitz S, Becker G, Schiefer U, Wilhelm H, Jeremic B, Bamberg M, Zrenner E (2002) Stereotactic fractionated irradiation of optic nerve sheath meningioma: a new treatment alternative. Br J Ophthalmol 86:1265–1268

Romanelli P, Adler JR Jr (2008) Technology Insight: image-guided robotic radiosurgery–a new approach for noninvasive ablation of spinal lesions. Nat Clin Pract Oncol 5:405–414

Romanelli P, Wowra B, Muacevic A (2007) Multisession CyberKnife radiosurgery for optic nerve sheath meningiomas. Neurosurg Focus 23:E11

Romanelli P, Conti A, Pontoriero A, Ricciardi GK, Tomasello F, De Renzis C, Innocenzi G, Esposito V, Cantore G (2009) Role of stereotactic radiosurgery and fractionated stereotactic radiotherapy for the treatment of recurrent glioblastoma multiforme. Neurosurg Focus 27:E8

Romanelli P, Bianchi L, Muacevic A, Beltramo G (2011) Staged image guided robotic radiosurgery for optic nerve sheath meningiomas. Comput Aided Surg 16:257–266

Shimano H, Nagasawa S, Kawabata S, Ogawa R, Ohta T (2000) Surgical strategy for meningioma extension into the optic canal. Neurol Med Chir (Tokyo) 40:447–451, discussion 451–442

Smee RI, Schneider M, Williams JR (2009) Optic nerve sheath meningiomas–non-surgical treatment. Clin Oncol (R Coll Radiol) 21:8–13

Stafford SL, Pollock BE, Leavitt JA, Foote RL, Brown PD, Link MJ, Gorman DA, Schomberg PJ (2003) A study on the radiation tolerance of the optic nerves and chiasm after stereotactic radiosurgery. Int J Radiat Oncol Biol Phys 55:1177–1181

Subramanian PS, Bressler NM, Miller NR (2004) Radiation retinopathy after fractionated stereotactic radiotherapy for optic nerve sheath meningioma. Ophthalmology 111:565–567

Turbin RE, Thompson CR, Kennerdell JS, Cockerham KP, Kupersmith MJ (2002) A long-term visual outcome comparison in patients with optic nerve sheath meningioma managed with observation, surgery, radiotherapy, or surgery and radiotherapy. Ophthalmology 109:890–899, discussion 899–900

Brain Metastases: The Application of Stereotactic Radiosurgery and Technological Advances

30

Siavash Jabbari, Lijun Ma, Paul Sanghera, Eric L. Chang, Sam T. Chao, Alex Karotki, Hany Soliman, Simon S. Lo, Daniel Letourneau, James Perry, David A. Larson, and Arjun Sahgal

Contents

Abstract

The purpose of this chapter is to provide a comprehensive review of the use of stereotactic radiosurgery (SRS) in patients with brain metastases. We focus only on level 1 evidence from randomized controlled trials and meta-analyses. A discussion on SRS technology follows and focuses on Gamma-Knife, Cyberknife, and modern linac-based SRS technologies.

Introduction

As the most common intracranial malignancy, brain metastases are frequently diagnosed in the general cancer patient population with an annual incidence of approximately 170,000 in the United States. Historically, the diagnosis of brain metastases was thought to confer a uniformly poor prognosis, and whole brain radiation (WBRT, Fig. 30.1) or even supportive care alone had

S. Jabbari
Department of Radiation Oncology, The Doug and Nancy Barnhart Cancer Center, Sharp Chula Vista Medical Center, Chula Vista, CA, USA

L. Ma • D.A. Larson
Department of Radiation Oncology, University of California San Francisco, San Francisco, CA, USA

P. Sanghera
Department of Radiation Oncology, Hall-Edwards Radiotherapy Research Group, University Hospital Birmingham, Birmingham, United Kingdom

E.L. Chang
Department of Radiation Oncology, University of Southern California, Los Angeles, CA, USA

S.T. Chao
Department of Radiation Oncology, Cleveland Clinic, Cleveland, OH, USA

A. Karotki • H. Soliman • J. Perry
Department of Radiation Oncology, Sunnybrook Health Sciences Centre, University of Toronto, Toronto, ON, Canada

M.A. Hayat (ed.), *Tumors of the Central Nervous System, Volume 12*,
DOI 10.1007/978-94-007-7217-5_30,

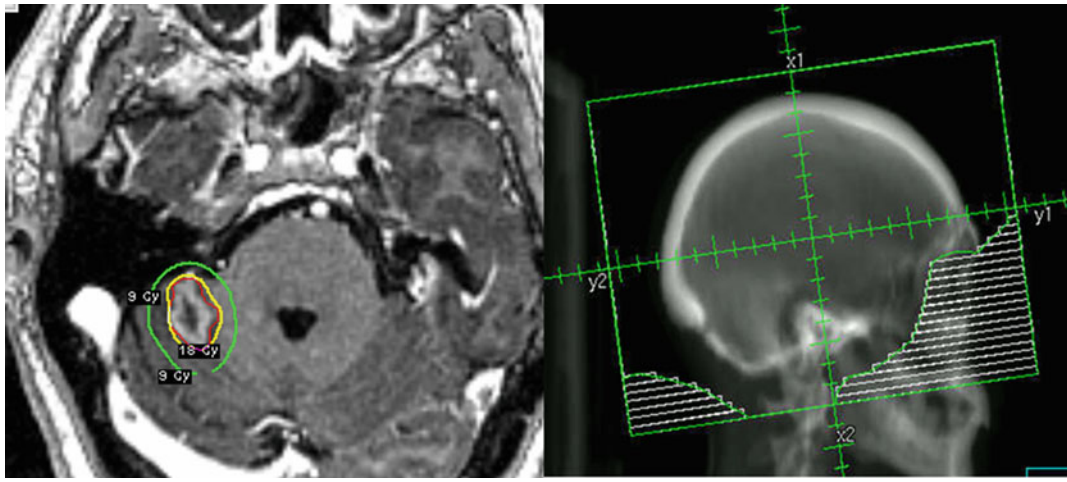

Fig. 30.1 An example of a cerebellar metastasis treated with 18 Gy in a single fraction, and the 18 Gy isodose line in *yellow* conforms around the target. Despite a small solitary lesion, prior to SRS this patient's whole head would have been radiated and on the *right* is a typical whole brain radiation portal

remained the only commonly available treatments for such patients for decades. However, with advances in MRI, brain metastases are commonly diagnosed during early and often asymptomatic stages of CNS disease progression, and advances in systemic therapy in conjunction with the above have generally improved the expected duration of survival post-diagnosis.

For years, the Recursive Partitioning Analysis (RPA) scoring system was the standard by which patients were prognosticated to guide treatment options and patients were grouped simply into three RPA classes based on performance status, stability of extracranial disease, and age with resultant median survival times of 7 months, 3–6 months, and, ~2 months (Gaspar et al. 1997). However, in contemporary oncology practice, we do not infrequently observe that patients with brain metastases may have an extended survival of several years post-diagnosis, and newer and more accurate prognostic indices have been developed, including the Graded Prognostic Assessment (GPA) and diagnosis-specific GPA (DS-GPA) scoring systems, and these now even incorporate tumour molecular profiles (Sperduto et al. 2008, 2010). As a result, we are now better equipped to select patients for focal stereotactic radiosurgery (SRS) (Fig. 30.1) and/or surgery, where the aim is to maximize local control rather than to simply temporize brain control with WBRT. Stereotactic radiosurgery is defined as the use of 1–5 fractions of high dose radiation delivered to a well-defined three dimensional target using a radiation delivery system that permits sub-millimeter delivery accuracy. An example of a SRS dose distribution is shown in Fig. 30.1.

Over the last 5 years, there has been a major shift in the management of brain metastases as we now have the randomized data and meta-analyses to support SRS alone or in conjunction with WBRT for patients presenting with up to four metastases (Aoyama et al. 2006; Kocher

S.S. Lo
Department of Radiation Oncology, University Hospitals Seidman Cancer Center, Case Comprehensive Cancer Center, Case Western Reserve University, Cleveland, OH, USA

D. Letourneau
Department of Radiation Oncology, Princess Margaret Hospital, University of Toronto, Toronto, ON, Canada

A. Sahgal (✉)
Department of Radiation Oncology, Sunnybrook Health Sciences Centre, Princess Margaret Hospital, University of Toronto, 610 University Avenue, M6G 2M5 Toronto, ON, Canada
e-mail: Arjun.sahgal@rmp.uhn.on.ca

et al. 2010; Chang et al. 2009; Tsao et al. 2012a, 2012b). The success of SRS has broadened its application to even the postoperative patient where historical dogma favoured postoperative WBRT without consideration of focal therapy (Roberge et al. 2012). This review will summarize the latest evidence formulating today's standards of care in the clinical management of brain metastasis, and detail recent technological advances specific to SRS.

Clinical Outcomes and Standards of Care Based on Randomized Controlled Trials and Meta-Analysis

Steroid therapy is the first line of management for symptomatic brain metastasis, and dexamethasone is the drug of choice given its relatively low mineralcorticoid effects. Steroids often improve symptoms related to cerebral edema. Steroid dose should be tapered as tolerated post CNS directed therapy.

Surgical resection, WBRT, SRS, or combinations of these therapeutic options are the standard CNS directed therapies for brain metastasis (Sahgal et al. 2012). Although some controversy exists as to the optimal therapeutic choice or choices, the treatment strategy has generally been dictated by the number of brain lesions at presentation and patient- and cancer-related prognostic factors. Currently available randomized trial data do not deal with poor-prognosis patients, patients with low KPS, or patients with a large number of brain mets, but they do deal with a select patient cohort with high performance status, relatively controlled low burden of extracranial disease, and a limited number of brain lesions. The following discussion is focused on evaluating treatment options with a focus on only these randomized trial data.

The Role of Surgery in the Management of Brain Metastasis

A practice-altering phase III trial randomized 54 patients with a Karnofsky Performance Status (KPS) over 70 and a solitary brain lesion (no other site of metastatic disease) to surgical resection vs. brain biopsy, in either case followed by WBRT (Patchell et al. 1990). All outcomes favoured the surgical group, including recurrence at original site of disease (20 % vs. 50 %), time to recurrence, median survival (10 vs. 4.2 months), time to death from neurological cause, and preservation of performance status (8.7 vs. 1.8 months). These findings were essentially confirmed by a second randomized trial (Vecht et al. 1993; Noordijk et al. 1994). In the third trial evaluating the same question, a survival benefit was not observed largely due to the selection criteria that allowed patients with poorer performance status to be included (Mintz and Cairncross 1998). Accordingly, surgical resection in the setting of a solitary site of brain disease is considered standard of care. What is not known is if SRS can replace surgery in these patients without compromising a potential gain in overall survival, and this will be discussed further in this chapter. However, for large metastases (typically >3 cm) and those resulting in significant edema and neurologic deficit, surgery is the best option to not only remove the tumour burden but relieve symptoms (Table 30.1).

WBRT in the Postoperative Patient

Patchell et al. (1998) also reported a phase III study evaluating the role of postoperative WBRT by randomizing 95 patients with a solitary brain lesion treated with surgical resection to WBRT vs. observation alone. Postoperative WBRT was found to significantly reduce both the rate of local recurrence (10 % vs. 46 %) and distant brain failures (14 % vs. 37 %), and deaths due to neurological causes (14 % vs. 44 %). However, overall survival and duration of functional independence were similar between the two cohorts. This study concluded that postoperative WBRT was the standard of care.

A more recent randomized trial published by Kocher et al. (2010) evaluated the role of WBRT vs. observation following either surgery or SRS. In the surgical cohort (160 patients), outcomes were similar to those observed in the Patchel

Table 30.1 Summary of the phase III randomized controlled studies evaluation SRS and WBRT

RCT	% Single brain metastases	Performance status	Tumour size	Primary endpoint	Local control	Distant control	OS
Aoyama: SRS (n=67) vs. WBRT+SRS (n=65)	49 % vs. 48 %	52 % KPS 90–100 vs. 66 % KPS 90–100	Median: 1.3 cm vs. 1.4 cm	Brain tumour recurrence	72.5 % vs. 88.7 % at 1 yr (p=0.002)	36.3 % vs. 58.5 % at 1 yr (p=0.003)	28.4 % vs. 38.5 % at 1 yr (p=0.42)
Chang: SRS (n=30) vs. WBRT+SRS (n=28)	60 % vs. 54 %	100 % KPS ≥70 (each arm)	Median TV: 1.4 cc vs. 2.3 cc	Neurocognition: HVLT scores at 4 months	67 % vs. 100 % at 1 yr (p=0.012)	45 % vs. 73 % at 1 yr (p=0.02)	63 % vs. 21 % at 1 yr (p=0.003)
Kocher: SRS (n=100) vs. WBRT+SRS (n=99)	68 % vs. 66 %	100 % WHO status 0–2 (in each arm)	Median: 2.0 cm vs. 1.8 cm	Duration of functional independence	69 % vs. 81 % at 2 yr (p=0.008)	52 % vs. 67 % at 2 yr (p=0.023)	Median: 10.9mo vs. 10.7mo (NSIG)
Kondziolka: WBRT+SRS (n=13) vs. WBRT (n=14)	0 %	100 % KPS ≥70 (each arm)	All tumors <2.5 cm	Local Control	92 % vs. 0 % at 1 yr (p=0.0016)	NR	Median: 11mo vs. 7.5mo (NSIG)
Andrews: WBRT+SRS (n=164) vs. WBRT (n=167)	56 % vs. 56 %	57 % KPS 90–100 vs. 63 % KPS 90–100	50.5 % ≤2 cm vs. 59 % ≤2 cm	Overall Survival	82 % vs. 71 % at 1 yr (p=0.01)	NR	Median Single mets:6.5mo vs. 4.9mo (p=0.04) Multiple mets: NSIG

WBRT whole brain radiotherapy, *SRS* stereotactic radiosurgery, *NSIG* not significant, *KPS* karnofsky performance status, *NR* not reported, *HVLT* Hopkins verbal learning test, *mo* months, *yr* year, *TV* total volume

et al. (1990) trial. Postoperative WBRT decreased intracranial disease progression at 24 months (31 % vs. 54 %, respectively) and the risk of neurological death (25 % vs. 43 %), while not impacting overall survival or preservation of performance status.

Stereotactic Radiosurgery as an Alternative to Surgery

As of yet, no completed randomized trials have directly compared surgical resection to SRS. The study by Muacevic et al. (2008) came closest, and randomized patients with a single resectable brain metastasis measuring 3 cm or smaller to microsurgery plus WBRT vs. SRS alone. This trial was closed early due to poor accrual, but the results of 64 randomized patients were reported in 2008 with overall survival, neurological death rates, and local control appearing similar in the two groups. The patients randomized to SRS alone were observed to have more distant brain recurrences, although this difference was no longer observed when accounting for salvage SRS. As compared to surgical resection and WBRT, SRS alone was also associated with a shorter hospital stay, less frequent and shorter use of steroids, decreased CNS toxicity, and improved quality of life scores at 6 weeks post therapy (this effect was no longer observed at 6 months). Coupled with the favourable local control results observed in the randomized studies evaluating SRS alone (summarized in the following sections), most believe that SRS is a reasonable alternative to surgery except for large lesions.

WBRT with or Without SRS

In the early years of SRS it was recognized that local control may not be optimal with WBRT alone. Therefore, it was important to clarify the role of SRS as a boost to WBRT in patients preseting with up to three metastases. Andrews et al. (2004) published the landmark trial based on 331 patients randomized to WBRT plus or minus SRS as a boost. Stereotactic radiosurgery was shown to improve local control, KPS, and for patients with a single brain metastasis, a statistically significant improvement in OS (6.5 months with SRS + WBRT vs. 4.9 months WBRT alone). In addition, a trend to support a median survival advantage for RPA class one patients (11.6 vs. 9.6 months), lung histology (5.9 vs. 3.9 months), and tumour size >2 cm (6.5 vs. 5.3 months) was observed in sub-group analysis.

An earlier but small study of 27 patients with 2–4 brain metastasis was published (Kondziolka et al. 1999). Patients were randomized to WBRT alone vs. WBRT and SRS. Local failure was 100 % at 1 year in patients treated with WBRT alone, and only 8 % progressed in those boosted with SRS. A statistically non-significant OS benefit was observed in the SRS group (MS 7.5 vs. 11 months). This study is controversial in that 100 % local failure in the WBRT alone cohort may reflect selection bias or bias associated with a small sample size.

A meta-analysis of these two studies concluded there was no difference in OS, with a hazard ratio (HR) of 1.63 (95 % CI 0.72–3.69, $p = 0.24$), while LC significantly favoured WBRT plus SRS with a HR of 2.88 (95 % CI 1.63–5.08, $p = 0.003$) (Tsao et al. 2012a).

SRS with or Without WBRT

The next question was the role of SRS alone while deferring WBRT to salvage therapy upon brain progression. This strategy was driven largely over concerns related to WBRT-associated neurotoxicity. Three randomized studies have been reported evaluating SRS alone to WBRT plus SRS as a boost in patients with up to 3–4 metastases (Aoyama et al. 2006; Kocher et al. 2010; Chang et al. 2009).

Aoyama et al. (2006) published the first study based on 132 patients with 1–4 lesions randomized to SRS alone vs. WBRT plus SRS boost. Whole brain radiotherapy was observed to reduce the risk of developing new brain metastasis (63.7 % vs. 41.5 %) and improve the 1-year local control rate (72.5 % vs. 88.7 %); however, no difference in OS (8.0 vs. 7.5 months). Neurocognitive

function changes were tested using the mini-mental status examination (MMSE) with no significant differences observed bewteen the two arms. However, neuropsychologists do not recognize the MMSE as an adequate test for assessing those neurocognitive functions most likely to be damaged by radiation.

In order to study neurocognitive changes associated with WBRT, a trial evaluating 58 patients with 1–3 metastases randomizing to SRS alone vs. WBRT plus SRS with the primary endpoint of neurocognition changes at 4 months (Chang et al. 2009). They used a validated neurocognitive outcome tool, namely the Hopkins Verbal Learning Test (HVLT), as opposed to the insensitive MMSE previously described in the Aoyama et al. (2006) RCT. Chang et al. (2009) reported worse neurocognitive function with respect to memory at 4 months following treatment in the WBRT plus SRS cohort. This impairment in memory was observed despite the better local and distant brain tumour control seen in that cohort. Although there were several limitations in this study that could have also contributed to the poorer neurocognitive outcomes in the WBRT group, such as greater extra-cranial and intra-cranial disease burden and more deaths at the 4 month interval, this study was the first to provide level 1 evidence that WBRT independently and adversely impacts neurocognition. A larger study by Brown et al. (2009) is currently accruing with neurocognition as the primary endpoint which will hopefully provide the much needed confirmatory evidence to support or refute the Chang study.

Nevertheless, Chang's conclusion is supported by a recent randomized trial of prophylactic cranial WBRT (PC-WBRT) in patients with non-small cell lung cancer (NSCLC) (Sun et al. 2011). Based on HVLT assessments, PC-WBRT was shown to adversely impact memory both at 6 months and 1 year despite a reduction in the risk of development of brain metastases in the PC-WBRT group (Sun et al. 2011). What both these RCTs suggest, is that recurrence is not the only cause of neurocognitive decline, but WBRT independently impairs memory function.

A recent meta-analysis of the Aoyama and Chang study by Tsao et al. (2012a), found no difference in OS between the two arms with a HR of 0.98 (95 % CI 0.71–1.35, $p=0.88$). Therefore, it is unlikely that SRS alone adversely impacts survival. The outcomes for local control and distant brain control from these two studies were pooled with the SRS alone vs. SRS plus WBRT arms within the Kocher et al. (2010) RCT (this was not possible for survival analysis due to the way in which the data were reported). It was observed that the addition of WBRT improved local control and distant brain control vs. SRS alone. The HR for local control was 2.61 (95 % CI 1.68–4.06, $p<0.0001$) and for distant brain control 2.15 (95 % CI 1.55–2.99, $p<0.00001$) (Tsao et al. 2012b). If the aim is to preserve neurocognition, then SRS alone is the preferred therapeutic option. If the patient is more focused on brain control and less concerned with neurocognition, then WBRT plus SRS is the preferred strategy. In either case, close imaging-based follow-up is required, to provide salvage therapy as needed.

The Evolving Role of SRS to the Resection Cavity as an Alternative to WBRT in the Postoperative Patient

Due to concerns of WBRT-related neurotoxicity, some investigators applied SRS to the postoperative surgical bed or surgical cavity, as opposed to treating with WBRT (Roberge and Souhami 2010; Roberge et al. 2012). A review by Roberge et al. (2012) analyzed 492 postoperative patients treated with SRS to the resection cavity in non-randomized trials. Crude LC was 79 %, and the risk of radiation necrosis was estimated at ~5 %. Randomized trials are underway to compare WBRT to postoperative cavity radiation, and clearly this is the current question that needs an answer (Roberge et al. 2012).

There are challenges with treating cavities with SRS due to the relatively large size and irregularity of the cavity shape, such that the SRS dose is typically compromised due to the principle of reducing the dose prescribed with increasing volume to repect safety. This has led some centers to treat with focal hypofractionated radiosurgery (3–5 fractions) to minimize risks of

normal tissue toxicity. Some preliminary data support a hypofractionated approach both for postoperative patients (Katz et al. 2012) and also for intact metastases (Kim et al. 2011). The ability to deliver hypofractionated SRS is largely due to advances in SRS technology and this will be discussed in the subsequent sections.

SRS Technology

Gamma Knife Technology

Intracranial SRS was pioneered in the 1950s by Sweedish neurosurgeon Lars Leksell, initially as a therapeutic approach for functional brain disorders, and subsequently for tumours. Certainly the largest application of SRS is now in the treatment of brain metastases. Ultimately, Leksell developed a self-contained SRS unit that is now known as the Gamma Knife. Gamma Knife (Eletka AB). Stereotactic radiosurgery is based on localizing and fixing the target in three-dimensions, such that target motion during treatment is negligible. The treatment process begins with the patient's skull fixed and indexed in three-dimensional space using a stereotactic metal head frame screwed to the outer calvarium.

Over the following several decades, small improvements were made to the original Gamma Knife system that included an automatic patient positioning system (APS), and improved treatment planning software; however, the limitations of manually changing collimator helmets to vary shot size and selective blocking requiring manual plugging of individual collimator holes remained. The latest model, the Leksell Gamma Knife (LGK) Perfexion (Elekta, Nocross, GA), is a major engineering advance that allows a versatility in treatment planning and delivery not previously possible (Sahgal et al. 2009). One key feature is the larger treatment volume space such that tumours along the base of skull, or at extreme lateral locations within the cranium typically not reachable (or treatable only with use of manually positioned trunions) with the pre-LGK Perfexion models, are now treatable. The second and major advancement is the single tungsten collimator helmet that is now embedded into the unit and computer controlled. The design is based on multiple rings of collimating holes drilled directly into the one tungsten piece creating nominal beam sizes of 16-mm, 8-mm, and 4-mm in diameter at the isocenter. An eight sliding sector design allows each sector to slide along the outside surface of the tungsten collimator and align with the different rings of predrilled holes to allow for 192 sixteen-millimeter diameter focused beams, 192 eight-millimeter diameter focused beams, or 192 four-millimeter diameter focused beams. Blocking is no longer based on manual plugging of individual collimator holes, instead, individual sectors are blocked. Ultimately, shots can be a composite of any of the three beam diameters or zero within any of the eight sectors, and results in significant gains in the flexibility of treatment planning, for complex lesions.

The latest innovations include an integrated relocatable head-frame that allows for fractionated SRS and the integration of image-guidance with an on-board cone-beam CT unit (Ruschin et al. 2010, 2013). Therefore, the technology has adapted to allow for frameless SRS and treatments like 30 Gy in 5 fractions which would otherwise require a linac-based system.

Robotic Linac-Based SRS: CyberKnife Technology

The CyberKnife (Accuray, Sunnyvale, CA, USA), developed by the neurosurgeon John Adler as an alternative to the Gamma Knife to deliver frameless SRS, has been an equally revolutionary SRS technology, with the central paradigm of allowing frameless treatment delivery for both intra- and extra-cranial (body) lesions (Sahgal et al. 2009; Dieterich and Gibbs 2011). This system is based on a compact mini linear accelerator mounted onto a high-accuracy robotic arm capable of moving accelerator with all six degrees of freedom. A near real-time stereoscopic image guidance and automated robotic

beam adjustment system allows for precision in treatment delivery with approximately 1 mm and 1 degree precision (Murphy 2009).

The paradigm shift with respect to brain SRS, is that a patient can be immobilized in a simple non-invasive head mask as opposed to the traditional invasive metal frame. With the ability to reliably deliver SRS doses without a frame, the initiative to fractionate and deliver a high dose per fraction SRS in a few treatments (typically 2–5 fractions) became an active area of practice. In fact, many fractionation schemes like 30–35 Gy in 5 fractions, 17–24 Gy in 3 fractions, and 24 Gy in 2 fractions were adopted without randomized evidence to support efficacy and toxicity. Institutional series are being reported and support fractionated SRS (Kim et al. 2011), but a randomized trial is needed to be definitive. Certainly for large lesions otherwise not treatable with SRS, or treatable to only a low single fraction dose, it is prudent to fractionate, but the optimal dosing has not been evaluated in either Phase 1 trials or RCT.

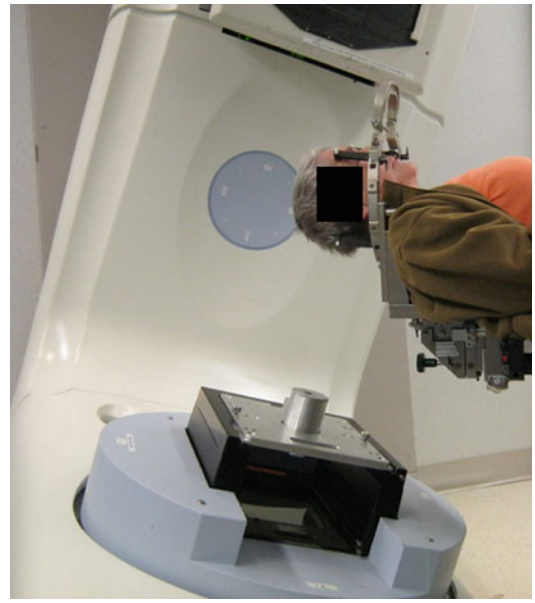

Fig. 30.2 A linac-based treatment unit with the circular tertiary collimator add-on visible. The patient is immobilized in an invasive head frame

Linear Accelerator-Based SRS

Linear Accelerator (linac)-based SRS was first developed by adding a tertiary circular collimator onto an existing linac head (and even removing the flattening filter in some cases) to yield small circular beams with a minimum diameter of 0.5–1 cm (Fig. 30.2). Modifications to the treatment couch and the in-room laser system were also required to ensure sub-millimeter precision in delivery. The treatment planning strategy was based on delivering multiple beam arcs with the focal point being the linac isocenter. Similar to Gamma Knife based SRS, an invasive head frame was required for both immobilization and stereotaxy. As the technology improved and SRS was increasingly being applied to tumours, manufacturers invested in the technique and one of the first dedicated linac systems built for intra-cranial SRS was the Novalis BrainLAB (Varian Medical Systems, California, USA). This unit was also one of the first to integrate a stereoscopic x-ray system into the delivery process to ensure precision and ultimately frameless SRS.

Modern linac systems are now developing with the intent of delivering high precision radiation as a matter of routine practice with the integration of intensity modulated radiotherapy (IMRT), multi-leaf collimators, image-guidance, and robotic couch technology. Therefore, no longer are dedicated boutique units required for SRS and, ultimately, these advances have increased the capacity in the community to deliver SRS.

Image-guidance is the major advance to be incorporated into linac-SRS delivery, and includes either (or even both) a stereoscopic x-ray or an on-board CT based system (Sahgal et al. 2009). Stereoscopic x-ray systems are based on a pair of orthogonal images that are processed to yield spatial co-ordinates of the anatomy to be tracked (Sahgal et al. 2009). Therefore, the image-guidance solution is fundamentally based on tracking bone or a visible fiducial, unlike the direct acquisition of three-dimensional images inherent to CT based solutions. The process of stereoscopic x-ray image guidance is based on the x-rays taken before treatment to ensure the target is positioned correctly and then several times per minute during the beam delivery to

ensure that the patient's position remains stable. The images are processed via automatic registration software and registered to the digitally reconstructed radiographs (DRR) taken at the time of simulation. If deviations in position are detected beyond tolerance, then either the linac position itself is adjusted, which is how the Cyberknife system works, or the patient's position is adjusted via couch shifts, or both.

On-line CT based image-guidance has almost completely taken the form of cone-beam CT units (CBCT) (Sahgal et al. 2009). Elekta was one of the pioneers in the technology. The key advantage is the acquisition of high quality kilovoltage or megavoltage three-dimensional images such that the tumour itself can be matched to the fan-beam based treatment planning CT, and directly verified at the unit console. The disadvantage to CBCT image-guidance is the time required for image acquisition such that the treatment beam has to be stopped, and real-time image-guidance is generally not possible. Furthermore, multiple CBCTs during delivery are not practical as the treatment time would be prohibitively long. Therefore, stringent immobilization systems are more important to maintaining high precision when relying on CBCT alone, rather than with stereoscopic imaging systems which verify the position of the target in near-real time.

With respect to frameless brain SRS, in-room infra-red (IR) camera guidance is gaining acceptance and becoming incorporated into modern linac systems. The technology relies on reflective fiducial markers placed on the patient's immobilization device (ex. bite plate) which are tracked continuously via in-room infra-red cameras during treatment. The markers provide stereotactic feedback information on the patient's position which is relayed to the beam delivery system and registered with the original stereotactic coordinates obtained during simulation. In the event of a deviation beyond pre-set thresholds, treatment delivery is automatically halted to allow for adjustments and patient repositioning as needed.

Long treatment times are still a major challenge to SRS delivery as the chance of positional deviation increases. The current focus of linac-based SRS research and development has been on how to deliver treatment faster. Volumetric modulated arc therapy (VMAT) has been incorporated into mainstream linac delivery and practically a full IMRT plan that took 15–20 min can now be delivered in a single near 360° gantry rotation. Treatment times have been shown to be approximately 50 % less than those of traditional step-and-shoot deliveries, but varies according to treatment sites (Davidson et al. 2012). The latest development in improving efficiency has been focused on increasing machine output. Flattening filter-free SRS technology is available with 1400–2400 MU/min output. Now 24 Gy in a single fraction can be delivered in minutes. There is a point of caution as we do not know the biologic effects with these unprecedented dose rates and there is potential for increased biological potency to favourably impact the tumour, but negatively impact the normal tissues.

The last point to discuss lies in the use of tertiary cones for SRS (Fig. 30.2). There is no doubt that add-on collimators to existing linacs require stringent quality assurance measures to avoid catastrophic errors in delivery. With micro-MLC technology, the use of cones is being phased out, and intensity modulated radiosurgery (IMRS) has been shown to yield improved target conformality and reduce treatment times for complex and multiple lesions (Tanyi et al. 2011). It should be noted, however, that for lesions measuring less than 0.5–1 cm, inherent uncertainties in small-field dosimetry and beam shaping concerns due to finite leaf widths limit the use of MLC for accurate treatments, and cones are still required for the treatment of such targets.

Future Directions

The field of brain metastases research largely develops in parallel with technologic innovations in delivery. Certainly for multiple metastases (>4 tumours), the aim is to test SRS alone to WBRT and determine whether or not these patients can be effectively spared WBRT. The intent is to treat patients with 5–10 metastases, and then even more lesions, with SRS alone.

This is possible with the advent of the LGK Perfexion as it is a machine geared to treat multiple metastases. They have developed software to keep track of treated lesions with respect to subsequent post-SRS diagnostic scans, to overcome the barriers associated with the clinical and imaging complexities of treating such cases. Linac SRS technology is also evolving, and allowing for multiple lesions to be safely treated with SRS alone in a single session and a single isocenter (Nath et al. 2010); however, one concern is the integral dose within the brain as it is greater with non-Gamma Knife technologies (Ma et al. 2011). With respect to focal therapy, the use of hypofractionated SRS will continue in community practice due to the inherent safety associated with fractionation, and the comfort in delivering focal high dose treatment without an invasive frame. Eventually, those common hypofractionated doses in current practice (35 Gy in 5 fractions, 24 Gy in 3 fractions) will be tested in a RCT to determine if in fact efficacy is improved for those tumours that would have otherwise been treated with single fraction SRS alone. For large tumours (>3 cm), the practice of hypofractionated SRS is evolving as routine practice despite the lack of evidence, and this stems from the limitations of single fraction SRS. The trials that will be needed in this population will be geared to surgery plus SRS (either a single or hypofractionated cavity treatment) to hypofractionated SRS alone. This has a chance to finish accrual as compared to the previously attempted SRS alone vs. surgery for small (<2 cm) lesions, as patients inherently would rather be spared surgery for lesions that are not threatening.

With respect to WBRT, developments are occurring to develop this technique beyond simply washing the entire brain with the palliative dose. Hippocampal sparing WBRT is being tested in a randomized trial, and has the potential to reduce the neurocognitive side effects of WBRT while providing the advantage of reducing the risk of new brain metastases emerging (Gondi et al. 2010). In addition, the use of WBRT with simultaneous integrated boosts to visible tumour is evolving, as it is well known that local control is sub-optimal with WBRT alone.

Areas that are difficult to investigate due to traditionally poor survival outcomes and difficulty in data collection inherent to the population include the optimal therapy for the patient with a poor performance status and/or short life expectancy (i.e., <3 months). Still many treat with WBRT, and in these patients supportive care alone may be more appropriate as the impact of WBRT on survival is questionable, and WBRT does result in acute declines with respect to energy levels, hair loss, and appetite loss (Slotman et al. 2007). Therefore, in these patients if therapy is indicated, it may be in fact more sensible to offer focal therapy like SRS to reduce the potential for these side effects and allow patients to pass with dignity with their faculties intact. In fact, the Chang RCT primary endpoint was neurocognitive decline at 4 months (Chang et al. 2009); therefore, this reinforces that the effects of WBRT on cognition are still relatively early post-WBRT, and SRS alone may be just as appropriate in the patient with a poor prognosis as compared to those patients with an extended good prognosis. The other challenging population to study is the patient with prior WBRT who develops recurrent brain metastases. Traditionally, this has been thought to be a fatal development; however, data support prolonged survival with the use of salvage focal SRS and these patients should be treated aggressively (Follwell et al. 2012). The first step in studying this population is to obtain good neurocognitive functioning data to then base further studies upon. At this time, there is no data reported in the literature using validated neurocognitive testing. It is a major challenge as most neurocognitive tests are labour intensive, and difficult for patients to complete. Furthermore, to randomize patients to repeat WBRT is a major barrier for the patient presenting with a limited number of recurrent tumours as the consequences of repeat WBRT can be severe with respect to cognition. Therefore, we will likely have to obtain good quality Phase II data on ideal patients with recurrent brain metastases before we can develop the ideal question to answer in a RCT.

The corresponding author of this chapter uses the available technology to treat as aggressively as possible those patients with recurrent brain

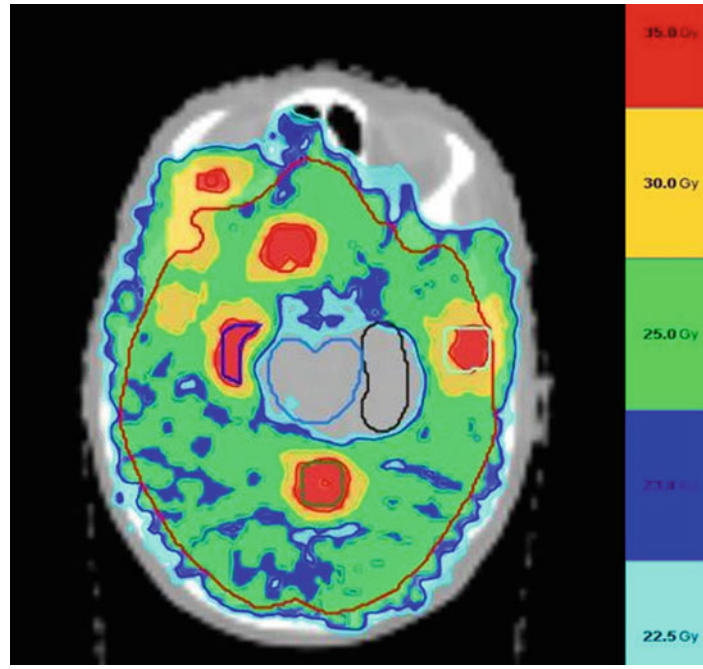

Fig. 30.3 An axial CT slice for a patient treated with repeat 25 Gy in 10 fraction WBRT (prior 30 Gy in 10 fraction WBRT 3 months prior). The brainstem region is spared to no more than 10 Gy as the patient had SRS to a brainstem lesion with 15 Gy in a single fraction just a week before. We spared the ipsilateral hippocampus to a mean dose of 10 Gy. In addition, all 32 cerebral metastases were simultaneously boosted to a total dose of 35 Gy. This patient was treated with the TomoTherapy (Accuray, Sunnyvale, California) system

metastases with expected good prognosis. Certainly when few lesions are present, focal SRS is reasonable and the treatment of choice (Follwell et al. 2012). For the patient with multiple progressing tumours and new metastases where repeat WBRT is indicated, the challenge is to treat effectively while minimizing cognitive dysfunction. For example, a patient with metastatic colon cancer previously treated with WBRT presented with a progressive brainstem metastases in addition to several progressive and new cerebral lesions just 3 months following initial WBRT. In total, the patient had 32 lesions distributed throughout the brain and a brainstem metastasis. The approach was to treat the brainstem lesion with 15 Gy in a single fraction using SRS, and then repeat WBRT with 25 Gy in 10 fractions and a simultaneous integrated boost to the gross disease to a total dose of 35 Gy using TomoTherapy. Therefore, the repeat WBRT plan had to spare the treated brainstem lesion and we restricted dose to a total dose of 10 Gy while also boosting each of the 32 metastases simultaneously to a total dose of 35 Gy, and we spared the ipsilateral hippocampus (lesion in contralateral hippocampus). An axial representative dose distribution is shown in Fig. 30.3. The patient remains controlled now 6 months following this repeat-patient specific WBRT, and a complete response in ~70 % of boosted tumours. This case highlights the power of modern radiation technology to think beyond traditional WBRT practice even when it is indicated.

Conclusion

The treatment of brain metastases has evolved beyond the reflexive use of WBRT for all patients. Now selected patients can be spared the neurocognitive consequences of WBRT, and treated with SRS alone with WBRT reserved as a salvage therapy. As linac technology has matured to routinely incorporate image-guidance and deliver high precision radiation for all patients, the application of SRS will only increase in the community. In time, postoperative patients will routinely be offered cavity SRS as either a single hypofractionated course, or repeat WBRT reserved as a salvage therapy. Even for patients

with 5, 10, 20, or more metastases, the technology is evolving to allow for focal treatment alone and give these patients the chance to retain as much neurocognitive function as possible during their cancer journey.

References

Andrews DW, Scott CB, Sperduto PW, Flanders AE, Gaspar LE, Schell MC, Werner-Wasik M, Demas W, Ryu J, Bahary JP, Souhami L, Rotman M, Mehta MP, Curran WJ Jr (2004) Whole brain radiation therapy with or without stereotactic radiosurgery boost for patients with one to three brain metastases: phase III results of the RTOG 9508 randomised trial. Lancet 363:1665–1672

Aoyama H, Shirato H, Tago M, Nakagawa K, Toyoda T, Hatano K, Kenjyo M, Oya N, Hirota S, Shioura H, Kunieda E, Inomata T, Hayakawa K, Katoh N, Kobashi G (2006) Stereotactic radiosurgery plus whole-brain radiation therapy vs stereotactic radiosurgery alone for treatment of brain metastases: a randomized controlled trial. JAMA 295:2483–2491

Brown PD, Kee AY, Eshleman JS, Fiveash JB (2009) Adjuvant whole brain radiotherapy: strong emotions decide but rationale studies are needed: in regard to Brown et al. (Int J Radiat Oncol Biol Phys 2008;70:1305–1309). In reply to Drs. Larson and Sahgal. Int J Radiat Oncol Biol Phys 75:316–317

Chang EL, Wefel JS, Hess KR, Allen PK, Lang FF, Kornguth DG, Arbuckle RB, Swint JM, Shiu AS, Maor MH, Meyers CA (2009) Neurocognition in patients with brain metastases treated with radiosurgery or radiosurgery plus whole-brain irradiation: a randomised controlled trial. Lancet Oncol 10:1037–1044

Davidson MT, Masucci GL, Follwell M, Blake SJ, Xu W, Moseley DJ, Sanghera P, Wong CS, Perry J, Tsao M, Sahgal A (2012) Single arc volumetric modulated arc therapy for complex brain gliomas: is there an advantage as compared to intensity modulated radiotherapy or by adding a partial arc? Technol Cancer Res Treat 11:211–220

Dieterich S, Gibbs IC (2011) The CyberKnife in clinical use: current roles, future expectations. Front Radiat Ther Oncol 43:181–194

Follwell MJ, Khu KJ, Cheng L, Xu W, Mikulis DJ, Millar BA, Tsao MN, Laperriere NJ, Bernstein M, Sahgal A (2012) Volume specific response criteria for brain metastases following salvage stereotactic radiosurgery and associated predictors of response. Acta Oncol 51:629–635

Gaspar L, Scott C, Rotman M, Asbell S, Phillips T, Wasserman T, McKenna WG, Byhardt R (1997) Recursive partitioning analysis (RPA) of prognostic factors in three radiation therapy oncology group (RTOG) brain metastases trials. Int J Radiat Oncol Biol Phys 37:745–751.33

Gondi V, Tolakanahalli R, Mehta MP, Tewatia D, Rowley H, Kuo JS, Khuntia D, Tomé WA (2010) Hippocampal-sparing whole-brain radiotherapy: a "How-To" technique using helical tomotherapy and linear accelerator-based intensity-modulated radiotherapy. Int J Radiat Oncol Biol Phys 78:1244–1252

Katz J, Knisely J, Ghaly M, Shulder M (2012) Adjuvant tumor bed radiosurgery following surgical resection of intracranial metastases. J. Neurooncol (in press)

Kim YJ, Cho KH, Kim JY, Lim YK, Min HS, Lee SH, Kim HJ, Gwak HS, Yoo H, Lee SH (2011) Single-dose versus fractionated stereotactic radiotherapy for brain metastases. Int J Radiat Oncol Biol Phys 81:483–489

Kocher M, Soffietti R, Abacioglu U, Villa S, Fauchon F, Baumert BG, Fariselli L, Tzuk-Shina T, Kortmann RD, Carrie C, Ben Hassel M, Kouri M, Valeinis E, van den Berge D, Collette S, Collette L, Mueller RP (2010) Adjuvant whole-brain radiotherapy versus observation after radiosurgery or surgical resection of one to three cerebral metastases: results of the EORTC 22952–26001 study. J Clin Oncol 29:134–141

Kondziolka D, Patel A, Lunsford LD, Kassam A, Flickinger JC (1999) Stereotactic radiosurgery plus whole brain radiotherapy versus radiotherapy alone for patients with multiple brain metastases. Int J Radiat Oncol Biol Phys 45:427–434

Ma L, Petti P, Wang B, Descovich M, Chuang C, Barani IJ, Kunwar S, Shrieve DC, Sahgal A, Larson DA (2011) Apparatus dependence of normal brain tissue dose in stereotactic radiosurgery for multiple brain metastases. J Neurosurg 114:1580–1584

Mintz AP, Cairncross JG (1998) Treatment of a single brain metastasis: the role of radiation following surgical resection. JAMA 280:1527–1529

Muacevic A, Wowra B, Siefert A, Tonn JC, Steiger HJ, Kreth FW (2008) Microsurgery plus whole brain irradiation versus Gamma Knife surgery alone for treatment of single metastases to the brain: a randomized controlled multicentre phase III trial. J Neurooncol 87:299–307

Murphy M (2009) Intrafraction geometric uncertainties in frameless image-guided radiosurgery. Int J Radiat Oncol Biol Phys 73:1364–1368

Nath SK, Lawson JD, Simpson DR, Vanderspek L, Wang JZ, Alksne JF, Ciacci J, Mundt AJ, Murphy KT (2010) Single-isocenter frameless intensity-modulated stereotactic radiosurgery for simultaneous treatment of multiple brain metastases: clinical experience. Int J Radiat Oncol Biol Phys 78:91–97

Noordijk EM, Vecht CJ, Haaxma-Reiche H, Padberg GW, Voormolen JH, Hoekstra FH, Tans JT, Lambooij N, Metsaars JA, Wattendorff AR, Brand R, Hermans J (1994) The choice of treatment of single brain metastasis should be based on extracranial tumor activity and age. Int J Radiat Oncol Biol Phys 29:711–717

Patchell RA, Tibbs PA, Walsh JW, Dempsey RJ, Maruyama Y, Kryscio RJ, Markesbery WR, Macdonald JS, Young B (1990) A randomized trial of surgery in the treatment of single metastases to the brain. N Engl J Med 322:494–500

Patchell RA, Tibbs PA, Regine WF, Dempsey RJ, Mohiuddin M, Kryscio RJ, Markesbery WR, Foon KA, Young B (1998) Postoperative radiotherapy in the treatment of single metastases to the brain: a randomized trial. JAMA 280:1485–1489

Roberge D, Souhami L (2010) Tumor bed radiosurgery following resection of brain metastases: a review. Technol Cancer Res Treat 9:597–602

Roberge D, Parney I, Brown PD (2012) Radiosurgery to the postoperative surgical cavity: who needs evidence? Int J Radiat Oncol Biol Phys 83:486–493

Ruschin M, Nayebi N, Carlsson P, Brown K, Tamerou M, Li W, Laperriere N, Sahgal A, Cho YB, Ménard C, Jaffray D (2010) Performance of a novel repositioning head frame for Gamma Knife perfexion and image-guided linac-based intracranial stereotactic radiotherapy. Int J Radiat Oncol Biol Phys 78:306–313

Ruschin M, Komljenovic PT, Ansell S, Menard C, Bootsma G, Cho YB, Chung C, Jaffray D (2013) Cone beam computed tomography image guidance system for a dedicated intracranial radiosurgery treatment unit. Int J Radiat Oncol Biol Phys 85:243–250

Sahgal A, Ma L, Chang E, Shiu A, Larson DA, Laperriere N, Yin FF, Tsao M, Menard C, Basran P, Létourneau D, Heydarian M, Beachey D, Shukla V, Cusimano M, Hodaie M, Zadeh G, Bernstein M, Schwartz M (2009) Advances in technology for intracranial stereotactic radiosurgery. Technol Cancer Res Treat 8:271–280

Sahgal A, Soliman H, Larson DA (2012) Whole-brain radiation therapy of brain metastasis. Prog Neurol Surg 25:82–95

Slotman B, Faivre-Finn C, Kramer G, Rankin E, Snee M, Hatton M, Postmus P, Collette L, Musat E, Senan S, EORTC Radiation Oncology Group and Lung Cancer Group (2007) Prophylactic cranial irradiation in extensive small-cell lung cancer. N Engl J Med 357:664–672

Sperduto PW, Berkey B, Gaspar LE, Mehta M, Curran W (2008) A new prognostic index and comparison to three other indices for patients with brain metastases: an analysis of 1,960 patients in the RTOG database. Int J Radiat Oncol Biol Phys 70:510–514

Sperduto PW, Chao ST, Sneed PK, Luo X, Suh J, Roberge D, Bhatt A, Jensen AW, Brown PD, Shih H, Kirkpatrick J, Schwer A, Gaspar LE, Fiveash JB, Chiang V, Knisely J, Sperduto CM, Mehta M (2010) Diagnosis-specific prognostic factors, indexes, and treatment outcomes for patients with newly diagnosed brain metastases: a multi-institutional analysis of 4,259 patients. Int J Radiat Oncol Biol Phys 77:655–661

Sun A, Bae K, Gore EM, Movsas B, Wong SJ, Meyers CA, Bonner JA, Schild SE, Gaspar LE, Bogart JA, Werner-Wasik M, Choy H (2011) Phase III trial of prophylactic cranial irradiation compared with observation in patients with locally advanced non-small-cell lung cancer: neurocognitive and quality-of-life analysis. J Clin Oncol 29:279–286

Tanyi JA, Kato CM, Chen Y, Chen Z, Fuss M (2011) Impact of the high-definition multileaf collimator on linear accelerator-based intracranial stereotactic radiosurgery. Br J Radiol 84:629–638

Tsao M, Xu W, Sahgal A (2012a) A meta-analysis evaluating stereotactic radiosurgery, whole-brain radiotherapy, or both for patients presenting with a limited number of brain metastases. Cancer 118:2486–2493

Tsao MN, Lloyd N, Wong RK, Chow E, Rakovitch E, Laperriere N, Xu W, Sahgal A (2012b) Whole brain radiotherapy for the treatment of newly diagnosed multiple brain metastases. Cochrane Database Syst Rev 4:CD003869

Vecht CJ, Haaxma-Reiche H, Noordijk EM, Padberg GW, Voormolen JH, Hoekstra FH, Tans JT, Lambooij N, Metsaars JA, Wattendorff AR, Brand R, Hermans J (1993) Treatment of single brain metastasis: radiotherapy alone or combined with neurosurgery? Ann Neurol 33:583–590

Treatment of Chordomas by Stereotactic Radiosurgery with a Linear Accelerator: Comparison with Other Modes

31

Fraser C. Henderson Sr., Kyle McCool, Juliet Seigle, and Gregory J. Gagnon

Contents

Abstract

This study was to determine the efficacy and safety of chordoma and chondrosarcoma treatment with CyberKnife Stereotactic Radiosurgery. Eighteen patients diagnosed with chordoma were treated with CSRS as a primary adjuvant treatment (17), or only treatment (1) for the tumor. They were followed at 6 month intervals with neurological examination, testing for pain (VAS), Quality of Life (SF-12) and MRI. Six patients were treated with other radiation modalities prior to CyberKnife: 2 patients had external beam irradiation (EBIR); 1 had proton beam radiation (PBR); 1 had EBIR and chemotherapy; 1 received heavy particle therapy (HPT) with helium ions as well as EBIR; and 1 had Gamma Knife irradiation. The series includes 28 tumor treatments for a total of 24 lesions among 18 patients with chordoma, median age 60 years (24–85 years), and 3 metastatic chordomas were treated solely with surgery. Tumor origin was weighted to the mobile spine (44 %), with 39 % intracranial and 17 % sacral. Male-to-female incidence for chordoma was 1:1. Mean tumor volume was 128.0 cm^3 (12.0–457.3 cm^3), median tumor radiation dose of 35 Gy (24.0–40 Gy) in five stages. Patients were followed for a median of 46 months (7–65 months) after CSRS treatment. There were 3 significant complications in patients with previous irradiation: infection in the surgical/radiation site (2), and decreased vision (1). Improvement in pain and the physical component of quality of life reached statistical

F.C. Henderson Sr. (✉)
Metropolitan Neurosurgery Group, Chevy Chase, Lanham, MD, USA
e-mail: Henderson@fraserhendersonmd.com

K. McCool
Department of Neurosurgery, Georgetown University Hospital, Washington, DC, USA

J. Seigle • G.J. Gagnon
Radiation Oncology, Georgetown University Hospital, Washington, DC, USA

M.A. Hayat (ed.), *Tumors of the Central Nervous System, Volume 12*,
DOI 10.1007/978-94-007-7217-5_31,

significance (p.05); neurological exam was maintained throughout follow-up. Histological change included: a 10 % MIB index in a marginal recurrence; apoptosis (semi-quantitative studies underway). Seven individuals experienced recurrence at a median post-radiation interval of 10 months (5–38 months), and 4 patients presenting with disseminated tumor died 7–48 months post-therapy. Two patients demonstrated significant reduction of tumor volume (reduction from 13.4 to 2.5 cm^3 at 3 years), while 9 others remained stationary with no evidence of recurrence. There has been no evidence of recurrence in one patient treated with CSRS alone (5 years), and no recurrences in spinal chordomas totally resected and irradiated with margin (37.5 Gy to the margin) with CyberKnife. Overall, the local control rate with recurrence free survival to date is 69.57 %. The CSRS safety and efficacy profile compares favorably with other treatment delivery systems. CSRS appears to reduce tumor volume with adequate dose, and the authors recommend treatment with 40 Gy in five stages to the margin of involved tissue (enhancing tumor with 1 cm margin).

Introduction

Chordomas are rare, slow-growing neoplasms. They represent less than 1 % of all intracranial tumors and 6 % of primitive cranial base lesions. Chordomas account for less than 4 % of all primary bone tumors. These malignant tumors arise from the embryonic elements of the primitive notochord, which is a cell line that develops the skull base and vertebral column. The notochordal remnants usually remain entrapped within the bone of the axial skeleton near the midline. Thus, chordomas may form from the intracranial clivus down to the sacrum of the lower spine. Chordomas statistically occur along an even distribution of 50 % in the sacrococcygeal region, 35 % in the cranial base, and 15 % in vertebrae. There is a 1.7 ~ 3:1 male predilection, and an even higher male predominance of 3:1 in sacral chordoma cases. Chordomas arise primarily in adults and are most prevalent in patients of 40–50 years of age.

Symptoms occur insidiously and vary according to the location of the lesion, and the patient usually has a long history of symptoms due to the slow growth pattern of chordomas. Though they metastasize less frequently than other bone and soft tissue malignant tumors, the local invasiveness of chordomas near critical anatomic structures of the brain and spine and extremely high local recurrence rate makes treatment especially challenging. The tumors have a propensity for extensive local spread. Unfortunately, symptoms usually appear only when the lesion is very large, so that complete excision is often difficult or impossible. Chordomas have a tendency to expand toward the brainstem and upward to the optic chiasm (Al-Mefty and Borba 1997).

Chordoma is the most common primary sacral neoplasm, but early diagnosis is almost impossible because its onset tends to be asymptomatic. The extensive local spread of these tumors and involvement of sacral foramina can cause nerve root compression that leads to radicular pain in the sacrum irradiating to the lower limbs or sensitivity disorders in the perineum. There is high local recurrence due to the large size of the chordomas upon discovery and the complexity of sacral anatomy. Options for treatment of patients with residual or recurrent cranial base chordomas or chondrosarcoma include radiation treatment, with or without resection: single fraction treatment with cobalt beam, fractionated proton beam radiation therapy, carbon ion irradiation, or hypo-fractionated irradiation with linear accelerator.

Radiosurgery Systems

Many linear accelerator systems have been used effectively in the treatment of chordoma. Though the authors' experience is limited to the CyberKnife, many of the systems share common principles. The CyberKnife is presented as emblematic of a robotic, image-guided stereotactic radiosurgery system (Fig. 31.1). Using a 6-MV X-band linear accelerator mounted on a

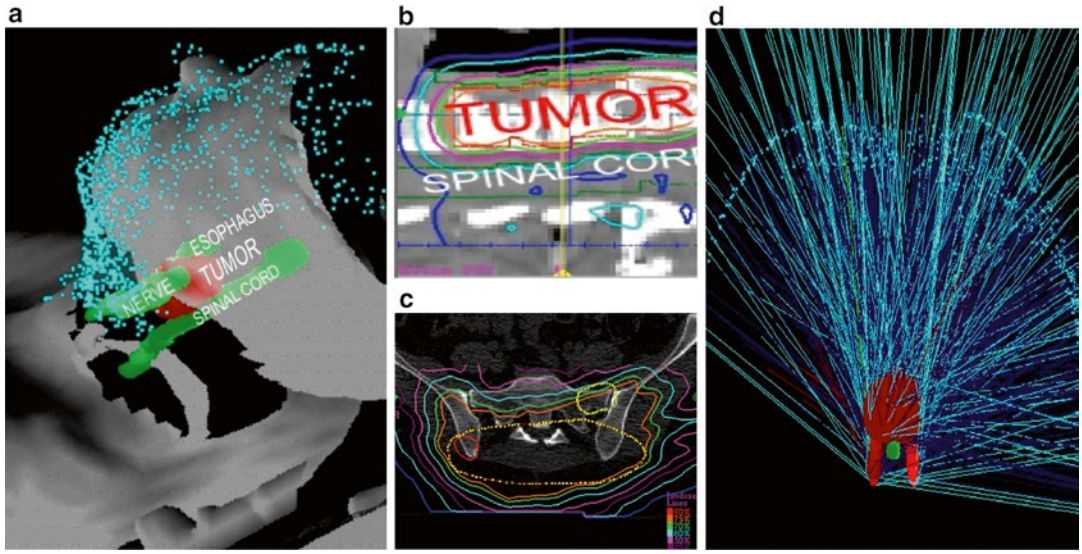

Fig. 31.1 CyberKnife Stereotactic Radiosurgery utilizes a noninvasive technique of imaging the patient, including lesion and critical structures, with several x-ray cameras to deliver the radiation dose precisely to the targeted lesion volume in real-time. (**a**) Three-dimensional model of contoured cervical lesion, highlighting radiosensitive structures such as spinal cord, esophagus, and vagus nerve. (**b**, **c**) Lesion is contoured in transverse, coronal, and sagittal planes. (**d**) Non-isocentric treatment delivery typically results in highly conformal coverage and rapid dose fall-off outside the target

fully articulated robotic arm, the CyberKnife is capable of rotational and translational movements to target tumors without rigid external fixation. Treatment planning utilizes non-isocentric delivery and an inverse treatment planning process. Optimization algorithms choose the appropriate beams from a total library of approximately 1,200 beams, depending on system configuration. Optimization proceeds according to the constraints provided for targets and critical structures, usually returning a solution that consists of approximately 150–200 beams, appropriately weighted to satisfy the constraints supplied. Non-isocentric treatment delivery typically results in highly conformal coverage and rapid dose fall-off outside the target.

The technique for planning and contouring has been described (Degen et al. 2005). Patients are generally placed supine in a vacuum-bag immobilizer with head and knee support. Thin-sliced CT scans (1.25-mm slice thickness and spacing), centered on the target, are used for contouring and treatment planning. In some cases, image fusion with MRI or PET is performed to assist in target delineation. Contouring is performed by the neurosurgeon. The volume targeted for treatment with the prescription dose is the clinical treatment volume (CTV). The CTV encompasses the Gross Tumor Volume (GTV), as identified on CT and/or MRI, plus a margin (ideally up to 10-mm for chordoma) to allow for microscopic disease extension. Tracking systems, such as Xsight® Spine (Accuray) compare digitally reconstructed radiographs (DRRs) generated from preoperative CT scans with frequently acquired intraoperative radiographs of the spine to identify any 3-D target displacements and global rotations of spinal structures. Translations and global rotations are aligned during patient setup, and automatically corrected during treatment delivery. Critical structures (including spinal cord, cauda equina, nerve roots, intestines, esophagus, trachea, kidneys, and heart) are delineated by the neurosurgeon and the radiation oncologist. An inverse treatment planning algorithm using linear optimization is used to generate a treatment plan with non-isocentric targeting. Plans are created and prescribed

individually for each patient based on isodose coverage, dose-volume histograms (DVHs), normal individual tissue doses, and other clinical considerations. Additionally, dose and fractionation prescriptions are shaped by dose volume constraints for the adjacent normal tissues. Treatment margins are added to GTVs based on clinical presentation, histology, and proximity to critical structures. Patients were treated daily, up to 5 days per week. Patients are offered mild sedation, such as benzodiazepines, during the treatment. The use of pre-treatment steroids, anti-emetics, nonsteroidal anti-inflammatory medications, and narcotics are determined according to the individual clinical presentation, proximity of critical structures, and risk of complicating edema.

Recurrence and Survival Outcome

The Georgetown University experience encompassed adult 18 patients. *Radiation Dosimetry* Depending upon previous irradiation, chordomas were treated on average with a regimen of 5×700 cGy to the margin. The isodose lines selected for individual tumors ranged from 60 % to 84 % (median 75 %). Median conformity index was 1.67, median coverage index 90.9 %. The average tumor volume (CTV) was 128 cm^3 (range 12.0–457.3 cm^3). At a mean follow-up duration of 5.8 years (range, 12 months to 18 years) from diagnosis, 14 patients were alive and 4 patients had died. Patients were followed after CK/SRS for a median of 45.5 months (range, 7–65 months). Overall survival rate by the Kaplan-Meier method was 74.3 % at 5 years after CK/SRS.

The actuarial local control rate was 59.1 % at 5 years. Seven of the eighteen patients (39 %) experienced recurrence at a mean 16 months after CK/SRS (range, 5–38); three of these same patients had recurrences prior to CK/SRS. Four patients were diagnosed with metastases after having undergone previous irradiation (3 CK/SRS, 1 EBRT) to the primary lesion. The disease-specific survival rate was 88.9 % at 5 years. Two of the four deaths were unrelated to chordoma, occurring in the absence of any evidence of disease; one death occurred at 7 months of unknown etiology, but was attributed to the chordoma; and one patient died of pulmonary complications following chordoma recurrence. There has been no evidence of recurrence of spinal chordoma in any patient in whom the tumor was totally resected and tumor site irradiated with 37.5 Gy to the tumor margin.

Quality of Life and Pain: The mean physical component of quality of life improved. Scores for the mental component of quality of life remained stable, regardless of whether the patients had undergone surgery and CK/SRS, or irradiation alone. Overall, the mean PCS and MCS scores of patients improved from 33.7 to 57.1 and from 50.3 to 58.4, respectively, and sustained a durable improvement throughout the period of observation. The mean pain score for patients prior to CK/SRS treatment was 40, which decreased to 3 for patients reaching 6 years of follow-up, reflecting a trend for the VAS to decrease ($p=0.11$). Most patients were managed with narcotic analgesics and NSAIDS. There was a tendency for MCS scores to increase following surgery ($p=0.09$); however, patients varied considerably in their responses over time.

Complications: There were no disabling (Grade 3 or 4) complications noted in this series. Three patients with previously irradiated clival chordomas (1 PBRT, 1 Gamma Knife, 1 EBRT), exhibited decreased vision or diplopia, but not blindness; two of these also had lower cranial nerve palsies. After surgery *but before* CK/SRS, two patients were hypoesthetic from lumbar and two from sacral radiculopathy; one developed a neurogenic bladder; and one urinary urgency. One patient (Illustrative Case #2) developed a neurological change after CK/SRS; she had been treated with 37.5 Gy to C3 and C4, and manifested hypoesthesia due to C4 radiculopathy and transient paresthesias possibly due to excessive spinal cord dose, although there were no findings on neurological exam. Two patients who received preoperative CK/SRS developed abdominal infections.

Results of Hypo-Fractionated Irradition

The GUH series shows an actuarial local control rate at 5 years between 50 % and 60 % for the typical fractionation scheme of 700 cGy × 5 fractions = 3,500 cGy. Single-fraction data are available from a Gamma Knife study (Krishnan et al. 2005). In that series of 25 chordomas, the 5-year local control was 32 % with a median dose of 15 Gy to the margin. Martin et al. (2007) reported on a Pittsburgh series of 18 chordomas treated with the Gamma Knife and found a 5-year actuarial local-control rate of 62.9 % for a mean tumor dose of 16 Gy to the margin. Standard fractionated radiation series, where the fraction dose is typically 1.8–2.0 Gy per fraction, have reviewed the published literature on fractionated radiation for chordomas. Their data includes dose, fraction and follow-up sufficient to determine 5-year local control with standard fractionation schemes. Tai et al. (2005). Although their analysis did not observe a dose–response relationship for local control, when the patient data were limited to standard fractionation (1.8–2.1 Gy fractions) and combined with further data from Douglas and Fowler (1976), a dose–response relationship for this fraction size did become evident: doses less than 50 Gy resulted in 5-year local control in 25 % (2/8), dose of 50–60 Gy resulted in 47 % local control (8/17), and doses in excess of 60 Gy resulted in 60 % local control (3/5).

Optimal Radiation Strategy

The rationale for treatment of chordoma should be founded upon the understanding of radiation's effect on tumor cells. The α/β ratio is a mathematical expression of a particular tissue's sensitivity to fractionated irradiation, represented in Gray (Gy). α/β ratio represents the fractionation sensitivity to low-dose fractions relative to high-dose fractions. It is not a measure of overall radiation sensitivity, but rather the sensitivity to varying the dose-per-fraction. The response of cancer cells, as well as normal cells, are typically modeled mathematically by a two-parameter model consisting of α and β, with the α component reflecting the contribution of single-hit radiation effects and β representing multiple-hit effects on a cellular target. The effect of radiation is dependent on this linear (α) component of fraction dose and a quadratic (β) component of fraction dose, and therefore radiation sensitivity can be determined by these parameters with the biological effect being proportional to $\alpha d + \beta d^2$, where d is radiation dose (Douglas and Fowler 1976). The α/β ratio represents the dose where biological effects, such as cell killing, are equally contributed by linear (α) effects and quadratic (β) effects. Tumors with a low α/β ratio (i.e. <4 Gy) will be more sensitive to the effects of a few high-dose fractions; a tumor with a high α/β ratio (i.e. >8 Gy) will be more sensitive to multiple-fractions. Most metastatic cancers are believed to have relatively high α/β ratios, which motivates the current standard radiation therapy treatment protocols that typically use 20–40 smaller dose fractions (Douglas and Fowler 1976). Some tumors, however, have low α/β ratios, such as prostate cancer, which is believed to have an α/β ratio perhaps as low as 1.5 Gy (King and Fowler 2001) and liposarcoma, which appears to have an α/β ratio less than 1 Gy (Thames and Suit 1986). These tumors would be expected to be sensitive to the effects of large fraction doses typical of single-fraction or staged radiosurgery. The α/β ratio of chordoma is unknown, though various ratios have been assigned, based on limited data, ranging from 7 to 10 Gy (Tai et al. 1995; Gwak et al. 2006). We determined this ratio for chordomas using the current series data with other published series of chordoma irradiation. Although relatively elegant in concept, determination of the α/β ratio for tumors is fraught with statistical uncertainties. Typically, this ratio is determined by a Fractionation Equivalent (FE) plot. To use this plot, the dose–response relationship is used:

$$S = e^{-\alpha d - \beta D2},$$

where *S* is the fraction of cells surviving a radiation dose *D*. Dividing this dose into n equal fractions gives:

$$S = e^{-\alpha nd - \beta nd2}$$

Illustrative Case # 1

A 53-year-old woman presented at another institution with primary complaints of perineal numbness, bladder dysfunction, and pain in her lower back and buttocks, which worsened upon sitting. MRI revealed what initially appeared to be a pseudomeningeocele secondary to a sacral cyst, but sacral laminectomy and biopsy revealed a chordoma. Two weeks later, she undewrwent intralesional resection of the dorsal portion of the chordoma (~30 % tumor volume removed) down to the level of the sacral roots. 2 months after surgery, her symptoms resolved, and she was referred for CK/SRS at GUH (Fig. 31.2a). Treatment was administered in 5 sessions of 750 cGy to the 75 % isodose line around a target volume (CTV) of 457.3 cm^3 with 90.5 % tumor coverage. MRI imaging revealed decreased size of the anterior spherical mass of irradiated chordoma from 13.4 to 2.5 cm^3 at 3 years of follow-up (Fig. 31.2b). At this point, the patient developed a marginal recurrence at the L5 level; further treatment was recommended, but the patient, who lived in a remote location, unilaterally decided upon hospice.

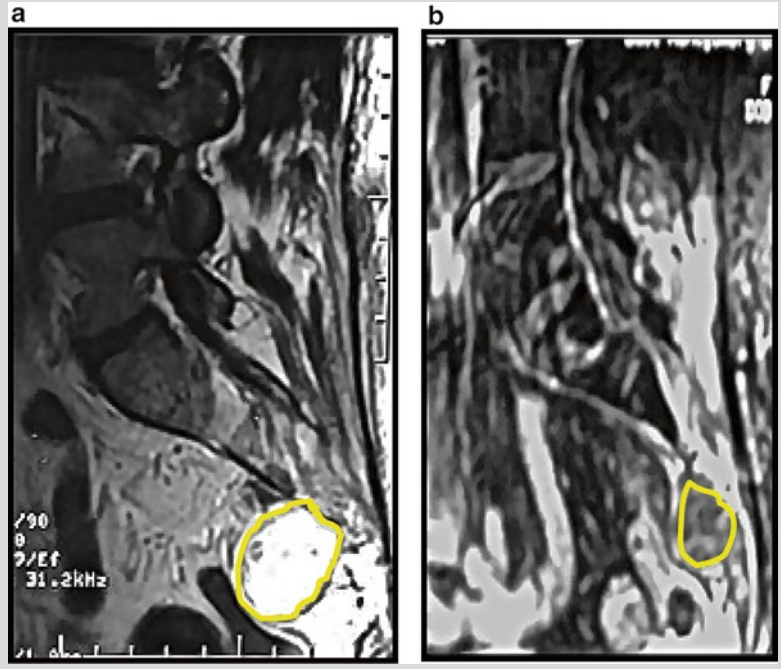

Fig. 31.2 MRI, Sagittal views, of sacrum in a 53 year old woman with sacral chordoma. (**a**) Patient underwent sacral laminectomy and resection of the dorsal component of the chordoma (approximately 1/3 tumor mass) down the level of the lumbosacral nerve roots. MRI shows the remaining spherical, pre-sacral component of chordomas (arrows) with a volume 13.4 cm^3, treated with 37.5 Gy in 5 sessions to the margin. (**b**) At 3 years, the pre-sacral mass (outlined) has reduced in size to 2.5 cm^3 3 years post-CK/SRS

Illustrative Case #2

A 29-year-old woman presented with right-shoulder and arm pain, and MRI revealed a 22.9-cm^3 lesion on the left side of C3-4 vertebrae (Fig. 31.3a). Biopsy demonstrated a chordoma. She was referred for CK/SRS and

received five fractions of 750 cGy (37.5-Gy total dose) to the 75 % isodose line with a coverage index of 89.04 %. Subsequently, she experienced C4 radiculopathy and mild, transient paresthesias. At 67 months, she had no pain, no neurological deficits, and no evidence of chordoma recurrence by MRI (Fig. 31.3b).

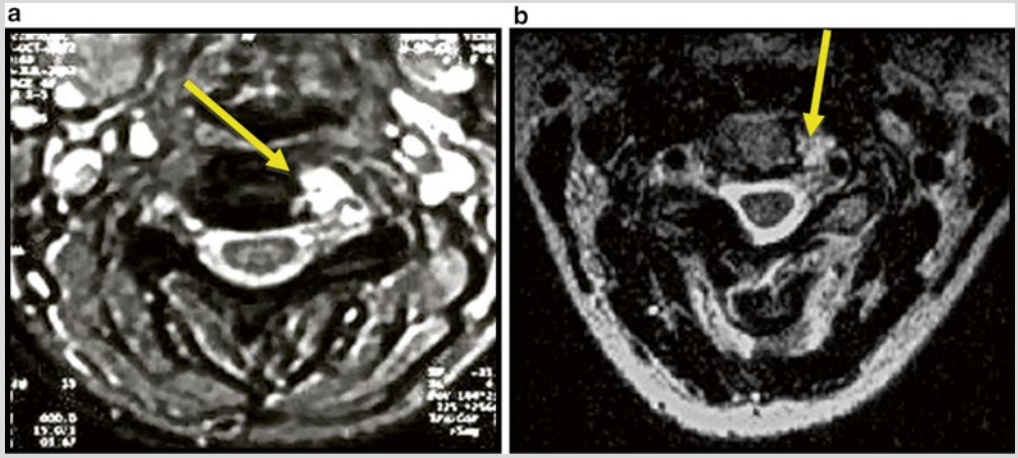

Fig. 31.3 MRI, Axial views, C3 level, T2 weighted images of a 29 year old woman who presented with right shoulder and arm pain; MRI revealed a left C3-4 chordoma (arrows) (**a**) She received 37.5Gy in five sessions of 750 cGy to 75 % isodose line; (**b**) At 67 months there is no pain, mild left C4 hypoesthesia, and no evidence of chordoma recurrence

Where *d* represents dose-per-fraction and *n* is the number of fractions. Taking the logarithm of both sides and rearranging yield:

$$-\log_e(S)/nd = \alpha + \beta d$$

This function is linear if *d* is plotted as an independent variable and 1/nd (reciprocal of the total dose) is plotted as a dependent variable, given similar outcomes (isoeffects). While the value of $\log_e(S)$ is indeterminable, the slope of the resulting line is equal to $\beta/\log_e(S)$ and the y-intercept is equal to $\alpha/\log_e(S)$. The ratio of the y-intercept over the slope therefore yields the α/β ratio. To use this technique for α/β determination, it is necessary to find clinical series using different dose and fraction schemes, but with similar local control rates. These series can yield a value through the FE plot. It is reasonable to assign a dose of ~60 Gy in 30 (2-Gy) fractions as equivalent to 16 Gy in a single fraction and equivalent to 35 Gy in 5 (7 Gy) fractions, for a 5-year local control endpoint. These three data points yield a linear regression line of reciprocal dose/fraction = 0.0033(total dose) + 0.0081 with a high R^2 value of 0.988 indicating an excellent linear fit. The ratio of y-intercept to slope yields 0.0081/0.0033, or a calculated α/β value of 2.45 Gy, a value considered low and supporting high-dose fractionation of these tumors, either with single or multiple high-dose fractions. Others recommend limited surgery to resect tumor away from critical structures to facilitate safe administration of very high doses of RT (Hug et al. 1999).

Rationale for Staging or Fractionation of Irradiation of Chordomas

The authors' rationale for multiple fractions is to minimize toxicity to CNS and maximize dose to the tumor. The calculated biological equivalent dose (BED) to the CNS decreases with respect to most tumors with increased fractionation. Furthermore, normal cells more faithfully undergo

the reparative process than tumor cells after irradiation-induced sub-lethal chromosomal injury. There are also theoretical advantages in terms of efficacy: Fowler et al. (1976) demonstrated greater tumor-cell kill with three fractions than a single dose, and attributed this increased efficacy to the increased radiosensitivity of tumor cells in the pre-mitotic phases following the first dose of irradiation; cells in these phases (late G2 and M) are more vulnerable to successive irradiation (Sinclair 1968). Oxygenation enhancement that follows the early stages of irradiation also increases the efficacy of irradiation (Howes 1969; Palcic and Skarsgard 1984).

Allowing that the α/β ratio for chordoma is 2.45 Gy derived above, the hypofractionation regimen employed in this study of 7.0 Gy×5 to the margin gives a BED to the chordoma of

$$\begin{aligned}\mathrm{BED}_{\alpha/\beta=2.45\ \mathrm{Gy}} &= 5\times 7.0\mathrm{Gy}(1+7.0\mathrm{Gy}/2.45\mathrm{Gy})\\ &= 135\mathrm{Gy}\end{aligned}$$

The dose used in this study is similar to the standard regimen of PBRT fractionation –76 Cobalt Gray Equivalents, or CGE- (Munzenrider and Liebsch 1999), where the formalism yields:

$$\begin{aligned}\mathrm{PBRT\ BED}_{\alpha/\beta=2.45\ \mathrm{Gy}} &= 38\times 2.0\ \mathrm{Gy}\\ &\quad (1+2.0/2.45\ \mathrm{Gy})\\ &= 138\mathrm{Gy}\end{aligned}$$

The CK/SRS dose used is also substantially greater than that used with EBRT fractionation (60 Gy in 30 fractions), where the BED is:

$$\begin{aligned}\mathrm{EBRT\ BED}_{\alpha/\beta=2.45\ \mathrm{Gy}} &= 30\times 2.0\ \mathrm{Gy}\\ &\quad (1+2.0/2.45\ \mathrm{Gy})\\ &= 109\mathrm{Gy}\end{aligned}$$

The authors recommend increasing the total treatment dose to 40 Gy (in 5 sessions) to the margin of the clinical treatment volume (CTV). For a chordoma α/β = 2.45Gy, a regimen of 5×8.0 Gy to the margins yields:

$$\begin{aligned}\mathrm{CyberKnife\ BED}_{\alpha/\beta=2.45\ \mathrm{Gy}} &= 5\times 8.0\ \mathrm{Gy}\\ &\quad (1+8.0/2.45\ \mathrm{Gy})\\ &= 171\mathrm{Gy}\end{aligned}$$

This regimen would yield a significantly higher dose than the standard proton-beam fractionation schedule.

Efficacy

The Georgetown University 5-year local-control rate of 59.1 %, overall-survival rate of 74.3 % and disease-specific survival rate of 88.9 % compare favorably with other series. Austin Seymour reported 5 and 10 year survival rates of 82 % and 58 % respectively; but this series of 68 patients included 28 with low grade chondrosarcoma and 4 with chondroid chordoma, which are noted for improved prognosis (Austin–Seymour et al. 1989). Munzenrider (MGH) achieved 4 year local control in 70 % (including chondrosarcomas), treated with a median dose 69 CGE (70–100 % by protons) (Munzenrider and Liebsch 1999). Others report Proton Beam Radiation (PBR) 5 year disease-free survival of 42 % (Igaki et al. 2004), and 59 % (Berson et al. 1988; Hug et al. 1999). Noel reported on 100 consecutive chordomas treated with PBR: the median interval from treatment to recurrence was 26 months, the 4 year disease free survival rate was 53.8 %, with a 5 year overall survival rate of 80.5 % (Noel et al. 2005). The Proton beam advantage is related to the steep dose gradient achieved with rapid fall off after Bragg Peak, which allows relatively precise tumor targeting and the ability to deliver high doses to the target (Munzenrider and Liebsch 1999). Single fraction treatment with Gamma Knife has resulted in local control rates 66 % at 40 months, (Muthukumar et al. 1998) for chordomas and chondrosarcoma using a median dose of 16.5 and 18.0 Gy respectively. The authors attributed failures to inadequate margin and inadequate dose.

In the GUH experience, tumors treated with >35 Gy (in 5 stages) to the margin exhibited no recurrence. However, treatment doses of less than 3,500 cGy (in 5 stages) resulted in a 31 % marginal recurrence rate, and all tumors receiving 3,000 cGy or less to the margin recurred.

Pain and Quality of Life After CK/SRS

The GUH experience showed that quality of life was maintained or improved in every patient, in terms of both the physical component and the mental component. Though pain and quality of life have not been generally reported in other series, Muthukumar reported neurological improvement of cranial nerve deficits with single fraction

Gamma Knife series, using a median dose of 18 Gy (Muthukumar et al. 1998), but Krishnan reported worsening of neurological symptoms in 24 % of patients with Gamma Knife (Krishnan et al. 2005). Imai reported stable Karnofsky performance scores and reduction of narcotic use in 6 of 14 patients undergoing carbon ion therapy (Imai et al. 2004). Other heavy particle series reported 13–20 % rate of severe complications, including myelitis, brain stem injury and brachial plexopathy (Castro et al. 1989; Berson et al. 1988).

In a series of 35 patients undergoing *en bloc* resection followed by EBIR, patients reported that pain was "incapacitating or severe" in 80 %, and mild or none in 20 % (Boriani et al. 2006). The largest series of extirpative clival surgery followed by proton beam, Gamma Knife or EBIR, demonstrated excellent survival but significant decrease in functional outcome (40 % by the Karnofsky Performance score) (Gay et al. 1995). Similarly, excellent survival outcomes after sacrectomy were attended by decreased neurological function in 20/27 cases (75 %) (York et al. 1999).

Complications

Total dose is limited by the potential for radiation toxicity, exemplified by radiation myelitis. The use of hypo-fractionated, or multi-session- stereotactic radiosurgery results in minor paresthesias in the cervical, lumbar and sacral nerve roots, but radiation myelitis is rare. On the other hand, Marucci reported 4 cases of radiation myelitis in patients who received 70 CGE to the spine (Marucci et al. 2004). Skull base irradiation with protons resulted in significant neurological worsening (Austin–Seymour et al. 1989), and a 42 % incidence of pituitary complications (Munzenrider et al. 1999). Others report grade 3, 4 toxicity (Hug et al. 1999), blindness and delayed optic neuropathy (Bowyer et al. 2003). Helium ion yielded a 27 % complication rate (Castro et al. 1994).

The Fowler linear quadratic formalism may be used to compare the relative biological equivalent doses (BED) administered in the various treatment regimens (Douglas and Fowler 1976). The α/β ratio is generally given as 2.2 Gy for central nervous system and peripheral nerves. The maximum safe dose (TD1 %, or Tolerance Dose with 1 % Complication Rate) for the spinal cord with standard fractionation (1.8 Gy×30 fractions) results in a Biological Equivalent Dose (BED):

$$\begin{aligned} \mathrm{BED}_{\alpha/\beta=2.2\,\mathrm{Gy}} &= 30\times 1.8\mathrm{Gy}(1+1.8/2.2\mathrm{Gy}) \\ &= \mathbf{98Gy} \end{aligned}$$

Therefore, a fractionation regimen resulting in a BED of 98 Gy is theoretically encumbered by a risk of radiation myelitis of no greater than 1 %. The CK Inverse Treatment Planning (minimizing dose to critical structures) and steep fall-off of irradiation (due to conformality of CK irradiation) allows a 8 % fall-off of maximum dose to CNS for every millimeter. The CNS is exposed to approximately 60 % of prescription dose for an epidural tumor. Thus, for a single fraction of 8.0 Gy administered to the tumor, only 4.8 Gy (i.e. 0.6×8.0 Gy=4.8 Gy) actually impacts the cord. Therefore, the proposed regimen (5×8.0 Gy) yields:

$$\begin{aligned} \mathrm{BED}_{\alpha/\beta=2.2\,\mathrm{Gy}} &= 5\times 4.8\mathrm{Gy}(1+4.8\mathrm{Gy}/2.2\mathrm{Gy}) \\ &= \mathbf{76Gy} \end{aligned}$$

which remains well under the TD1 % of the spinal cord.

In conclusion, disease-specific survival rate of 88.9 % in the GUH experience suggests that hypo-fractionated stereotaxic radiosurgery (multi-session stereotaxic radiosurgery offers promise in the treatment of chordomas. The proposed increase to 40 Gy to the margin in 5 sessions appears to promise a favorable BED to the chordomas with relative sparing of the adjacent critical structures. The estimation of the $\alpha/\beta=2.45$ Gy predicts improved outcomes with large doses in a hypo-fractionation regimen. Durable maintenance in pain and quality of life are generally recorded after treatment with CK/SRS. Results indicate that CK/SRS's safety and efficacy profile compares favorably with other modalities in the treatment of chordomas.

References

Al-Mefty O, Borba LAB (1997) Skull base chordomas: a management challenge. J Neurosurg 86:182–189

Austin–Seymour M, Menzenrider J, Goitein M, Verhey L, Urie M, Gentry R, Birnbaum S, Ruotolo D, McManus

P, Skates S et al (1989) Fractionated proton radiation therapy of chordoma and low-grade chondrosarcoma of the base of the skull. J Neurosurg 70:13–17

Berson AM, Casrtro JR, Petti P, Phillips TL, Gauger GE, Gutin P, Collier JM (1988) Charged particle irradiation of the chordomas and chondrosarcoma of the base of the skull and cervical spine. Int J Neurosurg 70:13–17

Boriani S, Bandiera S, Biagini R, Bacchini P, Boriani L, Cappuccio M, Chevalley F, Gasbarrini A, Picci P, Weinstein JN (2006) Chordoma of the mobile spine: fifty years of experience. Spine 31(4):493–503

Bowyer J, Natha S, Marsh I, Foy P (2003) Visual complications of proton beam therapy for clival chordoma. J Eye 17(3):318–323

Castro JR, Collier M, Petti PL (1989) Charged particle radiotherapy for lesions encircling the brainstem or spinal cord. J Int Radiat Oncol Biol Phys 17:477–484

Castro JR, Linstadt DE, Bahary JP (1994) Experience in charged particle irradiation of tumors of the skull base. Int J Radiol Oncol Biol Phys 29:647–655

Degen JW, Gagnon GJ, Voyadzis JM, McRae DA, Lunsden M, Dieterich S, Molzahn I, Henderson FC (2005) CyberKnife stereotactic radiosurgical treatment of spinal tumors for pain control and quality of life. J Neurosurg Spine 2(5):540–549

Douglas BG, Fowler JR (1976) The effect of multiple small doses of x rays on skin reactions in the mouse and a basic interpretation. Radiat Res 66:401

Fowler JF (1983) Dose response curves for organ function or cell survival. Br J Radiol 56(667):497–500

Fowler JF, Sheldon PW, Denekamp JA, Field SB (1976) Optimum fractionation of the C3H mouse mammary carcinoma using x-rays, the hypoxic-cell radiosensitizer Ro-07–0582, or fast neutrons. Int J Radiat Oncol Biol Phys 1(7–8):579–592

Fuller DB, Bloom JG (1988) Radiotherapy for chordoma. Int J Radiat Oncol Biol Phys 15(2):331–339

Gay E, Sekhar LN, Rubinstein E, Wright DC, Sen C, Janecka IP, Snyderman CH (1995) Chordomas and chondrosarcomas of the cranial base: results and follow-up of 60 patients. Neurosurgery 36(5):887–896, discussion 896–897

Gwak HS, Yoo HJ, Youn SM, Chang U, Lee DH, Yoo SY, Rhee CH (2006) Hypofractionated stereotactic radiation therapy for skull base and upper cervical chordoma and chondrosarcoma: preliminary results. Stereotact Funct Neurosurg 83(5–6):233–243

Howes AE (1969) An estimation of changes in the proportions and absolute numbers of hypoxic cells after irradiation of transplanted C3H mousemammary tumours. Br J Radiol 42(498):441–447

Hug EB, Loredo LN, Slater JD, DeVries A, Grove RI, Schaefer RA, Rosenberg AE, Slater JM (1999) Proton radiation therapy for chordomas and chondrosarcomas of the skull base. J Neurosurg 91(3):432–439

Igaki H, Tokuuye K, Okumura T, Sugahara S, Kagei K, Hata M, Ohara K, Hashimoto T, Tsuboi K, Takano S, Matsumura A, Akine Y (2004) Clinical results of proton beam therapy for skull base chordoma. Int J Radiat Oncl Biol Phys 60(4):1120–1126

Imai R, Kamada T, Tsuji H, Yanagi T, Baba M, Miyamoto T, Kato S, Kandatsu S, Mizoe JE, Tsujii H, Tatezaki S (2004) Working Group for Bone, Soft Tissue Sarcomas. Carbon ion radiotherapy for unresectable sacral chordomas. Clin Cancer Res 10(17): 5741–5746

King CR, Fowler JF (2001) A simple analytic derivation suggests that prostate cancer alpha/beta ratio is low. Int J Radiat Oncol Biol Phys 51(1):213–214

Krishnan S, Foote RL, Brown PD, Pollock BE, Link MJ, Garces YI (2005) Radiosurgery for cranial base chordomas and chondrosarcomas. Neurosurgery 56(4):777–784, discussion 777–784

Martin JJ, Niranjan A, Lunsford LD (2007) Radiosurgery for chordomas and chondrosarcomas of the skull base. J Neurosurg 107(4):758–764

Marucci L, Niemierko A, Liebsch NJ, Aboubaker F, Liu MC, Munzenrider JE (2004) Spinal cord tolerance to high-dose fractionated 3D conformal proton-photon irradiation as evaluated by equivalent uniform dose and dose volume histogram analysis. Int J Radiat Oncol Biol Phys 59(2):551–555

Munzenrider JE, Liebsch NJ (1999) Proton therapy for tumors of the skull base. Strahlenther Onkol 175(suppl 2):57–63

Muthukumar N, Kondziolka D, Lunsford LD, Flickinger JC (1998) Stereotactic radiosurgery for chordoma and chondrosarcoma: further experiences. Int J Radiat Oncol Biol Phys 41(2):387–392

Noel G, Feuvret L, Calugaru V, Dhermain F, Mammar H, Haie-Meder C, Ponvert D, Hasboun D, Ferrand R, Nauraye C, Boisserie G, Beaudre A, Gaboriaud G, Maza LA, Habrand JL, Mazeron JJ (2005) Chordomas of the base of the skull and upper cervical spine. One hundred patients irradiated by a 3D conformal technique combining photon and proton beams. Acta Oncol 44(7):700–708

Palcic B, Skarsgard LD (1984) Reduced oxygen enhancement ratio at low doses of ionizing radiation. Radiat Res 100(2):328–339

Sinclair WK (1968) Cyclic x-ray responses in mammalian cells in vitro. Radiat Res 33(3):620–643

Tai PT, Craighead P, Bagdon F (1995) Optimization of radiotherapy for patients with cranial chordoma. A review of dose–response ratios for photon techniques. Cancer 75(3):749–756

Thames HD, Suit HD (1986) Tumor radioresponsiveness versus fractionation sensitivity. Int J Radiat Oncol Biol Phys 12(4):687–691

York JE, Kaczaraj A, Abi-Said D, Fuller GN, Skibber JM, Janjan NA, Gokaslan ZL (1999) Sacral chordoma: 40-year experience at a major cancer center. Neurosurgery 44(1):74–79, discussion 79–80

Index

M.A. Hayat (ed.), *Tumors of the Central Nervous System, Volume 12*,
DOI 10.1007/978-94-007-7217-5, © Springer Science+Business Media Dordrecht 2014

F